PRINCIPLES OF STRUCTURAL INTEGRITY TECHNOLOGY

Office of Naval Research
Arlington, Va.

exclude many useful metals, and (b) they require the assumption that all structures are

PRINCIPLES OF STRUCTURAL INTEGRITY TECHNOLOGY

William S. Pellini

Superintendent Metallurgy Division (Retired)
Naval Research Laboratory

Adjunct Professor of Mechanical Engineering
Catholic University of America

1976

316 p.

N0014-75-C-0917

Office of Naval Research
Arlington, Va.

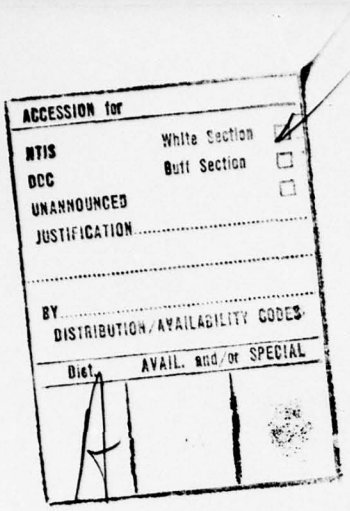

To
Kathryn and Mary

Sponsored by the Office of Naval Research
Contract No. N00014-75-C-0917

Library of Congress Catalog Number
76-50534

Available through the U.S. Department of Commerce, National Technical Information Service,
5285 Port Royal Road, Springfield, Va. 22161.

FOREWORD

This book is a rare achievement, summarizing coherently more than 25 years of groundbreaking research on real problems. During those years the author, by virtue of his ability to see past the immediate symptoms of engineering problems to their root causes, originated radically new principles for structural reliability assurance in engineering design and made possible practical application of the many new materials and engineering techniques.

These advanced materials and methods enormously improved the performance of naval vehicles and other structures, but they often at the same time presented engineers and designers with serious difficulties that blocked their practical use. Fortunately, Mr. Pellini was in a unique position to be aware of and deal with many of the most crucial engineering and design problems. In his work at the Naval Research Laboratory he was able to solve the most troublesome of these problems and to advance basic technological capabilities.

His status was not accidental. Mr. Pellini early gained the respect of both engineers and designers by his desire to deal with real problems and to direct research at meaningful goals. Beginning with the widely known brittle failures of ships and tankers, in which entire ships sometimes fractured in calm water at dockside, and continuing to the present age of high-performance ships, aircraft, and missiles, he has shown a remarkable ability to resolve the basic engineering issues. For example, in the ship failures the problem was metallurgical in nature. New laboratory test methods were needed, to demonstrate the true nature of the problem, before any realistic solution could be undertaken.

Mr. Pellini's involvement in this effort led to invention of the Drop-Weight NDT test, which was the first new Standard Method for characterizing fracture resistance of metals adopted by the ASTM in 30 years. At the same time, his broad-scope research in brittle fracture of steels culminated in the Fracture Analysis Diagram, which became the criteria-setting standard for design of steel structures. After this, the introduction of new high-strength metals and the maturity of general fracture mechanics led to Ratio Analysis Diagram concept, which has proved invaluable in selecting material systems.

A major contribution of Mr. Pellini has been his synthesis of the many variables affecting material performance into rational and coherent engineering approaches that can be understood and applied by designers. A large part of this book concerns translation of the physical phenomena of fracture and crack growth to a format that facilitates engineering analysis. Particularly important is the integration of material, fracture, design, fabrication, and environmental loading concepts into the total *Structural Integrity* approach to design. The principles developed by Mr. Pellini are now being invoked in contracts for design and construction of the future high-performance ship fleet and form the foundation for application of Structural Integrity Technology in other areas. All the answers are not yet available; developmental programs continue to identify new problems. However, the basic technology laid down here will be as valid in the future as in the past and will be the cornerstone of materials structures and engineering developments for many years.

The accolades and awards bestowed on Mr. Pellini highlight the value of his efforts to the entire scientific and engineering community of the nation. The highest Department of Defense and the Navy awards for scientific and engineering achievement are matched by the highest honors of the Washington Academy of Science, the American Society of Naval Engineers, the American Foundrymen's Society, the American Welding Society, and the American Society for Metals. During his active Navy career he published more than 150 papers on many topics and lectured extensively in the United States, Western Europe, and Asia. In 1974 he crowned an illustrious career by being elected to the National Academy of Engineering.

PETER M. PALERMO
Assistant Chief Naval Architect
(Structures)

Hull Division
Naval Ship Engineering Center

CONTENTS

PREFACE viii
NOMENCLATURE xii

1. INTRODUCTION 1
   - Background 1
   - Development of SI methods 1
   - Design philosophy 2
   - General procedures 2
   - Certification objectives 4
   - Educational requirements 4

2. MICROMECHANICAL CRACK EXTENSION PROCESSES 7
   - Chain of events 7
   - Engineering significance of microfracture 13
   - Cleavage fracture 19
   - Effects of microfracture transitions 25
   - Micromechanisms of void growth 27

3. FRACTURE MECHANICS CRITERIA 31
   - Relationships to fracture state 31
   - Physical significance of constraint 32
   - Constraint relaxation 36
   - Significance of fracture states 38
   - Metallurgical aspects of constraint transitions 39
   - Fracture-extension processes 43
   - Section-size effects 45
   - Plane-strain transition effects 48
   - Definition of constraint capacity 49
   - Test methods featuring definable constraint 51

4. FRACTURE CHARACTERIZATION AND ANALYSIS FOR STEELS EXHIBITING TEMPERATURE TRANSITIONS 55
   - General principles 55
   - Statistical aspects of metal quality 59
   - Loading rate effects 59
   - Characteristic K_{Id} curve 61

5. FRACTURE CHARACTERIZATION AND ANALYSIS: STRENGTH-TRANSITION EFFECTS 63
   - Strength-scale reference 63
   - Introduction to the RAD 64
   - Generalized RAD procedures 67
   - Combined K_{Ic} and DT scales 71
   - Metallurgical basis of quality corridors 72

Statistical variance of properties 74
Titanium and aluminum alloys 79
Critical-edge concept 81
Standard RAD format 81

6. FRACTURE-CONTROL PRINCIPLES: TEMPERATURE-TRANSITION PROBLEMS 87
Early studies of initiation and arrest 87
Natural crack tests 94
Crack arrest tests 102
Fracture Analysis Diagram (FAD) 105
Evolution of DT test 114
Section-size effects 116
Expanded version of FAD 120
Deterministic analysis procedures 122

7. FRACTURE-CONTROL PRINCIPLES: STRENGTH-TRANSITION PROBLEMS .. 125
Developments in retrospect 125
Low range of strength transition 129
High range of strength transition 131
Intermediate range of strength transition 133
Cost Analysis 138
Role of metallurgical factors in inspection 140
Probability assessments 142

8. CHARACTERIZATION AND CONTROL OF CRACK STATES IN WELD REGIONS 145
Structural criticality of weld regions 145
Fracture properties of weld zones 148
Generic problems of weld zone cracking 155
Phenomena of hydrogen-assisted cracking 160
Phenomena of restraint cracking 162
Systems analysis of weld factors 164

ADDENDUM: INTRODUCTION TO WELDING METALLURGY AND WELDING PROCESSES 167
Welding metallurgy for steels 167
Pearlitic steels 169
Quenched and tempered alloy steels 171
Welding processes 174
Electrode specification and alloy compositions 180

9. ANALYTICAL CRITERIA FOR CRACK GROWTH UNDER SUSTAINED LOAD 183
Reference system 183
Characterization criteria 184
Analytical significance of K_{Iscc} transitions 190
Environmental effects 194
Growth-rate factors 198
Metallurgical considerations 199

10. CHARACTERIZATION AND TERMINAL-ENVELOPE ANALYSIS FOR FATIGUE AND CORROSION FATIGUE 203

Technological status 203
Characterization of cyclic crack growth 204
Combined analysis 211
SI objectives for fatigue analyses 214

11. SPECIALIZED STRUCTURAL PROBLEMS: FRACTURE CONTROL FOR PLASTIC-STRESS SYSTEMS 217
Background 217
Physical model of plastic fracture 219
Control principles for plastic fracture 224
Generic problem areas 225

12. ROLE OF ANALYTICAL PROCEDURES IN FORMAL CERTIFICATION OF STRUCTURAL RELIABILITY BY CODES, RULES, AND STANDARDS 233
Certification philosophy 233
Applications to codes, rules, and standards 235
Modernization of specification systems 236
Certification by analysis for existing structures 240
Technological benefits of formal certification—case example of reactor pressure vessels 242
Certification requirements for specialized problems of crack growth—case example of hydrofoil craft 245
Requirements for reference to fracture state—case examples of aerospace structures 247

APPENDIX A—Introduction to Linear-Elastic, Plane-Strain Fracture Mechanics 251
Theoretical principles 251
Plane-strain test procedures 256
Fracture mechanics terms and equations 260

APPENDIX B—Graphical Analysis by Reference to the Characteristic K_{Id} Curve 263
General methods 263
Case examples of graphical analysis 267

APPENDIX C—Strength Transition: Case Example and Reference Tables 277
Case example of design based on arrest and initiation principles 277
Reference tables—alloy compositions of high strength steels 280

APPENDIX D—Introduction to Structural Steels 285
Alloy compositions of standard-grade steels 285

APPENDIX E—Fundamental Significance of the R-Curve Expression for Fracture-Extension Resistance 289
Fracture mechanics theory 289
Physical significance of R curves 290
R-curve characterization 292
RAD consolidation of R_p data 298

BIBLIOGRAPHY 301

INDEX 309

PREFACE

BACKGROUND

The last decade's dramatic advances in structural engineering are the synergistic result of many technological efforts. The driving forces for the efforts have been structural performance objectives beyond the bounds of existing technology.

The structural performance and reliability objectives were established according to the needs of the many radically new engineering systems developed in the last 10 years. The efforts have resulted in traumatic failures as well as notable successes. The failures were particularly significant; they made gaps in engineering knowledge glaringly evident.

In general, the failures were in the analysis of fracture and crack growth in metal. Clearly, the procedures for design, metal selection, and fabrication were inadequate for analyzing or assuring structural reliability. Engineers were forced to revise technological principles in the light of a new base of information for characterization of fracture and crack growth.

The adoption of new, rational characterization methods was the key to subsequent rational development and selection of alloys. These developments, based on *formal analytical methods,* were profoundly significant to structural technology. Previous alloy development and selection practices had been guided mainly by strength level objectives.

Similarly, the bases for rational, advanced fabrication methods were clarified. The important milestone was the departure from the primary use of strength level as a guide in development and selection of weld metals.

The role of systems analysis in the coherent application of new rational principles cannot be overemphasized. It was most important that the research efforts in design, materials, and fabrication were combined into an integrated whole.

Objectives

The subject matter of this textbook precludes abstract presentation of the separate roles of the engineering fields that contribute to structural integrity (SI) technology. Specialized engineering fields must be examined in the context of rational certification of structural reliability, as related to fracture and crack growth.

The main objective is a realistic and informative exposition of the primary engineering areas that must be integrated in the design process.

All discussions are in the context of a total systems approach to the integration of the specialized fields. Scientific principles that must be described in specialized terms are discussed in appendixes.

The presentations are intended to provide a tutorial introduction for engineering students and practicing engineers. The subject is explained by sequential exposition of scientific fundamentals, engineering criteria, analytical procedures, case examples, generalized principles, and certification requirements.

The interactions of design, materials characterization, fabrication, and inspection are examined for various types of structures. The consistent connection of the sections into a cohesive treatment of the subject rests almost entirely on the use of fracture mechanics ratio analysis and fracture-state criteria. There is no other way to effectively cross-reference the full span of mechanical and metallurgical considerations.

Selective reading can provide a reasonable introduction for those who have a general interest in the subject. For example, the sections on engineering fracture mechanics are useful for those who need such clarification for general reasons. The sections on welding and welding metallurgy are a compact introduction to this field, which generally is not understood by those who have a background in a mechanical discipline.

For proficiency in the subject, it is expected that the material would be the basis for a full one-year engineering course. Careful reading of the text, plus an intensive, one- to three-day series of lectures, should provide a reasonable familiarity to general engineering audiences.

Combined Use of English and Metric Units

The material of this text is expected to be of immediate and long-range interest to diversified groups of practicing engineers and students. In deference to all interests, a balanced system of reference to English, metric, and metric (SI) units was adopted.

The nomograph on page ix presents approximate conversions for stress and stress intensity (K_I) values from English to metric or vice versa. Strength values are cited in the figures in terms of ksi and kg/mm^2 units, while the text uses ksi and MPa units. Values of stress intensity (K_I) are cited only in ksi$\sqrt{\text{in.}}$ units, with the exception of specialized tables.

Conversions of temperatures and dimensions are made to the same degree of approximation that is implied by the measurement.

These various decisions were made for purposes of simplification of the text, with retention of familiar systems of units for most readers.

Acknowledgments

The origins of the technology that is the subject of this textbook may be assigned to research activities at the Naval Research Laboratory (NRL), under sponsorship of the Office of Naval Research (ONR). For 25 years, from 1950 to 1975, the two organizations provided the necessary resources and research freedom for the development of these new technological principles of fracture mechanics and mechanical metallurgy.

The development of the scientific principles into a mature engineering technology was marked by direct applications to a great variety of structures of naval interest. The interest of

a succession of chief engineers in naval organizations was of paramount importance. In effect, the entire Navy hardware system was used to test the new principles.

From this basis of engineering applications, there was an ever-broadening expansion of applications within the Federal Government and in industry. The importance of these users cannot be overstated. Their experience is the basis for the present confidence in technological applications.

The direct costs of developing this system exceed $100 million. Laboratory research accounted for about one-fourth of the cost, and three-fourths involved experimental applications and trials.

The cost of initial applications to serial production of structures designed according to the new principles of reliability assurance (such as submarines and aircraft) is beyond measure. However, these applications provided convincing proof, in service, of the reliability of the new technology. The contributions of those who made these pioneering decisions is acknowledged with fond remembrance and gratitude.

From beginning to end of the activity, the initiative was provided by the superb combined research and engineering teams of the Metallurgy and Mechanics Divisions of NRL. It was my good fortune to be associated with the members of these two notable organizations, the finest in this field ever assembled. With their combination, NRL was recognized as the leading international center for the development of structural integrity technology. This leading position was held for more than 20 years.

The sponsorship of this textbook by the Material Sciences Division (Code 470) of ONR is acknowledged with sincere gratitude. The object was to make the textbook available, at the lowest possible cost, to practicing engineers and students who may exploit the technology in the future.

I wish to record my appreciation for leadership in developing analysis diagrams by my principal associates, R. J. Goode, R. W. Judy, E. A. Lange, P. P. Puzak, T. W. Crooker, F. J. Loss, and C. T. Fujii. These diagrams hold the essence of an enormous amount of scientific and engineering information. Their lectures, also, have contributed greatly to the structure of the book as a practical guide for engineers.

November 1976

WILLIAM S. PELLINI

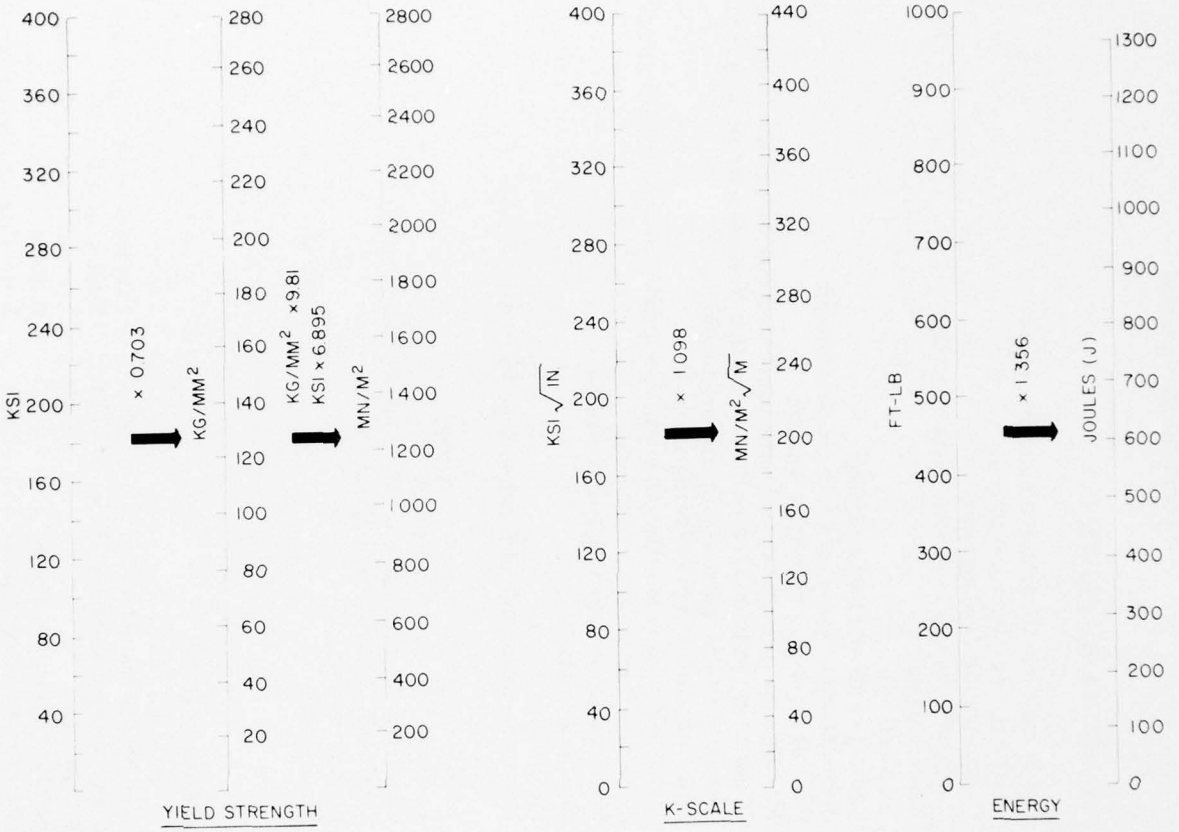
KSI
400
360
320
280
240
200
160
120
80
40
× 0703
KG/MM²
280
260
240
220
200
180
160
140
120
100
80
60
40
20
KG/MM² × 9.81
KSI × 6.895
MN/M²
2800
2600
2400
2200
2000
1800
1600
1400
1200
1000
800
600
400
200
YIELD STRENGTH
KSI √IN
400
360
320
280
240
200
160
120
80
40
0
× 1.098
MN/M² √M
440
400
360
320
280
240
200
160
120
80
40
0
K-SCALE
FT-LB
1000
900
800
700
600
500
400
300
200
100
0
× 1.356
JOULES (J)
1300
1200
1100
1000
900
800
700
600
500
400
300
200
100
0
ENERGY

NOMENCLATURE

FRACTURE MECHANICS TERMS

a	Depth, half length, or half diameter of crack
B	Thickness of plate or specimen
COD	Crack opening displacement
ΔK	Range of K values in fatigue-crack extension
E	Young's modulus
ϵ	Tensile strain
ϵ_c	Critical value of e for instability
$\mathcal{G}$	Strain energy release rate with crack extension
$\mathcal{G}_{Ic}$	Critical value of $\mathcal{G}$ for elastic fracture
K, K_I	Stress intensity factor (The subscript I denotes the opening mode of crack extension.)
K_c	Plane stress condition at crack tip for initiation; also crack conditions in propagation
K_{Ic}	Slow load (static) plane-strain fracture toughness
K_{Id}	Dynamic plane-strain fracture toughness
K_{Iscc}	Lowest value of K for slow extension of cracks in stress corrosion environments
J_c	J-integral fracture toughness index
L	Plane-strain limit by this fracture mode
PZS	Plastic-zone size
r	Plastic-zone radius
R_p	Numerical expression of R-curve slope for plastic fracture
σ, σ_N	Applied stress
σ_{yd}	Yield strength for dynamic loading
σ_{ys}	Yield strength for slow loading
R	Characteristic resistance to extension of plastic fracture
Ratio	Signifies K_{Ic}/σ_{ys}, K_{Id}/σ_{yd}, or K_{Iscc}/σ_{ys}
YC	Yield criterion
$2c$	Crack width

ENGINEERING TERMS

NDT	Nil ductility transition temperature obtained by drop weight test
FTE	Fracture transition elastic
FTP	Fracture transition plastic
DWT	Drop weight test
DT	Dynamic tear test
CAT	Robertson crack arrest temperature
C_v	Charpy-V test
ECST	Explosion crack starter test
ETT	Explosion tear test
FAD	Fracture analysis diagram
RAD	Ratio analysis diagram
IAD	Instability analysis diagram
PWE	Plastic work energy for fracture
TL-F	Technological limit for fracture properties (RAD)
NDI	Nondestructive inspection

CHAPTER 1

Introduction

BACKGROUND

In the past, engineers did not have an objective method for quantifying the fracture and crack-growth behavior of proposed structures. Instead, they had to rely on qualitative assessments by specialists. As a result, expensive retrofitting has often been necessary to correct failures that occurred in testing or in service.

Structural integrity (SI) technology—a new system of engineering methods—offers practical solutions to these problems. SI methods enable designers to certify before construction that a structure meets numerically expressed standards for structural integrity. The demand for such certification is growing, and, in many cases, SI certification is now a contractual requirement.

Structural integrity technology focuses on the effects of sharp cracks and metallurgical defects to which failures of massive structures can usually be traced. It is based on accurate measurement of fracture and crack-growth properties, using test methods adapted from fracture mechanics. By testing small specimens that have sharp notches and cracks, the cracking behavior of metals is quantified and used to predict conditions under which the metals will fail. The object is to compile standard system of numerical data that can be analyzed objectively. Such analysis can replace the traditional appeal to expert opinion and thus provide the basis for formal certification of structural integrity. Certification must be based on rational, numerical description of properties; qualitative assessments by specialists cannot be standardized.

Where the public interest and safety are affected, certification based on the use of SI principles may be required by statute. The principles provide the commonly understood references essential for the dialogue between those who impose standards and those who must meet them.

DEVELOPMENT OF SI METHODS

SI analysis has developed along a remarkably direct path. In the past two decades, one cycle of intense activity has followed another. Investigations of in-service failures established the importance of fracture properties, on the one hand, and of design and fabrication procedures, on the other. Studies of the mechanics of materials produced the science of fracture mechanics. Metallurgists developed reference systems for metal properties. Systems analysis integrated all these aspects of structural integrity, opening the way for formal, systematic codes, rules, and standards.

The early studies of in-service failures pointed clearly to the need for more exact determination of the crack sensitivities of metals. However, the success of fracture mechanics analytical procedures in quantifying fracture and crack growth raised objections as well as interest. It was objected that (a) the analyses are limited to brittle metals and therefore

exclude many useful metals, and (b) they require the assumption that all structures are defective.

Failure analyses and improved nondestructive inspection made it obvious that the crack states in a structure must be analyzed. They also encouraged acceptance of such analysis as part of design. After this general acceptance, the birth of formal SI procedures required only realistic criteria for fixing the statistical upper bound of crack size for design purposes. This depended on practical engineering experience with various types of structures and fabrication methods, plus the ability to quantify the capacity of inspection techniques to detect cracks.

DESIGN PHILOSOPHY

The fact that a critical stress intensity for crack extension is an inherent property of crack-sensitive metals does not restrict engineers to the use of crack-insensitive metals alone. SI technology establishes reliable procedures for using metals of intermediate crack sensitivity. In addition, the technology must establish the highest acceptable degree of crack sensitivity for specific structural design objectives. It provides the only engineering analysis and criteria base for most metals developed for high-performance structures.

The necessity of using metals with definable (that is, controlled) crack states and crack sensitivity leads to cross-reference analysis of limits. As the limit of crack-state stress intensity in a structure is permitted to increase, the crack sensitivity of the metal must decrease, and vice versa.

The engineering tradeoffs of cross-reference analyses must take into account design details and fabrication quality. These are of critical first-order importance. If structural details are poorly designed or fabricated, crack stress intensities will be high, and metals of low sensitivity to cracking must be used. Conversely, if connections are faired to provide smooth transfer of stress by details, forgings are normally used. This places the welds, which have intrinsically higher crack states, outside the regions of maximum stress. In this case, the intrinsic crack sensitivity of the metal may be permitted to be higher than if design and fabrication impose high crack stress intensities. For example, stronger (and more crack-sensitive) metals may be used safely.

SI technology requires iterative analysis of alternatives. Candidate metal systems, crack-state control, structural design details, and fabrication must all be considered. By tradeoffs among these factors, within limits of other functional and economic factors, a rational and accurate solution can be reached in the course of design. The procedures for making these tradeoffs must be formalized to meet the certification needs of structural engineering.

GENERAL PROCEDURES

Fracture and crack-growth control plans generally develop in steps closely linked to the stages of preliminary and detailed design. The complexity of the analysis depends on the given design problem. For novel structures and metals or complex design details, many analyses are required; alternate designs and fabrication methods must be considered, new data collected, and models tested. For conventional structures and materials, the problem is simply to select from among candidate metals according to existing data on their properties.

Metallurgical considerations are decisive in determining the complexity of the analysis. The most decisive metallurgical consideration is the *transitional* nature of all metal systems. Sharp transitions from low to high sensitivity to fracture and/or crack growth appear in all structural metals as their strength increases and, in steels, as temperature decreases.

Microstructural quality and section-size effects dictate the intrinsic crack sensitivity of a given metal at given temperatures and strength levels. To be useful in first-order analyses, these data must be systematized to present the range of crack sensitivities that apply at specific temperatures or strength levels.

Analysis diagrams of the type used in this text are essential for examining the range of properties in a given metal system (steels, aluminum, titanium) at specified strength levels. The consequences of raising or lowering yield strength are displayed by sharp transitions, and the benefits of shifting from low- to high-quality metals are indicated clearly.

The initial metallurgical analysis dictates the degree to which the SI plan must be applied in design and fabrication. This analysis indicates that the metal falls into one of three categories of crack sensitivity:

Insensitive—Structural reliability is inherent in the metal; the metal certifies the SI plan.

Highly sensitive—No reliable SI plan can be evolved except by designing for structural redundancy.

Moderately sensitive—Design and fabrication require exacting control, as indicated by the sensitivity level.

First-order metallurgical analyses are critical; they can lead to early adjustments in specified yield strength or metal quality. Many disasters with missiles, aircraft, and ships resulted from selecting metals mainly on the basis of strength level or cost. These criteria tended to result in selection of metals of excessive crack sensitivity. As a result, reliable SI plans could not be developed as retrofit solutions.

However, this unfortunate experience provides a major source of information for SI technology. The progress of SI technology would have been delayed without research effort and funds made available by crises due to structural failures.

The generalization of metallurgical analysis procedures is a major advance for SI technology. It is the most directly teachable part of the technology, which is fortunate, because it is the most fundamental.

The formalization of SI procedures for design and fabrication is more difficult to explain, because the procedures deal with specific certification objectives, which vary with the nature of the design problem. However, the general principles are explainable in terms of certification objectives for codes, rules, and standards.

CERTIFICATION OBJECTIVES

There are legal and contractual requirements for certification of the structural integrity of many structures. But even when not required, SI plans should be carried through as a matter of prudent engineering.

The aircraft and aerospace field has invoked increasingly rigorous certification requirements because of failures, mostly of structures and materials outside prior experience. Nuclear reactor design has long been subject to rigorous and conservative certification requirements. The Navy has an equally long history of using conservative SI principles in certifying ships. The requirements are kept up to date with developments in materials and design methods.

Structures that require very high strength metals (with correspondingly high crack sensitivity) generally need the most rigorous and thorough certification. The limits of crack sensitivity and inspection reliability must be fixed with great accuracy, and design and fabrication must be strictly controlled. Less crack-sensitive metals generally require a more modest degree of certification. These general requirements are modified, of course, by such factors as the possible consequences of a structure's failure or considerations of metal cost. Certification requirements are usually decided case by case, but a move toward more generalized practices is developing.

EDUCATIONAL REQUIREMENTS

The literature, textbooks, and university courses on structural reliability are generally narrow in scope and highly selective in content. The emphasis is on theoretical fracture mechanics, presented as an abstract engineering subject.

This background is useful, but it is not enough. In fact, overemphasis on fracture mechanics theory may be counterproductive, because the theory concentrates on linear-elastic (highly brittle) metals and ignores the more ductile elastic-plastic and plastic metals. SI technology permits selection from the entire range of engineering metals—linear-elastic, elastic-plastic, and plastic.

Test methods and interpretive procedures that apply to the full range of metal properties, from brittle to ductile, are necessary. These methods must be standardized by ASTM procedures to be acceptable for certification purposes. Moreover, a statistical data base of metal properties for analysis and selection is needed. It can be developed only by widespread use of standard test methods. Accordingly, standard engineering tests are essential.

Other examples of isolated and inadequate treatment of subject matter critical to SI engineering include

Metal-quality effects
Weldability
Statistical considerations of metal properties, stress distributions, and crack states.

These limitations present serious problems. In general, engineers cannot be expected to be conversant enough with various specialized fields to integrate the necessary mechanical, materials, and fabrication principles. However, each element that contributes to SI technology

can be reduced to engineering essentials and stripped of confusing details that are of only special interest.

There is no substitute for learning while doing, and proficiency requires an intern period with an SI technology team. However, a general introductory textbook is a prerequisite to an intern period.

Proof that the required educational background is not overwhelming is given by existing groups that specialize in SI technology. The memberships of these groups change, and new groupings emerge. This must require self-education. The groups generally include specialists in materials, design, fabrication, nondestructive inspection, and quality control. It is important that SI principles be understood by the team as a whole.

The separate disciplines of materials and structural engineering are no longer appropriate. A degree combining the two, plus minors in other important fields (such as weldability, design for welding, and nondestructive inspection) is an appropriate background for SI analysis. While the need for specialists will continue, there is an absolute necessity for generalists who can cover the whole field with various degrees of sophistication.

230-362 O - 77 - 2

CHAPTER 2

Micromechanical Crack-Extension Processes

CHAIN OF EVENTS

Catastrophic structural failures can be traced to micromechanical events involving minute volumes of metal. Cracks of millimeter dimensions have caused the fracture of ships, bridges, and other large structures. These fractures are due to inadequate ductility of small aggregates of metal grains at crack tips. This inadequacy is determined by events within the grains, close to the atomic level.

Figure 1 illustrates a typical failure that resulted from a design based solely on tensile test properties. A collar was welded to the mast to decrease the elastic stress at a site of corrosion pitting. The mast was ostensibly strengthened, but a weld crack caused plastic deformation at the crack tip, and as a consequence the metal grains developed microcracking. This mast, and others similarly "strengthened," fractured in a brittle manner because of the inadequate ductility of a few metal grains.

The point is that elastic strength is never a substitute for ductility in ensuring structural reliability. This knowledge is vital to designers and others concerned with the strength of materials and structural integrity.

Figure 2 introduces the chain of strength-ductility relationships that extends through the structural, macromechanical, micromechanical, and atomistic scales. Each scale range is pertinent to a different discipline, as indicated by the bracketed sections. The common interest of all the disciplines is in developing procedures for deducing conditions that determine strength.

Fig. 1—Ship mast failure by brittle fracture.

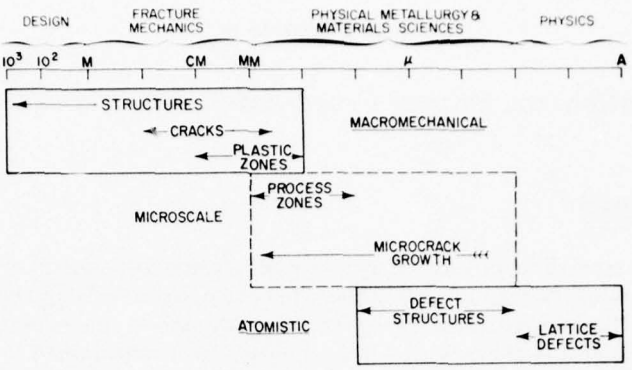

Fig. 2.—Scale of metal separation events, from angstroms to structural dimensions.

Except for purely brittle solids (so defined by smooth-body tension or torsion tests), microscale ductility controls cracked-body strength. All metals that yield in tension tests develop plasticity at crack tips. Figure 3 illustrates typical deformation patterns in the region of a crack subjected to load. At initial stages of loading, such patterns are developed by metals that would be classed as highly brittle in a fracture mechanics K_{Ic} test, and also by metals that would ultimately fail in a ductile mode. The difference between the two is the degree of local plastic deformation that precedes unstable crack extension or fully ductile rupture. The crack-tip deformation patterns are reproduced at all scale levels. The resistance to crack-opening forces is provided by plastic flow, to the limits of brittle or ductile behavior.

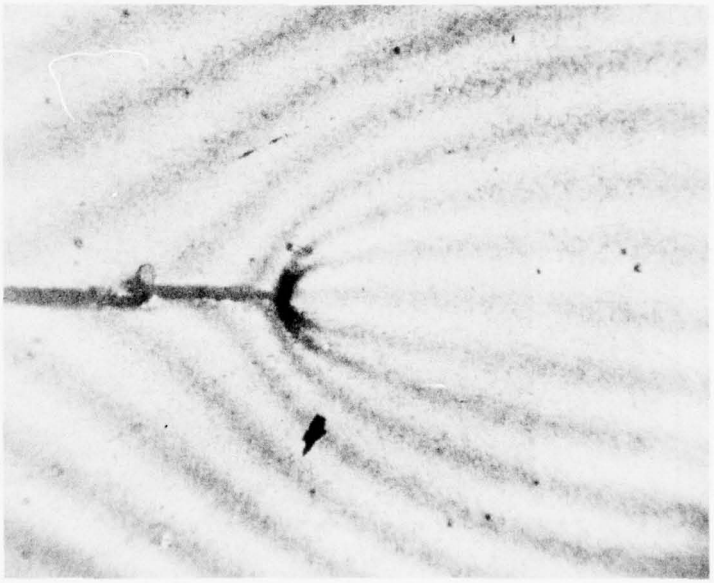

Fig. 3.—Moiré pattern of intense plasticity at crack tip.

Figure 2 illustrates the following sequence of events:

Microfracture begins at the lattice level, as metal-atom bonds split. The process may be "easy" or "difficult," i.e., near-elastic or highly plastic, according to the nature of the grains and phases.

Microcracking of individual grains does not result in fracture of the grain-aggregate structure as a whole unless the microcracks join together. Depending on phase types and distributions, the joining process at this larger scale may be easy or difficult (near-elastic or highly plastic) on a larger scale.

The plastic zone at the crack tip of a structural defect may be large or small at the time of fracture. The larger the plastic zone, the higher the resistance to fracture, and vice versa.

A small crack may be fracture-critical, and a large crack may be noncritical. This depends on the metal's potential for plastic flow at the crack tip. This potential ductility of crack-tip plastic zones is decided by microfracture processes.

Thus, the fundamental chain that determines the fracture reliability of a structure is always based on the behavior of minute volumes of metal. The scales of events cover more than 10 orders of magnitude, from angstroms to meters.

Figure 4 presents a generalized view of crack-front events for a small crack in a large structure. The crack-tip *plastic-zone* size is about 0.1 to 1 cm. The more ductile the metal, the

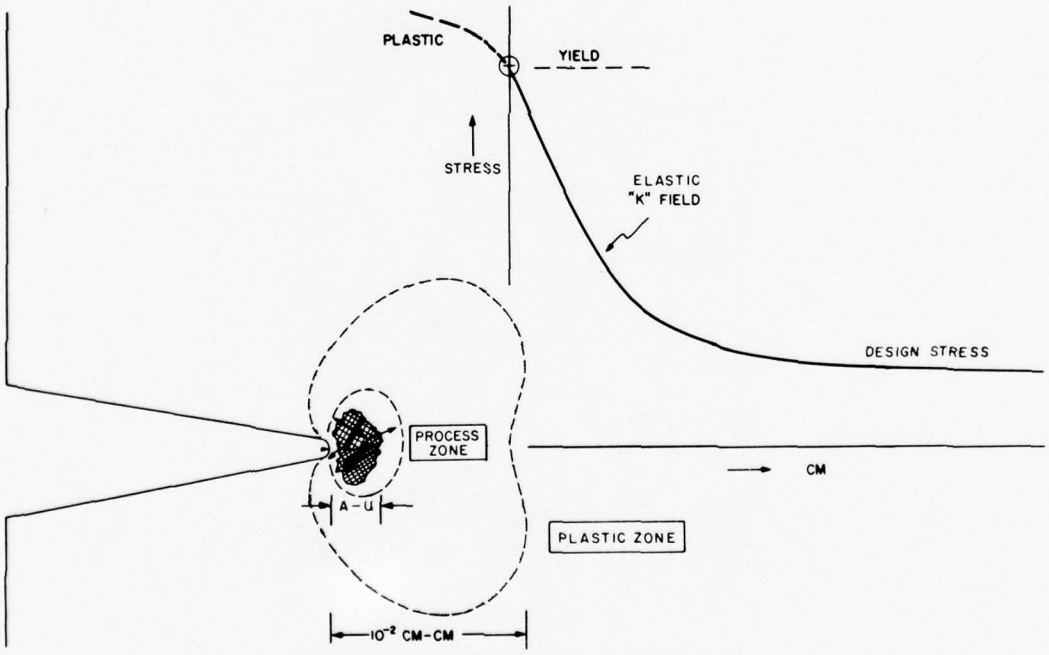

Fig. 4—Relationship of elastic force system to micromechanical plastic behavior of metal grains at crack tip.

larger the plastic zone. Within the plastic zone lies the *process zone,* where a few metal grains are undergoing the most intensive straining in the system. The atomistic events within the grains, which control grain cracking, are not illustrated in this figure because they take place on too small a scale. We will return to them later. The elastic-stress field K, or K-field, represents the rise in local elastic stress near the crack tip, compared to the nominal elastic load stress. This force system causes growth of the plastic zone.

Linear-elastic fracture mechanics avoids the complexities of analyzing the plastic zone by referring instead to the force system of the elastic-stress field. However, elastic analyses of the K-fields apply only to plane-strain (brittle) metals, which feature relatively small plastic zones.

The main features of this analytical treatment are illustrated in Fig. 5. Discussions to follow will describe it in detail. At this point, it suffices to say that the fracture strength of plane-strain (brittle) metals can be defined in terms of critical crack sizes for given elastic-stress loadings. The K_{Ic}/σ_{ys} ratio defines the characteristic fracture toughness of a metal.

Figure 6 illustrates the connection between microfracture processes, which are mainly of metallurgical interest, and the elastic force fields, which are the main reference of fracture mechanics. The enlargement of the plastic zones requires increasing the K-field intensity. If

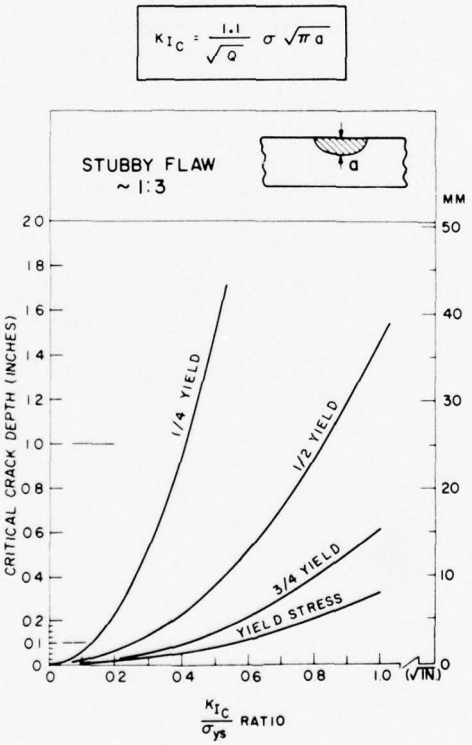

Fig. 5—Graphical analysis of critical crack size and stress combinations for brittle fracture initiation.

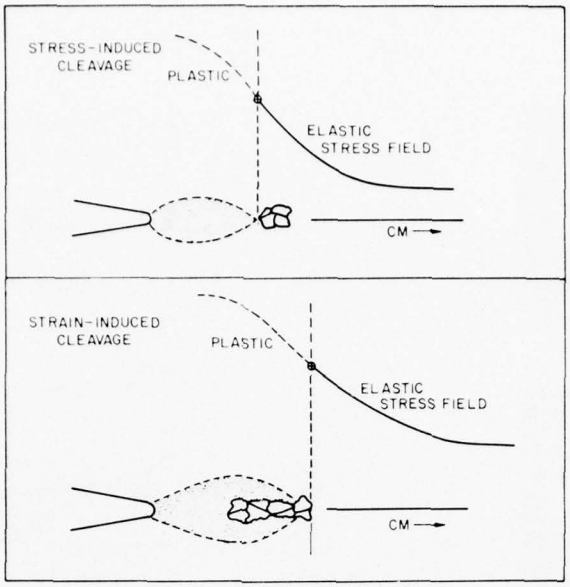

Fig. 6—Increase in elastic force field and plastic-zone size with increase in metal grain ductility.

microcracking develops early during plastic-zone growth, the K-field intensity at the time of fracture will be relatively low. Accordingly, K_{Ic}/σ_{ys}, as measured by the fracture test, will be low. Conversely, increased resistance to microcracking signifies that larger plastic zones will form and that the required K-field intensity will be higher As a result K_{Ic}/σ_{ys} will be greater, and the metal will have higher plane-strain fracture toughness.

These general features will be examined in greater detail for the case of cleavage-cracking processes, which determine the transition-temperature type of plane-strain fracture toughness of steels. Figure 6 provides an introduction to cleavage-cracking relationships, as follows:

Easy (near-elastic) cracking of grains takes place by stress-induced cleavage ahead of the plastic zone. It indicates a high degree of micromechanical brittleness and resultant low plane-strain fracture toughness.

More difficult (plastic) cracking of metal grains takes place in the plastic zone. It indicates strain-induced cleavage, i.e., relatively great micromechanical ductility. Nevertheless, the metal may remain brittle (albeit less so) in the sense that plane-strain (fast) fracture occurs.

Figure 7 illustrates metallurgy's essential dedication to ductility. The goal in steel improvement is to modify the microstructure so that grains do not cleave, but rather rupture in a ductile fashion, as individual tensile specimens. The corresponding effects on crack-tip plastic zones are indicated in the sketches. The important mechanical difference is the substitution of a large crack-tip plastic zone for a very small region of local deformation. Figure 8 illustrates

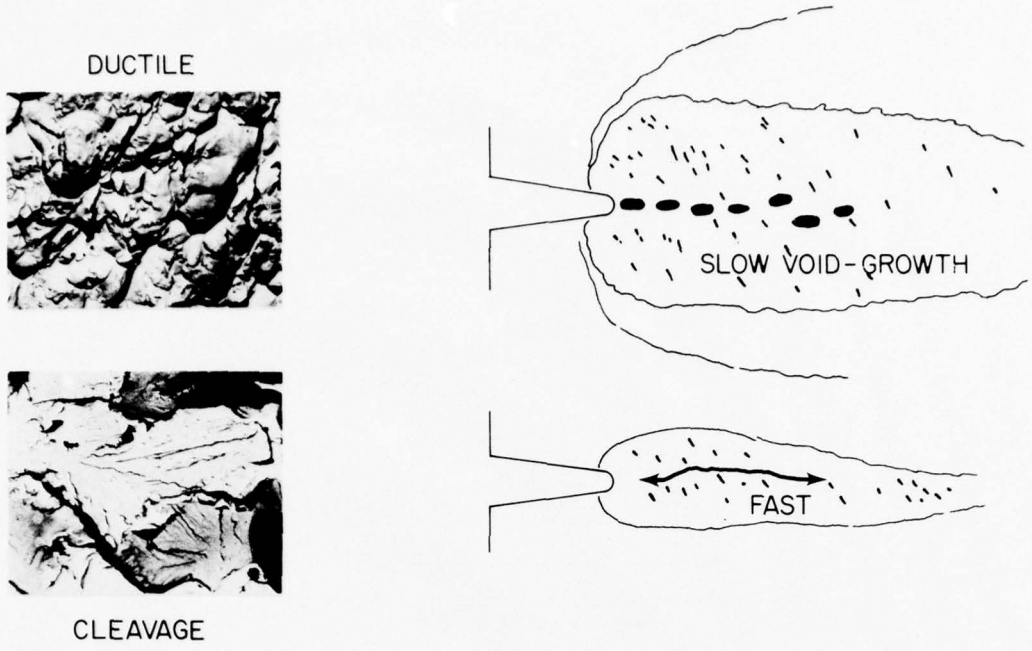

Fig. 7—Change from cleavage to ductile rupture of grains results in large increases in plastic-zone size, with corrolary effects on fracture extension.

the resulting change in fracture mode; the fracture-extension process changes from unstable (brittle) to ductile (plastic).

An understanding of cleavage processes requires examining events in the angstrom-to-micron range, i.e., within grains. These include events in the lattice bonds. Figure 9 illustrates cleavage and ductile performance of the grains. We draw a 1-μm circle and inquire as to the events within that led to cleavage or ductility. In particular, it is necessary to understand the role of defect structures in microcrack formation in grains.

Figure 10 is a schematic of lattice defects due to missing atoms or chains of atoms. The literature on this subject is vast. Figure 11 is an electron-microscope view of defect structures. Ductility at this scale is represented by "tangles" and brittleness by "pile-ups" that lead to microcracking.

The pile-ups are caused by glide along crystal planes. If this movement is blocked by grain boundaries, hard phases, or other discontinuities, a pile-up results. This results in intense elastic-stress fields, analogous to the K-fields of macroscopic cracks (Fig. 4). A plastic zone and process zone can even be visualized within the lattice of the crystal. This may stagger the imaginations of engineers familiar with macroscopic K-fields, but it is a normal reference for materials scientists and physicists concerned with strength at this small scale.

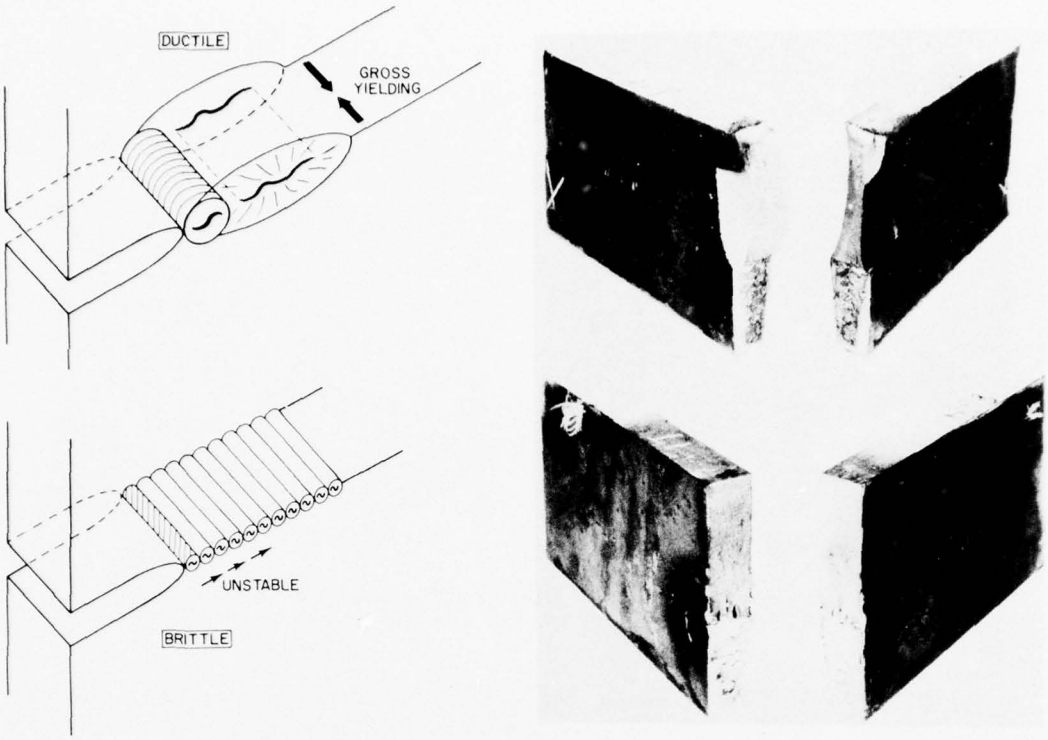

Fig. 8—Extreme limits of fracture modes—brittle and highly ductile fracture.

At all scales of reference, effects analogous to the K-field, plastic zone, and process zone can be found. Most important, at any scale there are limits beyond which elastic-plastic or plastic criteria, rather than elasticity theory, are appropriate. This applies to ultramicrocracks of micron or angstrom size as well as to large structural cracks.

ENGINEERING SIGNIFICANCE OF MICROFRACTURE

Knowledge of microfracture events provides the only rational explanation for very sharp transitions from brittle to ductile performance (in steels as a function of decreased temperature and in all structural metals as a function of increased strength). As an example, we shall discuss the events of such sharp transitions in temperature-sensitive structural mild steels. The failure of ships in winter and safe performance in summer will serve as the engineering example.

The only design factor that can explain this sharp temperature effect is microfracture ductility, as evidenced by fracture tests. The typical effect of temperature on the brittle-to-ductile transition of steels is illustrated in Fig. 12 by the Dynamic Tear (DT) test. The essential feature is the sharp change from plane-strain (brittle) to elastic-plastic (semiductile) fracture properties in a narrow temperature range. In brief, the metal becomes fracture-safe as a result of the elastic-plastic transition. The stress scale indexes the increase in elastic stress required to cause the extension of a fracture in the elastic-plastic temperature range.

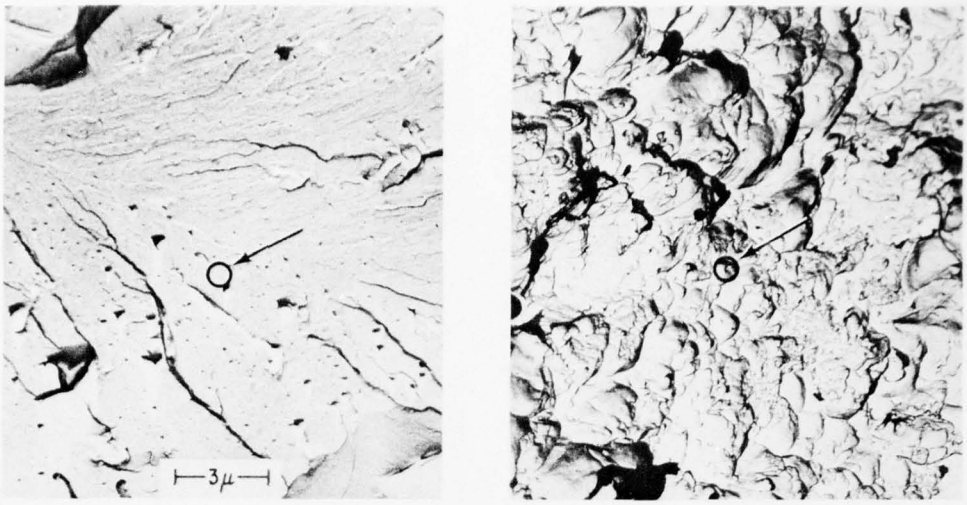

Fig. 9—Cleavage and dimple (ductile) fracture of individual grains at high magnification. The small circles represent 1-μm regions, within which the most basic processes of fracture—rupture of atom bonds—take place.

The NDT (Nil Ductility Transition) temperature signifies a degree of brittleness such that small cracks are critical for fracture initiation. It is possible to correlate ship-failure records with the NDT frequency distribution of the steels, as in Fig. 13. (Details are provided in Chapter 6.) At summer temperatures, the conditions for initiation and extension could not develop, and the metals were safe. At winter temperatures, essentially all of the steels could initiate and propagate fractures. This remarkable change takes place in a very narrow temperature interval.

Figure 14 (right) illustrates the cleavage of pearlite-ferrite grain aggregates that is characteristic of these steels at near-NDT and failure temperatures. Adjusting the C-Mn ratio by using lower carbon and higher manganese contents can alter the microstructure to make

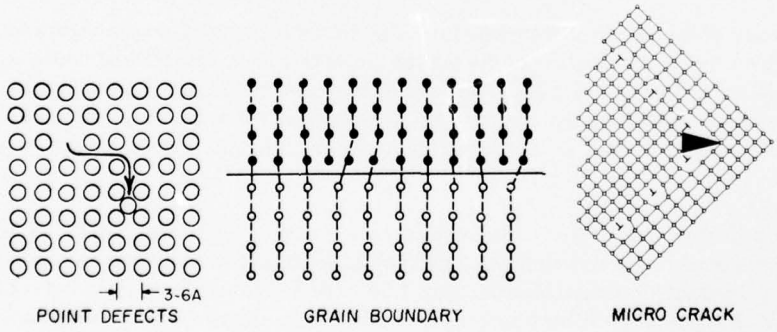

Fig. 10—Schematics of metal lattice defects, which are deviations from perfect periodicity of the atomic arrangement. Pile-up of defects, due to elastic stressing of the lattice, may result in microcracking.

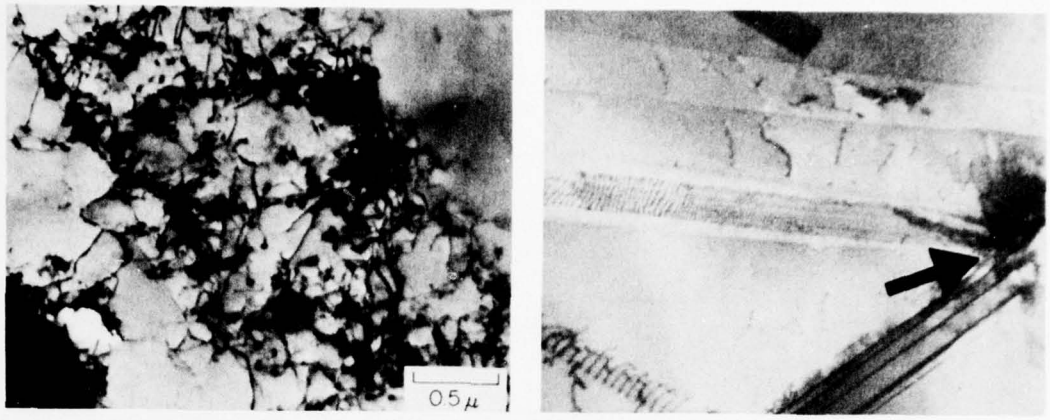

Fig. 11—Electron-microscope view of states of aggregation of lattice defects. If lattice ductility results in tangles, the grain as a whole behaves in ductile fashion. However, if pile-ups lead to microcracking, the grain undergoes cleavage.

cleavage more difficult, as explained in the next section. As a result, slip deformation is promoted at the crack tip, as in Fig. 14 (left). The important point is that cleavage suppression enhances microstructural ductility and causes a shift in the NDT population to lower temperatures, as noted in Fig. 13 for the improved fracture-resistant steels. This solution has been used for the ship-fracture problem. The improvement has been metallurgical, that is, at the scale level of grain size.

Figure 15 compares the scales of events that lead to brittle performance at winter temperatures and safe, ductile performance at summer temperatures.

At winter temperatures, the ship-failure steels developed easy incubation and extension of cleavage microcracking and, therefore, high sensitivity to fracture initiation due to small cracks. Fracture extension followed for this brittle state, which was common to the entire population of ship steels.

At summer temperatures, the same steels developed only isolated microcracks, which remained in a microstructurally arrested condition. As the result, the fracture performance of the steels was ductile, even in the presence of very large structural cracks, so that cracking in one plate would be arrested in the next.

Figure 16 shows a sailor repairing a partial crack; one very poor plate fractured, but the next arrested the crack. The temperature in this case was approximately 45°F (25°C). Temperatures only 10°F (5°C) lower might have resulted in complete fracture of the ship, which was then at sea. If the sailor had understood this, it is unlikely that the repair would have been made without an accurate thermometer nearby.

The doubler that he was adding would not serve the intended purpose at the lower temperatures. The real protection was the ductility of the crack-tip plastic zone. The relatively few grains in the process zone were behaving with enough ductility to hold the ship together.

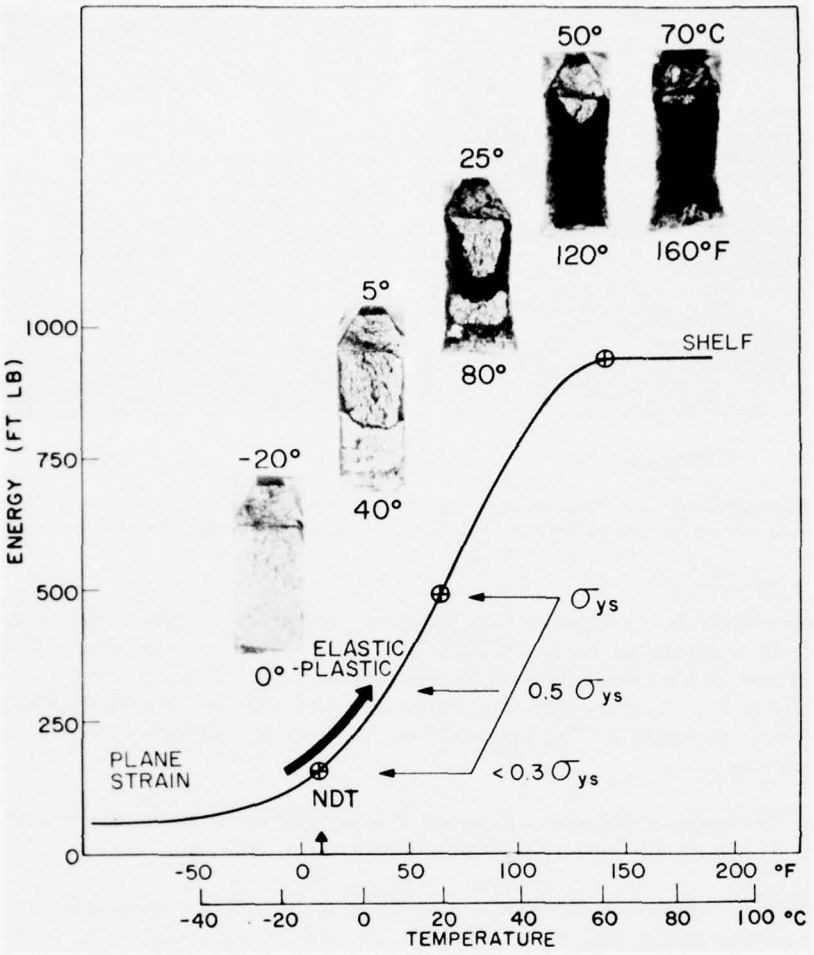

Fig. 12—Features of temperature-induced transition from plane-strain to plastic fracture properties.

The reader may figuratively exercise Fig. 15 by moving the bold arrows laterally, from the ductile to the brittle notations, retaining the slope. It will be evident that when microcracking develops and propagates easily at atomistic levels, then microcracking at microscale levels will extend and join up easily. The plastic zone will be small at the time of rupture, and the structure will fail catastrophically.

The reverse also holds; if the processes at atomistic levels are ductile (tangles) due to slip, then the entire chain of events will be ductile and the structure will be safe.

Metallurgists use these principles by adjusting microstructures, such as grain and phase sizes. They must use low-ductility (pearlitic) phases for strength. However, if these phases are made smaller and surrounded with ductile ferrite, microcrack incubation and joining-up can be suppressed. The carbon-manganese adjustment is a low-cost solution to the ship problem.

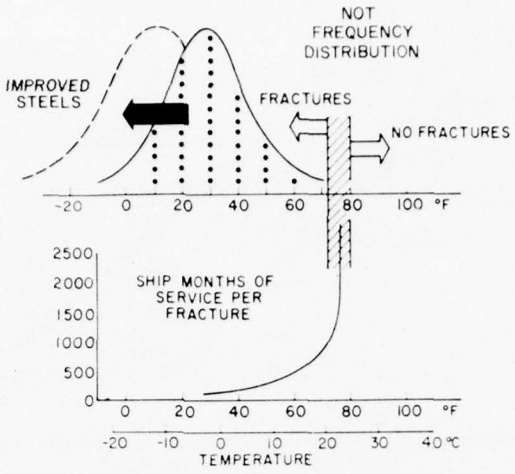

Fig. 13—Correlation of ship failure records with NDT frequency distributions of ship steels, as compared with improved steels.

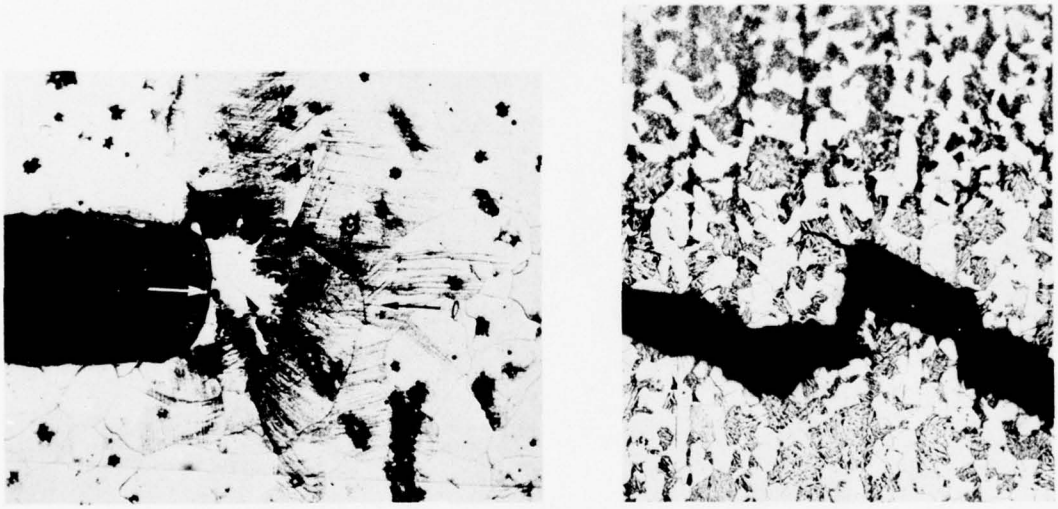

Fig. 14—(Left) Crack-tip deformation resulting from slip of lattice planes for individual grains (Hahn). (Right) Progression of brittle fracture by cleavage of ferrite-pearlite grain structures (200×).

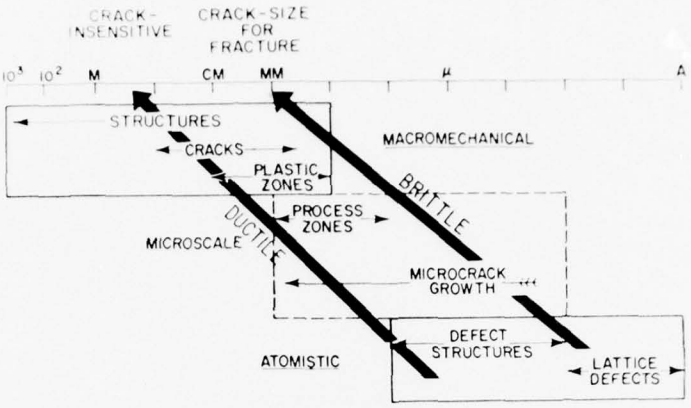

Fig. 15—Sequence of events that lead to crack sensitivity on the one hand and ductile performance on the other.

Fig. 16—At-sea repair of a single fractured plate. Continued propagation through the other plates was prevented by the fracture properties of the adjacent plate.

This general introduction indicates the importance of the following more detailed descriptions of micromechanical processes for temperature- and strength-induced transitions in fracture properties.

CLEAVAGE FRACTURE

Cleavage fracture in metals competes with slip processes. The critical cleavage stress for a single crystal may be attained in the elastic range if slip is prevented by defect structure locking mechanisms. In the absence of significant slip, cleavage may be said to be stress induced. Increased temperature provides the activation energy for decreasing the degree of locking of the slip systems. Accordingly, increased temperature decreases the stress required for slip.

The stress levels for yielding and subsequent plastic flow are influenced markedly by temperature; they fall off relatively rapidly with increasing temperature. The critical stress for cleavage is not strongly affected by temperature. The interrelationships of these effects determine the development of increased micromechanical ductility with increased temperature. The interrelationships are specific to single crystals, to aggregates of crystals, and to different degrees of mechanical constraint to plastic flow.

The exact form and relative slopes of the temperature dependence of the cleavage-stress and yield-stress curves, which are sketched in Figs. 17 to 24, may be debated. This is particularly true of the slope of cleavage-fracture stress. The point of incipience of plastic flow is a question of definition and of the scale level being considered. However, these are minor details. The important point is the experimentally confirmed concept of a crossover between these curves, which has major physical significance.

Figure 17 illustrates the effects of temperature in a single crystal. The crossover point of the cleavage-stress and yield-stress curves occurs at a critical temperature T_c. At temperatures below T_c, cleavage stress is reached before the stress required for yielding (induced by slip). For these conditions, cleavage fracture in a single crystal is said to be stress induced, i.e.,

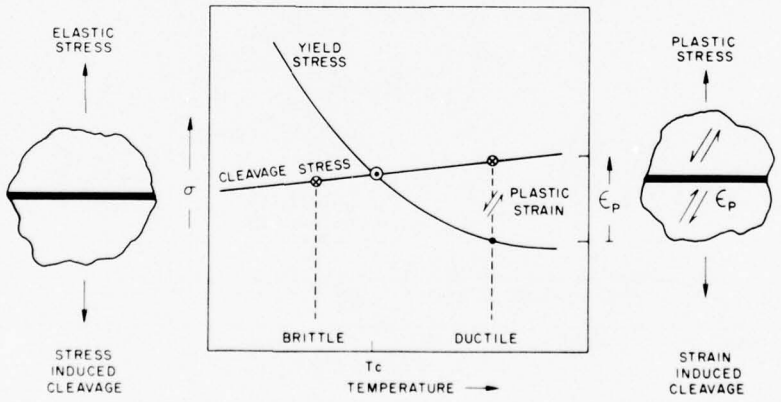

Fig. 17—Transition from stress-induced to strain-induced cleavage fracture in a single crystal.

brittle. At temperatures above T_c, yielding of the crystal occurs first, and plastic strain ϵ_p is developed to the extent required for elevating the flow stress (by work hardening) to the level of the cleavage stress. The term "strain-induced cleavage" defines ductile behavior; a critical level of plastic strain is required for the critical cleavage-stress level to be reached. Temperature T_c marks a transition from brittle to ductile cleavage fracture.

It is important to note that the differences in ductility are not involved in the actual cleavage of the crystal, but in the slip that occurs before the stress required for cleavage is reached. While it is not proper to speak of brittle cleavage or ductile cleavage (cleavage separation is always brittle), it is correct to speak of stress-induced and strain-induced cleavage. This is important because the appearance of cleavage on a fracture surface is often mistakenly thought to indicate brittleness. It may, however, reflect appreciable ductility, insofar as the total fracture process is concerned.

The ductility transition that takes place at very low temperatures for tensile stress provides a clear example of this fact. Figure 18 is a simplified replot of typical data of Cohen and associates, who clearly describe the micromechanisms of fracture in terms of cleavage. The data indicate a sharp increase in ductility and fracture stress as temperature increases. It is important to note that high elongation and reduction of area values are associated with

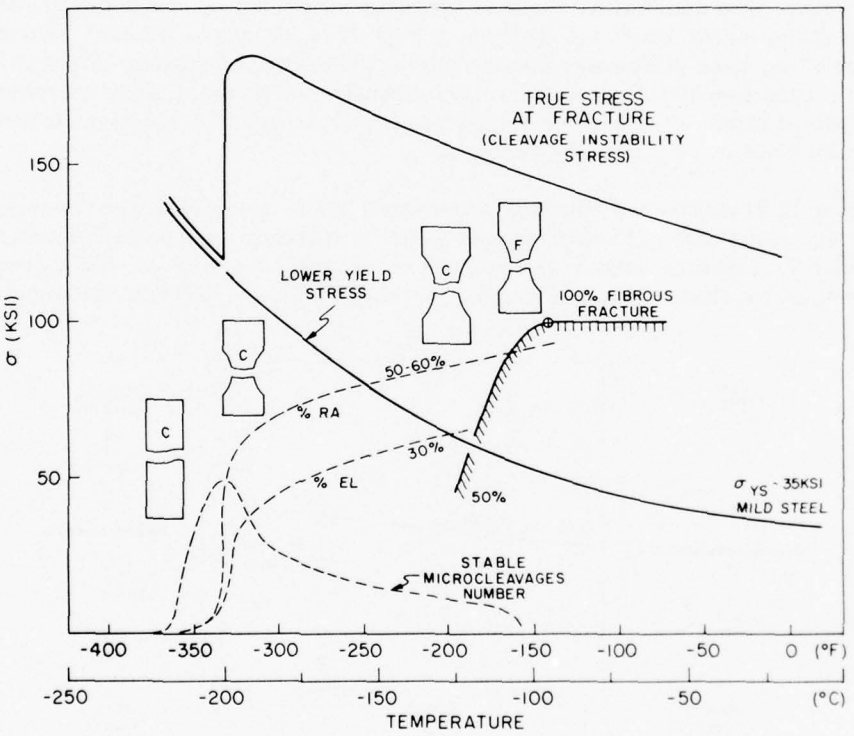

Fig. 18—Typical transition features for tensile specimens (Cohen). The three regimes of transition, as indicated by the elongation and reduction of area curves, are the toe region, the region of sharp rise, and the region of gradual completion of the transition.

cleavage fractures at intermediate and high temperatures in the tensile transition. Fibrous fracture takes place only after completion of the cleavage fracture transition. Indeed, the appearance of fibrous fracture in general marks the end of temperature transitions.

The development of cleavage for an aggregate of crystal grains must be considered in terms of the critical stress required for instability, i.e., for the unstable propagation of individual cleavage sites. For instability to occur, a critical microcrack length a_c must be attained, as well as a critical stress. Without the required combination of critical stress and critical microcrack length, cleavage will be stable and restricted to specific grains.

Figure 19 illustrates the conditions required for stress-induced and strain-induced cleavage instabilities in crystal aggregates. It should be noted that T_c for individual grains may vary according to the orientation of cleavage planes with respect to the stress direction. Some grains will be oriented favorably for stress-induced cleavage, while others may require plastic strain for cleavage. As temperature increases, all crystals will require plastic strain. According to crystal orientation, some will require more strain than others. As the average ductility of the grains increases, fewer individual cleavages will occur, and it will become more difficult to connect enough stable microcleavages to achieve critical microcrack length a_c.

Figure 19 illustrates brittleness at low temperatures; a grain of favorable orientation for stress-induced cleavage has split at the critical level of stress. Because of the low ductility of most other grains at the temperature, there is immediate instability, involving fast cleavage propagation through the entire grain matrix. At this temperature the critical microcrack length a_c is equal to one grain diameter. At a higher temperature, such that most grains are undergoing strain-induced cleavage, significant numbers of microcleavages do not appear until a higher cleavage stress level C_2 is reached. The higher level represents grains that are not favorably oriented and therefore require strain hardening before cleavage. At this level the aggregate contains separated microcleavages, which must be joined by breaking "plastic

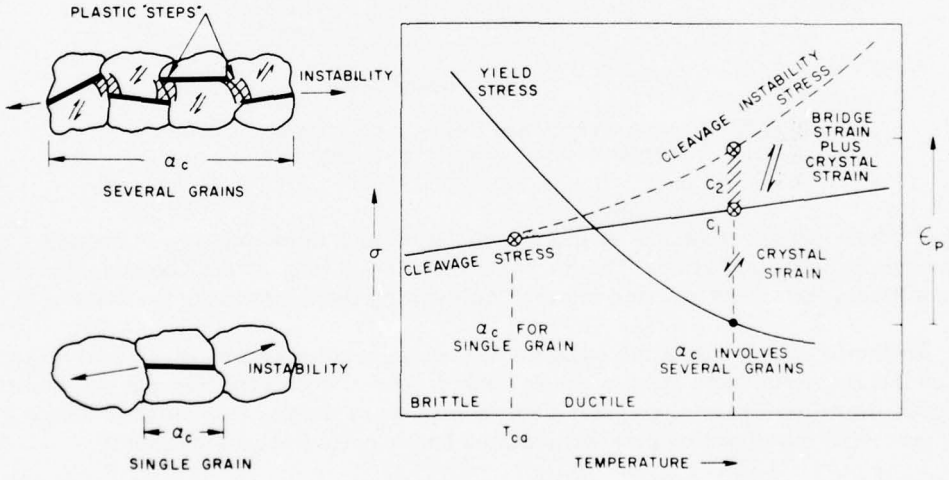

Fig. 19—Features of the brittle-to-ductile transition for grain aggregates. The effect of increasing temperature on the ductility of individual grains is amplified by the plastic strain required for the joining of individual microcleavages to reach critical microcrack size. Cleavage instability stress, critical strain level, and critical microcrack size increase gradually with increasing temperature.

230-362 O - 77 - 3

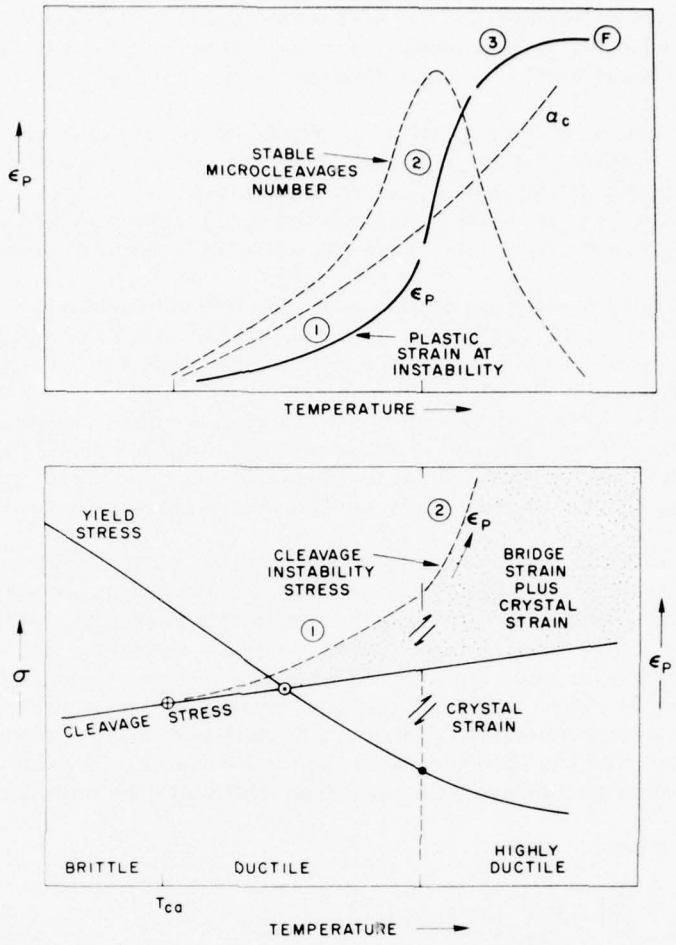

Fig. 20—Features of exponential change in critical cleavage instability stress and plastic strain for grain aggregates.

steps." These plastic steps are at grain boundaries and represent step mismatches of the cleavages in individual grains. The literature calls this "bridge strain," because it represents an additional increment of strain required for growing the microcracks to critical size.

Instability, then, is determined by the dashed curve noted as "cleavage instability stress," which lies above and has a steeper temperature dependence than the cleavage-stress curve for individual grains. Grain aggregates behave in a more ductile fashion than single grains because of the intergrain cooperation required for cleavage fracture instability.

The bottom of Fig. 20 is similar to Fig. 19, but the temperature scale is enlarged to illustrate a sharp rise in cleavage instability stress with increased temperature. The slope of instability stress is gradual at first but rises sharply in a critical temperature interval. The top of Fig. 20 explains the cause. The number of stable microcleavages first increases and then

decreases rapidly with increased temperature because of the general increase in ductility for all grains. Critical microcrack length a_c increases continuously, at a rate increasing with increased temperature, also because of increased ductility. Figure 18 provides experimental proof of the bell-shaped microcleavage number curve.

The illustration represents many low-temperature tensile tests. The counts are made by cross sectioning and metallographic polishing, followed by microscopic examination near the fracture surface. Since microcleavages noted after the fracture represent stable cleavages of individual crystals, the shape of the curve is important. At the start of the transition, the critical a_c size is equivalent to one grain diameter. This means that the first cleavage to develop will result in instability. This marks the point at which the cleavage count is near zero. The transition from a gradual to a sharp rise in microfracture ductility is related to the large increase in stable cleavages, which could not join up to reach the critical a_c size of several grain diameters. Other evidence for the sharp rise in ductility is provided by optical microscope observations of highly deformed grains between stable cleavages that could not be connected to a_c size, and also by the blunting of microcracks.

Following the sharp rise, ductility continues to increase as the number of microcleavages falls to very low levels. The microcleavages can never be joined to critical a_c size, even as small patches. Full fibrous microfracture develops.

The increase in plastic strain (microfracture ductility) is illustrated by the three regimes of the ϵ_p curves of Fig. 20, as follows:

Regime 1 is characterized by transition from stress-induced to strain-induced cleavage instability; the strain level rises gradually as critical length a_c increases.

Regime 2 is the region of transition to large a_c size and bridge-strain control; the strain level required for cleavage instability rises exponentially. Severe deformation of grains and blunting of microcracks develop.

Regime 3 is typified by saturation of processes required for development of cleavage instability and by transition to full fibrous fracture.

The temperature range of transition through these three microfracture regimes is characteristically narrow for any stress state (tensile or crack-tip). After the temperature of strain-induced cleavage for individual grains is reached, the interaction of the events described above leads to a cataclysmic rise in ductility at slightly higher temperatures. It is this chain of events that causes all temperature transitions to be sharp and irrepressible once started.

Microcleavage-number curves obtained for tensile tests of pure iron as well as for pearlitic steels show the same sequence of events. However, brittle carbide phases (pearlitic, etc.) serve as microcrack incubation sites and also promote joining of microcleavages. The tensile ductility curve is thus shifted to higher temperatures by the increased pearlite content. Fine grain sizes lower transition temperatures, and coarse grain sizes raise it. Fine and coarse distributions of ferrite-pearlite aggregates have corresponding effects. All of these effects influence the transition temperature by affecting the stress and strain conditions required for microfracture instability. In general, reduction in the unit-cell size of stable cleavage and decrease in the number and relative size of sites involving brittle phases lower the transition-

temperature range. Extensive studies of these interrelationships have been reported in the metallurgical literature and serve as the basic fund of knowledge of practical microstructural effects.

Before we discuss the effects of stress state (notches) on the transition, note that the effects of increased microfracture ductility are amplified by the presence of a notch. As the ductility transition develops at the tip of a notch, it leads to blunting of the notch and thus reduces constraint. In brief, unstable macroscopic fracture cannot develop above the temperature range of microfracture regime 2 because the large increase in microfracture ductility blunts the notch and thereby stimulates gross yielding of the metal in advance of the notch. The macroscopic fracture process then becomes ductile. Macroscopic instabilities are controlled by microscopic instabilities involving relatively few grains.

The effects of stress state on the specific temperature range of the microfracture transition are illustrated in Fig. 21. The average cleavage stress for single grains remains a main point of reference. The yield-stress (flow-stress) temperature-dependence curves are shown schematically for the tensile stress state and for a very sharp crack loaded statically and dynamically. Elevation of the flow stress at a crack tip results from the associated triaxial stress state. Additional elevation results from dynamic loading because slip is a time-dependent (viscoplastic) process. Higher stresses are required to activate slip in short times.

The elevations of the flow-stress curves increase the temperatures at which the curves fall below the cleavage stress curves, as indicated. The three critical temperatures for transi-

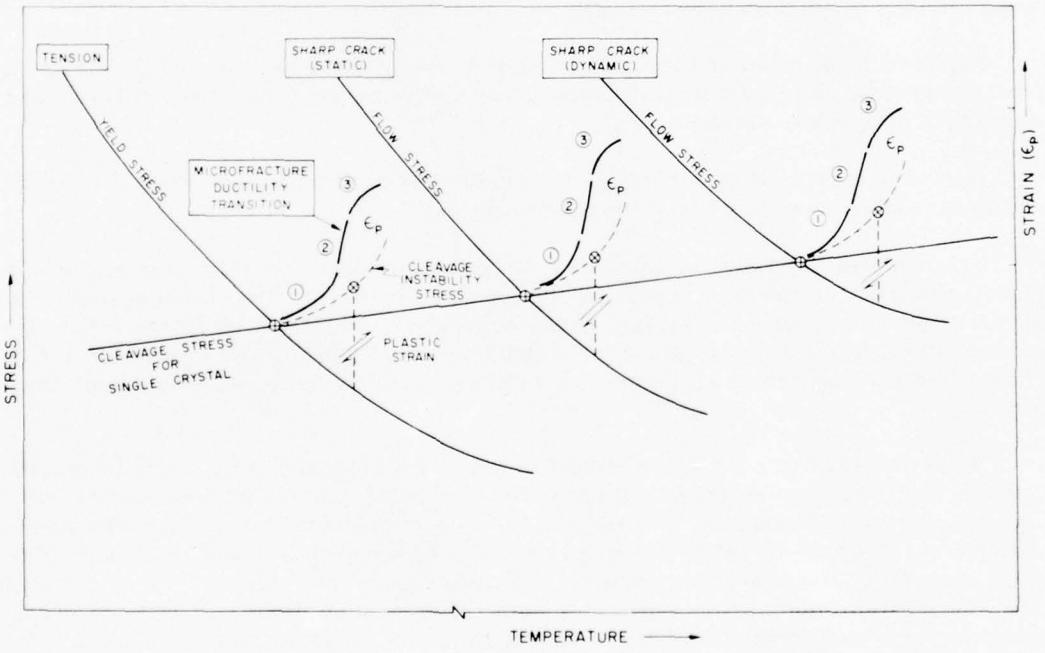

Fig. 21—*Effects of sharp cracks and dynamic loading.* These increase the stress required for plastic flow and thereby shift the intersections of the cleavage and flow stresses to higher temperatures.

tion from stress-induced to strain-induced cleavage instability are indicated in the figure by the crossover points of the curves. For each stress state cited, sharp microfracture ductility transitions develop in a narrow temperature range above the critical temperature.

More exactly, the transition begins at a somewhat lower temperature, due to the rise of the cleavage instability stress curve. (For simplicity, the dashed instability stress curves are shown to start at the crossover points.) Each of the microfracture ductility transitions includes microfracture regimes 1, 2, and 3 in close sequence. A change from cleavage to fibrous fracture occurs as each ductility transition is completed. The temperature intervals between the transitions are not at proper scale in Fig. 21 because that would complicate the illustration. The transitions for notches are relatively close together and occur at much higher temperatures than the tensile transitions.

EFFECTS OF MICROFRACTURE TRANSITIONS

Transition from stress-induced to strain-induced cleavage increases the plane-strain plastic-zone size, as shown in Fig. 22. The stress and strain fields normal to the crack are shown schematically to illustrate that maximum strain is attained near the crack tip and that maximum stress develops at the location of maximum triaxial constraint, which must be ahead of the crack tip.

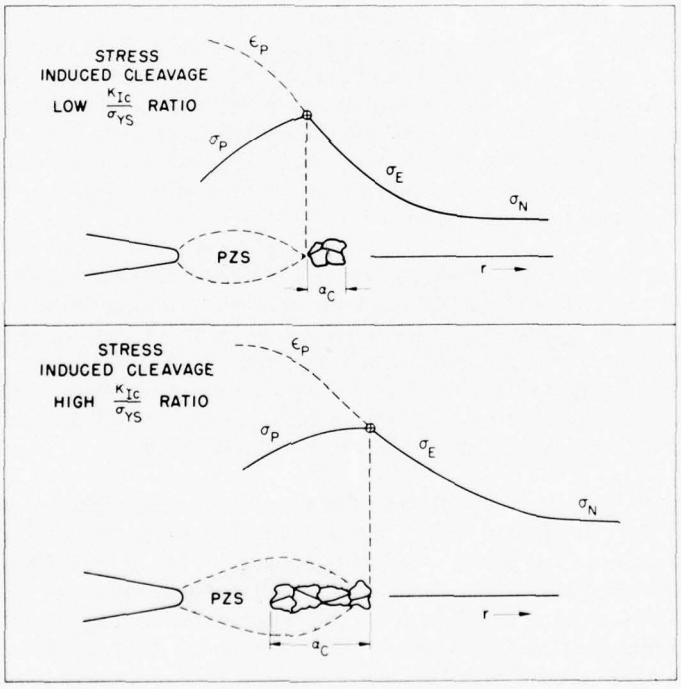

Fig. 22— Transition from stress-induced (top) to strain-induced (bottom) microfracture.

The upper part of Fig. 22 illustrates microfracture by stress-induced cleavage instability, requiring a small microcrack size a_c. The growth of the plastic zone is terminated early, as the elastic-stress field attains the required stress for cleavage instability. The fracture initiation point is located ahead of the elastic-plastic interface of the plastic zone. The stress field intensity K_{Ic}, and thus K_{Ic}/σ_{ys}, are low, indicating low plane-strain fracture toughness.

The lower part of the figure illustrates microfracture by strain-induced cleavage instability, which requires a large microcrack size a_c. The plastic zone must be larger to develop the high plastic-stress values required for cleavage instability. The fracture initiation point is inside the plastic zone. The values of K_{Ic} and thus K_{Ic}/σ_{ys} are higher for strain-induced cleavage, indicating higher plane-strain fracture toughness.

The increase in plane-strain fracture toughness results from the increased microfracture ductility. Retention of the plane-strain state requires increased mechanical constraint; increase in section size provides this constraint. However, a limit is reached, at which microfracture ductility can no longer be suppressed by mechanical constraint regardless of section size. Added constraint then can only expand the temperature interval over which the conditions of microfracture regime 1 apply. It is not possible to prevent the transition from regime 1 to regime 2.

Once the constraint barrier is breached, the rapid increase in ductility with increased temperature has a dramatic effect on macroscopic fracture toughness. First the plastic zone is enlarged because of rapid loss of triaxial stress field constraint. In effect, the elastic fields are replaced by plastic-strain fields as the crack-tip region becomes plastic. (This transition cannot be described quantitatively by the elastic-stress analysis basic to fracture mechanics.) The subsequent transition involves pronounced yielding in advance of the crack tip, accompanied by blunting of the crack. This results in through-thickness contraction, similar to the development of the neck region in tensile specimens. The neck is evidenced by dimpling of the surface in advance of the crack, like that generally associated with ductile tearing fracture. The volume of metal that undergoes through-thickness contraction is called a "plastic enclave." Plastic enclave conditions signify fracture processes that involve relatively large volumes of plastic deformation before rupture.

Figure 23 illustrates the sequence of macrofracture transition events, predicted on the basis of increased microfracture ductility as a function of increasing temperature. Two macrofracture transitions are shown, one for static and one for dynamic loading. We shall discuss the static K_{Ic} transition first. Temperature point L denotes the end of K_{Ic} plane-strain conditions and the start of a subsequent transition to a plastic enclave condition. Temperature limit L corresponds to a specimen thickness large enough to provide maximum constraint. Similar transitions occur at lower temperatures for thinner K_{Ic} specimens.

Dynamic loading involves parallel transition events. The dynamic transition starts sharply at the Nil Ductility Transition (NDT) temperature. Dynamically loaded K_{Ic} specimens of increasing section size are required to follow the course of the K_{Id} transition. If small specimens are used, the transition to plastic enclave conditions takes place at lower temperatures (close to NDT). The L point of the dynamic transition marks the highest temperature for the dynamic plane-strain condition, as found in large specimens. Above this temperature, plane-strain relaxation again occurs with the development of plastic enclave conditions and notch blunting. The transition from plane-strain to plastic enclave conditions develops over a rela-

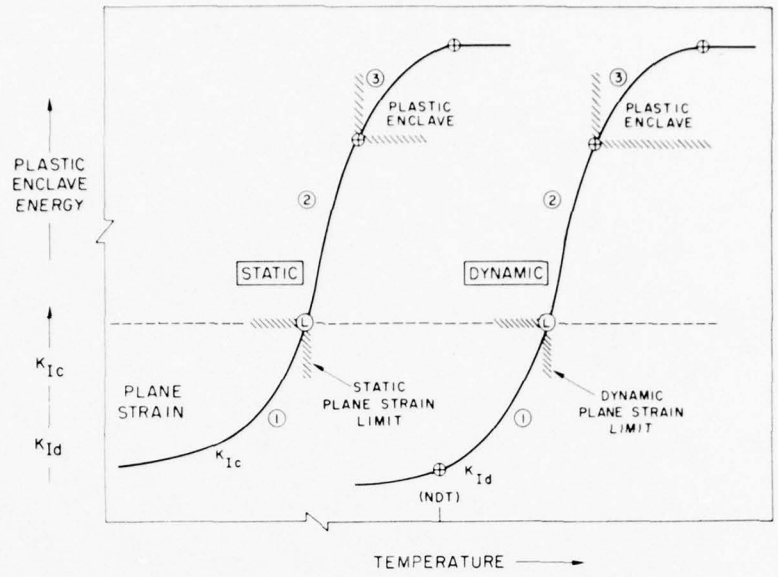

Fig. 23—Increased loading rate results in temperature displacement of microfracture-related fracture-mode transitions.

tively narrow temperature range and requires a change in definitions of fracture toughness, from fracture mechanics stress intensity indexing to plastic enclave energy indexing.

The dynamic transition may be referenced to critical temperatures marking the start of the plane-strain transition, the end of the transition, the early development of a plastic enclave, and the completion of plastic enclave growth to full ductility. These macromechanical transitions are results of entering microfracture regime 2, which features a large increase in ductility for a small increase in temperature. The ductility features of the three microfracture regimes are reproduced as macrofracture ductility events.

The main point of the metallurgical thesis is that if large additions of constraint are required to define the true K_{Ic} or K_{Id} temperature dependence in regime 1, this is a sign that microfracture ductility is increasing. Once microfracture regime 1 is entered, microfracture regime 2 can be suppressed only for a modest temperature range, at the price of large increases in mechanical constraint. At some point the additional constraint will be defeated by rapidly increasing microfracture ductility, and then plastic enclave conditions will develop.

Figure 24 serves as an introduction to fracture propagation tests. It is a general view of the significance of fracture energy transition curves as defined by dynamic fracture tests.

MICROMECHANISMS OF VOID GROWTH

The completion of the cleavage-to-ductile transition in low strength steel is ordinarily a mechanical condition of high shelf energy. The plastic enclave features gross plastic flow. Pronounced through-thickness yielding develops as a prerequisite for highly ductile fracture of slant type.

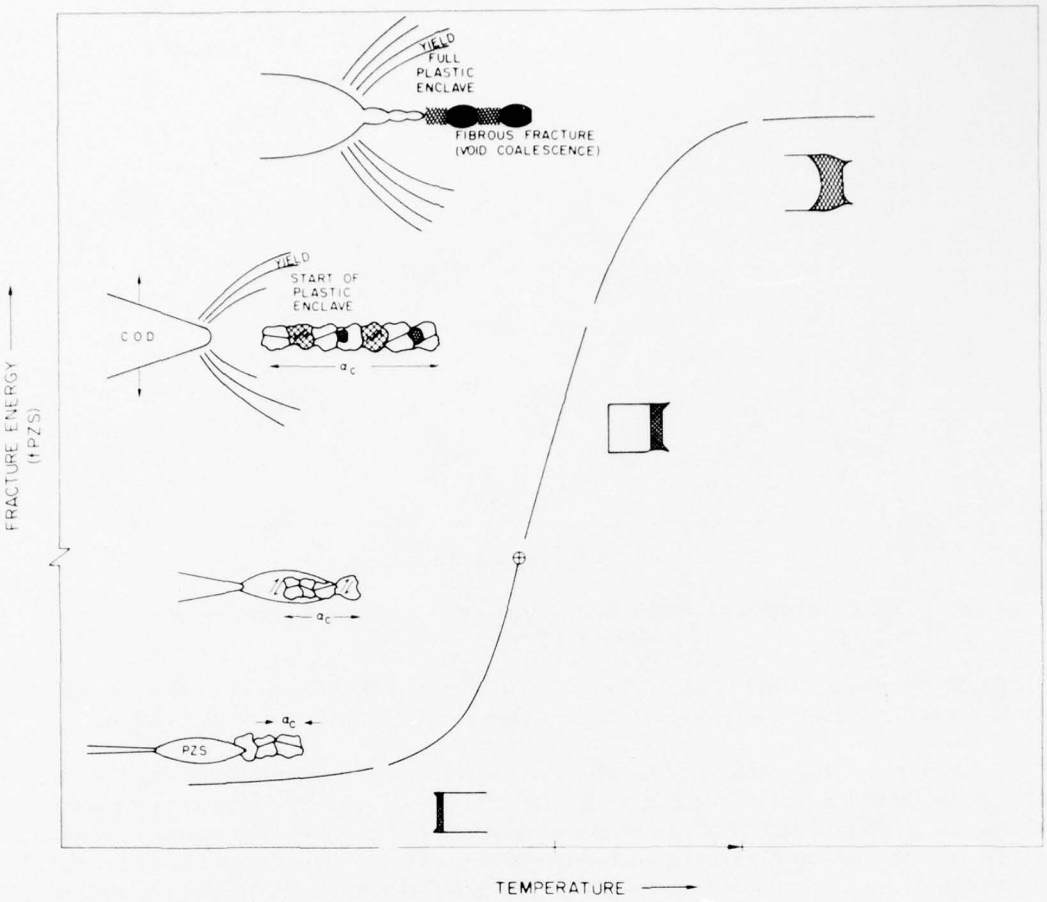

Fig. 24—Correspondence of microfracture processes to fracture-energy transition curves.

This mechanical behavior is the consequence of microfracture processes that involve the rupture of individual grains as tiny individual tensile specimens. Ductile rupture requires the opening of small voids between grains, particularly at the sites of nonmetallic inclusions. This takes place as microscopic voids develop, enlarge, and coalesce. The fracture appearance is termed "fibrous" when viewed by eye and "ductile-dimple" when observed at high magnification, as shown in Fig. 9. The dimples represent the sites of microscale grain ruptures.

The transition to fibrous fracture occurs as voids coalesce, as illustrated at the top of Fig. 24. The high shelf is represented by high levels of fracture energy. The gross plastic enclave and yielding are represented by the cross section of the fracture specimen.

Increasing the strength level of steels decreases the shelf energy and fracture ductility. A transition to low shelf levels is representative of temperature effects for relatively high strength steels.

The changes in microfracture void-growth processes that are responsible for these changes are general to all metals that do not undergo cleavage-related transitions due to temperature effects. With increased strength level in all metals, ductility as measured by tensile tests decreases, and the range between yield strength and tensile ultimate stress levels narrows. These observations indicate that the increased strength is developed by locking of slip systems in individual grains and grain aggregates, at the sacrifice of ductility.

These changes are reflected in the plastic-zone behavior of the grain aggregates at the crack tip. Void growth in the process zone requires increased plastic flow stresses with increased tensile yield stress. This means that the K-field stress is elevated, because the force system must increase to enlarge the plastic zone. However, decreased ductility results in earlier termination of void growth, i.e., rupture of the plastic zone. Thus, increased tensile strength decreases the critical terminal size of the plastic zone to the point at which plane-strain fracture can occur.

The conditions of stress-induced void-growth rupture are approached as K_{Ic}/σ_{ys} falls to very low values, and ruptures begin to occur at grain boundaries and other noncoherent microstructural regions such as carbide particles and hard phases. We may describe such events as rupture by suppressed void growth, or as a change to alternate microfracture mechanisms. Fractographic examination shows little or no evidence of void-growth dimples, and the featureless appearance of microfractures is termed "quasi-cleavage."

Mechanistically, this change from large-strain rupture to near-elastic-stress void-growth rupture is analogous to the change illustrated in Fig. 22 for cleavage. The rupture sites shift from within the plastic zone to the elastic-plastic border of the plastic zone, near the region of the elastic K-field.

Time-dependent crack-extension processes such as stress-corrosion cracking also can be understood by this model. A K-field that is below critical value for fracture may be at critical value for slow separation. For example, this happens as hydrogen is diffused into the plastic zone by corrosion in the crack-tip region. Hydrogen can activate microcracking at grain boundaries in high strength steels. Other more complex, non-void growth types of microcracking can occur in titanium and aluminum alloys.

An important general conclusion is that the nature and sites of microfracture separation events are changed by lowering critical K levels for crack extension.

CHAPTER 3

Fracture Mechanics Criteria

RELATIONSHIPS TO FRACTURE STATE

All aspects of fracture mechanics are referenced to three fundamental fracture states:

Plane strain
Elastic-plastic
Plastic.

The plane-strain fracture state applies to brittle materials characterized by linear-elastic fracture mechanics principles. The fracture surfaces are characteristically flat. The materials are frangible, and the metal separates purely by release of stored elastic energy.

The elastic-plastic fracture state is typical of semiductile materials. The fracture surfaces are flat, except for "fins" of slant fracture at the surfaces. Metal separation requires intermediate to high elastic stresses.

The plastic fracture state is typical of ductile materials. Fracture surfaces show considerable evidence of ductility, including slant fracture and yielding. Metal separation requires over-yield loading.

The fracture state of a metal is disclosed by appropriate test procedures. Fracture tests have structural meaning only when they place the level of fracture resistance within the range of a fracture state. For example, fracture properties of the elastic-plastic type automatically exclude plane-strain behavior. In general, the designated fracture state excludes lower orders and therefore places a lower limit on expected fracture performance.

The determination of the lower limits of reliability is the most crucial aspect of fracture-safe design. It defines the minimum guarantee provided and is therefore a primary reliability index.

In practice the minimum guarantee is given by selection of an appropriate fracture criterion. The criterion may be expressed in test specimen or structural design terms. It represents a fracture test value that specifies a level of fracture resistance within a fracture state. The level of fracture resistance then can be used in specifications. The criterion designation always signifies a specific fracture-state level, regardless of its reference to a test value or structural specification index.

There is growing awareness that the design of engineering structures should include documentation of fracture-control plans based on specific minimum criteria. Such requirements are being imposed as legally binding specifications. Thus, what was a professional responsibility is becoming a contractual obligation.

The plastic zone eventually becomes too large for unstable fracture extension, when the

Statistical data on fracture-state criteria must be collected. These data are essential for defining what is attainable for specific metals and specific design and specification purposes.

Engineers should be provided with unequivocal information on the criteria that can be met by standard-grade metals for specified temperatures and strength levels. Whether to use a metal of low, intermediate, or high fracture-state properties is an engineering question. For example, engineers should know how to specify a criterion that guarantees properties either low or high in the elastic-plastic fracture state, if service conditions require such properties.

The fundamentals of fracture mechanics are usually explained in terms of linear-elastic (purely elastic) stress-field analyses. The very low crack-tip ductility of plane-strain metals may be ignored, or corrected mathematically, in such analyses. An introduction to linear-elastic (plane-strain) fracture mechanics is presented in Appendix A.

The fundamental practical features of generalized fracture mechanics can be understood only in terms of constraint factors. Constraint is basic; if it is not understood there can be no rational beginning in understanding criteria. The reader is advised to study the following sections on constraint as a first step. The significance of Appendix A will be more obvious with this as background.

PHYSICAL SIGNIFICANCE OF CONSTRAINT

Plastic flow at crack borders develops following stress-strain relationships that are distinctly different from those of a smooth section. The difference is best explained by plots of true stress vs true strain, i.e., plastic-flow curves.

Exact definition of the flow curves for specific crack conditions is the subject of continuing research. We shall not attempt to describe the state of knowledge except to indicate that it suffices for generalizing constraint factors. These generalizations are well known to fracture research specialists and form the basic rationale for fracture mechanics theory.

Schematics will be used to explain constraint in terms of a physical model. The first step is to discuss the origins of constraint. Figure 25 illustrates that the introduction of a circular notch in a tensile bar causes a local elevation of the flow curve. We may describe the plastic flow of the smooth tensile bar as free, or unimpeded. Lateral contraction occurs with a minimum of opposition, allowing relatively free extension in the direction of loading.

The reduced section of the notched bar develops plastic deformation while the shoulders are stressed to elastic levels. Since the elastic contraction is small compared to the plastic contraction of the reduced section, plastic flow is opposed. The opposition is a reaction-stress system such that stresses in the σ_x- and σ_z- directions inhibit flow in the σ_y (load) direction. Thus, in contrast to the smooth bar's uniaxial tension system, the notched bar has a triaxial stress system. This triaxiality is what elevates the flow curve.

Constraint may be described as inhibition of plastic flow due to triaxial stress. The degree of inhibition is directly related to the degree of triaxiality, i.e., the degree to which σ_x and σ_z stresses approach the value of the σ_y stress. Exact equality of the three represents absolute constraint and absolutely prevents plastic flow. This condition is not attained in notched specimens because the stress system is always unbalanced. The σ_y stress is always greater,

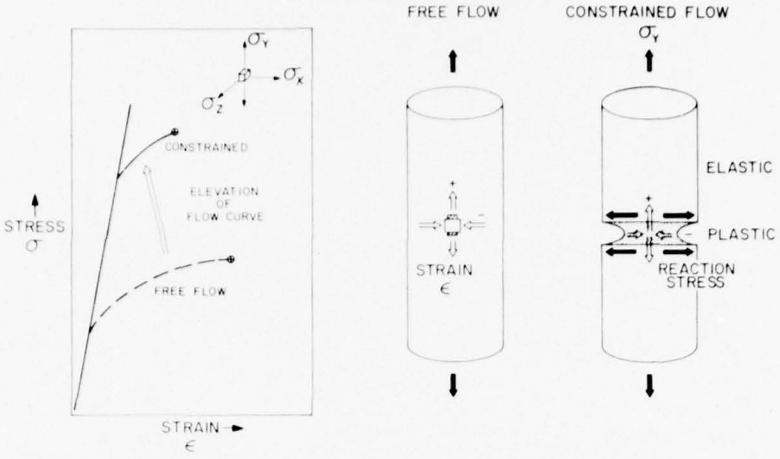

Fig. 25—Origins of constraint.

and thus flow takes place in the load direction. The important point is that flow inhibition subjects metal grains to abnormally high stresses compared to free flow in a tensile bar.

The origins of triaxial stress constraint may be traced to the elastically loaded metal that surrounds a volume of localized plastic flow. The effect is general, as indicated by the example of two pieces of hard steel bonded by a thin layer of soft braze metal. If sufficiently thin, the joint has a strength equal to that of the steel. This is due to the high level of constraint imposed on the flow of the soft metal by the elastically loaded hard metal. Mechanical constraint causes metal grains to act "stiffer." Thus, the flow behavior of metal grains is not intrinsic; it is a function of the degree of applied constraint. For example, if the brazed joint is made thicker, flow will be easier, due to decreased constraint.

The constraint-level-vs-stiffness relationship is basic to understanding the mechanical behavior of metal grains in crack-tip plastic zones. Increased mechanically induced "stiffness" decreases the ability of the grain structure to deform without microcracking.

Three separate stress systems are important in analyses of fracture conditions:

1. The nominal design stress, which is the usual engineering reference.

2. The stress that acts to open the crack. This stress should be examined as a function of structural geometry. For example, stresses at nozzles of pressure vessels may be three or four times the hoop-stress level. Such high stress is the nominal stress of interest if the crack is in such a high-stress region.

3. The localized stress at the crack tip that acts to rupture the grain structure. This stress can only be inferred indirectly, by reference to the constraint level.

Figure 26 illustrates the plastic-flow conditions at a crack tip in a tensile-loaded plate with a through-thickness edge crack. The plastic rod formed at the crack tip must increase in diameter, by σ_3-direction extension, with any increase in stress. However, this can happen

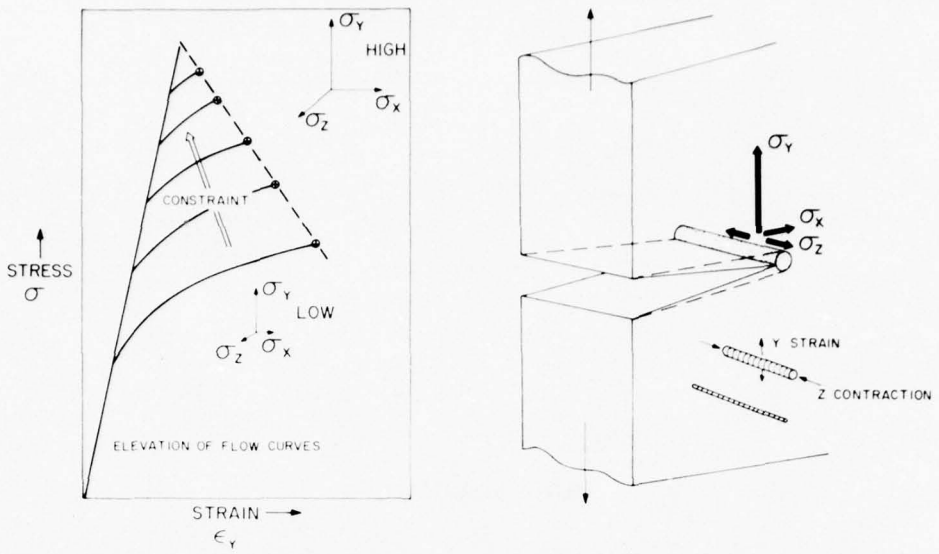

Fig. 26—Constraint conditions for through-thickness cracks. Increasing section size increases constraint, because crack-tip plastic flow is opposed by a greater length of surrounding elastically loaded metal.

only if σ_z-direction contraction occurs. The elastic material that surrounds the plastic rod opposes both σ_z- and σ_x-direction flow, producing a triaxial stress system.

The family of flow curves of Fig. 26 illustrates the effects of increasing the plate thickness. Constraint is increased, as indicated by higher flow curves, because triaxiality is increased by higher reaction stresses in the σ_z direction. In simple terms, the length of elastic material that envelops the crack is increased with crack-front size; therefore, the material's capacity for opposing enlargement of the plastic zone increases. It may be generalized that increasing crack-front size increases constraint. As a result, stress-strain relationships are changed so that higher σ_y stress levels are required to cause a unit increment of plastic flow at the crack tip. Thus, the metal behaves with increasing "stiffness" as crack-front size is increased.

A more generalized model of crack-front size effects for through-thickness cracks is presented in Fig. 27. Cracks of increasing size are represented for two plate thicknesses. There is an increase in flow-curve constraint with increasing crack size, to a limit level. This limit represents the maximum constraint capacity of a through-thickness crack. It is attained when crack dimensions exceed approximately twice the thickness (2 T). (This is a conservative estimate.) The concept of a *maximum-constraint crack for a given section size* is basic to the discussions that follow.

The reason for attainment of a maximum constraint capacity for a crack of this geometry can be explained in terms of the distance from free surfaces. Constraint to plastic flow is always highest at the center of the crack front. This region (represented by small squares in the figure) is farthest from the free surfaces. This means that plastic contraction (σ_z-direction flow) has the longest path and therefore experiences the highest resistance to plastic flow.

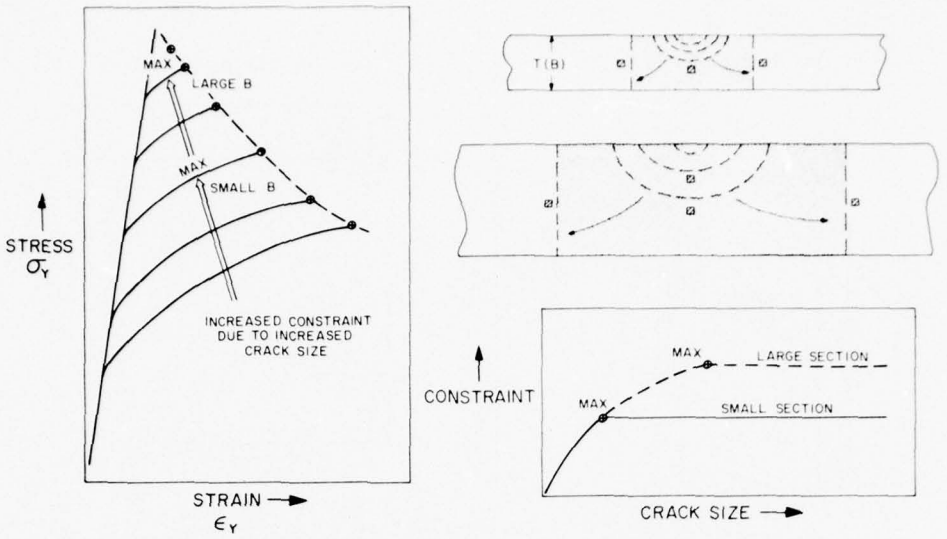

Fig. 27—Significance of maximum attainable constraint capacity for the section size, as related to maximum constraint cracks. The maximum constraint level developed by through-thickness cracks increases with section size because of the longer crack front.

Conversely, plastic contraction occurs most readily close to the free surface. In effect, the metal near the free surfaces experiences little triaxiality.

When a through-thickness crack attains a length of about 2 T, the minimum distance from the free surface is half the plate thickness (0.5 T), simply because all the other distances are now greater than 0.5 T. Thus, constraint can be increased only by expanding the 0.5-T distance by increasing the plate thickness. The fracture mechanics literature uses "B" to represent thickness because it indicates the crack-front *breadth* for through-thickness cracks and therefore indicates the free-surface distance. B is equivalent to T.

We may now generalize that maximum constraint capacity for a through-thickness crack is attained when the crack length is such that 0.5 T is the controlling distance from the free surfaces. This generalization is important to understanding the use of edge-cracked specimens in fracture testing. Edge-cracked specimens are designed for measuring the fracture resistance of a metal of specified thickness, under conditions of a maximum-constraint-capacity crack. The reason is that the lowest degree of ductile behavior that can be forced on the metal depends on maximized constraint. The metal cannot be forced mechanically to behave in a less ductile fashion than it exhibits under these conditions. The fracture resistance of the metal for this maximum imposed constraint is independent of further increases in crack size. Thus, maximum constraint is the basic scientific and engineering reference.

The connection between scientific and engineering aspects is illustrated in Fig. 28. The practical scientific interest is in measuring the minimum value of fracture resistance, as a standardized reference. With an increase in edge-crack depth a to approximate equality with specimen thickness, the limiting distance from the free surfaces becomes 0.5 T. Thus, constraint is maximized, as illustrated in the plot of constraint vs crack depth. Fracture tests

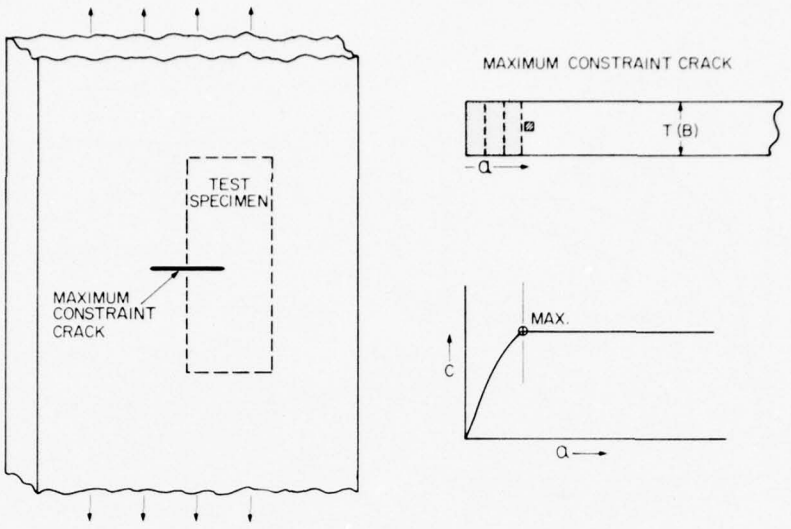

Fig. 28—Basis for design of fracture test specimens with maximum constraint cracks.

conducted with such a specimen measure the lowest level of fracture resistance (fracture state) for the metal, in the form of a specified section size T (B). The test thus identifies the lowest level of fracture that is *allowed to develop* by the intrinsic properties of the grain structure.

The edge crack may now be recognized as the equivalent of half the maximum-constraint crack introduced in a tensile-loaded flat plate. Only half is required, because the two ends of the crack are fully equivalent and subject to the same constraint. In effect the test specimen is a model of the maximum-constraint crack that controls the conditions of fracture extension in a structure. The lowest level of fracture state possible in the structure is the same as that characterized by the test specimen. The metal cannot be made to behave in a less ductile fashion.

CONSTRAINT RELAXATION

The object of fracture testing is to fix the constraint conditions and then observe the metal response as a dependent variable. The specimen is designed with a maximum-constraint crack; thus, the constraint capacity of the specimen is defined by the section size, and the metal response is the dependent variable.

Metal response is best understood in terms of the constraint definitions of fracture mechanics. These include (a) degree of applied constraint and (b) constraint-relaxation phenomena. Constraint capacity is defined in terms of *plane-strain* constraint, i.e., the capacity of the test for prevention of z-direction plastic flow. The fracture mechanics literature deals with constraint mainly under plane-strain conditions.

To understand constraint relaxation, we must consider crack acuity. The natural crack in a structure and the crack in the test specimen must be equally sharp; rounding off the crack tip decreases constraint. The development of plastic flow at a crack tip in the course of loading

causes some rounding off. For brittle metal crack blunting is very slight, and fracture extension occurs under conditions of continued crack sharpness. This behavior may be referred to as fracturing under conditions of plane-strain constraint. However, if the metal grain structure resists early rupture, the increase in plastic deformation results in blunting of the crack tip. As a result, the limit of plane-strain constraint capacity is exceeded. The effects are cumulative; crack blunting causes constraint relaxation, which causes increased plastic flow, leading to additional blunting, and so on, until a fracture state in excess of plane-strain conditions is reached.

These effects are illustrated by Fig. 29 in terms of decreasing flow-curve resistance, compared to the initially applied level. The degree of crack blunting determines the course of the flow curves. In effect, constraint relaxation, resulting from exceeding plane-strain capacity limits, decreases the effective stiffness of the metal at the crack tip, and contraction takes place in the through-thickness direction.

The resulting fracture states are illustrated in the figure. Plane-strain, elastic-plastic, and plastic fracture states are directly related to flow-curve behavior. Plane-strain states signify fracture extension without crack blunting (no relaxation of constraint); thus, the flow curve follows a course dictated by the degree of applied constraint. Elastic-plastic states imply significant decreases in flow-curve resistance due to constraint relaxation. Plastic states signify a major decrease or essential elimination of the applied constraint due to severe crack-tip blunting.

The sketch of the grain structure illustrates micromechanical behavior at crack tips. The parallel lines within grains indicate slip along crystal planes, which produces grain elongation. The deformation of individual grains is necessary for growth of a plastic zone at the crack

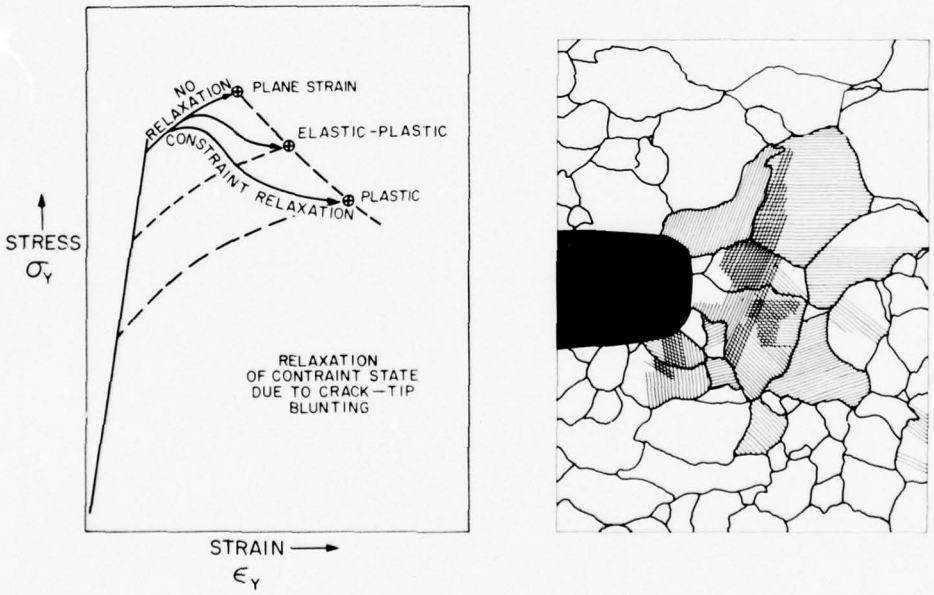

Fig. 29—Relaxation of plane-strain constraint by crack-tip blunting.

230-362 O - 77 - 4

tip. Slip processes compete with the development of cracks and/or voids in the grains or at grain boundaries.

Brittle metals develop microcracks or voids at early stages of plastic-zone growth. For these conditions the flow curve is terminated by early rupture. The *micromechanical* conditions that cause grain rupture are described as stress-induced fracture. The *macromechanical* behavior of the test specimen is called plane-strain fracture.

In ductile metals, grains continue to deform under further loading, causing the plastic zone to enlarge. If the crack tip is somewhat blunted, the grains sense decreased mechanical constraint and slip becomes easier. These facts indicate that a specific level of imposed constraint may be accepted or opposed by the grain structure. It should be noted that increasing constraint level signifies increasing constraint capacity. The two terms are related mechanical expressions of the test severity, for suppression of metal-grain ductility. "Level" and "capacity" are equivalent expressions for constraint.

The micromechanical response of metal to applied plane-strain constraint determines the macroscopic fracture state of the section size under test. The macroscopic fracture state determines the reaction of the metal to loading in the presence of a crack.

SIGNIFICANCE OF FRACTURE STATES

A physical model that explains the structural design significance of the fracture-state nomenclature is illustrated in Fig. 30. The figure indicates the range of metal responses to

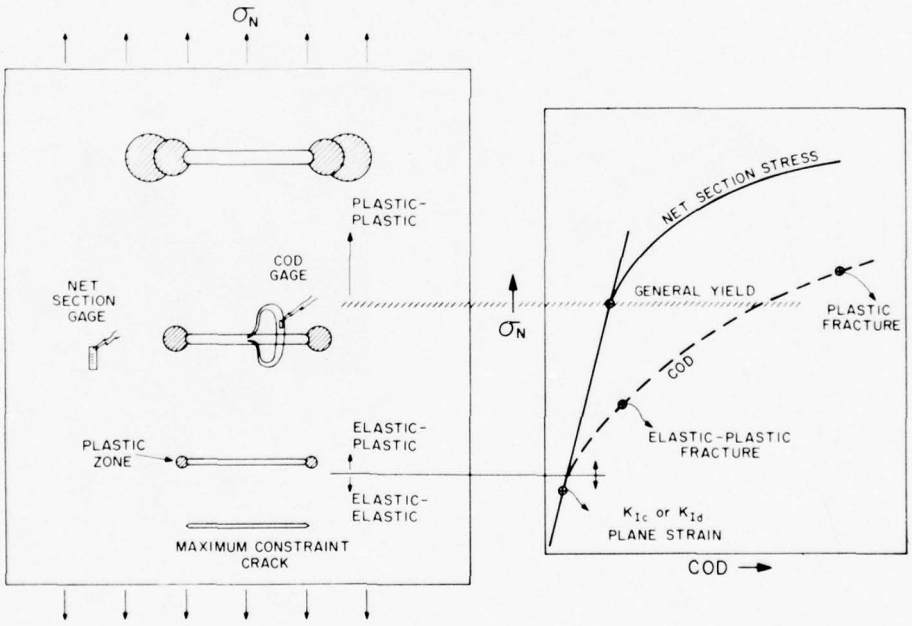

Fig. 30—Engineering significance of fracture-state nomenclature.

tensile loading of a flat plate with a maximum-constraint crack. The crack is considered to have a length of at least 2 T and to have a sharp edge. Two kinds of measurements are required: (a) a Crack-Opening Displacement (COD) gage measures the elastic or plastic behavior of the crack tip, and (b) a net-section gage measures the rise in nominal stress. The two quantities are plotted simultaneously in the figure. The points at which fracture occurs in metals of various fracture properties are indicated by the crossed points with the arrow designations.

If a metal fractures while the COD gage is indicating a linear response to increased nominal stress, it is deduced that the crack opening has been largely elastic. Since the nominal stress at failure, then, must be of the elastic level, the combined conditions could be described as "elastic-elastic." However, "plane-strain" is the conventional term. In effect, plane-strain constraint has been maintained to the point of fracture instability. K_{Ic} (or K_{Id}) may be calculated to define the level of plane-strain fracture resistance. The nominal engineering stress level at the point of fracture is generally *less than* 0.3 σ_{ys} for plane-strain fracture extension due to a through-thickness crack of a minimum 2- or 3-T length. This generalization is important to engineering use of all plane-strain metals (metals for which K_{Ic} and K_{Id} can be measured for the section size of interest).

The elastic-plastic fracture state indicates that significant ductility develops at the crack tip, as indicated by plastic response of the COD gage, but nominal fracture stress remains in the elastic range. In brief, the nomenclature signifies that plastic flow at the crack tip, due to constraint relaxation, is sufficient to raise the nominal fracture stress from 0.3 σ_{ys} to the limit of σ_{ys}.

The plastic fracture state means that the COD gage response is grossly plastic and that the nominal stress for fracture extension is elevated to the plastic range. In other words, plastic behavior is assured regardless of crack size for the section size of interest.

METALLURGICAL ASPECTS OF CONSTRAINT TRANSITIONS

The foregoing discussions have emphasized that a specifiable condition of constraint to plastic flow may be accepted or opposed by the intrinsic ductility of the metal grain structure.

It is desirable that the grain structure resist microcracking under localized, high-intensity crack-tip stresses. In other words, the grain structure must respond to increasing levels of plane-strain stress intensity K_I by continuing to activate slip systems within grains rather than forming microscopic voids between or within grains.

The macromechanical behavior of (a) a small test specimen with a maximum-constraint crack, (b) a large tensile-loaded plate with a crack of equivalent constraint, and (c) a structure with such a crack are all controlled *equivalently* by the metal grain structure. The critical factor in each case is the plastic-flow curve of a small volume of metal at the crack tip. Whether a huge structure such as a ship may be subject to fracture or is completely safe is decided by this microscopic volume of metal.

This information indicates that the microstructures of metals may be adjusted to provide constraint relaxation for specified imposed constraints. In other words, the structural behavior

of a metal of specified section size (and thus specified maximum constraint capacity) can be adjusted within known limits.

The basic procedure for characterizing the fracture state and interpreting the structural performance of a metal is illustrated in Fig. 31. The figure may be considered to represent a structural steel 1.0 in (25 mm) thick, for example. The problem is to define the temperature range of the constraint transition for the specific metal and thickness.

This can be done by using a large plate with a crack of maximum constraint capacity. The dynamic-load constraint transition (from plane-strain to elastic-plastic) controls fracture extension in rate-sensitive metals. Thus, loading of the plate must be applied by impact. If a series of such tests were conducted with increasing temperature, the results would be expected to follow the σ_N-vs-temperature relationship shown in the figure. The temperature scale is, in fact, a scale of increasing metal-grain microfracture ductility. Over a long range of "low" temperatures, say -200° to 0°F (-130° to 18°C), the fracture stress level changes little. This is the plane-strain (K_{Id}) temperature region, in which the imposed plane-strain constraint is enough to cause cracking of grains with very little localized deformation at the crack tip. Conversely, grain ductility is insufficient to cause constraint relaxation. The fracture surfaces are flat (brittle), with no thickness reduction, i.e., they show evidence of plane-strain fracture.

At a critical temperature specific to the steel and the section size, the effects of increasing temperature in promoting slip of the metal grains are manifested. At this point, the metal becomes ductile enough to develop some constraint relaxation; at this point the elastic-plastic state is entered. Accordingly, fracture stress begins to rise, and visible evidence of lateral

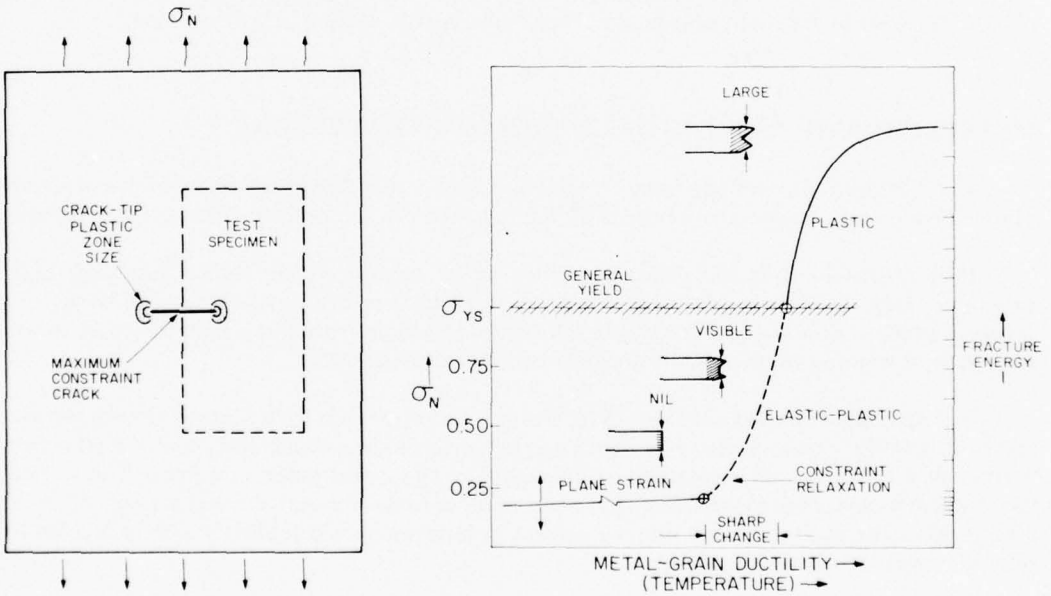

Fig. 31—Engineering significance of constraint transitions due to temperature-induced increase in metal-grain ductility.

contraction appears on the fracture surfaces. The first shear lips appear, indicating the start of mixed-mode fracture, characteristic of the elastic-plastic state. The constraint transition is remarkably sharp, and for the cited thickness, fracture-extension stress is raised from less than 0.3 σ_{ys} to 0.5 σ_{ys} in a 30°F (17°C) temperature span. It is then raised to yield-stress levels, with an additional temperature increment of this order.

Obviously, it is not practical to conduct tests of large plates for metal characterization. A properly designed small test specimen serves the same purpose, provided the constraint conditions are equivalent, as described previously. A fracture mechanics test specimen of 1.0-in (25 mm) section size serves for following the slight rise of fracture resistance in the plane-strain temperature region. The data plot will show a gradual rise of the K_{Id} curve with temperature increase. When the critical temperature for constraint relaxation is reached, K_{Id} can no longer be measured.

To use a small specimen above this temperature, it is necessary to measure the fracture behavior in terms of a ductility index. This measurement may be in terms of crack-tip lateral contraction or fracture energy. Thus, the fracture mechanics K_{Id} specimen may be fractured and indexed in terms of ductility. However, preparing a K_{Id} specimen is too expensive. The low-cost Dynamic Tear (DT) specimen provides the same information by identical ductility measurements. The most practical measurement is that of fracture energy for a standardized fracture path length. The main requirement is that the fracture path be long enough to permit development of the characteristic fracture mode (length approximately 2T or greater).

The reason that either K_{Id} or DT specimens may be used to provide an unequivocal measure of the constraint transition in terms of fracture energy is illustrated in Fig. 32. It shows the change in fracture mode associated with transition from plane-strain to plastic fracture. Both specimens have the same maximum-constraint crack (a slit with a sharpened edge). Thus they have the same constraint capacity, as determined by section size. The metal-grain ductility response to identical mechanical constraint is necessarily the same.

The changes in fracture mode are the result of progressively increasing plastic deformation of the crack tip, consequent to the constraint transition. The increased volume of metal that undergoes plastic deformation before fracture results in an increase in the fracture-energy reading as well as an increase in the degree of lateral contraction. Thus, the fracture-energy scale of Fig. 31 (right side) may be used to index a temperature-vs-energy curve, which has the same flat-plus-sharp-rise features as the temperature-vs-σ_y curve. The energy curve may be established easily by using the DT specimen. The temperature range of constraint relaxation for the specific steel and section size is thus defined by a test that is practical for general engineering use.

The fracture mode changes from flat to full-slant over the course of the constraint transition, and the transition may be indexed by plotting the percentage of slant fracture vs temperature. Such a plot shows a transition from zero (full flat) at plane-strain levels to 100% (full slant) at the completion of the transition. This degree of fracture-mode change is characteristic of metals featuring high-level plastic fracture states. Metals of lower plastic fracture resistance "shelf out" and retain a partly flat central region in the fracture surfaces.

The limiting degree of constraint relaxation determines whether a metal has high- or low-shelf features. There is a corresponding difference in lateral contraction or shelf fracture energy.

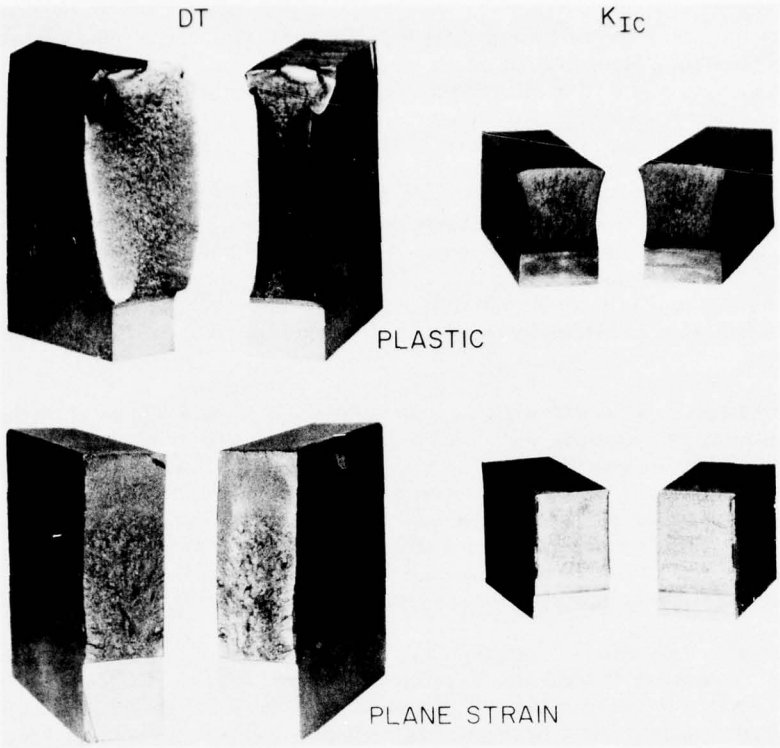

Fig. 32—Illustration of common features for the constraint transitions of K_{Ic} or K_{Id} and DT test specimens—section size 1.0 in. (25 mm).

From an engineering point of view, the essential characteristic is the specific temperature region of the elastic-plastic transition. *Very little is gained by small increases in* K_{Id} from very low temperatures to the temperature of constraint relaxation. Fracture-extension stress rises negligibly in the plane-strain region. The exact equivalence between the sharp rise in fracture-extension energy and the sharp rise in fracture-extension stress is the important engineering feature in Fig. 31.

The low-cost DT test is used to develop a data bank of metal properties. The various grades of engineering metals are thus classified by their characteristic constraint-transition temperatures, with due consideration for section size. Most important, the microstructural features required to locate the specific temperatures of constraint transition are accurately identified. Thus, it is feasible to "design" the metal for specific structural requirements, allowing for the lowest service temperatures.

Increasing strength level, for all metals, causes a decrease in metal-grain ductility. Thus, the curve in Fig. 31 may be considered to apply in reverse fashion. With increasing strength comes a drop from plastic to elastic-plastic and then to plane-strain fracture states.

The combined effects for steel are best illustrated by a tridimensional presentation like Fig. 33. The vertical scale is the energy-scale reference of Fig. 31; it may also be considered in terms of relative stress. Accordingly, it is the index of the constraint transition for a specific section size, for example, 1.0 in. (25 mm). The temperature and yield-strength scales are the usual reference planes for plotting constraint transitions. The important point is that the strength transition for steels must be discussed in terms of on-shelf properties, i.e., conditions at the completion of the temperature-induced transition. Note that high strength steels show small temperature effects.

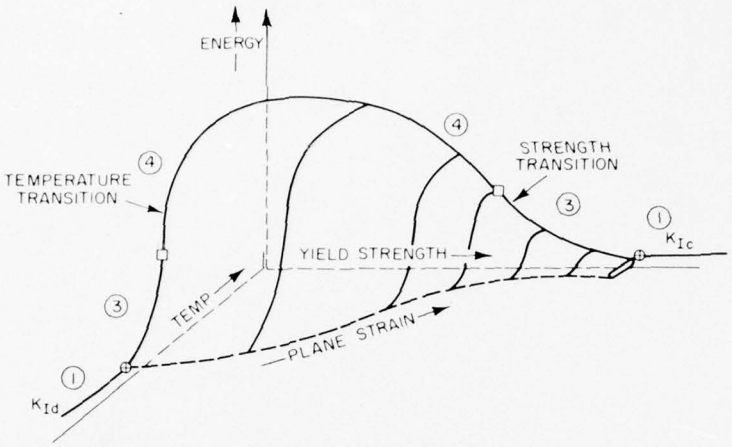

Fig. 33—Three-dimensional plot of temperature- and strength-induced constraint transitions for steels. The notations refer to fracture states, as follows: (1) plane strain, (3) elastic-plastic, and (4) plastic. (See Fig. 35 for significance of stage 2, which represents the special constraint transition for plane strain in thick sections.)

Nonferrous metals are relatively insensitive to temperature effects. Constraint transitions occur only as the result of strength-induced changes in metal-grain ductility.

FRACTURE-EXTENSION PROCESSES

Figure 34 illustrates the physical nature of fracture extension processes for plane-strain and plastic fracture states. The basic reason for the increase in fracture-extension stress during constraint transitions is revealed by considering these processes.

Plane-strain fracture indicates brittle behavior because fracture extension is of an unstable type. That is, as the initial small crack-tip plastic zone is ruptured, there is a release of elastic-strain energy, as if a spring were severed under stress. The crack remains sharp, and the next plastic zone that forms is likewise small and ruptures immediately on exposure to the high stress intensity (K_I) of the advancing crack tip. In effect, the fracture of the first "spring" releases elastic stress, which overloads the next, leading to its rupture. This process continues to total fracture.

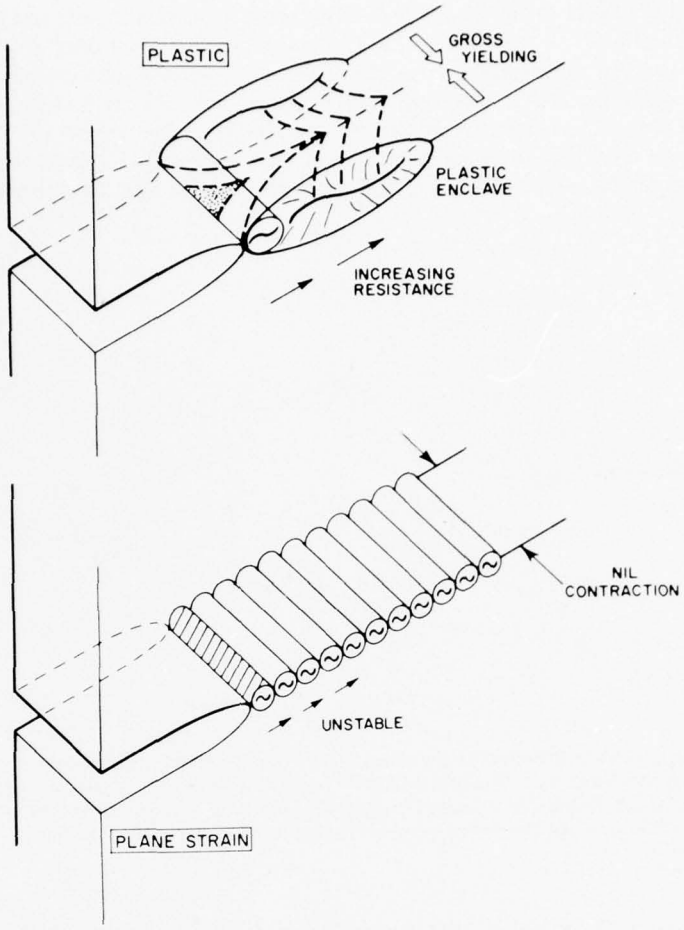

Fig. 34—Fracture extension for plane-strain and plastic fracture states.

The fracture, then, extends by repeated rupture of the crack-tip region. The nominal elastic-stress fields of the structure are important because they represent the degree of elastic extension of the long-range "spring" system and, therefore, the level of elastic-strain energy available for continued fracture extension. Low-level elastic-stress fields provide for release of the low elastic-strain energy required for plane-strain fracture. This is due to the small size of the plastic zones, which can absorb only small amounts of energy. Thus, in the usual nominal engineering design, elastic-stress fields on the order of 0.3 σ_{ys} are sufficient for continued unstable extension.

As the elastic-plastic region of the constraint transition is reached, the plastic zone gets larger, and more energy is required for rupture. Rupturing these larger plastic zones, therefore, takes a greater release of elastic-strain energy, which can be obtained only by raising the nominal stress. The extension process continues to be unstable (controlled by the elastic-strain-energy release) to the point that nominal stresses of yield magnitude are required.

The plastic zone eventually becomes too large for unstable fracture extension, when the increasing constraint relaxation produces a plastic-zone size that is not subject to rupture by release of elastic-strain energy. At this point, fracture extension cannot be induced or continued by elastic-stress fields; stresses of over-yield magnitude must be applied, and a plastic-strain field must be continually redeveloped in advance of the crack.

The constraint transition to high plastic-region levels is accompanied by increasingly large plastic-strain fields. The plastic-strain field, which must be evolved prior to the advance of ductile fractures, is illustrated by the condition termed "plastic enclave" in Fig. 34. Gross through-thickness yielding, which results in a dimple (lateral contraction), must take place in successive unit increments of rupture steps. Translation of a fracture by such high-ductility unit-increment processes requires stress fields of very high plastic level.

SECTION-SIZE EFFECTS

The very sharp transition from the plane-strain state to relatively high levels of the elastic-plastic state, illustrated by Fig. 31, is characteristic of all section sizes. The primary effect of large increases in section size, say from 1.0 to 12 in. (25 to 300 mm), is a K_{Ic} or K_{Id} transition. This type of transition does not represent a change in fracture state, as a constraint transition does, but rather a change in plane-strain fracture toughness. A sharp rise in K_{Ic} or K_{Id} takes place over a narrow range of temperature or yield strength, while the fracture state remains plane strain. Thus, this section-size effect represents a "plane-strain transition."

The engineering significance of this plane-strain transition in large sections is that it shifts the critical temperatures or strength levels of the constraint transition. In other words, plane-strain constraint is lost, and elastic-plastic fracture begins at higher temperatures and lower strength levels than with thin sections. This division between thin and thick sections is best placed at approximately 1.0 in. (25 mm).

Increases in section sizes from 1.0 to 12 in. (25 to 300 mm) result in very large increases in the constraint capacity of maximum-constraint cracks. That is, the size of the 0.5-B dimension of the crack front is increased enormously. Thus, metal grain ductility is suppressed to higher temperatures for cleavage fracture and to lower yield strength for void-growth fracture.

This suppression means that plane-strain conditions continue to apply in the sense that K_{Ic} or K_{Id} values can be measured. The sharp increase in K_{Ic} or K_{Id} indicates a large increase in plane-strain plastic-zone size. In effect, increasing metal-grain ductility in the plane-strain transition region is difficult to suppress, which is why large increases in section size are needed to provide the requisite constraint.

It should not be inferred that the plane-strain transition signifies an increase in fracture resistance equivalent to that of the constraint transition. It does not, because plane-strain measurements involve a fine-scale definition of the degree of brittleness. The plane-strain transition simply means that the measurement capacity is extended by increased section size. Moreover, a thick-section metal is not intrinsically of higher plane-strain fracture resistance than a thin-section metal. K_{Ic} or K_{Id} measurement at equal temperatures (provided such measurements are valid by ASTM practices), gives the same value for a thin specimen cut from a thick section as for the thick section itself.

The characteristic four parts of the temperature-transition curve for steels of very thick section are illustrated in Fig. 35. The 6- to 12-in. (150 to 300 mm) DT-test energy curves show a flat K_{Id}-related region (Part 1), followed by a modest rise in the K_{Id}-related plane-strain transition region (Part 2) and then a very sharp rise in the constraint-relaxation region (Parts 3 and 4). The lower half of the constraint-transition region represents the elastic-plastic fracture state (Part 3), and the upper half represents the plastic fracture state (Part 4).

The correlation to the K_{Id} curve includes a designation of the minimum section sizes (in inches) required for tracking this curve experimentally. Tracking the K_{Id} transition required an increase in section size from 1.0 to 8.0 in. (25 to 200 mm) in the range of 0° to 120°F (-18° to 50°C). At all temperatures below 0°F (-18°C), K_{Id} specimens 1.0 in. (25 mm) thick or smaller were adequate for tracking the low-slope portion of the curve. This clearly indicates the very large increases in constraint capacity that are required to maintain plane-strain conditions in the plane-strain transition-temperature range.

Another feature to note is the almost vertical rise of the K_{Id} curve as the constraint-transition temperature for the 12-in. (200 mm) section size is approached. This indicates that further increases in section size would provide a negligible increase in the temperature of K_{Id} measurement; a wall-like temperature limit is reached. In effect, the metal grain structure becomes too ductile for suppression to plane-strain levels by mechanical constraint.

The K_{Ic} curve for this same metal shows a similar exponential rise, but at temperatures about 70°F (40°C) lower. This displacement is evidence of a viscoplastic effect. At the low loading rates of K_{Ic} testing, time is allowed for slow (viscous) plastic flow. Accordingly, the flow-curve level is decreased, and thus the effective stiffness is decreased. It should be noted that

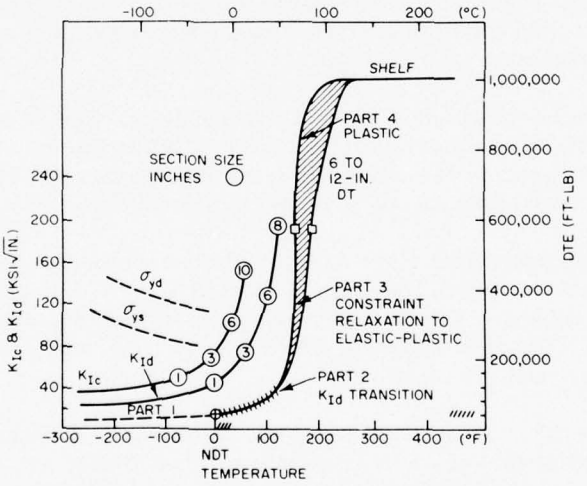

Fig. 35—Characteristics four-part constraint-transition curve for a 12-in.-thick (300 mm) plate of A533-B steel. The K_{Ic} and K_{Id} transitions are fully developed in the toe region of the DT-test curve for the full-section size. Circled numbers indicate (in inches) the increase in section size required to track the K_{Ic} and K_{Id} transitions. K_{Ic} and K_{Id} data from Wessel. (See Chapter 6.)

the K_{Id} curve is the controlling factor for rate-sensitive metals, as indicated by failure analyses of such structures as ships, pressure vessels, and bridges.

The characteristic three parts of the temperature transition curves for section sizes on the order of 0.6 to 1.0 in. (16 to 25 mm) are illustrated in Fig. 36. In this case, the plane-strain transition (Part 2) is essentially eliminated, due to the low constraint capacity of the 0.6-in. (16 mm) section size. For this low level of constraint, it is possible to measure only the nearly flat region of the K_{Id} curve (Part 1). The constraint transition (Parts 3 and 4) takes place with dramatic sharpness.

The experimental data of Figs. 35 and 36 are generalized in Fig. 37 (left side). In this case, plane-strain K_{Id} and constraint transitions develop as the result of increasing metal-grain ductility, which is due to increasing temperature. The right side of Fig. 37 is a generalized plot of section-size effects related to increasing metal-grain ductility due to decreasing yield strength. The K_{Ic} scale is used to indicate that the effects are common to steels as well as to non-rate-sensitive, nonferrous metals such as aluminum and titanium alloys. The figure illustrates that a family of transition curves, within the range of the two limiting curves, will develop as section size is increased from small to very large dimension.

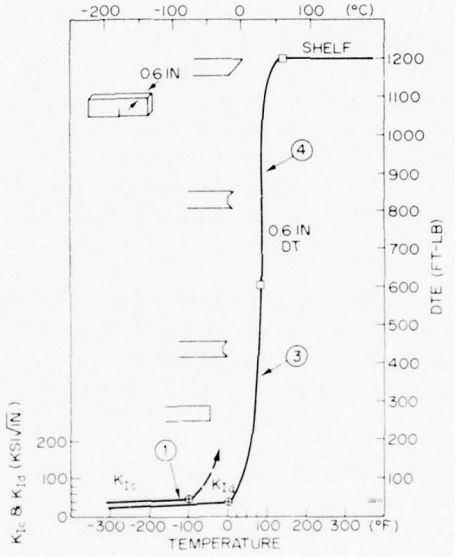

Fig. 36—Characteristic constraint-transition curve for conventional mild steels of 0.6-in. (16mm) section size. The K_{Id} and DT-test scales are adjusted to provide a common plot in the toe region of the DT curve. Note the sharp rise of DT fracture energy above the K_{Id}-limit temperature. Dashed line indicates start of plastic crack-opening displacement and lateral contraction for the K_{Ic} test, i.e., a ductility transition equivalent to that shown by the DT energy curve, but displaced to lower temperatures.

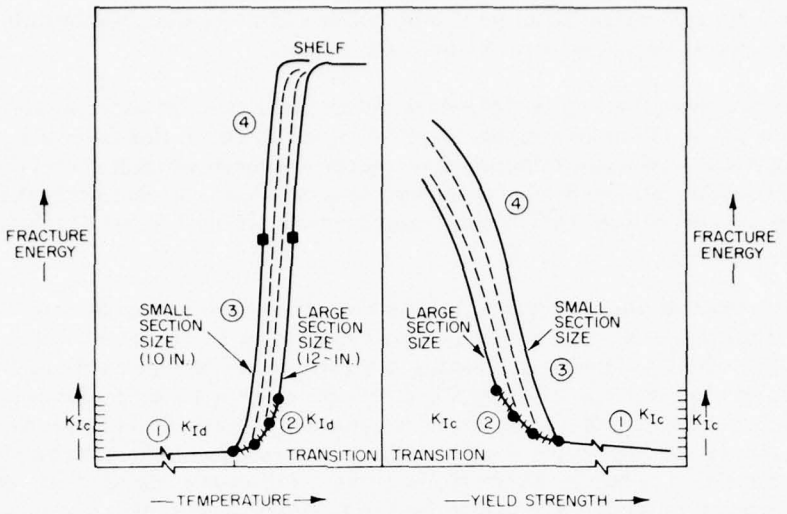

Fig. 37—Characteristic constraint-transition curves for small and very large sizes. Increasing section size results in shifts noted by dashed lines.

PLANE-STRAIN TRANSITION EFFECTS

Discussions of plane-strain transition effects in the scientific literature have centered on plotting the sharp rises in K_{Ic} and K_{Id} that may be observed in thick-section metals. By using an expanded K_I scale and omitting data on the rest of the transition to the elastic-plastic state, the curves give the impression of large increases in fracture resistance. By additional magnification of the scale, the curve may be shown to rise as the plane-strain limits of 1.0-in. (25 mm) section sizes are reached.

While these plots are defensible for scientific reasons (demonstrating the exact measurement of plane-strain properties), they have led to engineering confusion. In brief, engineers have misread the true significance of the plots. They do not demonstrate useful increases in fracture resistance; the differences they document are of minor engineering significance.

Fracture mechanics calculations reveal that the plane-strain transition for the case of thick sections has a small effect on the form of the fracture-extension stress curve for through-thickness cracks (Fig. 31). The following summations are of major engineering importance:

The fracture-extension stress level for the plane-strain state does not exceed 0.3 σ_{ys}, regardless of section size.

Increasing K_{Ic} or K_{Id} values to the constraint-capacity limit of the section size (the highest measurable value) increases fracture-extension stresses only in the range from $<0.1\ \sigma_{ys}$ to 0.3 σ_{ys}.

The plane-strain state always provides for catastrophic fracture extension at usual, nominal, design stress levels of 0.3 σ_{ys} to 0.5 σ_{ys}.

Protection from fracture extension (through usual structural stress fields) can be attained only by entering the elastic-plastic fracture state. The reason is indicated by the sharp rise of the fracture-extension stress, to over 0.5 σ_{ys}, in the elastic-plastic region.

The plane-strain state is always unacceptable if design requirements include positive prevention of catastrophic fracture.

By 1950, it was known from ship-fracture studies that small arc strikes could cause a pop-in to a through-thickness crack. Catastrophic fracture extension could then develop through the entire structure, despite the low nominal stress levels used in accordance with ship design rules. At the same time, Robertson CAT tests established that the fracture-extension stress in the plane-strain region could be as low as 5 to 8 ksi (35 to 55 MPa), i.e., below the normal design level of 0.3 σ_{ys}. These tests also indicated the rise in fracture stress for the elastic-plastic temperature region (Fig. 31).

Since 1950 fracture mechanics has evolved the analytical procedures summarized in the above list; they are obviously in agreement with prior knowledge. The 1950 solution to catastrophic problems is perfectly valid today. It involved the application of criteria that would document the use of metal with elastic-plastic properties, i.e., with fracture-extension levels of at least 0.5 σ_{ys}.

DEFINITION OF CONSTRAINT CAPACITY

Constraint capacity is best referenced to the plane-strain state. In a general sense, it is the capacity of a crack front to prevent constraint relaxation. In other words, it is the capacity for enforcing plane-strain conditions, i.e., essentially nil lateral contraction across the crack front.

The usual definition for this term, as given in the fracture mechanics literature, is "the capacity of the crack front for enforcing a plastic-zone size that is very small in relation to the section size." This definition is best understood in terms of a plastic zone at the crack front of a K_{Ic} specimen. If K_{Ic} (or K_{Id}) can be measured, then the plastic zone is very small, because plane-strain conditions apply. When constraint relaxation takes place, the plastic zone enlarges rapidly and eventually becomes very large in relation to the section size.

The idealized mathematical definition of plane-strain plastic-zone size r_p is given by

$$r_p = \frac{1}{6\pi}\left(\frac{K_{Ic}}{\sigma_{ys}}\right)^2 \qquad \text{or} \qquad r_p = \frac{1}{6\pi}\left(\frac{K_{Id}}{\sigma_{yd}}\right)^2$$

where σ_{ys} signifies the static (slow-loading) yield strength and σ_{yd} represents the dynamic value. As an approximation, $\sigma_{yd} = \sigma_{ys} + 30$ ksi (206 MPa) for steels of low or intermediate σ_{ys} levels. The important point is that K_{Ic}/σ_{ys} (or K_{Id}/σ_{yd}) defines plastic-zone size and thus ductility. The limit ratio that can be measured for a specific section size represents the limit plastic-zone size and constraint capacity of the plane-strain state for that section size.

It has been determined experimentally that the limit of plane-strain measurement is conservatively indicated by the following relationship to section size:

$$B \geqq 2.5\left(\frac{K_{Ic}}{\sigma_{ys}}\right)^2 ,$$

where B is the crack-front breadth for a K_{Ic} specimen, i.e., the section size T, expressed in inches.

For example, a constraint capacity of ratio value 1.0 is developed by a section size of 2.5 in. (62 mm). If the section thickness is less than this, the constraint capacity becomes inadequate to measure 1.0 ratio values, and constraint relaxation develops.

The plane-strain limit, expressed as a ratio, defines the constraint capacity of the section size. Tables 1 and 2 list the plane-strain limit ratios for various section sizes.

Table 1—Plane-strain limit ratio, section size as entry point

Section Size (in.)	Section Size (mm)	Ratio Limit (ksi $\sqrt{\text{in.}}$/ksi)
0.1	2.5	0.20
0.2	5	0.28
0.3	8	0.35
0.4	10	0.40
0.5	13	0.45
1.0	25	0.63
1.5	40	0.8
2.0	50	0.9
3.0	75	1.1
6.0	180	1.5
10.0	250	2.0

Table 2—Plane-strain limit ratio, ratio as entry point

Ratio Limit (ksi $\sqrt{\text{in.}}$/ksi)	Section Size (in.)	Section Size (mm)
0.1	0.03	0.6
0.2	0.1	2.5
0.3	0.2	6
0.4	0.4	10
0.5	0.63	16
0.63	1.0	25
1.0	2.5	64
1.5	6	142
2.0	10	254
2.5	16	386

The relationships between increased metal ductility (due to temperature or strength-level effects) and the mechanical constraint provided by given section sizes were defined during the late 1960s. The practical implications for engineering fracture-control plans are of wide scope.

The ratio limit for the section size has four engineering interpretations:

1. It represents the limit of plane-strain measurement for the section size.

2. It indexes the critical temperature or strength level for the transition from the plane-strain to the elastic-plastic fracture state.

3. It indicates that relatively small additional increases in temperature or decreases in yield strength have potent effects on fracture resistance. The sharp increase in fracture resistance is in the nature of a step function at these reference points.

4. Low-reliability plane-strain criteria for fracture-control plans are convertible to high-reliability elastic-plastic criteria within the span of the critical temperature or strength intervals.

The critical temperatures and strength levels of the elastic-plastic transitions for a given section size can be shifted within broad limits by known adjustments in metallurgical quality.

TEST METHODS FEATURING DEFINABLE CONSTRAINT

The various ASTM-standardized fracture mechanics tests are designed to exactly specified constraint capacities. The constraint limits for a specific specimen size B are defined by the formula cited in the prior section as

$$B \geq 2.5\left(\frac{K_{Ic}}{\sigma_{ys}}\right)^2 .$$

The maximum ratio value that can be measured for a specimen of specified section size is the index of constraint capacity.

The constraint developed by surface cracks may be defined exactly by reference to K_{Ic}/σ_{ys} or K_{Id}/σ_{yd}, as illustrated in Fig. 38. The section-size scale at the top of the figure indicates the minimum B dimension for test specimens featuring through-thickness cracks.

The equivalent curves for surface cracks indicate that specimens with surface cracks may be used to determine K_{Ic} and K_{Id} so long as the plane-strain constraint capacity of the crack is

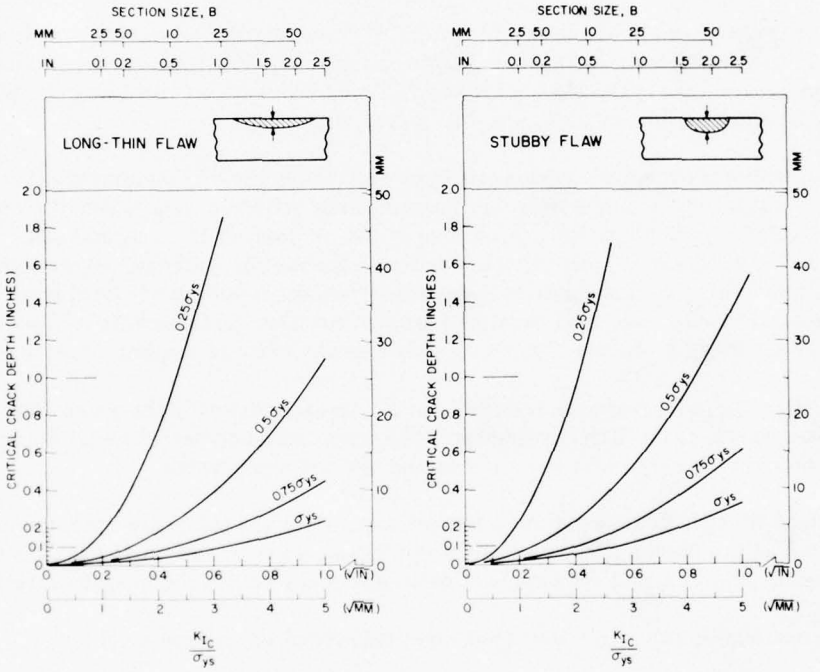

Fig. 38—Relationships of critical crack depth to relative stress and K_{Ic}/σ_{ys} (or K_{Id}/σ_{yd}). *Calculations apply only to the plane-strain state.* Note the limits of ratio measurement for specific sizes B.

not exceeded. That is, the crack should not exceed 0.6 T in depth, the noted fracture stress should not exceed σ_{ys}, and the COD-gage response should be elastic. This procedure is used experimentally, particularly in the aerospace industry. It has not been included in the ASTM standard practices, which are based solely on the use of maximum-constraint edge cracks, because the procedure requires expert knowledge in determining that plane-strain constraint capacities of the surface cracks are not exceeded.

K_c-testing (see Appendix A) extends fracture mechanics principles into the elastic-plastic state. The tests, which have not been standardized, are used mainly for specimens of sheet thickness. The problem is the requirement for defining a sheet width, in relation to the size of a through-thickness crack, that results in a valid K_c value; the required width increases rapidly with increase of K_c. Tests for metal of plate thickness would require the use of very large specimens, equal in size to commercial plate. Obviously, this would not be practical. Thus, other approaches must be used to characterize the elastic-plastic fracture state. The only practical approach is to characterize constraint-relaxation conditions in terms of *unattainable* plane-strain ratio values for the section size, as described below. This is simply a convenient means for continued reference to a standardized scale of known significance.

Constraint relaxation sufficient to cause nominal stresses to exceed yield should develop where

$$B \leqq 1.0(K_{Ic}/\sigma_{ys})^2$$

$$B \leqq 1.0(K_{Id}/\sigma_{yd})^2.$$

This conservative estimate of the "yield criterion" indicates that a section size less than 0.4 (1/2.5) times the minimum size for plane-strain constraint results in exceeding yield stress for fracture extension. This is the *constraint insufficiency* criterion for attaining the plastic fracture state. It is generally considered highly conservative.

To appreciate the meaning of this criterion, the reader should visualize measurement of a K_{Ic}/σ_{ys} ratio value using a specimen of the minimum required size. Then the specimen is reduced in thickness so that the section size is 0.4, or less, of the original size. The yield-criterion degree of constraint insufficiency is then attained. In practice, correlations to other tests of definable constraint are used to determine when the insufficiency level is reached. This is only one of the many roles that must be assumed by other tests because of fundamental or practical restrictions on the use of existing plane-strain fracture mechanics tests.

The direct use of fracture mechanics K_{Ic} or K_{Id} tests for defining the plane-strain limit for given section sizes is prohibitively expensive. The tests cannot be used directly for defining the yield criterion because the ratio values involved are not measurable.

We shall dismiss considerations of other tests that are not fully rational in terms of generalized fracture mechanics theory. At a minimum, any correlation to fracture mechanics tests should be based on test specimens of definable plane-strain constraint capacity.

Two practical engineering tests that meet this requirement are as follows:

•*Dynamic Tear-DT.* The geometric features of this test are the same as those of a side-bend, edge-cracked K_{Ic} or K_{Id} test specimen. Thus, the constraint capacity is definable by the

thickness dimension, as for fracture mechanics test specimens. The NRL-standardarized specimens of 0.6- and 1.0-in. (16 and 25 mm) thickness feature a K_{Ic}/σ_{ys} or K_{Id}/σ_{yd} constraint capacity of ratio 0.5 to 0.6, respectively. However, the DT test may be conducted for any size of interest, and the constraint capacity is definable in all cases.

• *Drop Weight-NDT.* The fixed size of the surface crack used for this test provides an effective K_{Id}/σ_{yd} constraint capacity of approximately 0.5 ratio.

The other engineering test that meets constraint-definability requirements is the Robertson test. The dynamic extension of a crack through a plate of specified thickness provides for definition of K_{Id}/σ_{yd}. For example, a 1.0-in. (25 mm) plate tested by the Robertson technique represents a K_{Id}/σ_{yd} constraint capacity of 0.6 ratio. The general form of the Robertson Crack-Arrest Temperature (CAT) curve is represented by Fig. 31. The lower toe of the CAT curve is the plane-strain (K_{Id}) region, and the elastic-plastic region is the rising part of the curve. In fact, the Robertson test is used specifically to determine the temperature range of elastic-plastic constraint transition for a specified section size. The CAT curve is defined by tracking the fracture-extension stress curve to the yield criterion (YC) point.

In practice, Robertson-type tests are usually conducted at a fixed nominal stress of 0.5 σ_{ys}. Several specimens are tested, over a range of temperatures, until fracture arrest is developed. The temperature of fracture arrest is the 0.5 σ_{ys} CAT. This is equivalent to a 0.5 YC point. The main drawback of the Robertson test is the cost. Low-cost engineering solutions for defining CAT-curve criteria are provided by DWT-NDT and DT tests. The primary criteria include the plane-strain limit L and the 0.5 YC and YC temperatures.

The Charpy V (C_v) test features an arbitrary notch and geometry of undefinable constraint capacity. Any attempt to modify this test to meet fracture mechanics rationality requirements results in a configuration equivalent to that of a small DT test.

Crack-Opening Displacement (COD) tests are basically side-bend-type K_{Ic} tests carried into the elastic-plastic and plastic range. The constraint capacity of a specimen is defined by the section size. The measurement index is the plastic displacement opening of the crack at the point of fracture extension. Other COD procedures involve measurements of lateral contraction at the crack tip.

In effect, a COD curve would follow the course of the dashed line that deviates from the K_{Ic} curve (shown in Fig. 36 for temperature transitions). The procedure has not been extended to include practical measurement for dynamic loading because of experimental difficulties related to dynamic measurement of the COD index. For the case of the strength transition, the COD measurements would follow the course of the curves in the elastic-plastic and plastic regions (Parts 3 and 4) in Fig. 37.

Current research on development of tests for indexing the elastic-plastic and plastic fracture states is aimed at achieving an analytical capability for surface cracks of the type shown in Fig. 38. This is a long-range goal, and such capabilities are not to be expected for at least a decade, if indeed they are feasible. Various types of J-integral tests are competing for use in developing such an index. The principal J-integral approach focuses on the use of a series of K_{Ic}-like specimens with different crack depths. The test procedures are in the very early stages of development.

230-362 O - 77 - 5

To calculate fracture-initiation conditions for surface cracks in the elastic-plastic or plastic range, it is necessary to use an exactly specified fracture property. This is similar to the procedure for plane-strain fracture testing.

The fundamental problem for any analytical approach to surface-crack calculations for elastic-plastic or plastic fracture is the dependence on geometry of these fracture states. Plane-strain fracture toughness is geometry-independent, i.e., K_{Ic} or K_{Id} are not functions of crack geometry. A critical K_I value for fracture initiation has the same meaning for through-thickness cracks as for surface cracks. This is not the case for measurements involving elastic-plastic or plastic fracture.

For elastic-plastic or plastic fracture, the only singular relationship between a crack in a test specimen and one in a structure is provided by a through-thickness crack under the same section-size conditions. The fracture property measured by the test specimen has the same significance in a structure if the mechanical conditions at the crack tip are the same. This exact similarity is provided by maximum-constraint through-thickness cracks.

The fundamental point of J-integral tests is that a measurement can be made by laboratory tests and then be converted analytically to surface crack conditions for fracture states other than plane strain. Approximate calculations could possibly be made for fracture levels moderately beyond plane-strain limits (low elastic-plastic). However, it is difficult to conceive that plastic fracture could be approached by such methods. The fundamental geometry-dependence problem for plastic fracture conditions is that resistance to fracture extension increases with extension (as described in Chapter 11) for all conditions of plastic fracture.

The constraint definitions provided by through-thickness cracks are fully adequate for analytical use in the case of elastic-plastic and plastic fracture. The fact that the elastic-plastic transition results in a sharp increase of the fracture-extension stress for through-thickness cracks satisfies normal engineering requirements for analytical use of fracture test data. The fracture-state level within the range of the elastic-plastic transition must be defined accurately by fracture tests. If it is known, engineering concern for surface cracks is eliminated. In general, the engineer should be concerned with surface cracks only for metals of plane-strain and very low elastic-plastic fracture properties.

CHAPTER 4

Fracture Characterization and Analysis for Steels Exhibiting Temperature Transitions

GENERAL PRINCIPLES

Constraint transitions in low and intermediate strength steels are associated with temperature-induced changes in microfracture ductility. Thus, fracture-state transition criteria must be referenced to the temperature scale. Fracture-state transition temperatures for standard-grade steels cover a wide range.

Specific transition features of a steel must also be referenced to the section size of interest, because of the effects of metallurgical quality and of differences in mechanical constraint.

Engineering use of transition data depends on exact definition of fracture-state properties. Formal fracture-control plans require sequential definition of (a) structural requirements (expressed in terms of a fracture-state criterion); (b) the metal grade selected to meet structural requirements at specified lowest service temperatures for the section size of interest; and (c) purchase specifications that provide a statistical guarantee that the requirements are met.

Such fracture-control plans depend on *standardized fracture tests* for certification that design criteria are met for the lowest service temperature. Characterization procedures must be exact and unambiguous.

The requirements for standardized fracture tests have practical engineering and contractual reasons. An additional requirement is that tests be as inexpensive as possible. In general, this means that relatively small, economical specimens must be used. The test results must be interpretable to the fracture-state transitions for any other section size. Such applicability depends on the rationality of the test with respect to fracture mechanics principles.

The standardized test specimen is cut to specified dimensions from the section size of interest. The characterization of metal quality in terms of the constraint-transition temperature is made in relation to the standardized section size. Since the constraint capacity of the specimen is known, adjustments may then be made to represent the effects of increasing constraint capacity to the limit imposed by the section size used in the structure.

For example, if the section size is that of a 3.0-in. (75 mm) plate, a 0.6- or 1.0-in. (16 or 25 mm) DT specimen (see Chapter 6) may be cut from the plate. The temperature range of the constraint transition for these standardized section sizes serves as the reference to metal quality. The constraint-transition temperature range is then shifted by a specific temperature increment Δt to represent the true transition temperature range for the 3.0-in. (75 mm) thickness.

The reason for general use of 0.6- and 1.0-in. (16 and 25 mm) DT specimens is that these fall into the lower range of the most widely used structural thicknesses. The two specimens have been used extensively to index the true transition-temperature range directly, for section sizes of 0.6 to 1.0 in. (16 to 25 mm). There is a small difference, on the order of 10°F (5°C), between the transition temperatures of these two section sizes. It is difficult to detect, because the test data reproducibility is of the same order, and ordinarily the curves superimpose. Adjustments of thickness effects to represent 2.0- and 3.0-in. (50 and 75 mm) section sizes involve relatively small shifts of the constraint-transition curve to higher temperatures, on the order of 20° to 40°F (10° to 22°C).

Metal of very thick section, say 6 to 12 in. (150 to 300 mm), requires shifts of 80° to 120°F (45° to 65°C). Through-thickness gradients of fracture properties due to metal quality differences may be present.

If it is determined that the through-thickness properties of the thick-section metal are uniform, it is possible to apply simple adjustment procedures over the full range of 1.0 to 12 in. (25 to 300 mm).

The procedure is illustrated in Fig. 39. The figure is based on data from limited sampling of 6- and 12-in. (150 and 300 mm) plates having relatively uniform through-thickness properties. Extensive information is available for 1.0- to 3.0-in. (25 to 75 mm) plates of a wide variety of conventional structural steels. The adjustment procedures are highly reliable, and they may be used with confidence in determining constraint-transition criteria for specific section sizes. They are accurate to ±10°F (±5°C) for the lower range of section sizes. Ordinarily, the true limiting factor in the application of this information is the estimate of lowest service temperature for engineering structures.

Figure 39 also illustrates the use of the constraint-capacity limits L for the section size as the basic reference for temperature-scale adjustment of the constraint transition. The limits are represented by the large circles, referenced to specific section sizes in ascending order of size. These are the critical temperatures at which dynamic plane-strain constraint is lost and constraint relaxation begins. The temperatures of initial rise into the elastic-plastic region are noted for 0.6-, 3.0-, 6.0-, and 12.0-in. (16, 75, 150, and 300 mm) section sizes. Conservative estimates of the yield criterion (YC) temperatures for the various section sizes are given by the midpoints of the DT test energy curves, as noted in the figure.

The family of curves represents a Δt matrix that indexes the mechanical effects of section size. Differences in metal quality shift the entire matrix up or down in temperature; the object of metal characterization is to locate the matrix on the temperature scale. It is important to recognize that the temperature position of the matrix is decided by metal quality.

Since the Δt relationships between matrix curves are fixed, the true temperature location of the matrix may be determined from data on any section size. The specific fracture-state criterion selected for reference is called the "entry point" for the matrix.

The practicality of the entry point selected is important. We may dismiss any entry point that uses large section sizes as impractical for routine engineering characterization purposes. Routine testing using small K_{Id} specimens is prohibitively expensive. Moreover, this procedure cannot produce a distinct entry point, because at temperature below the plane-strain limit for small section sizes the K_{Id} curve is nearly flat, as shown in Fig. 40. K_{Id} values are the same in

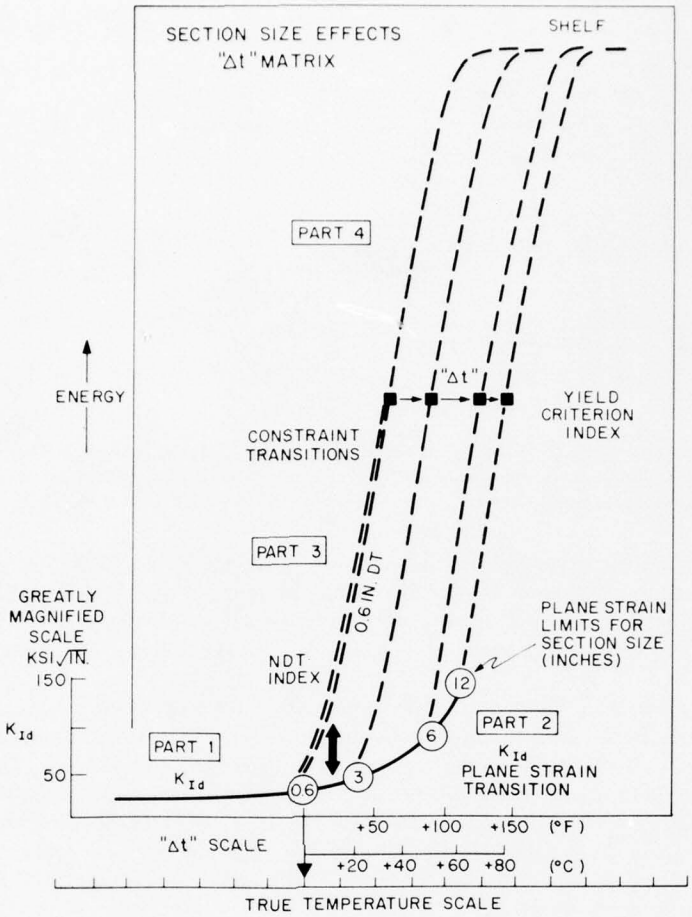

Fig. 39—Section-size effects represented by a family of transition curves with fixed Δt relationships.

the flat region for all conventional structural grades. The curve for one steel is reproduced by all others at this level, and it is impossible to find a characteristic entry point reference on a nearly flat curve. At a minimum, the K_{Id} curve must be followed to the point where it shows a distinct plane-strain transition-temperature rise. K_{Id} specimens for this determination must have section sizes larger than 1.0 in. (25 mm), as noted in Figs. 39 and 40.

The most practical way of locating the reference matrix is to establish the temperature range of the elastic-plastic transition, using a test specimen of small section size. The 0.6- or 1.0-in. (16 or 25 mm) DT specimens have elastic-plastic transition curves that serve this purpose; from their curves, all other elastic-plastic transition curves can be located in the temperature scale by adjusting Δt.

The midpoint of the DT test energy curve for 0.6-in. (16 mm) specimens is a reliable index of the temperature at which YC conditions are attained for this section size. Thus, the YC

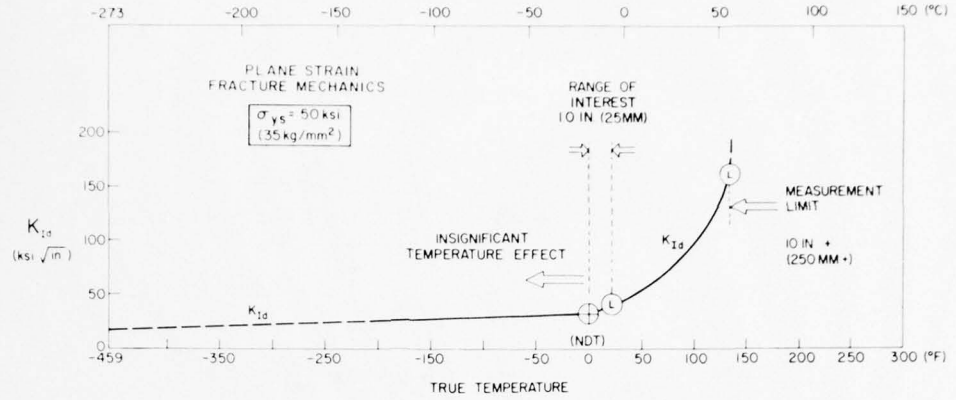

Fig. 40—Temperature range for plane-strain calculations based on K_{Id} transition curve. The range of interest for a 1.0-in. (25 mm) plate is compared to that of a 10-in. (250 mm) plate. The vertical rise at the high end of the K_{Id} curve indicates that increasing section size will not cause further extension of the K_{Id} curve.

point for the first curve of the matrix is the most practical indicator for locating the entire matrix in the temperature scale. The midpoint can be located with ease because of the steepness of elastic-plastic transition curves for conventional steels. Selection of a moderately higher or lower point results in negligible differences in the reference temperature.

The bold arrow of Fig. 39 indicates the temperature interval of vital engineering interest. It represents the critical temperature for the development of the elastic-plastic transition for small section sizes and the plane-strain transition for large section sizes. The two types of transition are related for reasons of mechanical constraint. Both must occur in this temperature region, because here microfracture ductility increases sharply. Metal quality determines the true temperatures of the transitions. At critical temperatures slip systems in the grains are activated, making it very difficult to increase the constraint capacity of the mechanical system and thus suppress ductility.

The specific constraint condition for the NDT temperature depends on the size of the surface crack formed by the brittle weld bead of the Drop Weight Test (DWT). The constraint capacity of the test is defined by the standardized crack size. The DWT develops a sharp transition from "break" to "no-break" within a 10°F (5°C) interval. The no-break condition provides definite evidence of constraint relaxation, i.e., evidence that the constraint-capacity limit of the crack has been exceeded. This is most evident at temperatures 10° to 20°F (5° to 10°C) above the NDT temperature, from the grossly deformed appearance of the crack border.

The no-break condition is first reached at the temperature at which K_{Id} specimens have K_{Id}/σ_{ys} ratios of 0.4 to 0.6. The effective constraint capacity of the DWT is thus verified as limited to approximately 0.5 ratio. The plane-strain transition takes place rapidly above the NDT temperature. Thus, much larger surface cracks would be required for fracture at temperatures significantly higher than the NDT temperature.

The unusual reproducibility of the NDT determination (±10°F; ±5°C) is best understood in terms of an effective constraint capacity, which determines the start of the plane-strain constraint transition. In brief, the NDT temperature pinpoints the rise in the K_{Id} curve. It

provides an excellent reference point for locating the true temperature positions of the matrix curves shown in Fig. 39.

STATISTICAL ASPECTS OF METAL QUALITY

Engineering characterization of a particular grade of structural steel is not accomplished by testing a single plate. Statistical testing must be done to determine the temperature range of metal-quality variance. For example, the NDT temperature may vary statistically from the mean value by ±20°F (±10°C), even in high-quality steels whose properties are rigidly controlled. The variance may be doubled for low-cost metal of open specification.

Statistical testing is generally required to define the high-end-of-the-population temperature for a specified criterion. The statistical reference temperature should be entered in engineering tables for the steel grade and thickness involved.

The most desirable characterization criteria for data bank purposes are those that provide a direct basis for engineering analysis of metal quality. From a scientific point of view, it does not matter whether the criterion cited is NDT, L, 0.5 YC, or YC. Each implies all of the others, and reference temperatures for the others may be defined by fairly simple analyses.

However, examination of data bank information is simplified if the need for analysis is eliminated for most cases of reference. The most significant criterion for general engineering problems is the 0.5 YC level of fracture properties, which is the midpoint of the elastic-plastic transition. Expressed statistically, as the temperature that guarantees fracture-extension resistance at the level of 0.5 σ_{ys}, it provides for direct interpretation in steel selection, as follows:

- It ensures that brittle fracture cannot develop in a structure, regardless of any crack that may be present. Since design stresses are generally based on 0.2 to 0.4 σ_{ys} levels, arrest protection is always present at temperatures above the reference temperature for 0.5 YC.

- It ensures that the steel selected is most economical, by preventing the use of steels with lower transition temperatures than needed. For most structural uses, the 0.5 YC level is sufficient and the YC levels serves no useful purpose.

It does not follow that the organization of data bank information in terms of 0.5 YC requires testing involving only 0.5 YC measurements. For example, a very large amount of NDT information is available for standard-grade steels, due to long and extensive use of the DWT. The NDT data bank can be translated into a 0.5 YC data bank by using the procedures described in this text. Dynamic Tear test data can be indexed directly to 0.5 YC temperatures. Robertson test data are ordinarily reported in terms of 0.5 YC, because this criterion is equivalent to the 0.5 σ_{ys} CAT. A large amount of 0.5 σ_{ys} CAT data have been gathered during the past 20 years in this country and particularly by investigators in Europe and Japan. Unfortunately, the data are scattered among many publications.

LOADING RATE EFFECTS

The engineering importance of dynamic fracture properties is well established for rate-sensitive metals. However, the reasons are often misunderstood. It is not a matter of loading

rate per se, but of microfracture processes. Minute volumes of metals that differ from the bulk of the host metal provide isolated brittle regions for microfracture initiation.

It is not practical to examine directly these isolated fracture initiation conditions; this would require microscopic search. However, their effect is to change macroscopic fracture-initiation conditions from static to dynamic, and dynamic fracture tests thus automatically reveal all unfavorable effects of localized brittle sites.

Dynamic testing is necessary for rate-sensitive steels, because their plane-strain transition curves for static and dynamic loading are displaced considerably along the temperature scale, as shown in Fig. 41. The development of an isolated region of microfracture causes a "jump" from the static to the dynamic curve. The result is a large decrease in plane-strain fracture properties. This is not the case for metals that are not rate-sensitive, and there is no need for dynamic testing of these metals.

A proper interpretation of fracture mechanics principles places all points that confuse technical discussions of rate factors in proper perspective with engineering considerations. The following points are of major engineering importance for structures that are not stress relieved:

- The K_{Ic} values of regions such as those that surround simple arc strikes or welds are not those of the base metal. The hardened material may have very much lower K_{Ic} values—as low as can be measured. Nonmetallic inclusions have similar effects.

- A metal of, say, 1.5 K_{Ic}/σ_{ys} ratio value can be transformed to 0.2 K_{Id}/σ_{yd} ratio value by localized dynamic loading.

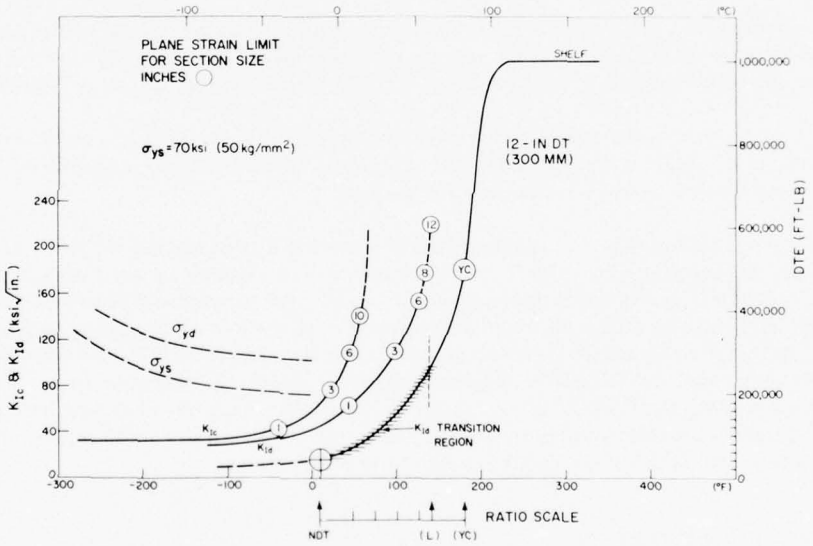

Fig. 41—K_{Ic} and K_{Id} transitions for a thick section size. A series of K_{Ic}-type specimens of increasing size was cut from the thick plate to establish the curves. The DT test was conducted for the full section size. (See Chapter 6 for test details.)

•The crucial loading rate is that of the localized pop-in. The sudden separation of a few metal grains means that dynamic loading rates thereafter control fracture extension. K_{Id} always determines fracture extension, regardless of initiation conditions.

•K_{Ic} values should not be used for statically loaded structures like bridges, ships, and pressure vessels. There is considerable evidence for initiation of catastrophic failure in such structures due to local metallurgical conditions.

•K_{Ic} measurement for the 1940-1945 ship failures would document *static elastic-plastic properties* at the failure temperature. (That is, the K_{Ic} measurement could not be made.) This applies even to ships that failed at the dock or on the ways before launching, due to arc strikes. Many similar situations could be documented for bridges, pressure vessels, and other large structures.

CHARACTERISTIC K_{Id} CURVE

The concept of a characteristic K_{Id} curve has emerged as a fundamental reference for plane-strain properties that may be analyzed in defining L and YC properties of specific section sizes. The fact that the temperature location of the K_{Id} curve may be indexed by the NDT criterion or by DT test criteria leads to practical procedures for metal characterization.

A section of the ASME Code adopted procedures in 1972 for metal characterization and structural integrity analysis based on an engineering version of the characteristic K_{Id} curve. This is a lower bound, conservative definition of the K_{Id} curve, and is cited as the K_{IR} (K_I reference) curve. The DWT test is used to define the NDT temperature and to locate the K_{IR} curve on the absolute temperature scale. The ASME procedures agree with the basic principles of characterization, discussed in regard to Fig. 39. Most important, the use of dynamic fracture properties represents recognition of the points discussed in the preceding section.

The ASME action suggests the potential for future engineering exploitation of the characteristic K_{Id} curve concept in other practical ways. This potential is illustrated by graphical analysis procedures presented in Appendix B.

The general form of the dynamic plane-strain transition of K_{Id} properties is illustrated in Fig. 41. The relationship of the K_{Id} curve to the static, plane-strain transition curve (K_{Ic}) and to the DT-test transition is clearly illustrated. There is a sharp rise in K_{Id} properties, in a temperature range that lies above the K_{Ic} transition. This range corresponds to the start of the DT curve transition for thick sections, at temperatures immediately above the NDT temperature.

The data were gathered by experiments described in Chapter 6. The slope of the K_{Id} curve with temperature from the NDT index point is believed to be characteristic for all low and intermediate strength steels. This feature has been documented by numerous K_{Id} curves, as determined by various laboratories for section sizes to 3.0 in. (75 mm). It is the basis for the K_{IR} approach used in the ASME Code. In comparison to the K_{Id} curve of the figure, the K_{IR} curve has a lower slope.

The characteristic K_{Id} curve used in Appendix B is of the same form and slope as that shown in Fig. 41. Verification of analyses presented in Appendix B confirms that the true form of the curve in Fig. 41 should be used to represent the characteristic curve.

CHAPTER 5

Fracture Characterization and Analysis: Strength-Transition Effects

STRENGTH-SCALE REFERENCE

Fracture-state transitions due to changes in strength level obviously must be referenced to the strength scale, just as temperature-transition effects must be referenced to the temperature scale. Changes in strength or temperature are the basic causes of changes in microfracture mechanisms and ductility.

The characterization practices for fracture testing involving strength- and temperature-induced effects differ from one another only in the sequence of test specimens that must be used to track the effects. The similarities and differences are as follows:

- For temperature-induced transitions, fracture-state transitions are tracked across the pertinent temperature range, using a test specimen of specified mechanical constraint capacity. A series of test specimens, cut from the steel of interest, suffices for this characterization. Only temperature must be varied.

- For strength-jnduced transitions, the fracture-state transitions are tracked across the pertinent strength range, using a specimen of specified constraint capacity. Test specimens are cut from samples of the metal that have been heat-treated to the appropriate range of strength levels.

The fracture research literature generally avoids discussing fracture-state transitions in terms of temperature and strength. The focus is mainly on the effects of changing constraint for a specific metal sample, i.e., on mechanics. However, the most elementary part of fracture-control planning is tradeoff analysis among available metals. Thus we arrive at a most important generalization:

> Metal selection must be based on structurally required fracture-state criteria for particular service temperatures or strength levels. Referring the fracture state of the metal to temperature and strength scales is the only way direct, rational connections can be made to structural requirements.

In brief, engineers must think in terms of fracture state, service temperature, and strength levels. Metal quality also should be indexed to fracture state for specific temperatures or strength levels.

INTRODUCTION TO THE RAD

The connection between fracture state and strength level is provided by the Ratio Analysis Diagram (RAD) procedure, as introduced in Fig. 42 for the case of steels. The temperature scale is replaced by the yield-strength scale, and changes in fracture resistance are plotted against this scale. For example, experience demonstrates that the best available steels follow the highest curve. This is the "technological-limit curve."

The poorest quality steels follow the lower bound curve. Steels of intermediate quality follow intermediate trend-line curves, as illustrated in the figure. The intrinsic fracture quality at any given level of yield strength is determined by the microfracture ductility for that strength level. A most important feature of the plot is that the attainable range of fracture quality narrows drastically as yield strength is increased above 160 ksi (1100 MPa). At strength levels above 230 ksi (1585 MPa), the range is very narrow.

Section size must be considered, because transitions in fracture state are a combined function of microfracture ductility and mechanical constraint capacity. Section-size effects are analyzed by inserting K_{Ic}/σ_{ys} ratio lines that indicate L and YC points for the specified section size.

The analyses of Fig. 42 are for a plate of 1.0-in. (25 mm) thickness. Therefore, the reference ratios for the plane-strain limit L and yield criterion YC are 0.63 and 1.0, respectively. The region between these two ratio lines represents the elastic-plastic fracture state. The intersections of the metal-quality trend lines with the two ratio lines define the yield-strength range of the elastic-plastic transition. Note that the specific yield-strength range is shifted to lower levels with decreases in metal quality.

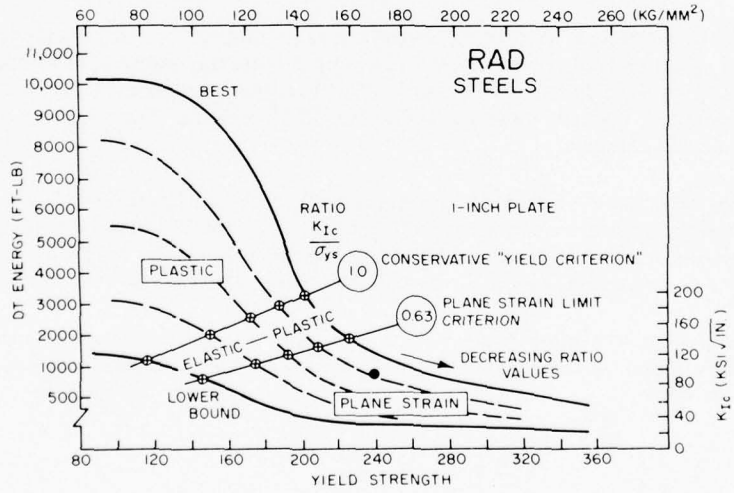

Fig. 42—Ratio analysis diagram (RAD) showing connection between fracture states and yield strength as a function of metal quality. Fracture states for a 1.0-in. (25 mm) section size are indicated by inserting appropriate ratio lines.

The benefits of metallurgical improvements that exceed the ratio limit for the section size

Test experience documents that for steels of the best attainable quality, a 1.0-in. (25 mm) K_{Ic} test specimen will track the K_{Ic} curve to approximately 230 ksi (1585 MPa) yield strength, exactly as noted. The limit of K_{Ic} measurement is reached at this strength level. Since the 1.0-in. (25 mm) K_{Ic} specimen provides insufficient constraint for measurement of higher K_{Ic} values, it develops elastic-plastic fracture in the yield-strength range between 230 and about 200 ksi (1585 to 1379 MPa). The K_{Ic} trend-line relationship to the yield-strength scale may be extended if section size is increased. A 2.5-in. (62 mm) section size permits plane-strain measurements of 1.0 ratio values. The trend line is referenced to the K_{Ic} scale, to the practical limits of this scale.

If the trend-line characteristics (quality level) of the steel are established, it is possible to extrapolate up or down from a fixed point. For example, assume that a steel 1.0 in. (25 mm) thick has been heat treated to 240 ksi (1655 MPa) yield strength. A K_{Ic} test is made, and the value (which may range from 30 to 110 ksi $\sqrt{\text{in.}}$) is determined to be 80 ksi $\sqrt{\text{in.}}$ This indicates a point in the RAD noted by the solid circle. The steel is of high, but not highest, quality. The trend line that applies is that of the dashed curve on which it falls.

The regions between the trend lines may be considered to represent metal-quality corridors. The metallurgical factors that determine whether a steel falls in a high or low corridor are well understood in terms of micromechanical ductility.

The various corridors of the RAD plot in Fig. 42 develop elastic-plastic transitions at yield strengths that are specific to the metallurgical quality. The circled points in the figure indicate the specific yield-strength values at which L and YC fracture properties are attained for the given section size.

The following observations are of major engineering importance:

The yield-strength range of specific L-to-YC transitions is on the order of 30 ksi (206 MPa).

The full range of the transitions (from best to worst quality) is on the order of 100 ksi (690 MPa).

The fracture properties at any specified yield strength in this range are strictly related to metallurgical quality.

It is obvious that selecting steels on the basis of fracture properties requires careful examination of the RAD plots. Strength level, relative metallurgical quality, and section size interact to establish fracture states and levels within states, and their interactions must be analyzed precisely. The RAD methods are unique tools for this kind of analysis. Their precision and reliability have been proven by extensive engineering use.

In addition, RAD procedures are powerful tools for analyzing design-criteria factors. For example, Fig. 43 illustrates the increase in fracture-extension stress that takes place for a through-thickness crack as a consequence of the L-to-YC fracture-state transition. The analysis is characteristic of all L-to-YC transitions, as described previously in general terms (Chapter 3). In this case, the fracture-extension stress is referenced to the true ratio values that lie below the plane-strain limit of Fig. 42. The term "true" signifies that the ratio values may be measured by K_{Ic} tests in the plane-strain region of the RAD.

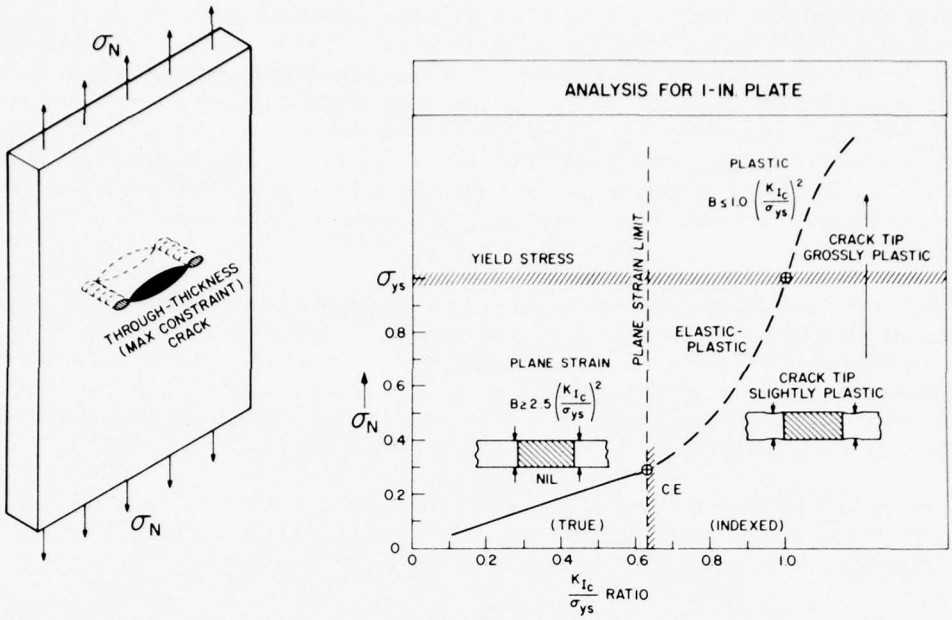

Fig. 43—Engineering significance of the L-to-YC transition. The curve represents fracture stress for a 3T (3.0-in.; 75 mm) through-thickness crack. The solid part is derived from calculations based on the measured K_{Ic} value, to its limit ratio of 0.63 for a 1.0-in. (25 mm) plate. The dashed line connects the limit ratio point to the yield criterion point.

The fracture-extension stress is limited to 0.3 σ_{ys} at the position of the 0.63 ratio line in the RAD plot. Increases of yield strength beyond this ratio line are accompanied by decreases in ratio values. Fracture-extension stress also decreases, to approximately 0.1 σ_{ys} at the highest levels of yield strength noted in the RAD. The plane-strain region of the RAD always corresponds to relatively low values of fracture-extension stress.

The elastic-plastic region, between the 0.63 and 1.0 ratio lines, involves ratios that cannot be measured by K_{Ic} tests of 1.0-in. (25 mm) section size. These ratios are cited in Fig. 43 as being indexed to the trend lines of the RAD. The indexing procedure defines a sharp increase in fracture-extension stress. This is due to constraint relaxation, as plane-strain fracture properties increase beyond the constraint capacity of the section size.

The reference to fracture properties in the elastic-plastic region is to plane-strain values that could be measured by using thicker section sizes. The elastic-plastic transition is a purely mechanical effect due to inadequate section size for retention of plane-strain constraint.

The specific yield-strength range that results in increasing ratio levels beyond the plane-strain limit is significant in the selection of design criteria. The relatively narrow strength range of 30 ksi (206 MPa) determines, among other things, the feasibility of using initiation or arrest criteria. If arrest criteria are desired, exact limits must be placed on the maximum level of yield strength that can be used in design. Since these limits change with metal-quality corridors, data on metallurgical quality is vital.

In preparation for more detailed discussions of RAD methods, it is important to examine the significance of design principles based on initiation or arrest criteria. The initiation principle can provide only provisional protection. It depends on control of crack size and stress level. The arrest principle provides positive protection without control of crack sizes. Use of the arrest principle limits design considerations to the level of nominal stress, which represents the long-range stress field. If the long-range stress field is insufficient to provide for fracture extension, cracks will be arrested and will be merely a nuisance.

In general, 0.3 σ_{ys} design stress is always adequate for fracture extension in the presence of through-thickness cracks if plane-strain conditions apply. This is the danger of using metals with plane-strain fracture properties; the only protection is preventing pop-in or growth of the surface crack. By contrast, when the elastic-plastic state is entered, fracture-extension stress rises rapidly, bringing into action the crack-arrest principle, which is highly reliable compared to the initiation principles. Detailed RAD examinations of design options based on initiation and arrest principles are described in Appendix C.

GENERALIZED RAD PROCEDURES

Engineering analyses of combined mechanical and metallurgical factors may be generalized by grid systems of ratio lines. Figure 44 illustrates a grid system for indexing the plane-strain ratio limits L of various section sizes. A similar grid system may be used to represent YC ratios for the same section sizes.

A grid system that provides a very large amount of analytical information is shown in Fig. 45, where the L and YC ratio lines define the elastic-plastic region. The ratio values are deduced from the plots of Fig. 46. A quick index can be made for the elastic-plastic region of

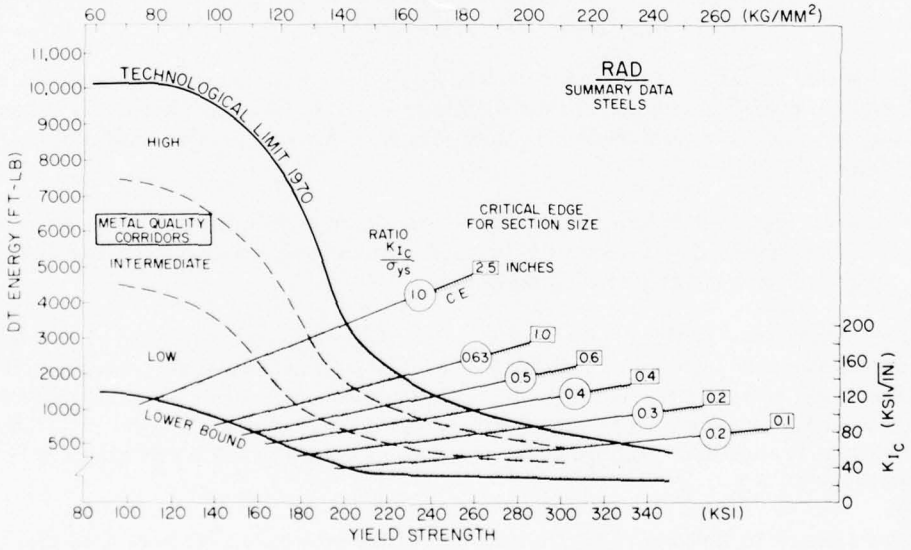

Fig. 44—Ratio-grid system with reference to the plane-strain limits of specific section sizes. Each ratio line represents a "critical edge" of transition to elastic-plastic fracture for the section size.

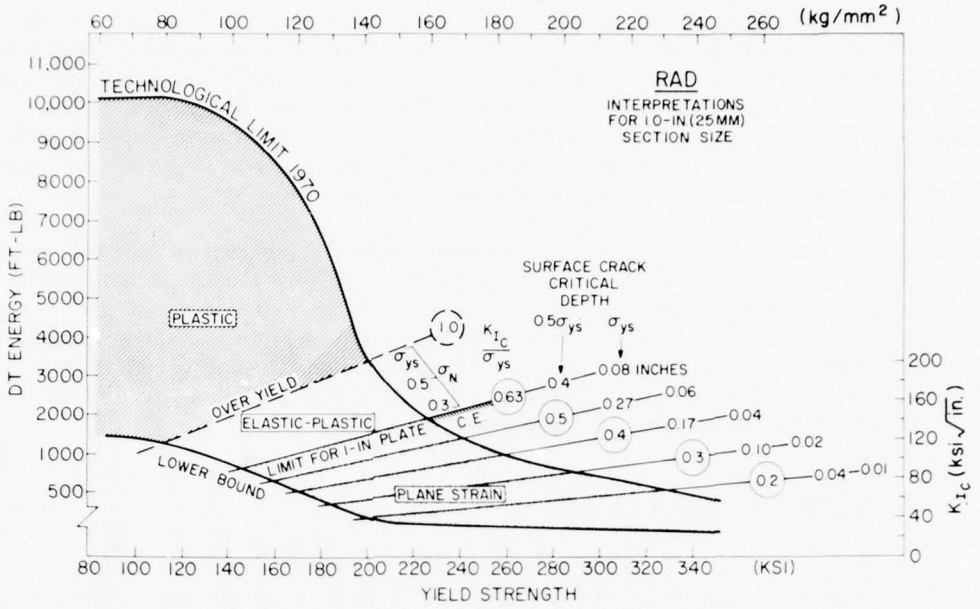

Fig. 45—Expansion of the analytical capabilities of the ratio grid system. The ratio lines for the plane-strain limit and yield criterion are drawn (for 1.0-in. (25 mm) section size) at 0.63 and 1.0, respectively. The increase in fracture stress for a through-thickness crack is indexed to the elastic-plastic region. Critical crack sizes in the plane-strain region are noted.

any section size by using a standard reference chart of ratio lines. The standard chart has a grid of ratio lines drawn in 0.1-ratio steps from 0.1 to 2.0 ratio values. The ratio values from Fig. 46 are traced from the standard chart by interpolation.

The L-and-YC analysis method is used to locate the elastic-plastic region for the section size of Fig. 45. Ratio lines that lie below the plane-strain limit are subsequently traced from the standard chart. The grid system is then complete, although other information may be added for specific purposes.

If desired, metal-quality corridors may be referenced in simplified fashion, as in Fig. 44. The three primary corridors represent high, intermediate, and low quality. Finer distinctions are not required for most engineering purposes.

The significance of the elastic-plastic region is interpreted in terms of the fracture-extension stress scale, inserted as noted in Fig. 45. The scale is deduced from the plot of Fig. 43. It applies to all section sizes and represents the increase in fracture-extension stress for a through-thickness crack with a length of three times the specimen's thickness ($3T$). The index is to 0.3 σ_{ys} at L and 1.0 σ_{ys} at YC, as described previously. The 0.5 σ_{ys} midpoint is found by interpolation.

There should be no concern for the accuracy of the inserted scale. Note from Fig. 45 that the increase from 0.3 to 1.0 σ_{ys} levels of fracture-extension stress must take place in a 30-ksi (206 MPa) yield-strength interval. Because the elastic-plastic transition is so narrow in terms

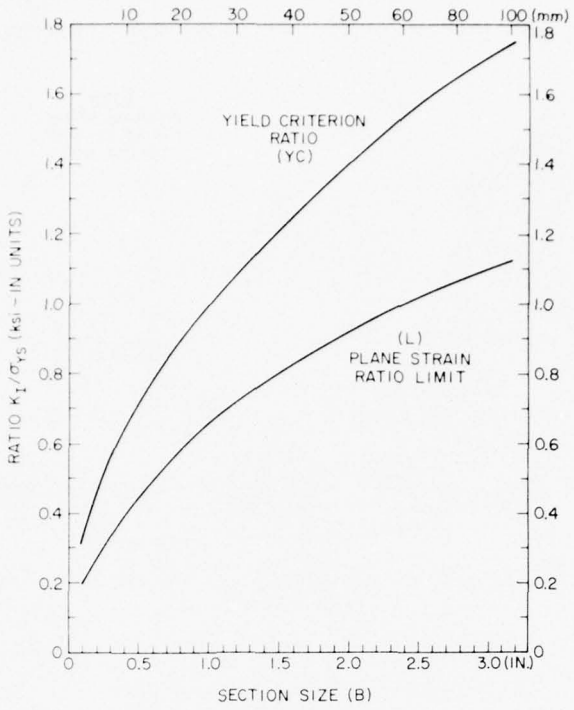

Fig. 46—Relationships of section size and ratio values for L and YC indexing of the elastic-plastic region in the RAD.

of yield strength, the true accuracy depends on the accuracy of statistical definition of yield strength by the tensile test.

The ratio lines in the plane-strain region of Fig. 45 are coded to notations of critical surface-crack depth for two levels of relative stress. The information is taken from the plots of Fig. 38 that apply only to the plane-strain region. The choice of 0.5 and 1.0 σ_{ys} relative stress for the references emphasizes the structural importance of high stress levels. These are the regions of geometric transition that decide the critical crack sizes of concern in engineering analyses based on initiation-control principles. Note that there is a sharp decrease in critical crack size with decreasing ratio value (increasing strength).

Specific RAD analyses are presented for section sizes of 0.5 and 2.5 in. (12.5 and 62 mm) in Figs. 47 and 48. These figures indicate the effects of decreasing and increasing section size. Comparing Figs. 47, 45, and 48 will illustrate section-size effects in ascending order of section size.

The main points made evident by examination of the RAD plots for increasing section sizes are as follows:

The elastic-plastic transition shifts to lower levels of yield strength.
The plane-strain region enlarges.

230-362 O - 77 - 6

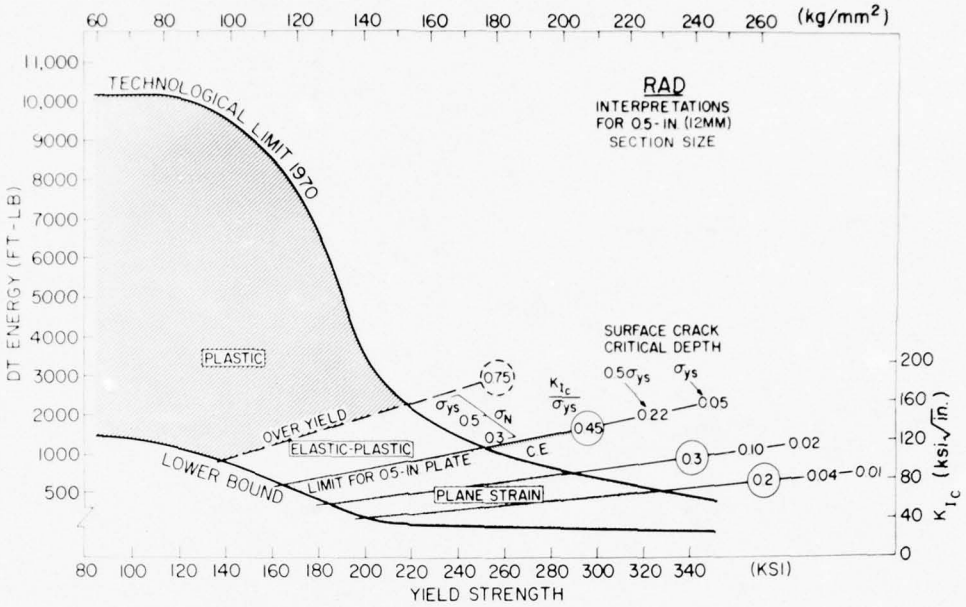

Fig. 47—Ratio analysis diagram (RAD) for 0.5-in. (12 mm) section size.

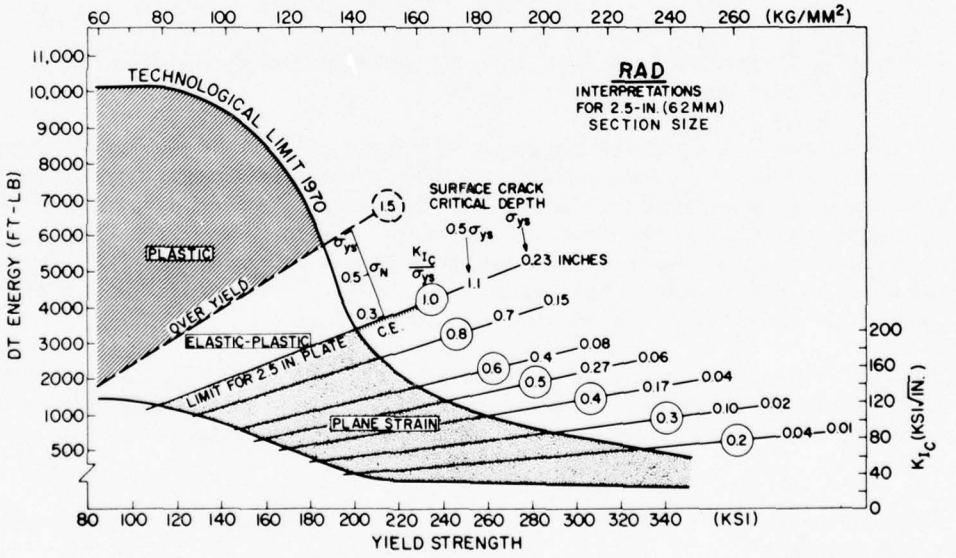

Fig. 48—Ratio analysis diagram (RAD) for 2.5-in. (62 mm) section size.

The plastic fracture region decreases in size.
The fracture-extension stress significance of the elastic-plastic transition is invariant.
The increase in critical crack sizes for 0.5 σ_{ys} stress levels is appreciable.
The increase in critical crack sizes for stresses close to yield levels is insignificant.

These mechanical effects may be analyzed in terms of metallurgical quality by examining the upper and lower bound trend lines. It is evident that the effects of decreased yield strength are very gradual and minimal for the lower bound trend line. For the technological-limit trend line they are relatively pronounced. Apparent for all section sizes are the effects of metallurgical cleanliness on the attainment of desirable fracture states to maximum yield-strength levels.

COMBINED K_{Ic} AND DT SCALES

The basis for plotting fracture properties in the RAD by dual reference to DT and K_{Ic} test scales is found in constraint. For example, a 1.0-in. (25 mm) DT test specimen and a K_{Ic} test specimen of the same section size have the same constraint capacity. The same section size and maximum-constraint crack are used; therefore, the same mechanical constraint is applied. In the RAD region below the 0.63 ratio line, the 1.0-in. (25 mm) DT specimen fractures in plane strain. In the region above the 0.63 ratio line, the fracture is of mixed-mode and then of full-slant type. The energy-to-fracture reading is a faithful reflection of the degree of constraint relaxation above the plane-strain limit for metal of 1.0-in. (25 mm) section size.

Correlations have been made between DT energy values and K_{Ic} test data; they document that an entry point from the DT energy scale predicts the K_{Ic} value (measured by valid ASTM procedures) within ± 15 ksi $\sqrt{\text{in.}}$ In fact, these correlations have been extended for specimens 2.0 to 3.0 in. (50 to 75 mm) thick. Thus, it is possible to index K_{Ic} values that would require the use of K_{Ic} specimens more than 1.0 in. (25 mm) thick.

The fracture energy of 1.0-in. (25 mm) DT specimens, cut from 2.5- to 3.0-in. (62 to 75 mm) or thicker plates, can provide for plane-strain fracture-toughness indexing for these section sizes. This reflects the fact that the degree of constraint relaxation (mixed-mode fracture) for the 1.0-in. (25 mm) section size is directly related to the constraint level of the thicker section. If the constraint level of the thicker section results in plane-strain fracture (for which K_{Ic} can be measured), then the degree of constraint relaxation for the 1.0-in. (25 mm) section size is determined by the closeness to which K_{Ic} approaches the limiting K_{Ic}/σ_{ys} ratio for the thick section. For example,

1. If the K_{Ic} value for the thick section is below 0.63 ratio, the 1.0-in. (25 mm) DT test will provide enough constraint for plane-strain fracture.

2. If the K_{Ic} value is close to the ratio limit for the thick section, the 1.0-in. (25 mm) DT test will develop mixed-mode fracture to a degree that depends on the difference in constraint between the two section sizes.

3. If the K_{Ic} value of the thick section is slightly above 0.63 ratio, the 1.0-in. (25 mm) DT test will show a small degree of mixed-mode fracture.

These various degrees of mixed-mode fracture in the 1.0-in. (25 mm) DT test will be reflected in the energy reading. Thus, the fracture energy is directly related to the K_{Ic}/σ_{ys} ratio that could be measured for section sizes that provide the necessary level of plane-strain constraint. Briefly, a specific intrinsic increase in metal ductility results in an increased K_{Ic}/σ_{ys} ratio (if constraint is adequate) or increased mixed-mode fracture energy (if constraint is inadequate). The two effects are relatable and rationalizable in fracture mechanics terms.

METALLURGICAL BASIS OF QUALITY CORRIDORS

The metal-quality corridors represent trend bands for fracture-property relationships to the yield-strength scale. The trend bands may be of high, intermediate, or low corridor type, depending on the "cleanliness" of the metal. "Cleanliness" refers to the density of nonmetallic particles such as oxides, sulphides, and carbides. These nonmetallic particles are brittle or noncoherent in comparison to the metal grain structure. They thus can undergo early cracking or separation from the surrounding metal grains in the process of crack-tip deformation. The microcracks or grain-boundary separations then can join to cause plastic-zone rupture. In effect, the deformation capacity of the grain aggregate is decreased by these particles. Cleanliness effects are important throughout the yield-strength range. However, increasing yield strength increases the severity of the effect.

Yield strength is increased by locking the slip systems of metal grains to increase the resistance of grain aggregates to plastic flow. The locking is accomplished by ultrafine dispersions of hard particles such as carbides. The price for increased resistance to plastic flow, however, is an unavoidable decrease in tensile ductility. This is accentuated in crack-tip plastic zones by elevation of plastic-flow stresses due to triaxial stresses (Chapter 3).

These phenomena dictate the decrease in fracture resistance with increased yield strength for ultraclean metals. Metallurgically dirty metals have lower fracture resistance at any yield strength than clean metals, the amount of difference depending on the number and type of brittle or noncoherent particles.

Increasing yield strength accentuates the steepness of the trend-band relation to yield strength, because of (a) decreased ductility of the host matrix and (b) premature microcracking due to foreign phases. Accordingly, increasing the density of nonmetallic particles shifts fracture-state transitions to lower yield-strength levels.

These phases, or foreign particles, that promote void-site nucleation in steels have the following two main sources.

Extrinsic nonmetallic particles are foreign bodies that may be traced to melting and deoxidation practices.

Intrinsic nonmetallic particles result from the formation of carbide phases during solidification, particularly in steels of high carbon content.

The improved steels developed during the past decade provide a basis for understanding the effects of deoxidation practices. These steels have intermediate or low carbon contents, to

promote weldability. Hardenability and strength are controlled by use of alloy elements; the high carbon contents of older steels are avoided. For these reasons the problems of intrinsic carbide phases have been eliminated.

These steels have the potential of attaining the highest corridor positions if the introduction of other nonmetallic phases can be avoided. Figure 49 is a summary of data for modern steels, melted according to various practices, as follows:

Conventional air-melt. Limited slag treatment results in relatively high phosphorus and sulfur contents (>0.015%). On solidification, phosphide and sulphide phases are formed. The addition of aluminum or other deoxidation agents produces Al_2O_3 or other nonmetallic phases. Thus, the void-site density is high.

Special slag, plus vacuum-arc remelting. Multiple slag melting practices are used to lower phosphorus and sulfur levels. Vacuum-arc remelting lowers oxygen content, eliminating the need for the deoxidation treatments cited above. Void-site density is decreased to intermediate levels.

Vacuum-induction melting, plus vacuum-arc remelting. Melting generally starts with an air-melt charge of special low-phosphorus and low-sulfur iron. Three or more slags may be used to lower phosphorus and sulfur levels. Alloy additions are made under vacuum, and the oxygen content is controlled by carbon deoxidation. The metal for the final vacuum-arc remelt is of very high purity. If properly processed, these steels are very clean, even when examined at high magnification.

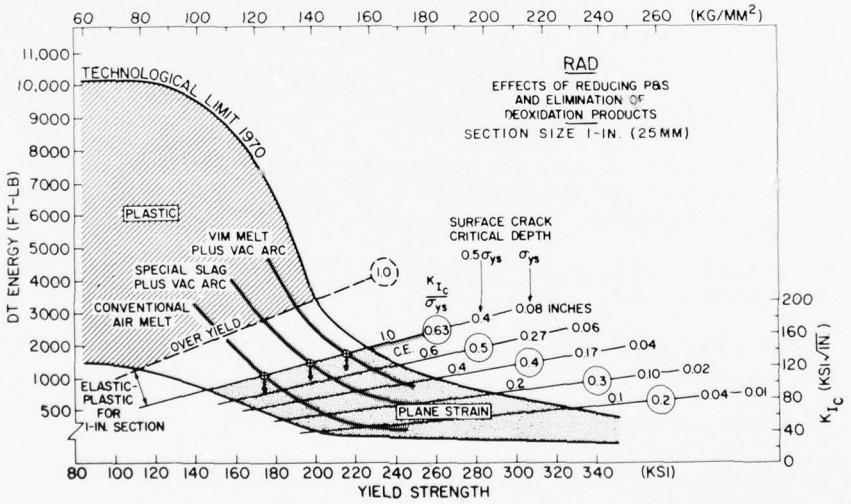

Fig. 49—Trend bands illustrating the effects of relative metallurgical cleanliness due to furnace-melting and deoxidation practices. The RAD indicates the significance of the metallurgical improvements.

Figure 49 is a plot of the trend-band properties of these steels. In fact, the top of the band represents the ceiling level attained by optimizing heat treatments to produce the maximum fracture properties for the given strength level. These data disclose that the ceiling level is built into the metal by the melting and deoxidation procedures. The relative cleanliness of the metal in the ingot determines the ceiling.

This is most important. It signifies that a small section of an ingot may be forged and evaluated as to corridor quality. Since a large ingot may cost $1.00 and a large forging $10 to $20 per pound, rejection of undesirable material at the ingot stage is economical.

The tremendous effects of metal quality on the fracture resistance of steels in the 180- to 220-ksi (1241 to 1517 MPa) yield-strength range is made clear by Fig. 49. For example, at 200-ksi (1379 MPa) yield strength, a 1.0-in (25 mm) plate may be of:

Elastic-plastic properties (if of high cleanliness),
Plane-strain limit (L) properties (if of intermediate cleanliness), or
Very low, 0.3 ratio, plane-strain properties (if of conventional cleanliness).
The correlative effects on critical flaw sizes are enormous, as indicated by RAD indexing.

The reader may analyze the larger range of effects for the 180-ksi (1241 MPa) level of yield strength. At this level, a 1.0-in. (25 mm) plate may vary among plastic, elastic-plastic, and low plane-strain ratio values, according to corridor quality.

In general, the older types of forging steels feature high carbon content coupled with strong carbide-forming alloy elements. The carbide particles that form during solidification are difficult to place back in solution during high-temperature heat treatment; they remain, to enforce low ceiling properties. Therefore, vacuum melting and other modern improvements in deoxidation practices cannot be expected to raise the metal quality to the higher corridor level.

STATISTICAL VARIANCE OF PROPERTIES

When a steel is purchased to a specified minimum value of yield strength, a range of yield strength and fracture properties will actually be present in the production lot or lots. The range of variation depends on the specification controls that are applied:

O—*Ordinary* metallurgical control, based on specification of composition and heat treatment, permits a wide range.

T—*Test* control, aimed at narrowing the property range by rejection, narrows the range to feasible limits, relatable to cost.

TL—*Test-limit* control is established by test reproducibility.

For example, yield-strength values for steels of over 170-ksi (1172 MPa) level may have the following ranges:

O—20 to 30 ksi (138 to 206 MPa)
T—10 ksi (68 MPa)
TL—5 ksi (34 MPa).

In the discussions to follow we shall consider ordinary O limits. The reader may analyze the effects on the statistical variances of reducing the range to T or TL limits. For guidance it may be cited that K_{Ic} test variations, in ASTM round-robin tests by different laboratories, were determined to be on the order of ±10%. This range is representative of the TL limits for K_{Ic} control.

Figure 50 presents a typical O-variance statistical box for forging-grade steel procured to minimum yield-strength specifications of 200 ksi (1379 MPa), with one of the following additional conditions:

Air-melt practices are used for the new steels.

The carbon content of the older steels is high enough to result in persistent alloy-carbide phases.

Either of these conditions results in the presence of nonmetallic phases that promote early void initiation during crack-tip plastic-zone growth. Thus, plane-strain fracture properties will be limited to low values. In effect, a low corridor ceiling is imposed on the metal.

The O-variance box illustrated in Fig. 50 may be shifted to below K_{Ic} ceiling levels for the corridor by off-optimum heat treatment, as indicated by the lower of the two superimposed boxes. A smaller box may be achieved by using T procedures to the TL limits. For example, the boxes shown may be decreased in size to about half the noted yield-strength and K_{Ic}-scale dimensions (see Fig. 53). It is impossible to decrease the box further. The important point is that the O-variance box provides the starting point for analyses of statistical variance.

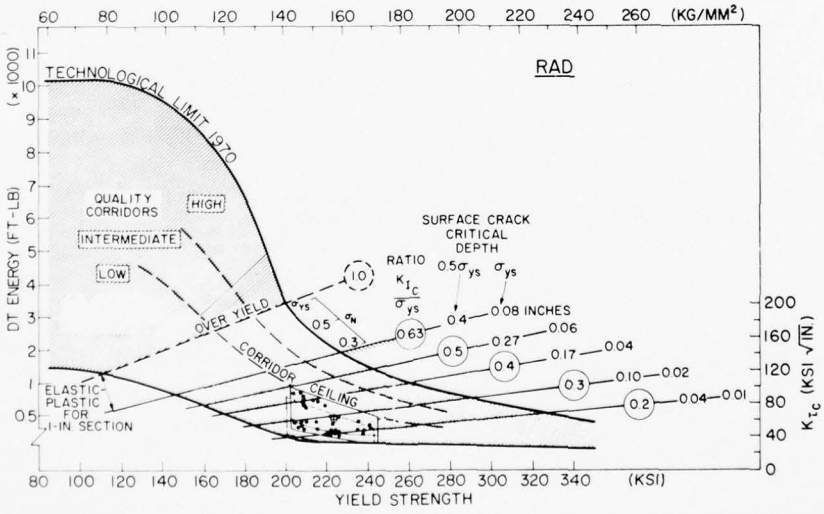

Fig. 50—Statistical-box estimate for a low corridor-quality steel, purchased to minimum yield strength specifications of 200 ksi (1379 MPa).

The statistical box indicates that design and purchase considerations must include appropriate lower bound values for K_{Ic}. This is a function of yield strength as well as of the narrowness of the yield-strength range. If the lower bound is placed at a relatively high K_{Ic} level for the population, a large fraction of the metal, as produced, will be eliminated.

We shall now examine the statistical population question in a broader context. Figure 51 illustrates the statistical boxes expected of metals purchased at various levels of minimum yield strength and metal quality. We estimate an O-variance yield-strength range of 25 to 30 ksi (172 to 206 MPa) above the specification minimum (the base of the box) and a K_{Ic}-ratio variance of two ratio lines (the height of the box). The latter is a conservative estimate. The circled crosses indicate mean expected values for yield strength and K_{Ic}.

Assume that any one of these boxes represents a design decision to procure steel at a specified minimum level of yield strength, say 200 ksi (1379 MPa). The following consequences emerge:

1. The high end of the yield-strength range of the population is 220 and 230 ksi (1517 to 1586 MPa).

2. The lower bound K_{Ic} value is defined by the lower corner of the boxes (shaded semicircles) for each of the three corridor levels.

3. The K_{Ic} design value must be the lower bound K_{Ic} value. The specific value is characteristic of the corridor quality.

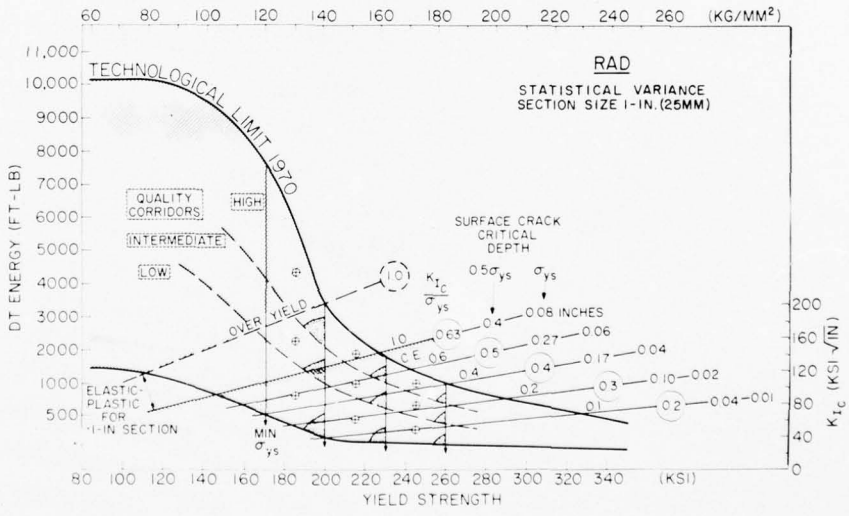

Fig. 51—Statistical-box estimates for steels purchased to four levels of minimum yield strength and three levels of melt quality. Crossed points indicate average expected properties. Dotted corner regions indicate minimum fracture properties, which can be specified or used in design.

4. The K_{Ic} value that would be acceptable to a steel producer for purchase specifications is likewise the specific lower bound value for the box.

It should be noted that with decreasing yield strength there is little increase in lower values for the low-corridor steels unless levels of less than 180 ksi (1241 MPa) are specified as minimun values. On the other hand, a rapid increase of the lower bound K_{Ic} value is caused by decreasing the yield-strength minimum below 230 ksi (1586 MPa) for high-quality, clean steels. Decreasing the yield-strength range by test control does not change these conclusions.

The increases become most significant when the lower bound K_{Ic} value approaches the ratio measurement limit for the section size. However, this means that steels featuring a lower bound K_{Ic} close to limiting ratio values may be used (and purchased) only if most of the population has fracture-resistance properties such that K_{Ic} measurements are not possible. This is the case if the plate section sizes are used as such in the structure. If considerable machining is done, ratio values in excess of the final section-size limits may be specified and measured. However, the fracture characteristics of the thinned sections may then be of the elastic-plastic type.

These analyses of metallurgical variance pose practical questions that emphasize the value of close control of metal quality and heat-treatment procedures. If the O-variance metallurgical control limits are not adequate, it is necessary to resort to metal rejection.

Regardless of whether metal is rejected before or after purchase, the cost of rejection must be assumed by the user. These analyses indicate that close to 50% rejection is necessary if K_{Ic} values equal to or exceeding the circles-cross mean points in Fig. 51 are established as purchase criteria. Decreasing the size of the statistical box only results in shifting the mean point; on a relative basis, the rejection statistics will continue to apply.

It should be noted that decreasing K_{Ic} requirements to 20 ksi $\sqrt{\text{in.}}$ below the mean points will reduce rejection rates by as much as 20%. However, the effects of such reductions on critical crack sizes, and therefore inspection costs, must be considered. In general, the related decrease in critical crack depths for regions of high stress is minor. In other words, relatively little is lost. This conclusion may appear appealing, but the small differences are really due to the fact that critical flaws are exceedingly small if stress levels are high. Little is lost because there is little to lose.

The analyses for regions of low stress are entirely different. Decreases of 20 ksi $\sqrt{\text{in.}}$ in these cases may be highly significant. Related decreases in critical crack depth may be very large or exceedingly minute, depending on ratio levels. A 0.1 ratio drop from 0.6 to 0.5 has a meaning completely different from a drop from 0.3 to 0.2. RAD coding to critical crack sizes clearly indicates this.

These analyses also disclose the benefits of shifting from low-corridor metals to clean metals of the highest corridor levels. Again, the benefits of such increases in K_{Ic} values are not particularly appealing. The reasons are basic to calculations of critical crack sizes for plane-strain metals.

The benefits of metallurgical improvements that exceed the ratio limit for the section size can be analyzed in terms of the elastic-plastic regime. The structural significance of entering and then exceeding this regime is best understood by reference to the stress level required for extension of a through-thickness crack, as discussed previously.

The metallurgical improvement necessary for crossing through the elastic-plastic regime pays high dividends by rapidly raising the nominal stress required for extension of through-thickness cracks. Moreover, the high costs of attempts to locate minute flaws, which are critical for high-stress regions, are eliminated. Modest increases in metal costs in this way can decrease costs and increase safety.

The kinds of tradeoff analyses that may be made between yield strength and metal corridor levels are indicated by the metallurgically zoned RAD in Fig. 52. The options that may be examined are indicated by the solid black squares and arrows. The design-strategy plotting-board uses of the RAD are thus indicated. The analyses can be performed in a few minutes, once the RAD is understood.

Figure 53 compares the location of the statistical box for the low-corridor steels of Fig. 50 with those for a series of new, premium steels of high-corridor features. The series is made up of steels with alloy contents varied to provide increasing levels of strength. The steels are strength-limited by the basic alloy formulation, i.e., they are specifically designed for the strength range indicated. In general, formulations that span a very broad range of strength levels are impossible because of microstructural conditions.

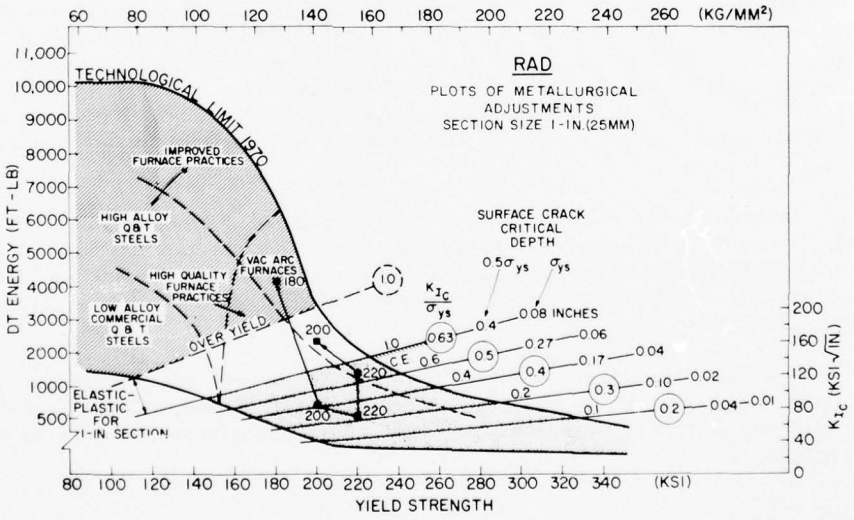

Fig. 52—One form of detailed metallurgical zoning of the RAD. Finer zoning, of primary interest to metallurgists, can be evolved. Trade-offs that may be made in design are indicated by the arrows.

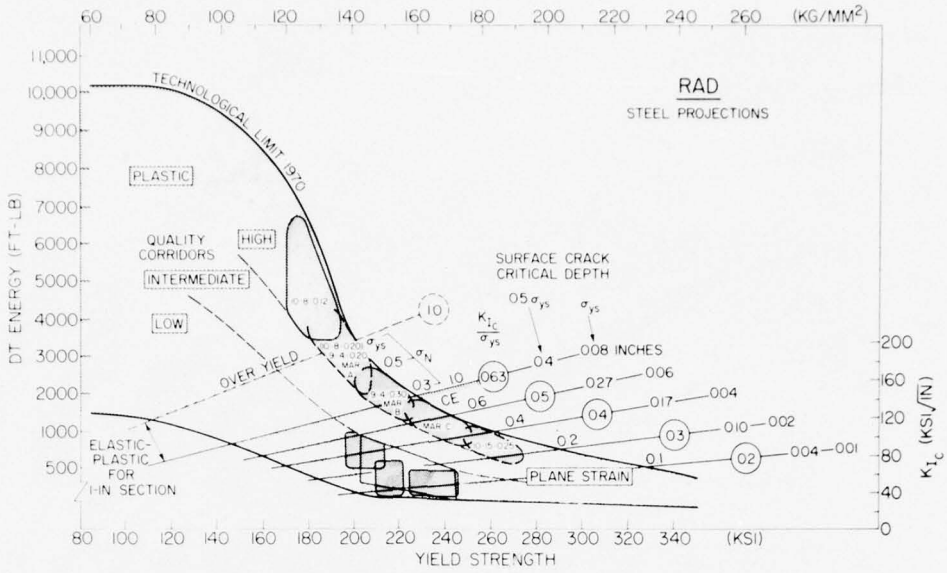

Fig. 53—RAD zoning for new, premium quality, high strength steel. The statistical-box for a low corridor-quality steel (as shown in Fig. 50) is inserted for comparison.

The mechanical-state analyses in Fig. 53 are specific to a 1.0-in. (25 mm) section size. However, the noted K_{Ic} scale-referenced properties for these steels are attainable in section sizes from 0.5 to 3.0 in. (12.5 to 75 mm). Specific types may be alloy-adjusted to provide the same properties for greater thicknesses.

TITANIUM AND ALUMINUM ALLOYS

Ratio analysis diagram summaries for commercial titanium and aluminum alloys are presented in Figs. 54 and 55. The significance of the ratio lines is the same as for steels, because fracture mechanics definitions of fracture properties do not depend on metal type. The metallurgical transitions from high to low fracture resistance are (as for steels) strength-related and may be modified considerably by metal quality.

The main metal-quality factor for titanium alloys is oxygen content, because these metals are ordinarily very clean due to vacuum-arc melting. The metallurgical problem is to avoid the embrittling effects of oxygen. The use of oxygen in small amounts to promote strengthening in the 120- to 140-ksi (827 to 965 MPa) yield-strength range is catastrophic to fracture resistance. The zones in Fig. 54 illustrate the expected fracture properties of titanium alloys produced to conventional commercial-purity oxygen levels, as compared to low-oxygen (less than 0.10%) alloys of slightly lower yield strength.

Special note should be taken of the combined effects of low-oxygen metal and decreases of 10 ksi (68 MPa) in minimum yield strength, from 125 to 115 ksi (861 to 792 MPa). Figure 54 illustrates that section sizes of 1.0 in (25 mm) undergo transitions from plane-strain to elastic-plastic or plastic fracture properties as the result of this combination.

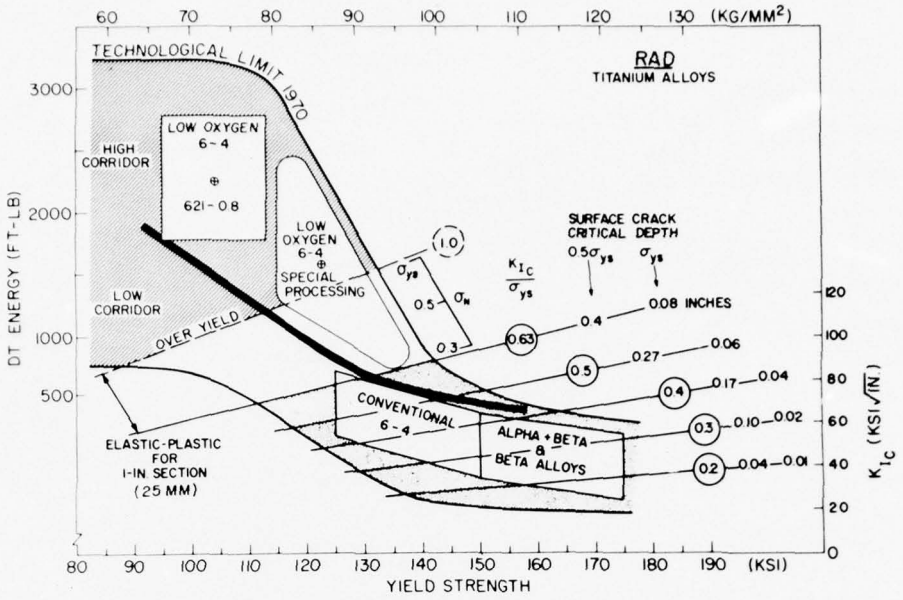

Fig. 54—RAD for titanium alloys; 1.0-in. (25 mm) section size.

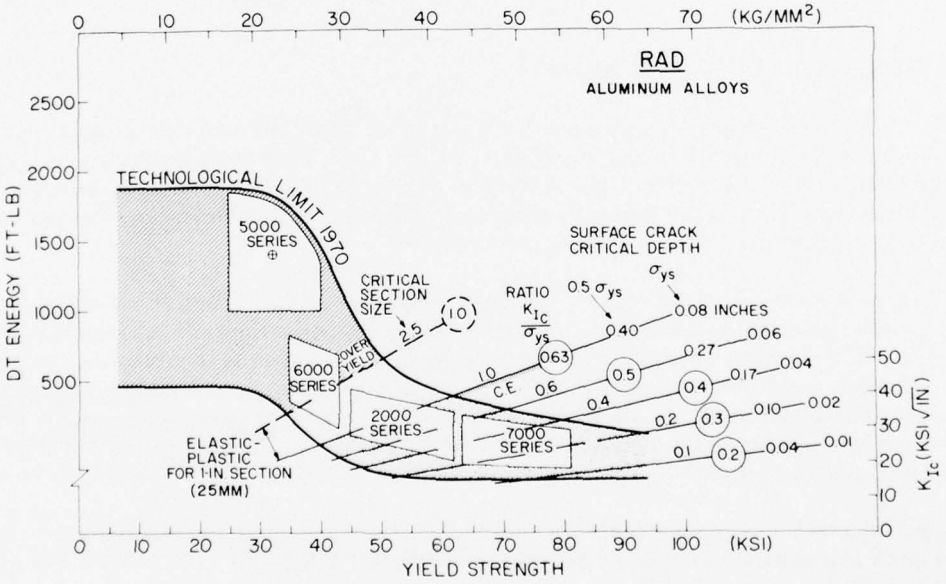

Fig. 55—RAD for aluminum alloys; 1.0-in. (25 mm) section size.

The dashed line in Fig. 54 represents the boundary between conventional and low-oxygen metal. The span between the dashed line and the technological limit represents improvements made between 1967 and 1970. There are sound metallurgical reasons for believing that additional improvements may be made by controlling texture and microstructure. Heat treatment and metal processing are particularly important for titanium alloys and have been only partly explored.

The RAD for aluminum alloys is presented in Fig. 55. The decrease in fracture resistance with increased yield strength is again evident. Aluminum alloys are metallurgically dirty and contain vast amounts of brittle intermetallic compounds that serve as sites for microcracking and void initiation. Because of this, *the true potential of aluminum alloys has not been* disclosed. Research in producing relatively clean metal should yield marked improvements. This is particularly true for the strength-transition range from 45- to 65-ksi (310 to 448 MPa) yield strength.

CRITICAL-EDGE CONCEPT

The foregoing discussions and analyses, based on the RAD system, lead to several important conclusions:

If the deciding factor in metal selection is the critical crack size for regions of high stress concentrations (K_t of 2.5 or greater), then plane-strain properties are undesirable because critical crack sizes will be below reliable inspection limits if the ratio value is 1.0 or less.

Metallurgical improvements that simply increase the measurable K_{Ic} value for a given section size provide small benefits in the above-cited case.

To achieve large returns from metallurgical improvement requires raising the intrinsic fracture resistance to above the plane-strain limit. *This is the critical-edge concept of transi*tion from plane-strain to elastic-plastic fracture properties.

The critical-edge concept provides important guidance to metallurgical research. It states that highly significant improvement in metal properties may be made in the strength-transition region. This is the region of rapid falloff of the RAD plot for each metal system. The improvement must be related to specific section sizes. Thus, the improvement possibilities are limited to lower yield-strength ranges for thick-section metal. With decreases in section size, higher yield-strength ranges provide the improvement challenge.

STANDARD RAD FORMAT

The foregoing discussions of RAD procedures indicate the wide variety of analyses and data-management methods made possible by the ratio-grid reference system. A standardized format for plotting and zoning mechanical and metallurgical conditions has been developed for use in structural integrity (SI) analyses.

The starting point for the SI format is the three-part zoning of the critical crack-size chart in Fig. 56. *The low-ratio zone indicates that critical crack sizes become exceedingly small, for* all stress levels, as the ratio decreases below 0.3 reference point. It is apparent that such

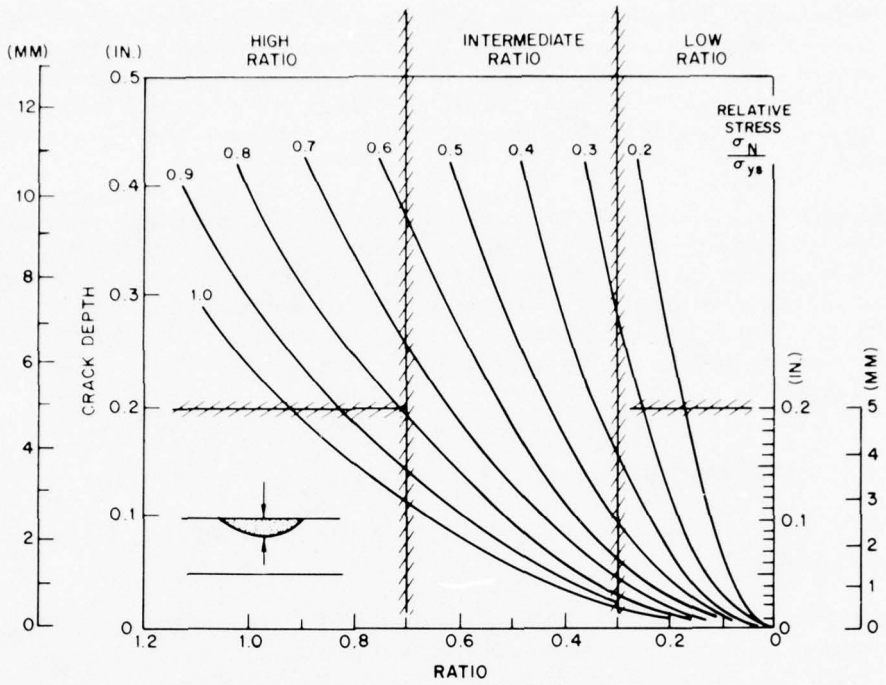

Fig. 56—Three-part zoning of critical crack-size diagram.

low-ratio metals do not provide reasonable latitude for detection or control of crack states. Accordingly, SI analyses must be highly pessimistic.

The high-ratio zone provides more latitude, depending on the stress level. Structural integrity analyses must be made case by case to determine whether other engineering considerations permit the required controls.

The intermediate-ratio zone should be analyzed in terms of high and low stress levels. For high stresses, the engineering problem becomes similar to that of the low-ratio zone; for low stresses it is similar to that of the high-ratio zone. Careful SI analyses must be made on a case basis to determine the feasibility of the required controls.

Ratio reference to the three zones, then, provides an immediate first-order analysis of the problem in using plane-strain metals. The three-zone system avoids the complication of referencing ratio lines to critical crack sizes (as presented in the introductory descriptions of RAD procedures).

Simplified three-part zoning of the RAD, in terms of low-, intermediate-, and high-ratio zones, is illustrated in Fig. 57. This is the standard format for SI analysis. The DT scale entry may be made to accommodate large (1.0-in.; 25 mm) or standard (0.6 in.; 16 mm) DT test specimens.

In using the SI RAD format, it is essential to place the ratio lines defining the elastic-plastic region for the particular section size. The appropriate ratio lines for L and YC boundaries can be found from Fig. 46.

Figures 58, 59, and 60 are SI diagrams of the elastic-plastic and plane-strain regions for 2.0-in., 1.0-in., and 0.5-in. (50 mm, 25 mm, and 12 mm) specimens, respectively. Note that a decrease in section size lowers the ratio range for the elastic-plastic region. Accordingly, the remaining plane-strain region is restricted to intermediate and very low ratio values by the zoning system of Fig. 56.

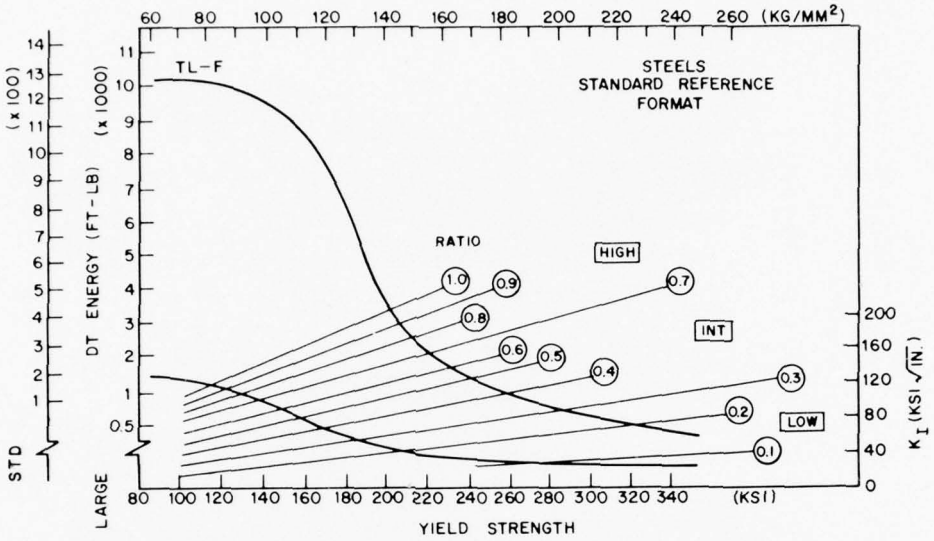

Fig. 57—Three-part zoning as applied to the RAD.

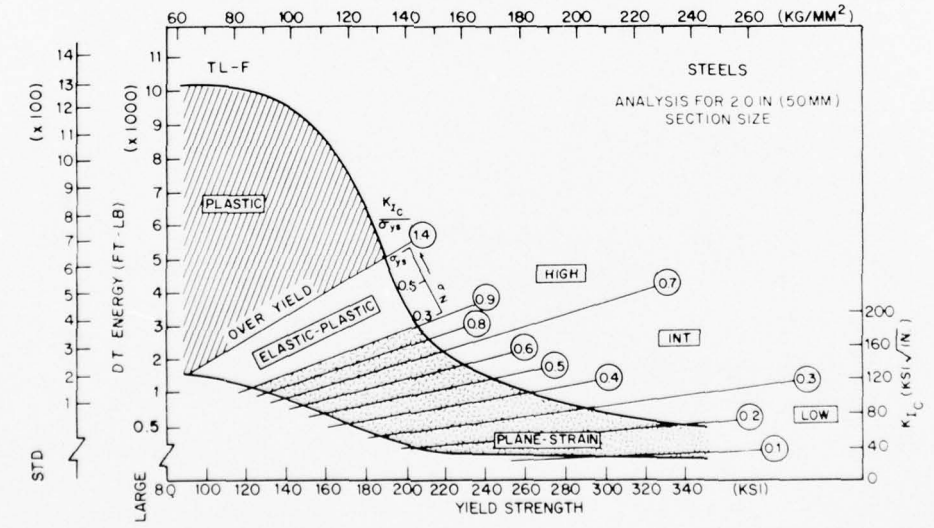

Fig. 58—Three-part zoning combined with fracture state analysis for 2-in. (50 mm) section size. Note range of ratio levels in plane-strain region.

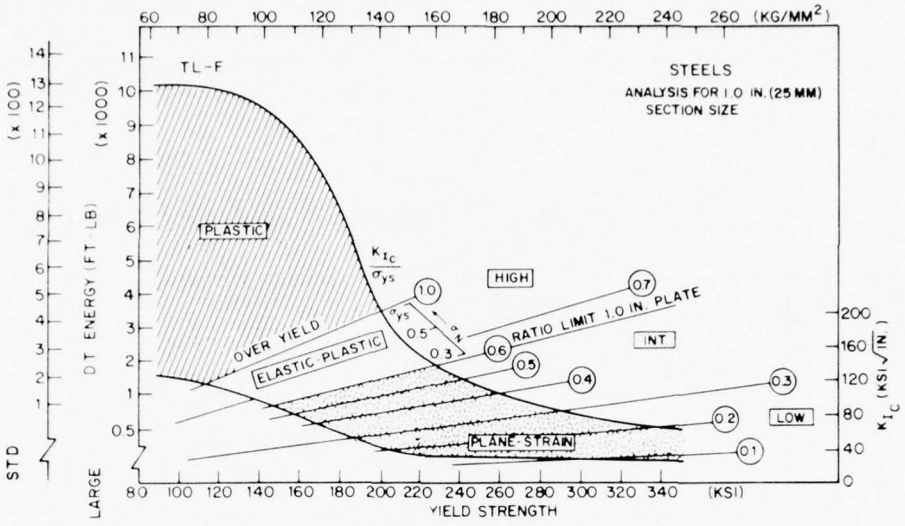

Fig. 59—Three-part zoning combined with fracture state analysis for 1-in. (25 mm) section size. Note range of ratio levels in plane-strain region.

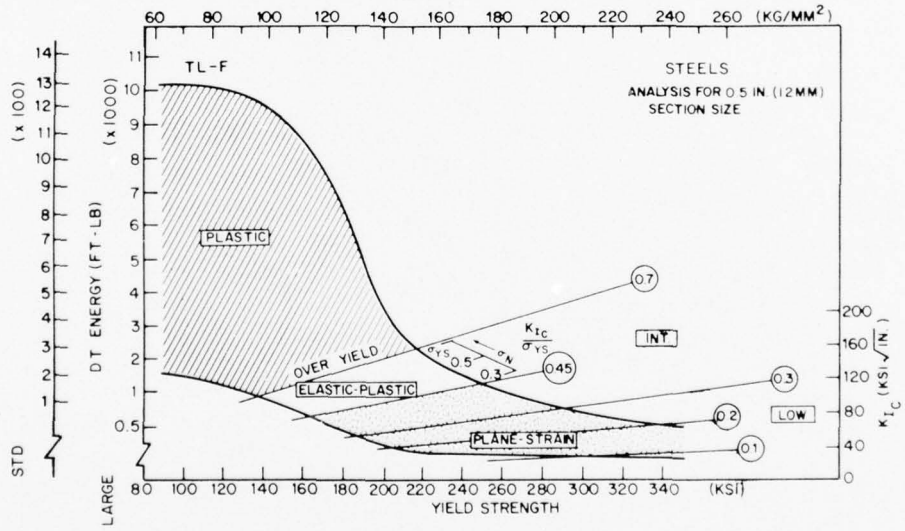

Fig. 60—Three-part zoning combined with fracture state analysis for 0.5-in. (12 mm) section size. Note limited range of ratio levels in plane-strain region.

Figure 61 represents an overlay, on the SI RAD, of quality corridors for steels. It is apparent that decreased quality may drastically change fracture state and decrease ratio values from intermediate to low.

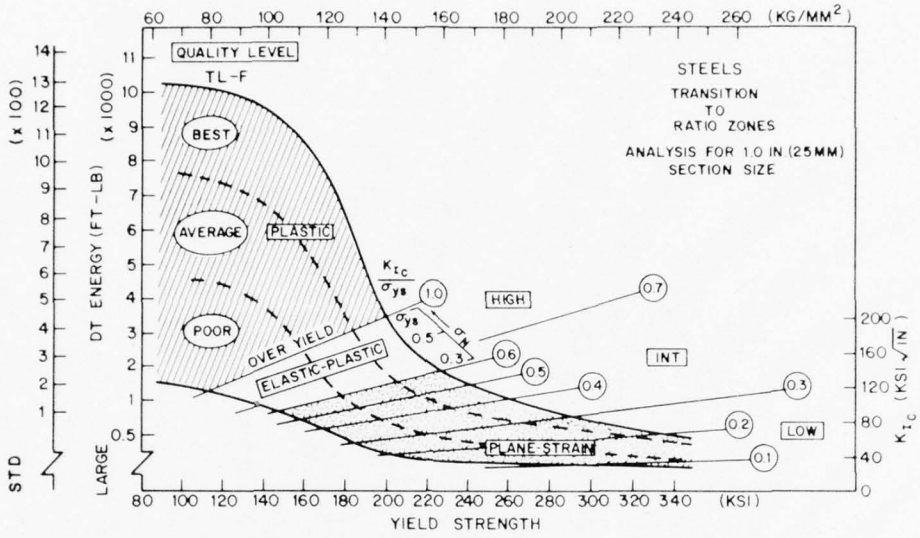

Fig. 61—Three-part zoning combined with fracture state analysis and metal-quality corridor analysis.

The three-part zoning method for indexing the RAD provides for rapid analysis of tradeoffs among engineering factors. In fact, any attempt to make analyses by any other method would require extracting information from RAD summaries of mechanical-metallurgical relationships.

CHAPTER 6

Fracture-Control Principles: Temperature-Transition Problems

EARLY STUDIES OF INITIATION AND ARREST

Until the 1940s, metal structures were generally fabricated by riveting and bolting. The failure of a component of such a structure is generally an isolated event and does not lead to total collapse. It was not appreciated that the monolithic nature of nonredundant welded structures provides continuity such that fracture initiation in even a small part can have catastrophic consequences. The failure of welded World War II ships made this fact appallingly clear. Fracture initiation was often followed by nearly instantaneous splitting of the entire ship (Fig. 62).

The problem was compounded by the lack of reliable information about metallurgical effects on the fracture sensitivity of steels. Thus, metallurgists could not immediately develop steels of improved fracture properties. Designers, also, had no basis for analyzing the relationship between crack size and stress for fracture initiation. The early welding engineers had been concerned mainly with welding procedures and not with fracture properties of the welds. Everyone relied on experience with riveted and bolted structures, which indicated that the elongation and reduction-of-area ductility parameters of the tensile test generally ensured ductile performance of the structure. Experience with welded ships, however, demonstrated that tensile test ductility was not sufficient for characterizing the structural reliability of steels.

Figure 63 illustrates the brittle fracture of a ship plate that displayed high tensile test ductility. Such glasslike fractures occurred only at temperatures below 60°F (15°C). The sharpness of the temperature effect led to the designation of the problem as a transition-temperature phenomenon.

Figure 64 illustrates a 1955 view of the effect of temperature on the tensile properties and fracture toughness of a typical ship steel. The smooth-body tensile specimen shows a ductile-to-brittle transition over a range of very low temperatures. In the presence of cracks, the transition from plastic to elastic levels of fracture strength takes place over a range of much higher temperatures. By the early 1940s it was recognized that the cracked-body transition-temperature range was the critical index for the loss of fracture strength in ship structures. It was then deemed essential to develop notch tests for determining this design parameter in the laboratory. Such tests would serve two purposes: (a) guiding designers, so that it could be known in advance if a contemplated structure was to be operated at temperatures below the cracked-body transition temperature, and (b) guiding metallurgists in developing steels of customized transition-temperature features.

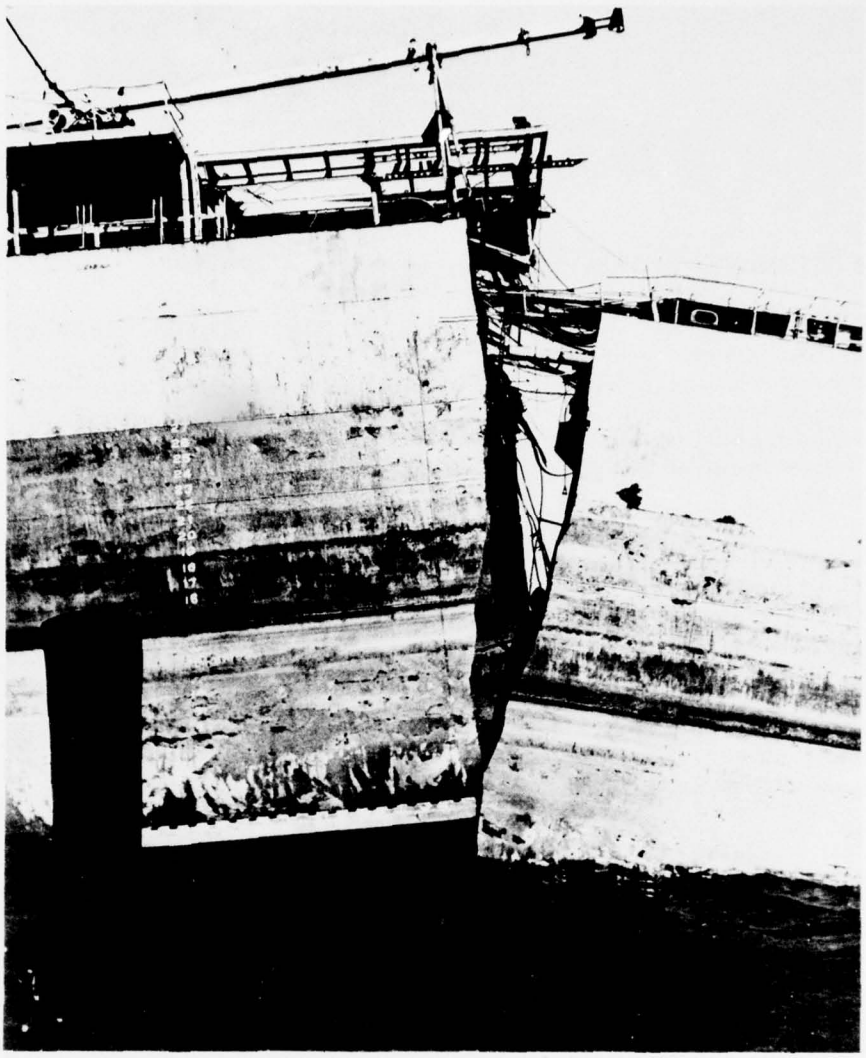

Fig. 62—Total fracture of ship, traceable to small defect.

Examinations of ship failures provided the first significant information about conditions for the initiation, propagation, and arrest of fractures. It was noted that the chevron markings shown in Fig. 63 pointed back to the exact location of fracture initiation. The initiation sites usually involved minute defects such as weld cracks or arc strikes (Fig. 65).

Surprisingly, large cracks several inches in length in the same plate were not responsible for the fractures. This confusing feature was clarified later, when it became evident that the large cracks represented incipient fractures that had been arrested and thus had blunted crack tips. These large cracks extended from corners or other welded details where stress levels were high. Arrests occurred when the crack entered regions of low nominal stress outside the area of the geometric detail. Many such cracks could be found on ships being built, indicating that

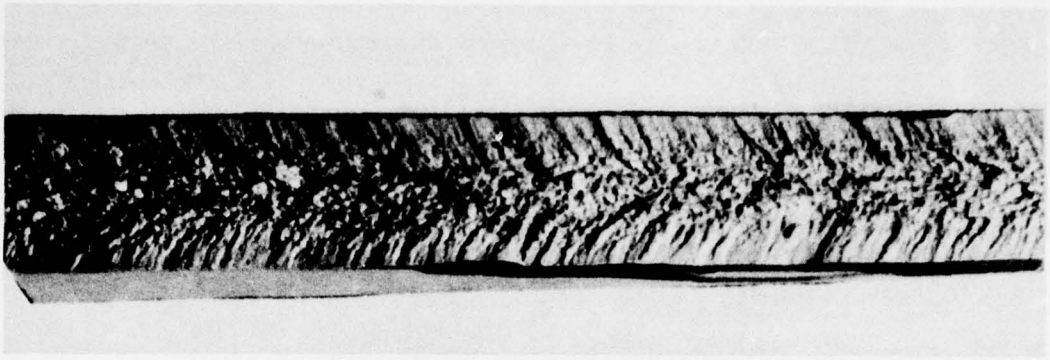

Fig. 63—Features of brittle ship plate fracture. The chevron markings point back to the site of the flaw responsible for fracture initiation.

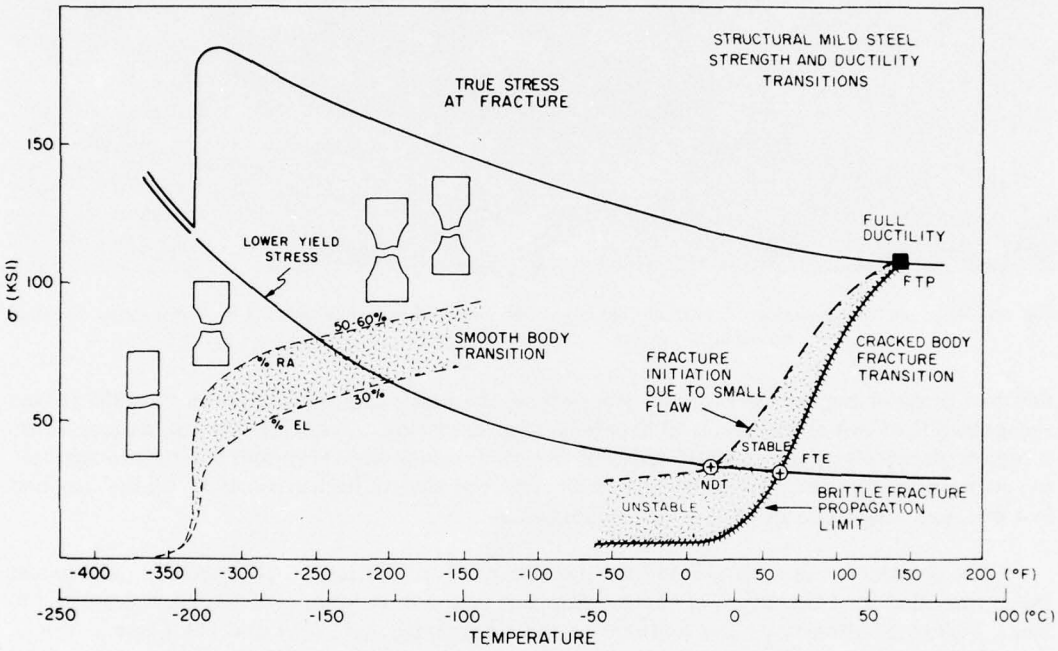

Fig. 64—Comparison (1955) of transition-temperature effects, defined by tensile and dynamic fracture tests of a typical structural mild steel.

their initiation had been spontaneous and strictly related to weld residual stresses. The combination of crack-tip blunting and low stresses prevented reinitiation of fractures.

It was then appreciated that the level of the elastic-stress field through which the crack was propagating had a bearing on the fracture problem. In a few cases it was noted that arrests had occurred in service when cracks entered new plates in regions that did not contain stress gradients. Figure 66 illustrates such an arrest. Note that the painted surface has crazed at the arrest point, indicating ductile behavior (yielding) of the metal. In this case, arrest is clearly

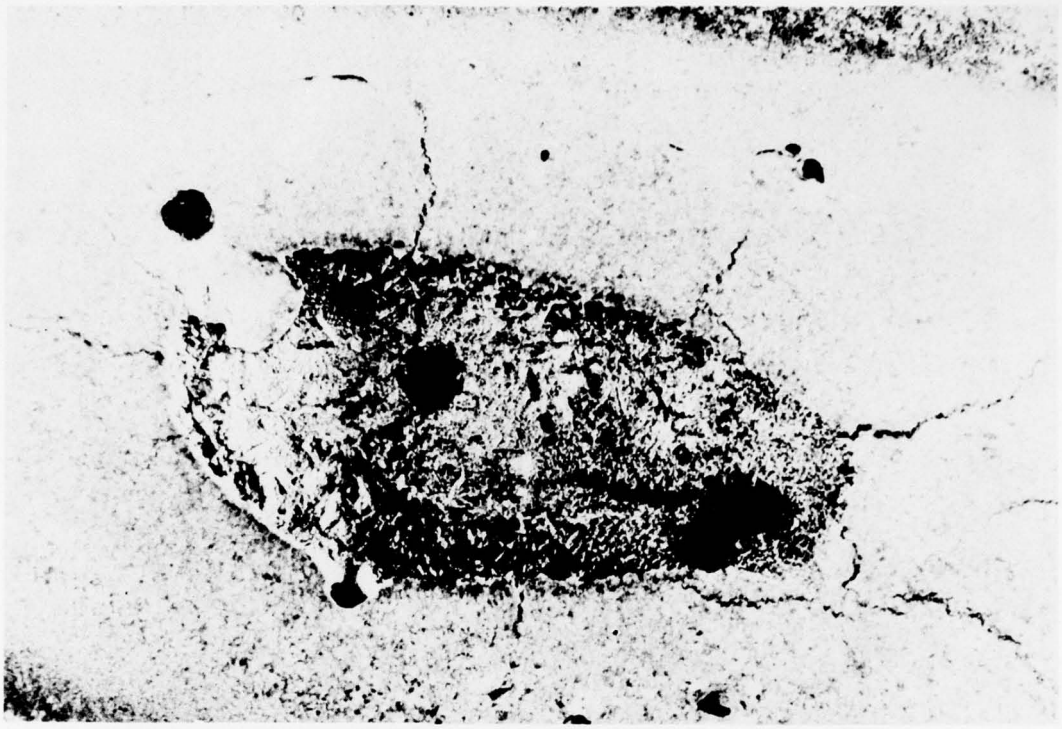

Fig. 65—Weld arc strike; small cracks extend from a solidified arc pool approximately 0.2 in. (5 mm) wide. Residual stress fields of close to yield level act across these cracks.

due to a plate of higher fracture toughness than the adjoining cracked plate. By 1950 it was recognized that two conditions lead to arrests of propagating cracks: (a) entry of the crack into a region of very low stress, and (b) entry of the crack into a plate of higher fracture toughness. Fracture initiation, then, could be expected to occur at sites of high stresses, in plates that had low fracture toughness at the service temperature.

The separation of ship plates into the categories of initiation, propagation, and arrest types provided for calibration of the significance of the only standardized notch tests of the time. Figure 67 illustrates the features of the Charpy-Keyhole (C_k) and the Charpy-V (C_v) tests. Both tests were developed in about 1905 and were used for qualitative assessment of the transition-temperature ranges of steels. There was no rational basis for using these tests to predict structural performance. In addition, it was not known whether fracture energy or some other criterion should be used in calibrating these tests.

Figure 68 illustrates typical C_k and C_v transition features for ship steels. Note that the energy-transition curves parallel the course of the fracture appearance and the notch-root contraction (ductility) transition curves. The energy curve provides the most direct definition of the transition features, and no advantage is gained by referring to the other measurements. However, these independent measurements clearly indicate that the basic reason for increasing fracture energy with increasing temperature is increasing ductility.

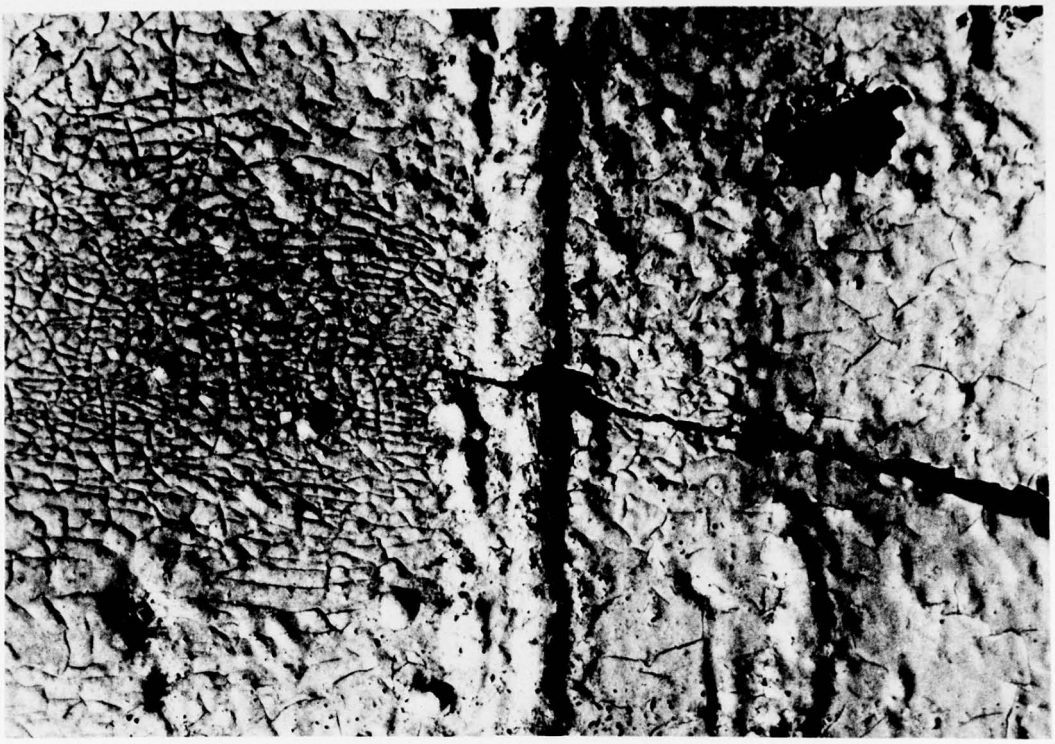

Fig. 66—Crack arrested on fracture entry into a plate of higher than average fracture toughness. Crazing of the painted surface indicates plastic deformation of the underlying metal.

By 1945, the C_k test was recognized as totally inadequate for defining the true in-service transition-temperature range. Because of its excessively blunt notch, it indicated a ductile-to-brittle fracture transition at temperatures much lower than those experienced by the ships. The C_k tests were discarded for studies of ship-failure steels by 1945. The C_v test offered better promise because its transition region includes the temperatures of ship fracture. Attention was directed to studies of the ship-failure steels by use of the C_v test.

By the late 1940s newly developed correlations disclosed that the fracture initiation, propagation, and arrest plates had distinctly different *maximum* values of C_v energy at the temperatures corresponding to the service fracture. The results were as follows:

Initiation plates—Maximum 10 ft-lb (14 J)
Propagation plates—Maximum 20 ft-lb (28 J)
Arrest plates—Energy values significantly in excess of 20 ft-lb (28 J) resulted in "yielding" arrests (see Fig. 66).

These statistics are summarized in Fig. 69 with reference to the position in the C_v energy-transition curve. Service temperatures below the 10-ft-lb (14 J) transition-temperature index provide for fracture initiation due to small cracks. Service temperatures below the

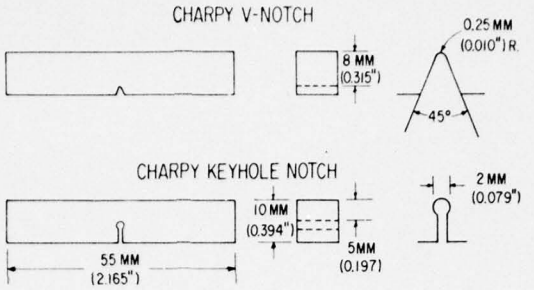

Fig. 67—Charpy-V and Charpy-Keyhole test specimens.

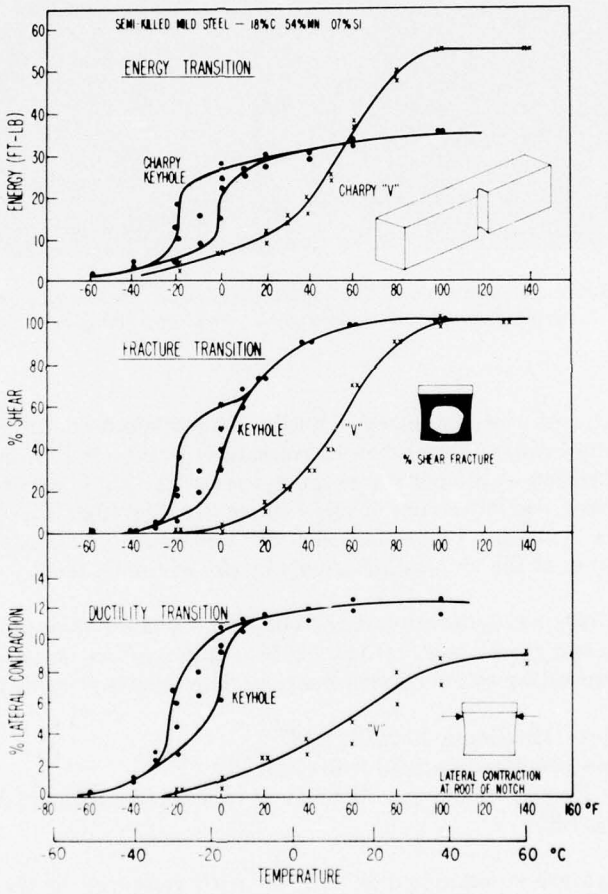

Fig. 68—Transition-temperature features of C_v and C_k tests as indexed by fracture energy, fracture appearance, and notch-root lateral contraction.

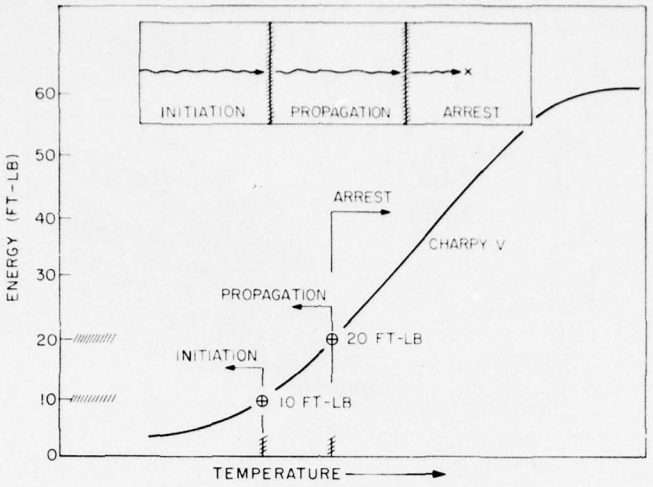

Fig. 69—Summary of C_v energy values for ship-fracture initiation, propagation, and arrest plates.

20-ft-lb (28 J) transition-temperature index provide for propagation except in areas of abnormally low stress. Service temperature in excess of the 20-ft-lb (28 J) transition-temperature index assure arrests due to metal ductility, as the fracture extends into a plate of such characteristics.

As the result of these studies, it became conventional to reference the transition-temperature range in terms of the 15-ft-lb (21 J) transition-temperature index, which represented a conservative definition of the highest temperature for fracture initiation.

It should be noted that the best of the ship plate steels features a 15-ft-lb (21 J) transition temperature at approximately 0°F (-18°C) and the worst at 140°F (60°C). The quality distribution was gaussian, as shown in Fig. 70, with a sharp peak at 65°F (18°C) and a high population density in the range of 35° to 90°F (2° to 32°C). The broadband distribution of the World War II ship plates results from poorly controlled metallurgical processes. With good mill control the range of variance can be kept within a 60°F (35°C) band.

By 1952 the 15-ft-lb (21 J) C_v transition temperature was accepted as the definitive criterion for design and as the guide for metallurgical studies. The effects of alloy elements, grain size, normalizing heat treatments, deoxidation practices, and so on were investigated in terms of their effect on shifting the 15-ft-lb (21 J) transition temperature. Figure 71 illustrates the shifts to lower transition temperatures, compared to those of the ship-fracture steels, that can be obtained by combining the benefits of decreased C-Mn ratio, aluminum deoxidation, and the use of normalizing heat treatments. Unfortunately, there was a basic error in the assumption that the 10- to 20-ft-lb (14 to 28 J) C_v energy range had the same significance for these modified steels. By 1953 it was demonstrated that the critical transition-temperature references moved to higher positions on the C_v energy curve (higher C_v energy indices) for many steels that differed from the original ship-fracture type. This finding destroyed the concept of an invariant reference to the C_v energy-transition curve. Clearly, the C_v test requires specific calibrations for different steels and thus poses unacceptable complications for general engineering use covering broad families of steels.

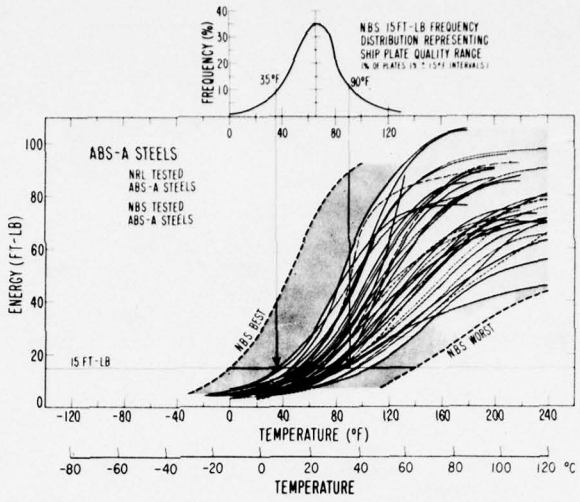

Fig. 70—Spread of C_v transition-vs-temperature characteristics of ship-fracture steels.

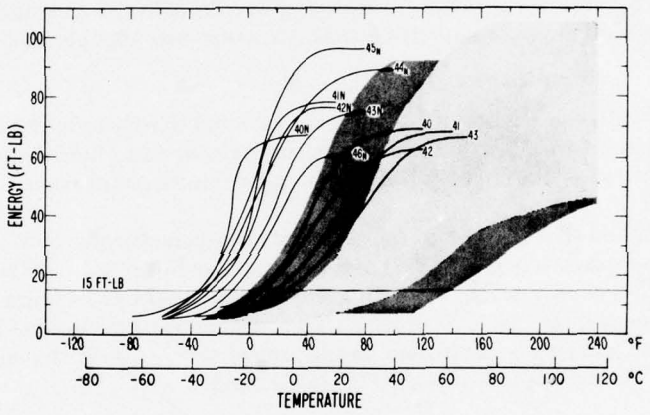

Fig. 71—Transition-vs-temperature characteristics of improved steels (curves) compared to those of fracture steels (shaded bands).

NATURAL CRACK TESTS

A wide variety of new fracture tests was developed during the 1940s. These tests can be separated into two basic types: (a) tests using tensile loading of small laboratory specimens with machine notches and (b) structural prototype tests of very large structures featuring machined notches and/or welds. The interest in large structural prototype tests resulted from the inability to reproduce ship-failure conditions at service temperatures in any of the small test specimens. Regardless of the acuity and depth of the machined notches, stresses over yielding were always required for initiation of fractures by the laboratory tests. In contrast, the initiation of in-service failures was always obtained at elastic-stress levels. Increasing the

size of the test plate did not modify this behavior. Again, in-service failure conditions could not be reproduced.

Obviously a fresh approach was required, because slow loading of specimens with machined notches did not reproduce the in-service conditions of fracture initiation. In view of the impasse that existed in 1950, investigations were redirected to fracture studies involving natural cracks. The basic premise guiding this approach was the recognition of the role of cleavage microfracture processes, which are inherent to metallurgical analysis of the problem. Such analysis had matured to suggest that cleavage fracture instability first develops in embrittled metal adjacent to the weld, i.e., in the heat-affected zone (HAZ). Once cleavage instability appears within the space of a relatively few grains in the embrittled heat-affected zone, the base metal grains in line are subjected to the dynamic extension of an ultrasharp natural crack. As a consequence, the structure as a whole behaves mechanically as it would under dynamic loading.

The mechanism of cleavage fracture is discussed in Chapter 2. The energy required for the propagation of unstable (fast) fracture is derived from elastic strain. The individual grains may be considered as loaded by elastic springs. As each grain cleaves, the release of elastic energy serves to increase the loading rate on the next grain in a dynamic fashion until cleavage occurs. The process continues indefinitely.

The cleavage of the first few grains is crucial for cleavage fracture; the mechanics of the cleavage process are dynamic thereafter. Thus, any form of metallurgical embrittlement, including strain aging of the crack-tip metal or the presence of brittle phases, can activate dynamic instability. Embrittlement of the heat-affected zone represents only one case. In the absence of such localized initiation conditions, the base metal responds to slow loading rates by behaving in a more ductile fashion. It is then more difficult to initiate cleavage fracture of the first grains. The engineering aspects of this problem are best considered in the light of the fact that micromechanical conditions controlling cleavage of the first grains also control the ductility and the effective strength of the structure as a whole.

There were two problems with the long-sought goal of initiating fracture at elastic levels in the presence of machined notches loaded at slow rates: (a) metal grains at the notch root are not subject to the same high degree of triaxial constraint to plastic flow provided by ultrasharp natural cracks, and (b) the slow loading rate favored extensive yielding before cleavage initiation in the first grains.

The highest temperature range for the initiation of cleavage fracture at elastic-stress levels must be determined by laboratory tests involving cracks of ultimate sharpness and the application of dynamic loading. These conditions ensure that the cleavage of the first grains develops under the most adverse conditions for suppression of microfracture ductility. The highest temperature at which a steel structure can be expected to fail is controlled by such worst-case conditions. By enforcing the worst case in laboratory tests, an exact match can be found to the highest temperatures of possible in-service failure at purely elastic load stresses.

The nature of the first experiments conducted with natural-crack tests is illustrated by Fig. 72. Arc strikes were applied to ship plate steels, and dynamic loading was developed by dropping weights in the center of the edge-supported plates. It was found that fracture initiation, for conditions of elastic loading, resulted at the ship-failure temperatures of 30° to 60°F (0° to 15°C) but not at higher temperatures, exactly as in the ship failures. The fractured plates

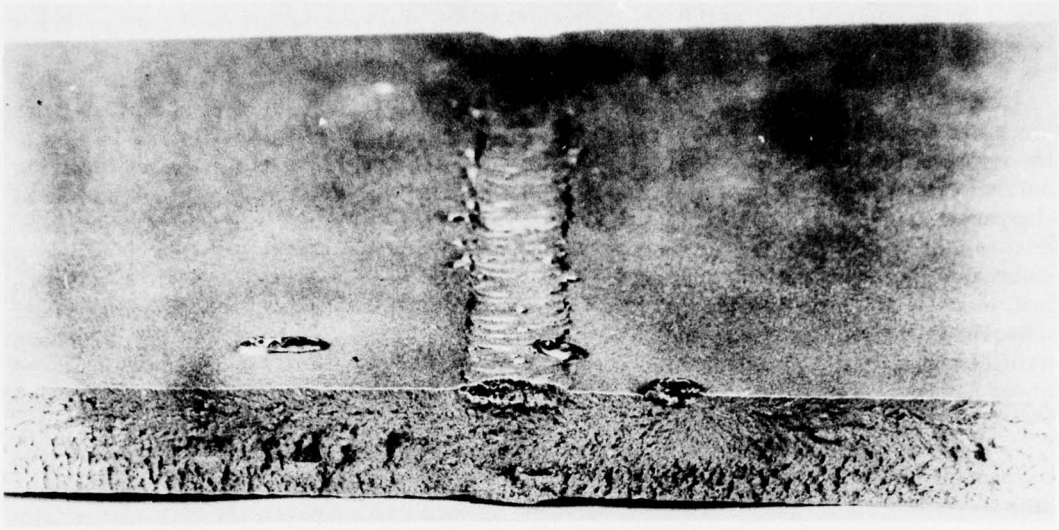

Fig. 72—Fracture of ship plate steel at elastic stress levels by dynamic loading *in the presence of small arc strike cracks.*

remained perfectly flat, indicating that the loading had not exceeded yield-stress levels. Explosion tests of the same plates without the arc strikes demonstrated great ductility at low temperatures, as predicted by the tensile tests. The dramatic effects of such tiny defects can be explained only by cleavage fracture instability processes of microscale dimensions. The volume of metal involved in the initiation of brittle fracture must always be smaller than the defect size.

These findings led to the development of the Explosion Crack Starter Test, which featured a short, brittle weld bead of hard surfacing type deposited on the plate surface. The plates were placed over a circular die and loaded by offset explosion. The intent was to observe the effects of increasing temperature on the propagation of the fractures. The function of the brittle weld bead was to introduce a small crack of natural sharpness, similar to the weld cracks or arc strikes of the ship failures. The reason for offset explosion loading was to ensure dynamic conditions for the initiation phase and to maintain soft-spring (continued) loading on the plate while the fracture propagated from the center to the edges. Temperature control was obtained by conditioning the test plate and then quickly placing it on the die for explosion loading.

The results of typical series of ship plate tests (1954) conducted over a range of temperatures are shown in Fig. 73. The series present a clear panorama of the effects of temperature on the initiation and propagation features of the steel, in the service temperature range of the ships. At 20°F (-8°C) a flat break is obtained (elastic fracture), while at temperatures of 40°F (5°C) and higher increasing bulging (plastic overload) indicates increased resistance to initiation of fracture. The term Nil Ductility Transition (NDT) temperature was applied to the flat-break temperature. In other words, with descending temperature a critical transition point is reached, such that elastic fracture initiation (nil ductility) is possible in the presence of a dynamically loaded small crack.

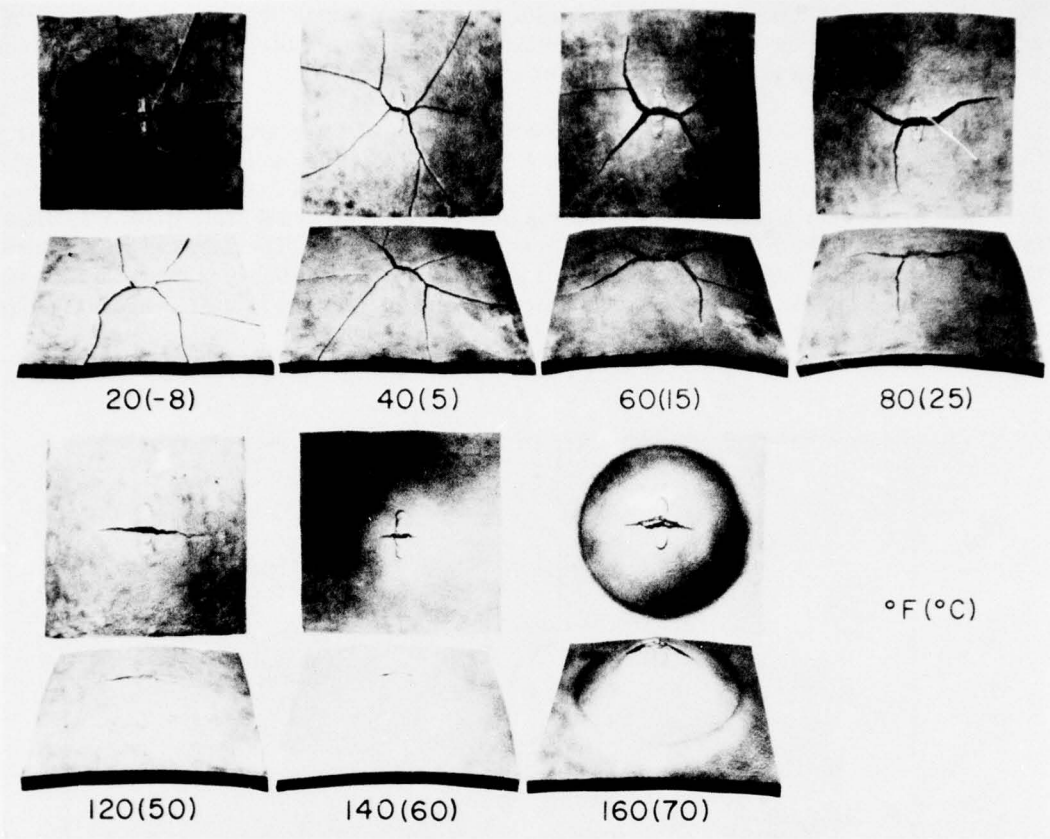

Fig. 73—Features of explosion crack starter tests of ship plate steels. The steel is representative of the best quality.

It should be noted that resistance to fracture propagation increases markedly with increasing temperature. Between 60° and 80°F (15° and 25°C) the fractures no longer run through the elastically loaded edge regions; however, continued propagation is obtained through the plastically loaded center regions. This temperature point is defined as the Fracture Transition Elastic (FTE) temperature; it signifies the highest possible temperature for unstable fracture propagation through elastic-stress fields. Ultimately, a higher temperature is reached, at which only ductile tearing is possible. Because of the high resistance to propagation of ductile fracture, the explosion loading resulted in a helmet-shaped bulge at 120°F (50°C) and above. The 160°F (70°C) bulge resulted from the use of a much larger explosive charge than was applied for the rest of the test series and illustrates the high degree of ductility. The temperature point of fully ductile tearing is called the Fracture Transition Plastic (FTP) temperature. The current, equivalent nomenclature for FTE is yield criterion (YC).

The fracture panorama presented by many such test series clearly illustrated why ship fractures occurred only at winter temperatures. The significance of initiation, propagation, and arrest features also becomes clear. The controlling temperature for fracture initiation due

to small cracks is obviously the NDT temperature. Fracture due to small cracks could not be expected to initiate in ship structures above the NDT temperature because gross plastic overloads are required in the presence of small cracks.

Figure 74 illustrates a typical correlation of explosion-test fracture performance with the C_v energy-transition curve for ship-fracture steels. NDT fracture-initiation features are obtained as the explosion-test temperature falls below the 10-ft-lb (14 J) C_v transition temperature. The band superimposed on the C_v curve indicates that the FTE (YC) arrest transition takes place close to the 20-ft-lb (28 J) transition-temperature index. The temperature at which the C_v curve attains shelf values corresponds to the FTP or full-ductility temperature. Thus, the initiation, propagation, and arrest relationships of ship fractures to the C_v curve (Fig. 69) are clearly reproduced by the explosion-test series.

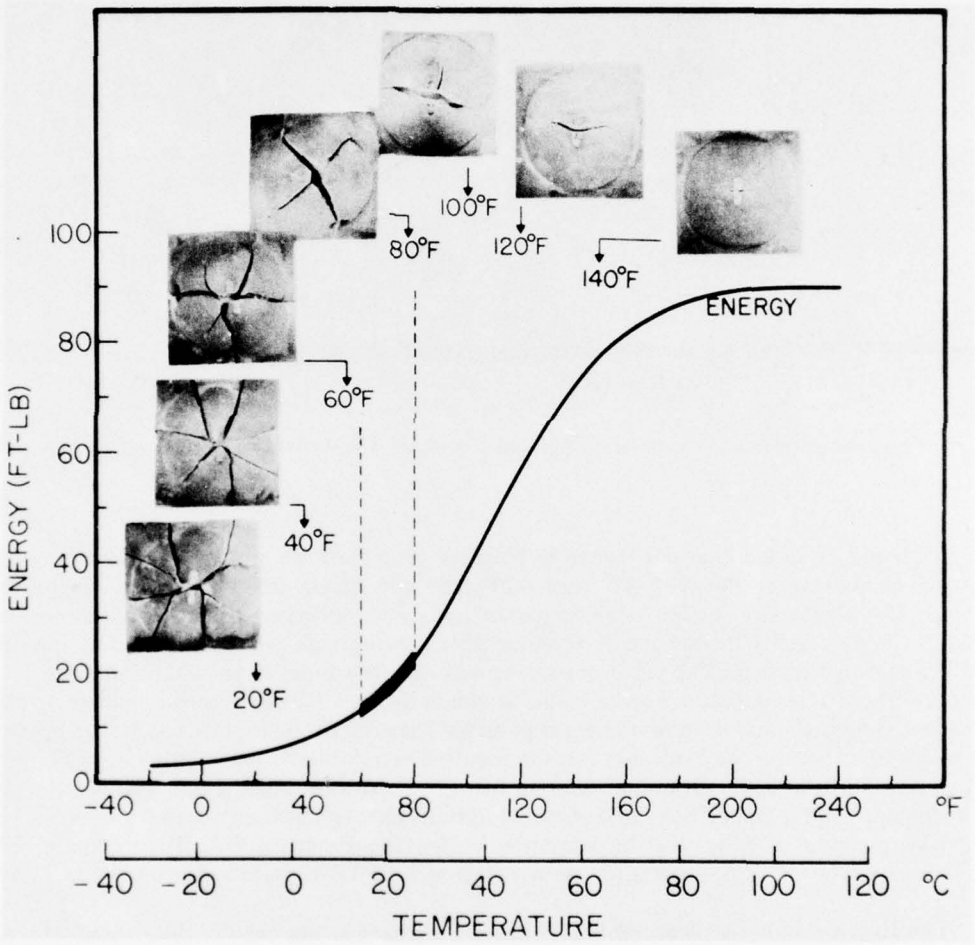

Fig. 74—Correlation of typical explosion crack starter test performance with C_v transition curves for ship-fracture steels.

The success of the explosion test in providing a direct correspondence to the service performance of the ship steels suggested its use on a broad front in studies of fracture initiation, propagation, and arrest. This was required in particular for the wide variety of steels for which there was no detailed documentation of in-service failure. These studies were also used to investigate whether the C_v curve predictions of initiation and arrest transition temperatures would hold for improved ship plate steels. Unfortunately, these and other steels indicated correlations indexed to much higher C_v fracture energies and therefore higher positions on the C_v curve, as illustrated in Fig. 75. These observations were important because they contradicted the then generally accepted conclusion that C_v transition-temperature indices would provide for invariant assessment of the service fracture characteristics of steels.

The failure of the C_v test to provide an invariant characterization method for the true transition-temperature range of steels emphasized the need for a simple natural-crack test for laboratory use. By 1953 this led to the invention and validation of the Drop Weight Test (DWT). The DWT was designed specifically for determining the NDT temperature. Figure 76 shows the DWT equipment.

Figure 77 illustrates the general features of the DWT specimen and the effect of temperature on its fracture characteristics. The specimen has the same brittle weld as the explosion-test specimen. A saw cut across the weld localizes the fracture of the weld bead to a single crack, at the exact center of the specimen. This crack provides the equivalent of a thumbnail-size crack with an ultrasharp tip. The brittle weld bead is fractured as near-yield-stress levels are attained, as a consequence of dynamic loading by a dropping weight. In practice, the DWT is conducted by loading the specimen as a simple edge-supported beam, with a stop placed under the center position. The stop restricts deformation to a very small amount; thus, deformation is kept constant for steels of different yield strengths.

Figure 77 (top) presents a typical test series that defines the NDT temperature as the highest temperature of nil-ductility break. The flat break signifies that fracture initiation due to the small crack occurred before the development of significant plastic deformation. Figure

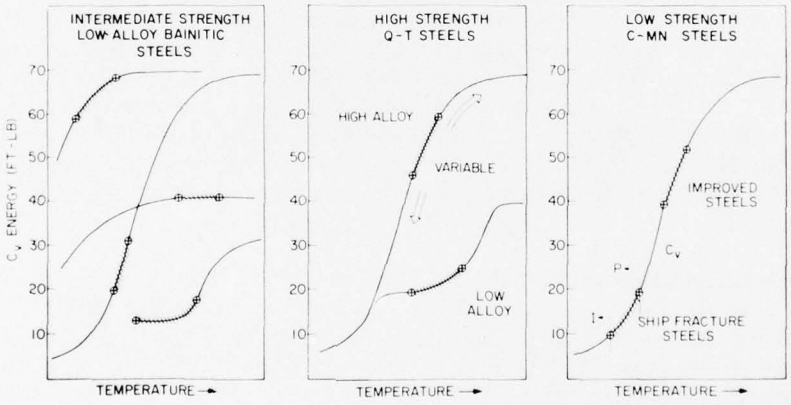

Fig. 75—Complications in the interpretation of C_v test transition temperature curves for different steels. The positions of the shaded initiation-to-arrest correlation bands (NDT to FTE) are shifted widely from their position in the toe region of the C_v curve (Fig. 13).

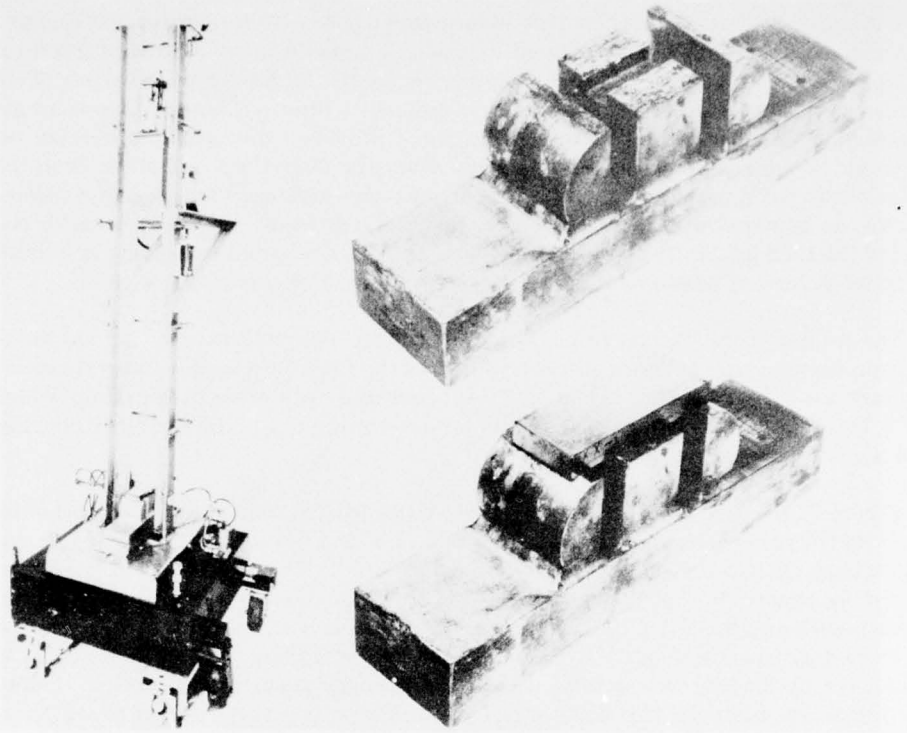

Fig. 76—Drop Weight Test equipment.

77 (bottom) illustrates tests conducted without the stop. At NDT + 20°F (NDT + 10°C) and NDT + 30°F (NDT + 17°C), the specimen can be deformed plastically without causing fracture. This clearly indicates that a sharp increase in dynamic fracture toughness takes place above the NDT temperature. Extensive use of the DWT has shown that the NDT reproducibility is within ±10°F (±5°C). This degree of reproducibility should not be surprising, in view of the pronounced effect of temperature at this critical point of the transition range. It should be noted that the NDT temperature is not affected by orientation of the test specimen with respect to the rolling direction, because brittle fractures are not influenced by the alinement of nonmetallic phases.

An early illustration of the capabilities of the DWT-NDT procedure for indexing in-service failure conditions is provided by Fig. 78. A statistical survey of the NDT temperature frequency distribution was made by random selection of World War II ship plate steels. The NDT temperatures range from 0°F (-18°C) for the best steels to 70°F (20°C) for the worst, with a gaussian distribution pattern at intermediate temperatures. It is evident from this figure that the dramatic increase in the rate of ship failures with falling temperatures, between 70° and 30°F (20° and 0°C), is directly related to the NDT temperature distribution of the steels. At temperatures above 70°F (20°C), essentially all of the steels are indicated to be above their NDT temperatures; no ship failures took place at these temperatures. At approximately 30°F

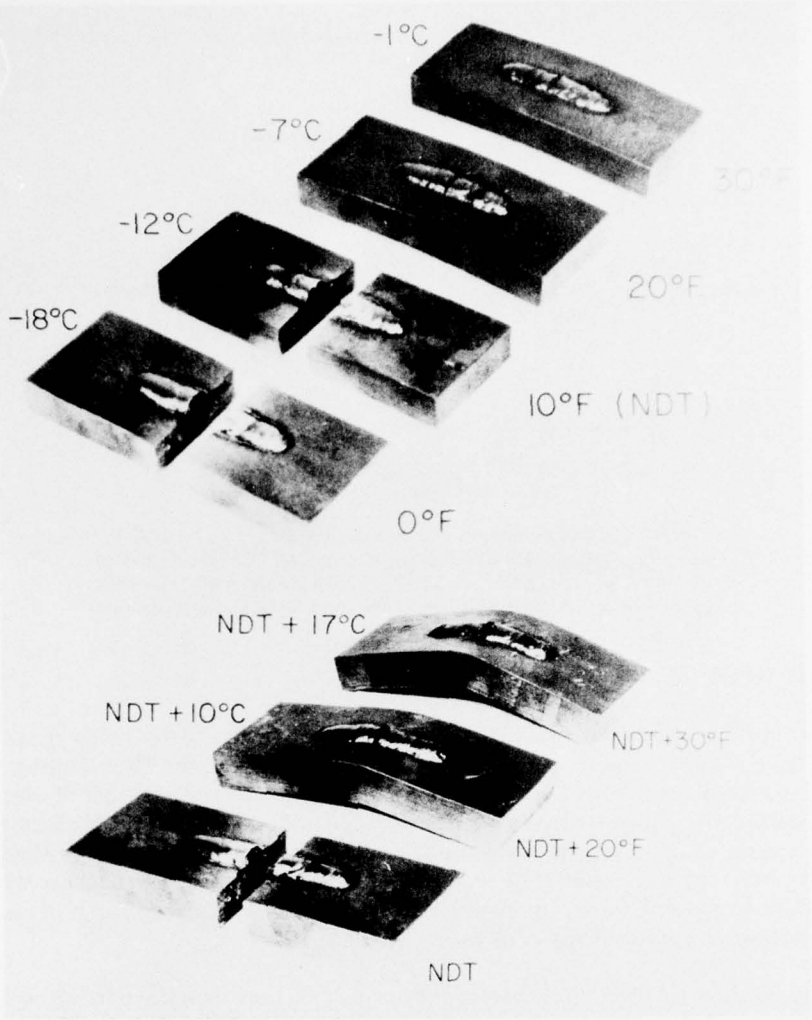

Fig. 77—Typical DWT series (top), which defines an NDT temperature of 10°F (–12°C). The sharp increase in dynamic fracture toughness of the metal, above the NDT temperature, is illustrated (bottom) by the tolerance for plastic deformation in tests conducted without a stop.

(0°C), essentially half of the population is at or below the NDT temperature, and the failure rate is very high.

It is apparent that a metallurgical improvement that would shift the NDT temperature frequency curve to lower temperatures by 40°F (25°C) would have prevented most of the ship failures. The NDT temperature of the worst steels would then be at the low end of the service temperature range. It is tragic to realize that the losses of lives and supplies that resulted from the ship failures could have been prevented by a small adjustment in the carbon and manganese contents of the steels. This adjustment provides the required shift in the NDT temperature distribution (see Fig. 89).

230-302 O - 77 - 8

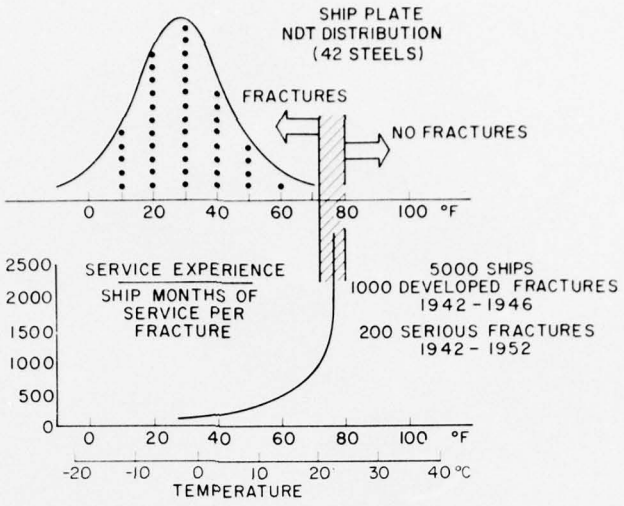

Fig. 78—Statistics of ship-fracture frequency, compared to the NDT-temperature frequency distribution of ship steels. Fracture rates increase rapidly as the fraction of the steel population with below-NDT properties is increased, as a result of decreasing service temperature.

CRACK ARREST TESTS

The evolution of the Robertson Crack-Arrest Test in the late 1940s marked another departure from conventional fracture studies. The importance of the Robertson test cannot be overestimated because it provided exact definitions of the relationships of stress level to crack-arrest features. Since its invention the test has taken various specific forms. However, the basic feature of all forms is forced initiation of the fracture, which is then caused to propagate (or not) through a flat plate, loaded to exactly defined levels of elastic stress. Figure 79 illustrates two types of Robertson tests. The tests are conducted over a range of temperatures, with either fixed or varied levels of stress.

Figure 80 shows typical data obtained from the test shown on the left side of Fig. 79. The first important feature to note is the nearly flat portion of the Robertson curve at low temperatures of the transition range. Temperature has little effect in this region, because the metal has very low dynamic fracture toughness. Fracture arrests are obtained for this highly brittle condition only if the stress level is reduced significantly below the 5- to 8-ksi (34 to 55 MPa) range. Obviously, this is too low to be used for fracture prevention in practical structures.

The part of the curve that rises markedly with increasing temperature represents the Robertson Crack Arrest Temperature (CAT) transition. In discussions of CAT-curve criteria, the FTE is equivalent to yield criterion (YC); the 0.5 σ_{ys} CAT is equivalent to the 0.5 σ_{ys} arrest criterion, as described in Chapter 3. Because of the strong temperature dependence of the stress level required for propagation, the CAT transition region provides a reliable method for fracture-safe design based on arrest properties. For example, the steel of Fig. 80 has a CAT of 60°F (15°C) for the 18-ksi (124 MPa) stress level. Structures designed for this level of stress

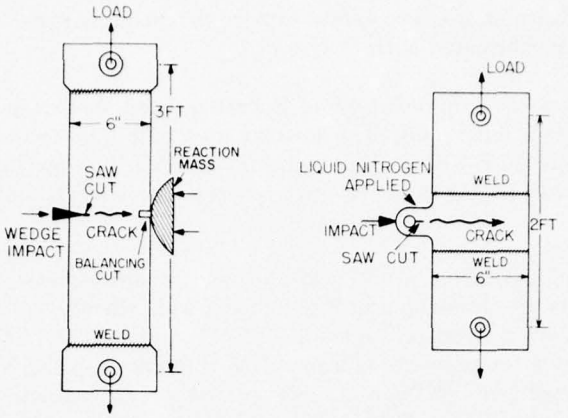

Fig. 79—Features of Robertson tests. In one type (left), fracture is initiated by plastic deformation of the saw cut region by wedge impact. In the original Robertson version, (right) a nub region is deformed by impact while being cooled to low temperatures. In both cases the crack traverses a region of fixed temperature and elastic stress.

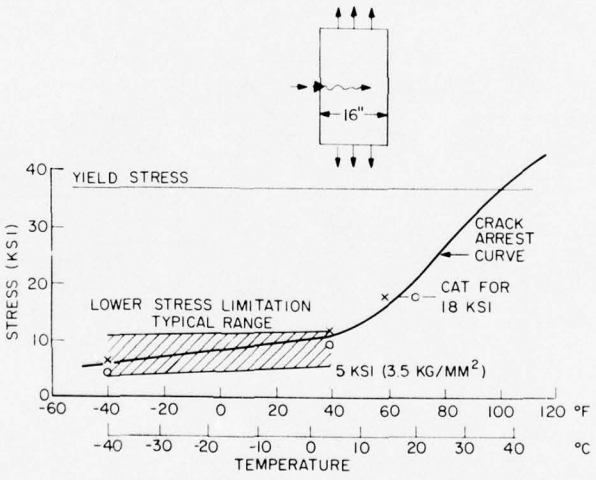

Fig. 80—Typical Crack Arrest Temperature (CAT) transition curve, as defined by Robertson tests. The x signifies propagation with total fracture of the specimen, and the circle signifies fracture arrest.

give positive assurance of fracture safety (due to arrest properties) at service temperatures above 60°F (15°C), if fabricated with this steel.

Figure 81 illustrates another type of Robertson test, featuring fracture initiation in a brittle element of the test assembly. The data are for a high-quality modern ship plate. The 0.5 σ_{ys} CAT is noted to be 15°F (-10°C). This figure introduces the important observation that the NDT temperature marks the point of initial rise of the CAT transition curve from its toe region.

The results of extensive studies of the relationships between the DWT-NDT and Robertson CAT tests are illustrated in Fig. 82 for a wide variety of steels. Note that the CAT transition curve bears a fixed relationship to NDT temperature. This relationship may be expressed simply by a temperature increment Δt referenced to the NDT temperature. Thus, the simple and inexpensive DWT can reliably locate the CAT transition curve on the temperature scale. For example, NDT + 30°F (NDT + 17°C) provides a conservative index of the CAT for the 0.5 σ_{ys} stress level (0.5 YC), and NDT + 60°F (NDT + 33°C) provides a similar index for the yield-stress level, i.e., the FTE, or YC. Unstable fracture propagation through elastic-stress regions, with characteristic velocities of several thousand feet per second, is not possible at temperatures above the FTE (YC). The propagation rate at over-yield stress levels is controlled by the rate of application of the plastic load in advance of the crack front.

These findings were of major consequence because they disclosed specific relationships between initiation and arrest of unstable fractures. These relationships are evident from the temperature dependence of two curves plotted in Fig. 82. The upper curve plots the rise in the stress level required for dynamic fracture initiation due to a small crack. It is important to note that the rise of this curve represents a transition from elastic to plastic levels of fracture-initiation stress. The NDT indexes the temperature of the initial rise of this curve to over-yield

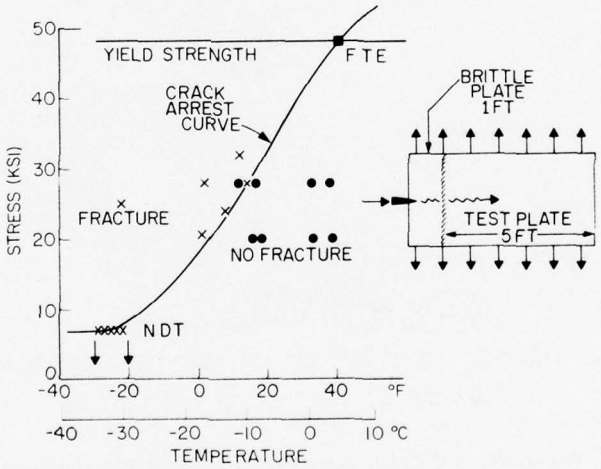

Fig. 81—Wide-plate Robertson test featuring fracture initiation in a brittle plate that is welded to the test plate. The CAT for 0.5 σ_{ys} is indicated as 15°F (-10°C). The NDT temperature, as determined by the DWT, indexes the temperature at which the Robertson CAT curve begins to rise.

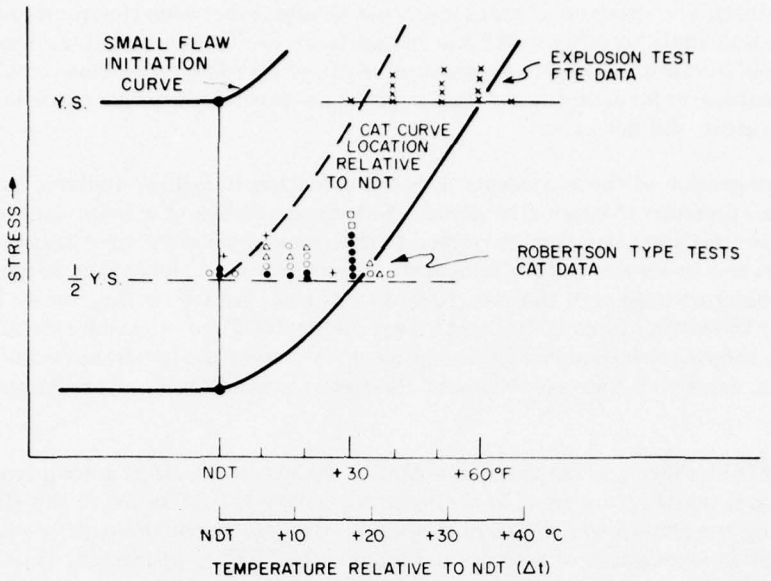

Fig. 32—Summary of tests for a wide variety of steels; the tests indicate that the CAT curve bears a fixed Δt relation to the NDT temperature.

stress levels. The sharp rise of the CAT curve also starts at the NDT temperature. The curves show a simultaneous rise above the NDT temperature, because the dynamic fracture toughness of the metal develops a strong temperature dependence at this temperature. Both curves are controlled by the same basic microfracture factor, the increase in dynamic cleavage fracture ductility of the metal grains.

Since the CAT curve defines the course of the stress-vs-temperature relationship for arrest, it should also define the limiting stress-vs-temperature relationship for the initiation of unstable fracture. Fracture initiation could be expected only for conditions that provide for propagation, i.e., in the region to the left of the CAT curve. Thus, increasing crack size lowers the stress required for fracture initiation from plastic levels to the limit elastic-stress level defined by the CAT curve. This effect may be viewed as a shift of the fracture-initiation curve with increasing crack size, from the small-crack curve position to near the CAT curve position as a limit. From these considerations, it became apparent that the corridor between small-crack and CAT curves should encompass a family of curves of similar form, but representing a spectrum of crack sizes.

FRACTURE ANALYSIS DIAGRAM (FAD)

The coupling of crack-size and transition-temperature considerations took place as the engineering significance of fracture mechanics definitions of stress-intensity factors began to be appreciated. For a brittle metal, the stress required for initiation should decrease in proportion to the increase in the square root of the crack size. Thus, very large increases in crack size should be required for fracture initiation as stress decreases from yield magnitude to low levels

of nominal stress. The spectrum of crack sizes that should lie between the small-crack and CAT-limit curves was qualitatively predictable on this basis. Unfortunately, at the time the experimental data of fracture mechanics parameters required for calculating these crack sizes at the NDT temperature, or for establishing the temperature-dependence of the stress level above the NDT temperature, did not exist.

The integration of these concepts directed attention to failure analysis as a means for defining the spectrum of crack-size curves. Extensive studies of service failures were conducted and carefully cataloged with respect to the crack size for fracture initiation, the NDT temperature, the in-service failure temperature, and the stress level that before failure had applied to the crack region of the structure. In addition, data from large-scale tests became available for the effect of increasing crack sizes (below NDT) for ship plate steels. These data provided the information required for assigning crack-size values for the curves of the diagram shown in Fig. 83, which was evolved about 1960 and is called the Fracture Analysis Diagram (FAD).

The FAD provides a generalized description of the relationships among crack size, relative stress, and temperature by a Δt temperature-increment reference to the NDT temperature. Locating the generalized diagram at specific positions in the temperature scale requires experimental determination of a single parameter, the NDT temperature. Thus, simply conducting a DWT allows the other factors to be revealed by the FAD.

Extensive international use of the FAD has positively documented its practicality. All known structural failures by unstable fracture conform to the limits predicted by the FAD. Continuing research on the transition-temperature fracture problem has confirmed its validity. The DWT, basic to FAD analysis, attained the status of an ASTM standard practice method in 1963.

We shall now discuss details of the use of the FAD. The most important is the requirement for careful consideration of the stress level that must be used in entering the FAD. Quantitative definitions of stress relationships apply only up to the limit of yielding, and FAD

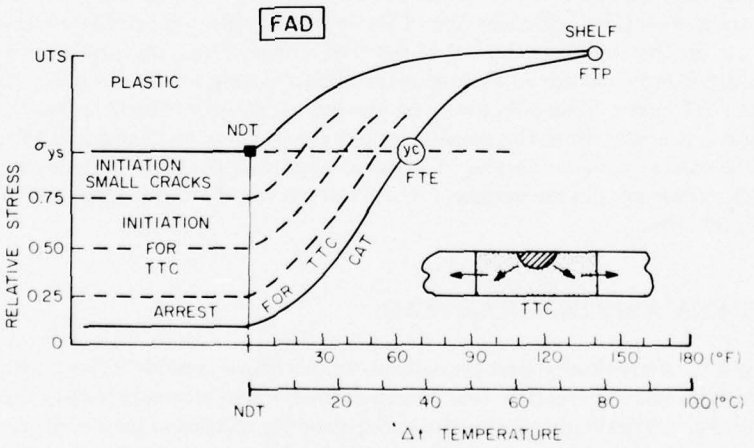

Fig. 83—Fracture Analysis Diagram (FAD).

extrapolations into the plastic region are not indexed specifically. These extrapolations can only indicate that the level of plastic stress should increase with increased temperature. Plastic-stress levels are not indexed, because there are no calculation procedures or failure experiences to indicate specific relationships.

The stress scale is referenced to the relative value of nominal engineering stress. If the crack is small and is entirely in a region of geometric detail, such as a sharp corner or the nozzle junction of a pressure vessel, the applicable stress is the geometrically intensified local stress field of the region. For example, in a pressure vessel, a nozzle region where stress is intensified by a factor of three or four should be considered as loaded to yield-stress levels for a nominal hoop-stress condition of $0.3\sigma_{ys}$. Since the best nozzle designs feature a minimum 3× intensification, cracks in nozzle regions should be considered subject to yield-stress levels. Such rudimentary stress analyses suffice, because conventional structures normally feature two general levels of stress: (a) the nominal design stress at regions of smooth section and (b) yield-stress levels at most regions of geometric transition.

A special consideration applies to as-welded (not stress-relieved) structures, due to the presence of yield-level residual stresses near the heat-affected zone (HAZ). These localized stress fields act in a direction parallel to the weld, as illustrated in Fig. 84. They result from restraint of longitudinal shrinkage during cooling of the weld area. The peak stress region is on the order of 1 to 2 weld widths and thus can only contain small cracks oriented in a direction normal to the peak stress. These localized residual stresses should not be confused with general weld-construction stresses, which may extend in any direction through the entire structure. Such long-range stresses do not normally exceed 0.5 σ_{ys}.

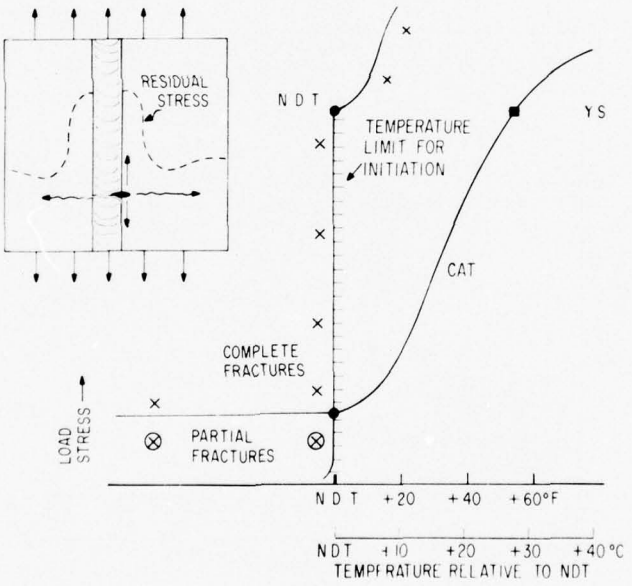

Fig. 84—Transition-temperature features of low-stress fractures resulting from weld residual stresses and small cracks.

Because of the highly localized residual stress field, small cracks in the weld or the heat-affected zone are effectively subjected to yield-stress levels, even in the absence of structural loads. As a result, welded structures that are not stress relieved may initiate fractures at small cracks in weld regions, for a wide range of nominal stresses, provided the in-service temperature is below the NDT. Fractures are therefore possible at very low levels of applied load. At temperatures above the NDT, such low-stress fractures cannot develop, because severe plastic loading is necessary for fracture initiation, as noted in Fig. 77.

Experimental verification of these predictions is presented in Fig. 85, which illustrates typical results of buried-flaw tests. These tests simulate weld cracks with sharp notches cut in the beveled edges of the plates before they are joined by a butt weld. After the weld, the notch tips are in the region of the embrittled heat-affected zone, as indicated by the drawing at the top of the figure, and are subject to high residual stresses. When such welded plates are loaded in tension, a sharp transition in fracture stress takes place, as noted by the arrow. At temperatures slightly above the NDT, the fracture load stress is above yielding. At temperatures below the NDT, the fracture load stress may fall to very low values. In the latter case, the load stress simply adds a small increment to the already existing residual stress, which may be close to yield levels. Buried-flaw tests have been conducted extensively to determine the critical temperature below which low-stress fracture is possible. It is apparent that this information may also be obtained from the DWT-NDT.

If fracture initiation is attained in the buried-flaw tests at load stresses below the level of the Robertson lower toe region, i.e., less than 8 ksi (55 MPa), arrest is obtained after a run of only a few inches, as the crack moves out of the weld residual stress field and enters the region

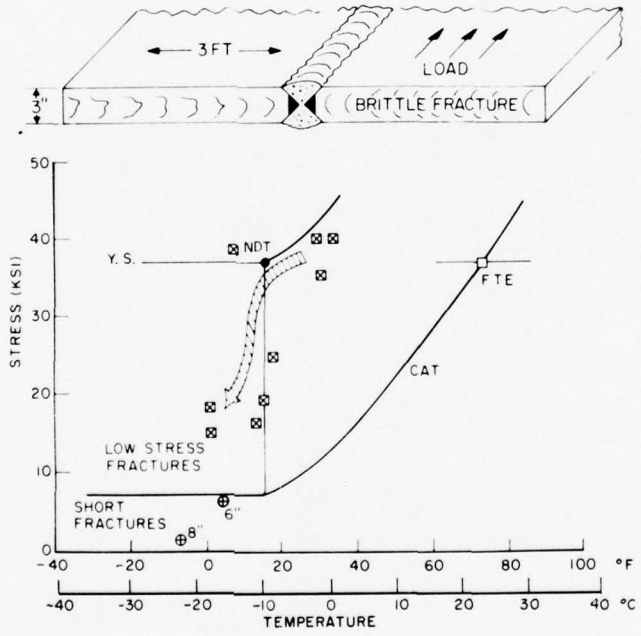

Fig. 85—Typical experimental data (Wells) from Buried-Flaw Tests, which define the critical temperature for low-stress fractures.

of low load stress. This is predicted by the Robertson tests. The existence of short cracks in the ship structures is thus explained.

Effective stress relief eliminates the high peak values of the localized weld residual stresses. Warm mechanical prestressing (loading at temperatures above the NDT) is also effective in preventing low-stress fractures due to crack-tip blunting. The benefits of warm prestressing do not apply to structures loaded randomly, because the prestress must be applied in the direction of the load stress.

In using the FAD, small cracks in the heat-affected zone or in the welds of as-welded (not stress-relieved) structures should be considered to be loaded to yield-stress levels, because this is the applicable stress acting on the small flaws in such locations. A structural failure that originated as the result of weld residual stresses is illustrated by Fig. 86, which represents a typical ship fracture. The fracture originated at the toe of a fillet weld joining a chock bracket to the deck. An arc strike at this spot provided the small, sharp cracks that served as the initiation site. The fillet weld provided the residual stress field. The conditions of fracture initiation for this case are predicted by the FAD. Since the failure temperature was slightly below the NDT, all the necessary FAD conditions of a small crack, loaded to yield stress at a temperature below the NDT, were met.

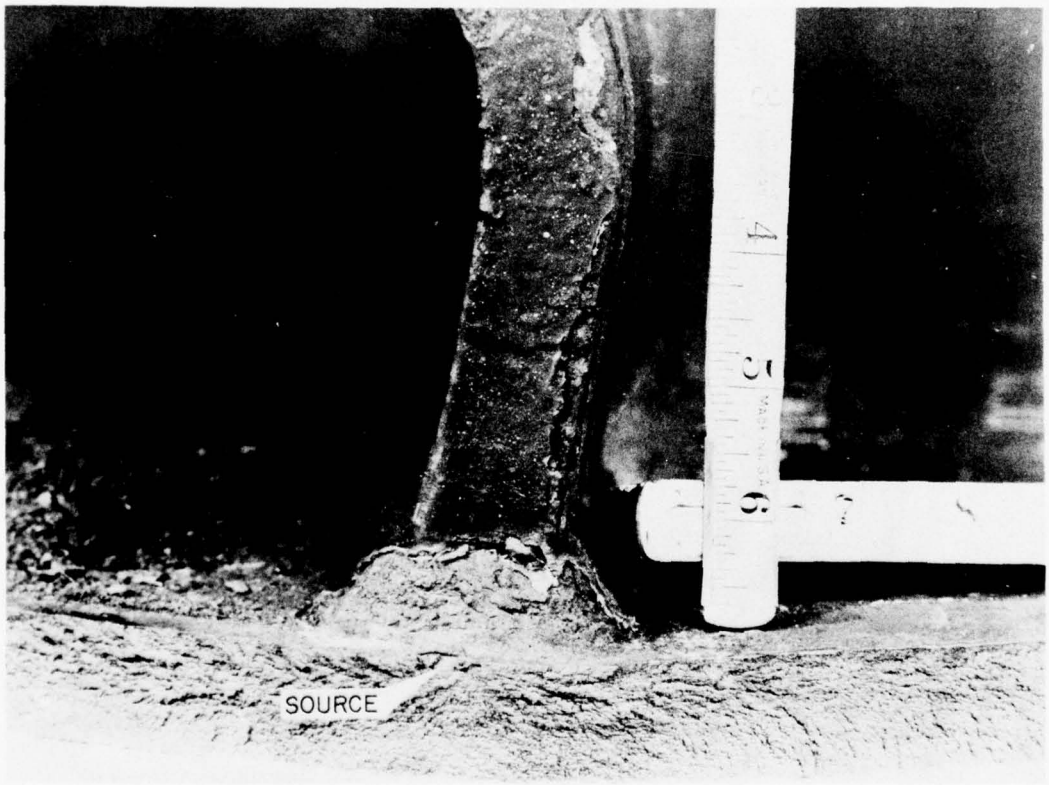

Fig. 86—Arc strike—the source of a ship fracture.

The nominal load stress of the ship structure was of consequence only in that it exceeded 8 ksi (55 MPa) and thus ensured uninterrupted propagation. At the 35°F (2°C) failure temperature, all plates in line would be expected to be below their respective CAT temperatures. In fact, half the population would be below NDT at the failure temperature (see Fig. 78). Because the CAT temperature for low nominal stresses is on the order of 20° to 30°F (12° to 18°C) above the NDT temperature, the probability of intersecting a plate of close-to-arrest properties would be very low, at a service temperature close to the midpoint of the NDT frequency distribution. Thus, the failure conforms to FAD predictions and also to NDT ship plate statistics.

Figure 87 illustrates another example of a small-crack, high-residual-stress fracture initiation below the NDT temperature, the failure of a massive shrink-fit ring for an extrusion press. Thermocouples had been brazed to the ring forging, and this resulted in small, liquid-metal corrosion cracks contained in a small region of high residual stress, due to rapid cooling of the metal at this spot. The fracture occurred spontaneously during cooling of the press from the high extrusion service temperatures. At failure, the ring was below the NDT temperature, and the necessary conditions of a small crack loaded to near-yield stress levels were met. It is important to note that the effective stress acting on the tiny crack in the braze region was the

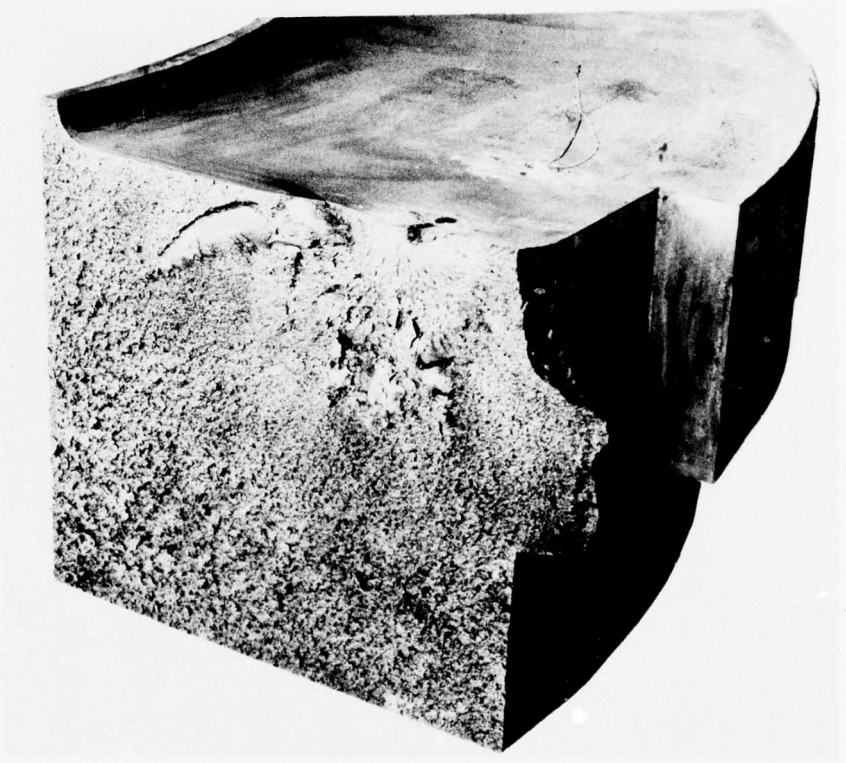

Fig. 87—Fracture of massive ring forging, 12 × 13 in. (300 × 325 mm) in cross-section, caused by tiny cracks subjected to high residual stress. The dark spot in the smooth region of the fracture (upper right corner) marks the position of a thermocouple braze that contained tiny cracks.

residual stress field of this small region. It was not the shrink-fit hoop stress (0.3 σ_{ys}), which represents the load applied to the ring. Again, the load stress was important only in that it ensured continued propagation as the fracture extended outside the localized residual stress field.

The critical importance of highly localized residual stress fields at temperatures below the NDT has been documented by many other failure analyses. In fact, this is the general condition responsible for ship fractures and explains why in-service failure statistics conform so exactly to the NDT temperature distribution of the steels. It should be noted that the existence of long-range weld residual stresses, in addition to highly localized residual stresses, may cause failure below NDT in the *absence* of load stresses. Such events are not uncommon. They have been documented dramatically by the fracture of ships under construction and of new gasoline storage tanks before filling, among other cases. Such spontaneous fractures are not possible above the NDT temperature.

The various temperature regions of the FAD also serve to define the nature of fracture to be expected. Below the NDT temperature the fracture appears flat and is devoid of surface shear lips; the ship fracture of Fig. 63 is representative. For flat-plate structures there is some tendency of the fracture to fork, leading to multiple propagation paths. In pressure vessels, forking is highly developed and leads to the extreme shattering shown in Fig. 88 (top).

The fracture features of the NDT-to-FTE (NDT-to-YC) region are also distinctive. Surface shear lips are easily visible at temperatures 10° to 20°F (5° to 12°C) above the NDT and increase progressively in thickness with increase of temperature to the FTE (YC). At temperatures above the midpoint of the elastic-plastic transition (0.5 YC), there is little tendency to fork, even in pressure vessels. A single straight fracture is the rule.

In the FTE-to-FTP (YC-to-shelf) region, a transition from shear lips to mixed-mode fracture and ultimately to slant fracture takes place. These changes are characteristic of the transition from elastic-plastic to plastic fracture states. For large thickness, slant fracture is not fully developed, because of high plastic constraint, and a partly flat, mixed-mode fracture is retained into the energy-shelf region.

An illustration of the changes in general fracture modes, developed in the NDT-to-shelf range, is provided by the failed pressure vessels in Fig. 88. The vessel at the top failed at the NDT temperature of the steel. The shattering is typical of failures in the NDT-to-0.5 YC (0.5 σ_{ys} CAT) temperature region. The other vessels represent examples from burst tests conducted at higher temperatures. The vessels featured a 20-in. (500 mm) slit, cut part way through the thickness, to simulate a long lamination responsible for the service failure. The high resistance to fracture propagation at temperatures slightly above the FTE (YC) is indicated by the arrested fracture of a hydrotest burst, in the center of Fig. 88.

The vessels were pressurized pneumatically to increase the test severity for bursts at FTP (shelf) temperatures. A number of revealing observations may be made for the FTP burst of Fig. 88 (bottom). Despite the huge size of the flaw, gross plastic bulging of the flaw region was required to force the extension of a ductile tear. This condition represents the application of a very high plastic overload to the flaw-tip region. The slant plastic fracture did not propagate in a straight line because the fracture resistance was too high. The very high energy available, due to the high-pressure gas, resulted in the pushing out of a flap, which remained attached to the vessel.

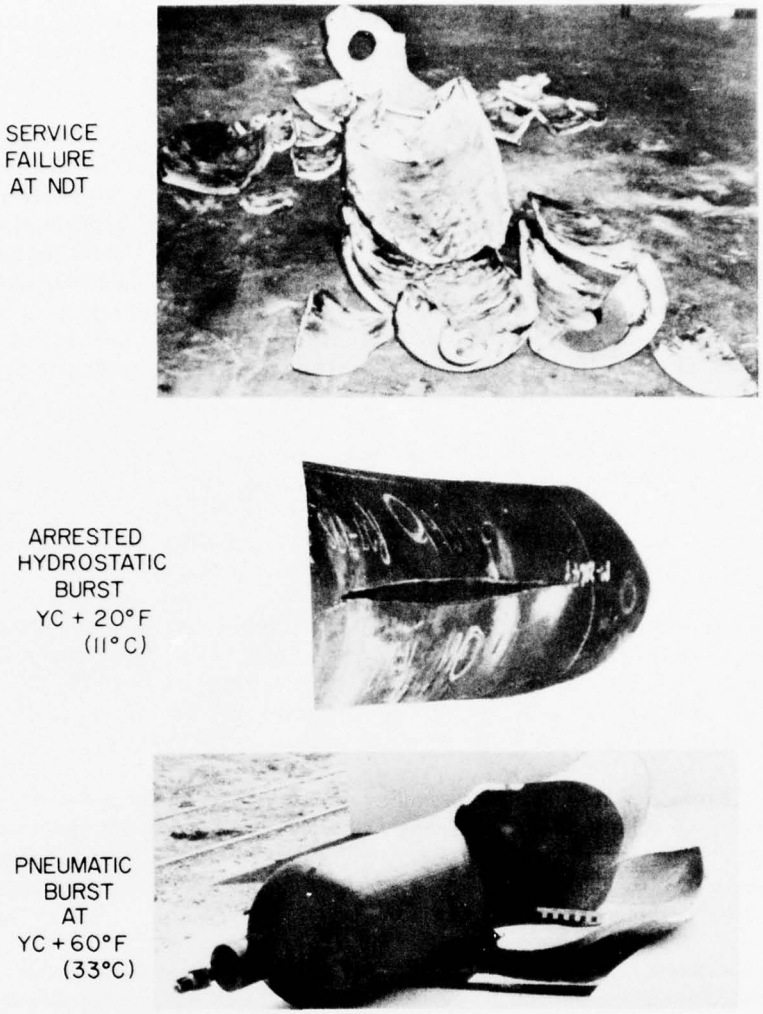

Fig. 88—Fracture modes of pressure vessel bursts, developed in the NDT-to-FTP (shelf) range.

The fracture characteristics of these three vessels, which correspond respectively to the initial, middle, and end points of the FAD, strikingly illustrate the progressive increase in fracture resistance over the temperature range of the diagram.

By 1963, all the information presented up to this point was available. The missing item was the effect of very large section size on the course of the crack-size curves and the CAT curve, at temperatures significantly above the NDT. Section-size effects will be described later in the context of 1968 developments. At this point we summarize the implications of the FAD as it applies to all section sizes at temperatures below the NDT and to section sizes not exceeding 2 to 3 in. (50 to 75 mm), for temperatures significantly above the NDT.

It should be noted that extensive engineering experience in the use of the new rational principles was gained between 1955 and 1965. At the start of this decade, there was total dependence on C_v correlations from ship-fracture studies. At the end of the period, the dominant engineering practices combined DWT characterization, NDT indexing of the CAT curve, and FAD interpretation procedures.

It was generally accepted that the FAD defines four main temperature-index points that serve as analytical design references:

1. NDT—Restricting service temperatures to slightly above the NDT protects against fracture initiation due to small cracks in regions of high local stress.

2. 0.5 σ_{ys} CAT (0.5 YC)—Restricting service temperatures to above this temperature point provides fracture-arrest protection if nominal stresses do not exceed 0.5 σ_{ys}.

3. FTE (YC)—Restricting service temperatures to above the FTE (YC) temperature provides fracture-arrest protection if nominal stresses do not exceed yield level.

4. FTP (shelf)—Restricting service temperatures to above the FTP temperature ensures that only fully ductile fracture is possible.

The degree of protection against fracture initiation and extension increases dramatically in the NDT-to-FTE (YC) regions. The assignment of subdesign points to this narrow temperature range would require very precise definitions of temperature, crack size, and stress. This observation is made to emphasize that finer divisions than the four design points of the FAD are not required for most engineering purposes. The large increases in fracture resistance that are obtained at 30°F (17°C) above the NDT reduce the problem of fracture-safe design to a temperature-reference system of utmost simplicity.

Making an appropriate choice of steel requires information on the expected NDT frequency distribution. Figure 89 presents typical frequency curves for a variety of conventional steels. This figure illustrates the wide range of properties available. It also emphasizes that metallurgical control of steel quality is essential to fracture-safe design. In general, the range of NDT temperatures is about 60°F (30°C), with a high concentration in a 30°F (17°C) span. If yield strength and thickness are specified, information on the average or the highest expected NDT temperature can be obtained from steel producers. Obviously, higher cost goes along with lower NDT temperature. Steels of lower NDT require normalizing, fine-grain practice, alloy additions, and ultimately quenched and tempered (Q&T) heat treatment, as indicated in the figure. Accordingly, design criteria in excess of real requirements should not be used, because they result in specifications of lower NDT and, therefore, increased costs.

The nomenclature of transition to a shelf level of fracture toughness was developed to refer to dynamic fracture conditions. The dynamic transition was defined as the limiting (highest possible) transition-temperature range. The shelf of the dynamic transition marks the attainment of a fully ductile mechanical state, independent of both temperature and strain rate.

For slow loading rates, the shelf condition is temperature-independent but not independent of strain rate. Increased loading rates may result in a dramatic change from static high-shelf ductility to a dynamic state of plane-strain brittle fracture. Thus, the full meaning of a shelf condition does not apply to the slow-loading case.

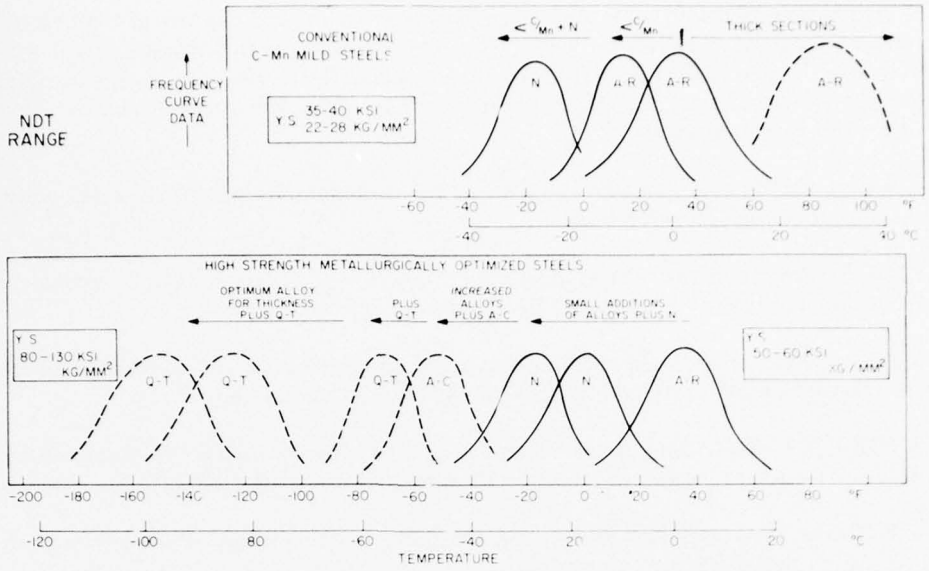

Fig. 89—Representative NDT frequency distribution of commercial structural steels. The various notations describe alloy contents and heat treatment conditions, as follows: <C-Mn, decreased C-to-Mn ratio; A-R, as rolled; N, normalized; A-C, accelerated cooling; and Q-T, quenched and tempered.

EVOLUTION OF DT TEST

The DWT defines the NDT temperature for steels that develop transitions to high-shelf ductility levels, i.e., low and intermediate strength steels. By 1962 it had become apparent that a new test of equally simple characteristics was required for investigating the properties of steels that exhibit low-shelf ductility. These include the high and ultrahigh strength steels, plus steels of intermediate strength levels that feature pronounced weak fracture directions. This need led to the development of a test at first called the Drop Weight Tear Test (DWTT). It used a notched brittle bar welded to a test section. The purpose of the brittle bar was to form a sharp natural crack. The composite specimen was tested with the DWT equipment, and the energy requirements for fracture were noted as a function of increasing temperature or increasing yield strength.

A modified version of an NRL DWTT test, which substituted a *shallow* surface-pressed notch for the brittle bar, was then developed by Battelle Memorial Institute investigators; it is known as the Battelle Drop Weight Tear Test (BDWTT). Until recently the BDWTT temperature-transition curve was plotted as a function of shear fraction (percent of fibrous fracture). This is satisfactory for defining the transition-temperature range from NDT to approximately the FTP for low strength steels. However, the fracture-appearance transition gives no indication of shelf level. The shelf features of strong and pronouncedly weak fracture directions are reported by the test as being exactly the same. Such a test is not appropriate for steels of intermediate or high strength, which may feature large decreases in shelf-level ductility, to a degree that may provide for propagation of fractures at elastic stress levels.

By 1964 the DWTT had been redesigned to eliminate the brittle crack starter bar, and the test was renamed the Dynamic Tear (DT) test. Figure 90 illustrates the features of 0.6-in. (16 mm) and 1.0-in. (25 mm) DT specimens. The original specimens had a deep, sharp crack introduced by an electron-beam weld, embrittled metallurgically by alloying. For example, a titanium wire added to the weld results in a brittle Fe-Ti alloy. The narrow weld is fractured easily in loading and thus provides a reproducible sharp crack. It was then established that equivalent results could be obtained by the use of a deep, sharp crack produced by fatigue or by slitting and then sharpening a deep notch by a pressed knife-edge, as in Fig. 91. DT specimens produced by any of these methods are tested over a range of temperatures, using the pendulum devices shown in Fig. 92. The upswing of the pendulum after the fracture indicates the energy absorbed in the fracture of the standardized test section.

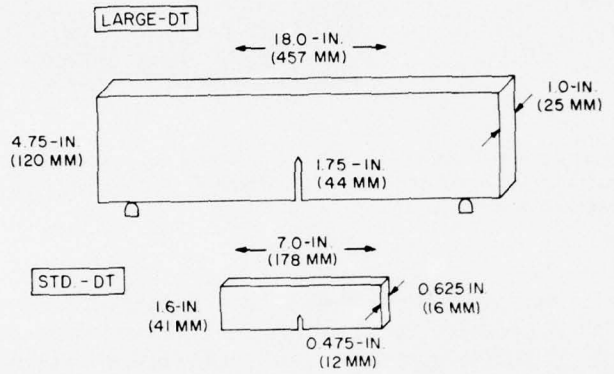

Fig. 90—Large and standard DT test specimens.

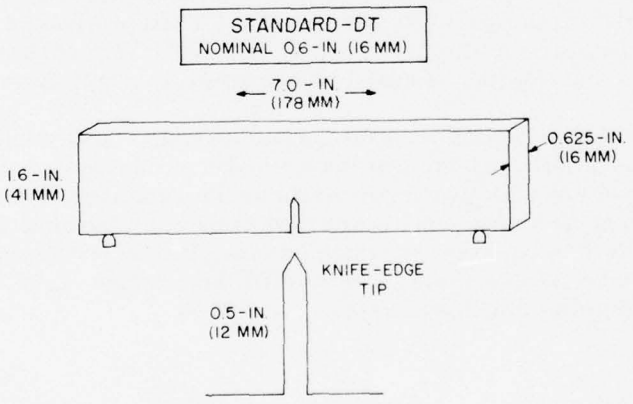

Fig. 91—Standard DT test specimen.

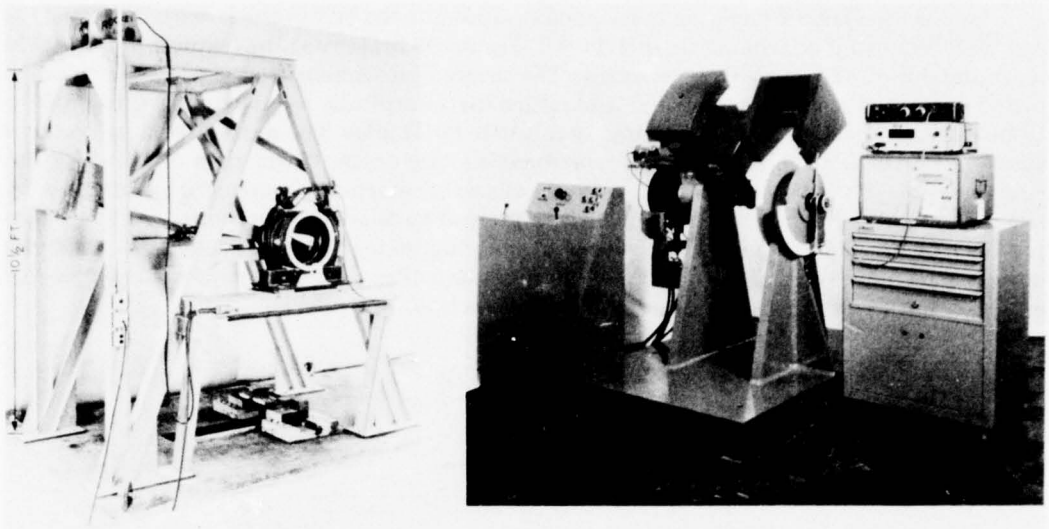

Fig. 92—DT test pendulum machines. The single-pendulum type of 5000 and 10 000 ft-lb (688 and 1375 kg-m) capacity is on the left. The instrumented double-pendulum type, of 2000 ft-lb (275 kg-m) capacity, on the right, allows shockless testing of standard DT specimens.

Figure 93 illustrates typical relationships of the DT energy-transition curve to the NDT, FTE (YC), and FTP (shelf) temperatures. The illustration is for a low strength steel of high-shelf fracture toughness. At the NDT temperature the fracture is brittle and shows a flat, featureless surface devoid of shear lips, exactly similar to the DWT fracture at NDT. A sharp increase in fracture energy is recorded above the NDT temperature, as increased ductility is developed by the metal grains prior to cleavage. The fracture surfaces develop visible shear lips as the NDT temperature is exceeded; these then become progressively thicker as the temperature is increased to FTE (YC) levels. At the shelf temperature, the fracture no longer shows signs of cleavage, but rather is of the ductile-dimple type. The DT test provides an inexpensive way to trace the course of fracture-state transitions from NDT to FTE (YC) and then to shelf. If the shelf is attained with partial retention of mixed-mode fracture, this is clearly evident.

Figure 93 indicates the conditions for the surface-crack fracture initiation of the DWT. Below the NDT, the surface crack initiates fractures when yield stresses are reached. Above the NDT, the surface crack requires plastic stresses for fracture initiation, because the plane-strain constraint capacity of the surface crack is exceeded. Conversely, the constraint capacity for the DT test is defined by the section size. For a small standardized DT test specimen like that shown in Fig. 91, constraint relaxation begins near the NDT temperature, as indicated by the elastic-plastic transition features drawn schematically in Fig. 93.

SECTION-SIZE EFFECTS

The main scientific issue between 1964 and 1968 was the effect of section size on the transition-temperature range. A fundamental question about plane-strain fracture tests and

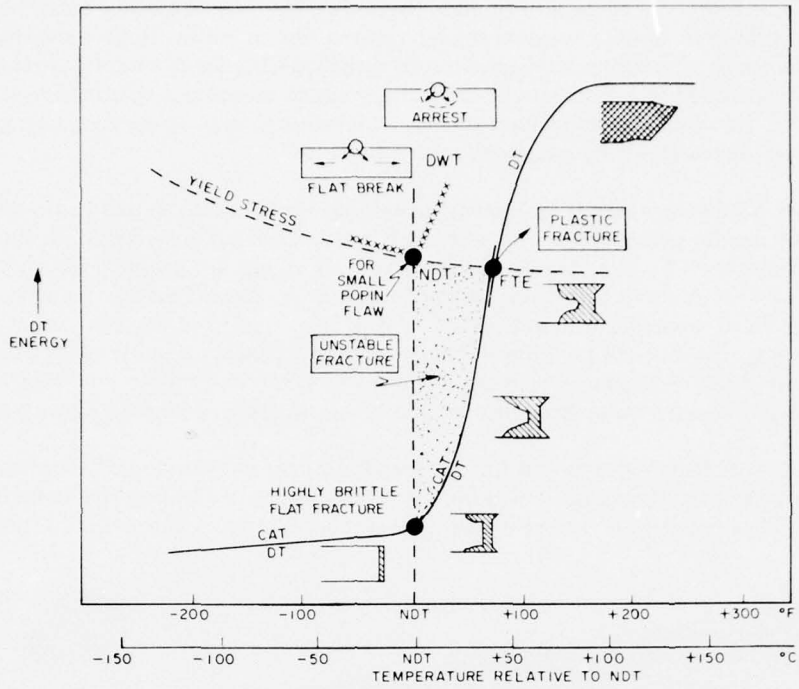

Fig. 93—Correspondence between DT, DWT, and Robertson CAT tests. The transition from plane-strain to plastic fracture properties is indicated by the change in fracture mode of the DT test and by the rise of the CAT curve. The NDT references the temperature of initial rise from plane-strain to elastic-plastic fracture states.

linear-elastic fracture mechanics theory was whether the temperature-induced transition from plane-strain to elastic-plastic fracture could be suppressed by very thick sections.

Constraint effects of section size had been explored extensively since the 1940s. By the mid-1950s it had been established that section-size effects result in large shifts of the transition range to lower temperatures as section size is decreased below 0.5 in. (12.5 mm). The effects of increasing section size to 2 in. (50 mm) are less pronounced. The amount of temperature shift Δt per unit thickness, as deduced from specific indices of the transition temperature (such as CAT for 0.5 σ_{ys}), decreases as thickness increases. This suggested an approach to saturation (relatively small further increases are possible) for section sizes greatly in excess of 3 in. (75 mm).

By 1964, theoretical fracture mechanics concepts of constraint effects predicted that increasing mechanical constraint would overcome increasing microfracture ductility. Accordingly, it was assumed that large increases in section size would *eliminate* the sharp rise in fracture toughness in the transition-temperature range. With the elimination of the transition features, the metal was expected to retain brittle plane-strain fracture properties to temperatures far above the NDT.

This assumption caused great concern with respect to reactor pressure vessels of thick wall sections, because it implied that brittle fracture could take place at service temperatures near

230-362 O - 77 - 9

500°F (260°C). In a broader context, it implied that all steels of thick section would be mechanically brittle regardless of metallurgical considerations. These implications were unacceptable because of basic microfracture considerations (discussed in Chapter 2) which state that fracture toughness is controlled at microscale. If true, the fracture mechanics assumption would have negated all of the carefully developed physical metallurgy principles that had guided the evolution of improved steels by control of microstructure.

The basic issues were settled in 1969 by investigations involving 6- and 12-in. (150 and 300 mm) plates of reactor-grade steels of the A533-B type. Westinghouse Research Laboratories studies by Wessel used K_{Ic} tests of full-size specimens. NRL studies used DT tests of specimens ranging from 0.6 in. (16 mm) to full size, as shown in Fig. 94. The DT energy-transition curve is shown in Fig. 95 in comparison with the K_{Ic} curve. It is evident that the fracture-state transitions due to temperature were not eliminated by increases in section size. Figure 96 illustrates the high plastic ductility of the DT specimen at 215°F (102°C). The plastic appearance indicates that propagation of a fracture through a structure would require loading above yield levels.

The transition features of the 0.6-in. (16 mm) DT test are noted in Fig. 97. The main effect of increasing section size is an expansion of the transition-temperature range by about 60° to 80°F (33° to 45°C). The transition of the thick plates is completed in the range of NDT + 180° to 220°F

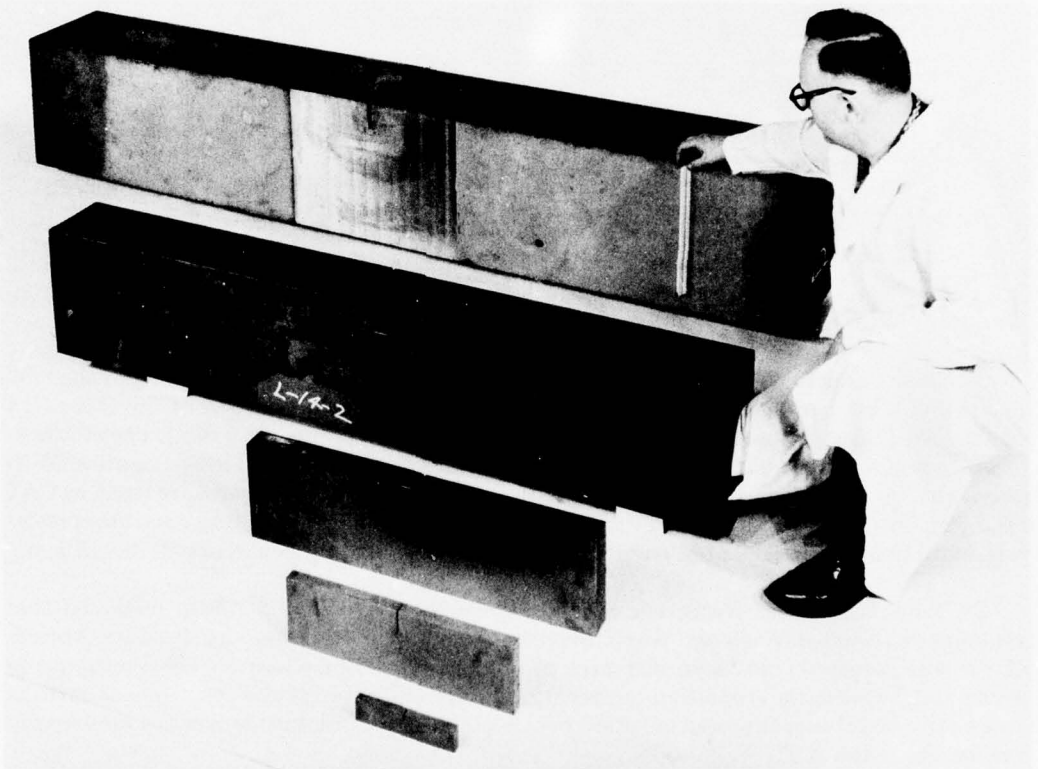

Fig. 94—Range of DT test specimens used for size-effect studies. All specimens have the brittle electron-beam weld crack starter.

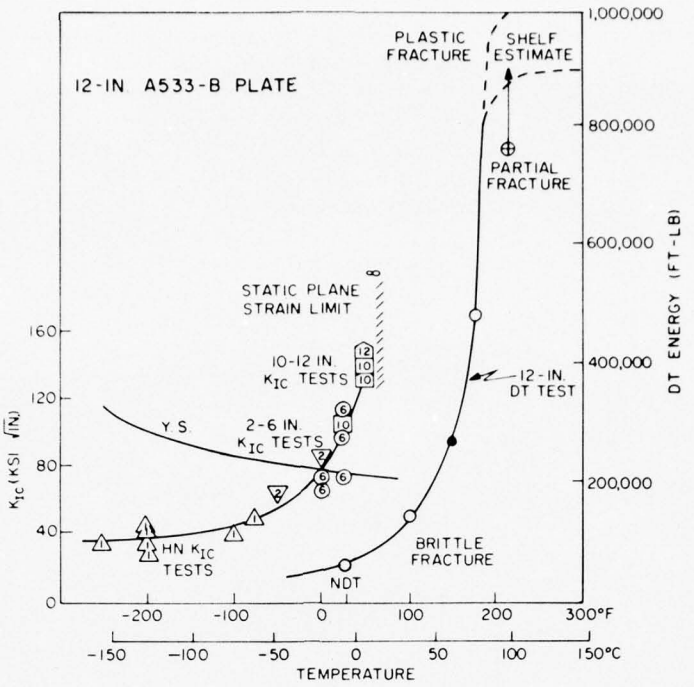

Fig. 95—Temperature transition of A533-B steel plate, as measured at full thickness by the 12-in. (300 mm) DT test. Results of K_{Ic} tests (Wessel) for the thick plate are plotted with notations of the specimen sizes required for the tests. The steepness of the K_{Ic} curve near NDT indicates a very sharp plane-strain transition.

(NDT + 100° to 120°C). The transition in both the thin- and thick-section DT test specimens starts at the NDT temperature. The effect of increased section size, then, is to expand (not shift) the transition-temperature range. The expansion of this interval for 6-in. (150 mm) specimens is slightly less than for 12-in (300 mm) ones. These results conform to expectations of saturation effects.

The K_{Ic} plot of Fig. 95 illustrates the increase in section size that was needed to follow the K_{Ic} plane-strain transition at temperatures close to the NDT temperature. The K_{Id} curve was estimated to develop a similar dynamic plane-strain transition in the toe region of the DT test energy curve. This estimate was based on the reasonable assumption that the K_{Id} curve should be limited to temperatures below the temperature midpoint of the DT test transition curve for thick sections. The DT test specimens exhibit pronounced through-thickness contraction and notch blunting above this temperature. The sequence of dynamic fracture events associated with all DT energy-transition curves is indicated by the photographs of Fig. 97 (for the small DT specimen). The sequence is common to all DT test transition curves that culminate at high levels of shelf fracture energy.

The investigations were completed in 1969-1970 by K_{Id} tests of very thick section (to 8 in.; 200 mm). The summary data presented in Fig. 41 confirmed predictions of the location of the K_{Id} plane-strain transition relative to the DT curve of Fig. 95.

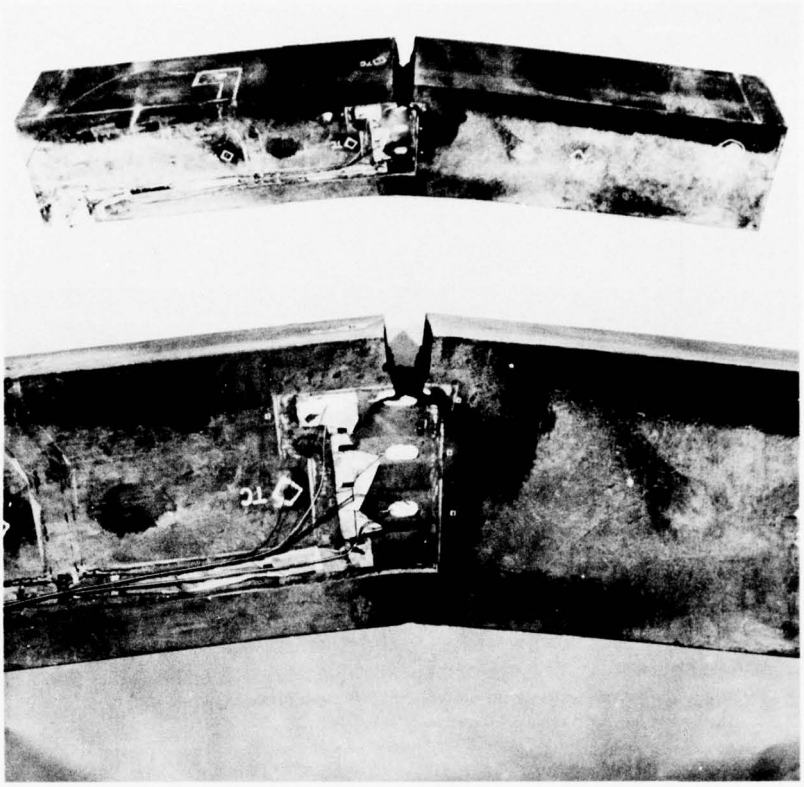

Fig. 96—Highly ductile performance of the 12-in. (300 mm) DT test specimen at 215°F (95°C). The size of the plastic enclave is indicated by the grossly dimpled region between the two tears that extend from the deformed crack root. The 750 000 ft-lb (104 000 kg-m) capacity of the equipment was insufficient to cause full fracture in this ductile mode.

The engineering implications of these studies are of major significance, as follows:

1. Below the NDT temperature, dynamic plane-strain fracture toughness is very low. The critical crack sizes at points of geometric changes that involve yield-level stresses are too small to be detected by inspection. While small K_{Id} test specimens may be used, this expensive test procedure yields little practical gain.

2. Huge K_{Ic} and K_{Id} specimens are required to plot the full temperature course of the static and dynamic plane-strain transitions. The costs of such tests are too high for most routine engineering purposes. Small specimens track the K_{Ic} and K_{Id} transition only to NDT or lower temperatures.

EXPANDED VERSION OF FAD

The information developed in the constraint-effects studies provided the basis for an expanded version of the FAD (Fig. 98). Three main points should be noted:

1. Section size has no effect on the small-crack curve of the FAD. The instability conditions for small cracks are controlled by the surface crack size, not the section size. For example, a very small surface crack does not recognize that it is located in a thin or thick section, if both are semi-infinite with respect to the crack size.

2. The instabilities of very large cracks are influenced by section size, because increasing size provides additional constraint for the large cracks. Thus, there is a moderate shift of the large-crack transition curves to higher temperatures, as indicated by the expanded FAD.

3. The rise of the CAT curves for thin and thick sections starts commonly at the NDT temperature. However, the rise is more gradual for thick sections because of the shift of the FTE (YC) to a higher relative temperature.

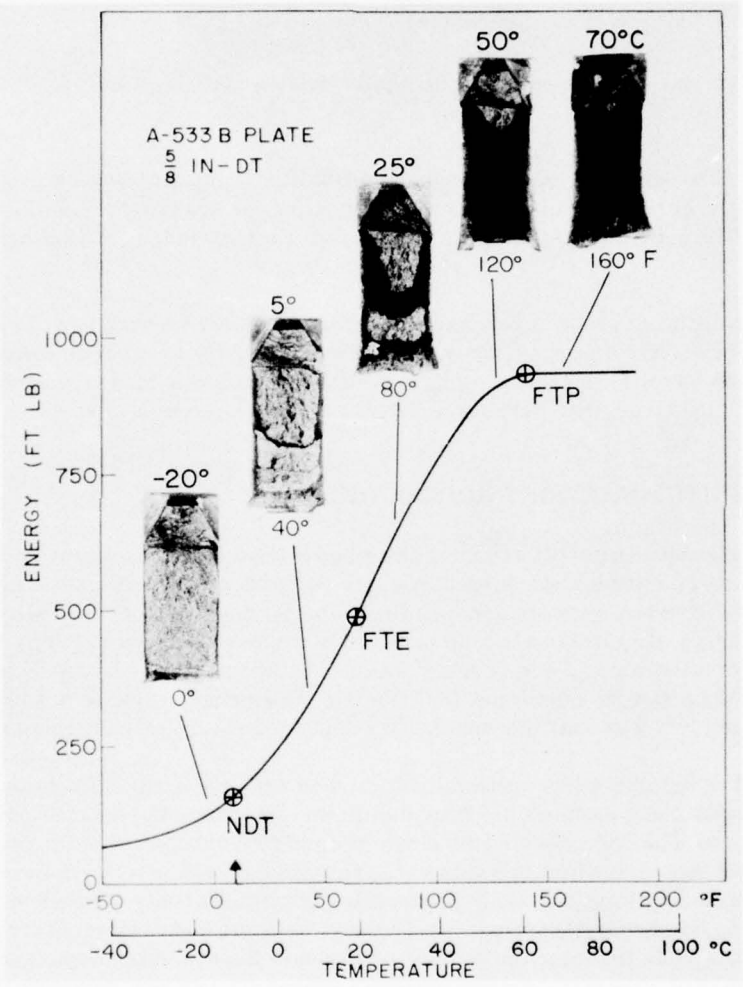

Fig. 97—Temperature transition of 0.6-in. (16 mm) DT test of the 12-in. (300 mm) A533-B steel plate. The NDT was indicated by the DWT to be 10° to 20°F (−21° to −7°C).

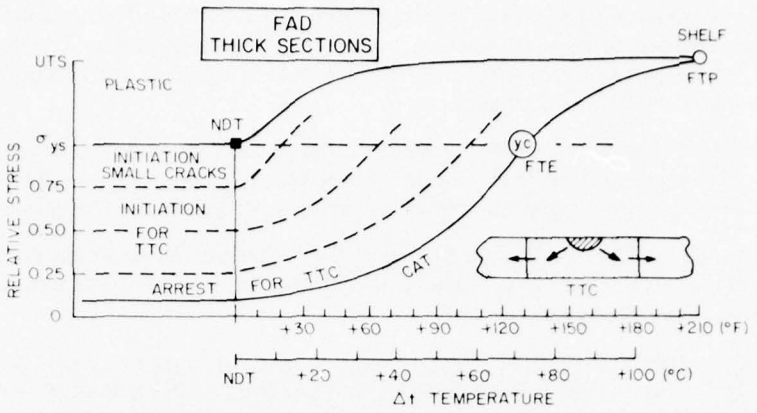

Fig. 98—FAD expansion to include the effects of very large section size.

The degree to which the crack-size curves are shifted to higher temperatures may be noted by comparing the Δt temperature at which the curves for various sizes intersect a specified level of stress. It will be apparent that all shifts are less than the shift in the CAT for the specified level of stress.

If uncertainties of stress levels and temperature are considered, it will be evident that adjustments of the FAD (due to section size) in excess of 30°F (17°C) are required only for special situations. These involve very large cracks in very thick sections loaded to relatively high levels of stress, i.e., huge structures, very large defects, and high stress levels.

DETERMINISTIC ANALYSIS PROCEDURES

An important feature of the advances described in the foregoing sections is the emphasis on the development of deterministic procedures that do not depend on opinion. The early studies (1945 to 1955) were a search for general directions of investigation. At first, the empirical correlations of C_v test properties to ship performance appeared promising, but it soon became evident that for scientific and engineering reasons this approach was wrong. Scientifically, the use of correlations was an admission that fundamental principles were not understood. The engineering problem was that the correlations depended excessively on opinion.

Rational design procedures generally depend on self-consistent calculations or graphical analysis methods. Such methods are fully definitive (deterministic) because opinion does not enter in their use. The only role of opinion is in the initial development of the procedure and in decisions on the degree to which it is subject to evaluation and technically defensible proof. The methods are tested by repeated use in engineering practice. If there are deficiencies, they are made evident by fixed analysis procedures. This was the route to development of classical design principles. Since 1955, the same route has been taken in the evolution of engineering fracture-control principles.

The following examples of test and analysis methods provide unequivocal design-criteria information. The procedure decides the answer that is obtained; case-by-case interpretation is

not necessary, as it is for the case of correlation. Thus, the methods are self-consistent for all determinations, or "deterministic."

Robertson Test CAT—The fracture-extension stress is related to specific design stresses and service temperatures. Definitions of propagation or arrest conditions are deterministic; they have been verified and are highly reliable for design use.

NDT Temperature for CAT Indexing—The benefits of CAT analysis are made available by standardized, low-cost fracture-test procedures. Statistical details of metal property variance can be included in the analysis, due to the ease with which such surveys can be made by the DWT.

FAD—This analytic method combines the use of CAT principles with those of dynamic fracture initiation due to small cracks. Because they are NDT-indexed and include statistical considerations, the procedures are entirely self-consistent.

Characteristic K_{Id} Curve—As described in Chapter 4, NDT-indexed K_{Id} curves may be converted analytically to define L and YC reference temperatures. Fracture-extension stress diagrams and surface-crack initiation diagrams are developed by formalized, fully deterministic methods.

DT Test Indexing of L and YC—As described in Chapter 4, section-size effects are analyzed in terms of fracture-state transitions. Applicable fracture-extension stress and surface-crack initiation diagrams may then be developed from the YC index to the temperature scale. Dynamic Tear specimens of small, standardized dimensions provide statistical data analyzable in terms of section sizes of interest. All steps are self-consistent in the context of basic principles.

The true mark of the dramatic advances made between 1955 and 1975 is the development of fracture-control plans that are not based primarily on opinion. Certification by analysis for the fracture-control plans also agrees with basic scientific principles. In fact, the analytical methods could not have survived the test of engineering application if they were not fundamentally rational.

The 0.5 YC (0.5 σ_{ys} CAT) criterion has been used consistently since 1955 to provide high assurance of structural reliability for temperature-transition problems. Engineering experience shows that the adoption of any criterion that permits use of low elastic-plastic or plane-strain levels provides insignificant protection.

Convincing certification of structural reliability can be made only if a large fraction of the steel population meets 0.5 YC properties at a conservatively defined lowest temperature of service. In brief, the certification must be statistically sound and must conform to fracture principles. In this respect, the conventional methods of reference to the fracture properties of standard-grade steels are both archaic and useless for design purposes. (See Chapter 12.) The improvements described in Chapter 4 would rationalize the reference procedures. Recent change in emphasis for reference of standard-grade steels, from C_v energy to C_v lateral expansion values, has no design merit. Figure 68 provides 1955 documentation of the fact that energy and expansion curves are strictly related, and not independent. This was well established by the mid-1950s but seems to have been forgotten. That the C_v test is not rational with respect to fracture mechanics principles is evident from Chapter 3 discussion of constraint reference requirements. The glaring failure of C_v definitions of fracture properties has been demonstrated

repeatedly. Recent documentation is provided in Fig. 178 (Chapter 12). There is no need for additional emphasis of this point; modernization of reference systems for fracture properties of standard-grade steels is overdue.

It should not be assumed that the standard-grade steels are not metallurgically rational because of the reference tables' deficiencies in rational characterization. As illustrated by Fig. 89, the steels provide a wide range of options for appropriate criteria. The problem is an imperfect reference system, which precludes direct interpretation of statistical properties in the context of modern principles. A description of the standard grade steels is given in Appendix D.

CHAPTER 7

Fracture-Control Principles: Strength-Transition Problems

DEVELOPMENTS IN RETROSPECT

As explained in prior discussions of mechanical and metallurgical principles, rational characterization of fracture properties is applicable to all metal systems. Design criteria have the same meanings for all systems; the only differences are in procedures for reference to temperature or strength scales to which fracture-state transitions of microfracture origin are indexed. This has become evident during the course of experience with temperature- and strength-induced transitions.

Developments in the solution of stength-transition problems can be reviewed only by referring to the present-day RAD format. The literature of the development period is difficult to follow because most publications were restricted to specific metals and strength levels. It is as if the RAD were cut into small parts, presented randomly, like a jigsaw puzzle. The presentations that follow describe the various apparently separate contributions to knowledge of the strength transitions of weldable steels.

The first rudimentary organization of information on the transitional features of high strength metals was developed for steels between 1960 and 1964. At the end of this period, a sharp transition in fracture properties, indicated by the present-day RAD plot of Fig. 99, was evident. (The RAD, of course, did not exist until 1968.)

The steels available in 1964 are represented by the two shaded zones of Fig. 99, plus the connecting zone indicated as "low-alloy modified." In the context of the RAD presentations, the fracture transition from low to high strength levels was exceedingly abrupt. Moreover, metals in the intermediate strength range were not used at the time for welding applications. Accordingly, in 1964 structural steels were separated into two general families—those with high fracture toughness at low strength levels and those with highly brittle properties at high strength levels.

The bimodal view of the strength transition was modified to the trend-band concept during the 1964-1968 period, as new steels were developed. The developments are indicated by the arrows pointing into the open region of the RAD, in the direction of the technological-limit curve for fracture properties (TL-F). Since 1968, the TL-F boundary has been relatively static.

New steels to complete the RAD zones were developed very quickly to meet the demand for high-performance military and aerospace structures. The development was limited by metallurgical factors related to the strength transition. Its achievement in the brief period of 4 years was possible only because of a new and substantial understanding of the connection between rational fracture-property characterization procedures and rational principles of metal improvement. RAD plots, developed by analytical steps, paced these developments and guided

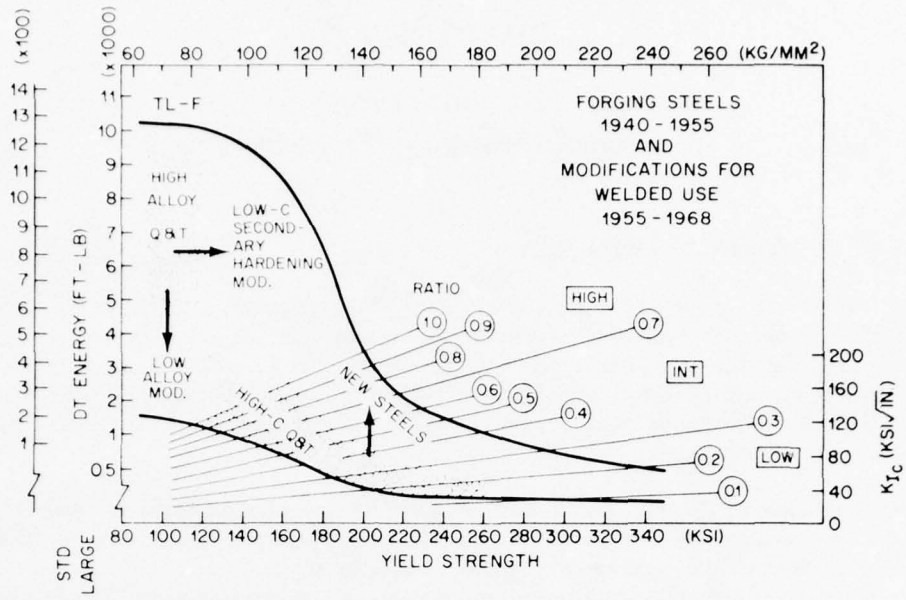

Fig. 99—RAD zoning of steels available prior to 1955 and those developed (arrows) between 1955 and 1968.

research. It is important to record that the completion of the RAD zones indicated in Figs. 100 and 101 was an organized team effort, deliberately focused on intermediate- and high-corridor fracture properties.

The scientific and engineering knowledge that provided the base for the advances of the mid-1960s was the result of the prior decade's research. The next decade fostered expertise in using the new principles. In all, the 1955-1975 period provided the following simultaneous new developments:

Rational fracture tests
Improved metal systems
Rational connection of mechanical and metallurgical factors
Novel high-performance, structural designs using the new principles
Procedures for certification of structures by analysis.

The preceding short history of the technological advances is preparation for the more detailed explanation to follow. However, a proper chronological account of the developments must mention the separation of engineering interest that persisted until about 1972. Until then, engineering groups and researchers specialized in studies of low, intermediate, or high ranges of the strength transition. The scientific and engineering literature appeared contradictory because of this specialization. In fact, unification was attained only as the interests of those concerned with low strength levels shifted to higher levels and as those concerned with higher levels shifted their attention to lower levels. The intermediate strength level provided a common ground.

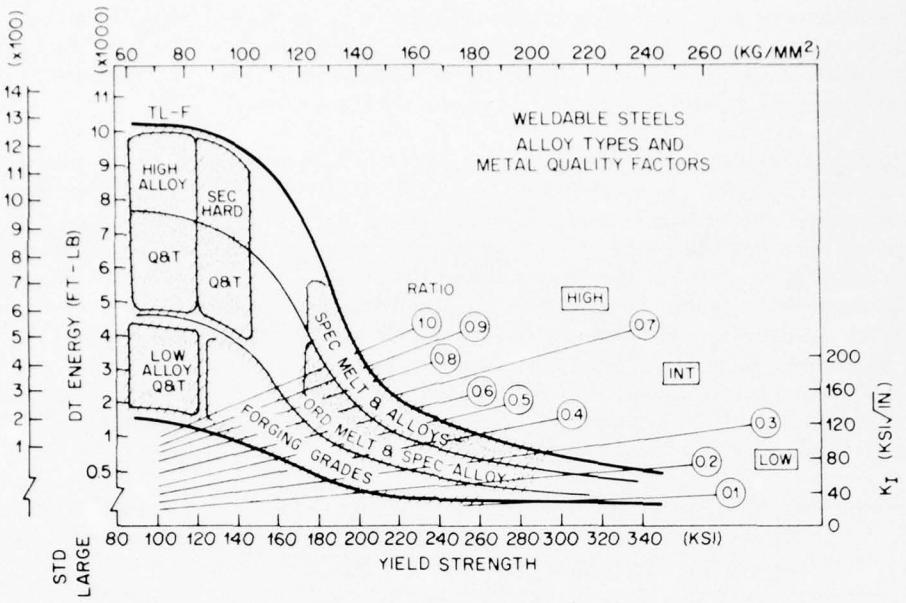

Fig. 100—RAD zoning of the new weldable steels, compared to older high strength forging grades.

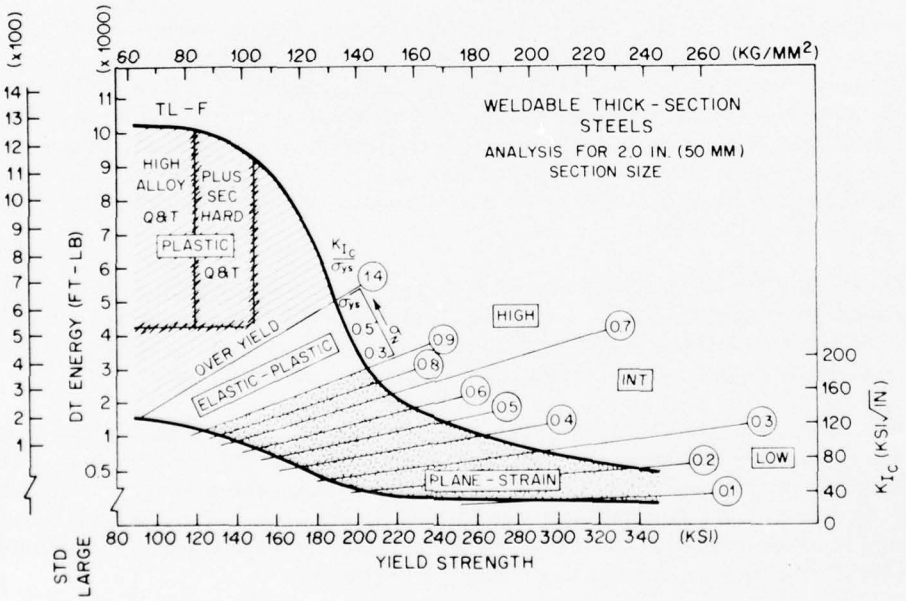

Fig. 101—RAD definition of plastic fracture properties for thick-section weldable steels.

The development of new steels to cover the entire range of the strength transition, with particular attention to weldability, was vital to the technological advances of the 1955-1970 period (Chapter 8). The new steels that completed the RAD were all developed for welded use. A brief account of the primary attention to welding is thus essential.

The high strength steels available before 1955 were developed for use as forgings and are known as forging grades. Figure 99 indicates the RAD locations of these steels. The high-alloy, quenched and tempered (Q&T) steels originated from high-quality forged armor steels. The development of armor steel (1910-1940) was directed by proof-test criteria for projectile and explosion-blast protection. Severe proof testing led to the use of exceptionally high-quality melting practices, alloy contents, and heat treatment. These practices were retained when armor steels were modified for welded use between 1954 and 1956. This modification is known as HY-80. The main compositional adjustment was decreasing carbon content from 0.30% to 0.18%. The HY-80 steel has the highest RAD position for its strength level because of the retention of the best possible metallurgical quality factors. It is now produced commercially (ASTM 543) at the intermediate RAD corridor position.

During the 1955-1962 period, other commercial modifications of armor steels emphasized low cost. These steels are indicated as "low-alloy modified" in Fig. 99. The low corridor position reflects the use of ordinary melting practices and limited alloy contents.

"Secondary-hardening" quenched and tempered steels represent another modification of armor steels (1963-1968), by addition of alloy elements that cause special hardening effects during tempering. The result is a modest increase in strength. Retention of high corridor position was ensured by more stringent control of metallurgical quality, beyond the limits of armor steels. For example, the permissible levels of sulfur and phosphorus impurities are lower than for HY-80 or armor steels.

The high strength forging grades (indicated as High-C, Q&T) were developed (1910-1940) for machinery applications, bolting and so on. They were used in aircraft components, mainly as unit forgings or bolted assemblies. Their very high carbon content (0.35% to 0.50%) precluded use in the as-welded condition. Fusion welding of these steels produces weld zones of very high hardness and therefore extreme brittleness. In general, welding of these steels must be followed by a full cycle of heat treatment. The low position in the RAD of the high-carbon grades is the result of excessive carbide particles in the microstructure. These steels cannot be elevated to higher positions in the RAD.

Use of high-carbon forging grades in rocket cases and aircraft (1958-1965) resulted in serious reliability problems (to be described). Eventually it became clear that entirely new steels were required for the higher strength range. The new weldable grades emerged during the period 1964-1968. Figure 100 is a present-day summary of weldable steels.

Developments in the low range of the strength transition were dictated by structural requirements entirely different from those of the high range. Moreover, the section sizes for the low strength levels involved thick plates and forgings as compared to sheets or thin plates of high strength metals. A compartmentalization of engineering experience developed because the low strength metals exhibited plastic fracture properties in thick sections and the high strength metals had plane-strain properties in relatively thin sections.

The development of generalized engineering principles effectively integrated experience with different combinations of strength level, section size, fracture-state properties, and functional requirements.

The most important developments must be described in terms of this experience, as follows:

- The low range of the strength transition (ships, submarines, and general structures)
- The ultrahigh range of the strength transition (aerospace structures)
- The intermediate range of the strength transition (aircraft and fast craft).

The object is to document by engineering experience the rationality of present principles over the strength-transition range.

LOW RANGE OF STRENGTH TRANSITION

The engineering teams that developed new technological capabilities for the low range of the strength transition had experience in establishing structural integrity principles for large, monolithic, welded structures. This background included experience with the ship fractures of 1942-1952 and specialized experience with combat ships and submarines.

Military service requirements directed attention to achieving plastic fracture properties for both base metal and weldments of welded structures. The arrest principle was understood by 1953, the time of the initial development work on the HY-80 steel weldment system. In brief, it was known that high resistance to plastic fracture required the use of steels that were "on-shelf" at service temperatures. This meant that the temperature transition to maximum fracture resistance must be completed (on-shelf) at service temperatures. The criteria were called at the time (1953-1956) on-shelf or high-shelf properties.

This was the first time a steel was developed according to design criteria tailored to specific functional requirements. It was also the first case in which weldability experts participated in a steel's development. Their prior experience included the first attempts to weld armor steels (1940-1952). Thus, it was well known that the available steels required modification for weldability. Metallurgical considerations dictated the first step of decreasing the carbon content of armor steels to prevent cracking in the heat-affected zone.

This brought into focus the remaining problems:

Development of entirely new, high-strength ferritic electrodes with high fracture properties and capabilities for highly restrained welding of thick sections (Chapter 8).

Development of structural prototype tests for confirming resistance to plastic fracture extension in the heat-affected zone and weld region.

The explosion crack starter test, previously used for ship steel studies (Chapter 6), was modified by placing the crack starter (brittle) weld of the DWT-NDT specimen directly on the

weld region. This introduced an initial sharp crack in the weld region to reveal the effect of welding procedures on the structural performance of the weldment.

The use of arrest principles and metallurgical considerations directed attention to section-size effects. At the time (1953-1956), the purely mechanical effects of constraint were not understood, but it was known that increasing section size could change cooling rates and produce poor microstructures. For example, the low-alloy modifications of armor steels (Fig. 99) have alloy contents generally adequate to produce plastic fracture properties at 1.0-in. (25 mm) section size. However, increasing section size to over 1.5 in. (37 mm) results in extreme brittleness at temperatures below 32°F (0°C).

The explosion crack starter tests were conducted at the section sizes of interest (1 to 3 in.; 25 to 75 mm). They therefore correctly defined the fracture-state properties of interest. The desired criteria of arrest properties for plastic overload conditions were documented for the plate, heat-affected zone, and weld. Most important, the HY-80 weldment system was compared rationally with other candidates. Those rejected for not attaining the desired reference criteria included the following:

Normalized C-Mn-V steels—brittle fracture of the plate at section sizes of interest.

The low-alloy modified steel (Fig. 99)—brittle or elastic-plastic levels of fracture extension resistance for sections thicker than 1.5 in. (37 mm), in plate and heat-affected zone.

Lower alloy modification of HY-80—brittle fracture of the plate at large section sizes.

Development was conducted under crash conditions, largely in 1955-1956. At the end of this period a commitment was made to fabricate immediately the new nuclear submarines in serial production. Accepting rational fracture criteria as justification for selecting HY-80 rather than another candidate was a monumental decision. An incorrect decision would have subjected at least 50 submarines to relatively brittle weldments before it could be corrected.

The rationale for assuming direct correspondence of laboratory prototype tests with structural performance remains valid. Because the fracture state is unique to the section size and steel of interest, it must apply equally to the fracture tests and to fracture extension in structures. This was well established among fracture specialists in the mid-1950s. However, the generality of the principle as a design criterion was accepted only after confirmation by structural performance at full scale. Confirmation for the case of submarines was established by full-scale explosion tests of fatigue-precracked submarine structures almost a decade after the crucial 1956 decision.

Between 1955 and 1960 the fundamental principles of fracture mechanics were established. Additional confirmation was gained largely from unfortunate experience with structural failures at the high end of the strength transition. At the low end, ductile fractures in laboratory specimens were matched with those in structures. Brittle fractures were similarly matched at the high end of the transition. These correlations were essential proof of the generalized principles.

HIGH RANGE OF STRENGTH TRANSITION

The engineering teams that developed the new capabilities for design and welding of ultrahigh strength metals had no prior experience with welded structures. Their experience in the aircraft field was based on riveted and bolted construction. The changes from riveted ships to welded ships and from riveted and bolted aircraft to welded rocket cases are strikingly parallel. In each case, welded monolithic construction was an unforgiving test of structural integrity principles.

Figure 102 illustrates the all-too-frequent results of hydrotesting rocket cases (Polaris and other types) during 1957-1960. The only ultrahigh strength steels available at the time were the high-carbon, quenched and tempered forging grades noted in Fig. 99. The strength range was first selected according to the principles of highest attainable yield strength (240 to 280 ksi; 1655 to 1931 MPa). No consideration was given at first to fracture properties.

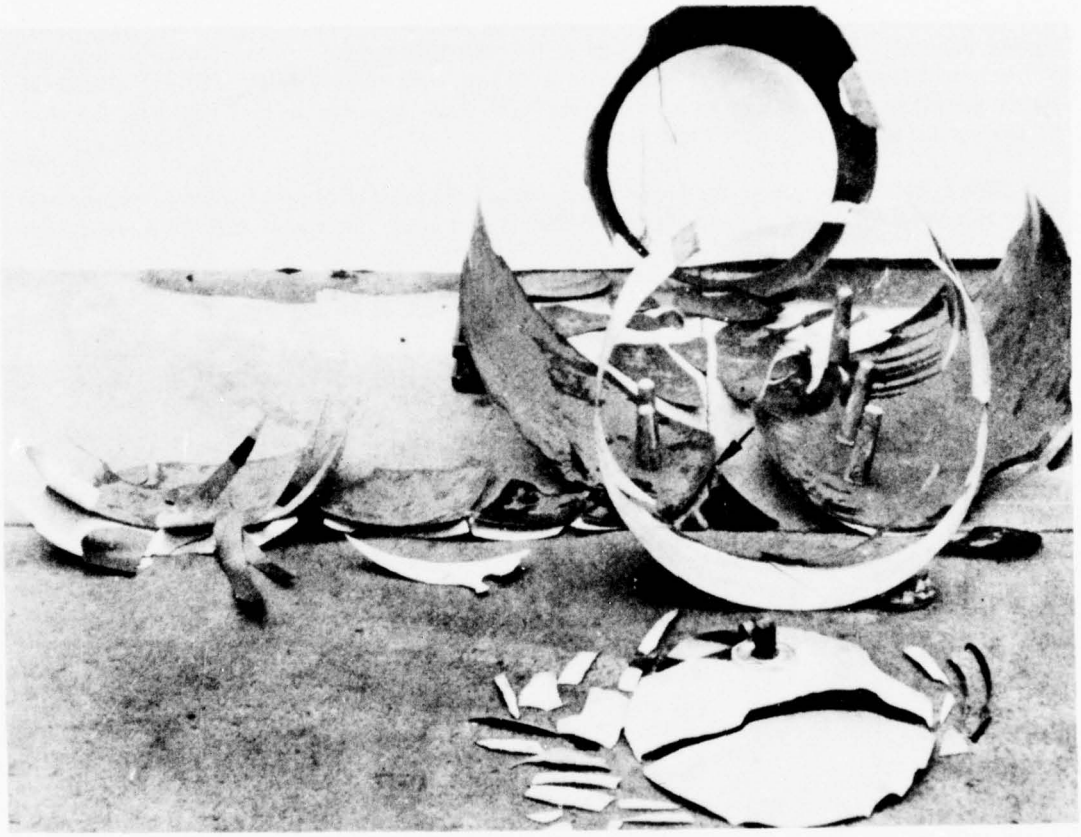

Fig. 102—Typical failure of rocket cases during hydrotesting.

Figure 103 is a retrospective RAD display of the problem. Fracture properties of these steels are in the low-ratio range (plane strain) for section sizes of approximately 0.2 in. (5 mm). The critical crack sizes for high hoop stresses (service and hydrotesting) may be deduced from Fig. 56. Microscopic examination was necessary to reveal the nature of very small defects that initiated the failures.

Experience disclosed that failure rates could be reduced by decreasing the strength range to 190-220 ksi (1310 to 1517 MPa). This elevates the fracture state for this section size to the elastic-plastic range (Fig. 103). However, part of the steel population remained in the plane-strain range. Another empirical solution was the metallurgical trick of decarburizing the surface. In effect, this decreased the strength level of the surface layer to 140 to 180 ksi (965 to 1241 MPa). By these methods, the hydrostatic test failure rates were reduced but not eliminated. The reason is stress-corrosion cracking (SCC) due to hydrotesting with water (Chapter 9). It was necessary to hydrotest with oil to eliminate fracture initiation by cracks due to stress-corrosion cracking.

Similar aerospace experience was involved with high strength titanium tanks for a variety of fluids. For example, stress-corrosion cracking by methanol and nitrogen tetroxide (fuels) caused dramatic failures of Apollo tankage in 1963-1964, aided by the low-ratio fracture properties of the titanium alloys used. The solutions were to modify the fuels to eliminate stress-corrosion cracking and to decrease strength levels to provide elastic-plastic fracture properties for the section sizes involved.

The general principle evolved from this experience is that the plane-strain metals must not be used in relatively thin section sizes. The reason is that thin sections limit the plane-strain

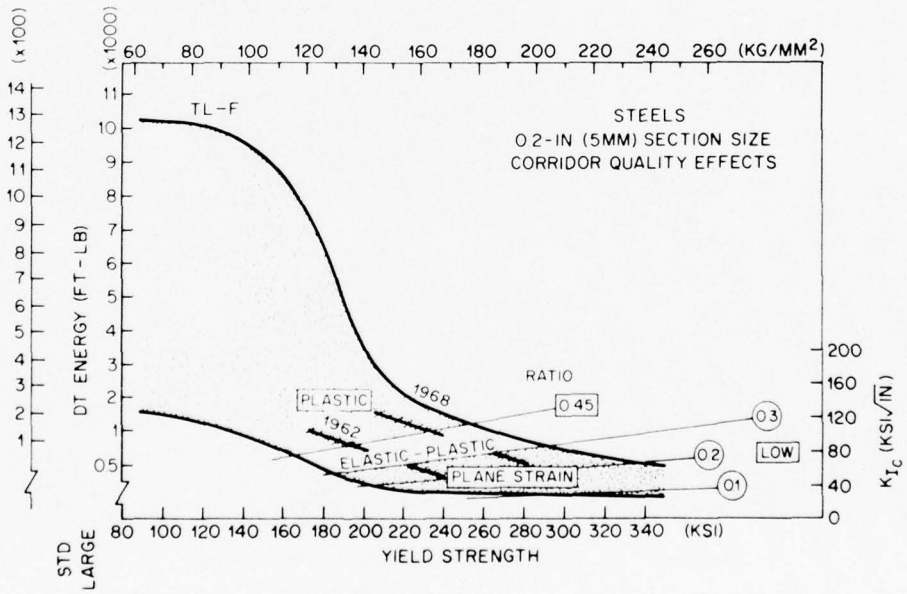

Fig. 103—Analysis of rocket case experience in terms of low-corridor steels used prior to 1962.

state to very low ratio values. The critical crack sizes that correspond to these low ratios are beyond reasonable detectability or control (see Fig. 56).

Accordingly, it is necessary to use metals of the highest possible corridor quality and to place a maximum on yield strength, so that high-level elastic-plastic properties can be retained.

The analyses in Appendix C provide the proper guides in reference to these principles. Polaris-type rocket cases could be fabricated, according to these principles, to a maximum of 240 ksi (1655 MPa) yield strength (Fig. 103). However, the new steels were not developed until 1965-1968, and the option of high corridor quality was not available at the time of the Polaris experience.

These experiences with the low and high ranges of the strength transition document the importance of arrest criteria. To date, no reliable fracture-control plan uses initiation-control principles for plane-strain metals subject to tensile loading. This statement applies to the high and low strength extremes of the strength transition for different reasons:

- Severe service conditions and low-cost fabrication requirements for typical structures of the low strength range (large-complex, monolithic, etc.)

- Low-ratio plane-strain properties for the high range.

The assertion that aircraft landing gears are an exception for the ultrahigh strength range is debatable. Their generally compressive stresses plus essentially monoblock features and unusual inspectability are not typical. While this case has been cited in the literature as demonstrating initiation control for low-ratio plane-strain metal, it is not a satisfying case for generalization. It is a special case that documents the severe engineering constraints that must be imposed in any attempt to use low-ratio plane-strain metals.

Only for the intermediate range of the strength transition can a case be made for using initiation-control principles. This range offers intermediate- and high-ratio properties, and therefore the advantages described in reference to Fig. 56 apply. However, this range also offers a wide choice of elastic-plastic and plastic metals for the section sizes of structures that are typically related to the intermediate range of the strength transition.

INTERMEDIATE RANGE OF STRENGTH TRANSITION

Interest in the intermediate range evolved during 1964-1970. The initial explorations were the result of Navy programs in deep submergence of small research submarines. Later interest centered on advanced aircraft and hydrofoils, the main components of which have section sizes of 1 to 2 in. (25 to 50 mm). However, the steels have potential for use in thicker sections, based on elastic-plastic criteria.

The exploration of this range was largely based on the first use of rational laboratory fracture tests. The DT and K_{ν} tests were used as appropriate for the fracture-state properties in question. Structural prototype tests of the explosion crack starter type were used to a limited extent, mainly to confirm the predictions of the laboratory tests.

230-362 O - 77 - 10

The striking correspondence between the fracture-state definitions of the DT laboratory test and those of the structural prototype test is illustrated in Figs. 104 and 105. The important point is the faithful definition of performance with respect to extension of through-thickness cracks in plastic, elastic-plastic, or plane-strain modes. Figure 105 also illustrates the major metallurgical effort of 1964-1968 in charting the strength transition. New steels in the intermediate yield-strength range of 120 to 200 ksi (827 to 1379 MPa) were investigated. The section sizes were normally 1 to 2 in. (25 to 50 mm), but selected tests of thicker sections were performed. Most of the new steels were purchased to specifications issued by the technology development

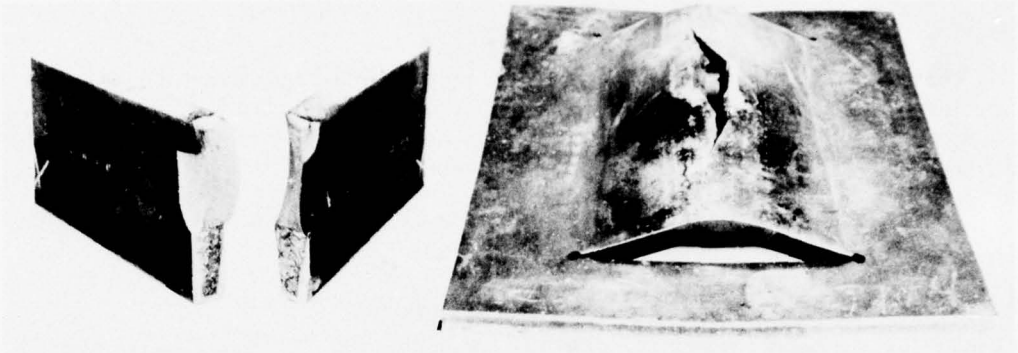

Fig. 104—Exact DT test reproduction of the characteristic fracture mode developed in explosion crack starter tests with through-thickness cracks.

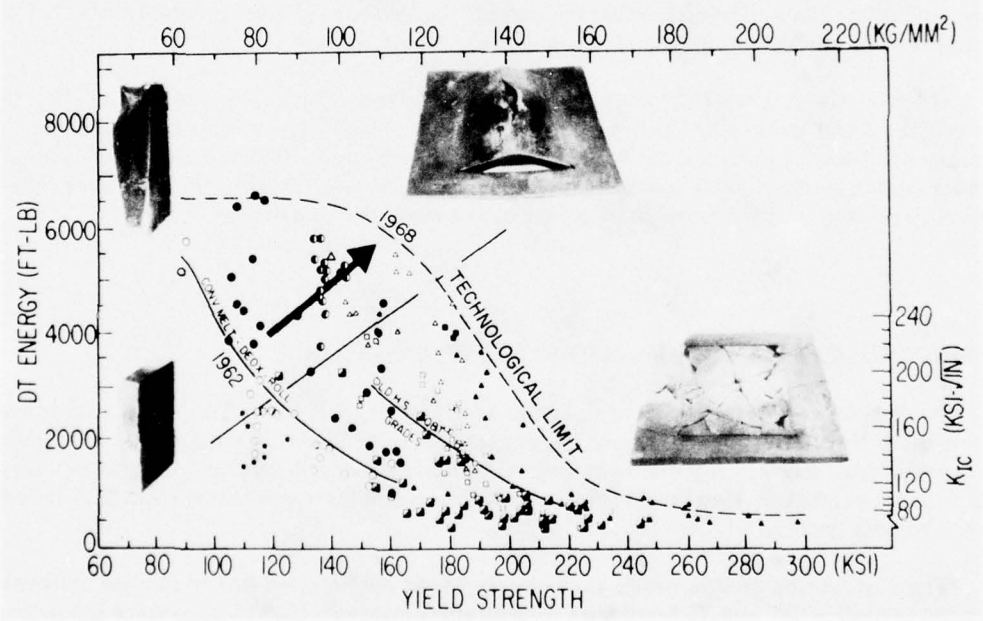

Fig. 105—Strength-transition analyses as described by a 1968 illustration, emphasizing the development of improved steels from 1962 to 1968.

teams, guided by rational tests. These steels are thus the first high strength metals developed by rational laboratory test methods that included analysis of mechanical constraint.

The need to examine both metallurgical and mechanical section-size effects dictated the use of full-thickness DT tests as well as DT tests of standard (small) dimensions. Figures 106 and 107 illustrate the range of instrumented DT test machines for large-size testing. Figure 108 shows a Japanese DT machine of recent (1972) construction.

Fig. 106—Large drop-weight DT test machine for tests of 2- to 4-in. (50 to 100 mm) section sizes.

Fig. 107—DT test machine for 6- to 12-in. (150 to 300 mm) section sizes.

The concentration on metallurgical quality resulted in a rational definition of practical limits for the high- and intermediate-quality corridors of the strength transition (Fig. 109). The information provides a rational basis for changes in selection criteria for such structures as advanced aircraft. The lower boxes represent the properties expected for steels of 1-in. (25 mm) section size, based on the old (pre-1965) selection principle of minimum yield strength. The low corridor position was enforced because these were the only steels available at the time. As a result, low-ratio plane-strain properties were developed, although not specified.

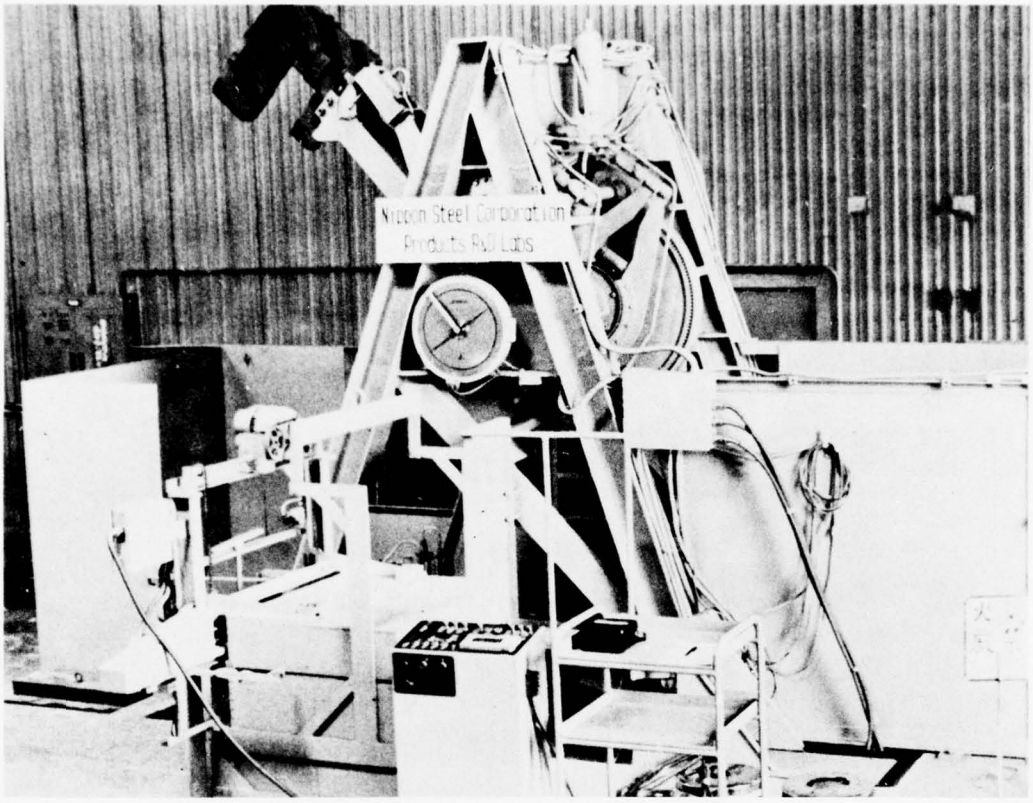

Fig. 108—Japanese pendulum-type DT test machine, which permits testing of high strength steels of section sizes up to 3 in. (75 mm). It is completely automatic, including self-loading from temperature-controlled chambers. (Photo courtesy of Nippon Steel Corp.)

Present criteria for structural strength members of advanced aircraft include (a) the use of metals of highest corridor quality and (b) the setting of a maximum on yield strength, decided by elastic-plastic properties and referenced to the given section size.

In addition, structurally redundant design features are emphasized for all strength-critical components. The same structural integrity principles are applied to other structures, such as fast craft and deep-diving research submarines. The reason for avoiding plane-strain properties is that the plane-strain state for intermediate strength levels is of intermediate ratio value. In principle, this allows much greater latitude in flaw detection and control than permitted by thin-section metals (low-ratio plane strain). However, the practicality of such control during fabrication and in service is the deciding SI technology question. The cost of using plane-strain metals of intermediate ratio value may be made unbearable by the costs of inspection, quality control, and documentation.

Developments of 1970-1975 have generally been directed to avoiding the use of initiation-control principles. No modern design criteria permit the use of plane-strain metals in fracture-critical locations of high-performance aircraft, fast craft, or aerospace structures.

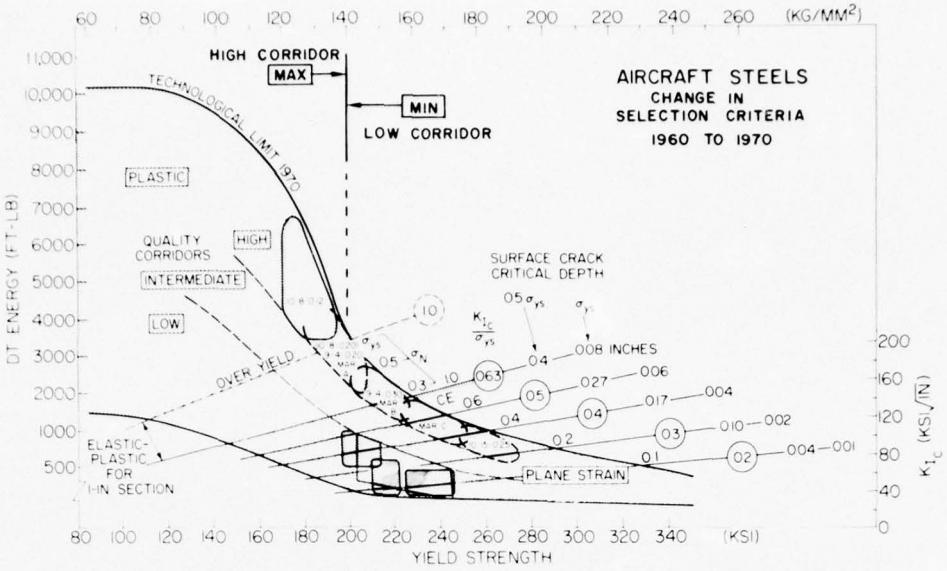

Fig. 109—Comparison of old and new selection criteria for aircraft steels.

Reports of K_{Ic} values for metals so used are misleading in their indications of design criteria. While the values may in fact be measured for thick forging stock, machining reduces the section sizes to levels at which elastic-plastic or plastic fracture properties apply. Section size must be considered in examining such inferences and interpreted by the RAD in terms of the section sizes used in the structures.

COST ANALYSIS

The use of SI principles in structural design is usually influenced by cost. The significance of cost depends on the intent of fracture-control plans and the specific contractual requirements.

The genesis of plane-strain fracture mechanics in the mid-1950s was stimulated by cost issues. In the early literature, it was cited as "procedures that would provide for fracture-safe design using brittle metals." In effect, the hope was that less expensive metals of plane-strain properties could be used, according to calculations of critical crack sizes for fracture initiation.

Paradoxically, engineering experience with plane-strain metals (using initiation control) demonstrates that the true cost question is exactly opposed to the original issue. The cost of using plane-strain metals may be rendered prohibitive by the need for tests, quality control, inspection, and lifetime surveillance. This inversion results from acceptance by users and regulatory authorities of plane-strain fracture mechanics definitions of critical crack sizes. If assurance of structural reliability is a contractual obligation, then

Statistical tests of plane-strain properties must be made at very high cost.

Quality control must be much more rigorous than for crack-tolerant metals.

Inspection requirements generally exceed capabilities.

Thus, escalating costs of structural certification will reduce questions of initial metal costs to relative insignificance. Contractual obligations to validate structural performance in terms of crack-initiation control make use of elastic-plastic metals the low-cost solution in most cases.

The certification costs of traversing the elastic-plastic regions of the strength transition are illustrated in Fig. 110. The relationships of increasing certification cost to the YC and L criteria and to decreasing ratios in the plane-strain region are illustrated by the inset graph (log scale). The important point is the rise of certification costs in the plane-strain region.

The arrows indicate the strength ranges for this escalation of certification costs, for both low- and high-corridor metals. Metal of highest corridor quality extends low-cost certification procedures to higher yield-strength levels. Exceeding these limits results in cost escalations to a degree that depends on the criticality of the structure and the potential effects of structural failures. That is, the more serious the consequences, the greater the cost of assurance that critical crack sizes do not develop. Lifetime surveillance of potentially staggering proportions is necessary.

The transition of stress-corrosion cracking properties to intermediate and low ratio values (see Chapter 9) may take place over a strength range lower than for fracture. This signifies that maintenance and repair problems may develop. While not catastrophic, the cost may be serious.

The analyses of Fig. 110 are specific to a 1.0-in. (25 mm) section size; adjustments for section-size effects may be made as described previously. Also, relative structural complexity dictates the rise of certification costs with decrease in ratio.

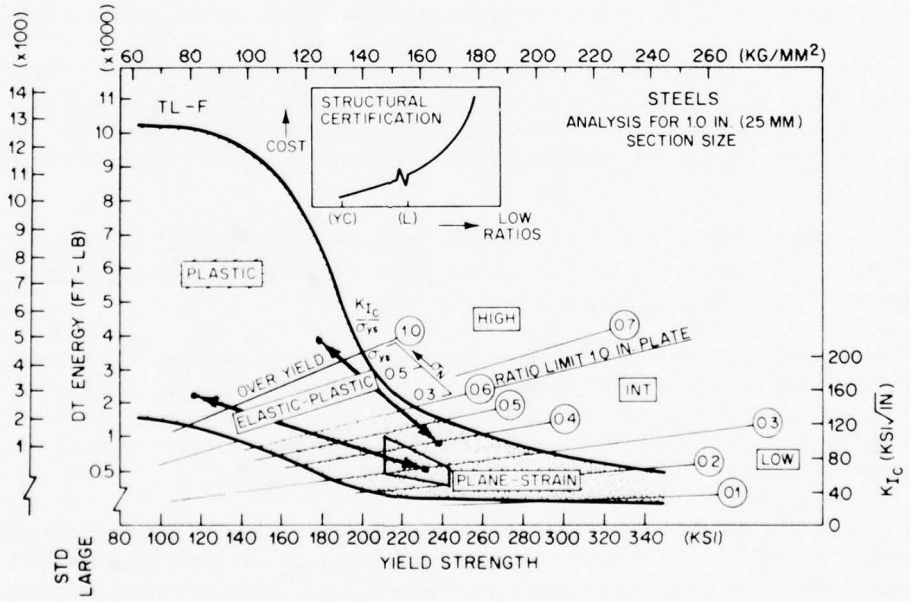

Fig. 110—Schematic of potential order-of-magnitude escalation of structural certification costs due to transition to plane-strain properties.

Engineering realities of metal properties should be considered in establishing nondestructive inspection (NDI) procedures for plane-strain metals. The predictions of critical crack sizes are upper bound estimates derived from linear-elastic theory. These predictions are accurate provided the metal properties are as measured by K_{Ic} (K_{Id}) tests. However, these analyses should take into account the fact that cracks may be in localized regions of metallurgical damage. The critical crack sizes then depend on the much lower K_{Ic} (K_{Id}) values for the regions of metallurgical damage.

A simple example suffices. Suppose that the properties for a weld are less than 0.3 ratio. The fact that the base metal features (say) 0.8 ratio properties is then irrelevant. The lower bound value for SI calculations of critical crack sizes is that of the weld and not the base metal.

It is noted that the critical SI need is nondestructive evaluation (NDE) of metallurgical damage regions, not NDI. The cost-escalation curves must include the total NDE problem, not merely the NDI part. The engineering experience of 1965-1975 gives ample evidence of the importance of NDE for high strength metals. In fact, the addition of rational metallurgical considerations in NDE analysis may be the most recent real advance in realistic probability assessment. In general, the credibility of fracture-control plans based on initiation control depends on probabilities of failure as determined by NDE.

ROLE OF METALLURGICAL FACTORS IN INSPECTION

Requirements for nondestructive crack inspection (NDI) cannot be established from purely abstract consideration of NDI capabilities. SI crack-inspection problems are generally decided by metallurgical factors according to the realities of nondestructive evaluation (NDE).

The term NDE refers to the entire system of inspection and quality-control (QC) procedures used throughout mill processing, forming, welding, machining, and installation. Many structural failures have been attributed to alloy impurities, improper heat treatment, improper welding, and other factors that influence fracture initiation but are not detectable by NDI for cracks.

The role of metallurgical factors may be analysed in terms of two broad categories: (a) *fracture state* (as related to critical crack size) and (b) *embrittlement sensitivity* (as related to the development of localized metallurgical damage).

Adverse combinations of metallurgical factors, such as plane-strain fracture properties coupled with high sensitivity to localized embrittlement, may make the NDE-QC problem insuperable. In such cases, practical control of effects that determine the development of minute critical cracks may not be feasible. Even if NDI capabilities are improved to cover microscopic crack sizes, control may be infeasible for other reasons.

A simple example, involving the standard-grade C-Mn (pearlitic) steels, indicates the generality of the NDE problem. Arc strikes at unexpected locations have triggered failures of many ships and other monolithic structures. Metallurgical "notches" representing hard or embrittled regions (the result of deviations from optimum weld control) can lead to fracture initiation due to intrinsic sensitivity of the steel to local damage.

Failure analysis by microscopic examination of the initiation site produces evidence that the initial defects can evolve spontaneously. The metallurgical notch conditions have a common feature—the crack site develops suddenly at the point of embrittlement. Crack-detection methods (including microscopic inspection) serve no purpose in these cases because there is no crack until the moment of failure.

Other conditions leading to metallurgical notches indicate the generality of the problem for metals of plane-strain fracture properties, as follows:

- In steels of intermediate strength and in titanium alloys, failure to provide gas coverage in gas-metal-arc (GMA) welding can result in severe local embrittlement.

- In high strength steels, proper techniques for starting the arc in stick-manual-arc (SMA) welds (moving backwards, then forward, to remelt the starting site) are essential to preclude severe embrittlement. When the arc is first struck there is no gas-shield protection by the electrode coating.

It is impossible to apply NDE controls to such embrittled sites; control of welding procedure must be relied on. Highly localized damage of this type is a problem only if the metal has plane-strain properties. For example, arc strikes are of no concern in metals of elastic-plastic fracture properties.

The embrittled region may have K_{Ic} or K_{Id} values much lower than those cited for the base metal—lower, in fact, than the limits of measurement of plane-strain properties. Ratio values of less than 0.1 may be inferred from the known effects of the embrittled regions. High residual stresses at the damage points (due to welding) can also reduce critical crack sizes in the damage region to microscopic dimensions. In fact, little tensile ductility may remain; this leads to spontaneous cracking in defect-free sites.

The search for improved NDI methods that can reliably identify cracks 0.2 in. (5 mm) or less in depth does not offer relief from such metallurgical notch problems. The reason is that the critical crack size for the base metal establishes the size of the volume of embrittled metal that is critical for metallurgical damage. If very small cracks are critical, then the critical volume of embrittled metal is very minute and beyond reasonable NDE-QC control. The problem becomes one of controlling metal hardness, quality, and cleanliness at the scale of 0.1 $in.^3$ (6 mm^3) or less for welds, heat-affected zones, machined surfaces, etc.

If critical crack sizes are 0.2 in. (5 mm) or larger, NDI detection and the use of NDE-QC become more realistic. The volume of metal that must be embrittled to produce spontaneous cracking becomes larger, and its development by failure of QC procedures becomes statistically less probable. The usual NDE methods may then suffice.

Experience supports the following general thesis: *When fracture safety necessitates NDI requirements of exceedingly minute crack sizes, NDE-QC is not feasible. Similar but unattainable exactness in processing, heat treatment, welding, etc., would be required.* The real problem of this near-microscopic crack-state control is the unattainable precision required of all NDE-QC procedures. The type of structure dictates whether procedures of extreme limits are feasible. For example, what is feasible for an aircraft landing gear may not be feasible for the box structure of a swept-wing aircraft. The inspectability and design simplicity of the structure have an important bearing on the attainable limits of metallurgical control in fabrication. The landing gear

Sensitivity to cracking may be inherent in the composition of the metal or may develop as

represents a highly refined, essentially unit-forging design. The box structure must be assembled from a variety of forged and plate subcomponents, and it features complex welded connections.

PROBABILITY ASSESSMENTS

Structural designs must approach imposed requirements within established limits. The general structural redundancy may be relatively fixed (pressure vessels) or subject to considerable adjustment (aircraft, ships, bridges, etc.). Reliabilty requirements may dominate, or they may be relaxed in favor of economic constraints.

In all cases, the designers must apply deterministic procedures to ensure structural reliability. These procedures require calculation of the load-bearing characteristics of the structure.

The early development of monolithic welded construction resulted in unexpected failures at relatively low elastic-stress levels. The randomness of these failures disclosed that reliability of structure could not be expressed in terms of probabilities. True control is exercised by purely random events, because random metallurgical damage dictates such performance.

The use of plane-strain metals poses serious problems of structural reliability certification. These metals have fast-fracture potential. Accordingly, failure probabilities exist, but their control is not in the province of the designer. The burden falls on others, who must verify fracture prevention by total control of crack-initiation conditions. Designers cannot verify by calculations the structural reliability of a specified structure.

It is really these probabilities, then, by which metal criteria are chosen. A design may be considered "probabilistic" if probabilities of failure by fast fracture exist. Ordinarily, failure probabilities are expected to be very low. If failure can be caused by purely random events (due to fabrication and quality-control deviations, or any other unpredictable circumstances), then probability definitions become stochastic (random). Proof that structural performance is not potentially controlled by stochastic circumstances should be part of fracture-control plans.

There is a distinct separation between fully deterministic solutions and probabilistic solutions. However, there is no definable point at which probabilistic solutions become stochastic. Thus, design solutions are either distinctly deterministic or potentially stochastic.

The use of plane-strain principles for controlling probabilistic events in plane-strain metals is feasible only under idealized conditions. In practice, it is the engineer's problem to document that SI requirements are met. Plane-strain fracture mechanics analyses do not specifically imply that plane-strain metals can be used safely. Conversely, such analyses may dictate consideration of other metals to suit the design configuration or the metal-selection process.

The designer has the choice of various procedures for ensuring that the design process is fully deterministic, as follows:

- Fracture-control plans may be based on *redundancy assurance,* if suitable to the structural configuration. This involves introducing multiple-load fracture paths, so that the failure of any one part does not result in a large reduction of structural strength.

- If redundancy assurance is not feasible, *fail-safe assurance* can be provided by the use of a metal that does not permit extension of fast fracture at nominal design stresses.

These design procedures may be classified as deterministic in that the design process, and not other factors, determines that the structure will not fail unexpectedly due to unstable fracture.

CHAPTER 8

Characterization and Control of Crack States in Weld Regions

STRUCTURAL CRITICALITY OF WELD REGIONS

The crack states of weld zones and the local stress systems that act to extend cracks are critical to fracture and crack-growth control plans. The conditions that may result from extension of a specific crack depend on, and must be deduced from, variations in metal properties along the path of extension.

Analyzing a homogeneous structure like a unit forging is relatively simple because there are no great variations in properties. All that is required is consideration of statistical fracture-property variances and selection of a suitable lower bound value for design reference. Analysis of a welded structure can be more complex because of possible sharp variations of fracture properties in weld zones. In addition, sharp variations in stress systems and in the paths for crack extension in weld-zone regions are possible.

The presence of welds means that a small volume of the metal in the structure may dominate reliability analysis. Welds often are metallurgically inferior and are frequently in the most stress-critical regions of the structure. However, welds have these effects only if the design for welding is inappropriate to the functional requirements of the structure. The first step in reliability analysis of a welded structure is to ensure that such adverse conditions are avoided. The object is to reduce the criticality of weld regions to the same level as that of the rest of the structure.

This is done for tensile properties by requiring a strength efficiency of welds equal to 1.0. This certifies that the welds are at least as strong as the base metal. However, equality of fracture or crack-growth properties may not suffice if the base metal has inadequate or marginal properties. Minor defects in welds, which have no effect on strength efficiency, may then be critical to fracture or crack growth, particularly if the welds are in regions that lead to high load-induced stresses or in configurations that result in high residual stresses.

The starting point in design for welding is to recognize that the defect state of welds is inferior to that of the base metal. Thus, designers must be more conservative about fracture and crack-growth properties of welds than about those of the base metal. The crack-state deficiency of a weld may be offset by properties of the weld metal that preclude extension of cracks. The crack-state deficiency also may be offset by reducing the maximum stress at the welds, as compared to the regions of highest stress in the base metal. Either method is good design for welding; the goal is to eliminate excessive dependence on the weld regions for structural reliability.

To establish whether weld regions are deciding factors for a specific design, it is essential to understand the main properties of these regions. The general principles are the same as those already described for the base metal; temperature- and strength-induced transitions are similar.

The main additional points are weld quality, as determined by welding processes; statistical variance of properties, as determined by fabrication controls; and residual stress systems due to welding procedures. All of these depend on in-situ melting, solidification, and transformations of the metal during joining. Weldability optimization by metallurgists for base and weld metals must presuppose a specific degree of quality control of welding processes. The specific lower bound fracture properties of weld can be characterized only if fabrication is firmly controlled. This is in contrast to the base metal, for which metal quality depends on mill-practice quality controls.

Such welding quality controls are feasible, as attested by fabrication specifications for critical structures. These document the standards and procedures of design for welding. The effects of temperature and strength transitions must be considered, because otherwise the specifications can present unrealistic engineering demands. That is, the controls may become too expensive or may be beyond the reach of technology.

To avoid exceeding practical limits, designers must consider the locations of welds in structures. Locating welds away from high stress or strain concentrations should be considered in terms of reliability and economic returns.

Fabrication quality control should assure that the metal properties of the weld zones are not grossly degraded with respect to base metal properties. The problem is that direct testing of properties before fabrication, as for base material, is impossible. Laboratory tests of welds made according to specified practices must be substituted. In practice, the welding procedures are "qualified" by the tests and then are duplicated during fabrication.

Another aspect of structural criticality involves limitations to stress analysis. Refined, computerized, finite-element analysis of stress or strain concentration are applied to selected critical regions, ordinarily called "K_t points of geometric transition." Moreover, these refinements are applied to critical structures with the object of increasing allowable stress. In general, regions so analyzed must be formed to exact configurations. The stress system in these regions must be derived from the loads analyses; residual stress fields due to welding may complicate or void the finite-element analyses.

In summary, placing welds, which may be more crack-critical than the base metal, in stress-critical regions of critical structures degrades reliability. Moreover, the higher than average crack-state probabilities of welds in such high-stress regions complicate crack inspection, both initially and in service, because smaller cracks must be detected with greater assurance than in the base metal.

All of these considerations are accentuated as the base metal goes from the plastic to the elastic-plastic and then to the plane-strain range. As the margin of reliability on which structural integrity plans are based is decreased, the importance of locating welds in regions of lower stress dominates the design process. Engineering experience in design for welding, gathered over the past two decades, is summarized in Figs. 111 and 112.

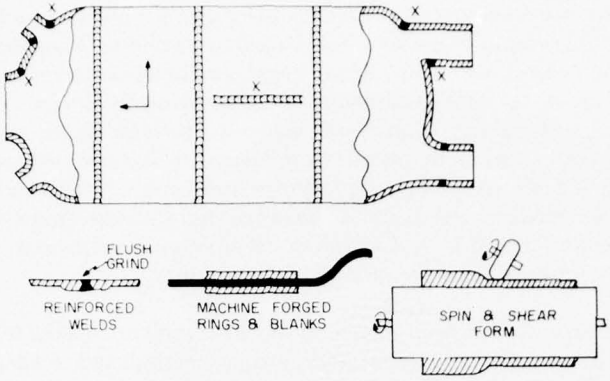

Fig. 111—Procedures for minimizing the criticality of weld regions in rocket case structures. The Xs represent locations of welds in high stress regions (or directions) that resulted in hydrotest failures. Welds without Xs indicate proper location, obtained by the use of ring forgings and forging inserts.

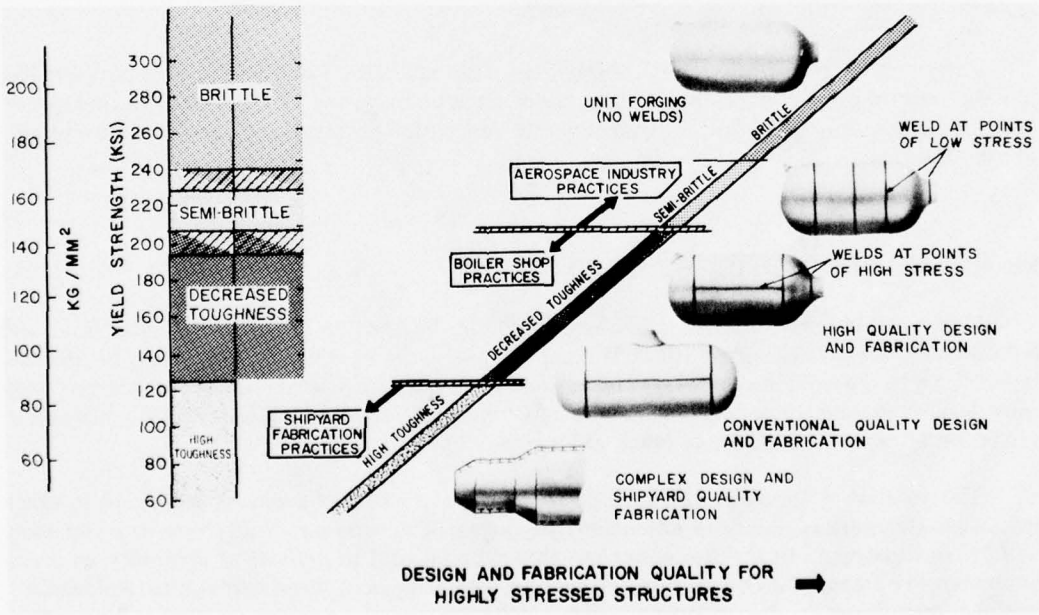

Fig. 112—Relationships of design and fabrication practices with strength transition regions.

Figure 111 illustrates the methods used by designers of rocket cases for dealing with weld criticality. Innumerable rocket cases were fabricated by varied welding techniques and adjustments of weld locations. Because of the high strength and limited fracture resistance of the base metals (Chapter 7), the welds were hypercritical in controlling failure rates in hydrotesting. The "X" notations of Fig. 111 indicate that welds subjected to high stresses by their locations at points of geometric transition or by orientation normal to the hoop stress are intolerable, as indicated by hydrotest failures. Using ring forgings and locating welds in low-stress regions of ports are necessary for rocket cases. It should be noted that hydrotesting was performed at close to service hoop stresses, 0.8 to 0.9 σ_{ys}. Critical crack sizes were very small, due to the combination of high stresses and low fracture properties.

Figure 112 indexes welding experience to the strength transitions of the base metals and matching weld metals. Design and fabrication quality are indexed to structural features, and typical practices are indicated.

The salient points of the figure are as follows:

Low range of strength transition—The base metal and welds have plastic fracture properties and are therefore insensitive to defects. Relatively crude design details, as well as low-cost welding and fabrication, are tolerable. Metal properties offset other factors that might otherwise require considerable design attention. An example is the HY-80 steels weldment system as used in submarine hull construction.

High range of strength transition—The base metal and welds have plane-strain fracture properties and therefore are highly sensitive to defects. Perfection of design details and welding practices must be emphasized, regardless of cost. The example represents rocket-case experience (Fig. 111).

Intermediate range of strength transition—The base metal and welds may have elastic-plastic fracture properties. However, because of other crack-growth factors (fatigue and stress-corrosion cracking), the high-quality design and fabrication practices typical of pressure vessels are essential.

FRACTURE PROPERTIES OF WELD ZONES

The weld region contains three separate metallurgical zones—weld, fusion line, and heat-affected zone (HAZ). In addition, it is contiguous to the base metal, which may be affected by cracking in the weld zones. Alloy composition, macrostructure, and microstructure may vary considerably among the zones. Residual stresses interact with load stresses to influence crack-initiation sites and directions of crack extension.

The relative volumes of the specific zones dictate whether fracture is limited to crack initiation (trigger) or includes extension (propagation or arrest). Weld geometry can vary widely, as illustrated in the Addendum to this chapter, and the effects of geometry on crack extension are important and require discussion. Metallurgical transformations (weldability) are also introduced in the Addendum.

The volumes of the weld zones dictate that the weld is the only zone that provides for characterization by the full range of fracture mechanics criteria. The K_{Ic}, DW, and DT tests may be used to establish a reference data base of rational criteria.

The heat-affected zone may be characterized by plane-strain criteria, if it is brittle enough to contain the small plastic zones involved. However, elastic-plastic and plastic transitions may increase plastic-zone size to exceed the dimensions of the heat-affected zone. If so, the weld and base metals become involved. The fracture property is then a complex value that integrates these various involvements. This would be the case for a simple, straight-sided (J) weld. For welds with sloping slides (V or VV), there are geometrical influences on fracture resistance; the result is analytically undecipherable.

Structural prototype tests (such as explosion-bulge tests) and structural models tested to force development of fracture paths form the basis for analyzing HAZ fracture characteristics. Figure 113 illustrates weld region fracture modes disclosed by explosion tests; Fig. 114 shows fracture paths in weld regions.

Conditions in which the fusion line can propagate fractures are rare. Because of protective geometry, the fusion line must be exceptionally brittle to pose a problem. The alloy factors that contribute to such a condition are readily identified and corrected.

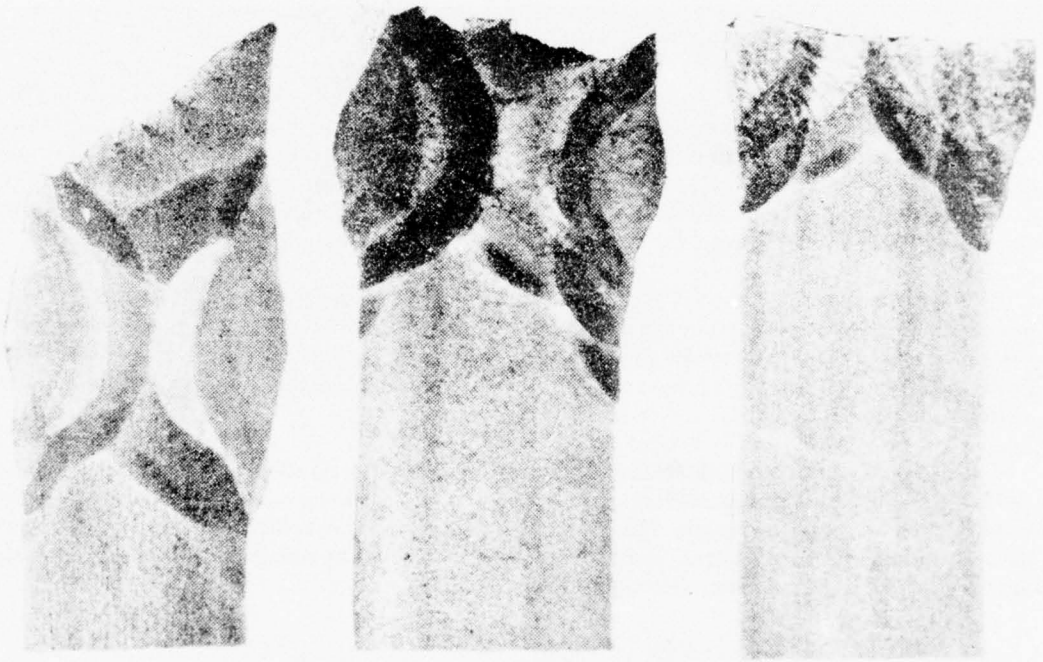

Fig. 113—Fracture modes in weldments of high strength steels—ductile fracture in base metal, brittle fracture of heat-affected zone, and brittle fracture of weld.

230-362 O - 77 - 11

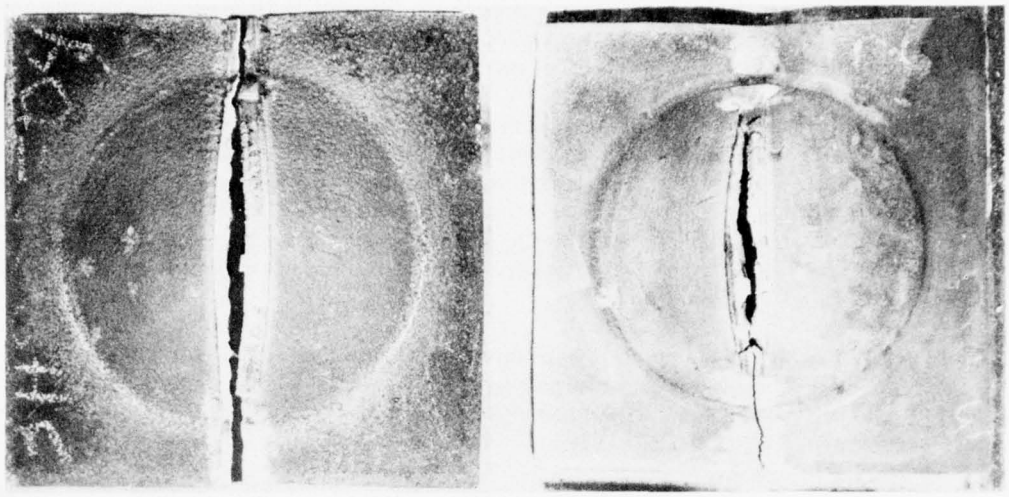

Fig. 114—Explosion bulge tests of 30 × 30 × 1-in. (75 × 75 × 2.5-cm) weldments of high strength steel, showing fractures of heat-affected zone and weld.

Strength Transition of Weld Properties

Figures 115, 116, and 117 summarize weld properties of high strength steel (K_{I_c} and DT). The three levels of corridor quality represent the same metallurgical conditions of relative cleanliness and microstructure that have been explained for forged or rolled steels. In addition, the microstructure of SMA welds results in sharper transitions than those of the base metal. GMA and gas-tungsten-arc (GTA) welds are microstructurally equivalent to the base steels. Accordingly, the different corridor levels reflect only varying cleanliness.

The low corridor position of SMA welds restricts plastic fracture properties to relatively low strength levels. Comparison of Figs. 115, 116, and 117 shows that reducing section size does not raise the elastic-plastic range significantly. The sharpness of the strength transition is the limiting factor, as it is for low-corridor steels. It is even more restrictive for SMA welds because of their sharper transitions.

The intermediate and high corridor positions of inert-gas-shielded welds provide for more gradual strength transitions. Reducing section size raises the elastic-plastic range to the same strength levels as for base metals. This is important; it allows the weld to be matched to the base metal fracture state at any strength level by appropriate welding procedures. Obviously proper alloying is a prerequisite for such matching.

Strength Transition of Heat-Affected Zone

The high-alloy steels that occupy the highest levels of plastic fracture properties in the RAD (Figs. 99 and 100) have excellent weldability where the heat-affected zone is concerned. By proper control of weld cooling rates, within reasonable engineering limits, highly ductile

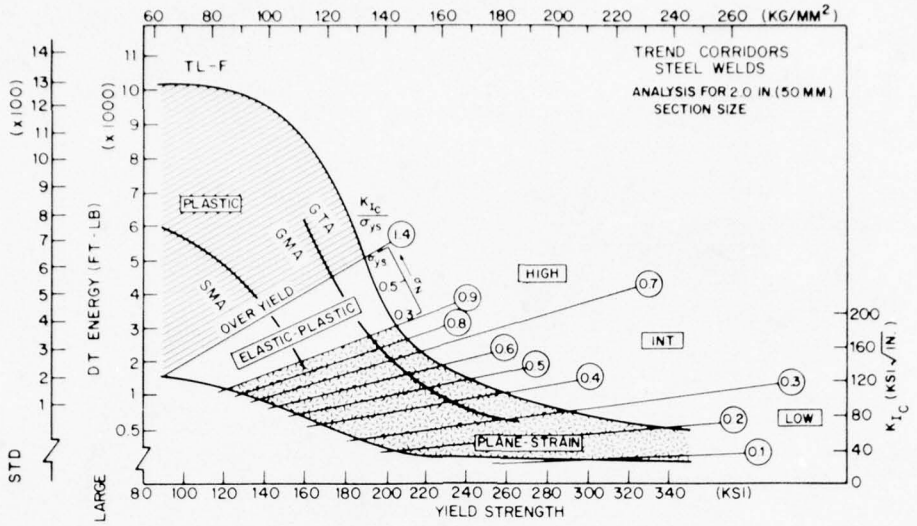

Fig. 115—Transition of fracture state for welds of 2-in. (50 mm) section size.

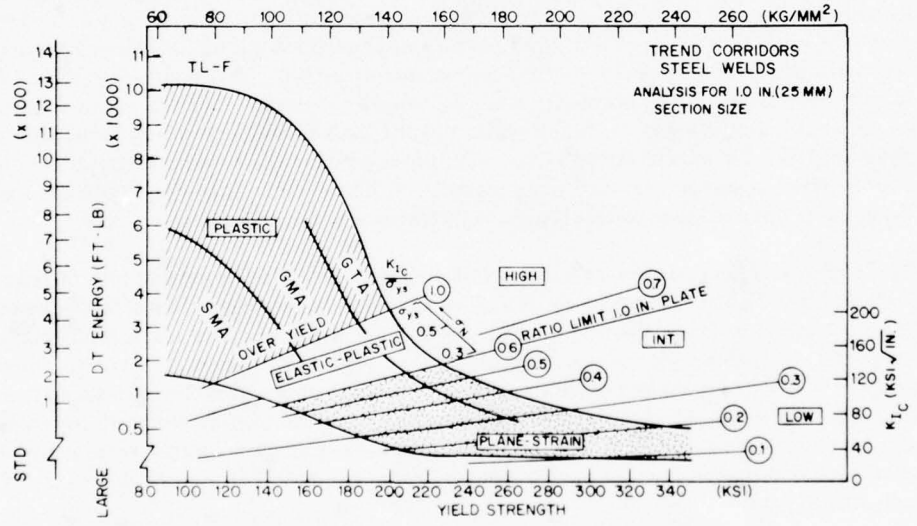

Fig. 116—Transition of fracture state for welds of 1-in. (25 mm) section size. Note that the elastic-plastic range is shifted to higher strength levels with decrease in section size. This is the result of mechanical constraint and does not reflect metallurgical differences.

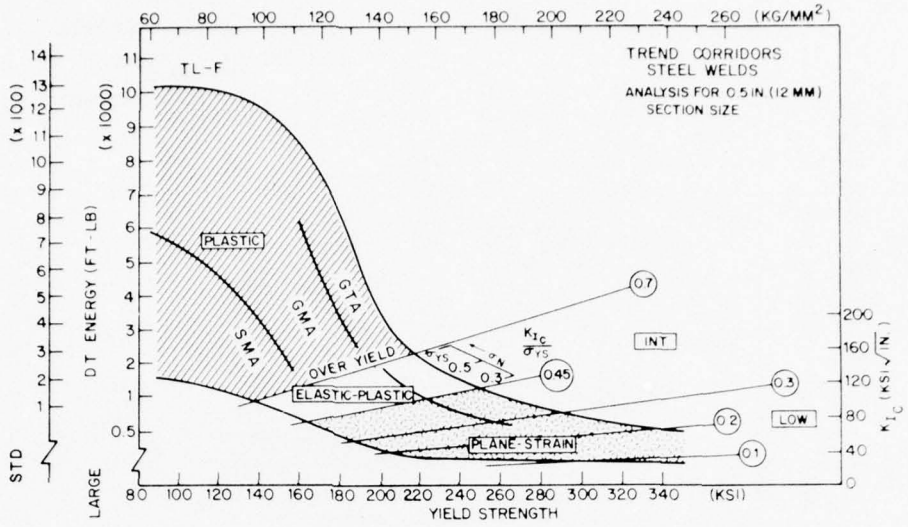

Fig. 117—Transition of fracture state for welds of 0.5-in. (12 mm) section size.

properties can be produced in the heat-affected zone. The explosion bulge in Fig. 118 illustrates the extreme resistance to plastic fracture typical of properly made HY-80 (ASTM A543) weldments, even in the heat-affected zone. In general, high-corridor metal has metallurgical characteristics that can produce high-corridor properties in the heat-affected zone. Conversely, a low-corridor base metal limits heat-affected zone properties under even the best welding procedures.

The low-alloy steels (Figs. 99 and 100) occupy the low corridor because of low-quality *melting practices for the strength* level. As described previously, the high density of void sites for microfracture initiation leads to low-shelf performance at the high end of the temperature-induced transition. The low alloy content has a separate effect; section size, for proper transformations to martensitic or bainitic microstructure, is limited generally (all grades) to 1 or 2 in. (25 to 50 mm). Quenching of thicker sections results in split transformations whose products include also upper bainites. The mixed structures when tempered have the proper strength level but are generally brittle. At normal service temperatures, thick sections may display plane-strain or elastic-plastic properties due to relatively high transition temperatures.

The separate effects of low-corridor position due to melting practices and of transition-temperature effects due to low alloy contents are reflected in the properties of the heat-affected zone. The range of weld cooling rates that provide for optimum transformation features is relatively narrow in low-alloy steels as compared to high-alloy steels. In principle low-alloy steels require more exact control of welding conditions, but in practice the economic reasons for selecting less expensive low-alloy steels also generally dictate minimized welding costs. As a consequence, welding processes with high deposition rates and slow cooling rates may be used. The split transformations due to the slow cooling rates can result in plane-strain properties of the heat-affected zone.

Ordinarily, the geometry of the weld (V or VV) protects the structure by preventing plane-strain fracture in the heat-affected zone. Plane-strain fracture ordinarily takes place only

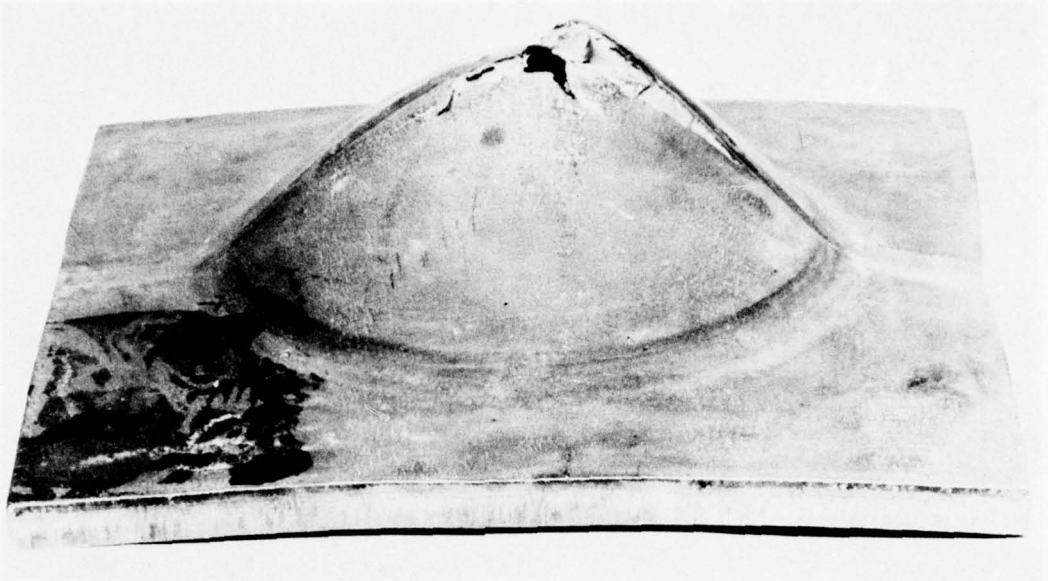

Fig. 118—Explosion bulge performance of properly fabricated high alloy, high RAD-position steels. All zones of the weld region have plastic fracture properties.

in the normal (90°) direction to the plate surface (flat fracture). Geometry precludes this mode of separation unless plastic loads are applied. For this kind of loading, the separation may be partly in the heat-affected zone and partly in the weld and base metal, with the heat-affected zone as the fracture-initiation site.

Joints produced by submerged-arc welding may feature straight-sided welds with relatively wide heat-affected zones (see Fig. 139). The protection sometimes due to weld geometry is not provided by this configuration. Fracture in the heat-affected zone at ordinary stress levels is thus possible if weld defects are present to serve as initiation sites.

An additional complexity is presented by the heat-affected zone in low-alloy, quenched and tempered steels. Stress relief is not appropriate or necessary for these steels because the main function of stress relief is to eliminate localized residual stresses in brittle steels. Stress relief is inappropriate also if vanadium is used as a strengthening element, because of stress-relief cracking of the heat-affected zone due to vanadium's tendency to increase creep strength at high temperatures. High creep strength results in preferential development of intergranular stress-rupture cracks.

Unfortunately, the codes for structures such as pressure vessels require stress relief (a holdover from practices long applied to pearlitic steels). Conforming to these codes can lead to serious stress-relief cracking in a plane-strain heat-affected zone, produced by inappropriate welding processes fully endorsed by the codes. This incorrect use of metallurgical principles in critical pressure vessels can result in the performance illustrated by Fig. 119. The experimental pressure vessel, fabricated for fatigue testing, was stress relieved as required by the codes. All features described previously were in evidence: a plane-strain heat-affected zone, extensive

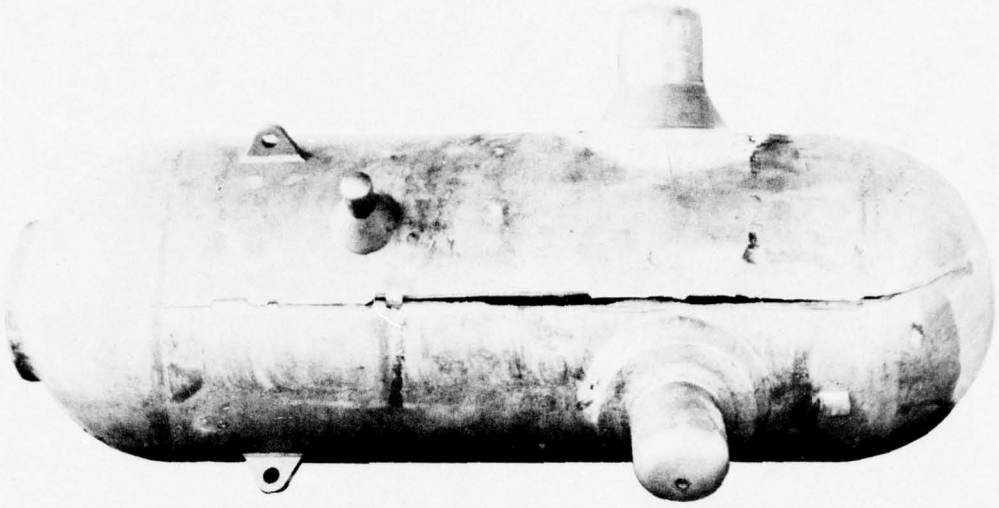

Fig. 119—Failure of an experimental pressure vessel, along the heat-affect zone of the weldment. The vessel is approximately 3 ft. (1 m) in diameter.

stress-relief fissuring of the heat-affected zone, fracture extension through the heat-affected zone at elastic hoop-stress levels, and a base metal of plastic fracture properties.

Design for welding must be based on intimate knowledge of weldability features of the steels involved. Procedures for high-alloy, quenched and tempered steels may not be proper for low-alloy steels and pearlitic steels.

Weldable steels of the intermediate and highest strength levels require exact control of welding so that weld properties are matched to the marginal base metal. Automatic GMA and GTA welding of this quality produces relatively small weld beads, as shown in Fig. 138; as a result, the heat-affected zone is very narrow. Also, the heat treatment of the heat-affected zone during welding duplicates the conditions for proper transformations of the base metal to martensites. Tempering the heat-affected zone by subsequent passes produces properties fully equivalent to those of the base metal and weld. Exact strength matching of the heat-affected zone to the base metal and weld is not vital because of the narrowness of the heat-affected zone.

For these reasons, the heat-affected zones of properly made welds in weldable high strength steels do not cause problems. If a proper welding procedure is used, heat-affected zone properties likewise will be proper.

Temperature Transition of Heat-Affected Zone

The characteristic role of the heat-affected zone in low strength, conventional (C-Mn) structural steels is crack initiation (trigger). Subsequent propagation or arrest depends on the base metal. Propagation of fractures along the heat-affected zone is rare in these steels because

of a combination of narrowness of the heat-affected zone, low residual stress for such paths, and weld geometry.

The trigger effects for fracture extension to the base metal (Fig. 129) are notorious for causing structural failures. Brittle heat-affected zones in pearlitic steels are due to excessively fast weld cooling rates, resulting in split transormations to pearlite-bainite-martensite microstructures. The relationship of hardness to brittleness in the heat-affected zone is very clear for these relatively soft steels. In fact, hardness testing is sufficient for optimizing welding procedures to eliminate excessively high crack-initiation properties.

The early weldability tests (Fig. 130) provide additional discrimination for heat-affected zone properties, if required. Figure 130 appears to show that the problem of brittleness in the heat-affected zone is temperature related. In fact, this is true for the test conditions only below the NDT temperature. Above the NDT temperature, cracking of the heat-affected zone is not transferred to the base metal and the test is no longer useful.

The use of base metals with elastic-plastic properties eliminates the heat-affected zone crack-initiation problem. Cracks originating in the heat-affected zone are arrested in the base metal.

The matching of weld and base metal properties for pearlitic steels may be analyzed in terms of NDT temperature or DT-related YC criteria. The welds ordinarily have lower transition temperatures because of their lower carbon content and relatively fast cooling rates. Improved structural steels that have lower transition temperatures are easy to match by adding alloys to the weld metal. Steels that have very low transition temperatures because of quenched and tempered heat treatment may be difficult to match; adding high-alloy contents to the weld may result in cracking due to the as-deposited hardness of weld beads. A tradeoff between cracking tendencies and low transition temperatures must be made for these steels.

GENERIC PROBLEMS OF WELD ZONE CRACKING

Cracking generally is due to an additive combination of causes. The main causes fall into two general categories—inherent metallurgical sensitivity and welding-derived stress or strain systems.

Seven principal types of cracking can occur during or after welding:

Solidification cracking (weld metal hot tearing)
Liquation cracking (heat-affected zone hot tearing)
Cold cracking (heat-affected zone)
Lamellar tearing (base metal)
Stress-relief cracking (heat-affected zone)
Hydrogen-assisted cracking (heat-affected zone and weld)
Restraint cracking (weld and heat-affected zone).

Short-range stress systems due to solidification and thermal shrinkage activate many of these cracking modes. Longer range stress systems due to restraint may then act to extend the cracks by the same or other modes.

Sensitivity to cracking may be inherent in the composition of the metal or may develop as the result of welding. High sensitivity develops if metallurgical and welding factors combine adversely.

In general, serious cracking problems arise when one of the additive causes becomes excessively dominant. Thus, the usual solution is to identify the critical factors and establish procedures for minimizing them. For example, hydrogen-assisted cracking problems are generally solved by lowering hydrogen content. Additional controls (stress, hardness of the heat-affected zone, etc.) are important but not decisive if the hydrogen content is high.

A physical sense of structural features that lead to high and low restraint stresses is provided by Figs. 120 and 121. Massive sections welded to rigid connection points develop high restraint. Thin sections welded to more compliant connection points develop low restraint. Massive structures tend to have restraint-cracking problems that are difficult to solve because of the high yield-level stresses on the weld regions. Changes in design of welded connections may be necessary for reliable solutions. For example, the structure shown in Fig. 120 could not be produced satisfactorily despite repeated repair attempts. A new design was required.

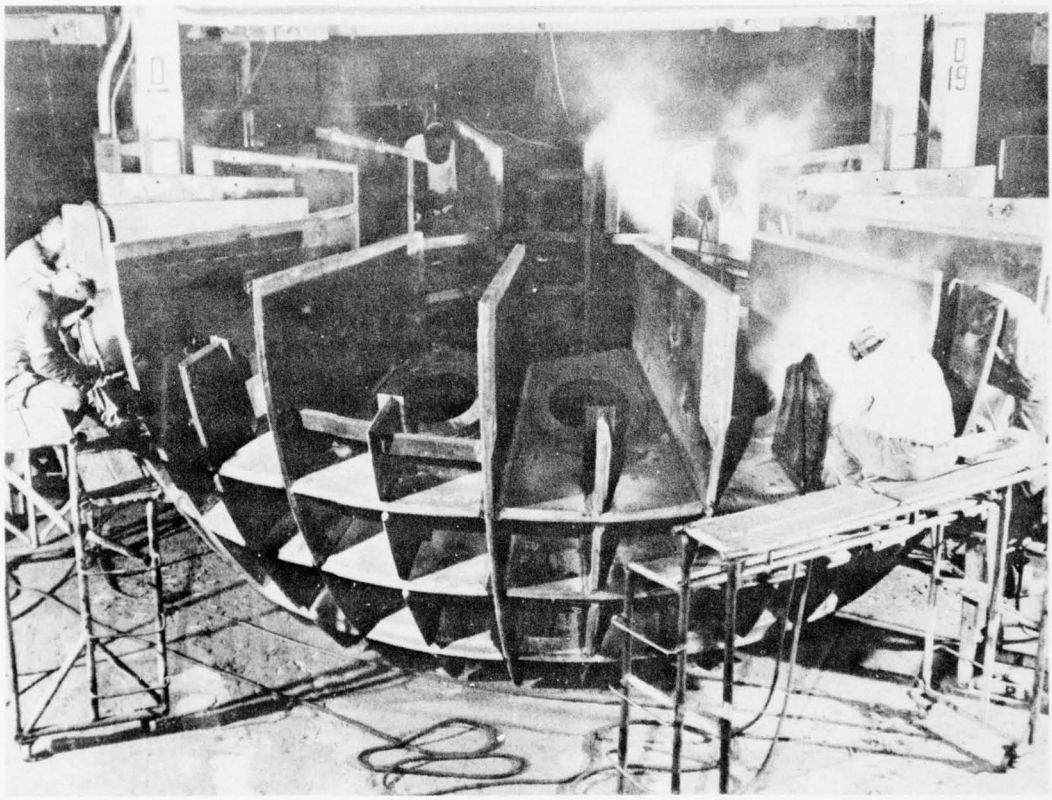

Fig. 120—Rigid structural features (T and cruciform connections of thick section) that provide high restraint to weld shrinkage, which results in plastic-level stressing of the weld, during and after solidification. This structure developed serious restraint cracking during fabrication.

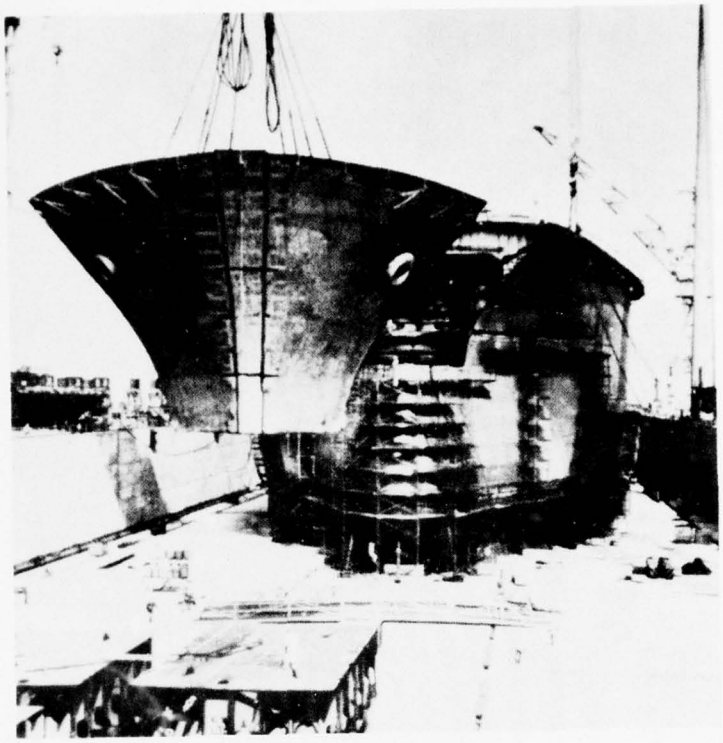

Fig. 121—Compliant structural features (butt welds of thin section), which provide low restraint to weld shrinkage.

Each cracking mode has its own metallurgical features. These are described in the following sections.

Solidification Cracking

As the pool of weld metal cools, columnar grains grow toward its center. Impurities or alloy elements are deposited between grains. Ultimately, a liquid-film condition, with little capacity for adjusting to contraction of the weld, is reached. As a consequence, the liquid film becomes the site of cracks, which may be longitudinal or transverse to the weld (Fig. 122), depending on the direction of restraint forces.

Sulfur and phosphorus impurities are critical to hot cracking for steels; small amounts suffice because the impurities are rejected and concentrated in the last remaining liquid films. The concentrated liquid has a lower freezing point than the steel. Thus, the liquid films persist while cooling strains continue to increase. Crack separation of the liquid films is strain controlled. The cracking mechanism is termed "hot tearing" because it occurs at high temperatures, before the metal develops appreciable strength.

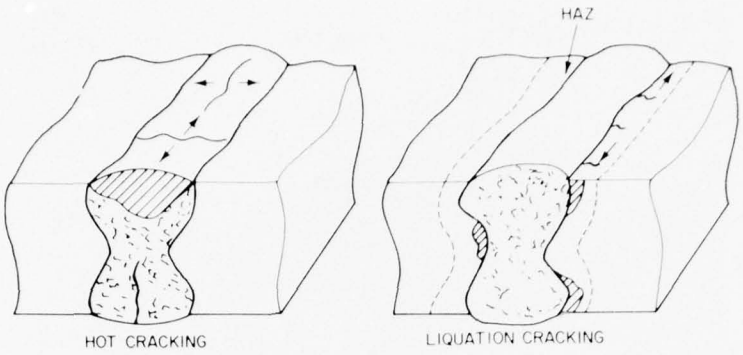

Fig. 122—Examples of cracking modes.

Liquation Cracking

The mechanism of liquation cracking (Fig. 122) is fundamentally the same as that of solidification cracking (strain-controlled cracking in the presence of liquid films). Liquid films develop at temperatures barely sufficient to melt film regions of sulfide segregation, but not high enough to melt the heat-affected zone of the base metal. The tensile strain system results from shrinkage of the heat-affected zone, impeded by the surrounding base metal. The liquation crack forms as the heat-affected zone begins to cool, after the arc pool has passed. The main solution is to lower the sulfur content of the steel.

Cold Cracking

In general, cold cracking (Fig. 123) takes place after a transformation that produces relatively hard products (bainite and martensites). Cold cracking is greatly enhanced if small

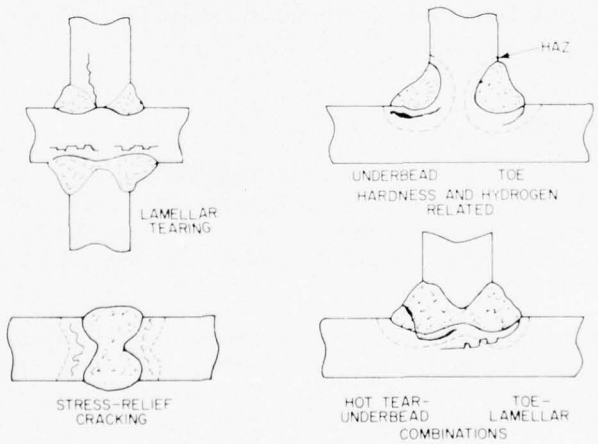

Fig. 123—Examples of cracking modes.

liquation cracks are present to serve as triggers. A combination of high carbon and sulfur contents is critical. The solution is to reduce hardness by increased preheating or by any other method that slows cooling. Shaping the weld bead to reduce local stresses is beneficial.

Stress-Relief Cracking

The fissure-like cracks of stress-relief cracking evolve by a stress-rupture mechanism, enhanced by carbon precipitation (Fig. 123). During welding, the heat-affected zone and the underlying weld bead are subject to high-temperature solution treatment, which allows carbides to be dissolved and taken back into solution. The relatively high weld cooling rate does not allow all carbides to be precipitated, and some remain in solution. Reheating the joint for stress relief causes carbide to precipitate during the creep phase; this leads to stress-rupture fissuring at grain boundaries. The grains are strengthened by the precipitation, and most of the creep strain is thus forced to the weaker grain boundaries, leading to rupture.

Lamellar Tearing

Lamellar tearing is separation of the base metal along planes of nonmetallic inclusions (on rolling planes), due to low ductility in the through-thickness direction. Ordinarily, this results from extension of other forms of cracks because of low-quality melting practices. The problem is most pronounced for fillet welds and highly restrained welds (Fig. 123).

Hydrogen-Assisted Cracking

The presence of hydrogen encourages fissuring in the plastic zones of crack tips. Hydrogen-assisted cracking merely extends other cracks that are already present. Thus, hot, liquation, or cold cracking can provide the conditions for this form of crack extension. The prior cracks may be exceedingly small, if strength levels and hydrogen contents are high. Short- or long-range high-intensity stress systems are critical, because they raise the K-force for crack growth to high values. Hydrogen-assisted crack extension tends to follow paths normal to the directions of stress (Fig. 123).

Restraint Cracking

The term "restraint cracking" does not signify a specific metallurgical mechanism; several may be involved. Restraint cracking is cracking for which restraint stress dominates in activating a particular mode of cracking. Modes most commonly associated with restraint cracking are hot tearing, hydrogen-assisted cracking, cold cracking, and lamellar tearing, singly or in combination.

Determination of the type or types of cracking generally requires removing a sample, cross-sectioning the crack, polishing and etching, then microscopically inspecting it at 50× to 250× magnification. Ordinary visual examination may be misleading. The difficulty of identification is made apparent by controlled experiments in crack development. Often it is necessary to deduce the cracking mechanism by observing the effects of welding variables and time-dependent effects. Combinations of mechanisms (such as initial fissuring by hot tearing and

extension by hydrogen-assisted cracking) may be perplexing unless the effects of procedural variables are examined. The opinions of experts, after simple examination of cracked samples, may be subject to debate. For these reasons, it is important to understand some of the main phenomena of hydrogen-assisted cracking and of restraint cracking.

Phenomena of Hydrogen-Assisted Cracking

The effects of strength level (hardness) on hydrogen-assisted cracking (HAC) are pronounced. The source of the hydrogen is not important, but the amount is crucial. Hydrogen contents from less than 1 ppm to approximately 5 ppm can trigger cracking. ("Low" contents are less than 1 ppm, "intermediate" contents are 1 to 2 ppm, and "high" contents are over 2 ppm.)

Figure 124 generalizes the effects of strength level on sensitivity to hydrogen-assisted cracking, in terms of the RAD. The same values apply for the heat-affected zone, as translated from hardness to the related strength level. Figure 124 also relates the sensitivity transition to hydrogen content. The summary is based on insensitivity levels known from service experience, plus fracture mechanics tests and other sharp-notch, sustained-load tests. The low end of the transition-corridor bands are referenced to K_{III} determinations involving the equivalent of K_{Iscc} tests (Chapter 9). The significance of K_{III} values can be translated by the ratio method to the RAD ratio scale in the same fashion as for K_{Iscc} values. The fall from insensitivity levels to low-ratio levels represents an extremely sharp strength transition. The transition is much sharper than for corridors of the fracture transitions. The same considerations apply to the heat-affected zone, as translated from the hardness values, which serve as the usual reference, to the equivalent strength levels.

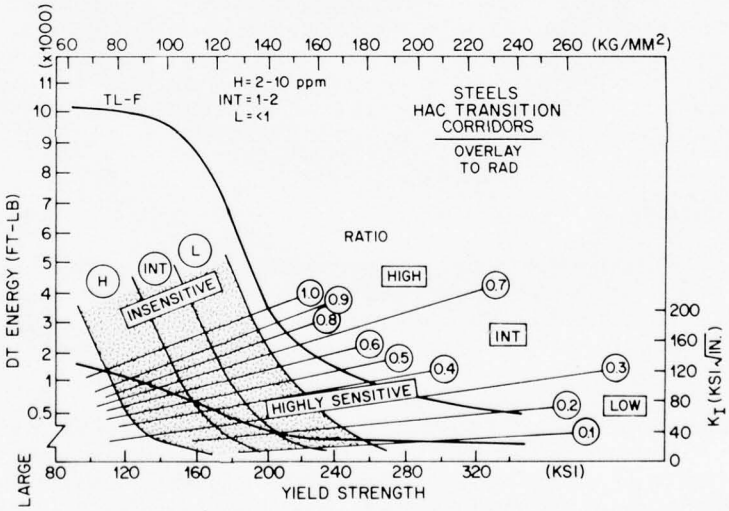

Fig. 124—Comparison of the very sharp transitions of sensitity to hydrogen-assisted cracking (HAC) with the strength transition of base steels and welds.

The significance to welding is now apparent. SMA electrodes of cellulosic type produce excessive hydrogen contamination of the weld pool and the heat-affected zone for all strength levels cited in the RAD plot. In fact, problems arise at strength levels above 50 ksi (344 MPa) if the heat-affected zone is transformed to pearlite-martensite combinations. For this reason, low-hydrogen SMA electrodes were developed to limit the hydrogen content of the solidified weld and heat-affected zone to about 1 to 2 ppm, depending on deposition procedures. This amount of hydrogen is excessive at strength levels of 120 to 150 ksi (827 to 1034 MPa) if restraint stresses are high.

The heat-affected zone for SMA welds is ordinarily excessively hard, before the tempering pass, for typical SMA hydrogen levels. Limiting the carbon content of the base plate and using high preheat temperatures are reasonable solutions to hydrogen-assisted cracking at the low end of the strength range cited above. As the strength level is increased, it becomes difficult to avoid cracking in SMA welds.

In general, hydrogen effects require a change from SMA to GMA welding at strength levels higher than 130 ksi (896 MPa) for high-restraint conditions and 150 ksi (1034 MPa) for low-restraint conditions. With proper precautions, the GMA weld pool may be limited to a hydrogen content of 1 ppm or lower, thus greatly reducing cracking sensitivity.

The strength level above which hydrogen cracking prohibits SMA welding is about the same as the strength-level limit defined by fracture properties if the welds feature reasonably moderate restraint. However, for conditions of high restraint the hydrogen-related limit of SMA welding is approximately 120 ksi (827 MPa). In brief, the hydrogen-sensitivity transition is sharper than the fracture-property transition for SMA welds.

One of the most insidious features of hydrogen-assisted cracking is delay. Extension of small fissures may take place over a period of hours, weeks, or months. As the strength level of the weld or heat-affected zone is increased, the delay becomes the most serious problem. The level of hydrogen that causes delayed cracking is much lower than that which causes immediate cracking. This complicates crack inspection.

This problem leads to consideration of hydrogen diffusion by high preheats (200° to 350°F; 95° to 180°C) and long-term soaking (6 to 12 h) at the same temperature. Such measures may be applied to SMA weld regions of high restraint in steels and weld metals of the 120- to 150-ksi (827 to 1034 MPa) strength level.

The economic disadvantages of these remedies and uncertainty about delayed cracking are important in design for welding. Since the cracking is concentrated in regions of high restraint, attention should be directed to selectively reducing the restraint stress and the hydrogen content of the welds at these locations. The following steps can accomplish this:

- Switch from SMA to GMA welding for rigidly connected massive sections.
- Use forgings at the point of connection and shift the weld to locations of smooth geometry, outside the connection point.

The rest of the structure may have SMA welds if desired. Automatic GMA welding can be used if the structure is suitable.

Phenomena of Restraint Cracking

Rationalizing restraint-cracking parameters requires understanding of the combined effects of restraint-stress level, preheat, and time. Diagrams developed by Japanese investigators illuminate the mechanisms involved; Figures 125 and 126 are generalized examples. Figure 127 illustrates weld metal restraint cracking.

Parametric studies of this type have been used to solve a variety of restraint-cracking problems. This approach defines a critical restraint intensity K_{cr} for cracking and a critical restraint stress σ_{wc}. Material and welding variables are assessed and compared by these parameters. The method uses a Y-groove weld restraint test that simultaneously tests the

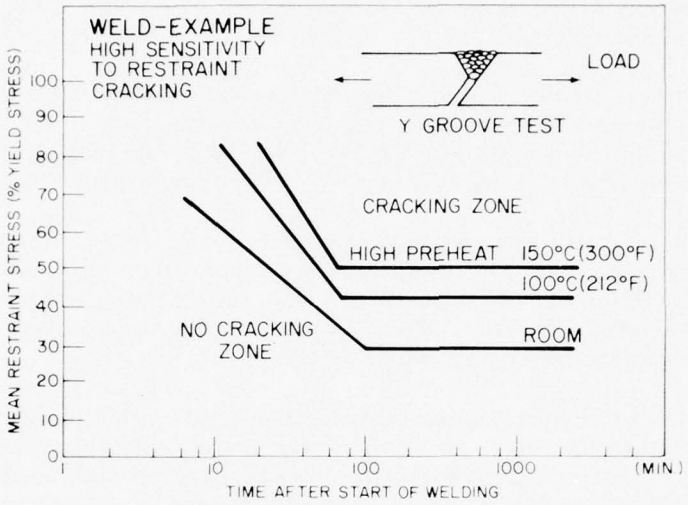

Fig. 125—Parametric relationships for restraint cracking in metallurgically sensitive weld metals.

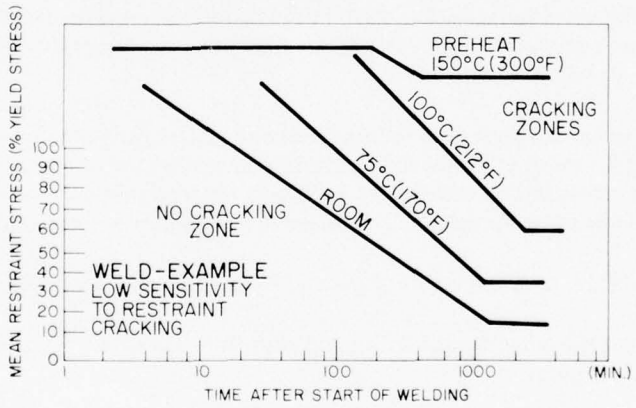

Fig. 126—Parametric relationships for restraint cracking in weld metals of low metallurgical sensitivity.

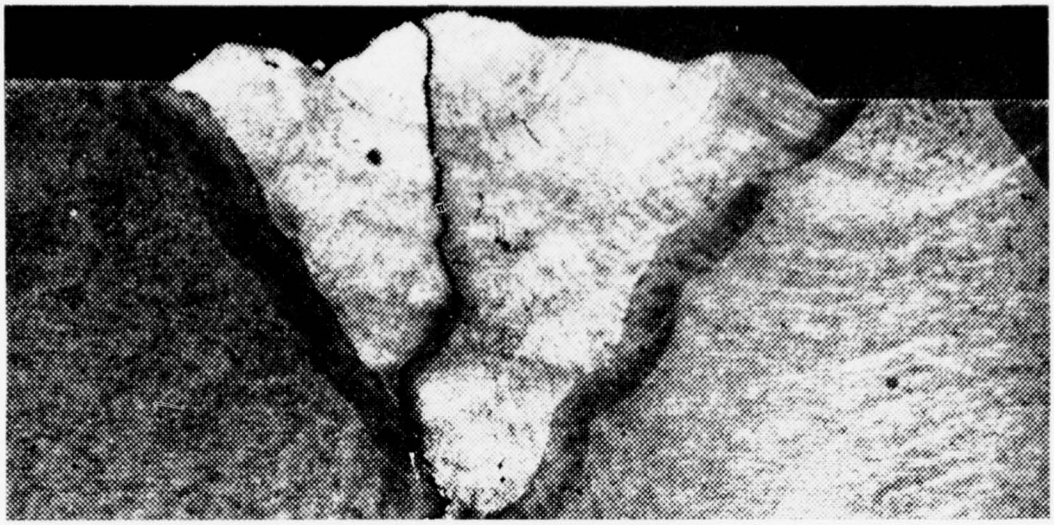

Fig. 127—Restraint crack in multiple-pass stick-manual-arc (SMA) weld.

cracking susceptibilities of the weld metal, the bond between weld metal and parent metal, and the heat-affected zone. One procedure, the Rigidly Restrained Cracking (RRC) test, restricts weld joint contraction during welding. A second, the Tensile Restraint Cracking (TRC) test, applies a fixed load to the weld joint immediately after welding.

The significance of a critical restraint stress for a given preheat temperature is that no weld cracking occurs at lower restraint stress, regardless of how long maintained. The minimum preheating temperature required for preventing cracking depends on the structural restraint condition and the weld zone material.

Figure 125 illustrates general relationships for weld metals with high sensitivity to restraint cracking of the type illustrated in Fig. 127. At the highest practical preheat of 300°F (150°C), delayed cracking results at low stresses (approximately 0.5 σ_{ys}). The delay indicates that hydrogen-assisted cracking was involved; the original fissures are considered to be the result of hot cracking.

Figure 126 illustrates general relationships between restraint stress and time for welds with lower sensitivity to delay cracking, if practical preheats of 212°F (100°C) are applied. Cracking is limited to severe restraint stresses in the plastic load range. Delay effects are obvious for low preheat temperatures, but high restraint levels are required.

Preheating eliminates hydrogen by diffusion. Delayed cracking in the presence of hydrogen demonstrates that the restraint system also produces hot-crack fissures, which are extended (or not) by hydrogen-assisted cracking. The extension depends on the hydrogen level and the strength level of the electrodes.

The combination of parameters that must be controlled, and the level of control, must be known in order to characterize the weld composition and welding procedure. The match to the structural restraint level must be made by assigning a critical restraint intensity K_{cr} to the joint.

For purposes of this discussion, we may categorize the K_{cr} values as follows:

- High values—Critical stresses close to or equal to σ_{ys}
- Intermediate values—Critical stresses equal to 0.5 σ_{ys}
- Low values—Critical stresses on the order of 0.25 σ_{ys}.

If information of the cracking diagram type is available, a reasonable selection will follow. The qualitative descriptions of Fig. 124 have been confirmed quantitatively by parametric studies of this type and by analysis of models.

SYSTEMS ANALYSIS OF WELD FACTORS

This section illustrates the logic of sequential analyses, conducted in iterative fashion, for solving weld criticality problems. The object is to preclude fracture or crack growth in weld regions. In a broader context, the welded regions of the structure are desired to have the same structural integrity as the rest of the structure.

At the outset, it should be emphasized that structural integrity (SI) solutions for the base material must be within the bounds of engineering reality. The solutions must be conservative; the object is not to prove the critical point for failure, but to stay on the positive, high-assurance side.

The first steps of the design process define desirable strength levels and section sizes. The function of the structure defines the configuration and the adjustability of features such as structural redundancy and location of geometric transitions at connections. The latitude for adjustment of these features must be understood.

For example, assume that preliminary design analyses have defined the following factors and options:

- The structure has features represented by Fig. 120, plates of 2-in. (50 mm) section size, and rigid connections. These combinations provide a worst-case situation of weld restraint.
- Steels of 120-, 140-, or 160-ksi (827, 965, or 1103 MPa) minimum yield strength may be chosen.
- Either SMA or semiautomatic GMA welds may be used at connection points.
- Forging inserts may be used at the sharp corners, to place the welds away from these high-stress positions.
- Matching-strength welds or welds of 20 ksi (138 MPa) lower strength than the base metal (undermatched to the next lower level) may be used.

Conservative SI objectives are established, as follows:

- High elastic-plastic fracture properties
- No weld restraint cracking, including delay effects (hydrogen-assisted cracking).

The analysis sequences are recorded in Tables 3 and 4 for fracture properties and hydrogen-assisted cracking, respectively. The tables indicate the minimum yield strength cited for the design objective and for the high end of the strength range expected in normal production.

Table 3—Fracture properties analysis for 2-in. (50 mm) section size

Properties	Low Option		Intermediate Option		High Option	
	(ksi)	(MPa)	(ksi)	(MPa)	(ksi)	(MPa)
Strength Reference						
Design σ_{ys} (min)	120	827	140	965	160	1103
Production σ_{ys} (max)	140	965	160	1103	180	1241
Analysis σ_{ys}	140	965	160	1103	180	1241
Material Reference						
Base steel (Intermediate corridor)	P		H/EP		PS	
SMA weld	H/EP		PS		PS	
GMA weld	P		H/EP		PS	

Code: P = Plastic
H/EP = High elastic-plastic (acceptability criterion)
PS = Plane strain (unacceptable)

Table 4—Hydrogen-assisted cracking analysis

Properties	Low Option		Intermediate Option		High Option	
	(ksi)	(MPa)	(ksi)	(MPa)	(ksi)	(MPa)
Strength Reference						
Design σ_{ys} (min)	120	827	140	965	160	1103
Production σ_{ys} (max)	140	965	160	1103	180	1241
Analysis σ_{ys}	140	965	160	1103	180	1241
Material Reference						
Base steel (low H_2)	I		I		I	
SMA weld (high H_2)	S		HS		HS	
SMA weld (intermediate H_2)	I		S		HS	
GMA weld (low H_2)	I		I		I	

Code: I = Insensitive (acceptable)
S = Sensitive (unacceptable)
HS = Highly sensitive (unacceptable)

230-362 O - 77 - 12

The high-end values are used for analysis because they are the controlling factors for the sharp strength transitions involved in the analyses.

Table 3 lists the fracture-state properties of the base metal and welds. The section size is 2 in. (50 mm). Data from Figs. 100 and 101 are used for the base metal analyses. The base metal is assumed to be of intermediate corridor quality. Figure 115 gives values for the weld metal analyses.

The high elastic-plastic condition is the minimum acceptable level for fracture properties. Table 3 indicates that this condition is met at the intermediate strength option by the base metal and the GMA weld, but not by the SMA weld. The high strength option does not meet this condition for base metal or welds.

It appears that the structure could be fabricated as follows:

- Strength-matching welds could be produced for the low strength option by the SMA weld and for the intermediate strength option by the GMA weld.

- Undermatching welds could be produced for the lowest strength option by the SMA weld in combination with intermediate strength base metal.

The acceptability of undermatching welds is a separate design question that will not be considered at this point because it involves fatigue considerations. According to fracture considerations, the lower strength weld is fully acceptable.

Table 4 presents the results of analyses of delayed hydrogen-assisted cracking. Since delayed cracking is a severe test of hydrogen effects, it is prudent to establish a criterion of insensitivity to hydrogen; for purposes of this analyses, information from Fig. 124 is used. Note that the hydrogen-sensitivity transitions are zoned at three levels: insensitivity, intermediate sensitivity, and high sensitivity. The trend bands for the transitions in sensitivity to hydrogen-assisted cracking are coded to high, intermediate, and low hydrogen content.

Using Fig. 124 necessitates consideration of typical hydrogen contents of base metal and specific welds; these are given in Table 4. It is also necessary to consider the degree of weld restraint. The initial analysis is for a highly restrained structure. Therefore, the insensitivity criterion cited above is mandatory.

Table 4 shows that analyses of the base metal and GMA weld indicate insensitivity to delayed cracking for all strength options. This is due to the very low levels of hydrogen, which direct the analyses to the L (highest) trend band of Fig. 124.

Table 4 also indicates that the SMA weld can be expected to meet the lowest strength option if hydrogen content is minimized at the intermediate level. It is not reasonable to expect that lower levels can be attained except by unusual practices, such as prolonged baking of the welds by strip heaters. By applying appropriate preheat, intermediate hydrogen contents can be attained; therefore, the intermediate trend band of Fig. 124 is used for the analysis. Ordinary SMA welds result in high hydrogen contents, which require reference to the H (lowest) trend band of Fig. 124.

The boundary indicated in Table 4 separates the acceptable (insensitive) from the unacceptable (sensitive) conditions for a highly restrained weld. If restraint is decreased by the use of insert forgings, the welds may then be acceptable at the sensitive, but not highly sensitive, degree of relative sensitivity. Insert forgings are of benefit only for SMA welds of minimized hydrogen content. The use of insert forgings raises the limit for the use of SMA welds from the lowest to the intermediate strength option.

Table 4 indicates that hydrogen-assisted cracking problems are of concern only if SMA welds are used. However, it does not imply that GMA welds always eliminate these problems. The GMA welds must be deposited under appropriate conditions, as cited in the following sections, and this requires precise quality control.

Considered together, Tables 3 and 4 indicate that the highest strength option is eliminated because of inadequate fracture properties of both base metal and welds. (In fact, the base metal analyses by itself is decisive.)

A final decision on using the intermediate option is fully decided by features of the weld, not the base metal. Careful design for welding is required in using the intermediate strength option. Relaxation of factors related to welding is allowed only by the lowest strength option.

This example of systems analysis indicates the importance of considering weld factors early in the design process.

ADDENDUM

INTRODUCTION TO WELDING METALLURGY AND WELDING PROCESSES

WELDING METALLURGY FOR STEELS

The microstructural state of a steel determines its strength level, hardness, and other mechanical properties. The alloy elements control the type of microstructure that is developed for any given cooling rate. Cooling rate, in turn, is determined by section size and heat-treatment procedure.

If the metal is air cooled from high temperatures (normalized), the cooling rate is relatively slow; the specific rate is strictly related to section size. The cooling rates due to quenching are much faster and are likewise related to section size and geometry. Flat plates quench-cool slower than bars, for example. The quenching medium may be varied, within limits, to influence cooling rates.

Relatively small differences in quench-cooling rates are important because they influence the nature of transformations (to a degree depending on the alloy). Some steels transform to desirable microstructure at a fairly wide range of quench-cooling rates; for others a very narrow range of cooling rate is critical. High-alloy steels are tolerant of variations in cooling rate, and low-alloy steels are more sensitive.

Differences in the cooling rate that develop in welding have similar effects. High-alloy steels are tolerant of a wider range of weld-cooling rates than low-alloy steels. Thus, the first step in welding metallurgy is understanding the alloy balance of the base steels.

Continuous-cooling transformation diagrams (Figs. 128 and 134) are the basic reference for the cooling transformations of the base steel. The transformations in the heat-affected zone may be deduced from these diagrams. For welds, a diagram specific to the weld alloy composition is a necessary reference.

The first step in heat treatment for normalizing or quenching is austenitization, i.e., heating to high temperatures, on the order of 1650°F (900°C). This puts the metal in a state of complete solid solution of the carbon and all alloy elements. This homogeneous phase is termed austenite.

When cooled below 1330°F (720°C), the austenite becomes unstable and transforms to a mixture of ferrite and carbides. The ferrite is a solid solution of carbon and some of the alloy elements in an iron matrix. The carbides are intermetallic compounds of iron with carbon and alloy elements, such as Fe_3C and more complex carbides of Mn, Cr, Mo, and V.

Strength is determined by the amount and distribution of the carbides. Coarse carbide structures result in low strength, and very fine dispersions of carbides result in high strength and hardness.

Normalizing leads to relatively coarse aggregates of ferrite and ferrite-plus-carbide (pearlitic) microstructures. The pearlite part consists of closely spaced platelets of iron carbide and ferrite. The microstructure is fully developed on cooling, and subsequent heating, as for stress relief, has no effect on microstructure.

Quenching ordinarily results in relatively hard microstructures called martensite and bainites. Martensite is a supersaturated phase of iron, containing much of the alloy elements

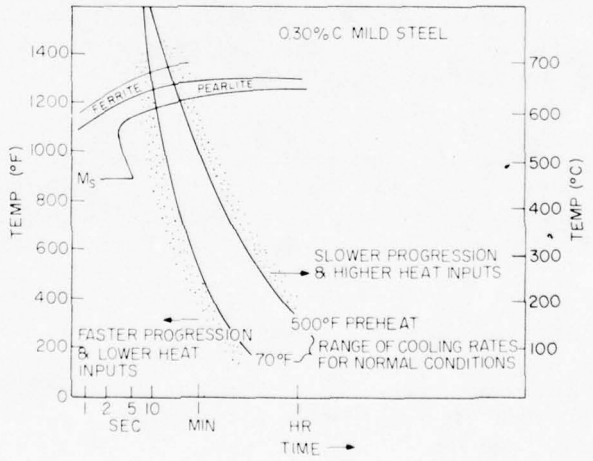

Fig. 128—Transformation features of low strength (C-Mn) pearlitic steels.

present in the austenite. On reheating (tempering) to temperatures below 1330°F (900°C), the unstable phase rejects alloy carbides in very fine dispersion. Bainites are acicular products that are finely dispersed on cooling, with some degree of remaining supersaturation. Subsequent tempering may cause additional rejection of finely dispersed carbide (secondary hardening). However, the other effect of tempering on martensite and bainites is agglomoration of fine carbides to larger particles. This softens the excessively hard phases to the desired level of hardness and strength. The as-quenched brittleness of the hard martensite and bainite structures is replaced by the as-tempered strength and ductility of the agglomorated fine carbide structures.

The implication to welding metallurgy is that heat-treatment effects of welding alloy steels take place in two stages. The resulting microstructure is the product of the quenching rate and the tempering effect of subsequent weld passes. For pearlitic steels, this tempering occurs only if the quenching rates have been fast enough to preclude pearlite formation and thus foster a martensite transformation.

The various types of transformations can be discussed in terms of the welding conditions that determine cooling rates and tempering effects in pearlitic and alloy steels.

PEARLITIC STEELS

The transformation features of C-Mn (pearlitic) steels are illustrated in Fig. 128. The cooling rates after normalizing result in transformation of some of the austenite to ferrite in the temperature range from about 1300° to 1200°F (700° to 650°C). The remainder of the austenite then transforms to pearlite in the range from 1200° to 1150°F (650° to 620°C). The resulting aggregate microstructure is illustrated in Fig. 14.

Increasing or decreasing cooling rates causes small but significant changes in the temperature range of the transformations. This feature may be noted by following the course of the ferrite and pearlite transformation zones in Fig. 128. Slower cooling, through higher temperature transformation regions, produces coarse pearlites of inferior fracture properties. Faster cooling, through lower temperature transformation regions, results in finer, more desirable pearlites and thus moderately increases strength and improves fracture properties.

Quenching small pieces of such steels in water results in cooling rates that cross the ferrite zone and then cut through line M_s, which represents transformation to martensite. This transformation takes place very rapidly at a critical temperature. Because there is no temperature range of transformation, as there is for pearlite, the process is almost instantaneous. If progressively larger pieces are quenched, cooling rates decrease and the transformations result in mixtures of ferrite, pearlite, and martensite. Eventually the martensite fraction is eliminated. These transformations are called split transformations; they produce mixtures of hard and soft products.

Moving slowly along the weld, using large electrodes and high heat inputs, results in slow cooling of the heat-affected zone. Accordingly, weak, coarse, ferrite and pearlite structures develop. The cooling rate is a function of the volume of metal heated to high temperatures (molten pool) and the volume of the heat sink, i.e., the thickness of the metal and the number of metal parts that comprise the weld joint. Fast progression, small electrodes, and low heat inputs

result in fast cooling rates for metals of thick section. Thin sections generally cool slowly because of the limited heat sink.

The main problem in the heat-affected zone for these steels is excessively fast cooling that results in total or split transformation through the M_s region. This makes the heat-affected zone hard and brittle compared to the base plate.

An arc strike or a small fillet weld produces a hard heat-affected zone. Therefore, these apparently minor fillet welds are dangerous because the surrounding heat-affected zone can initiate cracks if the base metal has plane-strain properties. Preheating before welding decreases cooling rates and thus avoids such transformations in the heat-affected zone. Arc strikes are harder to control because of their accidental origins.

The above discussion should emphasize that cooling rate quality control for the strength welds of the structure may be useless if minor welds are ignored. The minor welds can be critical in fracture and crack growth. Figure 129 illustrates the origin of a ship fracture traced to a clip weld.

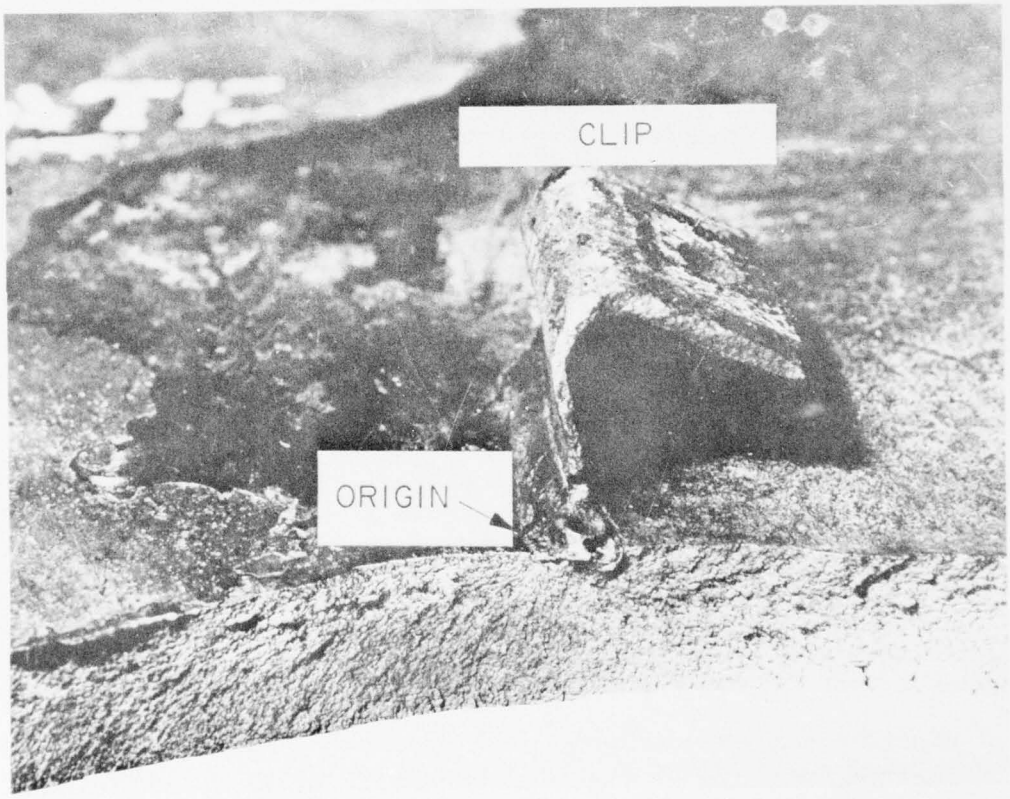

Fig. 129—Ship fracture origin due to a minor weld for attaching a clip. A great many structural failures of pearlitic steels have been traced to minor welds or accidental arc strikes.

The criticality of minor welds in pearlitic steels is a major problem for SI analyses. The only reliable solution is to avoid steels of plane-strain properties. If this is done, controlling the properties of the heat-affected zones of strength welds becomes a practical engineering goal.

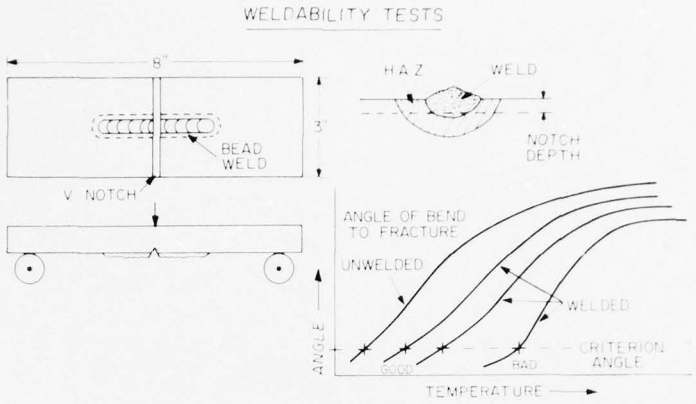

Fig. 130—Features of weldability tests, conducted to determine the effects of cooling rates on the heat-affected zone.

The importance of the heat-affected zone in promoting plate fracture led to the early development of "weldability tests" for indexing the degree of embrittlement in the heat-affected zone. These tests are performed to investigate the effects of weld deposition procedures and to assess the response to specific weld heating and cooling cycles. The tests generally feature bead-on-plate weld deposits somewhat similar in appearance to the weld bead of the DWT. Figure 130 illustrates the general features of weldability tests. A notch is cut across the weld bead and plate surface at the center of the specimen. The tests are conducted by slow bending using a roller anvil. The degree of bend angle at fracture is plotted as a function of temperature, which results in a transition curve. The relative embrittlement of the heat-affected zone is defined in terms of the transition temperature, indicated by a low bend angle, as noted in the figure. The series represents typical families of transitions for varying weld-deposition parameters.

QUENCHED AND TEMPERED ALLOY STEELS

The functions of typical alloy elements are illustrated in Fig. 131. Note that increased alloy content is required for desirable transformations with increased section size. Transformation diagrams for steels of this type generally feature a bainite zone, as noted in Fig. 132.

The base metal is heat treated by heating to austenitizing temperatures and then quenching in water. Quenching prevents transformation of the high-temperature austenite phase to undesirable pearlites and upper bainites, which are the normal products of transformation on slow cooling. These products have relatively coarse microstructures and so yield inferior strength and fracture toughness. Transformation to bainites and martensites is desirable

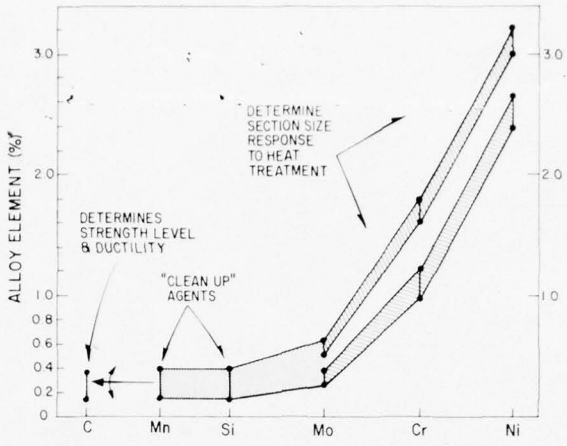

Fig. 131—Function of alloy elements in high-alloy Ni-Cr-Mo steels. Top band indicates alloy requirements for plates 2 to 3 in. (50 to 75 mm) thick. Bottom band is for plates 1 in. (25 mm) thick.

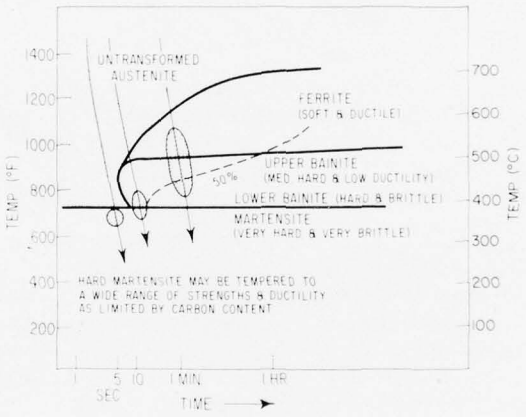

Fig. 132—Transformation features of high-alloy Ni-Cr-Mo steels.

because of their very fine microstructures. These products, which are called in general "martensites," are hard and brittle as quenched and require tempering to develop desirable combinations of strength and ductility. Tempering means reheating to temperatures in the range noted in Fig. 133 for periods that range from a fraction of an hour to several hours. The highest tempering temperatures produce lowest strength and maximum fracture toughness; the lowest temperatures result in highest strength with low fracture toughness.

The carbon content of the as-quenched martensites determines the strength level attained for a given tempering temperature and time. The effects of alloy elements, such as Cr, Ni, Mo,

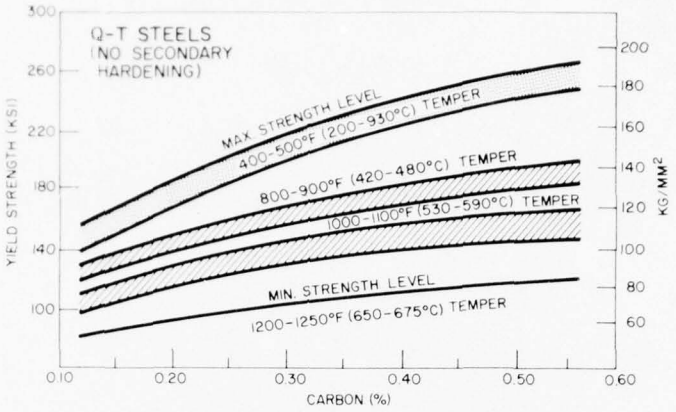

Fig. 133—Relationships of yield strength to carbon content and tempering temperature.

and Mn, on tempered strength are secondary compared to those of carbon. The major fuction of the alloy elements is to control the hardenability of the steel, i.e., the section thickness that can be quenched to martensite without partial transformation to pearlites and upper bainites.

In steels intended for welding and use in the as-welded state, it is generally necessary to restrict carbon content to below 0.20%. Hardness and relative brittleness of as-quenched martensites increase rapidly with increasing carbon content. The heat-affected zone, which transforms to martensite as the result of rapid cooling from high temperatures, tends to crack if its hardness exceeds specific levels that depend on the degree of weld restraint.

For this reason steels of approximately 90-ksi (621 MPa) strength level, intended for welding of complex structures, normally have carbon contents in the range of 0.12% to 0.18%. For steels of 140-ksi (965 MPa) strength level, it is advisable to lower the carbon content to about 0.10% to 0.14%. The limitations on carbon content require lower tempering temperatures for any specified level of strength. The lower temperatures tend to decrease fracture toughness. This effect may be countered by adding a strong carbide-forming element, such as vanadium, to promote retention of strength for tempering at higher temperatures than normal for vanadium-free steel of low carbon content.

Developing a customized steel to have the optimum combination of strength and fracture properties for a specific thickness is a fairly direct process based on well-established metallurgical principles. However, determining optimum welding conditions is much more complicated and requires consideration of weld cooling rates and degree of structural restraint (geometric complexity). As the alloy content (hardenability) and strength levels increase, optimization of welding conditions becomes more difficult. The use of such steels then depends on closely controlled welding procedures.

We may now discuss welding control in terms of cooling rates in the weld and the heat-affected zone. The essence of the problem is illustrated in Fig. 134 in relation to the transformation diagram of the base metal. The range of cooling rates for the normal operating

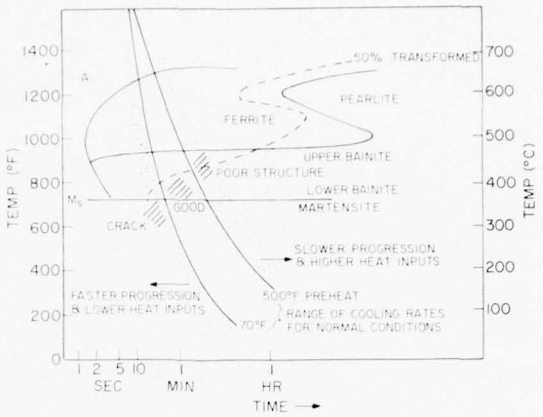

Fig. 134—Effects of weld cooling rates in preventing undesirable high-temperature transformation or crack formation.

conditions of stick electrodes is correlated with a range of preheats varying from no preheat to the normal maximum of 300°F (150°C). In this range, transformation products of good quality can be attained. Slower welding progression and higher heat input result in transformation to bainite structures of lower ductility. Faster progression and lower heat input result in the development of martensite, with consequent cracking of the heat-affected zone.

The normal trends in the development of higher strength steels shift the transformation diagram to the right, so that the kneelike region moves into the cooling-rate band for welds. This shift makes necessary more exact control of cooling rates to avoid cracking in the higher strength steels. In other words, the controls tend to move to limits that are narrow for human control and thus necessitate automatic, machine-controlled welding. Such welding cannot be done out of position (other than downhand) except by very difficult setup procedures. The 140-ksi (965 MPa) level is at the borderline of the need for automatic welding techniques similar to those used for rocket cases.

Another problem is the increased finesse required in tempering high strength steels that are heat treated to low tempering temperature. Figure 135 illustrates the effects of subsequent passes in tempering the hard martensite region created by the previous pass. Proper placement of the tempering pass is required to soften the hard zone, which would otherwise crack in service or on cooling. For steels tempered at high temperatures this is enough of a trick to call for expert welding and specified welding practices. For steels of higher strength, it is even more difficult and requires automatic welding. For steels above the 150-ksi (1034 MPa) level, manual welding is eliminated from consideration.

WELDING PROCESSES

The development of welding processes has been stimulated by the technological advances dealing with temperature and strength transitions. Investigations of structural failures of low strength pearlitic steels disclosed that the basic engineering problem was not preferential

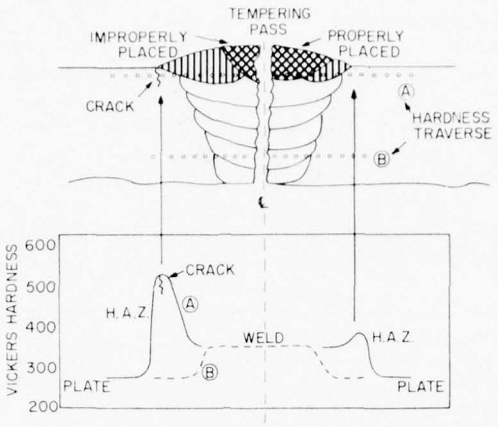

Fig. 135—The final tempering pass must be properly placed at the crown of the weld, to temper the heat-affected zone of the two prior passes at the edge of the weld.

fracture of weld zones but was inherent to the plane-strain properties of the base metal. The weld regions provided a trigger for initiating fractures, which could then extend through the base metal. When this was understood (1950), research was redirected to economic questions. Automatic welding was developed to minimize cost.

The high strength metals featured problems of fracture and crack growth in the weld and heat-affected zone. Accordingly, welding processes that emphasized quality were needed. Again, automatic welding was required, but it had to be different from the processes used for low strength steels. For high strength steels, a relatively large number of small beads are deposited, cooling rates are exactly controlled, and weld shrinkage stresses are minimized. Deposition rates are secondary to the quality control.

The various welding processes were developed to meet specific requirements. Accordingly, selection of welding processes is intrinsic to structural design. Different welding processes must be used for specific locations in complex structures, depending on accessibility of the joint, positioning of the work, local geometry of the weld-joint area, configuration of the joint, and other considerations determining whether specific types of automatic welding equipment can be used.

The fraction of the welding that is done by hand on a given structure is an index of the attention that has been given to design for welding. Manual welding is used only for welds not amenable to automatic welding. As the least controllable type of welding, it may be used when there is metallurgical tolerance for deviations from optimum macrostructural and microstructural conditions in the weld and heat-affected zone. To varying degrees, the manual weld joint is "designed" by the dexterity of the welder. If the plan calls for a difficult weld, the operator may be forced to an ad hoc solution of undesirable features.

The choice of welding processes is central to quality control. A visual estimate of relative quality may be made by referring to cross sections of representative welds. The poor quality that

may result from manual welding with stick electrodes is evident in Fig. 136. At the other extreme, Fig. 137 illustrates an almost invisible weld performed by electron-beam (EB) welding. From a mechanical point of view, the EB weld is nearly indistinguishable from the base metal. It is in this way somewhat similar to a braze joint for a high strength steel. The mechanical properties of a braze joint are not those of the low strength bond material (Cu alloy), but rather are equal to those of the steel (for reasons of mechanical constraint). For the same reasons, if a weld is narrow enough, then from an engineering point of view there is no weld.

Intermediate to these cases is the nearly perfect automatic weld of Fig. 138. Metallurgically and in regard to defects such welds can be almost exactly like the base metal.

The example of Fig. 138 is typical of requirements for welding high strength metals. Accurate fit-up and machining of the joint are essential. An exact relationship of the welding bead to the work is maintained by accurate control of the relative motion of work and tools. Welding shops qualified for such work have the general appearance of machine shops.

The conversion of conventional manual welding to mechanized welding (Fig. 139) is ordinarily not complete. Locations amenable to automatic welding are selected, and joints there are improved. The rest of the structure is welded manually. The desire to minimize weld joint preparation and fit-up can lead to problems such as those illustrated in Fig. 140. The automatic submerged-arc weld was subject to excessive shrinkage stresses and cracked as a result.

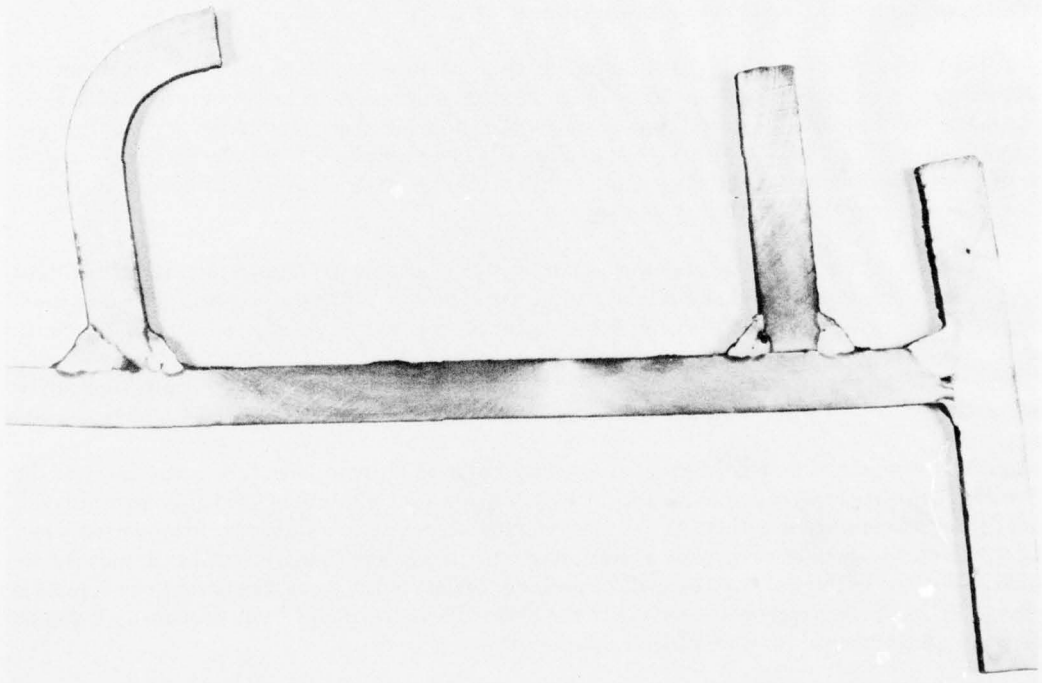

Fig. 136—Manual welds from 1942 ship structure.

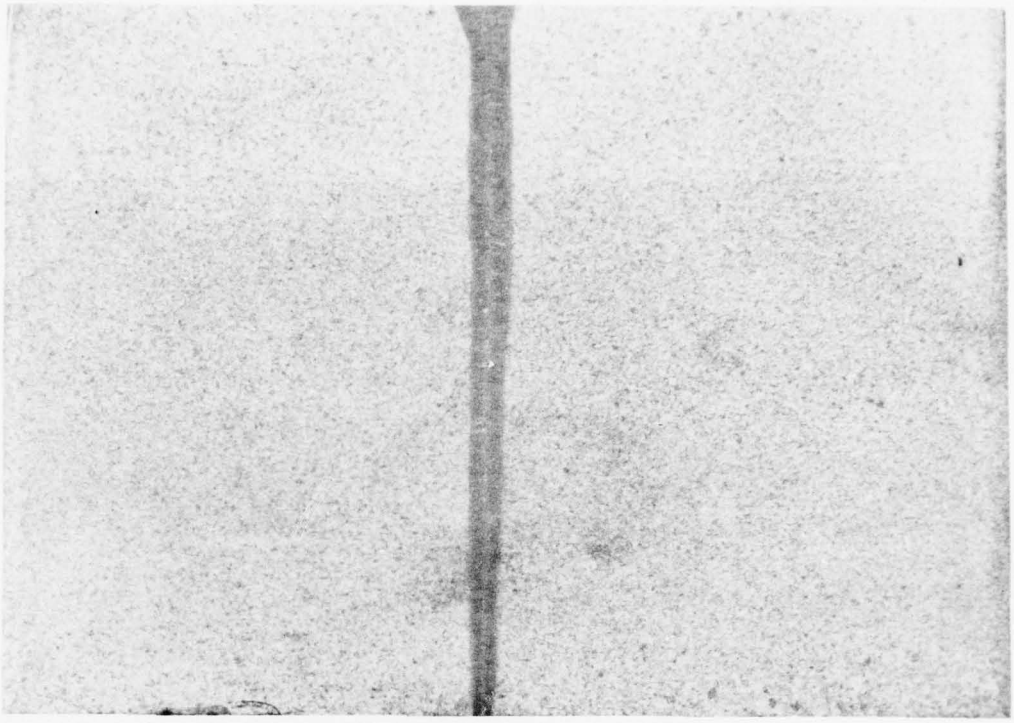

Fig. 137—Electron-beam (EB) welds require exact fit-up and machine preparation of the weld joint, plus precise positioning of the electron beam.

These discussions indicate that intelligent selection of welding processes, investment in positioning equipment, and proper design for welding are inseparable. The main welding processes are now described.

Shielded-Metal-Arc Welding

This is a manual stick welding process. The electrode is a flux-covered core wire of low-carbon iron. The alloy elements are present in the flux, which also controls arc atmosphere and provides flux protection of the molten metal. The protective CO_2 atmosphere of ordinary electrodes is from cellulose in the coating. Cellulose also provides considerable hydrogen; since hydrogen is undesirable for intermediate strength steels, a low-hydrogen coating is available. Low-hydrogen electrodes have a water content of 0.02% or less, compared to as much as 7% for cellulosic types. Special precautions, including baking and storage in ovens before use, are used to limit moisture content. However, these precautions are not sufficient to prevent hydrogen cracking of highly restrained welds where yield strength exceeds 120 ksi (827 MPa). High preheating temperatures and extended postweld soaking may then be necessary to eliminate hydrogen by diffusion. Quality control becomes difficult above the cited strength range if the structure has regions of high restraint.

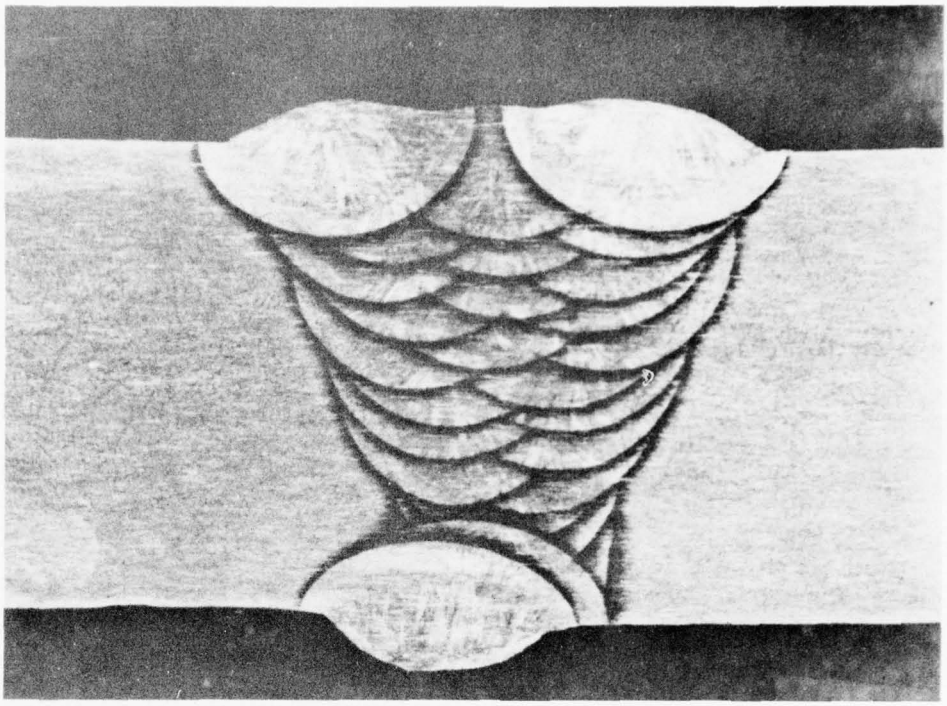

Fig. 138—Typical multipass, automatic GMA weld for high strength steels— 1-in. (25 mm) plate.

Submerged-Arc Welding

This process uses granular flux that forms a protective covering for the arc pool. Relatively large wire from a spool is fed to the arc between the electrode and the work piece. Alloy elements are introduced by the wire and the flux. The process allows relatively fast welding and deep penetration. Quality is generally intermediate between that of SMA and GMA welds. The main advantage is high deposition rates. However, emphasis on this may result in relatively low cooling rates, which are detrimental to high strength welds. Machine control features provide for better general quality than in SMA welds. Low-hydrogen welds of this type may be made if the water content of the flux is limited.

Gas-Metal-Arc Welding

In GMA welding, a relatively small wire from a spool is fed to the weld pool site. The arc and weld pool are shielded by inert gas from a nozzle surrounding the wire. Various forms of arc transfer—spray, pulse, or short-circuit—can be used, each of which implies a different mode of delivering the metal from the wire to the work. Automatic equipment and electronic controls allow wide latitude in controlling weld quality and in positioning work. The alloys are present in the wire and therefore provide exact control of composition. If the work and wire are very clean, the hydrogen content of the weld is very low (approaching that of hydrogen-degassed base

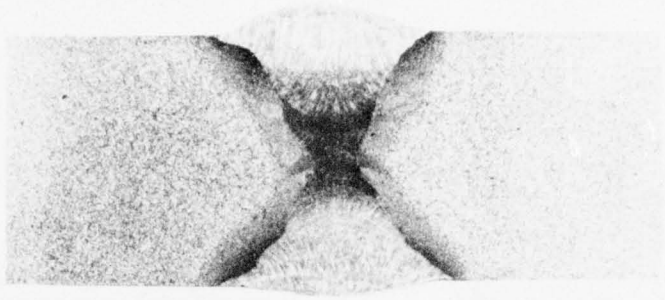

MANUAL - MULTIPASS

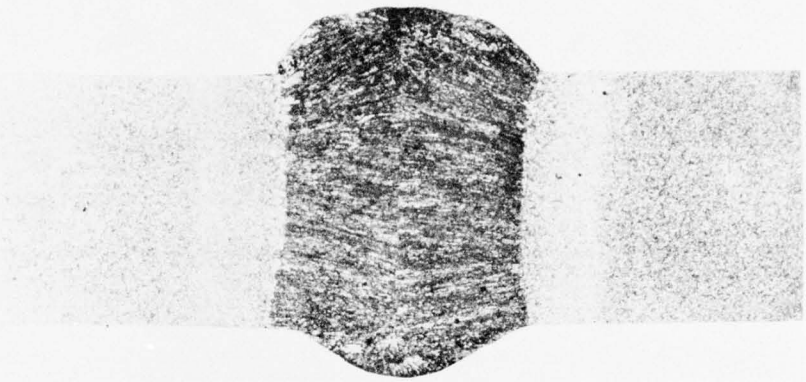

SUBMERGED ARC - SINGLE PASS

Fig. 139—Typical welds for conventional low and intermediate strength steels—1-in. (25 mm) plate.

metals). Accordingly, hydrogen-assisted cracking is minimized for high strength steels. In general, this process is required for steels with yield strength in excess of 150 ksi (1034 MPa).

Gas-Tungsten-Arc Welding

In GTA welding, a thin wire is fed to the arc between the joint and a nonconsumable tungsten electrode; inert gases provide shielding. The process may be manual or automatic. Very high quality welds of very low hydrogen content may be produced. Many variations of wire feed and electronic controls provide for exact adjustment of composition, cooling rate, etc.

The foregoing processes are only the primary welding processes of interest for welding throughout the range of the strength transition. The emphasis is on comparing features that

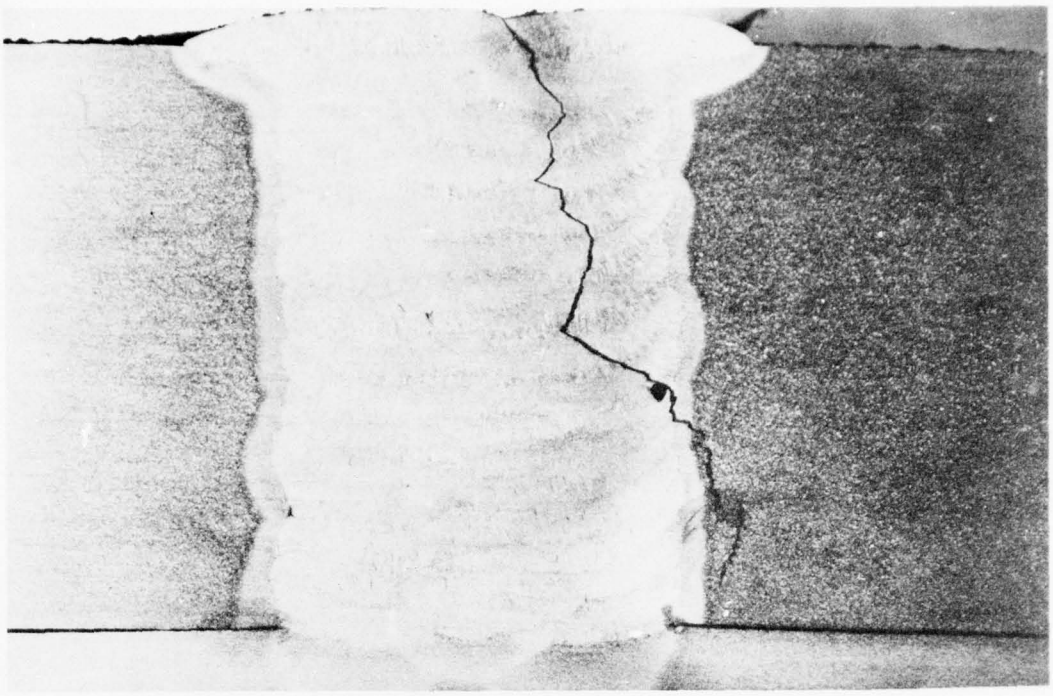

Fig. 140—Cracking of multipass, submerged arc weld due to high restraint—1.5-in. (37 mm) plate.

provide for control of metallurgical quality. In general, staying in the intermediate or high corridors of the high strength range requires fully automatic welding, with precautions to ensure cleanliness of consumables and work.

ELECTRODE SPECIFICATIONS AND ALLOY COMPOSITIONS

The combined AWS-ASTM specifications for mild steel welding electrodes are based on mechanical properties. Chemical analyses are not specified, except for special high strength electrodes.

Electrodes are classified according to the following coding system:

Exxxx	E	electrodes
E60xx	60	tensile strength (in ksi)
Exx1x	1	all-position electrode
Exx2x	2	horizontal- and flat-position electrode
Exx10	10	DCRP
Exx11	11	AC or DCRP
Exx12	12	DCSP or AC
Exx13	13	AC, DCRP, or DCSP

Exx14	14	iron powder coating
Exx15	15	low hydrogen—DCRP
Exx16	16	low hydrogen—AC or DCRP
Exx18	18	iron powder coating of 16 type.

The differences between AC and DC current and reverse and straight polarity (RP or SP) are significant in controlling arc transfer, penetration, and contour of the weld passes. Coating formulations are adjusted for usability.

The important point is that a rational system exists for selecting and using electrodes for particular kinds of welds. In addition, a system of standard welding symbols is used to indicate the joint configuration in design drawings.

Selecting proper proportions in preparing the joint for welding is also important, particularly as it affects accessibility by the electrode. Good accessibility and proper positioning of the work minimize defects and control distortion and residual stresses. All of these considerations are standardized for general reference to recommended practices.

Tables 5 and 6 list typical compositions and yield-strength levels of the electrodes commonly used for primary structural welds.

The chemical compositions listed disclose that general requirements for low carbon content (to preclude weld cracking) result in metallurgical dependence for strength on

- Solid-solution effects of manganese, silicon, and nickel

- Transformations and secondary hardening effects of chromium, molybdenum, and vanadium.

The compositions of intermediate strength welds differ from those of the base steels (see Appendixes C and D) mainly in significantly lower carbon content, much higher silicon content, and moderately higher manganese content.

For higher strength levels, the compositions of SMA welds are generally similar to those of GMA welds. The GMA compositions are the result of conventional alloys plus aluminum, titanium, and zirconium additions in the feed wire. In SMA electrodes, alloys are generally introduced from the coating; thus, greater local differences in alloy content may be expected in SMA welds.

Cooling rate affects the yield strength of the deposits. For example, large electrodes increase deposition rates but result in slower cooling and decreased strength. The weld alloy systems are mainly bainitic or martensitic; that is, they are hardenable steels. Cooling rates and subsequent tempering passes have a pronounced effect on the fracture properties of the weld alloy. Thus, decreasing yield strength by as little as 15 ksi (103 MPa) can produce major strength-transition benefits.

These considerations are important in deciding the specific strength matching of weld and base metal. At higher strength levels, overmatching may decrease fracture properties of the weld in comparison to the base metal.

230-362 O - 77 - 13

Table 5—Principal electrodes

Type	σ_{tu} (Minimum)		As-Welded σ_{ys} (Typical)	
	(ksi)	(MPa)	(ksi)	(MPa)
E6010	60	414	47	324
E6012	60	414	47	324
E6013	60	414	47	324
E7014	70	482	60	414
E7015	70	482	60	414
E7016	70	482	60	414
E7018	70	482	60	414
E8018	80	551	75	517
E9018	90	620	85	586
E11018	110	758	95	655
E12018	120	827	115	793

Table 6—Typical electrode compositions (%)

Type	C	Mn	Si	Ni	Cr	Mo	V
E60xx	0.08	0.40	0.15	—	—	—	—
E7016	0.08	0.70	0.60	0.20	0.10	0.20	0.02
E7018	0.09	0.70	0.60	0.20	0.10	0.20	0.02
E8018	0.09	0.80	0.60	0.90	0.10	0.20	0.03
E9018	0.07	1.00	0.60	1.60	0.10	0.20	0.03
E10018	0.07	1.10	0.50	1.80	0.25	0.40	0.04
E11018	0.07	1.10	0.50	2.00	0.30	0.40	0.04
E12018	0.07	1.90	0.50	2.00	1.10	0.40	0.04
GMA-100	0.07	1.40	0.40	1.80	0.20	0.40	0.04[a]
GMA-110	0.07	1.60	0.40	2.10	0.40	0.40	0.03[a]
GMA-120	0.07	1.60	0.50	2.40	0.50	0.50	0.02[a]

[a]Includes Al, Ti, and Zr at 0.10 levels.

The electrode usability definition systems for GMA and GTA welds are different from those of the SMA types. The various specifications cover the important details by appropriate standards. When attention to welding is critical, it is essential to reference the appropriate specifications in design documents.

CHAPTER 9

Analytical Criteria for Crack Growth Under Sustained Load

REFERENCE SYSTEM

Most engineering problems with sustained-load cracking (SLC) are traceable to strength-transition effects. The transitions from insensitivity to cracking to high sensitivity occur at lower yield strengths than do fracture transitions. Moreover, the sustained-load cracking transition in a given case is much sharper than the fracture transition.

The shift to lower strength ranges means that sustained-load cracking problems generally establish the lower limits for the permissible yield strength of a metal system. The exact limits for specific problems are determined by reference to both fracture and sustained-load cracking transitions. The combined reference is essential for two reasons:

1. The terminal condition for crack growth (arrest or fast fracture) is decided by fracture properties. Terminal events analyses indicate whether fast fracture or nuisance cracks requiring repair may result from sustained-load cracking.

2. The sustained-load cracking transitions are specific to metallurgical features, which thus must be exactly defined.

The situation is analogous to corridor trend bands for fracture. For example, depending on the severity of a given environmental effect, the slope of the sustained-load cracking trend band may vary with respect to the yield-strength scale. To varying degrees, the metal-quality trend bands interact with sustained-load cracking trend bands in establishing specific slopes.

Engineering analysis of these interacting effects presents formidable problems of data management and interpretation. The RAD system, extended to deal with both fracture and sustained-load cracking transitions, provides the only generalized method for such analyses. The basic RAD method has been proved by engineering experience. In general, only a modest extension of it is necessary for data management and analysis of crack-growth problems.

Precise knowledge of the specific cracking processes is important for all engineering analyses. The type of sustained-load cracking must be known if metal properties and structural reliability are to be assessed accurately. The first step is to establish any environmental effects. If any prevail, the environment becomes an important reference for characterization and analysis. Tests must be performed under closely controlled environmental conditions, and the analysis must reflect structural performance in that environment.

In the case of a liquid environment like water, the environmental effect is established by comparing tests in air with tests in the liquid. Generally, the *electrochemical* environment of the

liquid must be simulated in testing. For example, for freely corroding steel, seawater represents a specific electrochemical environment; the same steel coupled to a zinc cathodic protection system in seawater represents another environment. Both are cases of stress-corrosion cracking (SCC). The conventional terminology differentiates them by calling the first "stress-corrosion cracking for freely corroding conditions" and the second "stress-corrosion cracking for zinc coupling." The measured K_{Iscc} values are generally different and therefore specific to the electrochemical environment.

For air environments, hydrogen present in a steel due to melting practices may have important environmental effects. It may, for example, mask the effects of moisture in the air, which causes crack-tip corrosion and introduces additional hydrogen. Ultrahigh strength steels are highly susceptible to stress-corrosion cracking in air due to water vapor. Characterization of this environmental effect requires comparison of tests in vacuum with tests in air of controlled water-vapor content, so that stress-corrosion cracking conditions are characterized for air of specified water-vapor content. Baking test samples to fully eliminate hydrogen due to melting provides a point of reference in determining the full effect of the air environment.

The sustained-load cracking effects of in-situ hydrogen are called hydrogen-assisted cracking (HAC). The K_I crack-growth parameter for this kind of cracking is K_{IH}, which has the same mechanical meaning as K_{Iscc}.

Intermediate strength steels are not susceptible to water vapor in air. Thus, K_{IH} measurements comparing their baked and as-produced properties may be made in air. Such tests may be made to establish the presence of hydrogen deposited in weld metal by different welding processes. The pertinent sustained-load cracking tests are of the K_{IH} type, and test values are specific to the weld metal in the state of interest.

Environmental effects other than electrochemical may be involved when nonferrous alloys are exposed to various liquids in such structures as storage tanks. For example, nitrogen tetroxide and methanol have stress-corrosion cracking effects on high strength titanium alloys.

The presentations to follow do not cover all environmental effects. The object is rather to present general characterization and analysis methods for the sustained-load cracking effects of specific environments. Stress-corrosion cracking of steels in water is used to illustrate analytical criteria and engineering interpretations.

CHARACTERIZATION CRITERIA

The analysis requires that crack growth be characterized under crack-tip mechanical conditions of plane-strain constraint. The reason is that a connection must be established between K_I values of test specimens with maximum-constraint through-thickness cracks and K_I values for surface cracks of specific geometry. If this is not established, the measurements are of no value to engineering analysis.

To date, this equivalence has been established by laboratory tests that include surface cracks (to be described) and by examination of K_I conditions for crack growth in service (failure analysis). The evidence is that the same principles of mechanical constraint apply to both sustained-load cracking and fracture properties. That is, the significance of ratio values is the same, and therefore the analytical interpretations are the same.

It is essential to emphasize that relaxation of minimum section-size limits for test specimens does not necessarily indicate that the same relaxation of constraint rules applies to surface cracks. If this were the case, critical K_I values would be attained by smaller cracks than those observed in service.

This emphasis on plane-strain equivalence is important. There is considerable pressure to relax section-size requirements for K_{Iscc} testing, because of the difficulty of obtaining data for higher ratio values. The cost of experiments is increased by requirements for thick-section specimens. However, the object is analytical validity. Most of the K_{Iscc} data in the current literature provide no confidence for analysis, and the purpose of fracture mechanics characterization, of course, is analysis.

For these reasons, discussions of characterization will be restricted to precracked specimens designed to the same requirements as for K_{Ic} tests. Any RAD extrapolations beyond plane-strain limits for the section size will be reasonably validated by sharp transition features of trend bands.

The lowest value of stress intensity K_I that results in crack growth must be established by a series of tests. Figure 141 illustrates a K_{Iscc} determination for a high strength steel tested in synthetic seawater (3% NaCl) under freely corroding conditions. As noted, K_{Iscc} is an asymptotic value of K_I below which no crack growth takes place. The observation that the specimens did not break below this value, or that the clip gage did not show movement, is not sufficient for careful work. It is usually necessary to produce a fast fracture by increasing load, and then to visually examine the surfaces for evidence of crack growth.

The topography of crack growth by sustained-load cracking is distinctly different from that of fast fracture, as illustrated in Fig. 142. The absence of stress-corrosion cracking microfracture areas is evidence that no stress-corrosion cracking took place. The observation is made at the center region of the fatigue crack, where stress intensity is highest.

The K_{Iscc} value so established is examined for validity as related to the section size of the specimen. The minimum section size for valid measurement is calculated by the same formula

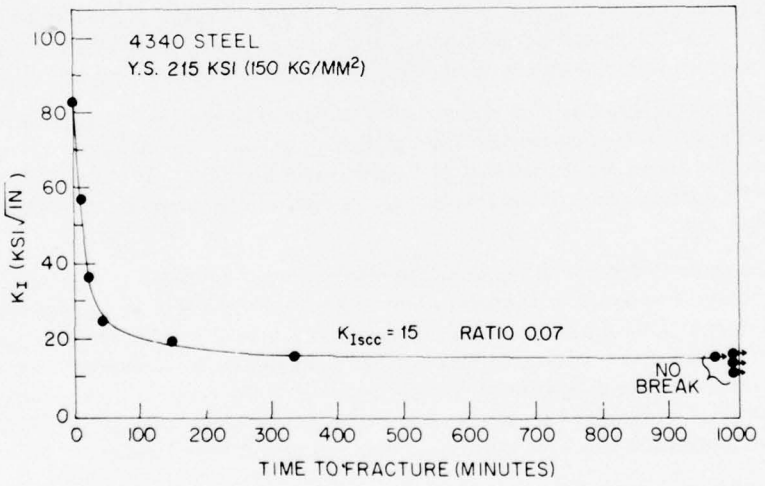

Fig. 141—Test procedure for establishing the lowest level of stress intensity that results in crack growth by stress corrosion cracking, or K_{Iscc}. The environmental condition is synthetic seawater (3% NaCl), freely corroding case.

Fig. 142—Typical topographic feature of stress corrosion crack growth—2.0-in. (50 mm) specimen.

as that used for establishing K_{Ic} validity, as follows:

$$B \geq 2.5\left(\frac{K_{Ic}}{\sigma_{ys}}\right)^2 \quad (K_{Ic} \text{ validity})$$

$$B \geq 2.5\left(\frac{K_{Iscc}}{\sigma_{ys}}\right)^2 \quad (K_{Iscc} \text{ validity}).$$

If the test specimen is of insufficient section size, the inferred K_I value for crack growth should be designated as invalid by established plane-strain standards. This signifies that crack growth took place but constraint was insufficient to provide known plane-strain conditions.

It is worth reemphasizing that the question of validity is crucial to calculations of critical conditions for growth of surface cracks. The analytical calculations are exactly the same as for K_{Ic} test values, and they presuppose that plane-strain conditions apply to both the characterization test and the surface crack. If conditions are not equivalent to plane strain, the calculations are not appropriate.

The requirement for use of appropriate section sizes for the K_{Iscc}/σ_{ys} ratio value poses practical problems. The usual test machines for deadweight loading are limited to about 1.0-in. (25 mm) specimens. This limits valid K_{Iscc} determination to 0.6 ratio. Determination of valid K_{Iscc} values in excess of this ratio requires impractical combinations of lever arm and weights. Use of tensile machine loading is not practical because of the long times involved. Figure 143 illustrates a special hydraulic-ram-loaded lever-arm machine for testing 2.0-in. (50 mm) specimens. This increases the limit for valid K_{Iscc} determination to 0.9 ratio.

Figure 144 summarizes K_{Iscc} data for steels; the data are strictly valid to 0.9 ratio. A modest extrapolation to 1.1 ratio values is indicated by consideration of the trend-band transition effects (to be described).

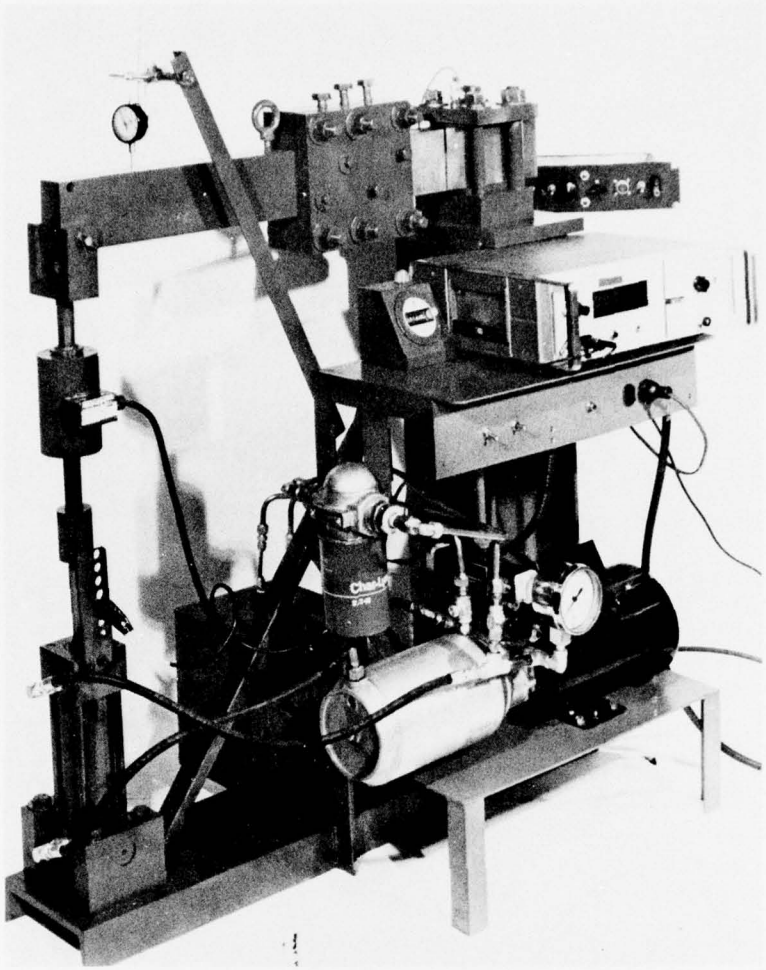

Fig. 143—Hydraulic-ram-loaded bend-type machine for K_{Iscc} testing of 2-in. (50 mm) specimens.

The stress-corrosion cracking data of Fig. 144 are plotted on the RAD display of lower and upper bounds for fracture properties. The following observations can be made:

The transition of K_{Iscc} properties is sharper than that of K_{Ic} properties.

The lower and upper bound curves K_{Iscc} are below those for K_{Ic}.

There are no valid K_{Iscc} data above 0.9 ratio. However, stress-corrosion cracking occurs up to limits estimated at 1.0 to 1.5 ratio. The estimates are made by trend-band procedures, as illustrated in Fig. 145. The three trend bands of relative stress-corrosion cracking quality corridors are evident from the data presented in Fig. 144 for ratios below 0.9. The bands are extrapolated to the 1.5 ratio level, based on evidence that stress-corrosion cracking occurs at

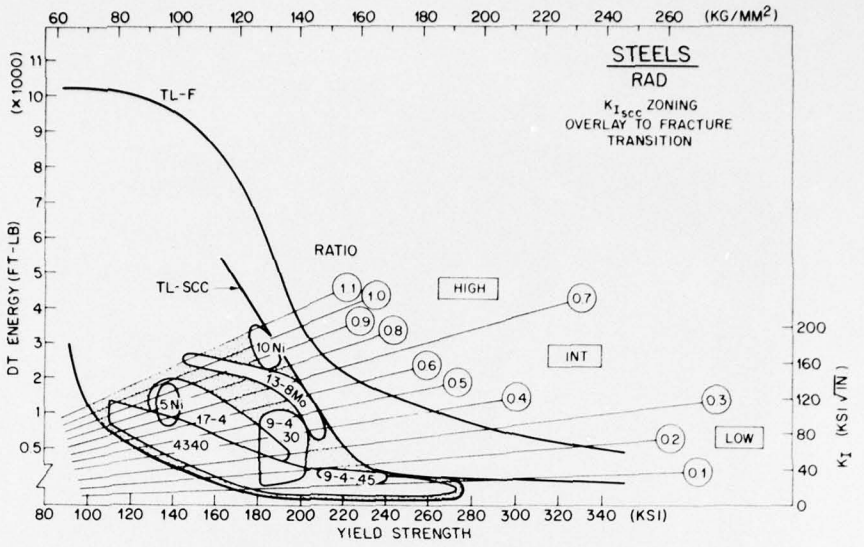

Fig. 144—RAD summary of K_{Iscc} data for steels. K_{Iscc} zones are plotted over fracture envelope limit curves. The K_I scale and ratio lines serve as common reference for K_{Iscc} and fracture properties. (Photo courtesy of C.T. Fujii).

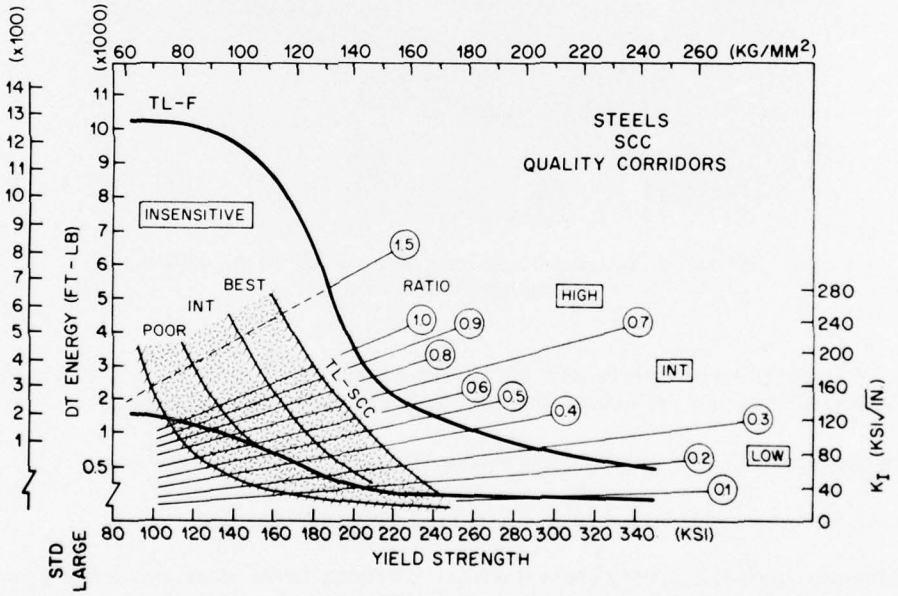

Fig. 145—Metal-quality corridors, as deduced from the data of Fig. 144. K_{Iscc} transitions from insensitivity to high sensitivity (low ratio) to stress corrosion cracking take place over a narrow range of yield strengths. Note technological limits, indicated by TL-F and TL-SCC (for fracture and stress corrosion cracking, respectively).

strength levels up to those intersected by the 1.5 ratio line. For example, poor-quality steels exhibit stress-corrosion cracking to a minimum strength level of about 100 ksi (689 MPa). Below this level, there is no evidence of stress-corrosion cracking, as illustrated in Fig. 146. Long-time tests result eventually in corrosion-blunting of the crack tip. This effect has been noted in steels after 1000 to 10 000 hours.

The strength transition of stress-corrosion cracking properties for poor quality steels is indicated by Fig. 145 (center of band) to have the following order:

Insensitive—below 100 ksi (689 MPa)
Ratio 1.5 (estimated)—at 110 ksi (758 MPa)
Ratio 0.6 (valid)—at 140 ksi (965 MPa)
Ratio 0.3 (valid)—at 170 ksi (1172 MPa).

Similar sharp transitions from insensitivity to stress-corrosion cracking to estimated and then to valid ratios may be deduced from the figure for intermediate- and high-quality steels. The transitions are displaced to higher strength levels by the effects of metallurgical quality. Above 220-ksi (1517 MPa) yield strength, all steels have the same very high sensitivity to stress-corrosion cracking, as indicated by ratios on the order of 0.2 to 0.1 or less.

The basis for development of the trend bands in Fig. 145 confirms the data's usefulness for generalized analysis. The trend bands may be used also for reference to specific effects of variations in the electrochemical environment, such as cathodic coupling as compared to freely

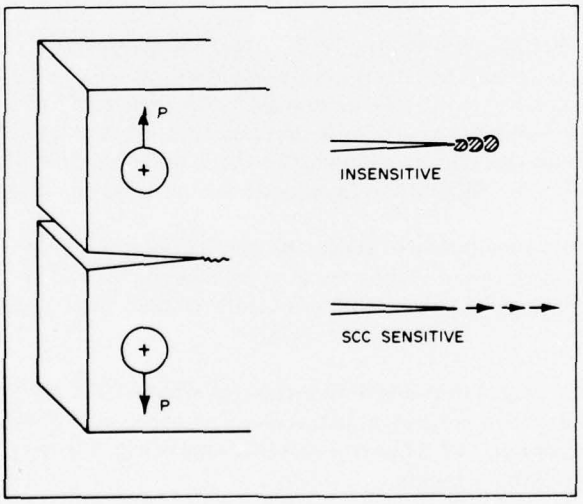

Fig. 146—Definition of insensitivity to stress corrosion cracking. The K_{Iscc} test specimen is held, at the highest K_I stress intensity that does not result in crack-tip yielding, for more than 1000 hours. The specimen is then broken to verify that no crack growth has taken place by stress-corrosion cracking. Crack-tip blunting by corrosion is usually noted when there is no crack growth.

corroding conditions. The plot of Fig. 145 represents freely corroding conditions for baseline reference purposes.

ANALYTICAL SIGNIFICANCE OF K_{Iscc} TRANSITIONS

Service experience and model tests of ultrahigh strength metals indicate that critical crack size and stress combinations for surface cracks could be calculated from K_{Iscc} test values. Observed crack sizes in structural failures due to stress-corrosion cracking matched these calculated values. However, the data were limited to stress-corrosion cracking properties of 0.3 or lower ratio value. The observation included steels and titanium and aluminum alloys.

Recent investigations have established that these analytical predictions for surface cracks are correct for ratio values up to the limit of valid data (0.9 ratio). The investigations involved surface-cracked fatigue test specimens loaded in a large tensile machine (Fig. 147). The screw-loaded machine was capable of holding a fixed stress level for long periods. The initial stress level was set significantly below the calculated stress intensity K_I for the surface-crack size of the specific test sample. The stress level was then increased in steps (with hold periods) to establish the minimum stress intensity for crack growth. Typical data points are plotted in Fig. 148. The reference curves and scales are exactly the same as those of Fig. 56. The significance of the three-part zoning of the ratio scale is the same as for fracture-related ratios.

The test results clearly indicate that the critical K_I conditions for crack growth match exactly the plane strain formula predictions on which the curves are based. These experiments provide convincing evidence for the general applicability of the plane-strain formula to extension of surface cracks by stress-corrosion cracking.

The data points include ratio values from 0.3 to 0.8 and relative stresses from 0.25 to 0.75. There is a considerable amount of failure-analysis data in the 0.1 to 0.3 ratio range, and for a wide range of service stresses, to fully document the low-ratio part of Fig. 148. Accordingly, there was no need for tests to validate the low-ratio predictions; the accuracy of the predictions for the low-ratio zones is well known. The experiments confirmed the validity of the predictions for the intermediate-ratio zone, for which there was little failure-analysis information.

At this point, the reader should examine the implications of Fig. 148. Detection and control of crack states can be expected only for metals of intermediate ratio values. Low-ratio metals present insuperable engineering problems because the critical crack sizes are very small for all levels of relative stress.

The trend bands of Fig. 145 indicate that the transitions from high to low ratio values are very sharp, as related to the yield-strength scale. The three-part RAD zoning of Fig. 145 is reflected in the zoning of Fig. 148. Thus, the implications of Fig. 148 may be translated directly to the RAD-defined transition bands.

The enormous effect of increasing yield strength by 20 to 30 ksi (138 to 206 MPa), which causes a fall from high to low ratios, is apparent. The engineering situation changes from reasonable expectations of crack-size control to complete uncertainty. There is little room for error, and the trend band that applies for a particular case must be established with accuracy. Figure 145 clearly indicates that assuming the wrong trend band leads to grossly incorrect SI analysis.

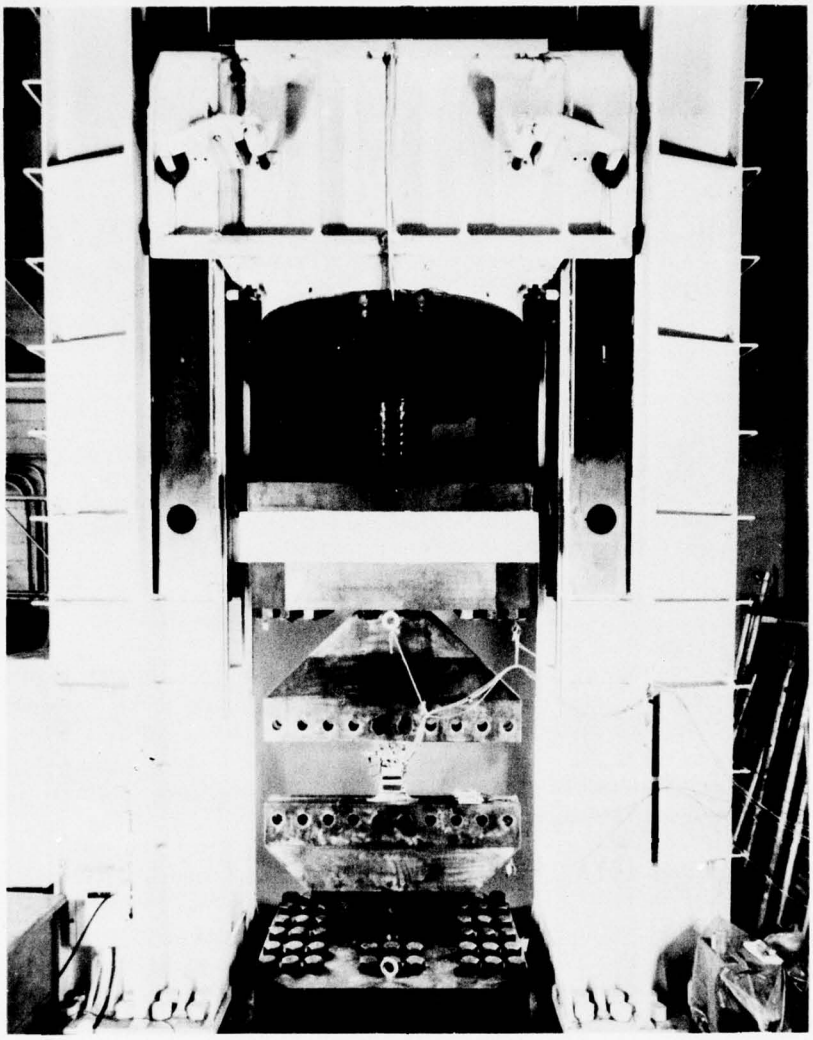

Fig. 147—Rigid (screw-loaded) machine for K_{Iscc} tests of surface-cracked specimens.

These considerations and the RAD procedures for stress-corrosion cracking analysis are exactly the same as for fracture analysis. Accordingly, simultaneous analyses may be made by reference to common features, as follows:

The K_I scale is used to plot both K_{Iscc} and K_{Ic}.

The three-part ratio zoning is common to both K_{Iscc} and K_{Ic} analyses.

The plane-strain limit for a given section size is the same for fracture and stress-corrosion cracking properties.

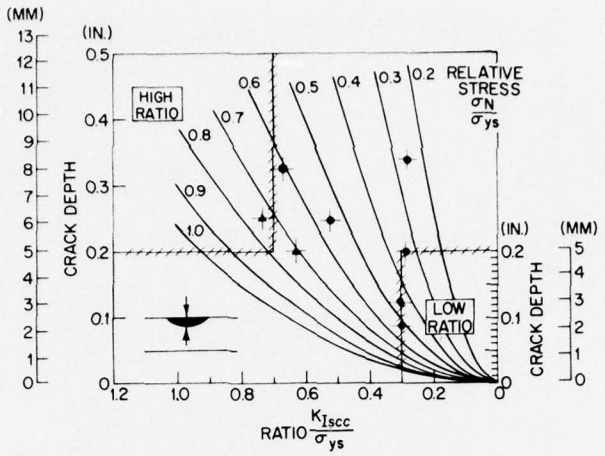

Fig. 148—Relationships of critical crack depth, relative stress, and K_{Iscc}/σ_{ys} ratio for crack growth by stress corrosion cracking. The three-part zoning of low, intermediate, and high ratios is the same as that used for fracture analysis in the RAD.

Figure 149 illustrates sequential SI analysis for the K_{Ic} and K_{Iscc} properties of a rocket case steel. Statistically reliable data from hydrotest failures of Polaris rocket cases (Fig. 150) are available to verify the RAD predictions.

The following steps depend on the RAD plot of Fig. 149 and the relationships of crack size and relative stress to the ratio values in Fig. 148:

- The statistical K_{Ic} and K_{Iscc} properties are plotted at appropriate strength levels.

- The elastic-plastic region for the statistical section size 0.25 in. (6.4 mm) is plotted at the appropriate ratio-line position. The K_{Ic} point, then, lies in the plane-strain region, and fast fracture is the predicted result of crack growth.

- The K_{Iscc} point is located at the 0.1 ratio line.

- For a 0.1 ratio value, Fig. 148 indicates that the critical crack depth for stress-corrosion cracking is about 0.01 in. (0.3 mm) or less for a stress level of 0.5 σ_{ys}. In effect, scratches could provide sufficient conditions for stress-corrosion cracking. Because hydrotesting was conducted in the range of 0.5 to 0.8 σ_{ys}, crack growth by stress-corrosion cracking due to the hydrotest water medium used could be expected to originate from minor defects or scratches.

The K_{Ic} point falls at the 0.22 ratio position. The critical crack depth for fast fracture is (Fig. 148) approximately 0.08 in. (2 mm) for a stress of 0.5 σ_{ys}.

- Crack growth by stress-corrosion cracking starting from defects of 0.01 in. (0.3 mm) or less should enlarge to a size of about 0.08 in. (2 mm), at which point fast fracture should be expected.

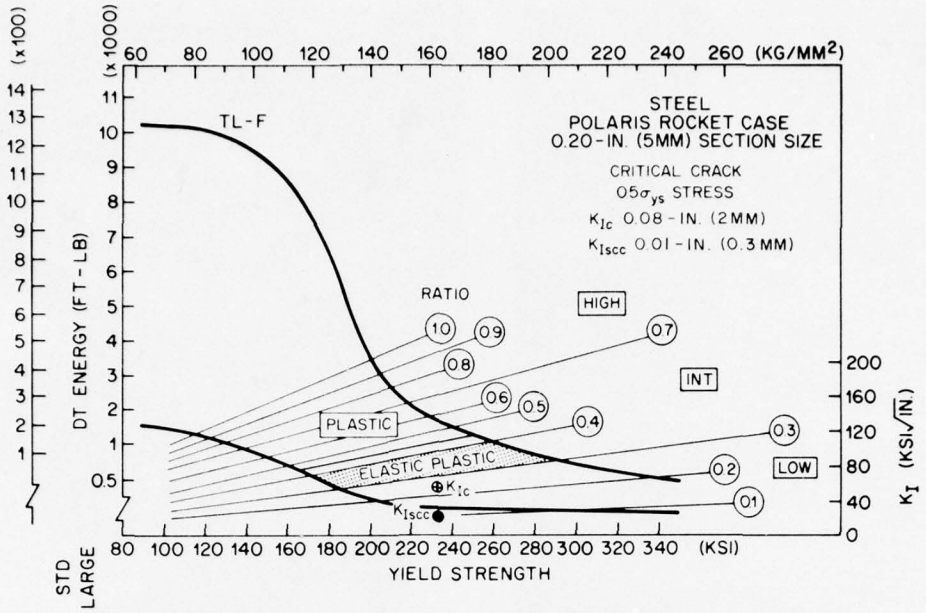

Fig. 149—Combined RAD analysis of fracture and stress corrosion cracking properties of a rocket case steel.

Figure 150 illustrates that the predictions were fully confirmed by hydrotest failures. The depth of the stress-corrosion cracking crack is noted to be about one-fourth of the section size, or 0.06 in (1.5 mm), at the point of fast fracture. There is no evidence of the defect that triggered stress-corrosion cracking; it was evidently very small, on the order of the size of scratches.

Other indirect predictions can be made from the very low K_{Iscc} and K_{Ic} ratios, as follows:

- Statistical probabilities for failure are very high. A large fraction of the rocket-case tests resulted in fracture.

- The time required for stress-corrosion cracks to grow to a terminal condition for fracture is short; the failures occurred during the brief period of hydrotesting (less than 10 minutes).

The practical solution to this problem at the time of the tests (1959-1962) was to use oil as the hydrotest medium. There was no requirement for stress-corrosion cracking properties related to service conditions; the rocket cases are not stressed until fired.

It is of interest to examine the rocket case problem in the context of present information. Figure 145 indicates that the cited K_{Iscc} value, as measured by the first stress-corrosion cracking tests during the early 1960s, are predicted by the RAD for a given strength level. It is now known that the type of steel involved follows the poor-quality trend band of Fig. 145. Thus, reducing stress-corrosion cracking sensitivity to ratio values greater than 0.3 would require a reduction of yield strength to 170 ksi (1172 MPa) or less. Because this is the highest value for the production range, it follows that the design value of minimum yield strength must be set at lower

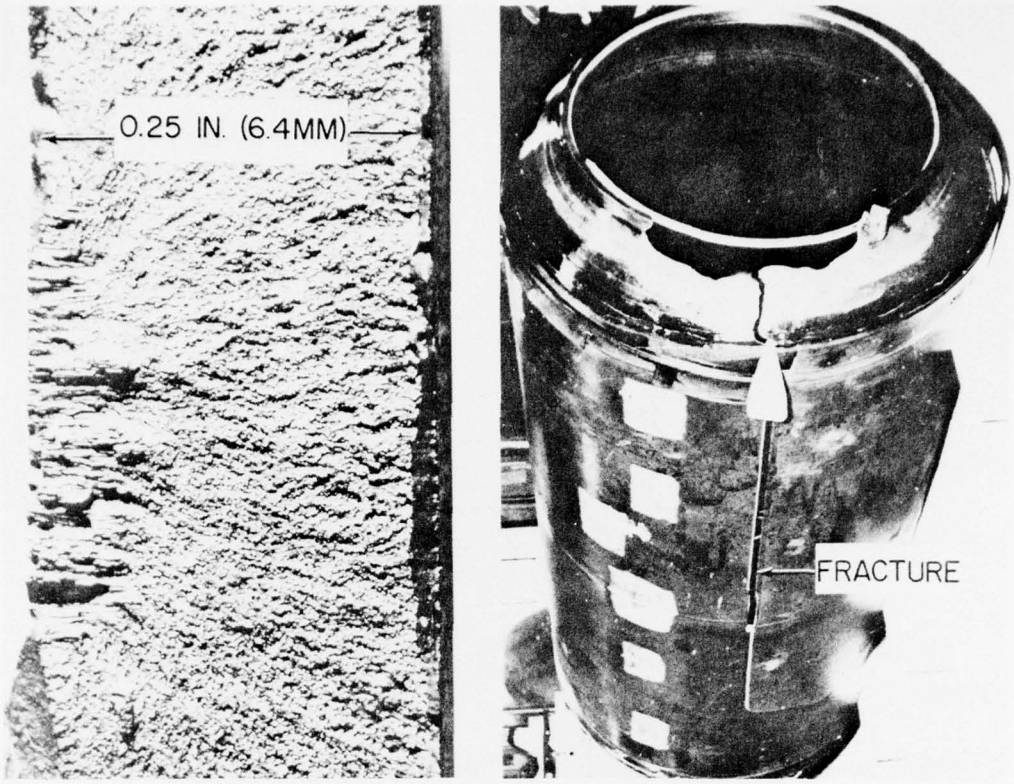

Fig. 150—Typical hydrotest failure of rocket cases. Note region of crack growth (by stress corrosion cracking) *to the critical size for fast fracture.*

levels than usual. In brief, the empirical solution, using oil, still makes sense for the rocket case steel. However, analyses today would indicate the desirability of shifting to improved steels, for reasons of both stress-corrosion cracking and fracture properties.

ENVIRONMENTAL EFFECTS

The mechanical consequences of environmental effects can be illustrated by shifts between corridors in Fig. 145. For the case of fracture, the trend corridors are established strictly by metal quality. In the case of stress-corrosion cracking (and sustained-load cracking in general) the trend-band corridors are determined by both metal quality and environmental influences; both must be dealt with in analysis.

The effects of environment on the microfracture processes of crack-tip plastic zones may be explained by extension of the fracture principles described in Chapter 2. At present, it is possible to provide fairly general descriptions of these processes.

Figure 151 is a gross enlargement of the plastic zone at a crack tip subject to load. The elastic K-field represents a stress intensity below the level required for fracture extension (K_{I_c}

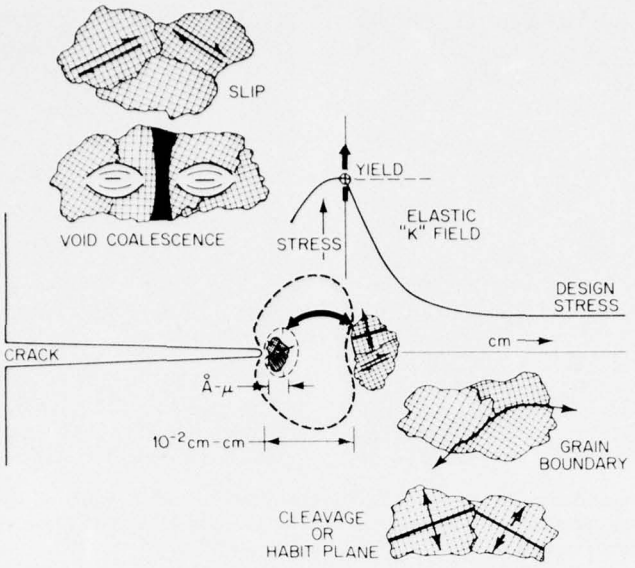

Fig. 151—Sites of metal grain separation for fast fracture (arrow-left) and for stress corrosion cracking (arrow-right). The difference is between a strain-induced mechanism for fracture in the plastic zone and a stress-induced mechanism for stress corrosion cracking in the elastic-plastic boundary. The microfracture processes are indicated by the sketches.

properties are assumed). Slip and void coalescence represent the mode of micromechanical separation, if stress intensity reaches K_{Ic} levels. The double-ended arrow in the plastic zone signifies that for K_{Ic} separation the process zone is close to the crack tip and within the plastic zone. The right-hand end of the arrow indicates that for K_{Iscc} conditions, the critical micromechanical separation processes may shift to the elastic-plastic interface of the plastic zone.

The time-dependent effects of stress-corrosion cracking separation may result from cracking along grain boundaries or on habit planes (similar to cleavage). These separation processes tend to be stress- rather than strain-critical. We now inquire as to the reasons that the K-field causes a different mode of metal separation for K_{Iscc} than for K_{Ic} conditions. First of all, the energy requirements for stress-induced separation along grain boundaries or habit planes are significantly less than for the void formation (slip) involved in strain-controlled separation. In brief, the effect of time on environmental effects is to permit less energetic processes to come into action. Thus, the K_I value for fracture is depressed to a lower K_{Iscc} value. In fact, a plastic fracture condition may be depressed (for crack growth) to a low-ratio K_{Iscc} value; the environmental effect is enormous in such cases. Figure 152 illustrates the dramatic differences in metal-grain separation processes that may be found in ductile plastic metals characterizable by valid K_{Iscc} values.

For steels, the electromechanical effect of stress-corrosion cracking acts in the grain structure, at the scale of microns. It is not an effect merely of corrosion at the crack tip; a diffusible corrosion product is evidently involved in steels. The agent is hydrogen, generated in the crack and diffusing into the plastic zone to promote grain-boundary fissuring.

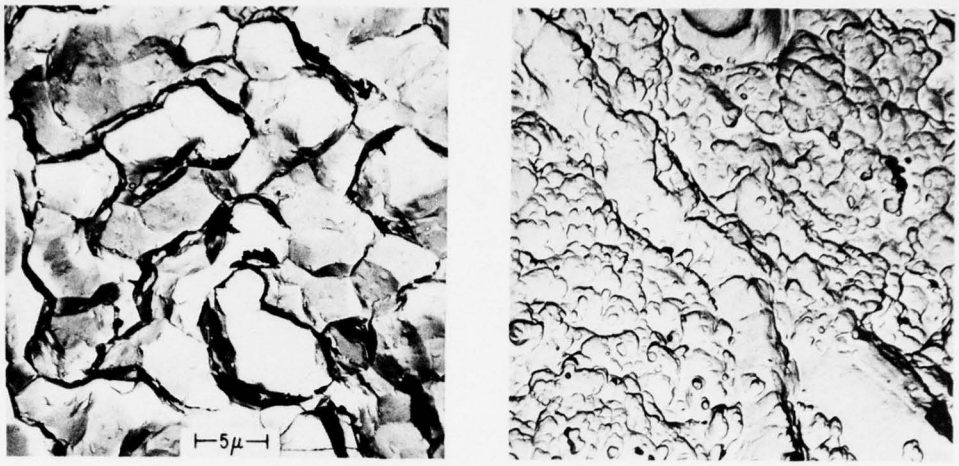

Fig. 152—High-magnification fractograph of K_{Iscc} test specimen surfaces. Crack growth by stress corrosion cracking (left) shows grain-boundary separations. Fast fracture (right) show ductile-dimple (void-growth) fracture of individual grains. The example is for an aluminum alloy.

The crack-tip solution chemistry is not that of the liquid outside the crack. For example, external pure water, when confined to the crack tip in a steel, changes into an acid solution of a pH characteristic of the alloy. (Values of pH from 3 to 5 are typical.) The plastic-zone material at the crack tip does not sense pure water in this case; corrosion at the crack tip is that of an acid solution. A relatively high hydrogen partial pressure develops, with consequent diffusion into the plastic zone. The effect is similar to that of a steel that has been charged to a high hydrogen content.

The similarity of the K_{Iscc} transitions for steels (Fig. 145) and the hydrogen-assisted cracking transitions illustrated in Fig. 124 are striking. In fact, these transitions are due to the same effects of hydrogen. In the case of in-situ hydrogen, the origins may be steelmaking practices or welding procedures.

The role of hydrogen explains specific additive effects of cathodic coupling in seawater. Figure 153 shows that the K_{Iscc} value for a high strength stainless steel of precipitation-hardening type (S-PH) is decreased by cathodic effects, from intermediate to very low ratio values. The decrease is directly related to the potential of the anode for releasing hydrogen at the cathodic surface of the S-PH steel. The increased hydrogen potential (pressure) is sensed in the crack and the plastic zone.

These cathodic effects result from using cathodic protection to prevent pitting corrosion. They may also be due to coupling of dissimilar metals for structural purposes. The example of Fig. 153 was investigated because an aluminum hydrofoil hull was coupled electrochemically to high strength stainless steel struts and to zinc and magnesium cathodic protection systems. The SI problem for a freely corroding strut is related to K_{Iscc} properties of 0.5 ratio. Figure 148 indicates that the critical crack size for crack growth at stresses of 0.5 σ_{ys} is about 0.3 in. (7.5 mm). This is a borderline size for in-service detection and control of critical cracks. However, when the steel is coupled to zinc or magnesium, the SI problem is related to K_{Iscc} properties of 0.2

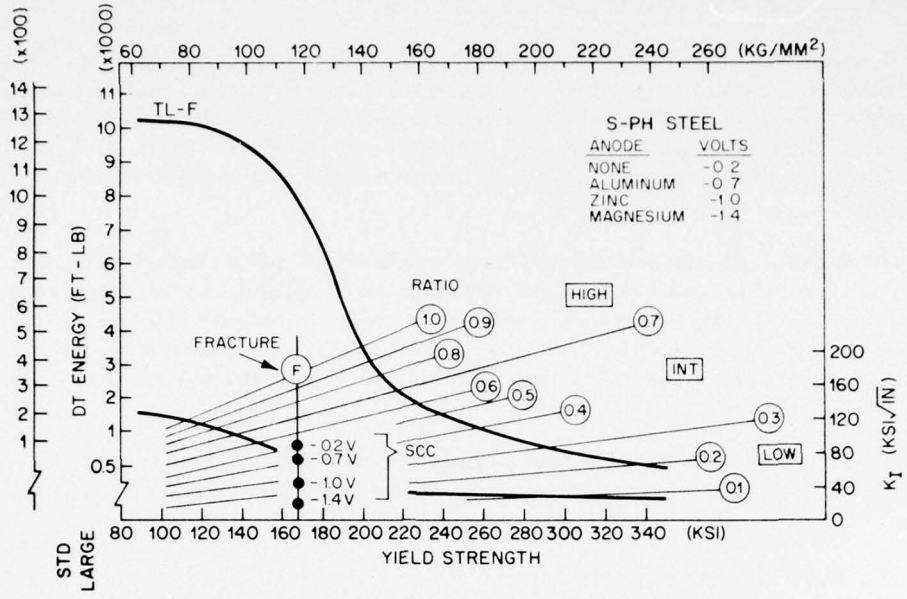

Fig. 153—Ratio analysis diagram (RAD) for high strength steel of precipitation hardening (S-PH) type, illustrating the effects of electrochemical environment (cathodic voltage), which results in increased pressure of hydrogen discharge and, therefore, in decreased K_{Iscc} for the hydrogen-sensitive steel. (Photo courtesy of C.T. Fujii and R.W. Judy, Jr.)

to 0.1 ratio value. At these low ratios, the critical crack sizes decrease to the range of 0.04 to 0.02 in. (1.2 to 0.5 mm). Detection or control of such small cracks is not feasible. Cathodic protection for pitting control thus changes the SI situation from marginal to completely impractical.

The S-PH steel features a strength transition, in terms of K_{Iscc} properties, indicated by the "poor" trend band of Fig. 145. The high end of the band represents the freely corroding condition, and the low end represents the zinc or magnesium coupling cases. Decreasing the strength level from 160 ksi (1103 MPa) to about 120 ksi (827 MPa) increases K_{Iscc} properties to 1.0 ratio or higher. As Figure 148 indicates, the critical crack size is increased to 0.5 in. (12 mm) or greater at a reference stress of 0.7 σ_{ys} and to about 1.0 in. (25 mm) for 0.5 σ_{ys} levels. Detecting or preventing cracks of this size is possible, and SI procedures based on this fact are practical.

In conclusion, the subject steel should not be used in seawater at yield-strength levels in excess of 120 ksi (827 MPa). The effects of cathodic coupling are an important reason for this limitation.

This example clearly indicates that analyses based on K_{Iscc} values must include coupling effects. Coupling is especially important at yield-strength levels in the strength-transition range for K_{Iscc}. The importance of a RAD system is evident, particularly for steels on which extensive data are not available. If the strength level of interest falls in a range where most steels show pronounced environment effects (Fig. 144), it is mandatory to develop specific data over a range of yield strength. The benefits of adjusting yield strength can then be assessed at the preliminary design stage.

230-362 O - 77 - 14

GROWTH-RATE FACTORS

The rate of crack growth for stress-corrosion cracking or other sustained-load cracking is of major interest. Quantitative predictions are beyond today's technology, but the general effects for steels are illustrated in Fig. 154 (for a low-ratio metal). The growth rate of a stress-corrosion cracking crack is increased as the K_I level acting on the crack rises above the K_{Iscc} threshold level. The figure illustrates crack growth up to the critical K_{Ic} value for fast fracture of the test specimens.

The increase in K_I stress intensity during the growth of surface cracks is a function of crack size, K_{Iscc} ratio value, and stress. If the metal has elastic-plastic or plastic properties, crack enlargement due to stress-corrosion cracking may lead to crack-tip yielding, particularly if stresses are high. As a result, the crack tip is blunted, and plane-strain constraint is lost. This is analagous to the constraint relaxation that invalidates K_{Ic} analysis as the elastic-plastic condition is entered.

The ratio level has a marked effect on crack growth. For stress intensities near K_{Iscc}, tests indicate that the time it takes for crack movement to begin is minutes or hours for very low ratio steels. For high ratios, incubation may take several days.

The time it takes to reach the terminal K_{Ic} stress intensities for fast fracture is the main consideration for low-ratio metal. If a low K_{Iscc} ratio is associated with a low K_{Ic} ratio, then fast fracture may occur very quickly. The rocket cases (Figs. 149 and 150) provide a clear example. Crack growth to the point of fast fracture took place during the hydrotest, which was about 10 minutes. The distance for growth to the point of fracture was exceedingly small, as described previously.

If a similar K_{Iscc} ratio of 0.1 to 0.2 is associated with a high K_{Ic} ratio, the distance may be very large. This combination may be developed for lower strength steels, as illustrated in Fig. 153. The fracture properties of the S-PH steel of this example are indicated by the ratio value of 1.0. Accordingly, a crack (at 0.5 to 0.7 σ_{ys}) must grow in depth from 0.02 in. (0.5 mm) to well over

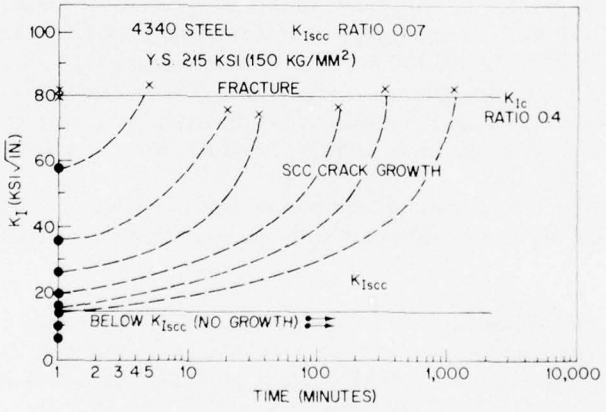

Fig. 154—Rate effects in extension of cracks, for K_{Iscc} test specimens loaded initially to different levels of stress intensity K_I. Note log scale for time reference.

0.5 in. (12 mm) before K_{Ic} conditions for fast fracture are reached (Fig. 148). The example assumes a metal of large enough section size to provide plane-strain conditions at the 1.0 ratio value for fracture.

When stress-corrosion cracking occurs in regions of residual stress such as welds, stress fields in the path of extension are decreased. The K_I value at the crack tip may then decrease with extension due to the decrease in stress, and extension will be limited to the regions of residual stress. The residual stress system in weld regions may be of very high elastic-stress level. This directs crack-growth analysis to the lower curves of Fig. 148; small cracks may be expected to grow for a wide range of K_{Iscc} ratio values. The stress gradient acts to arrest these cracks, and the result is a potential for many small cracks, which pose serious maintenance problems. Their repair by welding may lead to repeated cracking, particularly if field repairs are necessary.

METALLURGICAL CONSIDERATIONS

The characteristic locations of specific alloys in the RAD of Fig. 144 suggest microstructural effects in the intermediate strength range of K_{Iscc} transitions. For example, at 180-ksi (1241 MPa) yield strength, the range is from 0.1 to 1.0 ratio values. In this case, low- and high-ratio steels are markedly different in cleanliness, and correspondingly different in fracture properties. However, the apparent correspondence does not hold for the 140-ksi (965 MPa) yield-strength level. Steels of vastly different fracture properties have similar K_{Iscc} ratio properties. The key to these relationships is not cleanliness and microstructure alone. The specific alloy, microscale segregations of the alloy, texture, and many other qualities interact with the electrochemical environment in ways not fully understood.

Trend bands can be plotted, and specific alloys may be assigned characteristic positions in the trend bands (Fig. 145). However, it is impossible by adjusting alloys to shift to other trend bands, as can be done in the case of fracture properties. For example, it is not known how to elevate the 5Ni steel of Fig. 145 to higher ratio positions. (This is the secondary-hardening steel cited in Fig. 100.) The RAD plot suggests that steels of this strength level should have potential insensitivity to stress-corrosion cracking. However, this potential has not been realized to date for freely corroding conditions because of limited knowledge of alloy effects.

Metallurgical anisotrophy usually does not have pronounced effects on stress-corrosion cracking for steels. The reference data for Figs. 144 and 145 are reasonably representative of the different directions of conventional rolled or forged steels. However, directionality may be important for aluminum alloys and to a lesser degree for titanium alloys.

A RAD display of lower bound stress-corrosion cracking properties for aluminum and titanium alloys is presented in Figs. 155 and 156. As for steels, the strength transitions of K_{Iscc} are sharper than the fracture-state transitions. Crack-extension rates for these alloys are typically faster than for steels, at intermediate strength levels of the metals' respective strength transitions.

The RAD for aluminum alloys has a special metallurgical feature of major engineering consequence. The lower bound curve for the through-thickness direction is placed at very low ratio level. In fact, the transition is not developed to any significant degree. All major stress-corrosion cracking problems for intermediate and low strength aluminum alloys are due to this

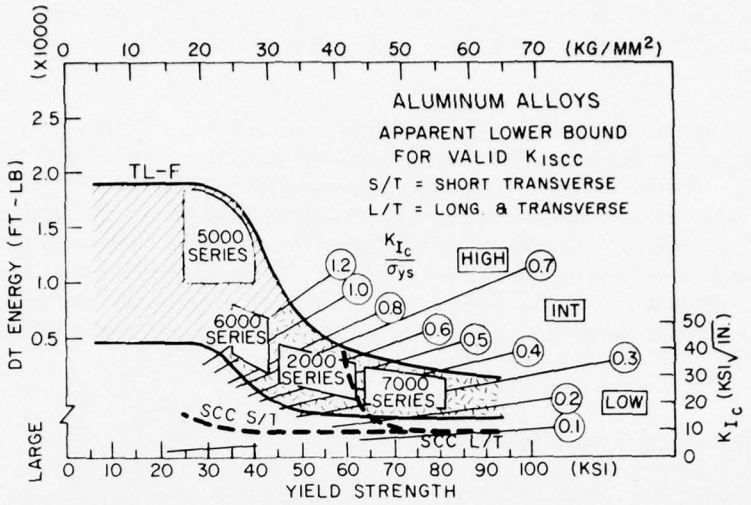

Fig. 155—Combined RAD display for fracture and lower bound stress corrosion cracking properties of aluminum alloys. The three ratio zones have the same meaning as for steels. (After R.W. Judy and R.J. Goode.)

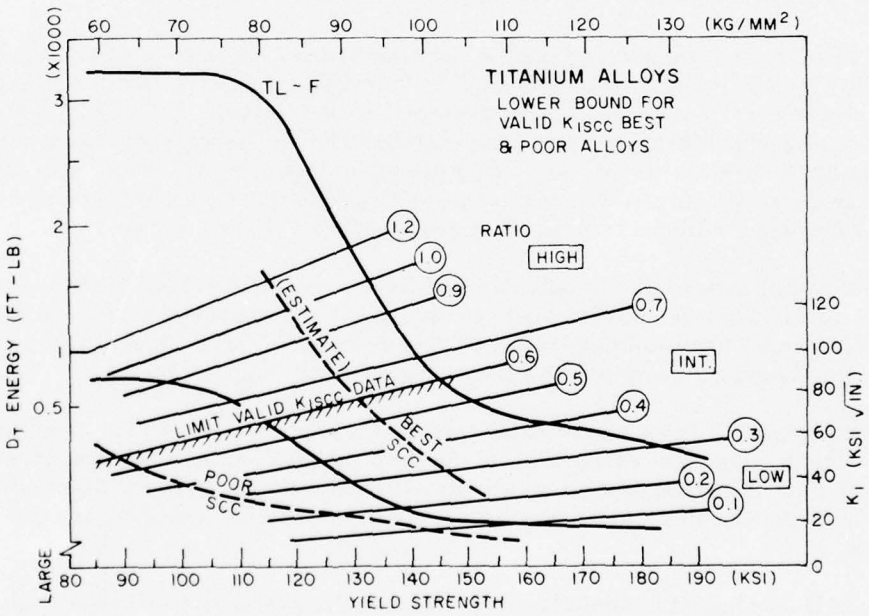

Fig. 156—Combined RAD display for fracture and lower bound stress corrosion cracking properties of titanium alloys. The three ratio zones have the same meaning as for steels. (After R.W. Judy and R.J. Goode.)

deficiency. The reason for this behavior is the relatively large amount of nonmetallic phases and alloy precipitates (due to heat treatment) that are preferentially alined on rolling planes. In effect, metal grains have low coherence on these planes, and this affects both fracture and stress-corrosion cracking.

A sharp transition develops only for the longitudinal and transverse (L and T) orientations, as shown in Fig. 155. The transition curve runs between the 2000 and 7000 series alloys. Special precautions are necessary if aluminum alloys are to be used under conditions leading to stress-corrosion cracking. Cracks have a pronounced tendency to rotate into alinement with rolling planes.

It should not be inferred that the lower bound curve for the short-transverse direction is characteristic of all aluminum alloys. As for steels, there are quality corridors that lie above the lower bound curve, even for the short-tranverse direction. For example, special processing and heat treatment can desensitize the short-transverse direction for some alloys. However, insufficient data exist for generalized zoning of the aluminum RAD. Accordingly, the presentation here is limited to upper and lower bound curves.

Metallurgical zoning of the titanium RAD is complicated by texture effects. It appears that a tendency for preferential alinement of grains in particular crystal directions affects stress-corrosion cracking and other sustained-load cracking properties of titanium alloys. In fact, the separation of stress-corrosion cracking from other forms of in-situ sustained-load cracking (probably due to hydrogen) is difficult for titanium alloys. Again, the lack of metallurgical information precludes generalized zoning, and the presentation is limited to upper and lower bound curves. There is no evidence of pronounced short-transverse direction effects for titanium alloys.

Specialized metallurgical studies have provided trend-band data for titanium alloys of specific section size, process history, and texture. Generalized metallurgical trend bands cannot be defined, however, and the data at present are of value only for special product forms.

While metallurgical effects are only partly understood for steels and for aluminum and titanium alloys, it is clear that strength-transition effects for stress-corrosion cracking are much sharper than for fracture. This statement applies not only to K_{Iscc} values, but also to other forms of sustained-load cracking, referenced as K_{Isle}. For example, hydrogen effects referenced to K_{IH} for steels are cited by K_{Isle} for titanium alloys. In both cases the important environmental effect is caused by in-situ hydrogen. In all strength transitions, the environmental effects are instrinsically related to microfracture processes in crack-tip plastic zones. Thus, all SI analyses for sustained-load cracking must consider these factors in an organized fashion, such as that presented by RAD plots. Specialized RAD plots should be prepared as required.

CHAPTER 10

Characterization And Terminal-Envelope Analysis For Fatigue And Corrosion Fatigue

TECHNOLOGICAL STATUS

The mechanics of crack growth under cyclic loading cannot be defined in terms of specific criteria. There is no single basic parameter that corresponds to K_{Ic}, and advances in standardization methods cannot be expected to supply one. The mechanical problem fundamentally is to integrate crack growth parameters between initial and terminal limits, i.e., from a source crack and to a critical crack size for structural failure. The most significant parameter is the rate of crack growth for specified conditions of load cycling. The growth rate determines the number of cycles to the terminal event.

The terminal event may be fatigue crack growth to metal separation, attainment of fast fracture, or rapid extension of stress-corrosion cracking, singly or in combination. The true limits of fatigue life may be set by a critical-size crack for fast fracture or stress-corrosion cracking.

These considerations have led to assertions that the technology of fatigue lags far behind that of fracture and that much remains to be done. While this is true in general, it is not realistic to expect fatigue analysis to achieve the same rigor as fracture analysis in the foreseeable future.

There is a strong element of systems analysis in every fracture analysis, even in scientific idealizations. The fracture problem has been overidealized in the literature, and systems analysis is required to place it in the context of engineering reality. In the case of fatigue, it is paradoxical that we must start with the literature's overpessimistic view of the analysis problem.

From the viewpoint of SI analysis, a very exact prediction of crack-growth rates is not the first consideration. Any estimate of service life includes assessments of safety, durability, and risk. Such an estimate must deal first with safety and risk; if these are not resolved adequately, formal calculations of crack growth are of academic interest.

In brief, the envelope of safe crack growth must be known with reasonable exactness and confidence. The rate of growth of fatigue cracks can then be expressed as the number of cycles required to breach the limits of the critical envelope. Due to the strength transition, the envelope limits for fatigue and stress-corrosion cracking become very small with increases in yield strength. The fact that fatigue lives become short is due more to this decrease in envelope size than to the acceleration of fatigue crack-growth rates by the increase in strength.

The envelope size may become so small that the initial crack size that is assumed for fatigue life calculations, as deduced from inspection capabilities, is critical for K_{Ic} fracture initiation or K_{Iscc} crack growth. If so, the fatigue life is one loading cycle, by definition of factors other than fatigue.

The structural safety and risk aspects of fatigue, then, depend on the size of this envelope. Safety and risk can be assessed with confidence by present technology, and this is of first-order importance for SI purposes. When structural reliability with respect to the envelope size is established, it is then possible to proceed with analysis of fatigue crack-growth rates. The scatter factor that must be applied to fatigue crack-growth analyses is determined by experience; it protects analysis from unconservative estimates of fatigue life. In any event, the scatter factor enters in establishing the envelope size. The true factor of safety or relative risk lies in the selection of appropriate latitude for crack enlargement (envelope size) for the problem of interest, not in the exactness of data on fatigue crack-growth rate or in the analytical treatment of the data.

The RAD system provides the essential reference base for terminal-events envelope analyses. Metal quality is an essential aspect of envelope analysis. Low rather than high corridor quality, for intermediate strength levels, can make the difference between one-cycle fatigue life and long, safe life of a structure.

The fatigue literature is correct in asserting that metal quality does not affect analysis of fatigue crack-growth rate except for corrosion fatigue. However, the statement is misleading in terms of systems analysis of SI problems. With increased yield strength, metal quality determines envelope-related risk assessments for fatigue analysis.

CHARACTERIZATION OF CYCLIC CRACK GROWTH

The main parameter for describing cyclic crack growth is the stress-intensity range factor ΔK. It represents the difference between upper and lower limits of crack-tip stress intensity resulting from cyclic loading.

Plane-strain conditions apply over a broad range of situations, because crack growth by fatigue can occur at much lower stress intensities than fracture. If plane-strain conditions apply, the calculations of K_I for cracks of specified size and geometry are of exactly the same form as those of subcritical K values for fracture. The additional requirement for valid K values is that nominal stresses be in the elastic range.

The test specimens may have edge, through-thickness, or surface cracks; test procedures are not yet standardized, as they are for K_{Ic} characterization.

The materials parameter measured in terms of the mechanical condition of ΔK is the crack-growth rate da/dN. This is expressed in terms of a power-law relationship, as

$$\frac{da}{dN} = C(\Delta K)^m,$$

where

a = depth of surface cracks or edge cracks
N = number of cycles
da/dN = crack-growth rate
C = numerical constant
ΔK = maximum K minus minimum K
m = numerical exponent.

The fatigue properties of a material cannot be characterized by a single materials parameter such as K_{Ic} or K_{Iscc}. The first step in characterization is determining a reference log-log curve of the type illustrated in Fig. 157. The loading is a simple zero-to-tension cycling in the absence of aggressive environmental effects such as corrosion. The reference curve provides a base of comparison in examining the effects of more complex loading cycles, with or without additional environmental factors. Figure 158 (left) compares the standard reference curve to a similar curve for loading in the presence of a corrosive environment (water); the right side presents a change in stress ratio R.

Stress ratio R is the ratio of minimum stress intensity to maximum stress intensity, as follows:

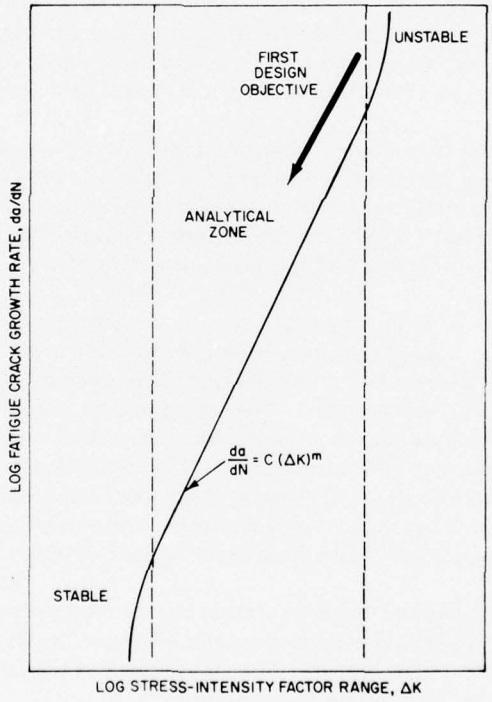

Fig. 157—Typical sigmoidal crack growth rate curve for structural steels ($R = 0$).

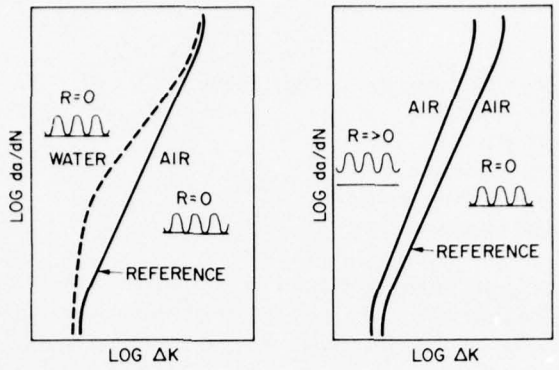

Fig. 158—Typical effects of load profile and corrosion environment, compared to the reference curve.

R = 0, for zero-to-tension
R = positive numerical value, for tension-to-tension
R = negative numerical value, for tension-to-compression.

Comparing these two curves with the reference curve (Fig. 157) discloses specific sensitivities of the material to changes in environment or stress ratio. Parametric data of this type have provided an important base of engineering information. For example, the effects of increasing strength levels for steels may be related to increased sensitivity to environmental effects and stress ratio. The effects on steels and aluminum and titanium alloys also may be compared.

These relative effects may cause order-of-magnitude differences in crack-propagation rates. Accordingly, the parametric data are important tools in assessing the scope of SI problems of fatigue or corrosion fatigue. However, when predictions of structural life (to the attainment of a defined crack state) are made, a "design" curve, characterizing the material under simulated load-vs-time profiles and taking the environment into account, is necessary.

The load-vs-time profile is an important means of characterization, based on structural simulation for complex loadings. Figure 159 illustrates that the *sequence* of variable-amplitude loadings can result in transient delay or transient acceleration of crack propagation. Peak tensile loads leave residual compressive stresses at crack tips, which delay crack extension at lower stress intensities for a number of subsequent cycles. Peak compressive loads, applied in variable-amplitude cycling, can produce opposite effects, accelerating crack extension for a number of cycles by eliminating residual stress systems due to previous peak tensile loads. Both types of effects are transient because crack extension eliminates the modified residual stress system, which is due to a change in the periodicity of peak loads.

Figure 160 presents baseline characterization curves for a precipitation-hardening stainless steel (S-PH) of 150-ksi (1034 MPa) yield strength. The baseline characterization of this steel is of the typical form illustrated in Fig. 157. The significance of the notations in Fig. 157 can be reexamined in terms of the Fig. 160 data, as follows:

- If $\Delta K < 10$, the cracks may be defined as stable, and no growth occurs.

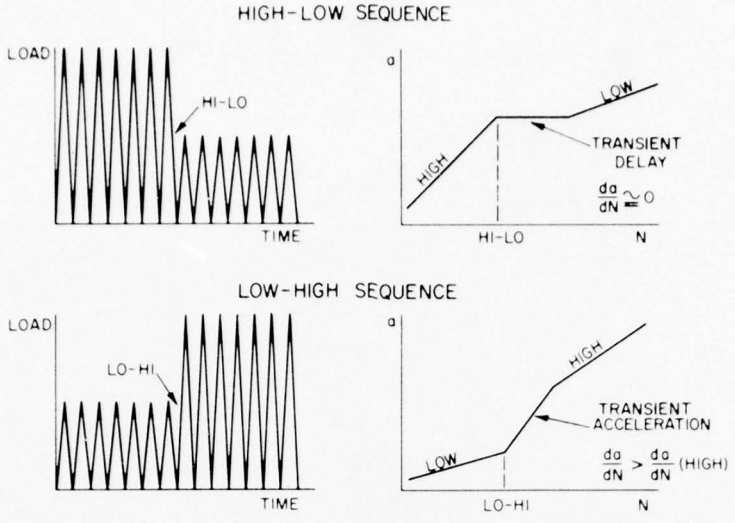

Fig. 159—Schematic illustration of load sequence effects on fatigue crack propagation.

• If ΔK is 10 to 80, the rate of crack growth increases as described by the power law $da/dN = C(\Delta K)^m$. This is the linear range that provides analytical data. Because this region is of greatest engineering interest, most da/dN-vs-ΔK data are confined to simple power-law relationships.

• If $\Delta K > 80$, the crack-growth rate increases rapidly, leading to terminal failure at high ΔK values. For design purposes, the growth must be regarded as the early onset of fracture, i.e., as unstable extension of the crack.

Seawater has a marked environmental effect, related to the electrochemical potential. Growth rates in the linear (power-law) range are increased by about five times in a seawater environment.

The baseline characterization data disclose that additional information about the cyclic rate is required. Because the metal is sensitive to stress-corrosion cracking (see Fig. 153), hold periods above K_{Iscc} can superimpose stress-corrosion crack growth, and slow cycling results in faster fatigue rates than fast cycling. The next (design curve) characterization step must simulate the load-vs-time profile for intended service conditions and for the section size of interest.

The baseline characterization indicates what subsequent tests must be made to assess effects that appear to be critical for the metal. For example, sensitivity to electrochemical effects directs attention to the cathodic protection system. If zinc is to be used, it must be used in the final simulation. The galvanic effect may be decreased by impressed-current systems. Attention to this could add significantly to the service life of the structure.

The final characterization step is intimately involved with the design phase. The first design objective is to limit crack-growth rates to the lowest practical level in the analytical zone of the power-law region (Fig. 157). This can be done by a number of methods, including change of

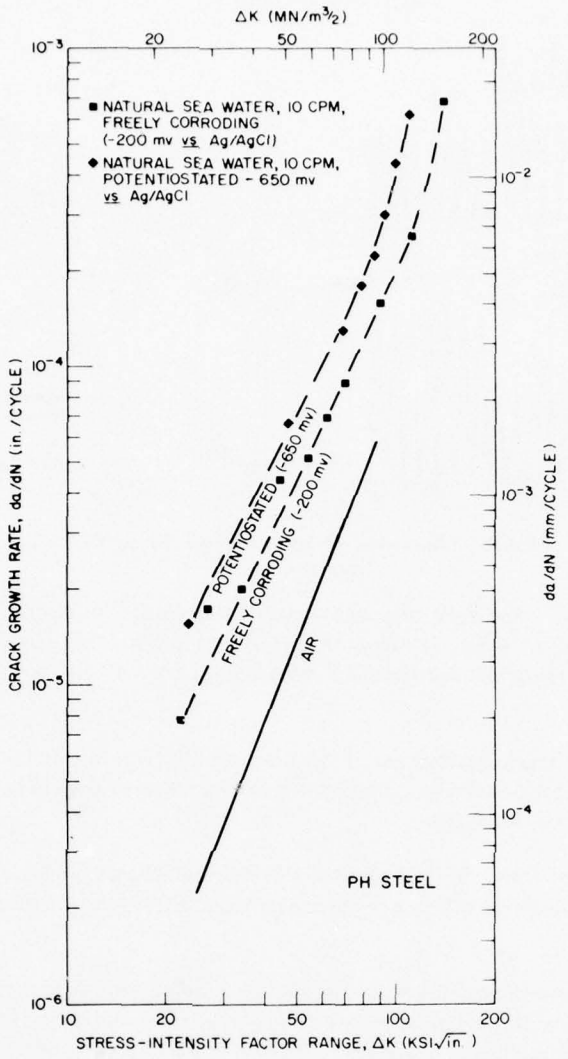

Fig. 160—Specific crack growth rate curve for high strength stainless steel of precipitation hardening (S-PH) type. (After T.W. Crooker.)

metals if necessary. At this stage, also, design details are refined to eliminate high ΔK conditions related to high stresses in regions of geometric transition. The baseline information is of critical importance to this analysis.

In general, the baseline characterization is restricted to the linear range, as indicated in Fig. 161. The figure illustrates the high reproducibility of the data and their adherence to the power-law relationship. Accordingly, it is unnecessary to conduct the large number of ΔK tests shown in this example. Research on a wide variety of metals documents that the da/dN-vs-ΔK curve is a simple and economical device for predicting service as follows:

•The da/dN-vs-ΔK curves for baseline reference and for design purposes can be established in the laboratory with relatively few measurements.

•Life predictions for precracked components may then be derived from the curves for any crack size or shape by integration:

$$N = \int_{a_0}^{a_f} f(\Delta K, R, E)da,$$

where

a_0 = initial crack size
a_f = terminal crack size of interest (such as a_f for K_{Ic} fracture, etc.)
$f(\Delta K, R, E)$ = function of ΔK, stress ratio, and environment.

Extensive investigations for high-quality, high strength steels indicate that scatterband limits are as illustrated in Fig. 162 for the basic reference curves. The average exponent is

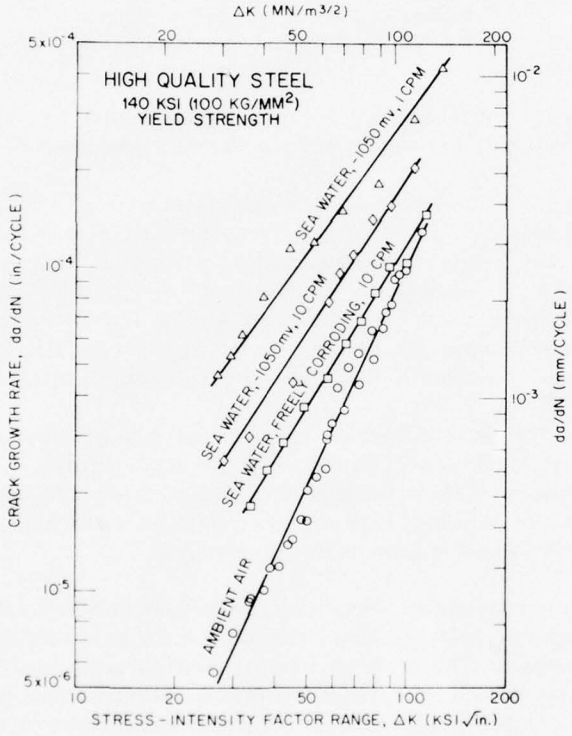

Fig. 161—Research-data curves for the linear da/dN-vs-ΔK region, representing environmental effects. (After T.W. Crooker.)

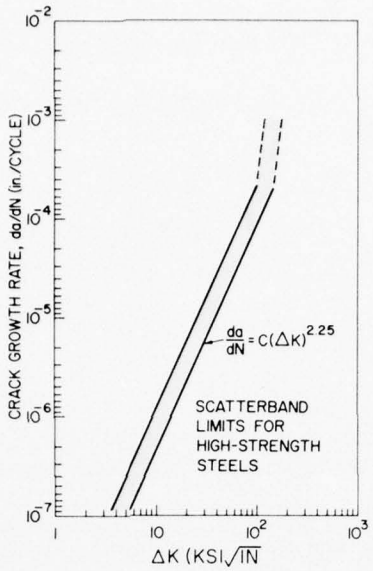

Fig. 162—Scatterband limits in linear region, for a broad sampling of high strength steels. (After T.W. Crooker.)

$m = 2.25$ This observation indicates that for high-quality metals, crack growth in the *linear range* is largely unaffected by variations in yield strength and fracture state.

The power-law regularity, over the entire range of yield strength for these metals, provides for analysis of K levels that are related to yield strength. With increase in yield strength, there is an increase in nominal design stresses. Accordingly, the K level for a given crack size increases with increased yield strength. In effect, as yield strength increases, the ΔK levels of interest rise along the slope of the band displayed in Fig. 160. The crack-propagation rates thus also increase with yield strength. In addition, the upper end of the band extends to higher ΔK levels because of the increased K limits of the high strength metals.

The interaction of fatigue and fracture properties also may be examined in terms of the linear range. The maximum value of K for the ΔK range may attain K_{Ic} values for fracture as a result of crack enlargement. This is the case if the metal has plane-strain properties at the section size of interest. For metals of high corridor positions in the RAD, fracture may not be possible and cracks may therefore grow to very large sizes.

The common reference to stress intensity K_I for fatigue and for fracture characterization allows both characterizations to be combined. Stress-corrosion cracking relationships may also be analyzed in the same terms. The combined analyses are best performed in sequence: fracture, stress-corrosion cracking, then fatigue. The fracture and stress-corrosion cracking analyses will indicate the criticality of fatigue properties for the performance expected under specified cyclic loading.

COMBINED ANALYSIS

The safe practice in fatigue analysis is to assume that cracks of size equal to the minimum detection capability of nondestructive testing exist at critical locations in the structure. Fatigue crack-growth calculations then can be based on this assumption.

For purposes of this discussion, we assume that the detection limit is represented by a semielliptical crack of 0.25 in. (6 mm) deep. The stress range is given by $R = 0$. The linear region of Fig. 162 is assumed for the reference curve for air, and a fivefold increase in crack-growth rates is assumed for the seawater environment. These assumptions generalize the analysis problem across the strength range; they are both reasonable and conservative.

The crack-size assumption provides for calculation of ΔK, which increases with increased yield strength for any level of relative stress. The results of increasing K for various fixed levels of relative stress are plotted in Fig. 163. The family of curves indicates that the rate of growth of the 0.25-in. (6 mm) crack is increased in proportion to the relative stress and the absolute level of yield strength. The increases occur smoothly over the range of the strength transition as displayed by superposition on the RAD limit curves.

Figure 164 presents similar curves for fatigue (freely corroding) in seawater. Note that the curves of relative stress are displaced to faster growth rates as compared to fatigue in air. The rate scale is inverted to emphasize this adverse effect.

Figure 165 introduces, as an example, the three-part zoning of the RAD, and assumes fatigue at 0.6 relative stress in seawater for specific combined analysis of fatigue and fracture properties.

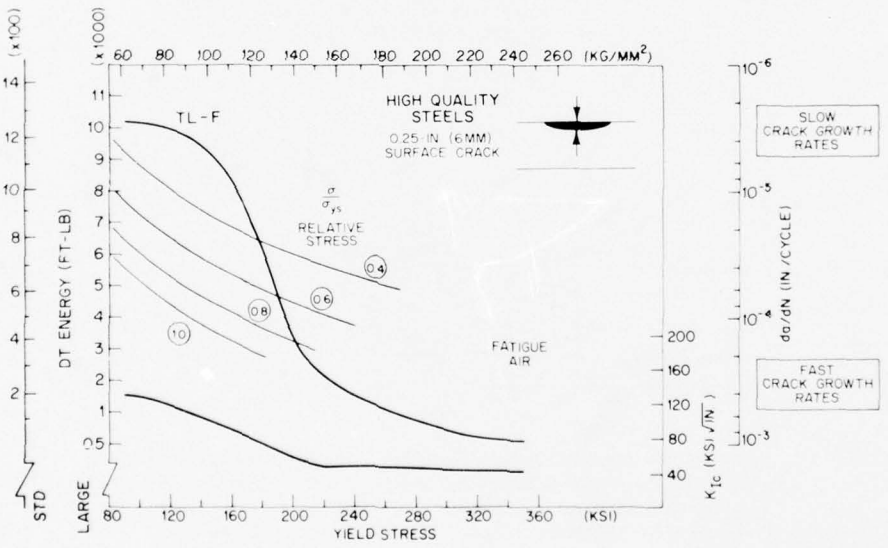

Fig. 163—Effect of yield strength, in the strength-transition range for fracture, on crack growth rates of a specified surface crack. Note inverted da/dN scale. Indexing crack enlargement to various levels of relative stress is appropriate because relative stress is a fixed design criterion.

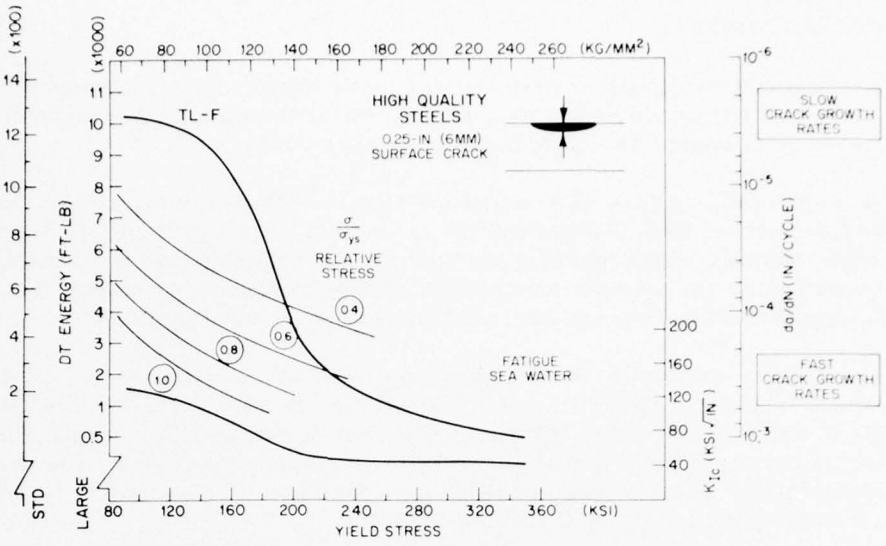

Fig. 164—Crack growth rates for the case of corrosion fatigue. Note substantial acceleration of crack growth, as compared to Fig. 163 data.

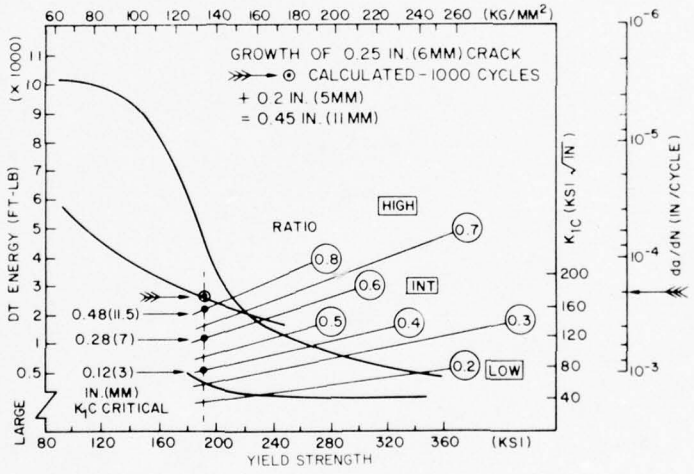

Fig. 165—The 0.6 relative stress level (Fig. 164) used as an example for analysis of fracture-envelope effects, at 190 ksi (1310 MPa) yield strength. The fatigue crack size at 1000 cycles is compared to the critical crack sizes for fracture (at 0.6 relative stress), for steels of various ratio levels.

The minimum possible growth (linear rate assumed) of the initial crack is cited for one level of yield strength as defined by the scale of crack-growth rate. At 190 ksi (1310 MPa), the crack will enlarge by about 0.2 in. (5 mm) in 1000 cycles.

The fracture properties of steels that lie in high, intermediate, and low RAD corridors are examined, according to the relationships of crack size and stress given by Fig. 56. The object is to deduce the critical crack sizes for K_{Ic} fracture initiation over the range of ratio values from 0.8 to 0.3, as noted for metal of this strength level. The following statements can be made (assuming a 0.6 relative stress) for the high, intermediate, and low ratios in this range:

- High corridor metal of 0.8 ratio, at 0.6 relative stress, features a 0.48-in. (11.5 mm) critical crack size for fracture. For the initial 0.25-in. (6 mm) crack, a crack growth of 0.2 in. (5 mm) indicates a close approach to the critical crack size after 1000 cycles.

- Intermediate-corridor metal of 0.6 ratio level features a critical crack size of 0.28 in. (7 mm). It is apparent that the minimum crack growth in 1000 cycles will exceed the critical crack size for fracture at 0.6 relative stress; fracture initiation can be expected.

- Low-corridor metal of 0.5 to 0.3 ratio value features critical crack sizes smaller than the assumed initial crack size for fatigue analysis. Thus, fatigue analysis is of merely academic interest because fracture can occur on the first cycle of loading.

This procedure may be used for analyzing any other combination of conditions for the cited crack size. New sets of curves would be required if the crack-size assumption were changed; this is a matter of calculation in terms of K_I. Analysis principles are the same.

Figure 166 extends the analysis, in principle, to the case of stress-corrosion cracking. For illustration purposes, we assume the same initial crack size as the prior example (Fig. 165). The

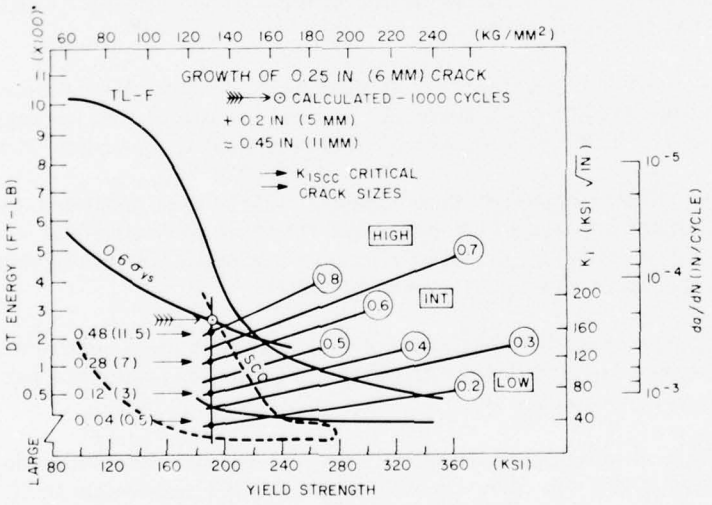

Fig. 166—Envelope analysis for stress corrosion cracking. The stress corrosion cracking envelope is more critical than the fracture envelope if holding periods are involved in the load sequence.

230-362 O - 77 - 15

only change is to add the upper and lower bounds of the K_{Iscc} range (see Fig. 144). Note that the K_{Iscc} range is depressed as compared to the ratio range for fracture.

The critical crack size at 0.6 relative stress may be deduced from Fig. 148 by reference to ratios from 0.5 to 0.2. However, the answer is apparent at this point because the K_{Iscc} calculations are the same as for the K_{Ic} case. The 0.25-in. (6 mm) crack is larger than necessary for a critical condition of crack growth by stress-corrosion cracking at all ratios cited.

The crack-growth problem in this case is dominated by the periods of "hold" at 0.6 relative stress, rather than by fatigue. It is necessary to consider whether the load profile of the structure includes holding periods. Attention should also be directed to regions of weld residual stresses, which may involve stresses of this magnitude. These questions should be resolved before fatigue crack-propagation rates are calculated. They may render such calculations unnecessary.

These procedures, based on RAD reference, simplify an otherwise overwhelming analysis of options. For example, the brief analyses described above may direct serious attention to limiting yield-strength objectives, for reasons of fatigue, stress-corrosion cracking, or fracture. The decrease in yield strength shifts ratio ranges for fracture and stress-corrosion cracking to higher values and therefore raises considerations of much larger critical crack sizes and elastic-plastic or plastic fracture properties (depending on section size). Sensitivity to fatigue will be decreased by lower crack-propagation rates in a broader envelope of terminal conditions. This may make the fatigue analyses meaningful in the context of service-life objectives. Blind calculations of fatigue life for structures limited by fracture or stress-corrosion cracking properties are futile.

SI OBJECTIVES FOR FATIGUE ANALYSES

If it is evident that envelope features do not limit structural integrity, design for fatigue life is practical. Again, we return to questions of geometric transition points and the presence or absence of welds at these locations.

Poor metal quality and poor design at points of geometric transition automatically place a structure at the high end of the ΔK curves. Figure 167 illustrates that the region of unstable fatigue crack growth will dominate the performance of such stress-critical locations.

The first SI objective for design improvement should be to bring these regions as much as possible into the linear ΔK range. This means that the crack population and stress levels must be decreased by high-quality design and fabrication of geometric transition points. Such refinements can increase fatigue life by a factor of 10 to 100.

As the ΔK range is increased by the use of high strength metals, such refinements become more critical. The decrease to the lower circled regions of Fig. 167 is required, particularly in the presence of corrosive environments.

If these refinements are not made, the fatigue life of the structure will be dominated by the nonanalytical part of the ΔK curve (unstable fatigue). If these fatigue-critical regions are neglected, fatigue analyses for the rest of the structure are of merely academic interest.

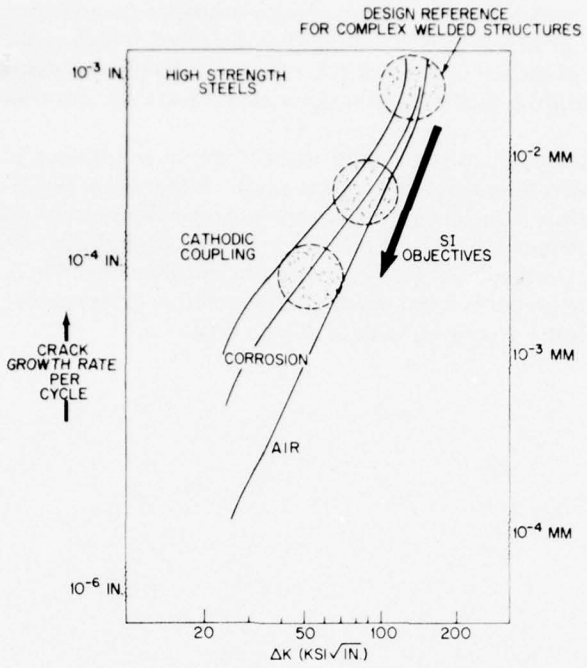

Fig. 167—Design and fabrication quality for points of geometric transition are critical to envelope and fatigue crack growth analyses. The circled regions indicate the shift from high to low crack groth rates that can result from use of appropriate SI principles.

The terminal envelope that applies for fracture and stress-corrosion cracking analysis at the level of nominal design stresses (0.5 to 0.6 maximum relative stress) does not apply to the regions of geometric transition. The stresses at such points may be equal to yield levels for poor design. The low-level, high-relative-stress curves of Fig. 56 and Fig. 164 are the appropriate references for critical crack size in fracture and stress-corrosion cracking analyses of envelope boundaries. These analyses lead to dismal predictions of envelope size if high strength metals are considered.

If the geometric transition points have welds of low corridor quality, the envelope predictions will be dismal even for intermediate strength metals. The reader is invited to make a quick analysis of these factors by reference to Figs. 165 and 166 plus fracture data presented in Chapter 8 for welds.

In general, the presence of SMA welds at poorly designed geometric transition points will involve terminal envelopes that define fracture and stress-corrosion cracking control for these points, if yield strength exceeds 120 ksi (827 MPa). No amount of model testing to investigate fatigue factors for steels of higher strength levels will obviate this conclusion. Reliable SI plans can thus be developed only if attention is first paid to the design and fabrication quality of the points of geometric transition. The increase in envelope then allows fatigue analysis and verifications by model tests, if required.

The emphasis on *model tests* for fatigue, because fatigue technology is not thought to be advanced enough for refined analysis, should be reconsidered. This reason may or may not be valid for structures of a given strength level. It is not valid if fracture of stress-corrosion cracking envelopes are the controlling factors, and fatigue model tests are not useful in this case.

SI analysis of model structures should precede any commitment to fabricate and test models for validation or refinement of fatigue analysis. Reliance on finite-element analysis of geometric transition points, which is limited to tensile properties, may or may not be defensible. For example, it is not defensible if the relative corridor quality of the metal at the structural points in question is not considered. It is important to consider whether the metal is of plane-strain or plastic fracture properties and whether it is sensitive to stress-corrosion cracking. The envelope must be analyzed according to data of this type.

CHAPTER 11

Specialized Structural Problems: Fracture Control For Plastic-Stress Systems

BACKGROUND

The loads applied to a structure may result in localized or general regions of plastic stress. These conditions must be considered in analyzing structures that may be fracture-critical in the presence of cracks.

Ordinary plastic-stress analyses do not take the presence of cracks into account. They are concerned more with K_t effects related to localized plastic strain. The work-hardening feature of metals is beneficial in limiting the increase in plastic-stress intensities for localized overstressing. The region of plastic stress tends to enlarge with increased load, rather than increase in intensity.

Cracks in regions of local deformation generally have adverse effects resulting in increased plastic stresses in the crack regions. The specific stresses that open the crack are also increased, because work-hardened metal can transfer stresses of higher intensity.

These structural conditions leading to increased fracture-extension forces are represented by geometric examples in Fig. 168 (right side). The conditions are compared to rigid structures that are the basis for prior discussions of fracture control, as follows:

Rigid structures have configurations of low compliance (high stiffness) that are load-limited to elastic-stress levels. The development or extension of a crack does not change the stress acting on the crack; it remains the nominal elastic stress of the structural location.

Compliant structures have configurations of low stiffness that are highly sensitive to changes in localized stresses acting to enlarge cracks. For example, if a crack develops in such a region, structural compliance is increased and yield stresses eventually are exceeded.

Geometric instability represents special cases of pressurized compliant structures (pressure vessels, side-pressurized plates, etc.). If the crack is long enough with respect to thickness, local plastic bulging will result and increase with crack extension.

Energy maximum represents structures intended to absorb finite levels of energy and to enter into some degree of general plastic deformation without failure by fracture (submarine hulls, highway guardrails, etc.). Components of ordinary structures may be subjected to similar conditions. For example, bending at hard-point locations may result in high localized deformation while the stress level of the structure as a whole remains in the elastic range.

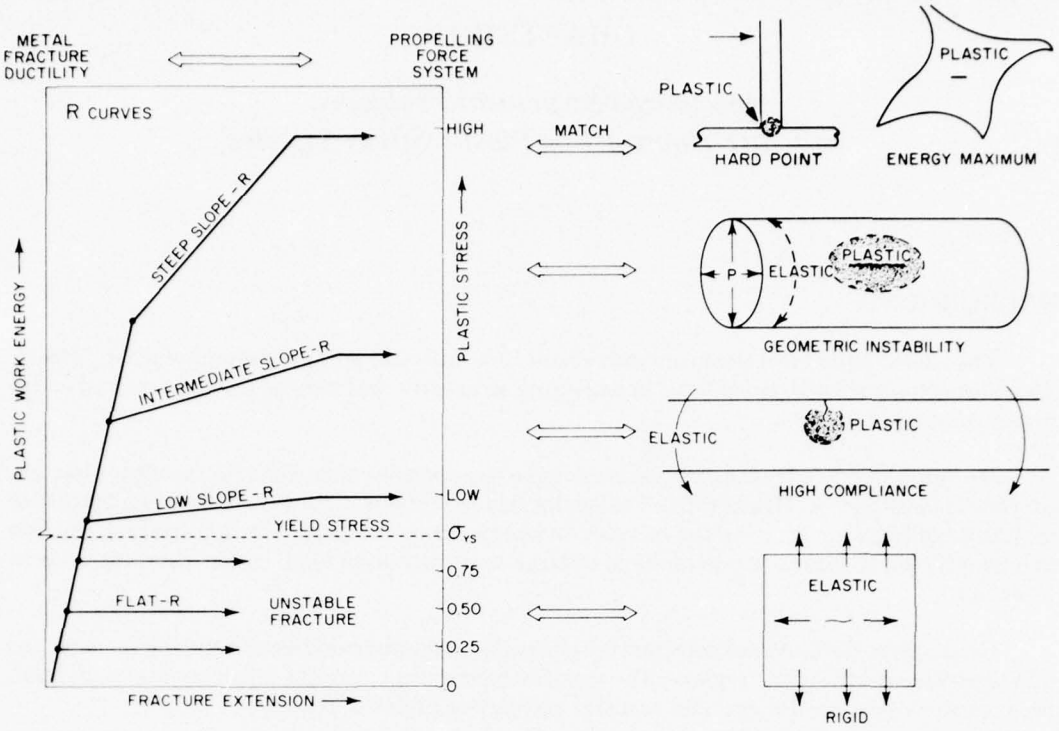

Fig. 168—Range of structural problems involving increased fracture extension stresses. The four arrows at center indicate the correspondence to the range of R-curve levels and slopes.

The propelling force for crack extension in these special cases may range from low to very high plastic stress. Defining limits is a difficult structural mechanics problem because crack size enters into the change in local compliance. These problems are generally treated by worst-case analyses that are credible for the given problem. For example, a fatigue or stress-corrosion crack may be assumed to generate a pressure vessel wall. The elliptical geometry of such a crack on penetration normally results in a crack length of about three to four times the wall thickness; an assumed $5T$ crack length is thus a realistic worst case. The degree of plastic bulging and the related plastic-stress levels may be calculated from this assumption.

In general, preliminary stress analyses will define plastic stresses of low, intermediate, and high levels. In many cases this is the best that can be done because of uncertainties in loads analyses.

As a second step, preliminary materials analyses must be made of candidate metals that are expected to feature plastic fracture properties of matching or overmatching resistance to fracture extension. In general, the search is for metals with clearly overmatching properties, if available. In many cases the problem involves an existing structure, and the analyses must take into account the maximum sizes of cracks that would be tolerable for the metal used. In cases of plastic instability due to cracks, it is necessary to characterize the metal's resistance to plastic fracture for the section size of interest.

The discussion to follow will describe the procedures for resistance-curve (R-curve) characterization of plastic fracture properties. The object is to provide rational connections among (a) fracture properties measured by laboratory tests of definable constraint capacity: (b) plastic-stress levels for fracture extension of maximum-constraint (through-thickness) cracks; and (c) structural performance (propagation or arrest) for specified section sizes.

The graph of Fig. 168 (left side) illustrates the broad range of plastic fracture properties in terms of plastic work energy, R-curve slope, and related plastic-stress levels for extension of through-thickness cracks. The connection to the structural problems illustrated on the right side is the subject of discussions to follow. Conditions of unstable fracture are included in the figure for purposes of comparison. The important difference is that unstable fracture does not permit plastic stresses to develop under conditions of maximum-constraint (through-thickness) cracks, as described previously.

All analyses for correspondence between fracture tests and structural performance must be made on the basis of maximum constraint cracks. This is a definable constraint state for plastic fracture, because section size is sufficient reference for defining this mechanical state. The constraint state for part-through cracks is not at present definable for plastic fracture.

The principles of ductile fracture have a history of engineering use that dates from the mid-1950s. While it is not an entirely new technology, recent advances in rational characterization and interpretation based on constraint state overshadow previous developments.

Understanding present technological capabilities in fracture control of ductile metals requires general knowledge of the mechanics of the fracture-mode transition that occurs with crack extension. The following section focuses on physical models. Appendix E explains fundamental fracture mechanics considerations and their application to rational R-curve characterization by laboratory tests.

PHYSICAL MODEL OF PLASTIC FRACTURE

The extension of plastic fracture has analogies to the elongation and reduction of area that precede rupture of tensile specimens. The comparison is illustrated in Fig. 169 for the special conditions that exist during initial extension of an existing sharp, through-thickness crack. The characteristics of the first stage include crack blunting, increased volume of the plastic enclave, increased plastic work energy for rupture, and transition in fracture mode.

In effect, the initial plastic constraint imposed by the sharp crack is relaxed to a stable state of decreased plastic constraint. Figure 170 illustrates the changes in crack-front configuration that lead to the development of stable slant and mixed-mode fracture. Slant fracture regions signify separation by shear forces (slip), while flat regions signify rupture by crack-opening extension. Full-slant fractures indicate a drastic change in constraint through the entire thickness. Mixed-mode fractures indicate that constraint is relaxed in large part at the free surfaces, while the central regions remain under the relatively high constraint imposed initially by the sharp crack.

The crack front leads in the central regions of high constraint. This is similar to the development of cup-and-cone fractures in tensile specimens. The flat central regions of the tensile fracture open first; then the sides undergo shear slip, which results in the cup-and-cone

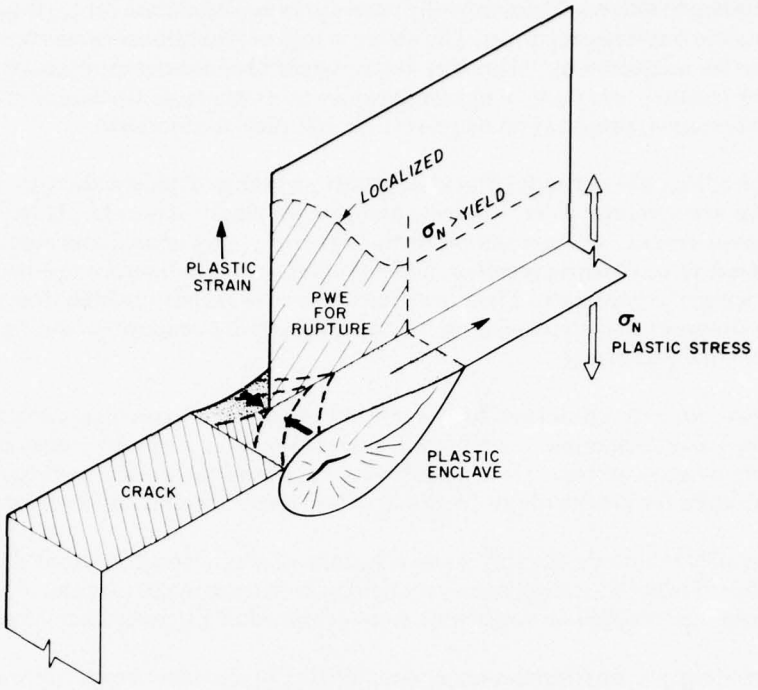

Fig. 169—Plastic work energy for plastic fracture increases with increase in size of the plastic enclave. Resistance to extension increases during the first states of internal rupture, as the initial plastic enclave enlarges. The nominal stress for fracture extension must exceed general yield.

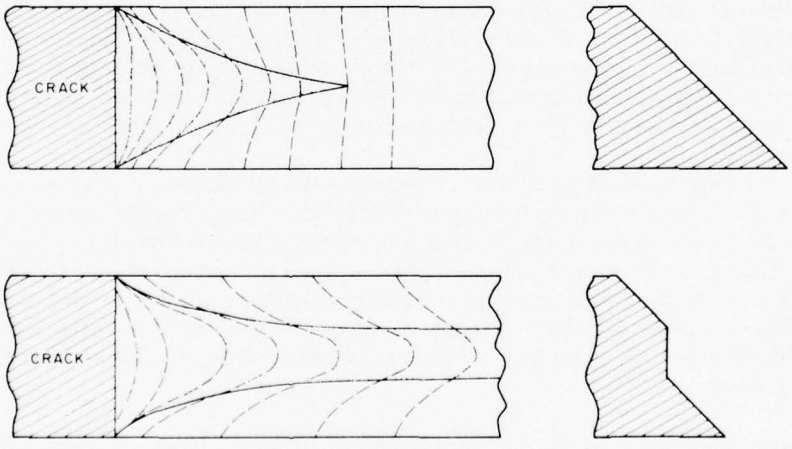

Fig. 170—Fracture extension sequences for metals of steep (top) and intermediate (bottom) R-curve slopes.

geometry. Elongation of the neck region of tensile specimens continues after the central flat region is developed: this produces extensive shear deformation for rupturing the sides. This analogy explains why the flat central regions (Fig. 170) extend to greater distances from the initial crack front than the surface regions of slant fractures. The central rupture develops in tunnel fashion when the plastic enclave is partly developed. Growth of the plastic enclave ends when slant fracture develops, as the last step of rupture.

The physical processes of increased resistance to fracture extension during the initial stages of extension may be explained in terms of visual appearance, stress state, and deformation. These are equivalent but appear different because they are described in different terms. It is important to clarify this point by explaining the various terminologies used.

Fracture-mode transition. This description of the constraint transition is the oldest and simplest. It stems from the visual observation that fracture extension is related to a transition from low-ductility flat fracture near the original crack tip to slant fracture involving a visibly greater degree of oblique slip. The transition may be complete (full-slant fracture) or partial (mixed-mode fracture). A partial transition is indicated by a combination of flat fracture at the center and slant fracture at the free surfaces.

Plane-strain to plane-stress transition. This description is in terms of fracture mechanics definitions of the mechanical constraint states that apply to the fracture-mode transition. The regions of flat fracture are considered to represent metal separation under plane-strain conditions (high triaxial constraint). The slant fracture regions indicate metal separation under plane-stress conditions (low triaxial constraint). The section as a whole is said to fracture in plane stress when a significant degree of slant fracture is attained; the exact distinction is a matter of arbitrary definition.

Through-thickness yielding transition. The constraint-transition events are related to an increase in the degree of yielding, as measured by lateral contraction. Increased contraction takes place in the course of the constraint transition because the degree of oblique slip increases as the triaxial stress state is relaxed.

Yield-zone size transition. This description is the formal fracture-mechanics definition of constraint-transition events. The reference is the ratio of yield zone r_y to section thickness T. A very small yield zone in proportion to thickness indicates plane strain. However, the exact r_y/T ratio that marks the constraint transition from plane strain to plane stress is a matter of arbitrary definition.

These various definitions illustrate the semantic problem involved in the use of the terms "plane strain" and "plane stress." It is necessary to consider what these terms imply.

Their origins are in abstract mathematical definitions of mechanical states in terms of two-dimensional stress or strain. The mathematician finds it easier to calculate load response in terms of idealized two-dimensional response (Poisson effects), eliminating troublesome geometrical features.

In mathematical usage, plane strain is defined as a condition of zero plastic flow parallel to the crack front. Plane stress is defined as zero stress in the same direction. The mathematical definitions represent extreme conceptual limits, ranging from total constraint to plastic flow to zero constraint.

In real metals, constraint cannot extend to either extreme. Brittle metals develop very little plastic flow and thus fracture under conditions close to idealized plane-strain constraint. Highly ductile metals develop large amounts of plastic flow, and they fracture under conditions that approximate idealized plane-stress constraint.

Engineers are advised to adopt the following simplified view of constraint states and constraint transitions:

Plane strain signifies fracture under high levels of triaxial constraint such that metal response is limited to flat fracture.

Plane stress signifies fracture under low levels of triaxial constraint as a consequence of metal response involving a high degree of oblique slip or total slant fracture.

Constraint transition signifies a marked change from plane-strain to plane-stress constraint.

The fracture-mode transition reflects the degree of oblique slip that occurs prior to separation, at the point of visual reference. Thus, a change in fracture appearance from flat to slant indicates a marked change in constraint. As such, it is an index of a marked increase in resistance to fracture extension. A metal that shows a distinct fracture-mode transition requires stresses in excess of yield to initiate or propagate cracking.

Figures E5 and E6, Appendix E, illustrate the development of characteristic fracture modes in metals of low and high plastic fracture ductility. In comparison, plane-strain fracture is characteristically totally flat. Elastic-plastic fracture is flat except for shear lips at free surfaces.

Figure 171 presents experimental DT test data that illustrate the relative increase in the energy required for through-thickness cracks to advance in metals of low and high R-curve slope.

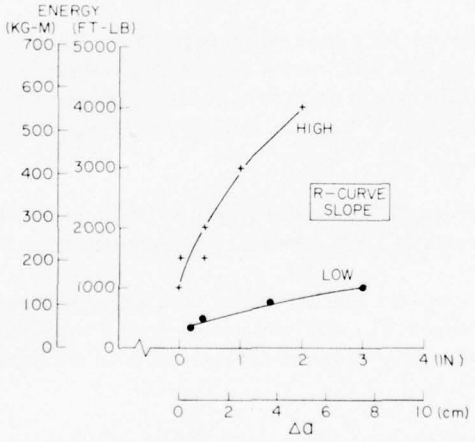

Fig. 171—Incremental additions Δa of impact energy required to advance the crack in DT test specimens for steels of high and low R-curve slope (1.0-in. (25 mm) section size).

Figure 172 illustrates the development of a huge plastic enclave prior to the advance of the crack at the free surfaces in a metal of high R-curve, plastic fracture (slant-mode) properties (Fig. 171). The physical reason for the steep R curve of such metals is the large size of the enclave. In comparison, metals of low (mixed-mode) plastic fracture properties develop fracture extension for enclave sizes that are intermediate between those shown in the two photographs of Fig. 172. As a result, the R-curve has low slope.

The foregoing discussions are based on plate metal of 1-in. (25 mm) section size. The absolute size of the plastic enclave, and the associated through-thickness contraction, scales with section size. As an approximation, the width of the plastic enclave for full-slant (plane-stress) fracture will be on the order of the section size. The lateral contraction may be one-tenth to one-fourth this size. It is obvious that the absolute volume of plastic deformation associated with full-slant, plane-stress fracture varies enormously from sheet to plate thicknesses.

The very small absolute size of the enclave in thin metals precludes the development of steep R-curve slopes. The main reason is that the plastic constraint level of thin sections is very low even for maximum-constraint cracks. Through-thickness yielding takes place with little resistance compared to the case of section sizes that feature high plastic constraint for similar cracks.

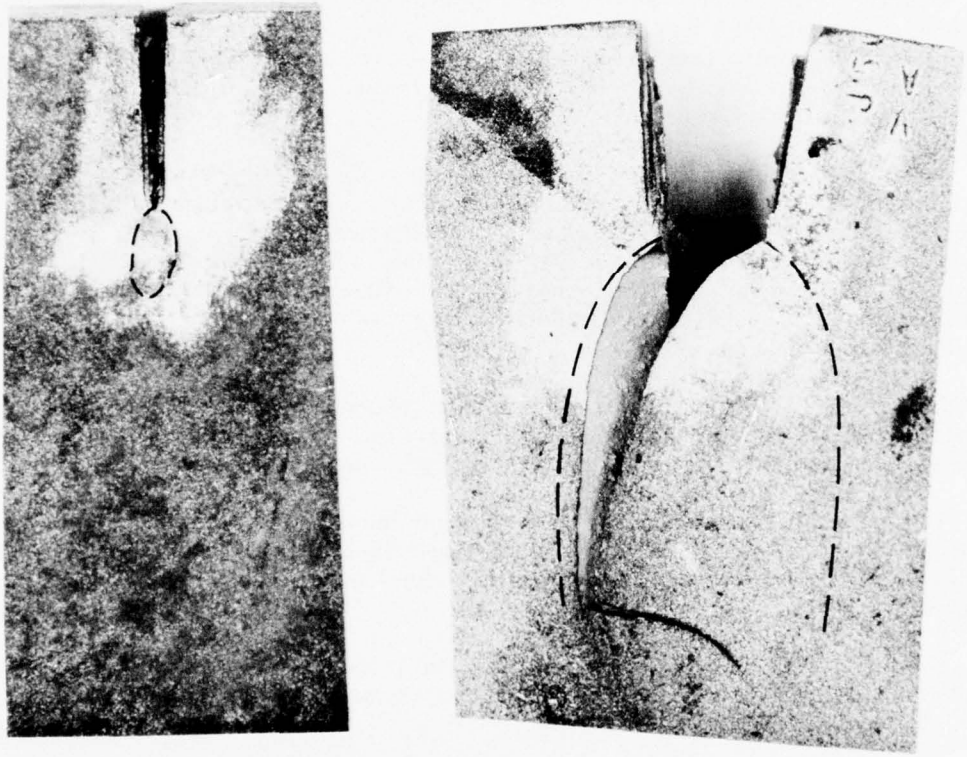

Fig. 172—Relative critical sizes of plastic enclaves developed prior to crack extension in steels of low (left) and high (right) R-curve slope.

Thus, the nominal stresses required to rupture the most ductile metals of thin sheet form will be much lower than for metals of plate section size. In general, full-slant fracture of plate thicknesses indicates that the nominal stress for crack extension will rise to high plastic levels as the fracture-mode transition develops (as the R-curve slope rises).

Metals of sheet form are limited to very low plastic stresses for extension of through-thickness cracks. In fact, very thin sheet thickness limits maximum stresses to the elastic range. This is called the thin-sheet plane-stress problem, because relatively small cracks (three to five times sheet thickness) may extend catastrophically at elastic stress levels, despite ductility sufficient for full-slant fracture.

CONTROL PRINCIPLES FOR PLASTIC FRACTURE

Fundamental barriers to idealized analyses of plastic fracture problems will exist into the foreseeable future, as they will for brittle fracture. In both cases, engineering principles can be applied with confidence only if conservative practices are used.

For brittle fracture, statistical metal variances limit analytical exactness. The scale of plane-strain fracture is highly compressed and requires high-precision measurement. Therefore, similar precision is necessary for metallurgical control of fracture properties. Fracture problems generally involve very small cracks that require great precision in detection. Because all considerations involve precision, engineering reality demands conservative solutions. The problem is solved in practice by the use of lower bound values for fracture properties and higher bound estimates of crack sizes and stress levels.

In the case of plastic fracture, the scale of R-curve slopes is very broad for plate metals. High-precision measurement is not required, and metallurgical control is simple compared to the problem of brittle fracture. The crack sizes of concern for plastic fracture are huge compared to critical crack sizes for brittle fracture (10^2 to 10^3 times larger). The basic analytical problem for plastic fracture is not exactness in measurement of fracture properties or crack sizes; the solutions are limited by the coarse-scale definition of stress levels. For this reason, conservative solutions are as a rule necessary.

In practice, plastic fracture problems are often treated in terms of strain and are related indirectly to plastic stress levels. Structural models must be used if strain predictions by finite-element analysis are inadequate for a given problem.

The discussions to follow focus on the fact that preliminary analyses for brittle fracture can be made relatively directly. For example, these analyses can easily provide for preliminary elimination of candidate metals, to allow more refined consideration of a small number of candidates.

For this analysis, a reference system of metal properties must be available. Fracture mechanics principles dictate that the following requirements must be met for rational data-bank characterization:

- Fracture properties must be referenced to specific section size.
- The fracture state must be defined.

- R-curve slopes must be converted to a numerical reference.

- The reference system must provide for mechanical analysis of section-size effects.

Fracture tests that satisfy these objectives must (a) use maximum constraint cracks for the section size of the test specimen, (b) use a fracture path long enough to allow the characteristic fracture mode to develop, and (c) measure R-curve slope in terms of work energy for complete extension through the critical stage of fracture-mode transition. These requirements are recognized as fundamental in $\mathcal{G}_c$ testing for sheet material (see Appendix E). However, $\mathcal{G}_c$ tests are not practical for sheet or plate because of their limitations on elastic stresses and the large size of test specimens.

Crack-opening displacement (COD) characterization methods (including the J_c approach) are in fundamental conflict with the R-curve aspects of $\mathcal{G}_c$ principles. The restriction of characterization to the first event of crack extension neglects the crucial R-curve slope and the fracture-mode transition to stable extension. These cannot be neglected for plastic fracture. The COD and J_c methods are useful for analyzing elastic-plastic fracture and the lowest levels of plastic fracture. In these cases R-curve slope is minimal, and there is little resistance to continued fracture extension for plastic stresses.

The DT test remains the only practical method that meets all of the fracture mechanics requirements outlined above. The ASTM proposed method (1975) for the 0.6-in. (small) DT test provides the required certification reference. Appendix E contains a comprehensive description of the significance of R-curve slope data from DT tests. Appendix E also explains the use of the RAD for (a) integrating plastic fracture and metal-quality data and (b) examining the structural mechanics significance of the data.

These developments provide the first generalized and procedurally simple engineering connection to structural performance, illustrated schematically in Fig. 168. The RAD methods provide enough quantitative information for most analyses of plastic fracture problems. As for brittle fracture, these analyses are crucial because they make possible rational selection of options for SI plans.

Engineering application of these principles to SI plastic fracture problems has been made with increasing sophistication since 1956. While the graphical analysis methods are relatively new, there is a vast store of prior experience with structures to confirm the validity of the methods.

GENERIC PROBLEM AREAS

Engineering experience in evaluating and applying plastic fracture criteria is examined in this section. It is assumed that the reader has reviewed Appendix E.

This experience may be described in terms of generic structural problems that involve unique combinations of configuration, section size, and loading systems, such as the following:

- Aircraft fuselage structures are representative of thin-section stiffened-sheet design.

• Ship and submarine structures are representative of thick sections subjected to explosion loading.

• Fluid and gas transport systems are representative of problems that may require control of pressure-release effects.

In addition, the general case of crack opening due to geometric instability is described in terms of parametric relationships among crack size, hoop stresses, and R-curve slope.

Thin-Sections—Aircraft

Explosive rupture of aircraft fuselages was experienced during the middle 1950s. This led to the first extensive investigations of fracture under conditions of geometric instability. The $\mathcal{G}_c$ research of the time provided the basic information for analysis. The aircraft failures were due in part to relatively brittle aluminum alloys of excessively high strength for the section size.

It was found that decreasing the strength level of the aluminum alloys to provide a full-slant, plane-stress fracture state (maximum possible fracture resistance) did not yield acceptable SI solutions. The internal pressurization of the thin-walled fuselage caused geometric instability for relatively short cracks. The rupture forces were then too high for the relatively low R-curve slopes of the metals. This was called the "thin-sheet plane-stress" problem. It was recognized that thin-sheet metal was limited to low-slope R-curves by section-size effects.

The practical engineering solution was use of plane-stress metal plus mechanical crack arrestors of riveted-stiffener type. The spacing of the arrestors was arrived at empirically by tests of models. The object was to limit the length of a crack so that geometric instability would not produce excessive forces. Metals of plane-strain or elastic-plastic fracture properties would allow crossing through the crack arrestors, so metal selection was restricted to plastic fracture properties. These SI solutions are still in force for all aircraft.

The characterization procedures for aluminum alloys used in aircraft depend on structural prototype tests. The tests are conducted for conditions of geometric instability and for varying crack lengths. There are no standard methods for characterizing plastic fracture properties by laboratory fracture tests. A great variety of modified $\mathcal{G}_c$ (K_c) tests and edge-notched tear tests have been used by the metals industry. As the result, the existing data are difficult to interpret.

The main problem for thin-sheet metals is the low R-curve slope resulting from geometric considerations. Recourse to measurement of extension stress by edge-notched tear tests does not provide increased sensitivity. Plastic stresses are confined to a narrow range and are geometry dependent.

A most significant feature of fracture tests of sheet metal is the visual indication of the fracture-mode transition. The first selection principle in SI analyses for sheet metal structures is restricting the candidate sheet metal to a full-slant, plane-stress fracture mode (for the thickness of interest). Mixed-mode fractures automatically indicate fracture extension at elastic-stress levels.

New characterization techniques based on laminated-type DT tests of the proposed ASTM (1975) configuration (see Appendix E) offer considerable promise for (a) definition of fracture

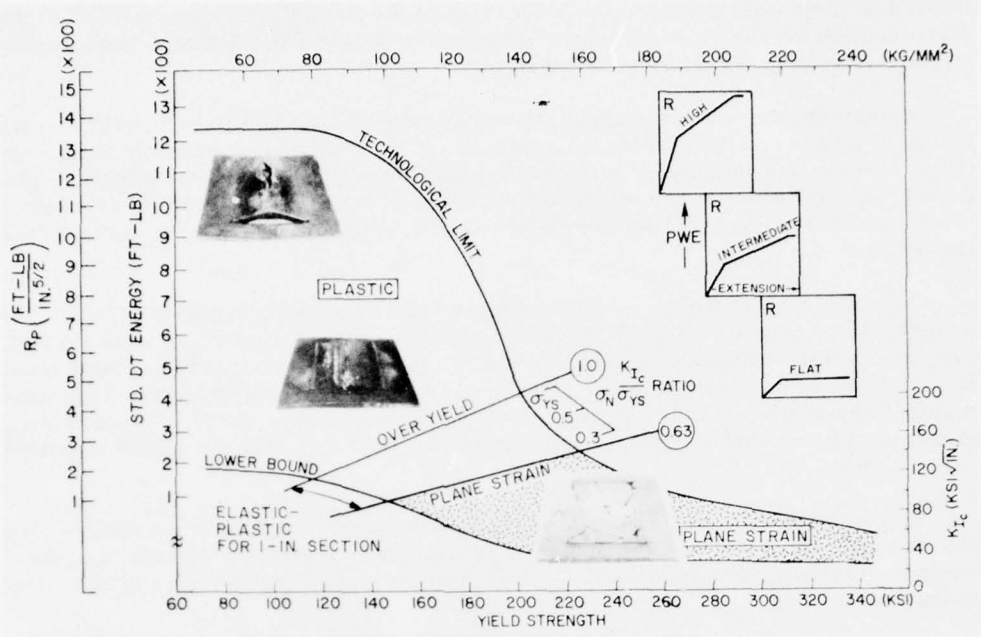

Fig. 173—Transition of plastic fracture properties, represented by the RAD scales of DT energy and the R_p parameter (see Appendix E).

mode, (b) measurement of small differences in R-curve slopes, (c) standardization of the data-bank reference system, and (d) systemization of data in the RAD format.

These advances are of major significance because thin-sheet characterization methods have not otherwise improved since the early 1960s.

Thick Section—Ships and Submarines

The early studies (1953-1956) for plate steels of 1- to 3-in. (25 to 75 mm) thickness were based on information provided by structural prototype tests of the explosion-bulge crack starter type (Chapter 7). The initial objective was direct simulation of localized explosion-load deformation of ship and submarine hull structures containing relatively small cracks. The simulation was extended later (1962) to represent maximum-constraint through-thickness cracks (see Fig. 104).

A new steel (HY-80) for submarine hull structures was selected in 1956, based on maximum resistance to fracture extension under conditions of geometric instability, hard-point deformation, and energy-maximum loading (Fig. 168). These structural mechanics considerations were well understood at the time.

The development of the extreme resistance to plastic fracture characteristic of HY-80 is illustrated in Fig. 173. The HY-80 steel has a nominal yield strength of 90 ksi (620 MPa). The

fracture properties are related to the lower range of the strength transition, which has the maximum metallurgical potential for plastic fracture resistance. This potential was achieved by proper melting, alloying, and heat treatment.

At this same strength level, metals of low alloy content or low melting-practice quality are limited to very low positions in the RAD scale. While the RAD was not available at the time (1956), the general metallurgical principles were understood. Proprietary low-alloy steel proposed by the steel industry were eliminated from consideration for submarine hulls because of inferior plastic fracture properties. The explosion crack starter tests confirmed the superiority of the HY-80 steel.

All of this new technology for SI planning was first developed and applied between 1953 and 1956. Serial construction of HY-80 submarines, based on the new principles, started in 1957. The urgency of this application did not allow time for testing full-scale structures. This was not done until the 1960s, when underwater explosion tests were made of fatigue-cracked full-scale models. The expense and time required for such tests preclude their use in selection of steel; metals must be selected according to rational fracture tests and relatively simple structural prototype tests.

Following the HY-80 experience, it was realized that a rational fracture test was essential if the strength transition for metal of plate thickness was to be explored. The explosion crack starter tests were to be used only as confirming evidence and for calibration of laboratory fracture tests.

This need stimulated the development of the DT test for characterizing fracture state by the rational principles of (a) maximum-constraint cracks and (b) sufficient fracture length to establish the characteristic fracture mode. Advanced methods evolved during the period from 1965 to 1970.

The general relationships of R-curve slopes and RAD DT test scale are illustrated in Fig. 173. For steels of 1-in. (25 mm) or greater thickness, a very broad range of R-curve slopes is metallurgically feasible, if strength levels are below about 150 ksi (1034 MPa). The range narrows rapidly as strength levels are increased to 200 ksi (1379 MPa). This can be read directly from the RAD by reference to the technological-limit curve.

The derivation and the significance of the R_{μ} scale are described in Appendix E. The R_{μ} parameter is a numerical expression of metallurgical quality that determines specific R-curve slopes for different section sizes.

Fluid or Gas Transport Systems

In the two prior cases, it is absolutely necessary to prevent the extension of plastic fracture. If extension occurs, the structure is lost, and there is no interest in secondary events.

The case of transport systems for combustible or toxic fluids and high-pressure gas is characteristically different. The events that follow the initial rupture are of major concern. In fact, the SI plans are generally aimed at controlling secondary events to feasible limits.

The first consideration in such plans is the relationship of the force system for fracture extension to the energy density and total energy of the contained fluid or gas. This analysis determines whether the force system has soft-, intermediate-, or stiff-spring characteristics.

Hydraulic loading presents a stiff-spring system. If the metal has a modest R-curve slope in the extension of through-thickness cracks, crack extension that leads to leakage is arrested by loss of the low-compressibility fluid. If the R-curve is flat (plane-strain properties), fragmentation by unstable elastic-stress propagation of the fracture will result. However, secondary events are minimal, because fragments simply fall or are pushed outward by the fluid.

Gas pockets in the hydrostatically loaded vessel give an intermediate-spring effect. For example, hydrotesting of pressure vessels may be dangerous if gas is not completely bled before full pressurization, when the R-curve slope is relatively low (elastic-plastic properties). For service conditions that involve the possibility of gas pockets in a hydrostatically loaded vessel, use of metals with plastic fracture properties must be considered. The object is to provide sufficient R-curve slope to limit fracture extension while relatively rapid depressurization takes place by leakage.

The soft-spring features of pneumatic loading provide for continuing effects of the force system on fracture extension.

The factors that determine the rate of depressurization through the rupture area include the following:

Energy density (pressure)
Gas volume
Possible side effects (detonation, etc.)
Rate of enlargement of rupture area
Limit size of rupture area (pipe or vessel diameter).

In general, analyses for these cases focus on events that result from a through-thickness crack, rather than on the initial cracking. The conditions that initiate the crack are matters of separate analysis. They may include laminations, poor welds, or accidental damage or puncture. Usually, it is difficult to reliably eliminate such possibilities. Accordingly, attention is directed to subsequent rupture extension, which represents the limiting conditions for SI protection.

Gas transmission lines provide an excellent example of the application of these principles. Because of the nature of construction and terrain, it is assumed that damage can occur, and that a rupture may be initiated. Experience confirms that it is not practical to prevent events leading to localized damage. While rupture of a gasline is undesirable, the real problem is arresting the fracture within a reasonably short distance.

The pipe diameter and pressure determine the depressurization rate for a rupture condition. The problem may be represented by pressure-vs-time decay curves for specific conditions. The SI solution involves the use of a metal with a crack-extension rate sufficiently slower than the depressurization rate to produce an arrest. The crack-extension rate is established by the work energy (plastic-enclave size) per unit increment of extension. This is directly related to the R-curve slope of the metal for the given section size.

Because of economic considerations, it may not be feasible to use metals of very high R-curve slopes. Achievement of an economically exact balance between minimum R-curve slope

230-362 O - 77 - 16

for arrest and specific pipeline requirements requires full-scale testing. It also requires statistical fracture data and quality control for candidate steels.

It should not be assumed that the procedures described above are to be followed generally as a guide for other cases. For example, a limited number of large pressure vessels may be of interest. Metal cost may then be less decisive. In this case, the choice of a metal with a very high R-curve slope is indicated.

The dramatic effects of very high R-curve slope are illustrated in Fig,. 174; the mechanical processes of forward fracture extension may be changed to produce another form of rupture. Regardless of the intensity of forces acting on the rupture region, it may be mechanically easier to develop a sidelobe type of petal, as illustrated in the figure. The forward-fracture process is thus converted to a shearing-type tear, which is self-limiting.

It is not necessary to use isotropic metals at the highest RAD level to develop sidelobe arresting effects. Rolling the metal to produce pronounced directionality can yield very high R-curve slopes in the direction transverse to the principal rolling direction. The direction of principal rolling will then feature low R-curve slopes. Appropriate placing of such directional metal in a cyclindrical pressure vessel produces the desired sidelobe petaling. For example, gas pipeline solutions could be obtained, in principle, by welding straight-away rolled plate in a spiral to form large-diameter gaslines.

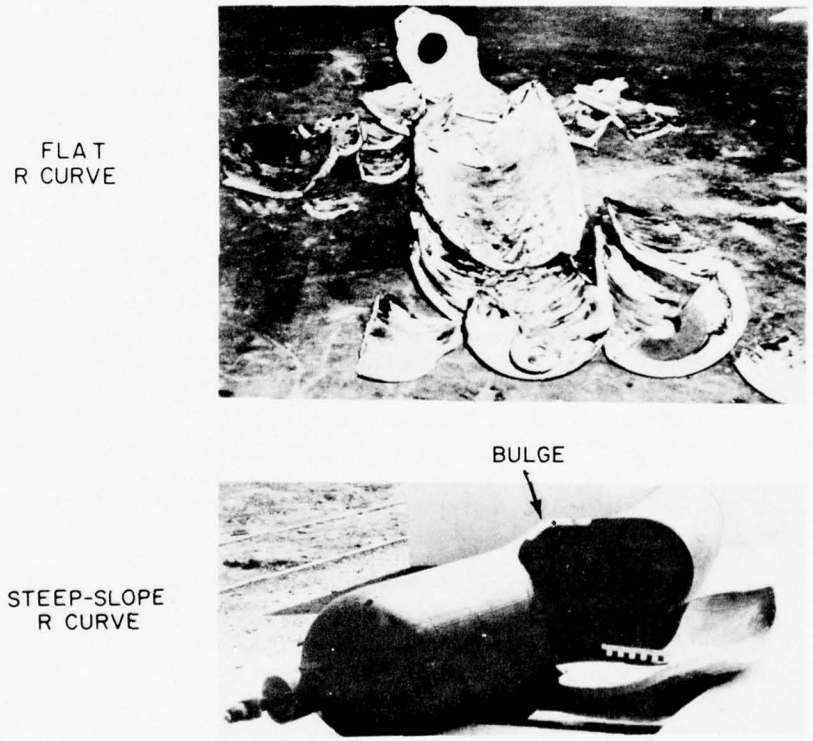

Fig. 174—Brittle service failure due to a long metal lamination in a high-pressure air flask of 1-in. (25 mm) wall thickness. The failure temperature was slightly below NDT (flat R-curve). The solution to the problem (bottom) was based on prevention of missile fragments.

Geometric Instability—Crack-Opening

The stress conditions that lead to the initial opening of cracklike defects are summarized in Fig. 175. The chart is based on general information obtained in burst tests of cylinders featuring lamination-type defects and/or part-through slits. It is not intended as a design guide but as an illustration of the type of information that should be developed.

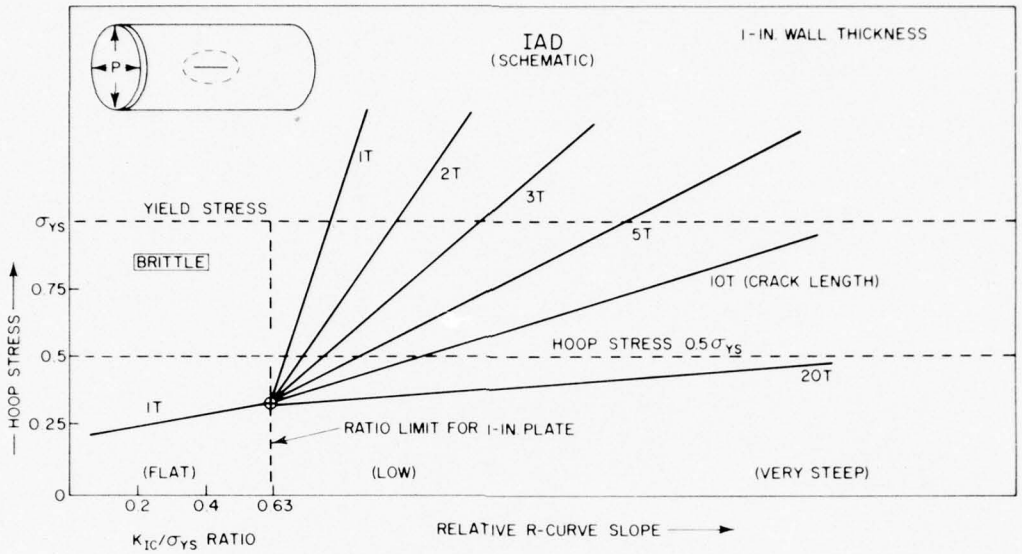

Fig. 175—Instability Analysis Diagram (IAD) illustrating general relationships of crack length, R-curve slope, and hoop stress combinations that result in crack opening rupture of cylindrical vessels

The figure includes a region that is referenced to the K_{Ic}/σ_{ys} ratio scale and, therefore, involves flat R-curves. The calculations of hoop stress for fracture derive from linear-elastic theory. At the ratio limit for the section size, the maximum elastic stress required for the initiation of unstable fracture is on the order of 0.3 σ_{ys}. Stress decreases slightly with decreasing ratio limit value L. The engineering interpretation is simply that the presence of a through-thickness crack results in fracture at low hoop stresses.

Analysis of the effects of R-curve slope starts at the ratio limit. It is indicated that very long cracks ($20T$) result in very high localized geometric instability forces, such that the hoop stress for crack opening remains low. Short cracks (1 to $3T$) result in lower geometric instability forces. As a result, the effect of increased R-curve slope is a function of relative crack length as indicated in the figure.

The fan of curves that relate hoop stress for fracture to relative crack lengths and R-curve slope (metal quality) is called an Instability Analysis Diagram (IAD). It should be noted that combined use of the RAD and the IAD leads to relatively simple parametric analyses that are useful in scoping crack-opening problems for pressure vessels. These analyses do not deal with questions of hydrostatic or pneumatic loading. The initial opening of the crack is not related to stored energy but solely to the intensity of localized plastic stresses.

CHAPTER 12

Role of Analytical Procedures in Formal Certification of Structural Reliability by Codes, Rules, and Standards

CERTIFICATION PHILOSOPHY

The purpose of certification is to ensure uniformity in design, fabrication, and inspection of structures. Various documents are used to define formal standards for certification. When legally adopted, the certification documents can assure uniform compliance.

The engineering considerations that dictate the objectives of certification documents are known as the philosophy, or intent, of the requirements. The intent is decided by the group responsible for imposing the standards (for example, an ASME code body for pressure vessels that must bear a stamp of approval).

The philosophy of these groups may be expected to change with improved design methods. In general, the intent is to use the best practical methods. Self-consistent quantitative procedures are preferable to those based on expert opinion and expressed by arbitrary rules.

Design factors that are deterministic (subject to numerical analysis) have always been considered certifiable to rational design rules. In this case, expert opinion is involved only in selection of accepted design methods from handbooks, codes, etc. In the past, fracture and crack-growth problems were considered purely qualitatively. Therefore, their solutions could not be classed as deterministic, and their certification depended entirely on expert opinion.

The most profound influence of the current rational quantification principles of fracture mechanics is on certification philosophy. Fracture and crack growth may now be treated as rationally as other design problems. Loose certification by expert opinion has been replaced by numerical criteria applied according to accepted methods. While the formula or graphical method selected for calculation may be a matter of expert opinion, the results are self-consistent; the analyses are deterministic, not matters of opinion.

These changes in philosophy are implemented by improvement of specific certification procedures prescribed in codes, rules, and standards. For example, the design agent may be required to comply with the following categories of provisions:

General—references to applicable design codes
Standards—documents for mechanical test procedures (ASTM, ASME, etc.)
Materials—specifications for standard-grade metals (ASTM, ASME, etc.)
Fabrication—references to standards for welding electrodes, welding procedures, and inspection of welds (AWS, etc.)

Supplementary—amendments to cited standards, which become part of the formal requirements.

All procedures in a specified combination of provisions must be uniformly rational. A mix of rational and arbitrary provisions cannot satisfy requirements for rational certification. The use of rational criteria for characterizing fracture and crack-growth properties requires rationality of other related provisions. For example, reference to a system of standard-grade metals should be based on rational fracture criteria.

The sequence of steps outlined in Fig. 176 should be followed in certifying structural reliability by rational principles. The certification sequence must be rational for all steps of characterization, analysis, and optimization of engineering factors.

The first step is based on rational fracture mechanics test methods and criteria for characterizing metal properties. The second step involves fracture mechanics analyses of fracture and crack growth. The graphical methods are simply an aid for rapid calculation of crack size and stress conditions and/or analysis of fracture state for the given section size. The important point is that the graphical methods conform with fracture mechanics principles. Accordingly, principles of fracture mechanics rationality are guaranteed to the user of the diagrams. Reference to the diagrams provides a basis for review of analytical methods and the resulting decisions. Documentation for review purposes is important for all rational provisions of codes.

The third step is based on rational integration of metallurgical, mechanical, and fabrication features. This step depends on the validity of the prior steps; if fracture mechanics details are not clarified, it is impossible to examine rational engineering tradeoffs involving fracture and crack-growth parameters.

The final step documents that certification is in conformance to all provisions for test, analysis, and engineering optimization. This step is equivalent to completion of a checklist to confirm that all appropriate documents have been followed. The degree of rigor for certification depends on the particular codes, rules, or standards.

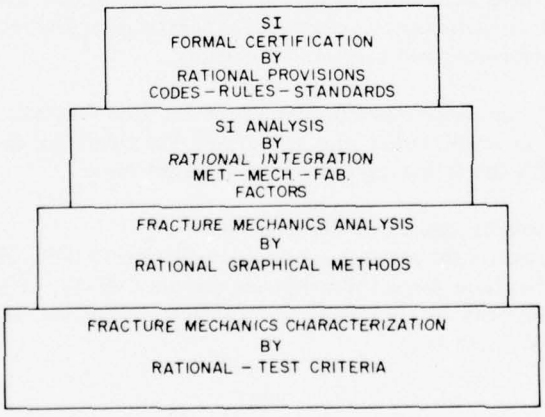

Fig. 176—Sequence of rational certification steps.

It should be noted that any amendments are legal or contractual requirements. Accordingly, the amendments must preserve the chain of rationality.

APPLICATIONS TO CODES, RULES, AND STANDARDS

Before 1970, the formal use of rational principles for fracture control was centered in aircraft, aerospace, and commercial nuclear power systems. A mechanism for promoting the use of new procedures existed in the form of a tradition of contractual specification by the user. Moreover, expert technical teams were associated with the development of the advanced systems. The use of rational principles for control of crack growth due to environmental effects and fatigue followed the use of rational fracture-control principles.

Between 1970 and 1975, there was a notable broadening of the formal use of these principles in codes, rules, and standards. The circumstances that have dictated more general use are of interest.

The most significant change in formal engineering practices is the adoption of analytical methods for various additional failure modes. Prior practices were formalized only for classical overload, buckling, plastic instability, and other failure modes related to tension or compression. Fracture and crack-growth failure modes can now be treated rationally.

Fracture and crack-growth control principles are formally applied by design agents, who are required by contract to use the appropriate provisions of codes, rules, or standards. Various examples will be cited to illustrate that there is no change in long-established formal engineering practices. The only change is in requirements for analysis of fracture and crack-growth problems.

A sound engineering basis must exist for including or excluding specific failure modes. In general, the first consideration is fracture. Crack-growth considerations are added if necessary. Accordingly, there is a logical separation between certification requirements for structures of low and high strength metals.

For example, commercial nuclear powerplants require consideration of failure modes that include fracture, crack growth, and the effects of neutron damage. The design agent is directed by the ASME Code and Federal standards to consider all of these. It should be noted that Federal standards do not dictate the ASME Code, which remains an independent document. This example is of interest because it indicates ASME action for modernization of the code, in addition to legal implementation.

The design bases for the pressure boundaries of commercial nuclear powerplants are defined by the *ASME Boiler and Pressure Vessel Code*, Section III, "Rules for Consideration of Nuclear Power Plant Components." The Section III rules were amended in 1972 to include advanced fracture mechanics principles for characterization and analysis. Other parts of the ASME Code did not, as of 1976, include these modern principles.

The ASME Rules for nuclear power plants have been made a matter of legal regulatory requirement by publication of stipulations to this effect in the *Federal Register*, plus amendments. For example, amendments cover neutron damage during the service life of the pressure vessel beltline.

This case illustrates the route by which the modernized Code has become a matter of law for designers, producers, and users of the structure. Formal certification is very stringent because of strict licensing requirements. Any questions of structural integrity that arise during the service life of the pressure boundary are also analyzed by reference to these standards. The point is that licensing is based on deterministic analyses, which do not depend on opinion. In Code terminology, the process is described as "certification by analysis," as distinguished from "certification by rule."

Other examples of legal requirements for certification that promote the modernization of codes, rules, and standards may be cited for ships, aircraft, bridges, fluid or gas transport systems, and other critical structures. The interesting feature of this general group is that the usual gradual nature of modernization may be altered on a case basis by enforced action. In general, a regulated industry tends to offer its own established specifications as a first solution to regulatory requirements. The industry specifications may be published in the *Federal Register* and thereby become law. They are then not subject to modification except by revision of the law. It is thus in the interest of both industry and regulatory authorities to adopt rational procedures. Thus, situations that could result in long-term impasses may be resolved expeditiously by consensus or by enforcement based on modification of the existing law. Public interest and criticality of failure consequences dictate whether gradual or immediate action is taken in a particular case.

The foregoing applies to structures that have common features and are ordinarily produced in commercial quantity. The use of modern certification principles has been most notable in radically new, high-performance, prototype or one-of-type structures. An example is provided by design competitions for high-performance aircraft. In this case, the designer is part of a team that must optimize the overall performance of the aircraft. The impact of SI principles in such cases has been great, because very specific aircraft standards are issued by procurement agencies as legally binding contractual requirements. For example, MIL STD-1530 (USAF) Military Standard—Aircraft Structural Integrity Program, Airplane Requirements (1972) and the related document, "*USAF Damage Tolerance Criteria*" (1972), have been used by the Air Force.

The importance of rational SI principles is evident from these contractual and legal applications. Moreover, the principles are a matter of engineering responsibility in general design. In the absence of specific contractual requirements, the implied legal responsibility for prudence and best practice remains. In cases of structural failures resulting in financial loss or injury, it must be proven that prudence and best practice were used, according to existing engineering knowledge.

MODERNIZATION OF SPECIFICATION SYSTEMS

The high strength steels that have been described in terms of RAD zonings have been adequately characterized in terms of rational fracture data. Their specialized use in critical structures has promoted exacting examination of their properties. Similar information is available for high strength aluminum and titanium alloys.

In general, the greatest need for rational characterization data, organized to provide ready reference to the designer, is for high-tonnage-use steels of low and intermediate strength. For example, the general specification system for standard-grade C-Mn (pearlitic) steels is complex

and has developed for a variety of reasons. The obvious categories are based on the following criteria:

Yield strength
C-Mn ratio and maximum Mn content
Open or tight specification ranges
Normalization or absence of it
Section-size range and limits
Special features of low-alloy additions.

To provide meaningful fracture data for metal selection from such listings, fracture properties must be cited in terms of rational criteria. Figure 177 illustrates minimum requirements for characterization. The fracture test value should indicate the position of the metal with respect to the six subdivisions of the fracture-state scale. In fact, the usual requirement is for definition of a level within the subdivision. For example, it is important to define levels within low and high elastic-plastic fracture states for purposes of establishing arrest criteria. The data must relate to specific section sizes and take into account statistical variances of metal properties. Obviously, considerable precision is necessary.

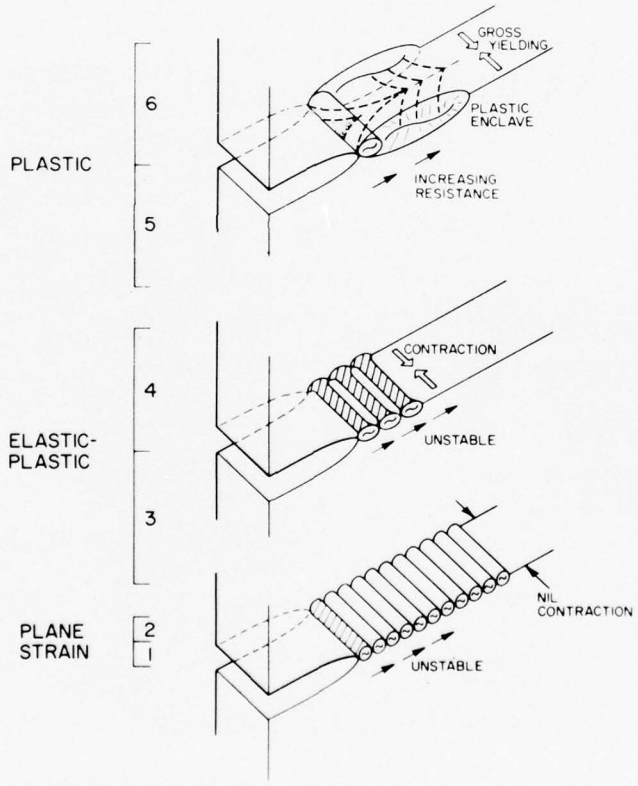

Fig. 177—Requirements for rational fracture state characterization of fracture properties. (See Chapter 3.)

These requirements are not met by the Charpy-V (C_v) reference system now used for standard-grade steels. Precise characterization is not possible for a test specimen that depends purely on correlation. Figure 178 illustrates that the C_v test does not develop the full range of fracture states. Constraint transitions are limited to a partially flat fracture with shear lips because of the small volume of metal behind the notch (see Chapter 11).

Specifications of minimum C_v properties for standard grades, as in ASTM publications, are established mainly for production quality control and not as design criteria. This is also the case for the more complex acceptance values for grade-thickness-temperature combinations, which are based on both C_v energy and lateral expansion. These values are the result of production experience, which proves that the values can be reliably attained. The only significance of the values, therefore, is for production quality control based on high statistical expectancy that the values will be met. The cost of the steel is based on this low rejection expectancy.

Experience confirms that C_v reference values as normally cited by standard-grade tables are inadequate for design. Figure 179 shows the fracture properties of a conventional standard-grade C-Mn (pearlitic) steel used in very large quantity. A complete brittle fracture of a large welded structure that included this metal occurred at the temperature noted. The source was traced to a very minute defect in the heat-affected zone of the weld, as deduced from the chevron markings on the fracture surfaces.

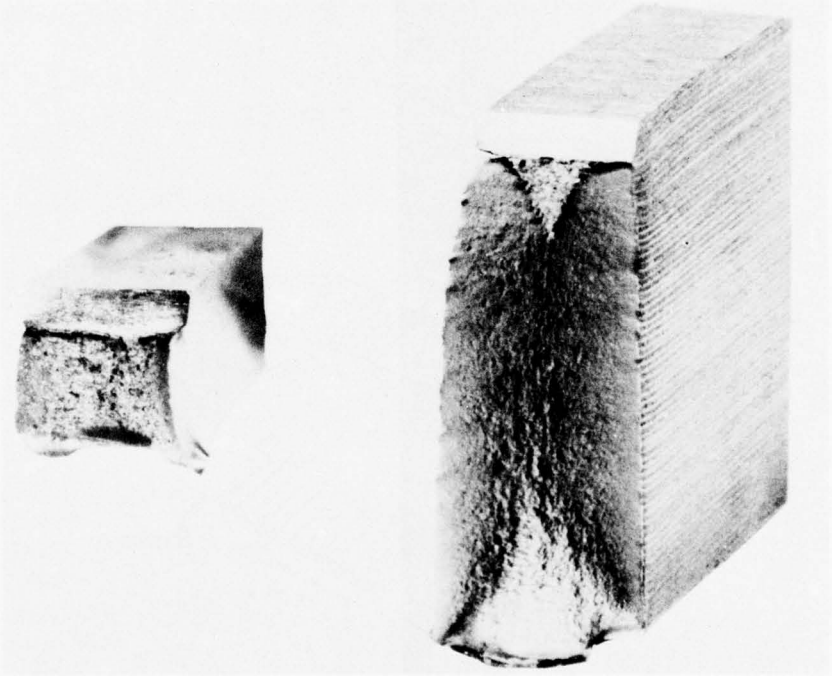

Fig. 178—C_v tests inherent inability to define fracture state (left). An increase in fracture path is necessary to disclose the fracture state of the metal, for the thickness of the C_v specimen (right).

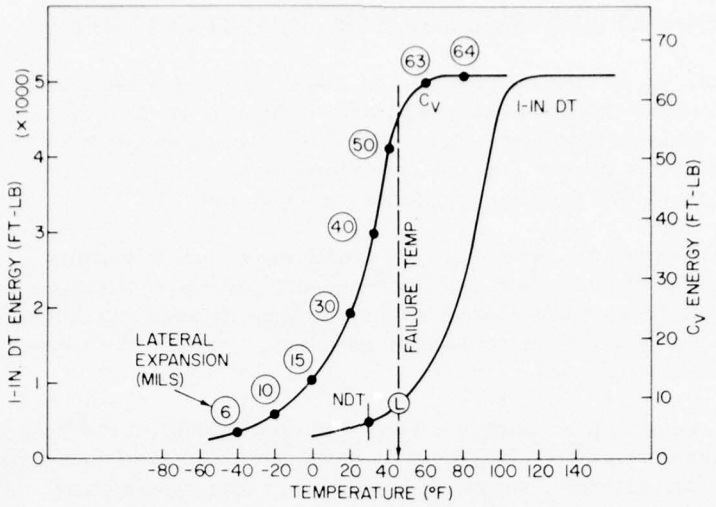

Fig. 179—Comparison of C_v and DT test fracture-properties characterization data, for a steel that failed in service (section size 1.0 in.; 25 mm).

The figure illustrates that

- The C_v energy and lateral expansion values at the failure temperature are very high—much higher than any ordinarily cited in standard-grade tables.

- The DT test, conducted at full thickness (1.0-in.; 25 mm), indicates that the fracture properties are essentially at the plane-strain limit at the failure temperature, as indicated by the circled "L" on the DT curve.

The dramatic differences in the C_v and DT characterizations are self-evident. However, it is more significant that the failure of the structure, at a temperature of high C_v fracture properties, startled the interested parties, including the regulatory authorities. This case illustrates the unfortunate association of fracture reliability with high C_v values for energy and lateral expansion. High C_v values can be totally misleading, as illustrated by this example and many similar cases.

Since the C_v values cited for standard-grade steels cannot be translated into fracture criteria at specific temperatures, they are useless for SI analysis. Because of this, designers ordinarily must search for other significant data. Serious application and documentation of an SI plan usually requires a fracture-test survey of candidate steels. In recent years, DWT-NDT and DT tests have been used increasingly for this purpose.

Expert mechanical metallurgists can accurately estimate NDT frequency distributions by referring to chemical composition, heat treatment, and section size, which yield estimates of the characteristic elastic-plastic transitions. Relatively few specialists are able to make these estimates with reasonable confidence. However, the fact that they can be made indicates that rational characterization data can be systematized with a reasonable statistical survey effort. Such systematization is badly needed by designers.

CERTIFICATION BY ANALYSIS FOR EXISTING STRUCTURES

The formal use of rational principles in the design of new structures has stimulated interest in their use for certifying existing structures. Also contributing to this interest has been the need for a common base of understanding between regulated industries and regulatory agencies. In such cases, the use of rational procedures is absolutely necessary. Analyses must be deterministic and beyond reproach of possible errors of opinions.

Most analyses are concerned with the possibility of brittle fracture in standard-grade steels. Considerable time and effort could be saved if the general predictions of fracture mechanics were relied on. For example, there is no rational basis for asserting that K_{Ic} criteria control the performance of welded C-Mn steels of plane-strain properties; experience dictates that K_{Id} properties control performance.

Localized metallurgical damage is the usual condition for brittle fracture initiation in structures of standard-grade C-Mn steels. A certain probability of such random damage is entailed in welding; rational certification by analysis, based on such purely random initiation events, is impossible. If appropriate analyses are made, the results automatically preclude certification.

Rational analysis of conditions for dynamic fracture initiation must be directed to the combined curves of critical crack size and arrest displayed in Fig. 180. The charts are explained in the discussion of the characteristic K_{Id} curve in Appendix B. The following features are important:

- Critical crack sizes for dynamic fracture initiation in regions of peak stresses are very small. They are impossible to reliably detect or prevent, even in the absence of metallurgical damage.

- The temperature range between L and YC criteria is relatively narrow for section sizes of less than 2 in. (50 mm).

- The 0.5 σ_{ys} (arrest) criterion is met at a temperature only slightly above the L criterion temperature.

- The arrest principle assures reliable fracture prevention for most structures. It does not depend on accidental metallurgical damage.

Because of these considerations, analysis for certification is generally aimed at documenting whether arrest protection is provided. Convincing proof can only be provided if the 0.5 σ_{ys} criterion is met.

One exception to this general rule is analysis of load stresses that are too low to sustain extension of brittle fracture. Another exception is structures of redundant design, in which fracture of a component does not necessarily lead to failure of the whole structure.

An interesting real-life example of certification by analysis is provided by large propane tanks (pressure vessels) that were load-limited to very low stresses. They were analyzed to determine whether stresses were, in fact, low enough to preclude brittle fracture. A general

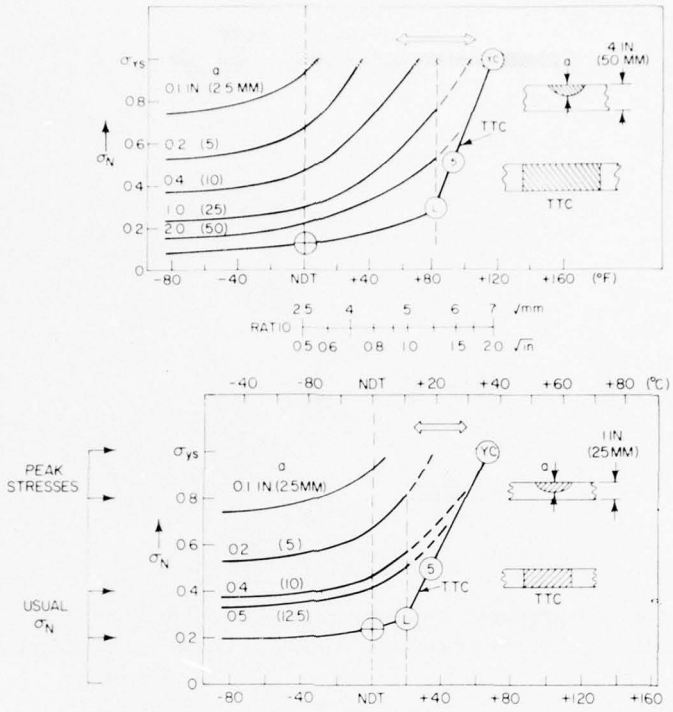

Fig. 180—Fracture mechanics analyses of dynamic initiation and arrest features, as reference to the K_{Id}/σ_{Id} ratio at the NDT temperature. (See Appendix B for ratio analysis procedure.)

consensus was attained among interested parties, including regulatory officials, that the structures could be certified safe by analysis.

The design criteria for the vessels resulted in hoop stresses that increase with temperature as shown in Fig. 181. The fracture analysis required examination of the temperature region of L-to-YC transition and the temperature region below the L point of the transition. A standard-grade C-Mn-V steel, of 0.6-in. (16 mm) section size was used.

Dynamic Tear and DWT-NDT fracture properties for the steel were surveyed statistically by random selection of samples from fabrication shops. This defined a statistical-expectancy band for the L and YC criteria, as illustrated in Fig. 181.

The L and YC relationships to the fracture-extension stress scale (σ_N) are described in Fig. B6 (Appendix B). Briefly, fracture-extension stress is referenced to an assumed condition of a through-thickness crack (TTC); since the crack provides maximum possible mechanical constraint (Chapter 3), the fracture extension stress is referenced to conditions that cannot be exceeded in structures. This is called limit analysis. The through-thickness crack assumption also provides a worst case for certification by analysis.

The problem was to determine the possibilities of extension of brittle fracture at all service temperatures, from -40° to 100°F (-40° to 38°C). The through-thickness crack assumption

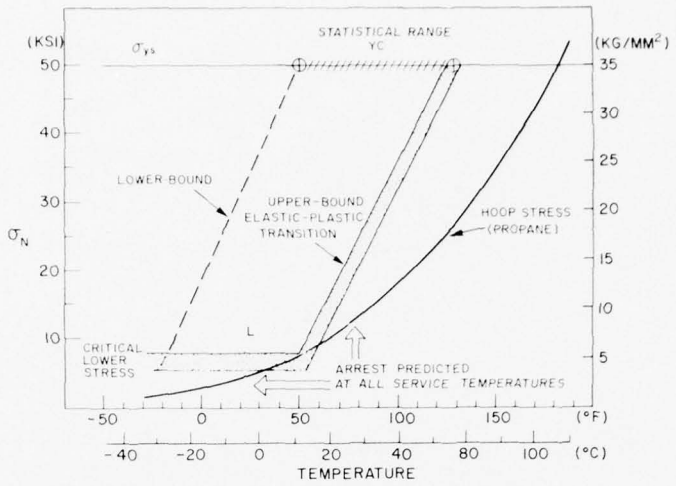

Fig. 181—Documentation for certification by analysis.

includes initiation conditions that involve punching penetration of the tank. It had to be proven that, regardless of damage, fracture extension would not follow. In effect, fracture arrest had to be demonstrated.

The fracture properties of the steel, examined on a statistical upper bound basis, were found to preclude fracture extension for through-thickness crack conditions, as follows:

At temperatures above 50°F (10°C), all steel plates of the population precluded fracture extension by virtue of elastic-plastic properties.

At lower temperatures, hoop stresses were below critical levels for extension of plane-strain (brittle) fracture.

The subject steel was used in as-rolled condition. A related question involved possible benefits of normalizing this steel, which would shift the upper bound elastic-plastic transition to the location corresponding to the lower bound curve of Fig. 181. This information was obtained in a related statistical survey; however, it was apparent that no benefits would result because the as-rolled steel is adequate to preclude brittle fracture for the cited hoop stresses.

This certification by analysis established a rational basis for examining the structural reliability of such vessels. Modifications of wall thickness and hoop stresses, due to changes in vessel size or in the liquified gas, must be examined in relation to specific curves of hoop stress vs temperature. The fracture properties must be matched to these curves in each case. The analyses cannot be made unless such data are developed as required.

TECHNOLOGICAL BENEFITS OF FORMAL CERTIFICATION—CASE EXAMPLE OF REACTOR PRESSURE VESSELS

Establishment of formal and rational certification procedures should not inhibit technological progress. In fact, synergistic effects of rational design promote technological advances.

CASE EXAMPLE: REACTOR PRESSURE VESSELS

The case of reactor pressure vessels is notable for the technological benefits of improved reactor steels, design criteria, and in-service operational techniques. There is long experience with legal enforcement of such critical SI objectives. Since this case of legal certification dates back more than 20 years, it is of interest to examine the beginning as well as the progress.

The beginning can be traced to failure analyses (1954) of conventional pressure vessels fabricated from A302-B steel, which was the most advanced pressure vessel material of the time. For this reason, the steel was of interest for the construction of the first commercial power reactors. Failures occurred while pressure vessels were being built for use in the elevator systems of aircraft carriers; Fig. 182 illustrates brittle fracture that took place during hydrotesting. There was an immediate investigation, but other failures took place within a few days as the result of weld residual stresses in partly finished companion vessels. This combination of events was startling and resulted in a searching analysis of causes and remedies.

The failures occurred at temperatures below the NDT temperatures of the steels, as expected. A statistical NDT frequency curve for A302-B steel was established from existing stocks, and the effects of improved normalizing heat treatment were examined. As a result, it was deemed practical to place a rigid maximum value on the NDT temperature of steels

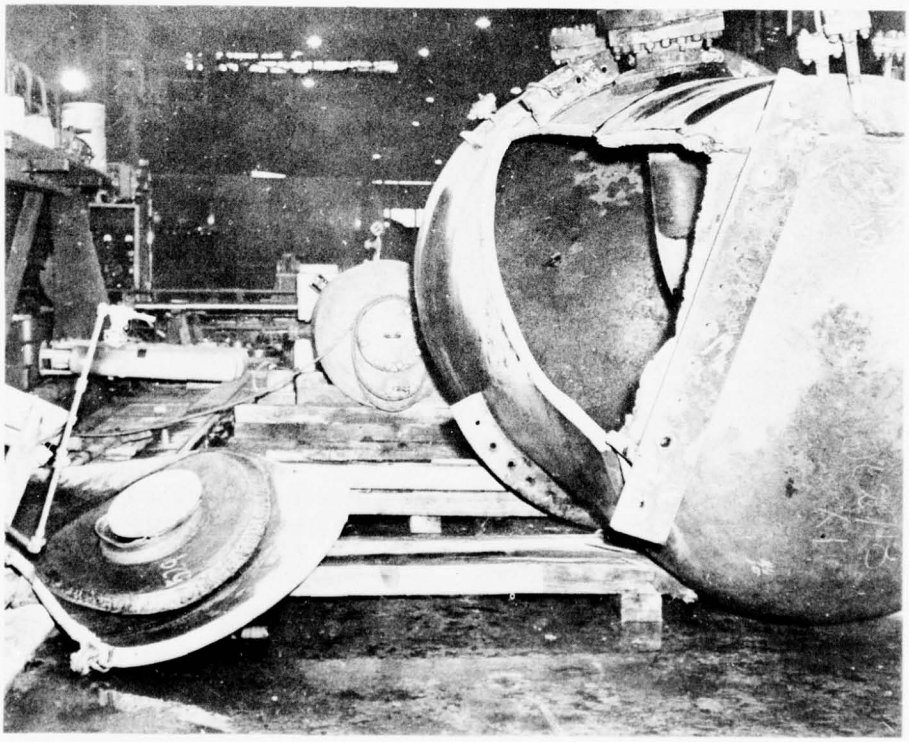

Fig. 182—Hydrotest failure of A302-B pressure vessel (1954) (section size 3.0 in.; 75 mm).

purchased for replacement of the pressure vessels. This ensured fracture-arrest properties at service temperatures and at hydrotest temperatures.

This experience with A302-B steel was the basis for establishing NDT specifications for the reactor pressure vessel of the first commercial nuclear powerplant in 1956. The object was to provide positive assurance of fracture-arrest properties at hydrotest temperatures. There was no concern for fracture at the high operating temperatures of the vessels. However, the possibility of brittle fracture in hydrotest was unacceptable because of the loss of public confidence that might result.

The following reference criteria were established;

Purchase specification: NDT = 10°F (−12°C)

Hydrotest temperature: FTE (YC) = 70°F (20°C).

The two criteria are in rational agreement because of Δt of 60°F (35°C) above the NDT temperature was used as reference to the lowest permissible hydrotest temperature. At the time, specifying a low fracture test temperature to guarantee fracture arrest at higher temperatures was a novel procedure. However, the procedure was used confidently because of experience with the Robertson CAT and with explosion crack starter tests (Chapter 6).

All commercial reactors constructed from 1956 to 1972 were designed to the NDT + 60°F (35°C) criterion for fracture-arrest properties at hydrotest temperature. The concept of a characteristic K_{Id} curve was added in 1972 to allow more detailed analysis in the startup temperature range. However, the NDT index remains the legal basis for certification of metal quality and for reference to the K_{Id} transition (Chapters 4 and 6).

Formal requirements for NDT temperature control, besides ensuring hydrotest reliability for more than 20 years in all commercial reactors, have other consequences worth examining. The first synergistic benefits involved the metallurgical quality of thick-section reactor vessels. The early A302-B reactor pressure vessels had relatively small diameters and section sizes compared to later designs. The escalation in pressure vessel wall thickness in the early 1960s, and particularly the very thick forgings for nozzles and head inserts, made the A302-B steel unacceptable. The NDT = 10°F (-12°C) criterion simply could not be met. As a result, the steel was modified to the present A533-B composition, and normalization was replaced by quenching and tempering heat treatment, which yielded better microstructure. The new steel was thus developed specifically to meet the fracture-arrest requirements of thick sections.

At the time, there was considerable questioning of this possibility by forging producers, who relied on inadequate background data. However, the improvement was feasible, and the forging industry accepted the specification requirements. In general, it spurred installation of improved quenching facilities, which otherwise would have been resisted.

By the early 1960s it became evident that the original NDT temperature could be elevated as much as several hundred degrees by neutron damage. Accordingly, it was possible to lose fracture-arrest protection at service temperatures, particularly during the startup phase of reactor operations. This was made glaringly evident by the rational criteria and analysis methods employed. This realization resulted in the benefits of prudent changes in pressurization and startup procedures for reactors that had seen enough service to suffer damage. Other

benefits included development of in-service annealing to eliminate such damage; this method was first applied, in about 1964, for the compact reactors used at remote Army installations.

Long-term relief from neutron damage problems was attained in 1970 as the result of investigations that isolated phosphorus and copper as the critical impurities for damage. The present specifications for pressure vessels, forgings, and weld metal emphasize the use of radiation-insensitive (low phosphorus and copper) metal. The NDT shift, as related to increases in the fracture-arrest criteria temperature, was used as the guide for this important metal-quality development.

The period from 1964 to 1969 was marked by serious concern about the effects of section size on temperature-induced transitions. As reported in Chapter 4, the issue was resolved by establishing the rationality of characterizing plane-strain transitions by reference to the characteristic K_{Id} curve as indexed to the NDT temperature. Thus, by 1972 the stage was set for action by the ASME Code in adopting improved analytical procedures based on these factors. To date, the ASME action is limited to sections of the Code dealing with the pressure boundaries of nuclear components. However, the discussions in Chapter 4 of generalized procedures for ratio analysis of characteristic K_{Id} curves presage more general use of these principles.

The tremendous effort required to resolve the thick-section constraint problem would probably not have been made had the question not been central to formal regulatory practices for reactor pressure vessels. Because it was, the effort involved the entire nuclear power industry. This advance, too, must be added to the list of the benefits of rational SI analysis.

CERTIFICATION REQUIREMENTS FOR SPECIAL PROBLEMS OF CRACK GROWTH—CASE EXAMPLE OF HYDROFOIL CRAFT

The basic procedures for establishing formal certification requirements for structural reliability with respect to crack growth are the same as for fracture. However, details tend to be specialized to the nature of the crack-growth problem. Most important, the definition of structural reliability requirements must include a broader range of factors, particularly with respect to environmental effects.

The essence of fracture prevention is avoiding catastrophic failure. In the case of crack growth, it is important to decide whether some degree of self-arresting crack growth that does not affect strength is acceptable. Obviously, nonarresting crack growth is not acceptable. Questions of self-arresting (localized) crack growth require detailed analysis before development of certification documents, particularly for new structural designs.

Criteria for eliminating catastrophic fracture dominated the SI analysis in the aircraft field until recently. However, with fracture issues resolved and reduced to general contractual documents, attention has turned to environmental crack growth effects. It is well known that stress-corrosion cracking and corrosion fatigue may pose very expensive maintenance problems for high-performance aircraft. For hydrofoil structures, contact with saltwater may make crack-growth problems crucial. A fleet of hydrofoil craft subject to grossly aggravated maintenance problems, as compared to aircraft, would not be economically acceptable.

Accordingly, formal documentation of performance must include credible evidence of reliability with respect to crack growth. The fact that such crack growth may be only a nuisance is not a satisfactory guarantee against unbearable maintenance costs during the life of the

230-362 O - 77 - 17

structure. This example is particularly important because much emphasis has been placed on avoiding catastrophic fracture. It is essential to include catastrophic economic consequences, loss of availability, and loss of confidence in structures that display visible cracks.

The elimination of all possible catastrophic consequences may be expected to guide developments for all structures subject to crack growth problems. Certification requirements are usually described in terms of general principles; specific cases require special provisions.

Figure 183 provides reference data for generalized discussions of crack-growth analysis. It is assumed that the criteria for stress-corrosion cracking, discussed in Chapter 9, are understood. The figure illustrates conditions for a commercial high strength stainless steel (S-PH) as heat treated over a wide range of yield strength.

The structural component of interest is a hydrofoil strut of stiffened-box construction, with section sizes of 1.0 in. (25 mm). Accordingly, the elastic-plastic region (L to YC) is located in the 0.63-to-1.0 ratio range of the RAD. The struts may collide with floating objects; thus, fracture properties of at least high elastic-plastic type are required. On this basis, it is evident from Fig. 182 that yield strength should be limited to a maximum of 170 ksi (1172 MPa).

The struts are assumed to be fabricated by electron-beam welding to produce minimum residual stresses and defects. If other methods are used for fabrication, the analysis must include higher residual stresses and larger defect sizes. These complications are avoided in this discussion.

Minimizing residual stresses and defect size renders it feasible to accept stress-corrosion cracking properties of intermediate and high ratio value. Low-ratio properties are unacceptable for reasons described in Chapter 9. On this basis, it is apparent from Fig. 183 that the stress-corrosion cracking analysis depends on whether cathodic coupling is involved. If so, the

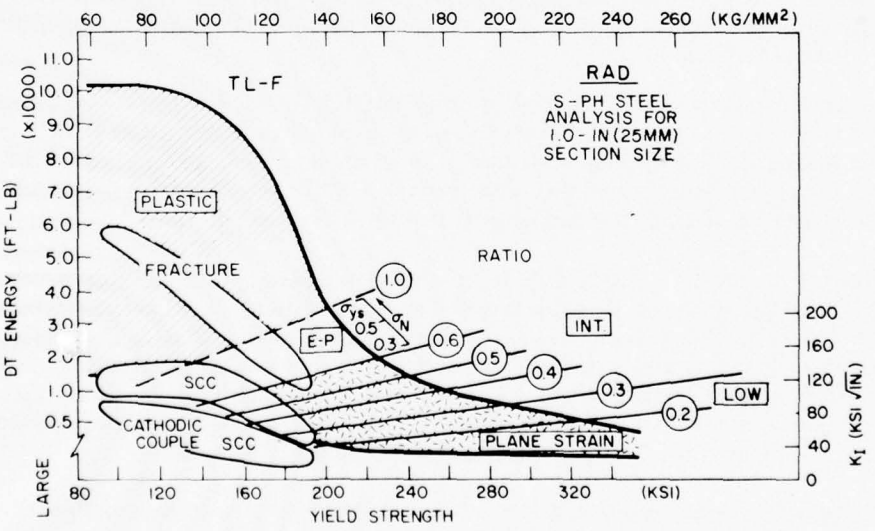

Fig. 183—Summary of fracture and stress corrosion cracking properties of high strength stainless steel (S-PH).

maximum yield strength must be set at 130 ksi (896 MPa). If not, it is feasible to use as an initial estimate the same maximum level established for fracture, 170 ksi (1172 MPa).

Questions of corrosion fatigue must also be examined (Chapter 10). However, these involve specific design details and load spectra beyond the scope of the present general description.

We now examine possible ways of establishing developmental goals and related certification requirements. It is necessary to consider the following possibilities:

- If the diagram (Fig. 183) is not available for the candidate metal system(s), the first requirement is the development of equivalent information.

- If the diagram is available, design requirements for yield strength should be tested against the implications of stress-corrosion cracking. Preliminary loads analyses provide for stress analysis and, therefore, indicate desirable yield strength objectives. If the implications of stress-corrosion cracking are adverse, reconsideration of either loads or stress analyses is necessary.

When feasibility is established, a prototype may be fabricated. The certification requirements are then extended to include NDE, QC, NDI, etc.

Reduction of these procedures to specific contractual documents obviously requires attention to details. Accordingly, the complete set of documents may cover different aspects of the problem. For example, the set may include (a) general requirements, (b) specific requirements for criteria and reliability plans, and (c) specific requirements for documentation and recordkeeping. This method is used for aircraft SI documents. General documents define the development objectives, and highly detailed documents cover specific aircraft designs.

In the case of hydrofoil craft, it is obvious that the specific documents for stress-corrosion cracking and corrosion fatigue are crucial. The SI analysis and certification problem is dominated by the crack-growth parameters defined by the two lower zones of the diagram in Fig. 183. A clear, formal definition of crack-growth control plans must be developed as a basis of contractual understanding. The crack-growth problem is decisive in development of hydrofoil systems.

The methods for prior analysis for crack-growth control requirements are general for all structures that use materials that are sensitive to crack growth. The relative degree of sensitivity determines whether crack-growth control is feasible. Feasibility is a crucial element of analyses that should be made before certification documents are issued.

REQUIREMENTS FOR REFERENCE TO FRACTURE STATE— CASE EXAMPLES OF AEROSPACE STRUCTURES

Specifications that cite plane-strain fracture properties K_{Ic} or K_{Id} are insufficient for establishing design criteria. For example, a given K_{Ic} value may represent plane-strain, elastic-platic, or plastic fracture properties, depending on section size and yield strength. A given K_{Id} value may represent different fracture states, depending on section size and temperature.

The complications that arise from specifications based solely on K_{Ic} or K_{Id} plane-strain values can be avoided by specific reference to the fracture state implied by the specification. This is important, and it should be considered in detail for rational specifications. Section size and yield strength are independent parameters and may be adjusted in the design process. If K_{Ic} is fixed, the adjustments can result in changes of fracture state. In this case, fracture state becomes a variable not controlled by the specification of K_{Ic}.

The problems that arise from failure to specify fracture state are evident from the fracture mechanics literature. By convention, most discussions are presented in terms of plane-strain properties and critical crack sizes. In some cases, failure to cite fracture states leads to incorrect assumptions by the reader. We cite two notable examples of insufficient discussion from an SI point of view:

1. The significance of steel selection procedures to the hydrotest failure of a large rocket case was not evident.

2. The significance of K_{Ic} specifications for high-performance aircraft was not discussed.

Figure 184 illustrates the dramatic failure of a very large rocket case during hydrotesting. This failure has been used repeatedly as a classic example for explaining the use of plane-strain fracture mechanics combined with precise methods of NDI. However, proper analysis in terms of fracture state changes the emphasis considerably.

The case in question was fabricated from air-melted maraging steel. The heat treatment resulted in a yield strength of 220 ksi (1517 MPa) and fracture properties on the order of 0.3 ratio. Weld defects, as shown in the figure, initiated the failure at a stress near 0.6 σ_{ys}. These defects defied NDI detection, both before and after the failure. The fracture properties of the weld were of the same order as those of the plate.

The literature's conclusions have emphasized the following:

Close correspondence to calculated critical crack sizes
The obvious importance of improving NDI capabilities
The importance of using plane-strain parameters for high strength metals.

All of these are proper, albeit limited, deductions. The rocket case in question was in development competition with that of another manufacturer. The companion case was fabricated from the same maraging steel and strength level, except that high-quality (vacuum-arc) melting was used rather than air melting. As a consequence, the steel had high-corridor elastic-plastic fracture properties. The failure steel had low-corridor fracture properties corresponding to a plane-strain fracture state. It was predictable that the high-quality steel would pass the hydrotest, as it did.

A correct failure analysis should consider both vessels, as follows:

- The failure of one vessel was due to inappropriate selection of air-melted steel, which resulted in a plane-strain fracture state for the section size and strength level.

- The reliable performance to be expected for serial production of the second case is directly related to elastic-plastic fracture properties for the same section size and strength level.

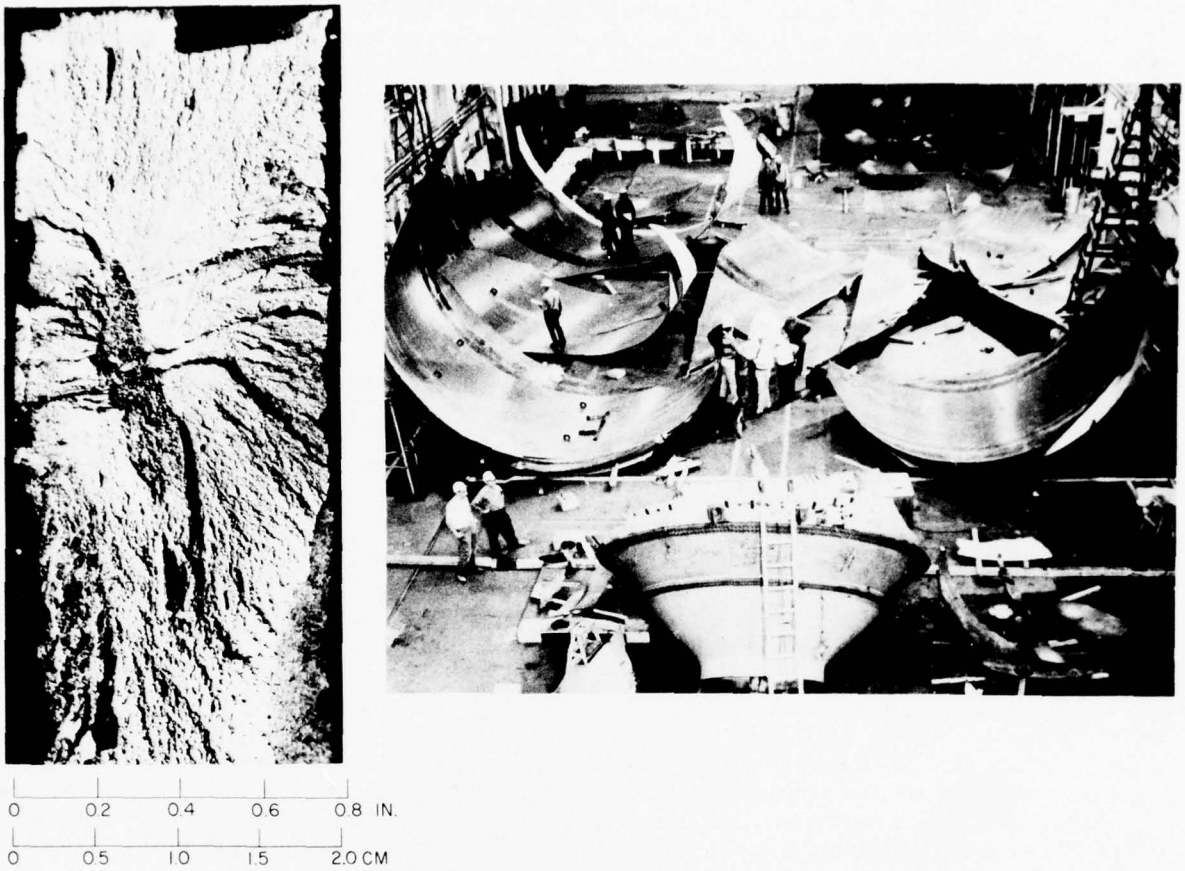

Fig. 184—Hydrotest failure of large rocket case.

The failure of the first case was statistically probable, but not certain. Even if the first case tested had not failed, there would be no guarantee of reliability for subsequent vessels. On the other hand, the elastic-plastic properties of the second case provide confidence of statistical reliability. In fact, at the time, prior analyses could have been made to predict the results of the hydrotest. The primary reliance on proof testing to establish reliability is outdated and potentially misleading. The purpose of proof testing should be examined in relation to fracture properties.

The construction of modern aircraft based on K_{Ic} requirements is another example that requires clarification by reference to fracture state. The emphasis on developing engineering-handbook data of K_{Ic} type for design purposes would seem to indicate plane-strain properties. However, the tests are conducted for thick sections of sufficient size for valid K_{Ic} characterization. The section sizes actually used in structures may be considerably below plane-strain limits, in which case the true fracture properties are of elastic-plastic or plastic type.

Figure 109 (Chapter 7) presents a RAD zoning for the new aircraft steels as compared to the old types. The specific mechanical differences are that (a) the old steels are characterized by plane-strain properties for section sizes of interest for strength members, and (b) the new steels are not characterizable by plane-strain K_{Ic} properties for equivalent section sizes. The RAD analysis is for a maximum yield strength of 220 ksi (1517 MPa) and section size of 1.0 in. (25 mm). If the maximum yield strength were limited to about 200 ksi (1379 MPa), elastic-plastic properties would be developed for the new steels for section sizes of 2 to 3 in. (50 to 75 mm).Thus, a modest adjustment of yield strength can ensure elastic-plastic properties in relatively thick sections. Accordingly, there is considerable latitude in designing strength members to avoid the problems of plane-strain metals. This fact has been used in the design of the latest high-performance aircraft. All fracture-critical locations are protected by the use of metals with high elastic-plastic or plastic fracture properties for the given section sizes.

It is proper to use K_{Ic} values for fracture property reference in handbooks. This is the same method of reference used for the data-storage (trend-line) system of the RAD. Either way, the true signficance of the K_{Ic} value must be analyzed in terms of section size. Otherwise, specific design criteria for the aircraft may not be appreciated as indicating elastic-plastic or plastic behavior.

K_{Ic} tests should not be used for purposes of quality control and certification documentation if the normal forging stock is not of sufficient section size for K_{Ic} tests. Processing special thick-section forging stocks solely for K_{Ic} tests is very expensive and not essential. A small DT test of standard size can be made, using samples machined from the forging stock, as for tensile tests. Thus, the certification and quality control function can be separated from the design handbook reference function.

The importance of a clear reference to the fracture state for the section size of interest cannot be overstated. There is no way to communicate the true intent of design criteria based on initiation or arrest principles except by explicit reference to fracture state. In fact, all aspects of structural reliability analysis depend fundamentally on appropriate consideration of the true fracture state.

APPENDIX A

Introduction to Linear-Elastic, Plane-Strain Fracture Mechanics

Theoretical Principles

To engineers, the most important aspect of linear-elastic fracture mechanics is the significance of the K parameter. This should be understood in relation to the plastic zones developed at crack tips. The K parameter defines the elastic-stress intensification in the region of the crack tip (Fig. A1). It is a function of the flaw geometry and the nominal stress acting in the region of the crack. The size of the plasticized region at the crack tip can be defined generally as a function of $K_{Ic}/\sigma_{ys})^2$. Except under extremely brittle conditions, fracture is initiated in this zone. The fracture instability event is basically related to a plastic-strain ductility limit of the metal crystals in the plastic zone.

Fracture mechanics avoids the complications of plastic-strain conditions by referring to the elastic-stress intensity K levels that are required for unstable crack movement. The critical K level, for mechanical constraint of maximum triaxiality (plane strain), that can be imposed on the crack-tip region is defined as K_{Ic}. The connection between K_{Ic} and the corresponding plastic-zone size (PZS) is crucial to ductility-limits interpretations of fracture toughness in terms of elastic-stress fields.

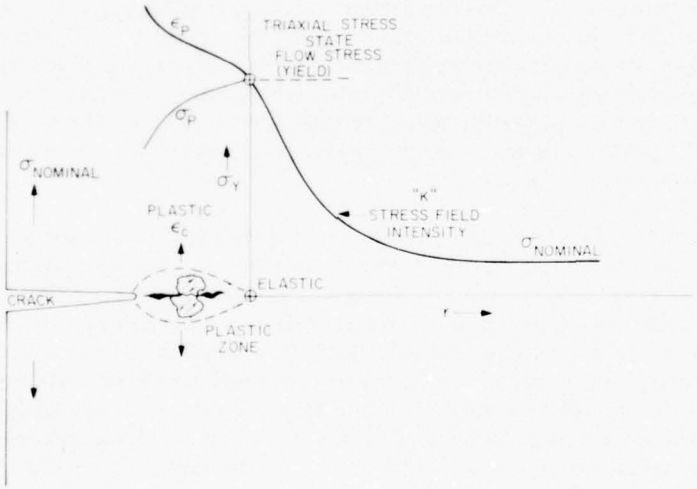

Fig. A1—Relationship of elastic and plastic stress fields to the plastic zone, for plane-strain constraint.

Unstable crack movement depends on the formation of a critical plastic-zone size; the larger the plastic-zone size at fracture, the tougher the material. Since the critical plastic-zone size is a function of $(K_{Ic}/\sigma_{ys})^2$, this ratio properly defines fracture toughness. For example, a low value of $(K_{Ic}/\sigma_{ys})^2$, or simply K_{Ic}/σ_{ys}, means a small plastic zone. This, in turn, means that little energy must be expended to develop the unstable crack; consequently, the material is brittle. The opposite is true for a high ratio.

It is impossible to gain such a simple physical insight into fracture conditions by sole consideration of K_{Ic} values. For instance, a K_{Ic} value of 60 ksi $\sqrt{\text{in.}}$ cannot be translated to fracture toughness if the yield stress is not specified. If the yield stress is 30 ksi (206 MPa), K_{Ic} value of 60 ksi $\sqrt{\text{in.}}$ denotes a very high fracture toughness because the critical plastic-zone size is large. The value of $(K_{Ic}/\sigma_{ys})^2$ is then equal to 4.0. If the yield strength is 180 ksi (1241 MPa), a K_{Ic} of 60 ksi $\sqrt{\text{in.}}$ indicates low toughness, because the critical plastic-zone size is very small. The value of $(K_{Ic}/\sigma_{ys})^2$ is then 0.09, which represents a plastic-zone size approximately 0.025 times that of the previously cited case. Metals of different yield strength will have the same level of fracture toughness if the ratio $(K_{Ic}/\sigma_{ys})^2$ is the same. The simple ratio K_{Ic}/σ_{ys} provides reference to this relationship and is the simplifying convention used the text.

The physical significance of plane strain is that it indicates maximum triaxial constraint to plastic flow. This means that the plane-strain plastic-zone size, at the point of fracture, cannot be made smaller by increasing the depth or size of a sharp crack. If the plastic-zone size cannot be made smaller, the fracture toughness measured is the lowest possible singular value for the metal. It is on this basis of singularity that K_{Ic} is considered a fundamental materials parameter.

The K definitions of elastic-stress fields at crack tips are appealing for stress analysis, because they allow fracture to be described solely in terms of crack-size and stress parameters. From a metallurgical viewpoint, the fracture toughness depends on the ability of metal grains to endure large plastic strains at the crack tip before separation takes place. The limit to the strain that can be developed under maximum triaxial constraint provides a connection between (a) ductility concepts of fracture toughness, which guide the metallurgist in improving the metal, and (b) the stress-intensity definitions of K values, which are used to calculate crack instabilities. Differences in fracture properties for different metals are expressible in terms of K values, but the physical interpretations of the metallurgical factors can be given only in terms of mechanically constrained ductility.

The stress intensity at the crack tip is a function of the depth and shape of the crack and the level of stress that acts to open the crack. A specific level of K_{Ic} stress intensity may be reached by combinations of large crack sizes and low stresses or small crack sizes and high stresses. These relationships provide the basis for linear-elastic fracture mechanics calculations of fracture instabilities. As the triaxially constrained plastic-flow ductility of the metal increases, the stress required for instability at the tip of a crack of specified dimensions will eventually exceed yielding. For a brittle metal, of small critical plastic-zone size, small cracks are severe enough for K_{Ic} stress-intensity levels to be reached at stresses below yielding. In a more ductile metal with a larger critical plastic-zone size, larger cracks will be required to cause failure at stresses below yielding. Increased ductility requires both increased mechanical constraint for retention of the plane-strain condition and increased crack severity for development of instability at elastic-stress levels.

The constraint on metal flow at crack tips is of geometric origin; it is related to inhibition of Poisson effects. The cracked area does not contract, because no longitudinal stresses act on it. It

tends to maintain its original dimensions while the metal in the plastic zone flows in the direction of the normal stress. To do so it must contract, by Poisson effects, in the plane of the crack. The metal contracting along the crack front must be connected physically to noncontracting cracked areas. The effect of the crack is to limit lateral contraction and thus limit extension in the normal direction. Increasing the size of the crack perimeter by increasing crack size provides increased constraint because the noncontracting area is larger; therefore the Poisson suppression effect is retained to larger plastic-zone sizes.

There are three requirements for the development of instability with retention of the plane-strain condition: (a) the volume of metal surrounding the crack must be large enough to contain the necessary triaxial elastic-stress fields, (b) the crack must be large enough to maintain adequate constraint for prevention of lateral contraction, and (c) crack depth must be sufficient to attain the critical K level for instability at stress levels below yielding.

The physical details of these relationships are evident in the features of ASTM-standardized K_{Ic} specimens, which are based on test experience:

$$B \geq 2.5\left(\frac{K_{Ic}}{\sigma_{ys}}\right)^2$$

where B represents specimen thickness in inches. The crack depth is suggested as 0.5 B for tension-loaded specimens, as is the uncracked ligament depth. These conditions provide the necessary constraint required by the level of fracture toughness defined by the K_{Ic}/σ_{ys} ratio. Increasing the crack depth while retaining the 0.5 ligament depth merely decreases the stress level at instability; the K_{Ic} value is not changed. Increasing B does not change the level of instability stress if the crack depth is held constant; K_{Ic} is not changed. If the ligament depth is less than the required size, the volume of metal surrounding the crack will be too small to contain the triaxial elastic-stress fields; plane-strain constraint will be lost, and K_c conditions will then apply. This will be the case even if the crack depth and B value meet the requirements.

A simplified physical interpretation of section-thickness and crack-size constraint relationships for surface cracks is presented in Fig. A2. The illustration superimposes two edge-cracked K_{Ic} specimens with two surface cracks. The thickness of the specimens B is assumed to be the minimum value. For a low K_{Ic}/σ_{ys} ratio a small B is adequate, and for a high ratio a larger B is required. It is assumed that the volume of metal below the K_{Ic} specimen and the surface cracks is large enough to contain the necessary elastic-stress fields. The size of surface cracks required for plane-strain fracture instability varies with the minimum B value. For maximum permissible near-yield stress loading, the critical crack size for metals with low K_{Ic}/σ_{ys} ratios is much smaller than for high-ratio metals. For lower stress levels, the crack sizes indicated schematically increase. However, for any relative stress, the critical crack size for low-ratio metals is always much smaller than for high-ratio metals.

Actually, the difference in relative sizes increases with decreasing stress level. However, the range of crack sizes for low-ratio metals is always relatively small, and that for high-ratio metals is relatively large. Small minimum B and small crack sizes go together; increasing B above the minimum limit does not change the critical size of surface cracks. Similarly, if a large B is required for constraint, only large cracks can cause instability; small cracks lead to over-yield stress levels.

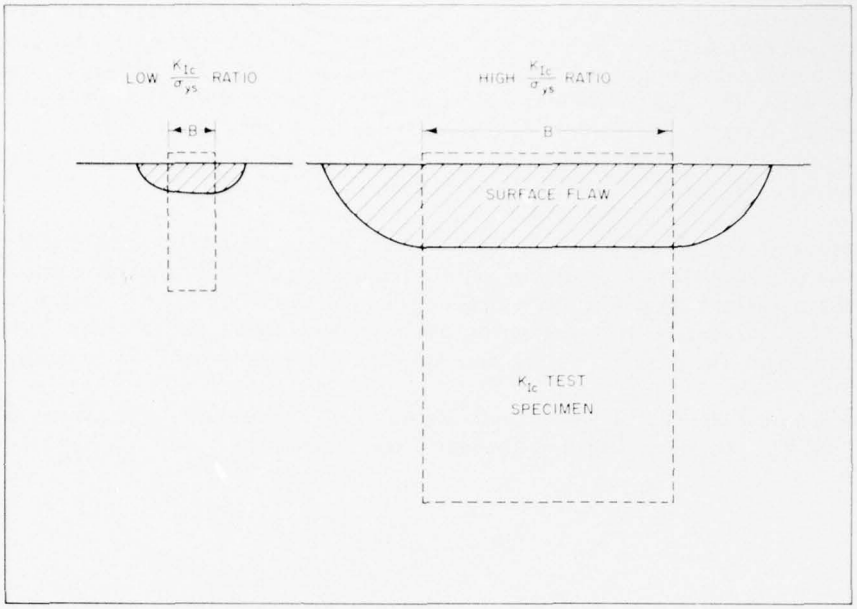

Fig. A2—Relative plane-strain constraint requirements, in terms of section thickness B and related surface crack sizes, for low- and high-ratio metals.

The geometry of the crack has a bearing on constraint levels—stubby cracks feature lower constraint severity as compared to long, thin cracks of equal depth. The reason is that the perimeter (which is a constraint index) is wider for long, thin cracks. Stubby cracks must be about two to three times deeper than long, thin cracks for equivalent severity. Though these complexities must be understood in principle, engineers need not become fracture mechanicians to use to concepts, which may be presented graphically in simple form.

The basis for calculating the graphical plots for semielliptical surface cracks in tension is provided by the crack-size-vs-stress relationship,

$$K_{Ic} = \frac{1.1}{\sqrt{Q}} \sigma \sqrt{\pi a},$$

where

a = crack depth
σ = nominal stress
Q = crack geometry parameter.

This relationship is simplified in the graphs of Fig. 38 (Chapter 3). The various curves relate critical crack depth to the K_{Ic}/σ_{ys} ratio for four levels of relative nominal stress. The stubby and long, thin crack geometries represent the two extremes of crack shapes. For most engineering purposes it is adequate to use one or the other of these extremes; others may be

interpolated if desired. The scales at the top of the figure index the minimum B thickness required for measurement of the specified ratios in K_{Ic} or K_{Id} tests. The subject diagrams apply generally to all metals.

The K_{Ic} parameter is the plane-strain fracture toughness under slow loading. Plane-strain fracture toughness for dynamic loading is defined as K_{Id} and the applicable fracture toughness parameter is then the K_{Id}/σ_{yd} ratio. Figure 38 also applies to the dynamic ratios; its use depends on determining K_{Id} and the dynamic yield strength.

The plane-strain condition is tolerated only by relatively brittle metals. An index of relative brittleness is provided by Table A1, which relates fracture mechanics calculations of plastic-zone size (used for plasticity corrections) to the K_{Ic}/σ_{ys} ratios and the minimum B for the K_{Ic} test specimens.

Table A1—Comparison of plane-strain constraint parameters

Minimum B		Maximum Ratio K_{Ic}/σ_{ys}	Critical Plastic-Zone Size for Plane-Strain Instability	
(in.)	(mm)		(in.)	(mm)
0.6	16	0.5	0.01	0.2
2.5	64	1.0	0.05	1.3
6.0	150	1.5	0.12	3.0
10.0	250	2.0	0.22	5.6

The increase in K_{Ic} specimen size required for retention of constraint conditions with increasing ratio values is striking. The relative dimensions of the critical plastic zones for each case are highly informative as to the degree of constraint to plastic flow that is involved for low and high ratios of plane-strain fracture toughness. It should be noted that exceeding plane-strain limits results in a very large increase in plastic-zone size, even for low ratio values.

If constraint is moderately inadequate, instability may still develop before yield-stress levels are reached. If it is grossly inadequate, the increase in plastic-zone size causes crack-tip yielding and blunting as load is increased in an attempt to reach fracture levels for elastic-plastic conditions. Stress levels then rise to conditions of general yielding. This physical interpretation is important in relation to the effects of the elastic-plastic transition. Once plane-strain constraint is lost due to increasing metal ductility, the plastic zone grows and causes crack-tip blunting. The blunted crack accentuates the plasticizing process. The region in advance of the blunted crack tip may then be described as a small plastic enclave. This may be visualized as the dimple of reduced section noted in advance of ductile fractures. The dimple region is similar to the neck region of a tensile specimen; it indicates that a relatively large volume of metal has been deformed. The energy required for fracture is increased, and eventually, as the transition to plastic fracture is reached, fracture instability cannot be attained.

Fracture mechanics plane-strain tests define fracture instability in terms of the elastic-stress field acting ahead of the crack-tip plastic zone. Figure A1 provides a schematic of a sharp

crack with a small plastic zone and the associated elastic-stress field. The intensity of the stress field, represented by the steepness of the stress curve on approach to the plastic zone, is defined by the parameter K_I. Linear-elastic analyses can relate crack depth, crack geometry, and nominal section stress to K_I. The K_I value at instability is defined as K_{Ic}, the critical value of K_I.

PLANE-STRAIN TEST PROCEDURES

A typical fracture mechanics test specimen is shown in Fig. A3. The specimen has a fatigue crack carefully prepared for maximum sharpness. The K_I stress intensity applied during the fatigue process must not exceed the minimum expected value of K_{Ic}. This is particularly important for the fatigue cracking at room temperature and for subsequent tests of the same specimen at low temperatures. The plastic zone developed at room temperature remains and precludes fracture with a smaller plastic zone at lower temperatures. This in turn precludes measurement of the correct K_{Ic} value at the lower temperature. A clip gage is mounted at the notch opening to monitor the crack opening displacement (COD).

For a valid K_{Ic} determination, it is necessary to document that instability develops at nominal elastic-stress levels, and that the clip-gage COD trace is recording in the elastic range. In general, instability signifies forward extension of the crack tip (which may be of minute dimensions) that is detectable by the COD gage. Such instability does not necessarily result in fracture of the specimen.

There are three types of instabilities:

1. A nonarrestable, pop-in type of instability leading to total fracture

2. A momentary pop-in instability, which is arrested and then requires increased load for further extension because the crack tip is blunted in the process of extension

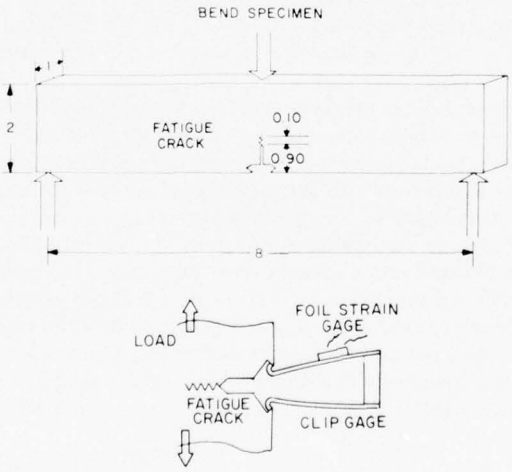

Fig. A3—General features of bend-type K_{Ic} test specimens.

3. A secant-offset instability, indicated by the COD gage as a deviation from elastic response, and by other evidence that the crack tip has moved slightly without becoming unstable.

These instabilities must be analyzed with care, in determination of valid K_{Ic} values according to ASTM practices. The critical K_I value signifies a measurement of the first separation of metal grains at the crack tip. It does not describe details of following events unless other information is provided. The engineering significance of nonarrestable pop-in K_{Ic} instability is clear—it defines fracture initiation followed by propagation through the test specimen or structure.

The general COD features that separate ASTM-validated K_{Ic} values from nonvalid K_{Ic} values are illustrated in Fig. A4. The drop-in-load instability indicated by K_{Ic} represents a valid type that leads to unstable fracture. The strictly nonvalid types are represented by the K_c and $K_?$ notation.

The test limitations for ASTM-validated determinations of K_{Ic} are necessary to ensure that elastic-stress field conditions apply at the time of instability. Evidence that the net section stress exceeds yield, or that the COD trace shows a nonlinear (plastic) response (K_c and $K_?$ notations), signifies that the crack-tip elastic-stress field was distorted or eliminated by excessive plasticity during the first extension of the crack tip. The various ASTM restrictions ensure that plane-strain tests apply only for metals that are brittle enough to initiate fracture with only a small amount of crack-tip plasticity.

The fracture mechanics term "plane strain" is applied to brittle fracture conditions mathematically definable by the K_{Ic} stress field parameter. The corresponding term for plastic fracture is "plane stress." The basic difference between plane-strain and plane-stress fractures may be visualized by considering the degree of through-thickness lateral contraction developed in the course of fracturing edge-cracked specimens of the K_{Ic} and DT types. In plane-strain fracture the lateral (through-thickness) contraction is very small. In plane-stress fracture the through-section yielding occurs with notch blunting (plastic COD). For the plane-stress case, the crack does not constrain the flow of metal to a small plastic zone.

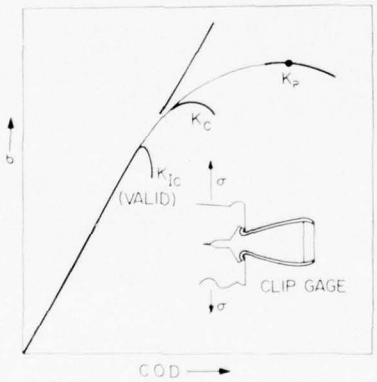

Fig. A4—Crack-Opening Displacement (COD) features of K_{Ic} test specimens.

Section size is important in K_{Ic} testing and in the engineering use of fracture mechanics principles. Section size establishes the maximum crack size that can be placed in a section and still allow retention of plane-strain conditions. Constraint to metal flow at crack tips is increased with increase in crack size, provided enough metal remains surrounding the flaw to contain the plane-strain, elastic stress fields. If plane-strain conditions are to apply, a significant part of the crack tip region must reside in the equivalent of a semi-infinite medium, which does not provide for mechanical sensing of free surfaces.

This is best understood by reference to the specimen size requirements for valid measurements of K_{Ic}. Figure A5 illustrates that the K_{Ic} measurement capacities of edge-cracked specimens increase with increasing section thickness. As the intrinsic metallurgical ductility of the metal is increased, the plane-strain fracture toughness and the section size of the specimen used for its measurement must increase also. If the intrinsic plane-strain fracture toughness of the metal is greater than can be measured for a given section size, the behavior of the metal will be characterized by plane stress (K_c) because of inadequate mechanical constraint. This is because the crack size controls the degree of constraint, and the section size controls the crack size that can be introduced. For thin sections the metal must be intrinsically extremely brittle to permit measurement of plane-strain fracture toughness.

The graphical procedures used to reduce test data, for bend and compact-tension specimens in K_{Ic} determinations, are illustrated in Figs. A6 and A7. The Y parameters were obtained by linear-elastic analyses, using computer programs that assume purely elastic behavior of the specimens, including the crack-tip region. Corrections are made for plastic zones by increasing the effective length of the crack, using a crack-length increment that is equal to the calculated plastic-zone size.

The graphical procedures for defining the Q parameter of a surface crack are illustrated in Fig. A8. The Q parameter describes the change in effective K_I of a surface crack, with changes in crack geometry and applied stress. It is the basic reason for the difference in the level of the

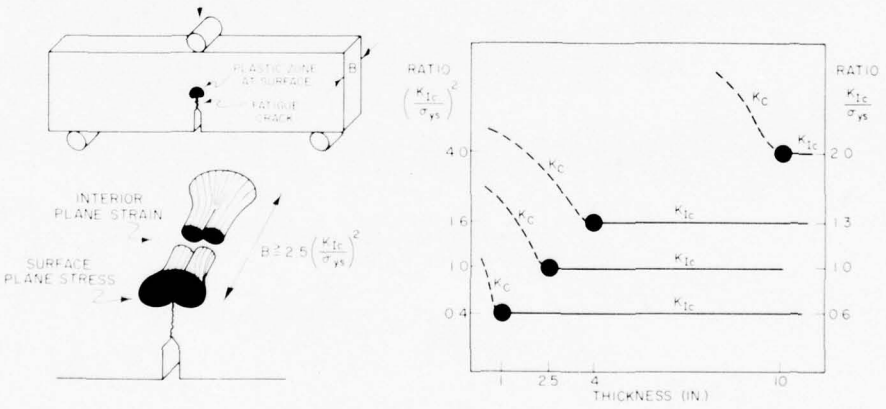

Fig. A5—Representative data illustrating why the K_{Ic} specimen's section size must be increased for measurement of increasing values of K_{Ic} and related K_{Ic}/σ_{ys} ratios.

•Complete fractures always developed at the low end of the 0.5 σ_{ys} (0.5 YC) frequency plot

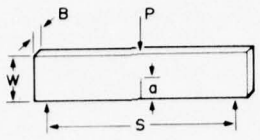

$$K_I = Y \cdot \frac{6Ma^{1/2}}{BW^2}$$

WHERE $Y = A_0 + A_1(a/W) + A_2(a/W)^2 + A_3(a/W)^3 + A_4(a/W)^4$
AND VALUES OF A VARY WITH LOADING:

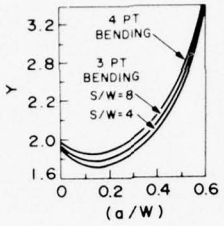

Fig. A6—K_{Ic} determination procedures for bend-type plane-strain test.

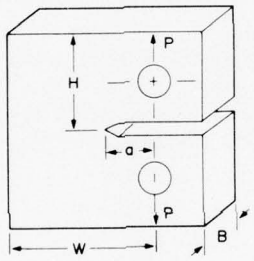

$$K_I = Y \cdot \frac{Pa^{1/2}}{BW}$$

WHERE $Y = A_0 + A_1(a/W) + A_2(a/W)^2 + A_3(a/W)^3 + A_4(a/W)^4$

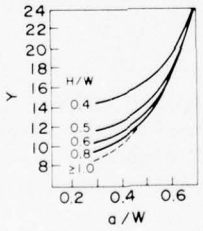

Fig. A7—K_{Ic} determination procedures for compact tension plane-strain test.

$$K_{Ic} = 1.1\sigma\sqrt{\pi a}$$

$$\left(\frac{K_{Ic}}{\sigma_{YS}}\right)^2 = 1.21\,\pi\left(\frac{\sigma}{\sigma_{YS}}\right)^2\left(\frac{a}{Q}\right)$$

RATIO $\frac{K_{Ic}}{\sigma_{YS}}$	CRITICAL CRACK DEPTH a			
	10:1		4:1	
	$0.5\sigma_{YS}$	σ_{YS}	$0.5\sigma_{YS}$	σ_{YS}
0.2	0.004	0.009	0.058	0.013
0.3	0.098	0.021	0.131	0.029
0.4	0.175	0.037	0.234	0.051
0.5	0.272	0.058	0.365	0.080
0.6	0.393	0.083	0.525	0.116
0.8	0.700	0.150	0.934	0.206
1.0	1.09	0.232	1.46	0.321
1.5	2.45	0.522	3.28	0.723

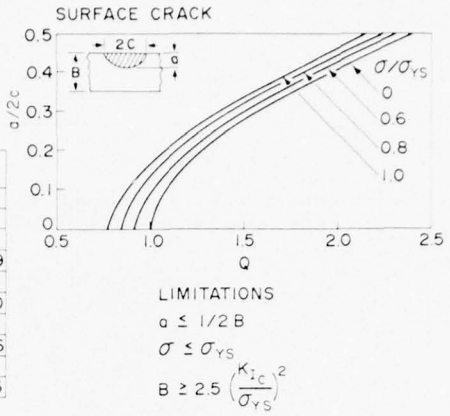

Fig. A8—Linear-elastic procedures for calculation of critical crack sizes for plane strain, surface crack conditions.

curves (Fig. 38) for stubby and long, thin cracks. The linear-elastic computer programs used to develop these relationships include the plastic-zone corrections described above.

The foregoing discussions have focused on plane strain. Fundamental discussions in terms of the plastic work-energy parameter $_c$ are presented in Appendix E. These discussions treat resistance to fracture extension, mainly for the case of plastic fracture.

FRACTURE MECHANICS TERMS AND EQUATIONS

Strain Energy Release Rate $\mathcal{G}$—This quantity represents energy released, per unit crack surface area, as the crack extends. The parameter $\mathcal{G}$ is a measure of the force driving the crack, such that

$$\mathcal{G} = \frac{\pi\sigma^2 a}{E}$$

where

a = one-half crack length for a through-thickness crack in a semi-infinite tension plate
σ = nominal applied prefracture stress
E = modulus.

Plastic Work Energy $\mathcal{G}_c$—$\mathcal{G}_c$ is a specific index of the material's resistance to crack extension; it is related to elastic energy absorbed, per unit area of new crack surface, in crack extension. Plastic work energy at the crack tip opposes the elastic energy release. At the point of instability, the elastic energy and the plastic work energy (resistance) are balanced, so that

$$\mathcal{G}_c = \frac{\pi\sigma_f^2 a}{E}$$

where

σ_f = nominal stress at crack extension for a through-thickness crack in a semi-infinite plate in tension
$\mathcal{G}_c$ = critical $\mathcal{G}$.

Stress-Intensity Factor K—K represents the elevation of stress in advance of the crack-tip plastic zone, which is related to the plastic work energy term as follows:

$$K = \left(\frac{E\mathcal{G}}{1-\nu^2}\right)^{1/2} \quad \text{(for plane strain)}$$

where ν = Poisson's ratio.

Plastic-Zone Correction—To correct for the presence of the plastic zone, an apparent increase in initial crack depth a_0 is applied by adding r_p (plastic-zone radius). The crack length then becomes $a = a_0 + r_p$, where the plastic-zone radius is

$$r_p = \frac{1}{6\pi}\left(\frac{K_{Ic}}{\sigma_{ys}}\right)^2 \quad \text{(for plane strain)}$$

Calculations for Plane-Strain Condition Cracks—In a generalized form,

$$K_{Ic} = a\beta\sigma\sqrt{\pi a}$$

where

σ = nominal stress applied under slow loading
a = crack depth or length
α = flaw geometry factor ranging from 1 to 3, approximately
β = function of crack-tip sharpness, loading rate, crack-tip metallurgical damage, etc. (Ranges from 0.5 to 2, approximately.)

The critical size of surface cracks may be influenced by combined α and β factors, which on the low side reduce the critical crack depth by a combined factor of 0.5 and on the high side increase the crack depth by a factor of 6.

Calculations for Plane-Strain Surface Cracks—The formal equation for a surface crack in a tension-loaded plate is

$$K_{Ic} = \frac{1.1\sigma\sqrt{\pi a}}{\sqrt{Q}}$$

230-362 O - 77 - 18

where

a = crack depth
σ = applied stress
$1.1/\sqrt{Q}$ = specimen and crack-shape factor obtained from charts.

This equation assumes K_{Ic} applies to either dynamic or static loading conditions. The calculated crack depths are based on the same assumption.

As a rough generalization for the same geometry, an internal crack depth, measured at the short dimension, requires a slightly higher stress for instability when the preceding equation is applied.

APPENDIX B

Graphical Analysis by Reference to the Characteristic K_{Id} Curve

GENERAL METHODS

The characteristic K_{Id} curve is plotted on an expanded scale in Fig. B1. The relative temperature scale is centered on the NDT temperature, the starting point for the dynamic plane-strain transition. The NDT index also locates the true temperature position of the K_{Id} curve for a specific steel. If the NDT temperature is known, the K_{Id} curve is fully established by the Δt plot. The procedure eliminates the need for expensive K_{Id} tests of each steel.

The ratio scale of Fig. B1 is derived by calculating dynamic K_{Id}/σ_{yd} ratios. The dynamic yield strength is defined as

$$\sigma_{yd} = \sigma_{ys} + 30 \text{ ksi (206 MPa)}.$$

This approximation is used in the fracture mechanics literature as a reasonable adjustment for the plastic-flow resistance of crack-tip plastic zones subjected to dynamic loading. The ratio scale of the figure is specific to a steel of low yield strength, as noted.

The ratio increases from a value of 0.5 at the NDT temperature to 2.0 at the high end of the curve. Since the K_{Id} curve is assumed to be of characteristic form, the ratio scale is equivalent to a ΔR scale (R represents "ratio") indexed to the NDT temperature. The Δt scale and the ΔR scale have a fixed relationship to each other and also to the NDT index temperature. This is the case for a fixed level of yield strength, as noted for Fig. B1. Relationships for a higher level of yield strength are presented in Fig. B2. Metric system relationships for the two respective levels of strength are presented in Figs. B3 and B4.

Two separate B scales, for section sizes corresponding to L and YC conditions, are at the tops of these plots of the characteristic curve. The section sizes are indexed to the ΔR scale in each figure, according to the descriptions in the legend of Fig. B5. The B dimensions of the YC scales are 0.4 times those of the L scales, as cited in Fig. B5. This fixed relationship signifies that the temperatures for attainment of L and YC conditions have a specific Δt with respect to the NDT temperature. The L and YC temperatures for specific section sizes are defined analytically by reference to the ΔR scale, which provides the appropriate Δt.

Figure B6 illustrates the basis for using L and YC temperatures to indicate the increase in fracture-extension stress of a through-thickness crack (TTC). The increase is a consequence of the L-to-YC transition. The fracture stress for a through-thickness crack with a length three

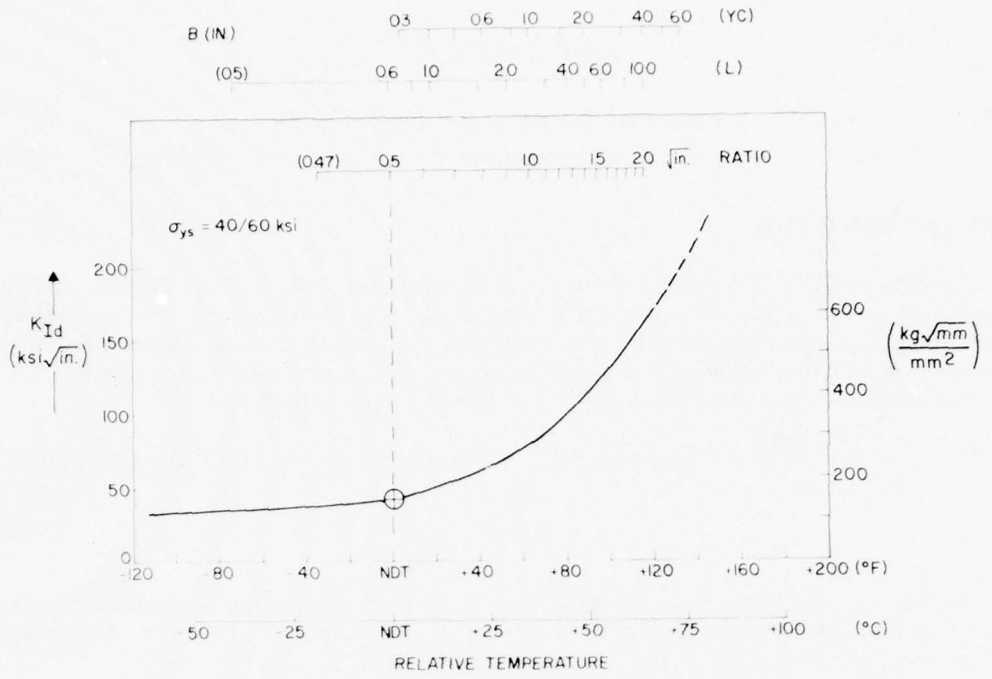

Fig. B1—Characteristic K_{Id} transition curve correlated with various reference scales. The K_{Id}/σ_{ys} ratio scale applies to steels with yield strengths of 40 to 60 ksi (172 to 275 MPa). (The ratio scale is in ksi-in. units.)

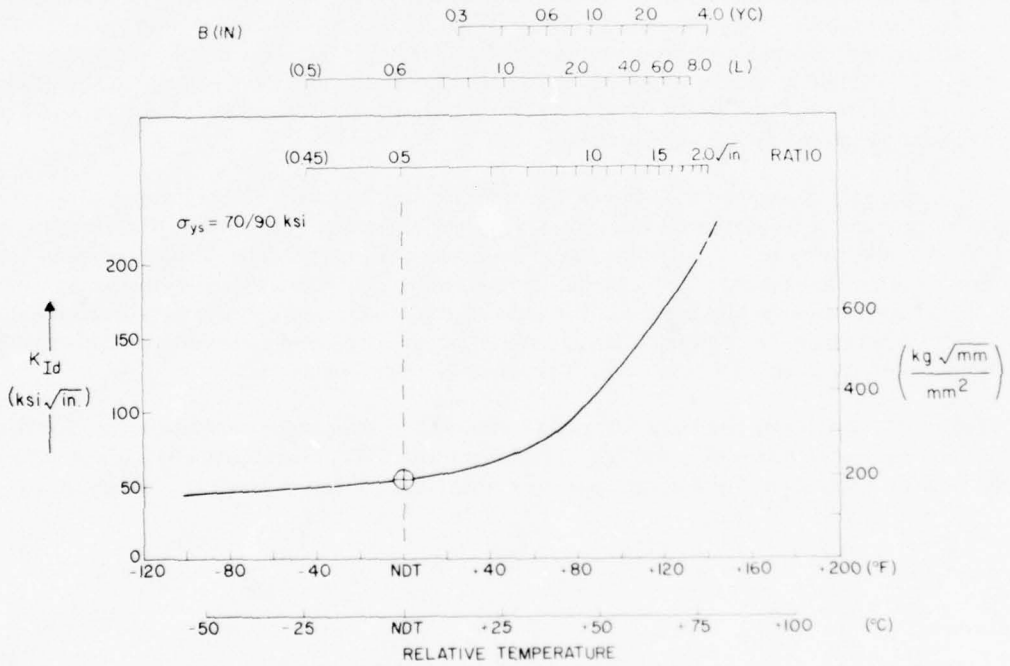

Fig. B2—Characteristics K_{Id} curve for high strength steels correlated with various analytical scales. (The ratio scale is in ksi-in. units.)

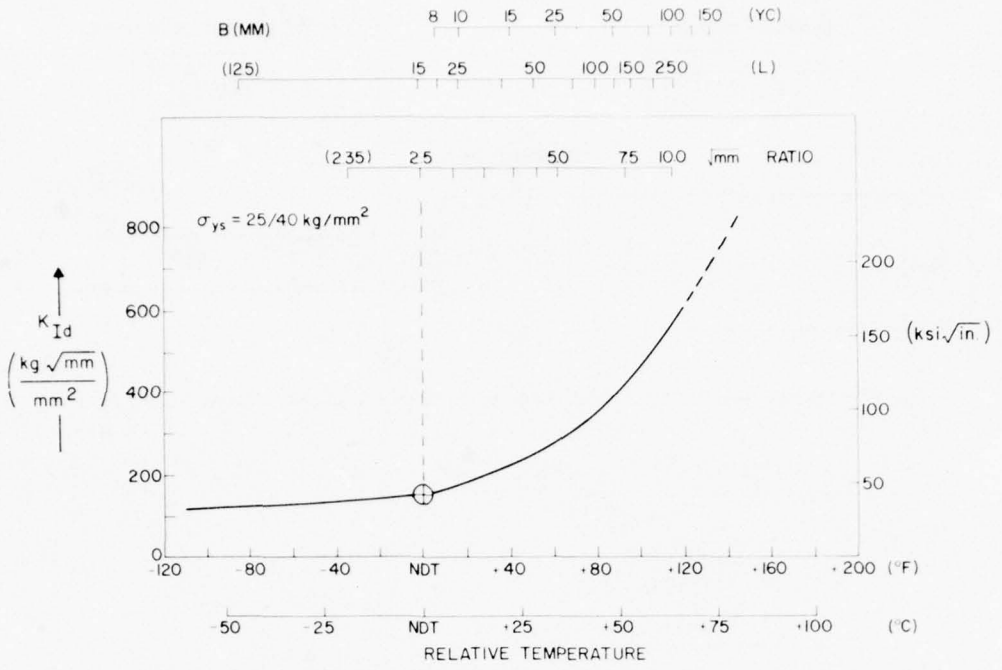

Fig. B3—Characteristic K_{Id} curve for low strength steels correlated with various analytical scales. (The ratio scale is in kg-mm units.)

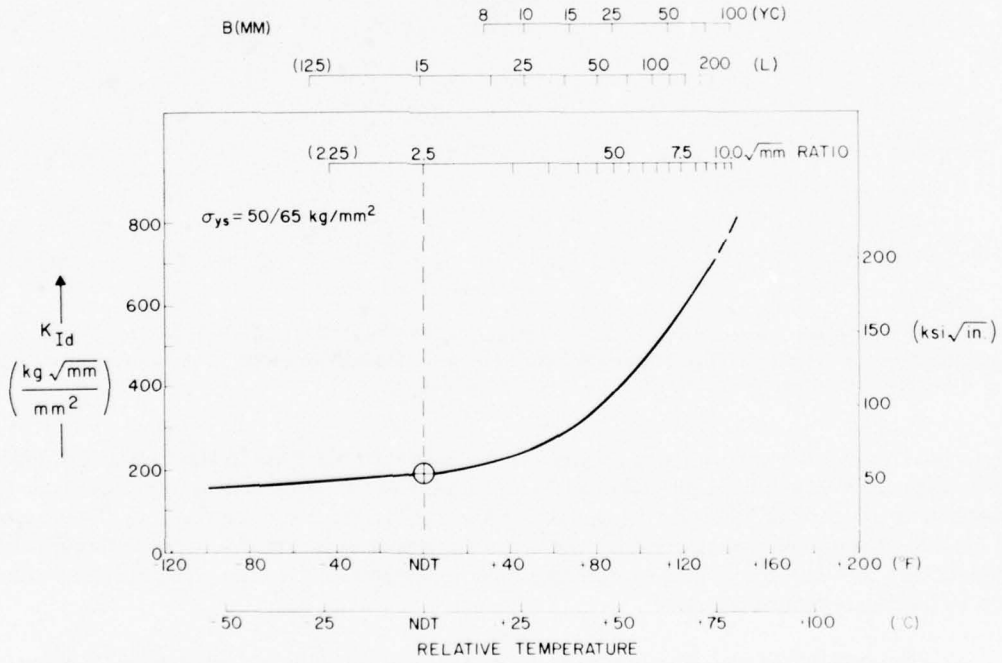

Fig. B4—Characteristic K_{Id} curve for high strength steels correlated with various analytical scales. (The ratio scale is in kg-mm units.)

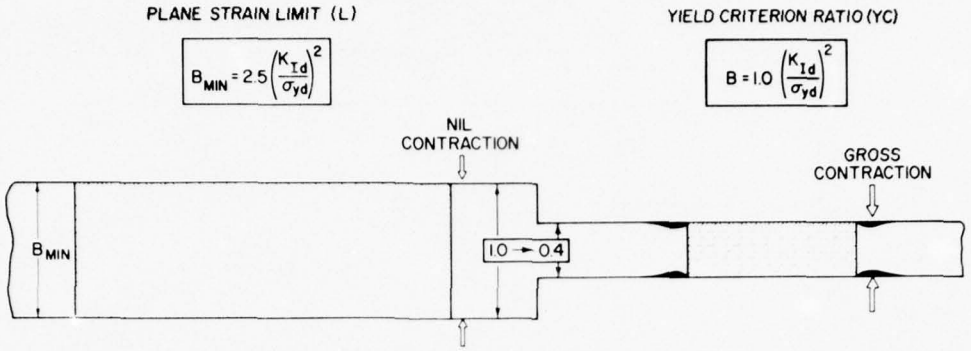

Fig. B5—Section-size difference corresponding to L and YC criteria for a specific K_{Id}/σ_{yd} ratio.

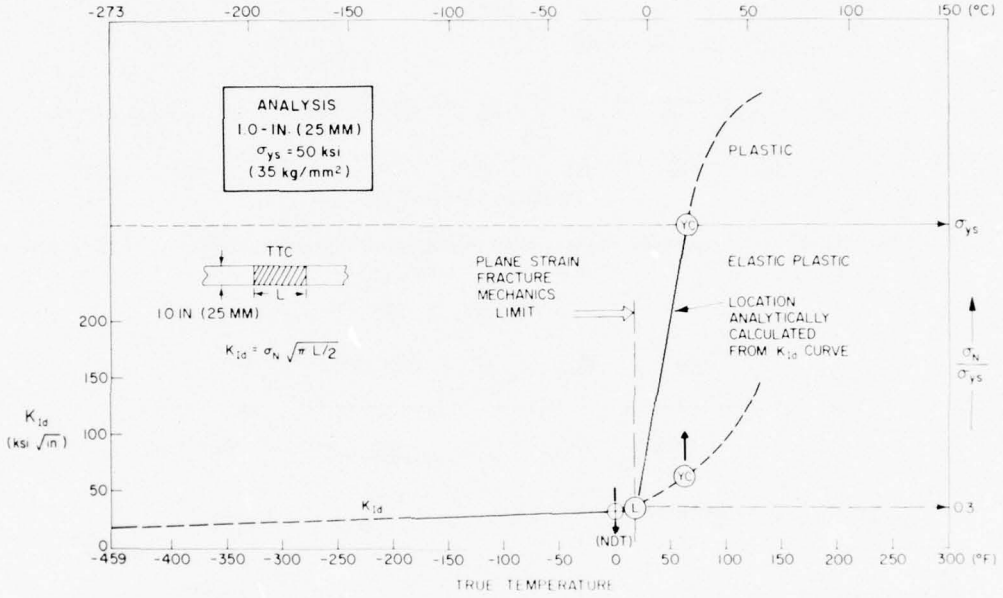

Fig. B6—Elastic-plastic transition for a 1.0-in. (25 mm) plate of 0°F (–18°C) NDT properties. the L and YC cirteria points are deduced from the K_{Id} curve by the ratio-scale procedure. The relative stress scale for fracture extension of a through-thickness crack is indexed to the L and YC points.

times the thickness is calculated from the plane-strain formula cited in the figure. The calculations are valid only to the L point, beyond which plane-strain conditions are lost due to elastic-plastic transition. The YC point in the nominal-stress-vs-temperature (σ_N – vs-t) plot must be located at the yield-stress level, by the basic definition of plastic fracture. A straight line connecting the L and YC points is used as a first approximation for the elastic-plastic transition in fracture-extension stress.

A more detailed examination of the σ_N – vs – t transition, as related to Δt and ΔR scales, is presented in Fig. B7. The figure indicates that the increase in fracture stress with temperature

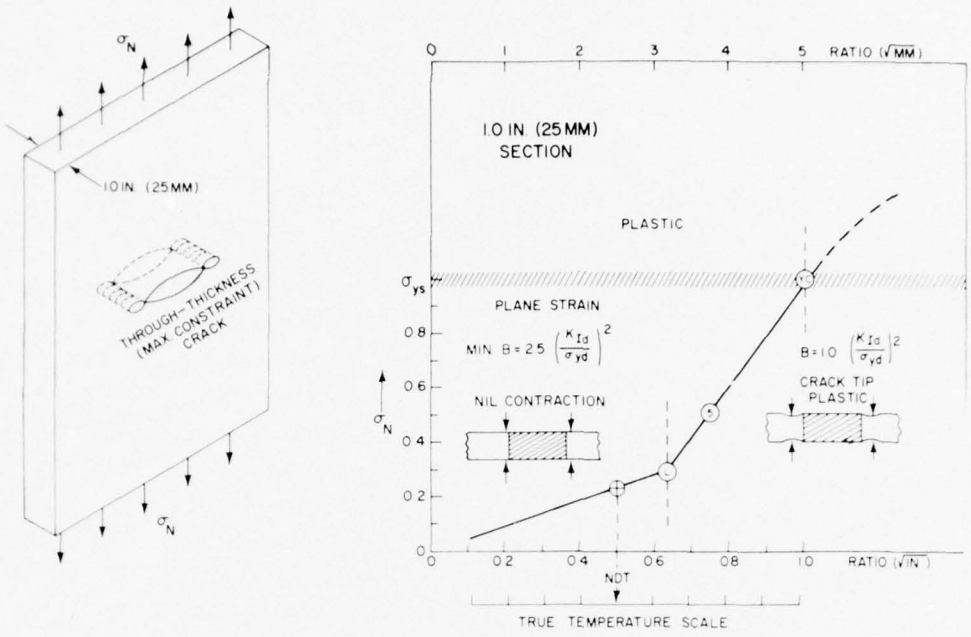

Fig. B7—Graphically indexing the σ_N-vs-t fracture stress curve to the characteristic K_{Id} curve, based on ΔR and Δt scales.

corresponds to a relatively shallow curve in the plane-strain region up to the L point, while the increase is sharp in the L-to-YC temperature-transition range. Calculations of fracture-extension stress due to a through-thickness crack longer than $3T$ result in a decreased slope in the plane-strain region, in accordance with the plane-strain formula of Fig. B6. From an engineering point of view, the decrease is insignificant; the fracture stress values for the $3T$ crack (the minimum length for through-thickness-crack analysis) are much too low to provide for arrest in ordinary structures. Arrest properties are attained only in the L-to-YC transition region. Because of the narrow temperature range of this transition, (see Fig. B6), crack length effects are overshadowed by the transition to plastic fracture.

It follows that precise location of L and YC temperatures are more important for engineering analyses than determination of crack size. Fortunately, the exactness of NDT definition and the reproducibility of the K_{Id} curve rate of rise above the NDT temperature provide adequate precision. Confirmation of this is provided by the graphical analysis, exact prediction of the location of Robertson CAT curves (see Fig. B11).

CASE EXAMPLES OF GRAPHICAL ANALYSIS

The procedure for locating L and YC temperatures is illustrated in Fig. B8 for a range of section sizes. The ΔR scale is used for locating the critical L and YC ratio from scales presented in appropriate figures. The ratio of interest is noted from the reference scales, and the temperature location of the ratio value is indexed to the K_{Id} curve. The vertical dashed lines mark the temperature locations of the ratio values. The Δt relationships of the NDT temperature with the L and YC points, for an ascending series of section sizes, are clearly evident.

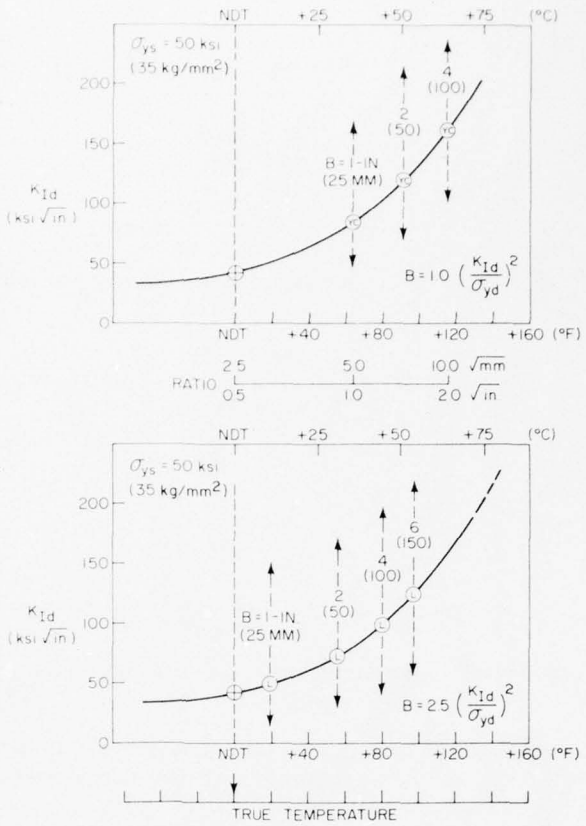

Fig. B8—Rise of the L and YC points on the K_{Id} curve as a function of increasing section size. The temperature locations are deduced by reference to the ratio scale, using the applicable B = 2.5 and B = 1.0 constants.

The sequence of plotting σ_N-vs-t transition curves is illustrated in Fig. B9 for a 1.0-in. (25 mm) section size. The first step (bottom) is indexing L and YC points by the procedure illustrated in Fig. B8. A projection is then made to the σ_N-vs-t plot (top), in accordance with the transfer method of Fig. B7.

The same procedures are used to locate the σ_N-vs-t curve for a 2.0-in. (50 mm) section size in Fig. B10.

It should be noted that the plots for the two section sizes apply generally to steels of low strength. Differences in NDT temperature simply indicate a temperature shift of the σ_N-vs-t curves. The only fracture test requirement is that the DWT be used to establish the NDT temperatures of specific steels that represent the two section sizes. The NDT temperatures may be different for such reasons as metallurgical quality or cooling rate. The thicker steel may have the same, higher, or lower NDT temperatures than the thinner steel. The NDT temperature differences between the two steels can exceed the L-to-YC temperature range of one of the steels. Accordingly, an accurate definition of the NDT temperatures is vital.

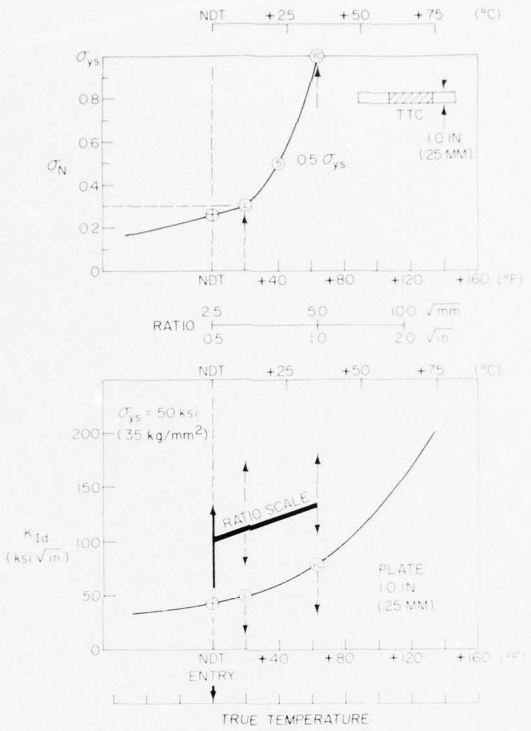

Fig. B9—Indexing the σ_N-vs-t curve (upper plot) to the K_{1d} scale, for 1.0-in. (25 mm) plate.

Figure B11 illustrates a test of the accuracy with which these analyses predict the true temperatures of L and YC. The figure is based on the NDT properties of steel plates used in Robertson CAT determinations, as reported in the literature. NDT temperatures are used to locate the σ_N-vs-t transition curve for elastic-plastic fracture, as described previously. The analysis is specific to the section size and low strength level of the steels and predicts the 0.5 YC temperature to within the experimental accuracy of the 0.5 σ_{ys} CAT determination; see Chapter 6 for details of the Robertson tests. This result confirms the correctness of the basic principles of the analysis.

Figure B12 illustrates the basis for extending the analysis methods to include the case of surface cracks. The ratio scale is referenced to the dynamic ratio K_{1d}/σ_{yd}. A specific ratio value may be indexed to the section size for L properties (top scale) or to the relative stress for fracture initiation at a specific surface-crack size. Interpolation may be used for stress levels that lie between any of the four levels noted in the figure.

Figure B13 is a plot of the increase in fracture stress for various surface-crack sizes, as a function of increasing ratio with respect to the K_{1d} curve. The ratio limits L for various section sizes are indicated in the figure. The critical L values establish a cutoff for the surface-crack calculations. This is illustrated in Fig. B14 for a 4.0-in (100 mm) section size. The curves for surface cracks

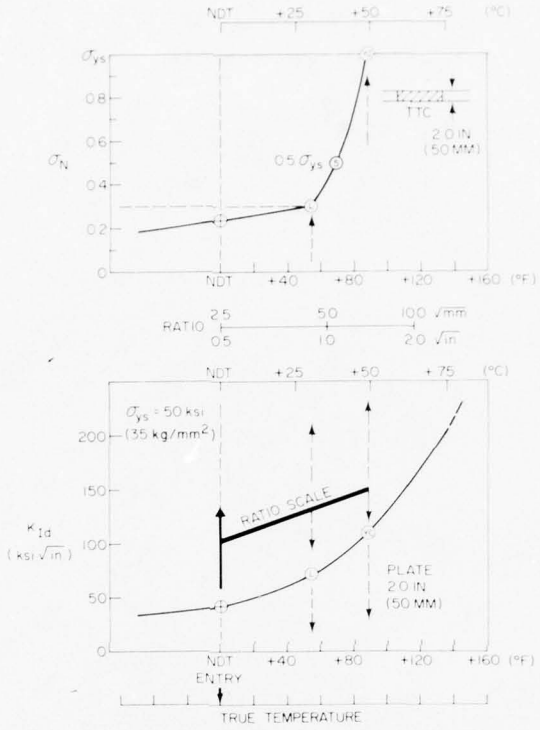

Fig. B10—Locating the σ_N-vs-t curve on the K_{Id} scale, for a 2.0-in. (50 mm) plate. Note shifts of L and YC points.

are not extended beyond the limits of the elastic-plastic transition, because the analysis is then dominated by the increase in fracture-extension stress for a through-thickness crack. Residual possibilities for the pop-in of surface cracks in regions of very high local stress are of no consequence because the elastic-plastic transition generally controls fracture reliability at temperatures above the 0.5 YC reference point. This fact is noted by dashing of the surface-crack curves at temperatures above this point.

Charts of this combined type may be developed for various section sizes. The charts bear a specific Δt relation to the NDT temperature. Thus, determination of the NDT temperature provides for indexing the charts to the true temperature scale. A large amount of information is provided by very simple chart adjustment to the temperature indicated by the NDT index.

An example of detailed statistical analysis is presented in Figs. B15 and B16. The analysis is started in Fig. B15 by plotting the known NDT frequency distribution curves of the steels involved in the 1940-1945 ship failures described in Chapter 6. The K_{Id} curves indicate the locations of characteristic K_{Id} curves related to low, intermediate, and high NDT temperatures of the frequency plot. From them, the L and YC frequency curves are established by use of the ΔR scale, according to previously described graphical methods.

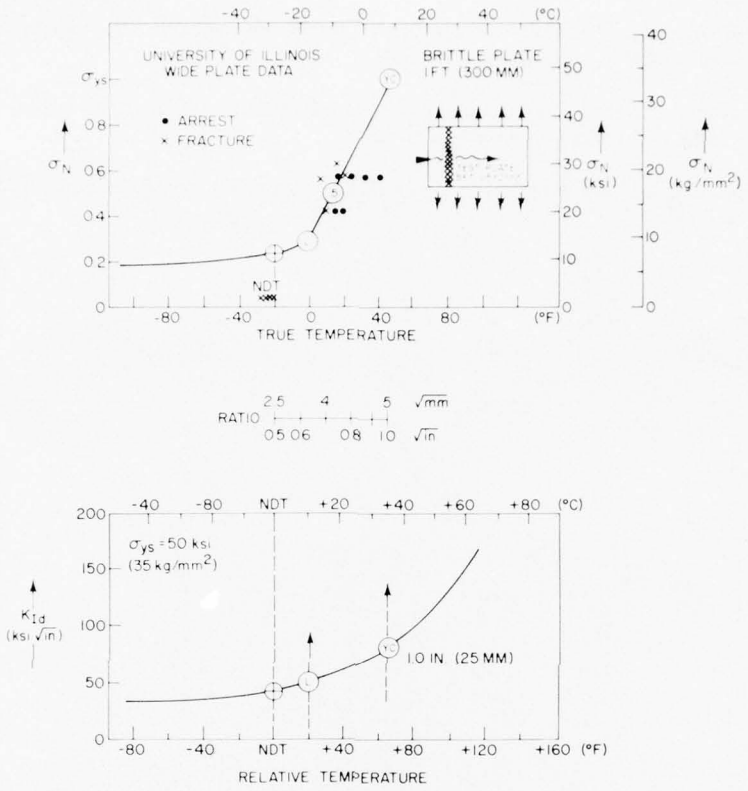

Fig. B11—Test of the accuracy of elastic-plastic analytical predictions by reference to wide-plate (Robertson test type) data. The NDT temperature of these plates is indicated by the Xs (for several tests) in the top graph. The bottom graph indexes the σ_N-vs-t curve to the K_{Id} scale.

The analysis is tested in Fig. B16, to determine whether the predictions are in accord with experience of ship fracture. The experimentally established NDT frequency curves are translated to graphically analyzed L, 0.5 YC, and YC frequency distributions, which are plotted at the top of the figure. The ship fracture experience is presented in the bottom graphs:

- Failure rates increase as most of the population becomes sensitive to small cracks in regions of high stress, i.e., as the number of members of the population subject to NDT and L conditions increases with decreasing temperature.

- No fractures occurred at the high end of the 0.5 σ_{ys} (0.5 YC) frequency plot. (All plates had positive arrest properties for the design level 0.2 to 0.3 σ_{ys}.)

•Complete fractures always developed at the low end of the 0.5 σ_{ys} (0.5 YC) frequency plot (all plates lacked suitable arrest properties).

•Partial fractures took place in the temperature region at which there was a high probability that the crack would run into an arrest plate.

It is apparent that the predictions are highly accurate. This confirms the validity of the analytical methods.

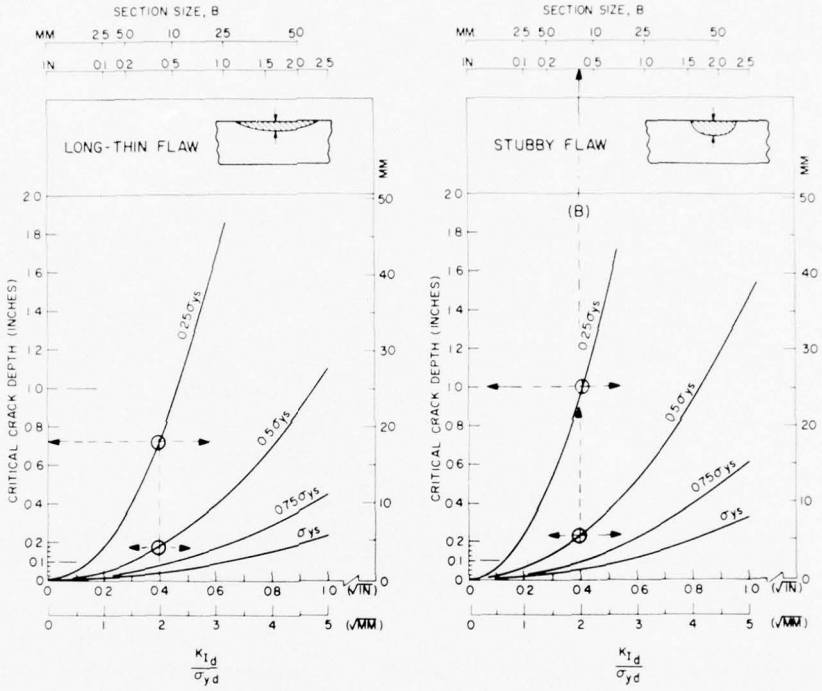

Fig. B12—Referencing the ratio scale to section size B for the L-criterion ratio, and simultaneously defining critical crack sizes for specific ratios.

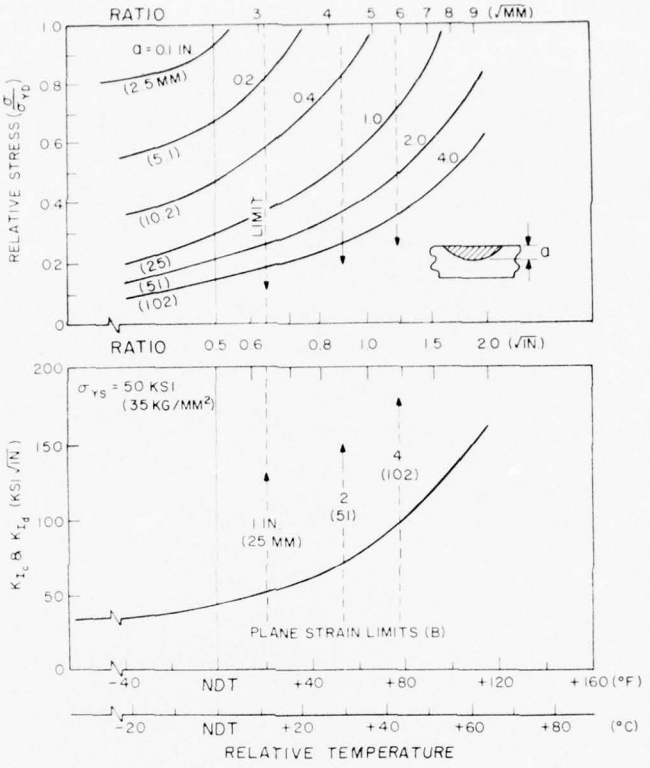

Fig. B13—Critical crack size-vs-stress diagrams evolved by indexing to the K_{Id} curve.

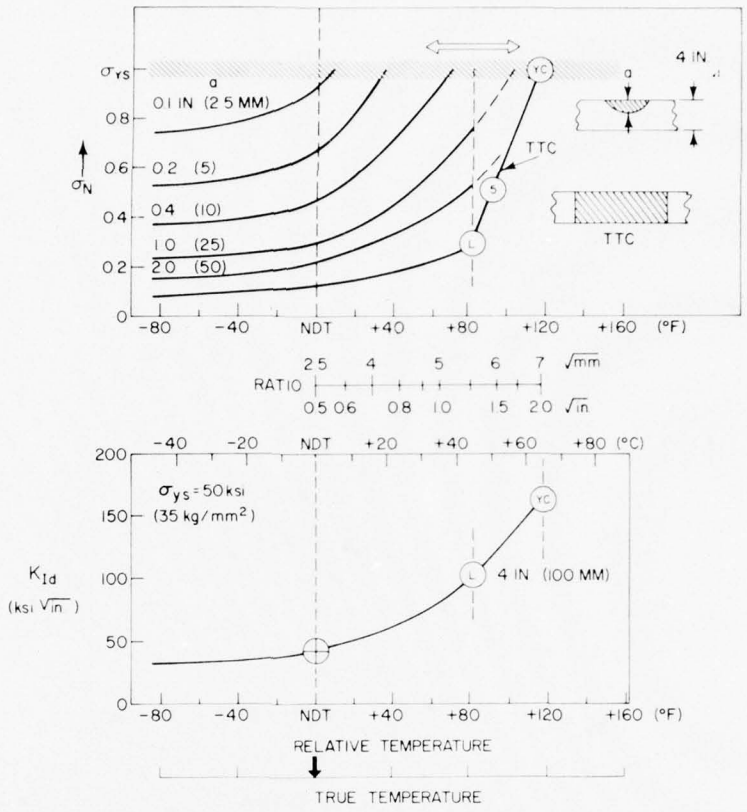

Fig. B14—Graphical analysis for surface cracks as applied for the case of a specific section size; also illustrates σ_Y-vs-t curve for a through-thickness crack.

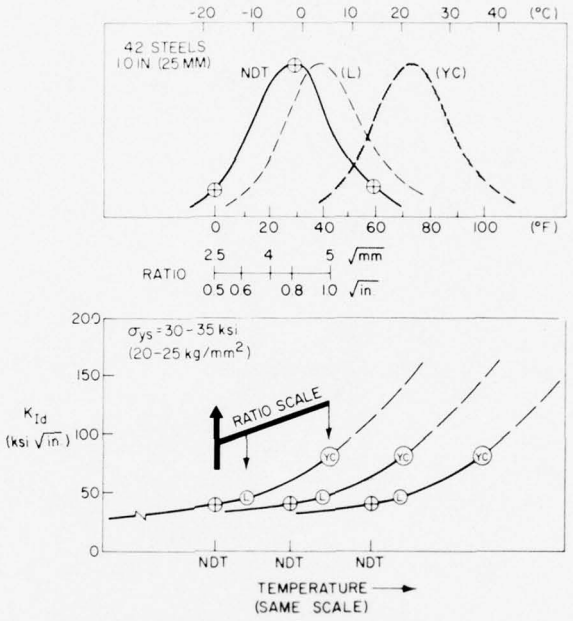

Fig. B15—Use of NDT-vs-frequency statistics, for the 1940-1945 ship-failure steel plates, to analyze L and YC statistics. The NDT distributions define the quality range of the steels used for ship construction during this period.

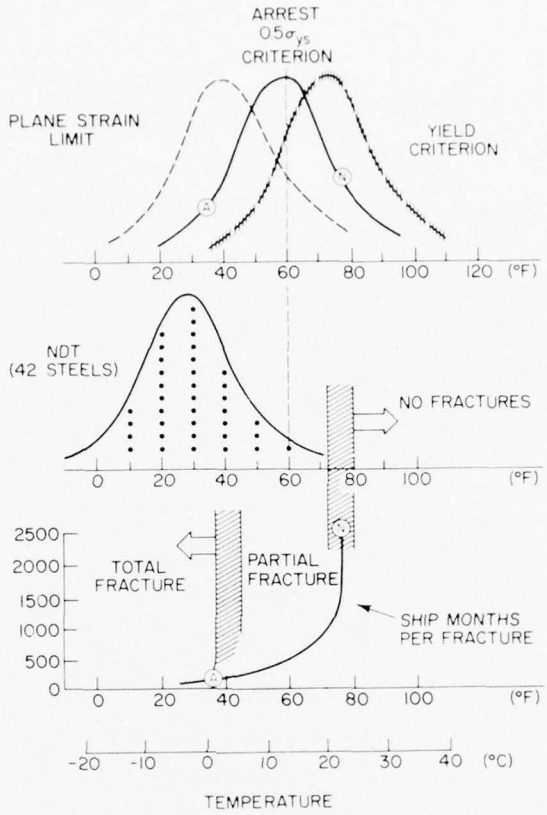

Fig. B16—The temperature-vs-frequency distributions (top) represent analytical predictions evolved by the ratio analysis presented in Fig. A15.

APPENDIX C

Strength Transition: Case Example and Reference Tables

CASE EXAMPLE OF DESIGN BASED ON ARREST AND INITIATION PRINCIPLES

Consider a thin-walled pressure vessel with walls, 0.15 in (4 mm) thick. The first problem is to determine the maximum yield strength that may be used with retention of fracture properties sufficient to preclude bursting in the presence of through-thickness cracks. The following considerations apply:

- The desired yield strength is in the range of 240 to 280 ksi (1655 to 1931 MPa).
- The steel is a maraging type and of high fracture quality.
- The nominal design stress is 0.3 σ_{ys}.
- Stress-corrosion cracking, leading to the development of through-thickness cracks, is possible.
- Leakage is acceptable, but bursting is not.

These considerations dictate that, for a crack that grows through the wall, the arrest principle of leak-before-fracture must be applied. The crack length may be expected to be in the range of 2 to 6 T, i.e., 0.30 to 0.90 in (7.5 to 22.5 mm) on penetration. For reliability, a fracture stress at least twice the design nominal stress (>0.6 σ_{ys}) should be necessary for bursting in the presence of through-thickness cracks.

The solution is reached by using the relationships illustrated in Fig. C1, keyed to the elastic-plastic region defined by the RAD in Fig. C2. The first step is to analyze the range of possible K_{Ic} values for the yield-strength range of 240 to 280 ksi (1655 to 1931 MPa). The RAD data bank provides for this analysis. The following conditions apply:

- At 240 ksi, (1655 MPa) the K_{Ic} range is from 30 to 140 ksi $\sqrt{\text{in.}}$
- At 280 ksi, (1931 MPa) the K_{Ic} range is from 30 to 90 ksi $\sqrt{\text{in.}}$
- The high ends of the K_{Ic} ranges are maximum recorded values. Reasonable expectations for high-quality metal are represented by the trend band.
- The reasonable-expectancy K_{Ic} range is 70 to 100 ksi $\sqrt{\text{in.}}$ at 240 ksi (1655 MPa) and 40 to 70 ksi $\sqrt{\text{in}}$ at 280 ksi (1931 MPa), as noted in Fig. C2 by the circled points.

230-362 O - 77 - 19

•The mean K_{Ic}/σ_{ys} ratio value falls from 0.4 to 0.2 as yield strength is raised from 240 to 280 ksi (1655 to 1931 MPa).

The significance of falling from 0.4 to 0.2 ratio value must be analyzed in terms of the specific section size. The plane-strain limit ratio is 0.25, and the yield criterion ratio is 0.38. These two critical ratio lines have been drawn across the diagram of Fig. C2 to locate the

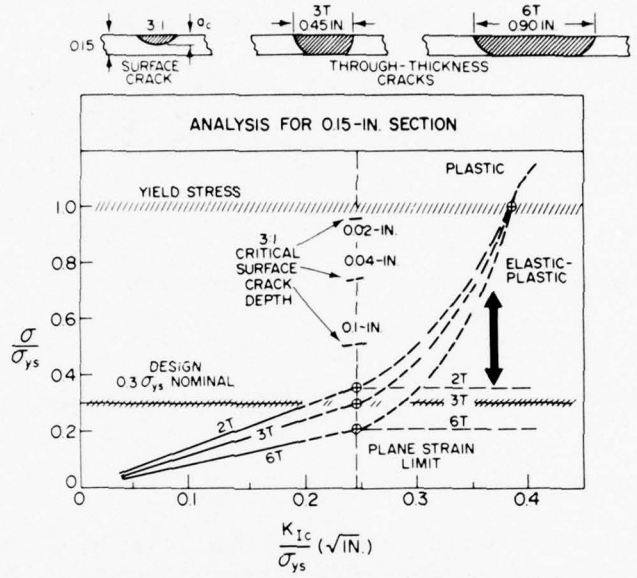

Fig. C1—Engineering analysis for a high strength steel of thin section. At the plane-strain limit for the section size, the fracture stress for the noted crack sizes (in terms of T) is always at the level indexed by the crossed circles.

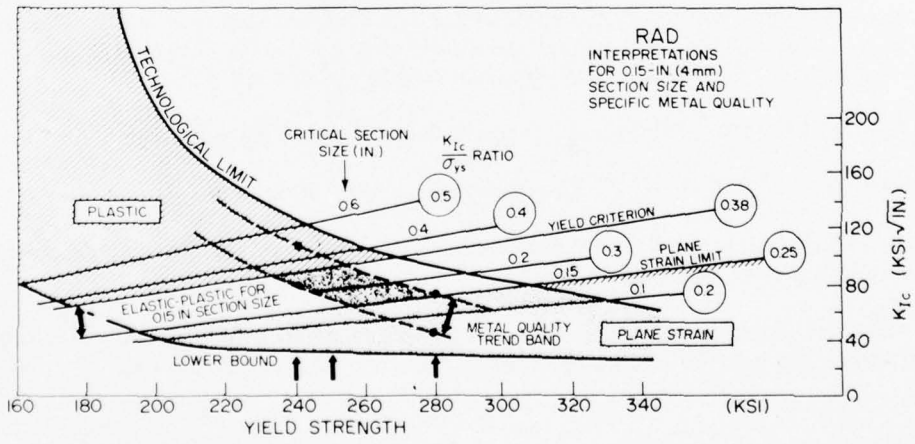

Fig. C2—Engineering analysis for 0.15-in. (4 mm) section size. Note that the analysis is specific to the cooridor quality of the metal.

elastic-plastic region. The following fracture states correspond to the strength levels indicated by the vertical hold arrows:

<240 ksi (1655 MPa)—plastic
250 ksi (1724 MPa)—high elastic-plastic
280 ksi (1931 MPa)—plane strain.

In the high range of the elastic-plastic state, stresses in excess of 0.5 σ_{ys} are required for fracture extension by through-thickness cracks. Thus, a maximum yield strength of 250 ksi (1724 MPa), for metal of this quality, fulfills the desired leak-before-failure fracture conditions. The fracture stress then will be at least 0.6 σ_{ys}. This meets the twice-nominal-stress requirement for safety margin.

The crack-length relationships to the relative fracture-stress scale are presented in Fig. C1. The solid curves define the effects of increasing K_{Ic} plane-strain properties to the plane-strain ratio limit (0.25) for this section size. At the plane-strain limit, the fracture-extension stresses for the various crack lengths are on the order of or below the nominal design level (0.3 σ_{ys}). Accordingly, bursting is to be expected if cracks penetrate the wall.

The set of rising curves indicates the effects of traversing the elastic-plastic region, to the yield criterion ratio value of 0.38. Fracture stresses in excess of 0.6 σ_{ys} are attained at the high end of the elastic-plastic range. Note that we may code the yield-strength scale to the rising values of the K_{Ic}/σ_{ys} ratios of this plot, as listed below.

Ratio	Yield Strength (ksi)	MPa
0.20	280	1931
0.25	270	1862
0.30	260	1793
0.35	255	1758
0.38	250	1724

This relationship is traced by the midcourse of the quality band of Fig. C2.

Proof of the validity of the trend-band curve is required for quality control and purchase specifications. This requirement is met by K_{Ic} tests, using section sizes that provide for valid K_{Ic} determination in the elastic-plastic region for a 0.15-in. (4 mm) section size. Specimens of 0.2- to 0.3-in. (5 to 7.5 mm) thickness are required. Alternatively, measurements are made for metal 0.15 in (4 mm) thick, at yield-strength levels high enough to allow valid K_{Ic} measurements. The trend band derived by either of these procedures verifies the desired trend-band level.

Consideration is often given to increasing the wall thickness for "added safety." In the examples of Fig. C1, increasing wall thickness while keeping yield strength constant at 240 ksi (1655 MPa) raises the plane-strain ratio limit and causes metal of 0.3 to 0.4 ratio value to assume plane-strain properties. In this case, the fracture-stress curves for $2T$, $3T$, and $6T$ flaws remain at the 0.2 to 0.3 σ_{ys} level. This is represented by the flat curves with the $2T$, $3T$, and $6T$ notations. Comparison of the fracture stresses for the plane-strain and elastic-plastic states, is provided by the two sets of curves in the figure. The bold arrow emphasizes the dramatic

differences. The importance of entering the elastic-plastic state is evident. Increasing wall thickness does not increase safety.

Ordinarily, increased wall thickness is used to reduce nominal stresses from the maximum allowable (0.5 σ_{ys} for pressure vessels). Figure C1 indicates that stress must be reduced to 0.25 σ_{ys} or less to effectively prevent fracture when cracks penetrate the pressure vessel wall. Reductions from, say, 0.5 σ_{ys} to 0.3 σ_{ys} do not provide added safety for such cases. Paradoxically, reductions in wall thickness that increase stresses above the allowable, to 0.6 or 0.7 σ_{ys} do provide safety if the reduction in thickness results in metal of high elastic-plastic fracture properties. In developing fracture-control plans, engineers must use completely new thinking with respect to factors of safety. Adherence to past conventions is dangerous.

Finally, we shall illustrate the low reliability that results from designing pressure vessels according to initiation criteria, i.e., by controlling surface-crack sizes. Again, new thinking is essential. We shall first assume that reliable inspection procedures are available for detecting or monitoring surface cracks in service. (In many cases such procedures are not available.)

The effect of relative stress level on the critical size of surface cracks of 3-to-1 length-to-depth geometry is indicated in Fig. C1 at the plane-strain limit value. Note that the critical crack depths are in the undetectable range of 0.02 to 0.1 in (0.5 to 2.5 mm) at a nozzle location, where stress is high. In the hoop-stress region of the vessel (0.3 σ_{ys}), surface cracks more than 0.2 in (2.5 mm) deep are required for fracture initiation at the plane-strain limit for the section size. For lower ratio values the critical crack size decreases rapidly at this stress level. In fact, it decreases to undetectable dimensions cited above for the nozzle. Thus,

- Reliable protection cannot be provided at nozzles for metal of the highest measurable plane-strain fracture properties.

- Similarly, reliable protection cannot be provided for other locations of the pressure vessel if the plane-strain value is significantly less than maximum for the section size.

To summarize an important and often neglected consideration in fracture-control planning based on prevention of fracture initiation, the critical crack size for any structure is defined by stress levels in the range of 0.75 to 1.0 σ_{ys}, *not* by nominal design stress levels.

The reason is that such high stress levels generally are present in structures due to regions of geometry transition. The most refined designs, such as those for nuclear reactor pressure vessel nozzles, result in stress-concentration effects of approximately 2.5. This means stresses 2.5 times the allowable 0.5 σ_{ys} result in exceeding yield levels. A gradient of stress from 1.0 to 0.5 σ_{ys} obviously exists in the nozzle transition region. The reader should now recognize the significance of the lower curves of Figs. 38 and 56. They define the usual and not the unusual requirements for crack-size surveillance. The literature's usual reference to nominal stress of less than 0.5 σ_{ys} level represents an unrealistic idealization of structural design problems.

Reference Tables—Alloy Compositions of High Strength Steels

The specifications for standard-grade steels, as well as other types of metal specifications, properly deal with details important in procurement. Because of these details, it is difficult to understand the metallurgical basis of the specification system for steels that cover the full

strength-transition range of the RAD. This presentation is aimed at explaining how chemical composition and heat treatment determine the location of steels in the RAD display.

Evidence that a sound metallurgical basis does exist is provided by the fact that an expert mechanical metallurgist can perform the following self-consistent analyses:

- Given a specific composition, section size, and melting procedure, the strength-transition corridor zone can be located in the RAD.

- Given a strength-transition corridor or a zone within the corridor, the general alloy composition and related metal-quality details can be described.

The compositions of typical steels corresponding to the various zones of the RAD are presented in Tables C1, C2, and C3. These tables are the key to understanding the RAD-related significance of standard grades and other specifications. They display the main alloy features of modern weldable steels, as compared to older steels developed for general use as rolled or forged products.

Table C1 illustrates that in the conventional rolled or forged steels relatively high carbon contents are used to vary yield strength over the full range of the RAD. The high carbon contents limit these steels to low corridor levels. Thus, for section sizes greater than 1 in. (25 mm), plane-strain fracture properties hold for intermediate and high strengths. Adjustments of the alloy content within the ranges cited may be expected to shift fracture properties up or down only within the low corridor.

Table C1—Representative compositions of quenched and tempered rolled and forging grade steels[a]

Steel	Composition (%)						
	C	Mn	Ni	Cr	Mo	V	Si
40xx (Mo Type)	0.25	0.8	—	—	0.25	—	0.25
	0.30	0.8	—	—	0.25	—	0.25
	0.40	0.8	—	—	0.25	—	0.25
41xx (Cr-Mo Type)	0.25	0.9	—	0.9	0.2	—	0.25
	0.30	0.9	—	0.9	0.2	—	0.25
	0.40	0.9	—	0.9	0.2	—	0.25
43xx (Ni-Cr-Mo Type)	0.20	0.7	1.8	0.7	0.25	—	0.25
	0.40	0.7	1.8	0.7	0.25	—	0.25
61xx (Cr-V Type)	0.20	0.8	—	0.9	—	0.10	0.25
	0.50	0.8	—	0.9	—	0.10	0.25
46xx and 48xx (High Ni-Mo Type)	0.20	0.8	1.8	—	0.25	—	0.25
	0.20	0.6	3.5	—	0.25	—	0.25

[a] Minimum σ_{ys} related to carbon content; maximum section size related to hardenability response.

230-362 O - 77 - 20

Table C2—Representative compositions of low-alloy quenched and tempered steels for welded use[a]

Thickness Limit		Composition (%)						
(in.)	(mm)	C	Mn	Ni	Cr	Mo	Other	Si
1.25	32	0.20	0.90	—	0.65	0.25	Zr-B	0.70
4.0	100	0.20	0.90	0.90	0.55	0.55	V-Cu-B	0.25
2.0	50	0.20	1.00	0.60	0.55	0.25	V-B	0.25
1.25	32	0.20	0.60	—	—	0.55	B	0.25
2.0	50	0.20	1.20	—	—	0.45	B	0.25
2.0	50	0.20	0.55	—	1.40	0.30	Ti-Cu-B	0.25
2.0	50	0.20	0.60	1.30	—	0.55	B	0.25
0.8	19	0.20	0.95	—	0.65	—	Zr-B	0.70
4.0	100	0.20	0.55	1.30	1.10	0.55	B	0.25

[a]Minimum σ_{ys} 100 ksi (689 MPa) to 2.25 in. (57 mm), 90 ksi (620 MPa) to 4.0 in. (100 mm)

Table C3—Representative compositions of high-alloy steels for welded use

Type	Thickness Limit		Minimum σ_{ys}		Composition (%)									
	(in.)	(mm)	(ksi)	(MPa)	C	Mn	Ni	Cr	Mo	Co	V	Si	Ti	Al
Quenched and Tempered Ni-Cr-Mo Type	<4	100	85	586	0.18	0.30	3.0	1.8	0.5	—	0.02	0.25	—	—
	>4	100	85	586	0.18	0.30	3.7	1.8	0.5	—	0.02	0.25	—	—
	<4	100	100	689	0.18	0.30	3.0	1.8	0.5	—	0.02	0.25	—	—
	>4	100	100	689	0.18	0.30	3.7	1.8	0.5	—	0.02	0.25	—	—
Quenched and Tempered Ni-High Co Type	<4	100	175	1207	0.20	0.30	9.0	0.8	1.0	4.5	0.08	0.08	—	—
	<4	100	175	1207	0.26	0.30	8.0	0.5	0.5	4.0	0.10	0.08	—	—
	<4	100	200	1379	0.32	0.30	7.0	1.0	1.0	4.5	0.10	0.08	—	—
Maraging Type	—	—	210	1448	0.02	0.08	18.0	—	4.3	8.0	—	0.08	0.15	0.10

The generally low alloy contents of these steels are due to cost-cutting efforts. The steels are designed to provide adequate hardenability and as-quenched hardness for desired yield-strength levels at specified section sizes. Carbon and alloy contents are increased in combination to meet the need for increase yield strength or the requirements of increased section size. The usual reference in selection of these steels is the guaranteed minimum tensile strength for the section size of interest, as measured at the quarter-thickness position of the product form.

This reference information may be used by plotting the corresponding statistical range for minimum and maximum yield strength in the RAD. The range of fracture properties is then

defined directly from the low-corridor, top and bottom limits. Inserting the elastic-plastic zone ratio lines for the section size completes the analysis. The fracture-state properties are defined accordingly, in terms of statistical-expectancy ranges.

Table C2 illustrates the compositions of standard-grade quenched and tempered steels developed specifically for welded use. The yield-strength range of these steels is fixed by the ASTM-specified minimum values. In comparison to the steels of Table C1, these steels cover a relatively narrow range of yield strength, as noted in RAD plots.

In these steels, alloy cost minimization is indicated by relatively low, conventional alloy content and by the use of special elements (Zr-B-V-Ti) to enhance hardenability, hardness, or grain refinement. The low corridor level of these steels is largely due to melting procedures dictated by economy. Further weldability and microstructure information pertinent to these steels is in Chapter 8.

The thickness limits noted in the table for these steels do not uniformly ensure elastic-plastic or plastic fracture properties. Considerable differences in fracture properties may be expected between the relatively thick and relatively thin section sizes, and caution should be used in selecting section sizes of 2 to 4 in. (50 to 100 mm). Individual fracture property determinations should be made to ascertain whether a steel is suitable for intended service. Prior experience with these steels in 1.25-in. (32 mm) section sizes should not be relied on for thicker sections. Experience with thinner sections is not translatable to thicker sections because of mechanical constraint effects due to section size, which may cause a shift from plastic to plane-strain properties.

Table C3 lists the compositions of representative high-alloy steels developed or modified for welded use. The steels have yield strengths that cover the full range of the intermediate and high RAD corridors. The high alloy contents are necessary for producing optimum metallurgical microstructures in relatively thick sections. The only special addition that is used for the Ni-Cr-Mo type steels is vanadium, which is a conventional strengthening agent. Carbon content is increased only for the higher strength ranges.

The maraging steels are special types that do not require quenching. Hardening takes place by precipitation of Ti-Al compounds, in a process similar to the age-hardening of aluminum alloys. The heat treatment entails solution treatment at 1500° to 1800°F (810° to 980°C) followed by cooling in air or water to room temperature. In this condition, the material is relatively soft. Age-hardening heat treatments involve reheating in the range of 875° to 950°F (470° to 500°C) for 2 to 3 hours.

Table C3 illustrates the composition for the lowest strength level of the standard grades of maraging type. Higher strength is achieved by increasing the titanium content to the 0.30% to 0.80% range and by adjusting the age-hardening temperatures and times. Thickness limits are not cited. The only requirement is for achieving the minimum strength levels of the specifications.

The literature on weldable high-alloy steels contains extensive references to U.S. Navy HY-steels. The original development of the commercial Ni-Cr-Mo and weldable nickel-high cobalt (Ni-High Co) types, cited in Table C3, was done to complete the HY series. (HY signifies "high-yield.") The HY-80, HY-100, and HY-180 steels correspond generally to the 85-, 100-, and 175-ksi (586, 689, and 1207 MPa) grades cited in Table C3. Military specifications are more

detailed than commercial standard-grade specifications, particularly with respect to quality factors that decide the location in the transition corridors of the RAD. The HY steels are premium versions of the commercial grades.

HY-130 is a recently developed steel not represented in the current listing of standard commercial grades. The specified minimum yield strength of 130 ksi (896 MPa) is achieved mainly by a modest increase in the conventional alloy content of the Ni-Cr-Mo steel of Table C3, plus a decrease in tempering temperature. The object is to evoke a secondary hardening response during tempering. Secondary hardening takes place by the precipitation of Cr-Mo-V carbides that strengthen the tempered martensite matrix of the steel while changing fracture properties little. In brief, the strength transition is shifted to higher strength levels. HY-130 steel retains the highest RAD corridor position currently achievable for the yield-strength range of 130 to 155 ksi (898 to 1069 MPa).

APPENDIX D

Introduction to Structural Steels

ALLOY COMPOSITIONS OF STANDARD-GRADE STEELS

The reference system for the standard-grade structural steels may be understood in general terms by examining representative alloy features, presented in Tables D1 and D2. All of these steels evolved from structural carbon steels. They differ in microstructure because of the combined effects of alloy additions and cooling rates. Section size is an important metallurgical reference because of its effect on cooling rates for any specified heat treatment.

Small additions of the alloy elements noted in the tables produce fine rather than coarse microstructures during air cooling. Finer microstructures increase yield strength and fracture properties. Carbon contents are generally kept below 0.25% to reduce cracking tendencies in welding and to offset requirements for high preheat temperatures.

Table D1—Representative compositions and yield strengths of structural steels

Type of Steel	Composition (%)					Minimum σ_{ys}	
	T[a]	C	Mn	Si	Condition[b]	(ksi)	(MPa)
Carbon Steels	B	0.28	0.40	0.05	AR	28	193
	A	0.22	0.60	0.05	AR	40	275
	B	0.24	0.95	0.15	AR or N	40	275
	C	0.25	0.95	0.15	AR or N	40	275
	C	0.15	1.20	0.20	AR or N	36	248
	B	0.22	1.10	0.20	AR or N	40	275
C-Mn-V Steels and Ni-Cr-Cu Modified Steels	A	0.25	1.20	0.20	0.5V AR or N	55	379
	A	0.25	1.20	0.20	0.5V AR or N	62	427
		(+0.2 Ni, 0.2 Cr, 0.2 Cu)					

[a]Thickness: A—1 in. (25 mm)
B—2 in. (50 mm)
C—4 in. (100 mm)

[b]AR—As Rolled
N—Normalized

Table D2—Representative compositions and yield strengths of structural Ni-Mo steels

Thickness		Composition (%)						Minimum σ_{ys}	
(in.)	(mm)	C	Mn	Si	Ni	Mo	HT[a]	(ksi)	(MPa)
To 2	50	0.15	0.60	0.20	2.20	—	N	45	310
To 6	150	0.25	0.60	0.20	3.50	—	N	45	310
To 2	50	0.20	0.80	0.20	—	0.50	N	42	289
To 6	150	0.25	0.80	0.20	—	0.50	N	42	289
To 4	200	0.20	1.30	0.20	0.90	0.50	N	55	379
To 6	150	0.20	1.30	0.20	0.60	0.50	AC	60	413
To 6	150	0.24	1.30	0.20	0.90	0.50	AC	75	517

[a]Heat Treatment: N—Normalized
AC—Accelerated Cooling (spray or quench)

The 1940 ship fracture steels (Table D1) provide a starting point for the discussions of alloy effects. These steels were developed for use in riveted structures. Their high carbon and low manganese contents result in coarse, pearlitic microstructures of low strength and high transition temperatures. The low silicon content results in a rimming steel of high oxygen content, unsuitable for normalizing. No benefit with respect to transition temperature would result from normalizing, because of the coarse austenitic grain sizes at the austenitizing temperatures of approximately 1650°F (900°C).

Modern weldable steels have silicon contents on the order of 0.20%. This produces a silicon-deoxidized steel to which more potent deoxidizers such as aluminum can be added. The notations of "fine-grain practice" in references to standard-grade steels indicate that the steel is deoxidized enough that normalizing will yield transition-temperature improvements. The expense of normalizing is justified only if the steel is made by fine-grain practices. Aluminum is added in usual amounts of 0.02% to 0.04% (acid soluble). Adding aluminum yields no significant benefits for conventional as-rolled steels, because the high rolling temperatures result in austenite grain-coarsening even in the presence of aluminum.

There generally is a striking difference in ferrite grain size between ordinary as-rolled steel and normalized steel that has been made by appropriate fine-grain practices. Optical microscope observations at 100× magnification disclose a coarse grain structure for the as-rolled material (ASTM ferrite grain size 5 to 8), as compared to the normalized steels (ASTM ferrite grain size 9.5 to 11.0). These grain-size differences are enough to place the expected DT transition-temperature curves in normalized steel statistical bands rather than (higher temperature) as-rolled steel statistical bands. In effect, microscopic examination can be translated directly to a reasonably precise definition of the DT transition curves and fracture-state criteria at specified temperatures. This rational connection between microstructure and fracture criteria requires consideration of mechanical section-size effects. For example, the predictions for 0.6-in. (16 mm) standard DT specimen section sizes must be adjusted, because of mechanical constraint, for thicker sections.

Table D1 illustrates that the carbon-manganese balance influences strength level. Carbon and manganese contents are increased in combination to attain higher levels of yield strength and to offset the effects of increased section size. The limits of this combined effect are reached at approximately 40 to 45 ksi (275 to 310 MPa). Vanadium additions are used for the next increment of strength increase. Vanadium steels can achieve yield-strength values of 55 to 65 ksi (379 to 448 MPa), with or without additions of nickel, chromium, and copper in small amounts (0.2%).

In the case of thick sections and requirements for low-temperature service, it is not appropriate to use vanadium strengthening, because thick sections have undesirable fracture properties. The sequential steps in alloy progression are illustrated in Table D2. The preferred alloy combinations feature nickel and molybdenum in the amounts cited. The table also indicates that for exceptionally thick sections, accelerated cooling (AC) must be used. Depending on the section size and desired strength level, it is necessary to shift progressively from normalizing to spray cooling and then to full-quench treatments, followed by appropriate tempering.

Nickel-molybdenum steels are not transformed to ferrite-pearlitic structures by accelerated cooling; the transformation products are largely of acicular upper-bainite types. The fine-scale distributions of ferrite and carbide particles of the bainitic microstructure are responsible for the relatively high strength of these thick-section steels. There is an additional benefit in retaining the desirable transition temperature features of the thinner (normalized) steels to the level of very thick sections noted in the table.

For these steels, extension of the thickness range from 6 in. (150 mm) to 12 in. (300 mm) results in surface-to-center gradients of fracture properties because of inadequate bainitic hardenability. The surface regions then have lower transition temperatures than the central regions.

The attainment of strength levels in excess of 80 ksi (551 MPa) requires quenching and tempering plus relatively high alloy contents and/or section-size limitations. The alloy features of the higher strength classes are described in Appendix C.

The sulfur and phosphorus contents of the steels in Tables D1 and D2 are generally limited to a maximum of 0.035% to 0.040%. In comparison, high strength steels of high coridor quality are limited to a maximum of 0.01% to 0.02%.

APPENDIX E

Fundamental Significance of the R-Curve Expression for Fracture-Extension Resistance

FRACTURE MECHANICS THEORY

Fracture mechanics research in the early 1960s concentrated on measurement of the fracture-extension resistance of metals, in terms of the plastic work-energy parameter $\mathcal{G}_c$. The basic features of the balance between the work $\mathcal{G}$ of the externally applied stress field and the characteristic resistance R of the material to fracture are illustrated in Fig. E1. The illustration is for the simple case of a two-dimensional body with a flaw of length $2a$, residing in an elastic tensile stress field.

The term $\mathcal{G}$ is the strain-energy release rate with crack extension (per unit length of crack border), or crack-extension force. R is the crack-extension resistance (of the material at the crack

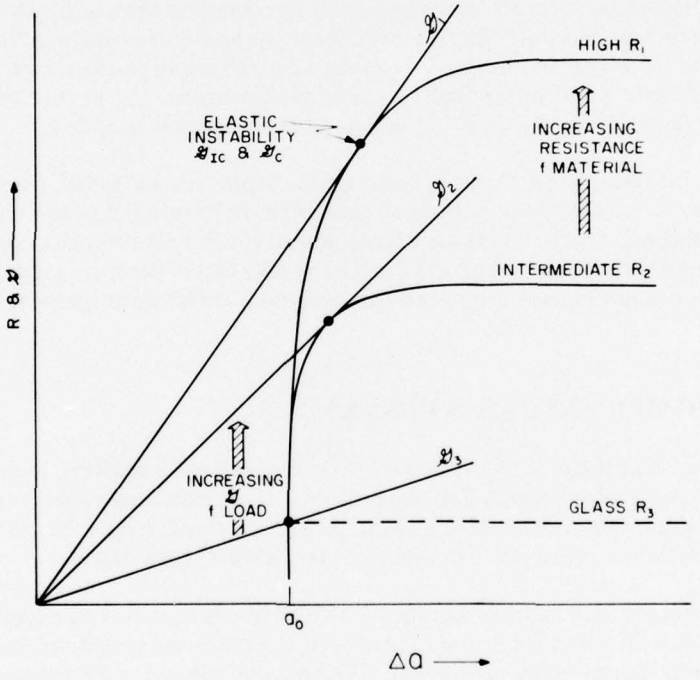

Fig. E1--Fracture mechanics definition of R-curve features in terms of rising $\mathcal{G}$ (to the point of instability $\mathcal{G}_c$). The mathematical analyses apply to elastic loading, but the basic concepts may be extended to plastic fracture.

tip) opposing $\mathcal{G}$. The strain energy produced by the stress field is represented by the straight line through the origin, while the slope of the line indicates the magnitude of $\mathcal{G}$. Characteristic R-curves for different materials are illustrated by the R traces for this simple case; however, the shape of the R-curves is influenced by geometrical considerations of the body, including flaw length, specimen width, thickness, and stress state.

The critical point in the energy balance system is the point where $\mathcal{G}$ and R are equal; this is visualized as the point of tangency for the two curves. This point represents the critical value of $\mathcal{G}$, which is denoted $\mathcal{G}_c$. The tangency implies that an excess of the strain energy $\mathcal{G}$ necessary to sustain the fracturing process is available, and therefore, the fracture will propagate. For this to be meaningful, the fracture, once initiated, must be self-sustaining (unstable). At $\mathcal{G}$ values less than $\mathcal{G}_c$, R is higher than $\mathcal{G}$, and crack initiation cannot occur because of insufficient driving energy. The R-curve for extremely brittle materials, such as glass, allows for no increase in R with crack movement. The other R-curves of Fig. E1 represent many real metals that tolerate a very small degree of crack movement without fracturing. The R-curves for materials that fracture elastically must, by definition, reach a point at which R does not increase with increasing crack length; this is not the case for ductile metals. Higher levels of $\mathcal{G}_c$ are required for the fracture of materials with higher characteristic resistance R, as shown in Fig. E1.

For maximum-constraint plane-strain conditions, the critical crack-extension energy is denoted by $\mathcal{G}_{Ic}$. Basic linear-elastic fracture mechanics equations relate $\mathcal{G}_{Ic}$ to the elastic-stress and flaw-size conditions necessary for fracture. These equations are usable in the practical sense only for the case of plane strain ($\mathcal{G}_{Ic}$), because of a strong dependence of $\mathcal{G}_c$ on specimen dimensions and basic materials properties. For plane strain, $\mathcal{G}_{Ic}$ is related to the critical stress-intensity factor K_I by $K_{Ic} = E\,\mathcal{G}_{Ic}$, where E is the elastic modulus.

When the limitations on thickness and crack depth are exceeded, even for the elastic loading case, the K parameter is subject to geometric influences, and the equations are not applicable. Thus, the K_c and $\mathcal{G}_c$ terms, which include all conditions other than plane strain, have no practical value as predictors of fracture conditions. The loss of accuracy is caused by the rising R-curve, which does not permit crack extension without continuous increases in energy.

PHYSICAL SIGNIFICANCE OF R CURVES

The physical significance of the slope of the R-curve with fracture extension should be understood in a generalized sense; Fig. E2 presents schematic illustrations. The figure illustrates a metal section containing a sharp elliptical surface crack, subject to tensile loading. The increments of crack extension are Δa, and a_0 is the initial crack depth.

The top graph of Fig. E2 illustrates the σ-vs-COD traces that may be expected for frangible metals and metals with rising R-curves. In principle, the crack-opening displacement (COD) can be related to the Δa extension by calibration. COD may be measured by a clip gage. For ductile metals, COD (and Δa) occurs with rising load into the plastic region (rising R) without evidence of unstable fracture extension. For a frangible metal, the COD gage detects an "instability" at elastic-stress levels, followed by unstable fracture.

The effects on crack-tip geometry are illustrated at the bottom of the figure by the r_n-vs-Δa plot, where r_n signifies the crack-tip radius. The important aspect is that very large differences

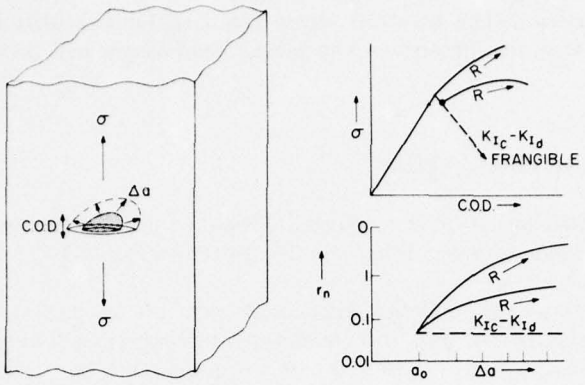

Fig. E2—Physical significance of increased resistance R to fracture extension for ductile metals (solid curves) and frangible metals (dashed curves). Note that K_{Ic} or K_{Id} parameters apply only for the frangible metals, which do not feature increased R. The important physical aspects are load stress σ and crack-tip blunting r_n.

in crack blunting result from extension of fractures for metals of different R-curve features, as follows:

Flat-slope R curve—Crack-tip sharpness is retained because the critical plastic-zone size is small.

Intermediate-slope R curve—Crack-tip blunting occurs gradually by a process of increasing plastic-zone size. The small degree of blunting developed in the first unit extension results in a larger plastic-zone size for the next step, which causes additional blunting and therefore an additional growth of the plastic-zone size, and so on. A stable condition is achieved, after which there is no further increase in r_n.

High-slope R curve—Crack-tip blunting occurs rapidly as the result of gross plasticizing of the zone in advance of the tip, starting with the first rupture increment. The effects are accentuated in further extension; again there is a leveling to a stable r_n configuration.

Increases in plastic work energy per unit extension (E/A) will develop due to the crack blunting and the increases in plastic-zone size. The specific E/A increases in the course of fracture extension for ductile metals are related to the slope of the R-curves.

The slope of the R curves will be reflected in the nominal engineering stress required for fracture extension, as follows

Flat-slope R-curve—Unstable fast fracture occurs at the level of nominal elastic stress required for initiation.

Intermediate-slope R-curve—The nominal stress required for stable crack extension increases gradually with extension. While the first extension may be at elastic-stress levels, continued extension may require over-yield stresses.

High-slope R-curve—The nominal stress required for the initial crack extension will exceed yield; after this, an increase of the plastic load stress will be required for continued extension.

R-CURVE CHARACTERIZATION

The fundamental barrier to characterizing R-curve slope by any test that does not permit the stable fracture mode to develop fully is illustrated in Fig. E3.

The figure illustrates the effects of fracture test configurations and procedures for indexing fracture-extension events. The flat-, intermediate-, and high-slope R-curves represent metals of plane-strain, low plastic, and high plastic fracture properties, respectively.

Fracture properties are measured under the following three conditions:

Full constraint—The tests focus entirely on the first detectable crack movement, under full constraint due to the existing crack.

Plane-strain configuration—Test specimen geometry limits the development of the fracture-mode transition. Accordingly, the measurement reflects fracture under conditions approximating plane-strain constraint.

Plane-stress configuration—Test specimen geometry allows full development of the fracture-mode transition. As a limit, the measurement reflects fracture under conditions approximating plane-stress constraint.

The figure illustrates that faithful measurement of intermediate-and high-slope R-curve fracture properties is possible only if the specimen configuration is of plane-stress type. Restricting the specimen configuration to plane-strain type or focusing on the first event of crack extension results in grossly inaccurate definition of plastic fracture properties.

The E/A or $\mathcal{G}$ scales are equivalent expressions of work energy for fracture extension. The $\mathcal{G}$ scale represents K_{Ic} test values converted to energy by the $K_{Ic} = E\mathcal{G}_{Ic}$ relationship. The E/A scale corresponds to the DT test values of energy, as measured for conditions of incremental crack extension.

The standard configuration of the DT test is defined as a plane-stress configuration, because it allows full development of this fracture mode. If the length of the fracture path is reduced, the DT test loses its ability to index the fracture-mode transition. Like the usual K_{Ic} and COD tests, it then indicates only conditions of initial extension, when the plane-strain stress state of the initial crack dominates fracture extension.

Figures E4, E5, and E6 provide experimental verification of the schematic illustration in Fig. E3. Series of modified DT test specimens, with ascending fracture path lengths, define the relative increase in E/A with fracture extension. The examples use a steel of 1-in. (25 mm) section size, heat treated to low, intermediate and high strength levels. The strength transition results in a corresponding change from high to intermediate and low fracture-extension resistance.

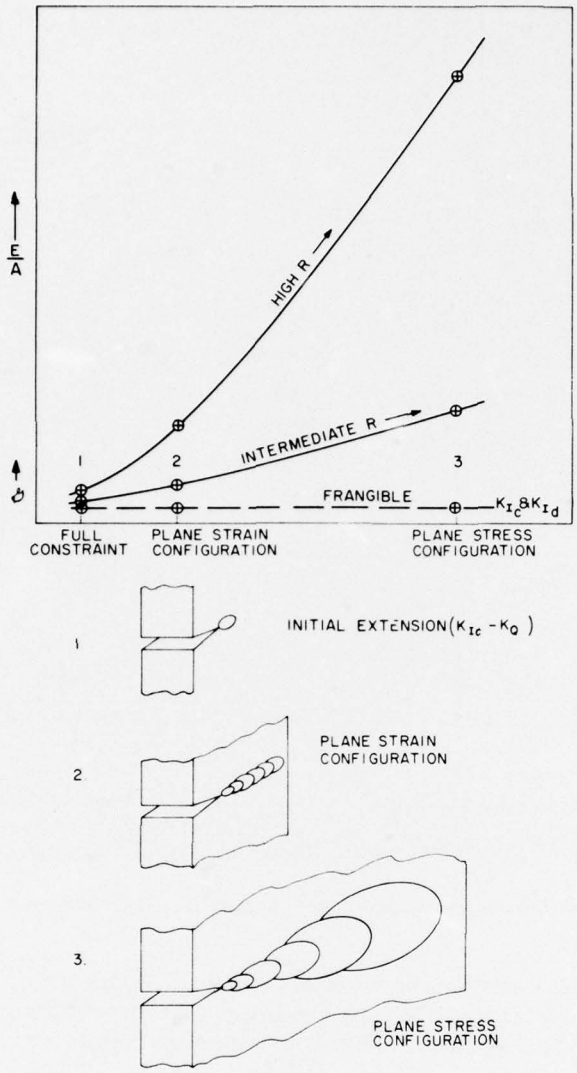

Fig. E3—Definition of R-curve features by (a) fracture mechanics tests which only measure features of initial extension, (b) the plane strain DT configuration test, and (c) the standard DT test which represents a plane stress configuration. Solid curves indicate increasing R, typical of ductile metal.

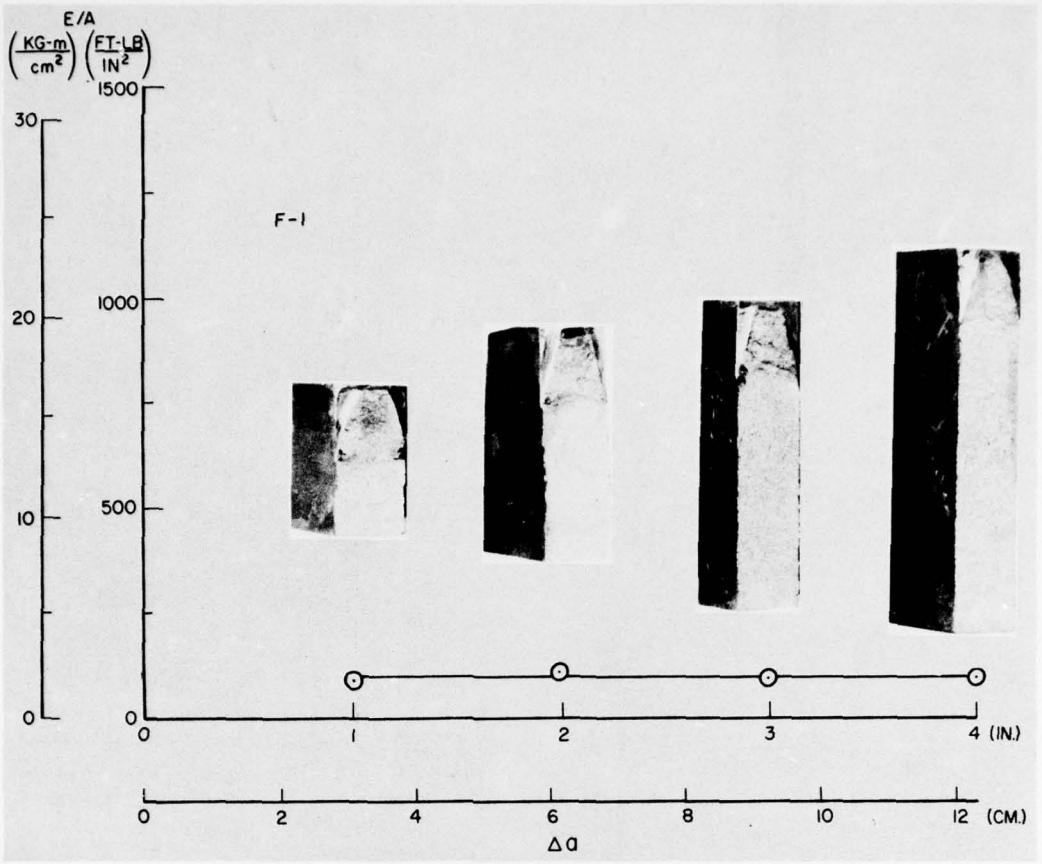

Fig. E4—Fracture appearance transition and R-curve features for steel of plane-strain fracture properties.

In effect, the series represents an experiment in tracking the strength transition in terms of R-curve slope. Characterizing the relation between decreasing R-curve slope and the development of strength transitions for specified section sizes defines an intrinsic metal-quality factor.

The object of R-curve characterization is to identify a metal-quality parameter from data that include mechanical information. Extensive studies have been conducted for a variety of steels and aluminum alloys, over a broad range of strength levels and section sizes.

Curve-fitting analyses of the type shown in Fig. E7 indicate that a material constant R_p may be derived from the data, as follows:

$$E = R_p \Delta a^2 f(B)$$

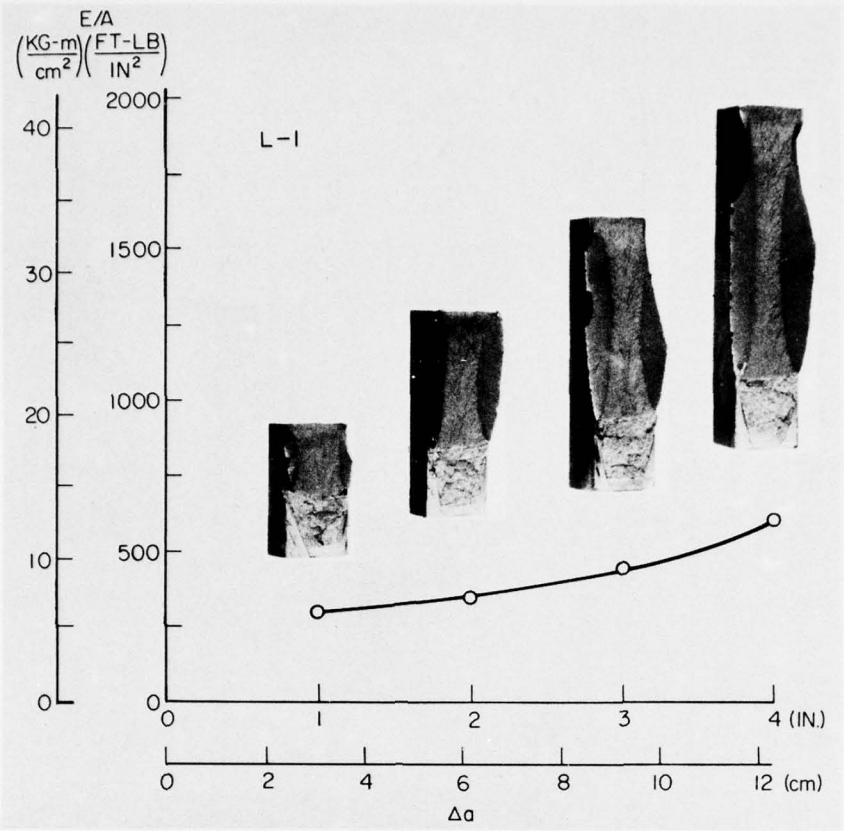

Fig. E5—Fracture appearance transition and R-curve features for steel of low-level plastic fracture properties.

where

R = energy per unit area (E/A)
Δa = crack-extension increment
$f(B)$ = function of section size B.

The R_p constant defines the position of the curve on the log-log plot, which is characteristic of the metal. Changes of section size affect the constraint state, purely as a mechanical factor. The interactions of metallurgical and mechanical factors decide the specific resistance R to fracture extension.

The general equation that defines the interactions of metallurgical and mechanical factors has the form

$$E = R_p \Delta a^x B^y .$$

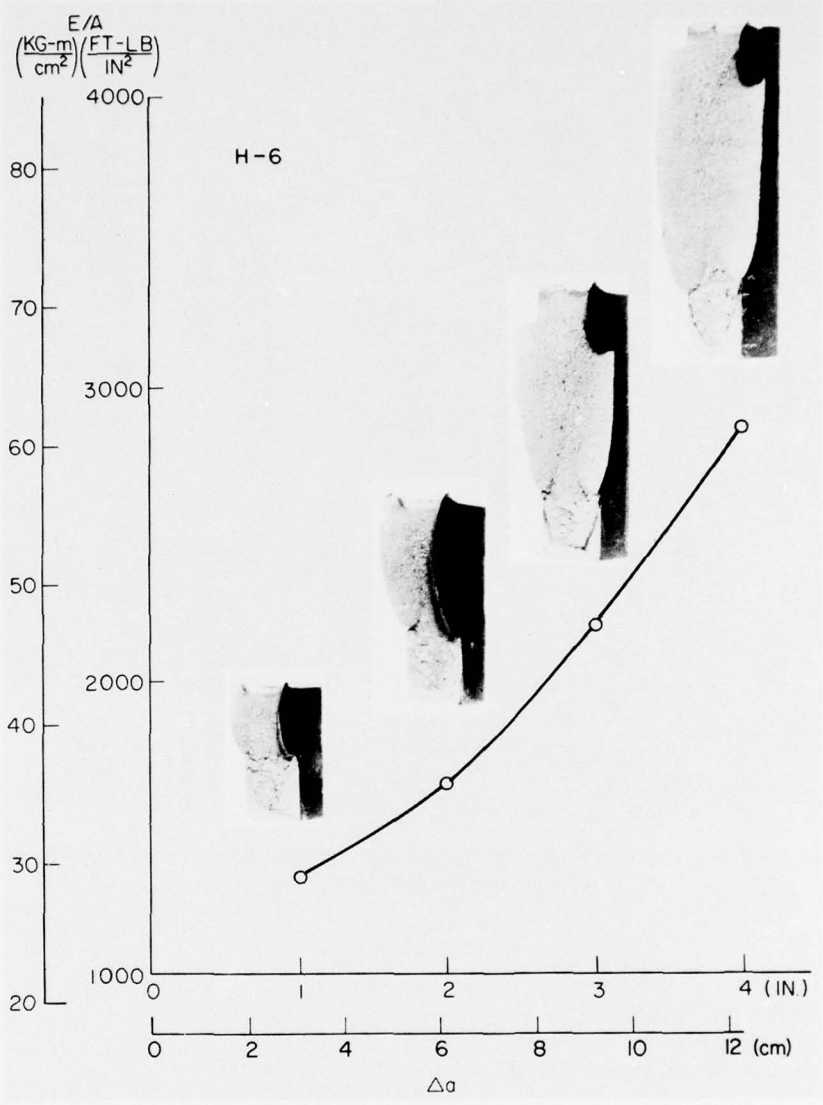

Fig. E6—Fracture appearance transition and R-curve features for steel of highly plastic fracture properties.

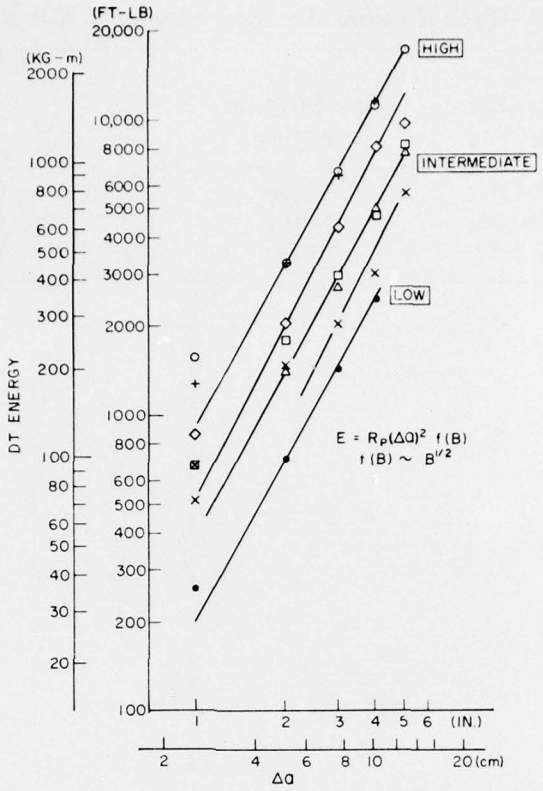

Fig. E7—Log-log plot of experimental data for five steels featuring low to high R-curve slope properties.

Studies of steels and aluminum and titanium alloys show that the exponents vary within the ranges noted in Table E1.

The generalized equation

$$E = R_p \Delta a^2 B^{0.5}$$

provides a reasonable approximation for characterizing metal properties. It has been used in developing a reference data bank for steels and aluminum alloys.

Information on titanium alloys suggests that the exponents should be adjusted for specific alloy systems. In general, it is recommended that new alloy systems be investigated to determine whether adjustments are required.

R_p characterization, for metals of thin section, may be performed by using a laminated version of the standardized DT test (Fig. E8). In this case, E/A and B are calculated on the basis

Table E1—Typical values of x and y exponents: $E = R_p (\Delta a)^x (B)^y$

Material	Section-Size Range (in.)	Yield Strength Range (ksi)	x	y	R_p Range (ft-lb/in.$^{5/2}$)
Steel	0.75-6.0	80-180	1.8-2.1	0.4-0.7	180-925
Titanium	0.10-0.50	120-160	1.8-2.1	0.4-0.7	30-180
Aluminum	0.10-3.0	27-78	1.6-2.1	0.4-0.9	50-200

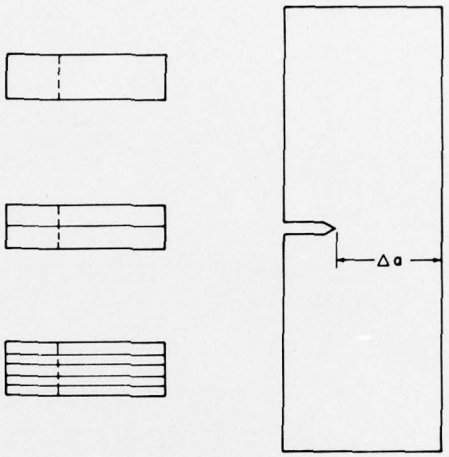

Fig. E8—Configuration of standard DT test specimens for full-section and laminate materials characterization.

of laminate dimensions. The only other requirement is adjustment of the DT specimen's thickness to the closest value attainable by stacking of the laminates. Figure E8 illustrates tests conducted with laminated DT specimens 0.5 in. (12.5 mm) thick.

Figure E9 shows results of full-section and reduced-section tests of four aluminum alloys. Since the laminates were cut from the same material used for the full-section tests, there is no change in the metal-quality parameter R_p. The characteristic value of R_p for each sample is noted at the top of the figure.

Ordinarily, a metallurgical effect may be expected of changes in section size for a given alloy, because of differences in metal working and grain structure. However, the strength-transition factor is dominant, and a low strength alloy of 5086 type should not be expected to develop low R_p properties like those of the high strength 7075 type. The order-of-magnitude decrease in R_p values represents a strength transition, for the plastic fracture properties of aluminum alloys, that is best represented by a RAD plot.

RAD CONSOLIDATION OF R_p DATA

Rational methods for R-curve characterization provide unified methods of data reference and interpretation, by RAD plotting and analysis. Figure 173 is an example for steels. Many

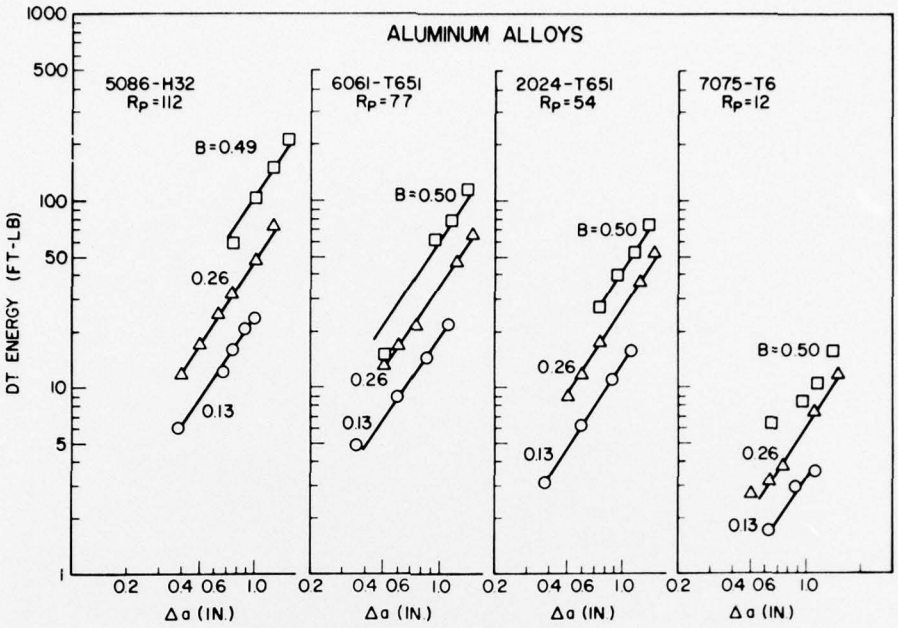

Fig. E9—Fracture data for full-section and reduced section (laminate) tests of four aluminum alloys. (After R.W. Judy, Jr., and R.J. Goode.)

examples for steels and for aluminum and titanium alloys may be found by reference to the bibliography. Note that the R_p scale has been added to the RAD. The R_p scale provides entry to the RAD plot for large or small DT test specimens or laminated versions of the small DT specimen (Fig. E8). In fact, any DT modification that retains the rational geometric features described previously may be used by reference to the R_p scale.

The RAD display defines the range of R-curve slopes that are metallurgically attainable for given strength levels and section sizes. The information is available for structural steels and for aluminum and titanium alloys. Questions of metal selection can be answered only if organized information of this type is used as reference.

Other test methods have been used empirically to develop a reference data bank for special applications. These tests, including the Charpy-V, have served for correlation with results obtained in structural prototype burst tests, such as those of gas line steels. However, there is no general analytical value that provides for transfer of the information to other metals or strength levels.

The RAD defines the best SI option for a particular case if metal properties are the dominant factor. In particular, the RAD serves as a warning if excessively high strength levels are involved in the initial consideration of candidate metals. For example, a modest decrease of strength level may increase the maximum attainable R-curve slope from low to very high. Purely mechanical effects of changing section size may be analyzed in similar terms.

BIBLIOGRAPHY

MICROFRACTURE MECHANISMS

A.S. Tetelman and A.J. McEvily, Jr., *Fracture of Structural Materials,* Wiley, New York, 1967.

B.L. Averback et al., "Fracture," in *Proceedings of International Conference on the Atomic Mechanisms of Fracture, Swampscott, Mass., Apr. 12-16, 1959,* Wiley, New York, 1959.

M. Cohen, "Metallurgical Structure and the Brittle Behavior of Steel," National Academy of Sciences, Ships Structure Committee, SSC Report 183, May 1968.

N.J. Petch, "The Ductile-Cleavage Transition in Alpha Iron," in *Fracture,* pp. 54-67, MIT Technology Press, Boston, Mass., 1959.

E. Orowan, "Classical and Dislocation Theories of Brittle Fracture," in *Fracture,* pp. 147-160, MIT Technology Press, Boston, Mass., 1959.

J.R. Low, Jr., "A Review of Microstructural Aspects of Cleavage Fracture," in *Fracture,* pp. 68-90, MIT Technology Press, Boston, Mass., 1959.

FRACTURE MECHANICS

G.R. Irwin, "Fracture," in *Encyclopedia of Physics,* Vol. VI, pp. 551-590, Springer, Berlin, 1958.

G.R. Irwin, J.A. Kies, and H.L. Smith, "Fracture Strengths Relative to Onset and Arrest of Crack Propagation," *Proc. ASTM,* 1958, vol. 58, pp. 640-660.

G.R. Irwin, "Fracture Mechanics," in *Structural Mechanics,* J.N. Goodier and N.J. Hoff, eds., p. 557, Pergamon Press, New York, 1960.

J.I. Bluhm, "A Model for the Effect of Thickness on Fracture Toughness," *Proc. ASTM,* 1961, vol. 61, pp. 1324-1331.

G.R. Irwin, "Crack-Extension Force for a Part-Through Crack in a Plate," *Trans. ASME,* 1962, vol. 29, ser. E, pp. 651-654.

G.R. Irwin, "Relation of Crack Toughness Measurements to Practical Applications," *Weld. J. Res. Suppl.,* Nov. 1962, vol. 41, (no. 11), pp. 519s-528s.

G.R. Irwin, "Crack-Toughness Testing of Strain-Rate Sensitive Materials," *Trans. ASME J. Eng. Power,* Oct. 1964, vol. 86, ser. A, pp. 444-450.

Fracture Toughness and Its Applications, American Society for Testing and Materials, ASTM STP 381, Philadelphia, Pa., 1965.

W.F. Brown, Jr., and J.E. Srawley, *Plane Strain Crack Toughness Testing of High Strength Metallic Materials,* ASTM STP 410, p. 126, American Society for Testing and Materials, Philadelphia, Pa., 1966.

E.T. Wessel, "State of the Art of the WOL Specimen for K_{Ic} Fracture Toughness Testing," *Eng. Fract. Mech.,* 1968, vol, 1, pp. 77-103.

W S. Pellini and F.L. Loss, "Integration of Metallurgical and Fracture Mechanics Concepts of Transition Temperature Factors Relating to Fracture-Safe Design for Structural Steels," pp. 1-38, *WRC Bulletin 141,* 1969.

Review of Developments in Plane Strain Fracture Toughness Testing, W.F. Brown, Jr., ed., ASTM STP 463, American Society for Testing and Materials, Philadelphia, Pa., 1970.

"Plain-Strain Fracture Toughness of Metallic Materials," in *Book of ASTM Standards (Part 10)*, ASTM Standard Method E399-72, p. 960, American Society for Testing and Materials, Philadelphia, Pa., 1975.

A.A. Wells, "Unstable Crack Propagation in Metals: Cleavage and Fast Fracture," *Proceedings of Crack Propagation Symposium, College of Aeronautics, Cranfield, England,* 1961, vol. I, pp. 210-230.

INVESTIGATIONS OF SHIP FRACTURE PROBLEM

M.L. Williams, "Analysis of Brittle Behavior in Ship Plates," in *Symposium on Effect of Temperature on the Brittle Behavior of Metals with Particular Reference to Low Temperatures,* ASTM STP 158, p. 11, American Society for Testing and Materials, Philadelphia, Pa., 1954.

M.L. Williams, "Investigation of Fractured Steel Plates Removed from Welded Ships," Report No. 3, National Bureau of Standards, Washington, D.C., June 1951.

M.L. Williams and G.A. Ellinger, "Investigation of Structural Failures of Welded Ships," *Weld. J.,* Oct. 1953, vol. 32, pp. 498s-527s.

"The Design and Methods of Construction of Welded Steel Merchant Vessels," Report of a Board of Investigation, U.S. Government Printing Office, Washington, D.C., July 1946.

P.P. Puzak, M.E. Schuster, and W.S. Pellini, "Crack-Starter Tests of Ship Fracture and Project Steels," *Weld, J. Res. Suppl.,* Oct. 1954, vol. 33, pp. 481s-495s.

GENERAL INVESTIGATIONS OF TRANSITION-TEMPERATURE PROBLEM (1950-1960)

P.P. Puzak, E.W. Eschbacher, and W.S. Pellini, "Initiation and Propagation of Brittle Fracture in Structural Steels," *Weld, J.,* Dec. 1952, vol. 31, pp. 561s-581s.

M. Gensamer, "General Survey of the Problem of Fatigue and Fracture of Metals," in *Fatigue and Fracture of Metals,* p. 1, MIT Technology Press and Wiley, New York, 1952.

W.S. Pellini, F.A. Brandt, and E.E. Layne, "Performance of Cast and Rolled Steels in Relation to the Problem of Brittle Fracture," *Trans. AFS,* 1953, vol. 61, pp. 243-262.

W.S. Pellini, "Evaluation of the Significance of Charpy Tests," in *Symposium on Effect of Temperature on the Brittle Behavior of Metals,* ASTM STP 158, p. 216, American Society for Testing and Materials, Philadelphia, Pa., 1954.

M.E. Shank, "A Critical Survey of Brittle Failure in Carbon Plate Steel Structures Other Than Ships," pp. 1-48, *WRC Bulletin 17,* Jan. 1954.

Control of Steel Construction to Avoid Brittle Failure, M.E. Shank, ed., Welding Research Council, New York, 1957.

E.R. Parker, *Brittle Behavior of Engineering Structures,* Wiley, New York, 1957.

P.P. Puzak, A.J. Babecki, and W.S. Pellini, "Correlations of Brittle-Fracture Service Failures with Laboratory Notch-Ductility Tests," *Weld, J. Res. Suppl.,* Sep. 1958, vol. 37, pp. 391s-410s.

H.H. Johnson and R.D. Stout, "Comparison and Analysis of Notch Toughness Tests for Steels in Welded Structures," pp. 1-28. *WRC Bulletin 62,* July 1960.

GENERAL INVESTIGATIONS OF TRANSITION-TEMPERATURE (1961-1975)

W.S. Pellini and P.P. Puzak, "Fracture Analysis Diagram Procedures for the Fracture-Safe Engineering Design of Steel Structures," pp. 1-28, *WRC Bulletin 88,* May 1963.

W.S. Pellini and P.P. Puzak, "Practical Considerations in Applying Laboratory Fracture Test Criteria to the Fracture-Safe Design of Pressure Vessels," *Trans. ASME J. Eng. Power,* 1964, vol. 86, ser., A, pp. 429-443.

E.H. Brubaker and J.D. Dennison, "Use of Battelle Drop-Weight Tear Test for Determining Notch Toughness of Line Pipe Steel," *J. Metals,* 1965, vol. 17, pp. 985-989.

F.M. Burdekin and D.E.W. Stone, "The Crack Opening Displacement Approach to Fracture Mechanics in Yielding Materials," *J. Strain Anal.,* 1966, vol. 1 (no. 2), pp. 14-153.

P.P. Puzak and E.A. Lange, "Standard Method for the 1-Inch Dynamic Tear (DT) Test," U.S. Naval Research Laboratory, NRL Report 6851, Feb. 1969.

F.J. Loss and W.S. Pellini, "Coupling of Fracture Mechanics and Transition Temperature Approaches to Fracture-Safe Design," U.S. Naval Research Laboratory, NRL Report 6913, Apr. 1969.

W.S. Pellini and F.J. Loss, "Integration of Metallurgical and Fracture Mechanics Concepts of Transition Temperature Factors Relating to Fracture-Safe Design for Structural Steels," pp. 1-38, *WRC Bulletin* 141, June 1969.

"Standard Method for Conducting Drop-Weight Test to Determine Nil-Ductility Transition Temperature of Ferritic Steels," in *Book of ASTM Standards (Part 10),* ASTM Designation E208-69, pp. 582-601, American Society for Testing and Materials, Philadelphia, Pa., July 1975.

Impact Testing of Metals, ASTM STP 466, American Society for Testing and Materials, Philadelphia, Pa., 1970.

W.G. Clark, Jr. and E.T. Wessel, "Application of Fracture Mechanics Technology to Medium Strength Steels," in *Review of Developments in Plane Strain Fracture Toughness Testing,* p. 160, ASTM STP 463, American Society for Testing and Materials, Philadelphia, Pa., 1970.

W.L. Server and A.S. Tetelman, "The Use of Pre-Cracked Charpy Specimens to Determine Dynamic Fracture Toughness," *Eng. Fract. Mech.,* 1972, vol. 4, p. 367.

ROBERTSON TEST AND RELATED INVESTIGATIONS

T.S. Robertson, "Propagation of Brittle Fracture in Steel," *J. Iron and Steel Inst.* (London), Dec. 1953, vol. 175, p. 361.

F.J. Feely, Jr. et al., "Studies on the Brittle Failure of Tankage Steel Plates," *Welding J.,* Dec. 1955, vol. 34 (no. 12), pp. 596s-607s.

H.M. Kihara and K. Masubuchi, "Effect of Residual Stress on Brittle Fracture—Studies on Brittle Fracture of Welded Structures at Low Stress Level," *J. Soc. Nav. Architects Japan,* July 1958, vol. 103, pp. 251-262.

R.J. Mosborg, "An Investigation of Welded Crack Arresters," *Weld. J.,* Jan. 1960, vol. 39 (no. 1), pp. 40s-48s.

A.A. Wells, "Brittle Fracture Strength of Welded Steel Plates," *Brit. Weld, J.,* May 1961, vol. 8, pp. 259-277.

W.J. Hall, W.J. Nordell, and W.H. Munse, "Studies of Welding Procedures," *Weld, J. Res. Suppl.,* 1962, vol. 41 (no. 11), pp. 505s-518s.

W.J. Hall, H. Kihara, W. Soete, and A.A. Wells, *Brittle Fracture of Welded Plate,* Prentice-Hall, Englewood Cliffs, N.J., 1967.

T. Kanazawa, S. Machida, and T. Miyata, "Brittle Fracture Initiation of Welded Steel Structures," in *The First International Symposium of the Japan Welding Society,* Japan Welding Society, Tokyo, 1971.

STRENGTH TRANSITION

P.P. Puzak and W.S. Pellini, "Evaluation of the Significance of Charpy Tests for Quenched and Tempered Steels," *Weld. J.,* June 1956, vol. 35 (no. 6), pp. 275s-290s.

A.J. Babecki, P.P. Puzak, and W.S. Pellini, "Report of Anomalous 'Brittle' Failures of Heavy Steel Forgings at Elevated Temperatures," ASME Publ. 59-Met-6, American Society for Testing and Materials, Philadelphia, Pa., May 1959.

H. Bernstein and J.A. Kies, "Crack Growth During Static Tests of Rocket Motor Cases," *Metal Progr.,* Aug. 1960, vol. 78, no. 2, p. 79.

W.S. Pellini, "Advances in Fracture Toughness Characterization Procedures and in Quantitative Interpretations to Fracture-Safe Design for Structural Steels," pp. 1-46, *WRC Bulletin 130,* May 1968.

R.J. Goode, R.W. Judy, Jr., and R.W. Huber, "Procedures for Fracture Toughness Characterization and Interpretation to Failure-safe Design for Structural Titanium Alloys," pp. 1-17, *WRC Bulletin 134,* 1968.

R.W. Judy, Jr., R.J. Goode, and C.N. Freed, "Fracture Toughness Characterization Procedures and Interpretations to Fracture-Safe Design for Structural Aluminum Alloys," pp. 1-16, *WRC Bulletin 140,* 1969.

C.F. Tiffany, "Fracture Control of Metallic Pressure Vessels," NASA SP-8040, NASA-Lewis Research Center, Cleveland, Ohio, May 1970.

L.A. Cooley and E.A. Lange, "Vertical Drop-Weight Machine for Conducting Drop-Weight NDT, Drop-Weight Tear, and Dynamic Tear Tests," U.S. Naval Research Laboratory, NRL Report 6993, Jan. 16, 1970.

W.S. Pellini, "Criteria for Fracture Control Plans," U.S. Naval Research Laboratory, NRL Report 7406, May 11, 1972.

Application of Fracture Prevention Principles to Aircraft, National Materials Advisory Board, NMAB-302, Feb. 1973.

U.S. Department of Defense, *Method for 5/8-Inch Dynamic Tear Testing of Metallic Materials,* MIL-STD-1601 (SHIPS), May 8, 1973.

WELD CHARACTERIZATION AND WELDING FACTORS

C.E. Hartbower and W.S. Pellini, "Investigation of Factors Which Determine the Performance of Weldments," *Weld. J.,* Oct. 1951, vol. 30, pp. 499s-511s.

W.R. Apblett, L.K. Poole, and W.S. Pellini, "The Continuous Cooling Transformations of Weld-Heat-Affected Zones," *Weld., J. Res. Suppl.,* Sept. 1952, vol. 31, pp. 421s-430s.

P.P. Puzak and W.S. Pellini, "Embrittlement of High Strength Ferritic Welds," *Weld, J. Res. Suppl.,* Nov. 1952, vol. 31, pp. 521s-526s.

W.S. Pellini and E.W. Eschbacher, "Ductility Transition of Weld Metal," *Weld, J. Res. Suppl.,* Jan. 1954, vol. 33, pp. 16s-20s.

W.J. Murphy and R.D. Stout, "Effect of Electrode Type in the Notch Slow-Bend Test," *Weld. J.,* July 1954, vol. 33 (no. 7), pp. 305s-310s.

Residual Stresses in Metals and Metal Construction, W.R. Osgood, ed., Reinhold, New York, 1954.

W.R. Apblett and W.S. Pellini, "Factors Which Influence Weld Hot Cracking," *Weld. J. Res. Sup.*, Feb. 1954, vol. 33, pp. 83s-90s.

W.S. Pellini, "Notch Ductility of Weld Metal," *Weld, J. Res. Sup.*, May 1956, vol. 35, pp. 217s-233s.

A.A. Wells, "Brittle Fracture Strength of Welded Steel Plates," *Brit. Weld. J.*, May 1961, vol. 8, pp. 259-277.

STRESS CORROSION CRACKING AND OTHER TYPES OF SUSTAINED LOAD CRACKING

B.F. Brown, "Notch Sensitivity Effects in Stress Corrosion and Hydrogen Embrittlement Tests on High Strength Steels," *Corrosion* Aug. 1959, vol. 15, pp. 399t-402t.

E.H. Phelps and A.W. Loginow, "Stress Corrosion of Steels for Aircraft and Missiles," *Corrosion* 16,pp. 325t-335t (1960).

C.J. Slunder and W.K. Boyd, "Environmental and Metallurgical Factors of Stress-Corrosion Cracking in High-Strength Steels," DMIC Report 151, Battelle Memorial Institute, Columbus, Ohio, 1961.

Stress Corrosion Testing, ASTM STP 425, American Society for Testing and Materials, Philadelphia, Pa., 1967.

B.F. Brown, "The Application of Fracture Mechanics to Stress Corrosion Cracking," *Met. Res.*, Dec. 1968, vol. 13 (no. 129), pp. 171-183.

R.W. Judy, Jr. and R.J. Goode, "Stress-Corrosion-Cracking Characterization Procedures and Interpretations to Failure-Safe Use of Titanium Alloys," *Trans. ASME J. Basic Eng.*, Dec. 1969, vol. 91, ser. D (no. 4), p. 614.

B.F. Brown, "Stress-Corrosion-Cracking—A Perspective Review of the Problem," Naval Research Laboratory, NRL Report 7130, June 16, 1970.

B.F. Brown and C.D. Beachem, "A Study of the Stress Factor in Corrosion Cracking by Use of the Pre-Cracked Cantilever Beam Specimen," *Corrosion Sci., 1965, vol. 5, pp. 745-750.*

J.G. Kaufman and M. Holt, "Fracture Characteristics of Aluminum Alloys," Alcoa Technical Paper 18, 1965.

B.F. Brown, "A New Stress-Corrosion Cracking Test for High-Strength Alloys," *Mater. Res. Stand.*, Mar. 1966, vol. 6 (no. 3), p. 129.

B.F. Brown, "ARPA Coupling Program on Stress-Corrosion Cracking," (Final Report), Naval Research Laboratory, NRL Report 7168, Sep. 1970.

D.O. Sprowls, M.B. Shumacher, and J.D. Walsh, "Evaluation of Stress-Corrosion Cracking Susceptibility Using Fracture Mechanics Techniques," Alcoa Report for Marshall Space Flight Center, Contract No. NAS-8-21487, May 1973.

M.F. McGuirre, A.R. Troiano, and R.F. Hehemann, "Stress Corrosion of Ferritic and Martensitic Stainless Steels in Saline Solutions," *Corrosion,* July 1973, vol. 29 (no. 7), pp. 268-271.

T.G. Gooch, "Stress Corrosion Cracking of Welded Joints in High Strength Steels," *Weld. J. Res. Sup.*, 1974, vol. 53 (no. 7) pp. 287s-298s, 306s.

R.W. Judy, Jr., and R.J. Goode, "Failure-Safe Design with High Strength Steels for Salt Water Applications," *Mater. Protect. and Performance,* Aug. 1970, vol. 9 (no. 8), p. 23.

H.L. Craig, Jr., D.O. Sprowls, and D.E. Piper, "Stress-Corrosion Cracking," in *Handbook on Corrosion Testing and Evaluation,* W.H. Ailor, ed., p. 231, Wiley, New York, 1971.

Stress Corrosion Cracking of Metals–A State of the Art, H.L. Craig, ed., ASTM STP 518, American Society for Testing and Materials, Philadelphia, Pa., 1972.

Stress-Corrosion Cracking in High Strength Steels and in Titanium and Aluminum Alloys, B.F. Brown, ed., U.S. Government Printing Office, Washington, D.C., 1972.

G.Sandoz, "A Unified Theory for Some Effects of Hydrogen Source, Alloying Elements, and Potential on Crack Growth in Martensitic AISI 4340 Steel," *Met. Trans.*, 1972, vol. 3, pp. 1169-1176.

R.W. Judy, Jr., and R.J. Goode, "Stress-Corrosion Cracking of High-Strength Steels and Titanium Alloys," Naval Research Laboratory, NRL Report 7371, Mar. 13, 1972.

FATIGUE AND CORROSION FATIGUE

R.G. Forman, V.E. Kearney, and R.M. Engle, "Numerical Analysis of Crack Propagation in Cyclic-Loaded Structures," *Trans. ASME J. Basic Eng.*, 1967, vol. 89 (no. 3), p. 459.

S.R. Swanson, "Random Load Fatigue Testing: A State of the Art Survey," *Mater. Res. Stand.*, Apr. 1968, vol. 8 (no. 4), p. 10.

J.T. Ryder and J.P. Gallagher, "Environmentally Controlled Fatigue Crack-Growth Rates in SAE 4340 Steel—Temperature Effects," *Trans. ASME J. Basic Eng.*, Mar. 1970, vol. 92 (no. 1), ser. D, p. 121.

T.W. Crooker and E.A. Lange, "How Yield Strength and Fracture Toughness Considerations Can Influence Fatigue Design Procedures for Structural Steels," *Weld. J. Res. Sup.*, Oct. 1970, vol. 49 (no. 10), pp. 488s-496s.

K. Walker, "The Effects of Stress Ratio During Crack Propagation and Fatigue for 2024-T3 and 7075-T6 Aluminum," in *Effects of Environment and Complex Loading History on Fatigue Life*, ASTM STP 462, p. 1, American Society for Testing and Materials, Philadelphia, Pa., 1970.

W. Breyan, "Effects of Block Size, Stress Level, and Loading Sequence on Fatigue Characteristics of Aluminum Alloy Box Beams," in *Effects of Environment and Complex Load History on Fatigue Life*, p. 127, ASTM STP 462, American Society for Testing and Materials, Philadelphia, Pa., 1970.

J.P. Gallagher and R.P. Wei, "Crack Propagation Behavior in Steels," *Proceedings of International Conference on Corrosion Fatigue, Storrs, Conn., 1971*, NACE, Houston, Tex., 1972.

T.R. Brussat, "An Approach to Predicting the Growth to Failure of Fatigue Cracks Subjected to Arbitrary Uniaxial Cyclic Loading," in *Damage Tolerance in Aircraft Structures*, ASTM STP 486, p. 122, American Society for Testing and Materials, Philadelphia, Pa., 1971.

T.W. Crooker, "The Role of Fracture Toughness in Low-Cycle Fatigue Crack Propagation for High-Strength Alloys," presented at Symposium on Fracture and Fatigue, Washington, D.C., 3-5 May 1972, *Eng. Frac. Mech.*, 1973, vol. 5, pp. 35-43.

T.W. Crooker, "Designing Against Structural Failure Caused by Fatigue Crack Propagation," *Nav. Eng. J.*, Dec. 1972, vol. 84 (no. 6), p. 46.

PLASTIC FRACTURE

G.R. Irwin, "Fracture Testing of High-Strength Sheet Materials Under Conditions Appropriate for Stress Analysis," Naval Research Laboratory, NRL Report 5486, July 27, 1960.

"Fracture Testing of High-Strength Sheet Materials: A Report of a Special ASTM Committee," ASTM Bulletins 243, pp. 29-40 (Jan. 1960) and 244, pp. 18-28 (Feb. 1960), American Society for Testing and Materials, Philadelphia, Pa.

J.I. Bluhm, "A Model for the Effect of Thickness on Fracture Toughness," *Proc. ASTM*, 1961, vol. 61, 1324.

J.G. Kaufman and A.H. Knoll, "Kahn-Type Tear Tests and Crack Toughness of Aluminum Alloy Sheet," *Mater. Res. Stand.*, 1964, vol. 4 (no. 5), p. 151.

J.E. Srawley and W.F. Brown, Jr., "Fracture Toughness Testing Methods," in *Fracture Toughness Testing and Its Applications,* ASTM STP 381, p. 133, American Society for Testing and Materials, Philadelphia, Pa., 1965.

D. Broek, "The Effect of the Sheet Thickness on the Fracture Toughness of Cracked Sheet," National Aerospace Laboratory (Amsterdam), Technical Report No. NLR-TR M.2160, Jan. 1966.

F.M. Burdekin and D.E.W. Stone, "The Crack Opening Displacement Approach to Fracture Mechanics in Yielding Materials," *J. Strain Anal.,* 1966, vol. 1 (no. 2), pp. 145-153.

R.W. Nichols, F.M. Burdekin, A. Cowan, D. Elliott, and T. Ingham, "The Use of Critical Crack Opening Displacement Techniques for the Selection of Fracture Resistant Materials," in *Practical Fracture Mechanics for Structural Steels,* pp. F1-F113, U.K. Atomic Energy Authority and Chapman and Hall, Ltd., London, 1969.

F.M. Burdekin, "Crack Opening Displacement—A Review of Principles and Methods," in *Practical Fracture Mechanics for Structural Steels,* pp. C1-C12, U.K. Atomic Energy Authority and Chapman and Hall, Ltd., London, 1969.

A.A. Wells, "Crack Opening Displacements from Elastic-Plastic Analyses of Externally Notched Tension Bars," *Eng. Fract. Mech.,* 1969, vol. 1, pp. 399-410.

A. Cowen and N. Kirby, "The Application of C.O.D. Measurements to Large Scale Test Behaviour," in *Practical Fracture Mechanics for Structural Steels,* pp. D1-D27, U.K. Atomic Energy Authority and Chapman and Hall, Ltd., London, 1969.

W.S. Pellini and R.W. Judy, Jr., "Significance of Fracture Extension Resistance (R Curve) Factors in Fracture-Safe Design for Nonfrangible Metals," pp. 1-20, *WRC Bulletin 157,* 1970.

R.J. Goode and R.W. Judy, Jr., "Fracture Extension Resistance (R-Curve) Features of Aluminum Alloys," *Metals Eng. Quart.,* 1971, vol. 11, (no. 4), p. 39.

R.W. Judy, Jr., and R.J. Goode, "Fracture Extension Resistance (R-Curve) Concepts for Fracture-Safe Design with Nonfrangible Titanium Alloys," Naval Research Laboratory, NRL Report 7313, Aug. 16, 1971.

C.N. Freed, A.M. Sullivan, and J. Stoop, "Influence of Dimensions of the Center-Cracked Tension Specimens on K_c," ASTM STP 514, pp. 98-113, American Society of Testing and Materials, Philadelphia, Pa., 1972.

A.M. Sullivan, J. Stoop, and C.N. Freed, "The Influence of Sheet Thickness Upon the Fracture Resistance of Structural Aluminum Alloys," ASTM STP 536, pp. 323-333, American Society for Testing and Materials, Philadelphia, Pa., 1973.

A.M. Sullivan, J. Stoop, and C.N. Freed, "Plane Stress Fracture Resistance of High-Strength Titanium Alloy Sheet," in *Titanium: Science and Technology; Proceedings, Second International Conference on Titanium,* pp. 1411-1426, Plenum Press, London, 1973.

R.W. Judy, Jr., and R.J. Goode, "Ductile Fracture Equation for High-Strength Structural Metals," Naval Research Laboratory, NRL Report 7557, April 3, 1973.

R.W. Judy, Jr., and C.A. Griffis, "Fracture Extension Resistance of Aluminum Alloys in Thin Sections," Naval Research Laboratory, NRL Report 7627, Oct. 12, 1973.

A.M. Sullivan and J. Stoop, "Further Aspects of Fracture Resistance Measurement on Thin Sheet Material: Yield Stress and Crack Length," in *Fracture Toughness and Slow Stable Cracking,* ASTM STP 559, p. 99, American Society for Testing and Materials, Philadelphia, Pa., 1975.

T. Swift, "Development of the Fail-Safe Design Features of the DC-10," *Damage Tolerance in Aircraft Structures,* ASTM STP 486, p. 164, American Society for Testing and Materials, Philadelphia, Pa., 1971.

Damage Tolerance in Aircraft Structures, ASTM STP 486, American Society for Testing and Materials, Philadelphia, Pa.,1971.

Fracture Toughness Evaluation by R-Curve Methods, ASTM STP 527, American Society for Testing and Materials, Philadelphia, Pa., 1973.

GENERAL

J.R. Hawthorne, L.E. Steele and W.S. Pellini, "Effects of Nuclear Radiation on the Properties of Reactor Structural Materials," ASME 61-WA-332, no. 28, 1961. Also, Naval Research Laboratory, NRL Report 5731, Jan. 22, 1962.

J.R. Hawthorne and F.J. Loss, "Fracture Toughness Characterization of Shipbuilding Steels," SCC-248, pp. 1-36, Ship Structure Committee, U.S. Coast Guard Headquarters, Washington, D.C., 1975.

S. T. Rolfe and J. M. Barsom, *Fracture and Fatigue Control in Structures—Applications of Fracture Mechanics,* Prentice-Hall, Englewood Cliffs, N.J., 1977.

INDEX

aircraft steels, 75–79, 250
alloy steels, 171, 281, 282
aluminum alloys, 79–81, 226
  R_p data, 298
  stress-corrosion cracking, 199, 200, 201
arc strikes, 60, 90, 109, 170
arrest criteria, 66–67, 133
arrest principle, 67, 130, 240, 277

buried-flaw test, 108

COD (*See* crack-opening displacement)
C_v test (*See* Charpy V test)
Certification, 4, 139, 233–234
  by analysis 240, 242
  stress corrosion cracking 184, 285
Charpy V test, 93, 123, 238
cleavage, 19–25
cold cracking, welds, 158
compliant structures, 217
constraint, 32–36
  maximum-constraint crack, 34–36
  relaxation, 36, 40–46, 52, 66, 71
  surface cracks, 51
constraint capacity, 34–47, 50, 53, 66
  Charpy V test, 53, 90, 92
  crack-opening displacement tests, 53
  Drop-Weight-NDT, 53–58, 99–105
constraint limits, 51, 56–60, 69
constraint transition, 33–45, 219–222
  microfracture relationships, 40
  tridimensional presentation, 43
continuous-cooling transformation diagrams, 168–172
corrosion fatigue
  crack-growth parameters, 230–207
crack growth
  sustained load characterization, 184–186
  cyclic characterization, 203–207
crack growth rates
  corrosion fatigue, 212
  stress-corrosion cracking, 198, 201–213
Crack-Opening Displacement
  tests, 39, 53, 225, 257

DT (*See also* Dynamic Tear test)
DT test
  index procedure, 57–60
  laminate materials, 298
  plastic fracture application, 225
DT test machines, 116, 135, 136
DWT (*See* Drop Weight test)
delayed cracking, welds, 161
design for welding, 145–146, 154
deterministic procedures
  design criteria, 122
  fracture analysis, 142
Drop-Weight test, 99–100, 114
dynamic fracture tests, rationale, 60
dynamic loading, 60, 255
Dynamic Tear (DT) test
  data bank use, 42, 59
  development, 114–137
  specimens, 115
dynamic yield strength
  definition, 49

elastic-plastic transition, 43–65
elastic stress, K-field, 10, 251–253
electrochemical environment, 183, 197
  K_{Iscc} relationship, 184
Explosion Crack Starter test, 96, 129, 134

FAD (*See also* Fracture Analysis Diagram)
fabrication specifications, 146
fatigue
  analysis, 203–214
  crack-growth parameters, 203–205
  electrochemical effects, 207
  power law, 204
flow curve, 32–38
Fracture Analysis Diagram, 105, 106, 109, 122
fracture-control plans
  cost analysis, 138
  deterministic analysis procedures, 55, 123, 142
fracture criteria, 31–36, 177
fracture-extension processes, 43, 241
fracture-extension stress, 48–68, 241
  RAD, 64–85
  ratio values reference, 65–69
fracture modes, 41, 111, 149
  transition, 221, 222

fracture properties, statistical variance, 24, 76, 237
fracture states, 31, 44, 248
  definition, 32–39
  scale, 237
  specifications, 247
  transition, 32–39, 266, 219–222
fracture stress, 40–42, 66
fracture tests,
  standardization requirements, 55
  structural meaning, 31–39
Fracture Transition Elastic (FTE), 97
Fracture Transition Plastic (FTP), 97

Geometric instability, 217–226, 230, 231

HAC (*See* hydrogen-assisted cracking)
HAZ (*See* heat-affected zone)
HY-80 steel, 128, 130, 148, 227, 283
HY-130 steel, 284
HY steels, 283
heat-affected zone, 150–170
  fracture properties, 149–152
high-alloy steels, composition, 282, 283
high strength steels, 128–141, 278–280
hydrogen-assisted cracking, 29, 159–184

IAD (*See* Instability Analysis Diagram)
initiation-control principles, 137, 277
Instability Analysis Diagram, 231

J-integral tests, 53–54, 225

K parameter, 251–253
K_c testing, 52, 253
K_{Ic} testing, section size, 46, 52–54, 258
K_{Ic}/σ_{ys} ratio, 51–54, 252–255
K_{Id}, section-size effects, temperature transition, 46, 116–120
K_{Id} characteristic curve, 263–267
  graphical analysis, 263–275
K-field, 10, 251–252

lamellar tearing, 159
lateral expansion, C_v test, 238, 239

metal improvement, rational principles, 125
metal quality
  RAD reference system, 64–78
  statistical analysis, 77
metal-quality corridors, 64–73
  steel-melting practices relationship, 73
  stress-corrosion cracking, 188–190
  weld properties, 150–155
microcracking, 9–29
  foreign phases, 72, 73
  grain-aggregate, 9–18
  hydrogen, 29
  stress corrosion cracking, 194–199

NDE (*See* Nondestructive Evaluation)
NDI (*See* Nondestructive Inspection)
NDT (*See also* Nil-Ductility Transition)
NDT determination, reproducibility, 58
NDT frequency distributions, 114
NDT temperature, 99–105
  specific constraint condition, 58
  statistical testing, 59
natural-crack tests, 94–104
neutron damage, 244
Nondestructive Evaluation, 140, 141
Nondestructive Inspection, 140, 141

PZS (*See* plastic zone size)
pearlitic steels, transformation features, 169
plane-strain
  definition, 221, 251–255
  constraint, 43, 141, 250–258
  limit, 50–69, 264–267
plane-strain surface cracks, calculations, 51, 260, 272
plane-strain test
  bend, 259
  compact tension, 259
plane-strain transition, 45–66, 117–122, 220–222
plane stress, 221, 257
plastic enclave, 26–28, 120, 223
plastic fracture, 217–225
plastic-zone size, 251–255
  definition, mathematical, 49
pneumatic loading, 111, 112, 228, 229
power law, fatigue relationship, 204–210
process zone, 10
prototype tests, 130

quenched and tempered steels, transformations, 171–174

R_p scale, RAD, 299
RAD (*See also* Ratio Analysis Diagram)
RAD summary, K_{Iscc} data for steels, 188
R-curve, 219, 291–294
R_p data
  aluminum alloys, 298
  steel alloys, 298
  titanium alloys, 298
  scale, 228, 297
rate-sensitive metals, 59–61

Ratio Analysis Diagram (RAD)
  aluminum alloys, 79, 80
  metallurgical zoning, 78
  procedures, 64–84
  steels, 64–84
  titanium alloys, 79, 80
ratio-grid system (RAD), 64–84
redundant design, 137, 240
residual stresses, 107, 199
  spontaneous fracture, 111
resistance curve (*See* R-curve)
restraint cracking, welds, 159, 162
restraint stresses, 156, 163
Robertson Crack-Arrest temperature, 102–104
Robertson Crack-Arrest test, 102–104

SI (*See* structural integrity)
SLC (*See* sustained-load cracking)
section size
  K_{Ic} testing, 258
  thickness effects, 56–64, 117–120
K_{Iscc} testing, 185–186
shelf
  dynamic transition, 113
  slow loading, 113
ship failure steels, 15, 87–109, 170
steel alloys, R_ρ data, 298
steel, thick section, temperature transition, 46, 117–119
steels
  high strength, 128–154, 278, 280
  HY-80, 128
  maraging, 283
  pearlitic, 169, 285
  ultrahigh strength, 131
  weldable, 126–128, 282
stress-corrosion cracking, 180–199
  aluminum alloys, 199–201
  microfracture processes, 194
  RAD procedures, 191–193
  titanium alloys, 200, 201
stress ratio, fatigue testing, 205
stress-relief cracking, welds, 159
structural prototype tests, 129–134
  weld regions, 149
structural redundancy, 142
structural steels, standard grade, reference system, 285
sustained-load cracking, 183–185

technological limit curve, 64, 125
tensile restraint cracking, welds, 163
tensile test transitions, 20
thin-sheet plane-stress problems, 224–226
titanium alloys, 79–81, 132, 141, 184
  R_ρ data, 298
  stress-corrosion cracking, 200, 201
trend band (RAD)
  steels, 65–76
  stress-corrosion cracking, 189, 199
    sustained-load cracking, 183, 184
triaxial stress system, cracks, 25–34, 251–252

void growth, processes, 27–29

warm mechanical prestressing, 109
weld geometry, 152
weld metals, strength transition, 148–153
weld regions, 147, 164
  crack states, 145, 166
  metallurgical zones, 148–153
weld zone cracking, categories, 155–160
weldability tests, 155, 171
weldable steels
  high strength, 126–128, 282
welding processes, 175–178
welding electrodes, 180–182
welding metallurgy, 169–170
welds
  cracking, 155–160
  design, 145–164
  fracture properties, 150–152
  residual stresses, 107, 108
  weldability optimization, 146–148

yield criterion (YC), 52, 66, 123, 266
  DT test indexing, 52, 56–57
  definition, 52

U. S. GOVERNMENT PRINTING OFFICE : 1977 O - 230-362